Chaitanya B. Pande
Kanak N. Moharir *Editors*

Groundwater Resources Development and Planning in the Semi-Arid Region

Springer

Groundwater Resources Development and Planning in the Semi-Arid Region

Chaitanya B. Pande • Kanak N. Moharir
Editors

Groundwater Resources Development and Planning in the Semi-Arid Region

Springer

Editors
Chaitanya B. Pande
Sant Gadge Baba Amravati University
Amravati, Maharashtra, India

Kanak N. Moharir
Sant Gadge Baba Amravati University
Amravati, Maharashtra, India

All India Coordinated Research Project
for Dryland Agriculture
Akola, Maharashtra, India

ISBN 978-3-030-68123-4 ISBN 978-3-030-68124-1 (eBook)
https://doi.org/10.1007/978-3-030-68124-1

This Springer imprint is published by the registered company Springer Nature Switzerland AG
The registered company address is: Gewerbestrasse 11, 6330 Cham, Switzerland

Dedicated to my parents and all my teachers

Preface

Semi-arid regions of the earth are today suffering from lack of sustainable water and groundwater. There is a growing demand throughout the world for sustainable watershed development, management, and planning. The demand is more significant in the rain-fed and drought-prone areas of earth surface, where watershed management is poorer and groundwater is limited. The primary focus of the book is the improvement of groundwater, aquifer mapping, soil and water conservation planning, suitable zones of groundwater development, flood mapping with surface runoff, trends of rainfall, land use impact on the groundwater, watershed development and planning, and water resource and environmental management. Conservation measures involve the preparation and implementation of various projects to improve the management of watershed functions that affect the plants, animals, and human communities within the watershed boundary. Rapid, accurate, and cost-effective latest technologies, Modflow software, machine learning, artificial intelligence, and geospatial technologies can be used for planning for groundwater development in the semi-arid region.

The book discusses on the groundwater related issues such as groundwater flow, watershed development, land use, rainfall, delineation of groundwater potential zones, soil and water conservation planning, and development of water and soil resources in the semi-arid region. The book highlights the recent application areas of groundwater flow modelling software, wavelets techniques, remote sensing, GIS, methods in rainfall trends, water conservation techniques in the field of watershed development, groundwater planning, changes of land use, monitoring and modelling of groundwater and aquifer mapping, hydrological modelling, and sustainable land management. This book has 26 chapters contributed by various researchers, scientists, and professors from various countries.

The book includes the research work of professors, planners, scientists, and research scholars from various universities, international organisation, and institutions from India as well as from other countries of the world, such as National

Institute of Hydrology, University of Bergen, Geophysical Institute, CIMA Research Foundation—International Centre on Environmental Monitoring, Helmholtz-Zentrum für Umweltforschung, Fiji National University, James Cook University, Australia, Bahir Dar University, University of Mumbai, Maulana Azad National Urdu University, Indian Institute Technology Roorkee, Indian Institute of Technology (BHU), Varanasi, École des mines d'Alès, avenue de Clavières, National Institute of Technology Raipur, Sathyabama Institute of Science and Technology, Bharathidasan University, All India Coordinated Research Project for Dryland Agriculture, Dr. Panjabrao Deshmukh Krishi Vidyapeeth, Akola, M. Kumarasamy College of Engineering, Chemiqua Water & Wastewater Company Kraków, University of Naples Federico II, RWTH Aachen University, National Centre for Earth Science Studies, University of Kerala, The Gandhigram Rural Institute-Deemed to be University, University of Lucknow, Indian Institute of Remote Sensing, ISRO, and Asian Institute of Technology, Bangkok.

Amravati, Maharashtra, India — Chaitanya Baliram Pande
Akola, Maharashtra, India — Kanak N. Moharir

Contents

1 **Issues and Challenges of Groundwater and Surface Water Management in Semi-Arid Regions** 1
Khadeeja Priyan

2 **Review of GIS Multi-Criteria Decision Analysis for Managed Aquifer Recharge in Semi-Arid Regions** 19
Sajad Fathi, Jenny Sjåstad Hagen, Alessia Matanó, and Guilherme E. H. Nogueira

3 **Robust Ensemble Modeling Paradigm for Groundwater Salinity Predictions in Complex Aquifer Systems** 53
Alvin Lal and Bithin Datta

4 **Modeling Landscape Dynamics, Erosion Risk, and Annual Sediment Yield in Guna-tana Watershed: A Contribution for Microwatershed Level Conservation Priority Area Identification** 73
Daniel Asfaw, Getachew Workineh Gella, and Mulualem Asfaw

5 **Evaluation of Multiwell Pumping Aquifer Tests in Unconfined Aquifer System by Neuman (1975) Method with Numerical Modeling** 93
Nitin Rane and Geetha K. Jayaraj

6 **Groundwater Remediation Design Strategies Using Finite Element Model** 107
S. M. V. Sharief and Mohammad Zakwan

7 **Modeling of Groundwater Level Using Artificial Neural Network Algorithm and WA-SVR Model** 129
Shishir Gaur, Anne Johannet, Didier Graillot, and Padam Jee Omar

8 Development of Conceptual Model and Groundwater Flow Modeling Using GMS Software: A Case Study for Dharsiwa Block, Chhattisgarh, India 151
Aman Kumar Bohidar and Ishtiyaq Ahmad

9 Numerical Modeling for Groundwater Recharge 165
Marykutty Abraham, Priyadarshini, and Kavisri Manikannan

10 Assessment of Aquifer Vulnerability for Sea-Water Intrusion in Nagapattinam Coast, Tamil Nadu, Using Geospatial Techniques 179
Rajesh Jayaraman and Lakshumanan Chokkalingam

11 Watershed Planning and Development Based on Morphometric Analysis and Remote Sensing and GIS Techniques: A Case Study of Semi-Arid Watershed in Maharashtra, India 199
Chaitanya B. Pande, Kanak N. Moharir, and SFR. Khadri

12 Correlation Between Land Surface Temperature and Vegetation Cover of Nagapattinam Coastal Zone, Tamil Nadu, Using Geospatial Techniques 221
Rajesh Jayaraman and Lakshumanan Chokkalingam

13 GIS-Based Legitimatic Evaluation of Groundwater's Health Risk and Irrigation Susceptibility Using Water Quality Index, Pollution Index, and Irrigation Indexes in Semiarid Region 239
Balamurugan Panneerselvam, Kirubakaran Muniraj, Maciej Thomas, and Nagavinothini Ravichandran

14 Hydrogeochemistry of Groundwater Quality in Amaravathi River Basin of Karur District (Tamilnadu) Using Graphical and Multivariate Statistical Methods 269
Jafar Ahamed A and Loganathan K

15 GIS-Based Assessment of Urban Groundwater Pollution Potential Using Water Quality Indices 293
Manish Kumar Sinha, Preeti Rajput, Klaus Baier, and Rafig Azzam

16 Multivariate Statistical Tools in Assessing the Quality of Water Resources in Netravati River Basin, Karnataka, India 315
S. Gayathri, A. Krishnakumar, K. Devi Chandana, Sibin Antony, Vinu V. Dev, V. Arun, and K. Anoop Krishnan

17 Seasonal Variation of Groundwater Quality in the Kallada Basin, Southern Western Ghats of India 335
Uma Mohan and A. Krishnakumar

18 GIS-Based Water Quality Assessment of Chalakudy River Basin, Southern Western Ghats, India 353
R. Resmi, A. Krishnakumar, and K. Anoop Krishnan

19 Groundwater Resources Management Using Remote Sensing and GIS 369
Rohit Sambare, Vishal Singh, and Sanjay Kumar Jain

20 Trend Analysis of Groundwater Level Using Innovative Trend Analysis 389
Mohammad Zakwan

21 Change Detection Analysis and Delineation of Artificial Groundwater Recharge Suitability Zone for Dindigul Block Using Geoinformatics Techniques 407
S. Arivazhagan, A. Karthi, M. Kirubakaran, and V. T. Mubasheer

22 Artificial Replenishment of Ground Water by Rain Water Harvesting: A Case Study 435
Sejal Desai

23 Reservoir Sedimentation Assessment of Rihand Reservoir Using Remote Sensing Technique 453
Smrati Singh, Abhishek Kumar Yadav, and Arun Pratap Mishra

24 A Coupled Hydrological and Hydrodynamic Model for Flood Mitigation 467
Triambak Baghel, Manish Kumar Sinha, Ishtiyaq Ahmad, and M. K. Verma

25 Modelling and Assessment of Flood Discharge Based on Intensity-Duration-Frequency Curves in Kuttanad District, Kerala, India 485
J. Brema and Minnu K. Benny

26 Groundwater Development and Planning Through Rainwater Harvesting Structures: A Case Study of Semi-arid Micro-watershed of Vidharbha Region in Maharashtra, India 513
R. S. Patode, Ranee Wankhade, Sumiran Dabrase, M. B. Nagdeve, Chaitanya B. Pande, V. V. Gabhane, A. B. Turkhede, R. S. Mali, and V. P. Pandagale

Index 559

About the Editors

Chaitanya B. Pande (Dr. PDKV, Akola) received his Ph.D. from Sant Gadge Baba Amravati University, Amravati. He has more than a decade of university, research, and industrial experience. Dr. Pande is a reviewer of *Earth Science Research Journal*, *American Journal of Geophysics, Geochemistry, and Geosystems*, *Sustainable Water Resources Management* (Springer journal), *Modeling Earth Systems and Environment* (Springer journal), *Applied Geomatics* (Springer journal), *Journal of Agriculture Sciences* (Bioinfo Publication), *Applied Water Science* (Springer), *Journal of the Institution of Engineers (India): series A* (Springer), *Groundwater Sustainable Development* (Elsevier journal), and *Environmental Sustainable Development* (Springer journal). He has published 40 research papers in international journals with Springer, Taylor and Francis, and Elsevier with citations more than 355. He has published one book with Springer. He has presented more than 20 research papers in national and international conferences. His research interests include remote sensing, GIS, watershed management, hydrogeology, hydrological modelling, land use and land cover analysis, groundwater quality, urban planning, hydro-geochemistry, groundwater modelling, geology, hyperspectral remote sensing, remote sensing and GIS application in natural resources management, watershed management, and environmental monitoring and assessment subjects.

Kanak N. Moharir works in the Department of Geology, Sant Gadge Baba Amravati University, Amravati, and is a Researcher in the Department of Geology at Amravati University, Amravati. With more than 6 years of teaching and research experience, she has published more than 37 research papers in various national and international journals and has presented 15 research papers in national and international conferences with citations more than 280. Her research interests include remote sensing, watershed management hydrology, land use and land cover, aquifer mapping, groundwater modelling, hydrogeology, geomorphology, and geology. She is a reviewer of eight springer journals and other journals.

Chapter 1
Issues and Challenges of Groundwater and Surface Water Management in Semi-Arid Regions

Khadeeja Priyan

Contents

1.1 Introduction 1
1.2 Semi-Arid Regions 4
1.3 Water Scarcity 4
1.4 Climate Change and Impact of Floods and Droughts 5
1.5 Issues and Challenges of Groundwater Management 6
1.6 Sustainable Water Management 9
1.7 Challenges for Sustainable Groundwater Management 9
1.8 Challenges in Surface Water Sources 12
1.9 Conclusion 14
References 14

1.1 Introduction

Water is an essential natural resource for survival and ecological development on Earth. Currently, all countries face surface water and groundwater problems, especially in semi-arid regions; these problems include water pollution, groundwater changes, lack of rainfall, declining agricultural production, and climate change–related factors (Pande et al. 2018a). Water is a scarce and, hence, precious resource as a result of human population expansion, industrialization, urbanization, and increased irrigated agriculture. Agriculture is the largest user of groundwater and surface water, but in the future other factors will place greater demands on water in

K. Priyan (✉)
Civil Engineering Department, G H Patel College of Engineering and Technology, Vallabh Vidyanagar, Gujarat, India
e-mail: khadeejapriyan@gcet.ac.in

C. B. Pande, K. N. Moharir (eds.), *Groundwater Resources Development and Planning in the Semi-Arid Region*, https://doi.org/10.1007/978-3-030-68124-1_1

semi-arid areas (Seckler et al. 1998), and water resources for agriculture will be overused or underused (Tanji and Kielen 2002). India has more than 17% of the world's population but only 4% of its water resources and 2.5% of its land resources. According to Nitiayog data, 20.92% of the population in India lives below the poverty line. Over the years, the demand for water has been increasing manyfold in various sectors, such as agriculture, domestic consumption, industry, and power generation as the population has increased. The demand for freshwater is increasing due to rapid and unplanned urbanization and economic growth (Sahasranaman and Arijit 2018). Since water is a precious resource in agriculture, every drop of water available for irrigation is significant for overall farming efficiency. Due to the challenges in groundwater and surface water resources, Indian agriculture faces water scarcity. Over the years, agricultural output in India has become less remunerative and more uncertain. This chapter discusses various issues and challenges connected to groundwater resources and planning in semi-arid regions.

Water is a common pooled resource that can be managed only when all stakeholders, such as residents, civil society and government, or a combination of all these, understand its importance as a common resource (water portal, 2020). The various governments involved are trying to implement sustainable water management policies. These policies mainly aim at the development and management of sustainable water resources. Several studies have looked at local demand and supply situations. Molden et al.'s (2001) investigation was based on various water-scarcity studies around the world. It classified water-scarcity areas into three categories: (1) water-scarce areas, (2) high potential areas, and (3) high need areas. Based on this classification, physical water scarcity is experienced in water-scarce areas, water logging and salinity problems are found in high potential areas, and water scarcity with respect to economic, financial, and skilled human resources is found in high need areas. Hence, there is no universal solution to global water crises. However, owing to large special and temporal variations, many regions experience water scarcity. Water-scarce regions lack adequate clean water to meet human drinking water and sanitation needs. This impacts human health, productivity, the environment, and ecosystems (Cosgrove and Loucks 2015). Growth in irrigated agriculture poses a serious threat to the environment in many places around the globe (Abdullaev 2004).

It has been estimated that the global supply of available water is more than sufficient to meet current and foreseeable demand in the world (Molden et al. 2001; Cosgrove and Loucks 2015). Its spatial and temporal distribution across the globe varies. About 60% of the annual precipitation on the Earth's surface, 108,000 km^3, evaporates into the atmosphere and the remaining flows towards the sea, of which about 20–25% could be managed effectively (Seckler et al. 1998). Freshwater requires meeting demand for domestic, economic development, and environmental needs. The available resources are inadequate in many parts of the world to meet these needs (Cosgrove and Loucks 2015).

Aquifers are vulnerable to pollution through porous media or through fractures or cavities. In urban areas, the presence of microorganisms poses a threat to the quality

of drinking water. Owing to intense agricultural activities and industrialization, contaminated water flows increasingly through subsurface layers into groundwater. Surface water resources are under stress due to the declining potential for augmenting existing supplies and the pollution of freshwater resources from domestic and industrial wastes. Efficient and effective water management techniques are of paramount importance for groundwater sustainability. All governments have initiated flagship programmes to implement sustainable water management programmes.

Demand for water continues to increase due to population growth, industrialization, and urbanization. As the supply of water decreases, increasing competition and growing conflicts between these sectors pose a significant threat to water management. Hence, water management needs to address the balance between water demand and supply. Semi-arid regions are categorized according to whether they are in developed or underdeveloped countries, but the bottom line is that they are regions which receive little rainfall in a given year. Although this may seem like an ideal scenario, the drawbacks of semi-arid regions stem from the unreliability of water availability throughout the year. Water is a scarce economic commodity, and climate change affects both special and temporal variability. Groundwater or subsurface water is defined as the total water found beneath the surface of the ground and is considered part of the hydrologic cycle (Fig. 1.1). This chapter discusses the issues and challenges of water management (both groundwater and surface water) on both the supply and demand sides in the face of climate change. The study mainly highlights the issues and challenges faced in semi-arid regions in India, as well as

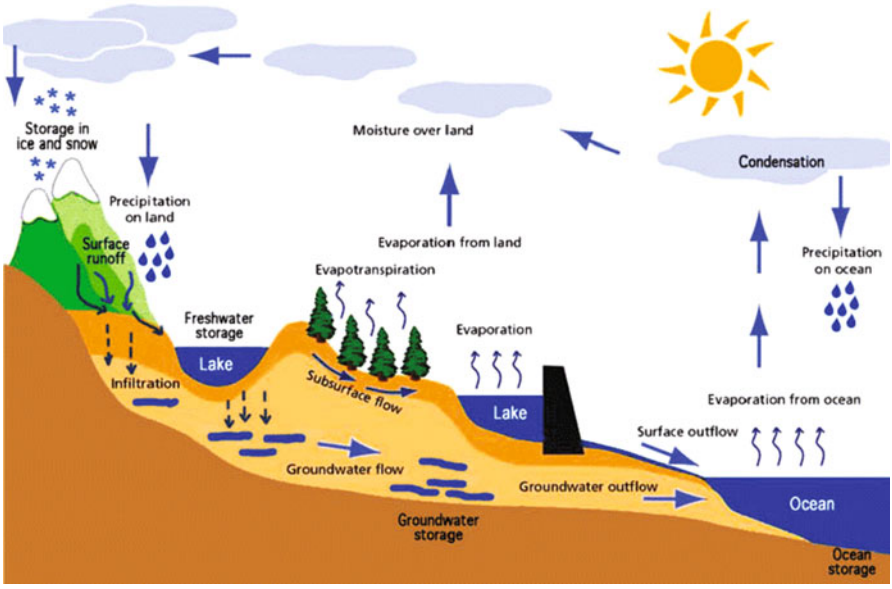

Fig. 1.1 Schematic diagram of hydrologic cycle

initiatives taken by the country for sustainable development. It also focuses on the scope and limitations of supply- and demand-side approaches to water management.

1.2 Semi-Arid Regions

Water is a precious natural resource which is severely stressed in many parts of the world. Because water scarcity is a major concern in many semi-arid regions lacking perennial sources of water, managing the available usable water is crucial. Generally, these regions experience water scarcity due to low levels of rainfall and high evapotranspiration rates, and they face drought, low precipitation, and acute water shortages. Since the late nineteenth century, large-scale irrigation has been practised in many arid and semi-arid regions (Tanji and Kielen 2002; Pande and Moharir 2015). Groundwater is a reliable source of water in arid and semi-arid regions and has been widely consumed for irrigation, domestic, and industrial uses. Exhaustive water abstraction has led to aquifer overexploitation and resulted in a lowering of the water table at alarming rates. The northern and western parts of Gujarat state are semi-arid regions in India. These regions experience highly erratic rainfall with very high evaporation rates. The percolation of water to the groundwater table takes place mainly through fractures and fissures present in hard rock, which leads to a deep water table. All rivers are seasonal rivers. Stream orders were identified in between 1–6. Groundwater in key aquifers is rapidly depleted, which results in the degradation of aquifers. Generally, the upper reaches of river basins in semi-arid regions contain steep topographic gradients, which cause high runoff. The groundwater recharge potential is very low because of insufficient rainfall, watershed planning, and low storage capcity. Many semi-arid areas have compact and fissured rocks and the aquifers results under the moderate water yield potential. The lower reaches of semi-arid regions have good groundwater potential, but they also suffer from salinity problems.

1.3 Water Scarcity

Water is a scarce economic commodity. Since water shortage is experienced in different seasons, augmentation techniques are adopted on both the supply and demand sides of water management. As challenges in water development and management increase, the quality and quantity of freshwater are also affected. Many of the world's watershed areas and river basins are overexploited and in a state of chronic water stress. The permanent depletion of groundwater resources could have severe consequences with associated environmental impacts. It has also been observed that in coastal areas, due to excessive pumping and deepening of aquifers, freshwater aquifers have been contaminated by sea water. Rapid urbanization and land-use changes have resulted in reductions in the natural infiltration or

recharge of aquifers. Similarly, in inland regions, especially alluvial areas, irrigation with high total dissolved solids from deep aquifers causes land degradation. In hard-rock areas of Saurashtra, excessive pumping has led to the drying up of wells and acute shortages of water for drinking and irrigation purposes (Kumar 2001; Khadri and Moharir 2016). There is thus an urgent need to augment valuable water resources, i.e., groundwater and surface water resources. This has led to various problems related to the quantity and quality of water and issues such as the deterioration of surface water quality, water levels, and the depletion of groundwater sources. A realistic approach to water management takes into consideration social and economic aspects. Freshwater demand in the world doubles every 21 years. To achieve effective utilization of available water resources, Keller et al. (1996) observed discharges could be captured effectively to meet demand growth in basin area.

1.4 Climate Change and Impact of Floods and Droughts

Climate change has significant negative impacts that pose a major economic threat in the world that will last into the next decade (CSE 2020). According to the CSE's report, the top risk in the past 4 years stemmed from extreme weather events, and the failure of climate change mitigation and adaptation will have a huge impact on the global economy. In 2019, around 2359 per 100,000 people were affected by climate change disasters. Most Indian cities are vulnerable to flooding in monsoon months due to the non-availability of proper stormwater management systems. According to the 2011 census, Indian cities are home to 31% of the total population and their GDP contribution is 63%. It is estimated that by 2030, India's urban population will become 40% of the total with a GDP contribution of 75%. This may result in a huge demand for urban infrastructure. Urban growth development often results in an uncontrolled rise in peak flood hydrographs. Hence, stormwater management poses a significant challenge for urban developers like civic authorities, consultants, and landowners. Innovative stormwater management techniques are essential to solve the problems associated with this challenge, such as reduced groundwater recharge, which leads to a lowering of the groundwater table at an alarming rate and environmental pollution. Water is considered the first line of defence against climate change (water portal, April 2020). People experience difficulty on a daily basis accessing water due to climate change. The water crisis can be tackled by judicious utilization of this precious resource by promoting water conservation and sustainable water-use techniques. Water quality management should be effectively integrating by wastewater treatment systems. Sahasranaman and Arijit (2018) argue that 'clean India' and 'Swachh Bharat' campaign will be successful if proper sanitation measures are implemented successfully.

Many cities have conventional stormwater practices in the form of drainage through sewers. However, all smart city proposals emphasize above all landscape development. Proposals incorporate the need for rainwater harvesting and

stormwater management for reuse and conserved water in aquifers (www.smartcities.gov.in). Low impact development (LID) for stormwater management is an innovative initiative of green infrastructure that originated in 1990 to mitigate climate change and pollution control. Green infrastructure ensures the sustainable management of limited open spaces available in urban areas and provides a good opportunity for developing and preserving urban landscapes. This strategy uses various techniques to mitigate the impact of increased urban stormwater runoff near the sources and brings certain ecological advantages. It includes different site design strategies which will be helpful for better hydrological components, for example infiltration, evapotranspiration, filtration, harvesting, and retention. This will be helpful in controlling flooding resulting from improper stormwater management. The hydrological impacts of LID are peak discharge control, improved groundwater infiltration, and improved evapotranspiration.

Various structural and non-structural best management practices (BMPs) have been studied, and these practices have been adopted in the USA, Canada, UK, and other countries. Landscape-based LID techniques, in the form of, for example, green roofs, rainwater harvesting, grass swales and dry swales, bioretention, permeable pavement, perforated pipe systems, and soakaways, have been designed and adopted in various countries. Bioretention or raingardens have been adopted as an effective BMP in the USA (Davis et al. 2009). Bioretention is an effective method whereby all the physical, chemical, and biological processes of a natural hydrologic system are performed. The quality of infiltrated water will improve once it passes through different porous soil media. Bioretention is one of the popular stormwater management practices for addressing urban non-point pollution in New England (Dehais 2011).

1.5 Issues and Challenges of Groundwater Management

Groundwater recharge of rainwater through soil contributes to the rise of the groundwater table and is a reliable source of water in semi-arid regions. Groundwater caters to the demand of the country's ever-growing domestic, agricultural, and industrial sectors and is extensively exploited by various users. The accumulation of groundwater also happens from recharge brought about by seepage losses from irrigation networks and deep percolation from farm irrigation (Tanji and Kielen 2002). Irrigation through all sources has contributed significantly to agricultural production in arid and semi-arid regions. Because rivers are seasonal in these regions, groundwater is the only dependable source of water. Wells are observed in many parts of semi-arid regions, especially on the upstream sides of the river basins located in semi-arid regions. Large seasonal drops in groundwater levels are observed in these regions, which face acute water issues, in terms of both quantity and quality (Pande et al. 2019a; Moharir et al. 2019).

India's irrigation agriculture has two components: (1) surface (canal) irrigation development and (2) groundwater resource development. Surface (canal) irrigation

development requires high public investment by the states, whereas groundwater resource development involves private tube well development. The share of groundwater sources for irrigation has increased from 28.7% (1950–1951) to 62.4% (2012–2013), but the share of canals in net irrigated areas has decreased from 39.8 to 23.6%.

The mechanized pumping technologies which emerged in the mid-twentieth century caused widespread drawdown externalities, and this resulted in the overdevelopment of groundwater resources, which led to the depletion of shallow aquifers (FAO 2003). The increased application of engineering approaches is a viable way to achieve economic returns in water productivity. Raising the physical productivity of water in crops without due consideration to economics will have little relevance for small farmers in developing countries (Kumar and Van Dam 2013, b).

1.5.1 Overexploitation of Groundwater Sources

Perennial sources of surface water are not available in most semi-arid regions. The groundwater table declines when discharge is higher than recharge. Deeper water levels are observed in overexploited parts of semi-arid regions. Deep confined aquifers, which are grouped into, first, aquifers whose depth varies from 78 m below groundwater level (bgl) and, second, aquifers varying from 154 to 274 m bgl, which existin in North Gujarat (CGWB 2018). According to the CGWB report, steep declines have been noticed during the last 5 years in North Gujarat. The groundwater level is declining at an average rate of 2 m per year in deeper aquifers. Two distinct hydrogeological rock units, such as hard rock and soft rock, have been identified (Khadri and Pande 2016b)

The scale and rate of abstraction due to massive expansion in pumping capacity and the rate of groundwater level decline have made the aquifer system vulnerable to overabstraction. Groundwater recharge and conservation programmes are needed in the Saurashtra, North Gujarat, and Kachchh regions. In these areas, groundwater recharge through artificial recharging techniques should be enhanced. Irrigation is the single largest user of water, accounting for more than 70% of the world's supplies of developed water (Seckler et al. 1998). The negative impacts of groundwater exploitation include (1) a declining groundwater level, (2) groundwater contamination, (3) decreased crop yields, (4) land subsidence, and (5) a reduction in environmental flows (Khadri and Pande 2016a; Patode et al. 2016).

FAO (2003) identifies the following consequences of groundwater exploitation:

- Changes in flow patterns in nearby aquifers;
- Reduction in water usage for ecological purposes, such as base flows in streams and wetlands, and damage to ecosystems and downstream users;
- Increased pumping costs and energy usage;
- Land subsidence and damage to surface infrastructure.

1.5.1.1 Declining Groundwater Tables

Due to the mechanized pumping technologies which emerged in the mid-twentieth century, widespread drawdown externalities have occurred, resulting in the depletion of shallow aquifers (FAO 2003). Groundwater levels have declined at an alarming rate, and proper control measures and planning should be put in place to conserve water in aquifers. Adequate augmentation of groundwater recharge schemes should be implemented through artificial recharging methods.

1.5.1.2 Pollution in Aquifers

Degradation of aquifers is caused mainly by the disposal of human and industrial waste and the percolation of pesticides and herbicides. Aquifers are vulnerable to pollution through porous media or fractures/cavities (Moharir et al. 2020). Generally, the quality of deep aquifers is better than that of shallow aquifers. In subsurface layers, bacteria can survive up to 50 days, but a virus can survive for longer. In urban areas, the presence of microorganisms is a threat to the quality of drinking water. Due to intensified agricultural activities and industrialization, contaminated water flows are increasingly finding their way to subsurface layers and into groundwater (Moharir et al. 2017; Khadri and Moharir 2016; Pande et al. 2018b).

Sources of pollution:

- Agricultural pollution
  - Extensive use of agricultural chemicals
  - Non-point sources pollution, predominantly in agriculture rather than industry and municipal sewage systems as large coverage of area.
  - Fertilizer
  - Nitrate concentration (Gujarat) and other nutrient pollution
  - Extensive irrigation
- Urban pollution
  - Leaking sewers and other wastewater sources
  - Urban flooding
  - Construction materials
  - Domestic wastewater disposal

Impact of groundwater pollution:

- Water-borne diseases, e.g. cholera
- Pollution externalities
- Major causes of groundwater contamination

1.6 Sustainable Water Management

India faces challenges in achieving 9 out of 17 sustainable development goals (CSE 2020). There is a need to develop strategies to reduce water stresses. Al-Jawad et al. (2019) suggested through their modelling approach in the Diyala River Basin in Iraq that to achieve sustainability within the next 25 years, strategies need to be developed to reduce water stresses by 45%. Sustainable Development Goals (SDGs) use various indicators for water resource management. These indicators are source augmentation and restoration of water bodies, source augmentation (groundwater), large- and medium-scale irrigation (supply-side management), watershed development (supply-side management), participatory irrigation practices (demand-side management), sustainable on-farm water use practices (demand-side management), rural drinking water, urban water supply and sanitation, and policy and governance. With respect to these indicators, Gujarat ranks first, with 7.5 points. The country average is 4.52 and the water metric includes surface water and groundwater (Pande et al. 2017).

1.7 Challenges for Sustainable Groundwater Management

Because India is an agrarian country, the present and future challenges of sustainable agricultural demand can be met by technological innovation. To improve crop productivity, efficient irrigation techniques are needed to raise yield production. Over the years it has been seen that Indian agriculture is beset with water scarcity and has become less profitable and more uncertain. Hence, there is a prudent and urgent need to use available water efficiently; micro-irrigation is one innovative technology that holds great promise in terms of raising crop yields. Because land and water are basic needs in the agricultural and economic development of any country, 70% of India's population is dependent on agriculture for their livelihood. Gujarat has many hectares of unused cultivable land (Pande and Moharir 2018).

Timplementation of sustainable groundwater management faces several challenges. For sustainable groundwater management, adequate scientific data are required on the following matters: (1) Annual water balance of recharge and abstraction; (2) inter-annual variability of replenished water through recharge since variability is very high; (3) reliability and productivity of wells in terms of water levels and water quantity and quality; (4) availability of reliable time-series data of groundwater level in specific aquifers; (5) quantifying aquifer recharges; (6) sustainability of socio-economic activities in relation to falling groundwater levels, which is complex; (7) groundwater overdraft and declining quality; (8) groundwater pollution, including urban wastewater discharges and industrial pollution; (9) overstressing of local aquifers in urban areas—struggling to maintain water quality; (10) groundwater pollution from agricultural chemicals; (11) cost of pollution control and aquifer remediation; (12) salinity and waterlogging; (13) deaths

related to water pollution; (14) soil and groundwater contamination due to industrialization and population growth; (15) patterns and management of groundwater use—socio-economic development, urban vs. rural use, including irrigated agriculture; (16) decision-making framework; (17) assessment system; and (18) long-term effects of climate change and global warming. The sustainable yield of an aquifer must be estimated to determine the nature and variability of aquifer recharge, quality of recharge water, control of aquifer degradation, techniques to enhance recharge, and patterns and intensity of groundwater use. Some of these data are technical, whereas others are socio-economic in nature. Scientists and researchers should give priority to both these types of data if they wish to obtain reliable and accurate results (Pande 2020a).

A good assessment system is required to determine groundwater availability and productivity. Legislation should be put in place to prevent unauthorized drilling or deepening of wells and pumping of water. At the farm level, low-flow irrigation networks are required for sustainability water conservation. Micro-irrigation techniques, such as drip irrigation, sprinkler irrigation, and others, are common methods used in precision farming and sustainable agriculture development (Pande 2020c). This techniques can be adopted by farmers. This methods can be reduce loss of water during irrigation. To reduce evaporation loss from the soil using this method, mulching can also be used. This can help to improve crop yields and optimize water use. Usually plastic mulches are used, but their disposal is very harmful. Micro-irrigation techniques have advantages and disadvantages. Its advantages are as follows: (1) water application efficiency is high; (2) fields with irregular shapes can be easily irrigated; (3) recycled non-potable water can be safely used; (4) soil type plays a less important role in the frequency of irrigation; (5) fertilizer application efficiency is high because it can be mixed with water before application; (6) soil erosion is reduced; (7) weed growth is controlled; (8) water distribution efficiency is highly uniform, controlled by the output of each nozzle; (9) labour costs are lower than other irrigation methods; (10) variation in supply can be managed by regulating valves and drippers; and (11) it is usually performed at lower pressure than other types of pressurized irrigation, reducing energy costs (Pande 2020d).

Drip irrigation's disadvantages are as follows: (1) the initial costs can be more than those of overhead systems; (2) the pipes should be clogged and the water is not properly filtered by equipment; (3) water, time, and harvests will be wasted if the system is not installed properly; and (4) the all PVC pipes often suffer from rodent damage, requiring the replacement of the entire pipes and increasing expenses. These systems require careful study of all the relevant factors, like topography, soil, water, crop and agro-climatic conditions, and the suitability of a drip irrigation system and its components.

Though technology holds great promise and benefits, according to the report published by IAI et al. (2016), the national schemes initiated since 2006 have not addressed the following important issues related to planning and implementation of the technology: (1) inadequate focus on nationwide spread of micro-irrigation technology; (2) inefficiency in implementation as the responsible agency changed it from a dedicated programme to a component part of National Mission For

Sustainable Agriculture (NMSA) under Pradhan Mantri Krishi Sinchayee Yojana (PMKSY). In many states, allocated funds were not used properly due to a lack of implementation strategy; (3) lack of reliable guidelines and delay in government orders; (4) unavailability of subsidy funds for installation as subsidies reduced from 50% to 35% and the allocation of funds under various schemes was cut; and (5) the very difficult for securing the financial support by financial services and banks. It was reported that a lower adoption rate was due to budget cuts during the period 2013–2016.

Meti (2012) conducted a study on bananas in Dharwad, Karnaka, and stated the various constraints of adopting drip irrigation: (1) complicated loan application process and delays in receiving the funds, (2) non-availability of soluble fertilizers, (3) inadequate supply of electricity, (4) high capital investments, (5) inadequate follow-up services by drip agencies, and (6) non-availability of quality materials and damage to laterals by rodents. The policy and implementation strategies should be revised for better penetration of this technology.

The noted benefits due to micro-irrigation technology are increases in yield, improvement in water use efficiency, reduction in the cost of water, fertilizers, and manure, and weed removal. All these add up to an increase in the overall economic benefits from the optimum use of water since the technology offers greater benefits like irrigation efficiency (50–90%), fertilizer (28.5%), and energy (30.5%) (IAI 2016). This technology is highly relevant and praiseworthy. Micro-irrigation is an intervention that can address various issues of agricultural growth and hence is considered a technology that can be leveraged to achieve sustainable agriculture. Farmers have been adopted the advanced technology for farming and then farmers income is increased due to technology in in any areas. Hence economic considerations can be incorporated into engineering approaches to emphasize the importance of water productivity.

Real water savings can be realized from irrigation efficiency at the field level. To improve water productivity in agriculture, initiatives can be taken at the field level and the saved water can be used for the irrigation of additional acreage or for environmental and social needs. Kumar et al. (2008) proposed various factors, such as type of crop and spacing between them, type of micro-irrigation technology, soil type, climate, and geo-hydrology, in real water savings through the use of micro-irrigation technologies (Khadri et al. 2013).

In India, if an agricultural area under irrigation is less than or equal to 30% of the net sown area, it is referred to as a rainfed area, and if more than 30%, it is an irrigated area. Massive public investments have been made, mainly in watershed development and management, to improve rainfed agriculture using irrigation structures. However, the interventions in rainfed areas have had limited success due to lower levels of rainfall and to the aridity. Hence proper interventions are required based on the agro-ecology and hydro-meteorology of the region (Kumar et al. 2017). Reliable and adequate water supply and water delivery control can increase water productivity at the farm level and lead to real water savings. The benefits of micro-irrigation technology are increased yield, improvement in water use efficiency, reduction in the cost of water, fertilizers, and manure, and weed removal. All these

add up to an increase in the overall economic benefits from the optimum use of water. The real water savings from the use of micro-irrigation technologies mainly stem from savings from non-beneficial evaporation and non-recoverable deep percolation. Hence the water efficiency due to real water savings is very different from the savings in applied water (notional water saving).

The present chapter is to appraise drip irrigation with mulching as an innovative technology for sustainable agriculture in India and its significant impact on water productivity and land productivity. Various studies are available on the effect of drip irrigation and mulching on different crops (Tiwari et al. 2014; Biswas et al. 2015). These studies provide benefits in terms of yield increase, economic returns, and water use efficiency in connection with applied water. But real water savings are not discussed in existing studies. This chapter assesses the current status and technologies of micro-irrigation and evaluates the future prospects of micro-irrigation adoption in India. Drip irrigation has delivered many benefits with respect to water resource utilization as well as overall economic value. The yield from mulched treatments for all levels of water application are considerably higher than non-mulched treatments (GOI 2005; National Water Policy 2012; Moharir et al. 2020).

SDGs use various indicators for water resource management. These indicators include source augmentation and restoration of water bodies, source augmentation (groundwater), large- and medium-scale irrigation (supply-side management), watershed development (supply-side management), participatory irrigation practices (demand-side management), sustainable on-farm water use practices (demand-side management), rural drinking water, urban water supply and sanitation, and policy and governance. Gujarat ranks first on these indicators with 7.5 points. The country average is 4.52 and the water metric includes surface water and groundwater (CSE 2020).

1.8 Challenges in Surface Water Sources

Many large water projects exist in various parts of the world. Large dams cause various environmental and ecological problems. Large-scale land submergence leads to the need for rehabilitation and resettlement of people, loss of valuable ecosystems, prevention of ecological flows of water at the downstream of the dams, and loss of flora and fauna downstream, for example. Reservoir siltation and soil erosion are other major problems that arise in connection with large-scale surface water projects. Other impacts include soil salinization, declining ecological flows, and land subsidence, for example (Pande et al. 2019b).

Over the past few decades, extreme flood events have become more frequent due to the effects of urbanization and climate change. This has caused even the most well-planned drainage systems to be inefficient in performing their functions. Flood risk management, computation of flood water contamination with sewage water, and analysis of extreme flood events are some of the critical areas to be evaluated.

Conventional drainage systems focus on removing excess stormwater from drainage basins as quickly as possible. However, due to recent changes in climate and an increased requirement of water quantity as a result of population growth, drainage systems should be designed such that water can be collected, stored, and used for other purposes. Current drainage systems should be analysed, evaluated for their performance during monsoons, and modified with the help of recent technologies, case studies, and software in the most cost-effective way (Pande 2020b).

Due to increased urbanization, permanent road surfaces, existing buildings, and pavements are causing decreases in the percolation of water into soil. This is due to the fact that pucca road surfaces and other infrastructures will not allow water to permeate materials, leading to the requirement of drainage lines on the sides of roads. Because water must be carried by drainage lines, attempts have been made to carry large quantities of water away from streets such that the water does not remain on surfaces for a long time and hinder traffic and other activities. In this scenario, water tries to quickly escape a given area without taking into account the necessity of maintaining groundwater levels for the use of bore wells, recreational activities, and other uses. Many countries have devised solutions involving low-impact development for stormwater management, a stormwater management technique that aims to manage runoff water using distributed and decentralized micro-scale controls (Khadri and Pande 2015).

Floods have many causes, including heavy rainfall, unusually high tides, tsunamis, and failure of hydraulic structures, for example. Periodic floods occur in many Indian rivers due to heavy rainfall in catchment areas. Flood plains exist on most of the major rivers in India, which can cause large-scale damage to property and crops. Waterlogged and poorly drained areas are the worst affected. Tanji and Kielen (2002) showed that a very high rising water table results in water logging and associated salinity problems. In conventional drainage systems, less importance is given to water quality, services, and recreational uses. Moreover, conventional drainage systems have limited capacity and constraints that make them inflexible. Contemporary requirements for urban stormwater management relate to runoff quality, esthetics, recreational value, environmental protection, and a variety of water uses. Hence, an integrated and transdisciplinary approach will be necessary to take into account these various factors in a common platform to facilitate innovative and sustainable solutions. A combination of centralized and decentralized systems will also be necessary to combine the best of the different systems and enhance their synergy for sustainable design. To achieve these goals, a design framework integrating technical, social, environmental, economic, legal, and institutional aspects will be crucial. Stormwater should be treated as a positive source in sustainable drainage systems. Despite advancements in techniques and tools for sustainable urban drainage systems (SUDS), the implementation of sustainable drainage remains a very challenging task in reality. Many practical implementations of SUDS tend to underestimate their complexity, so the resulting performance is often unsatisfactory with respect to SUDS operation and maintenance, little to no co-ordination of interaction with other water bodies, and institutional impediments and barriers to SUDS practices.

Deep aquifers take time to replenish because water takes more time, perhaps weeks or even months, to move through unsaturated soil. If a surface water source is polluted, clean-up actions can be carried out without much difficulty, but remediation of a polluted aquifer is very difficult and expensive—or even impossible. FAO (2003) states that there is an inverse relationship between the vulnerability of aquifers to pollution and the difficulty of remediation. This is because fractured aquifers are more vulnerable to pollution and so permit rapid flow compared to the slow movement that occurs in porous media. Efficient and effective water management techniques are of paramount importance for groundwater sustainability (Patode et al. 2017). Adequate groundwater availability and sustainability can be ensured by proper public awareness and other appropriate measures (CGWB 2018).

1.9 Conclusion

Rainwater is the major source of recharge for surface and subsurface water. In semi-arid regions, groundwater and surface water sources have been exploited almost to the point of exhaustion. The main reasons for this are increased demand for water from various sectors and competition for water use in these sectors. Groundwater is a major source of water for drinking and irrigation purposes, but groundwater levels decrease daily due to climate change and high demand from industry and society. The overexploitation of groundwater sources has resulted in the lowering of water tables at alarming rates and the deterioration of water quality in aquifers. Surface water resources are also under threat because of their misuse. The quality of surface water resources is affected by industrial waste disposal and siltation due to heavy floods. Floods are common phenomena in Indian rivers. All these factors affect per-capita water availability in semi-arid regions. All governments promote water use efficiency in the irrigation sector. But there are many challenges in implementing micro-irrigation techniques to improve agricultural efficiency. To mitigate groundwater depletion and achieve sustainability, conjunctive use of surface and groundwater is an effective method where possible.

References

Abdullaev, I. (2004). The analysis of water management in Bukhara Oasis of Uzbekistan; historical and territorial trends. *International Water Resources Association, Water International, 29*(1), 20–26.

Al-Jawad, J. Y., Al-Jawad, B. S., & Kalin, R. M. (2019). Decision-making challenges of sustainable groundwater strategy under multi-event pressure in arid environments: The Diyala River Basin in Iraq. *Water, 11*, 2160. MDPI.

Biswas, S. K., Akanda, A. R., Rahman, M. S., & Hossain, M. A. (2015). Effect of drip irrigation and mulching on yield, water-use efficiency and economics of tomato. *Plant Soil and Environment, 61*(3), 97–102.

Centre for Science and Environment. (2020). *State of India's environment 2020 in figures. A down to Earth annual*, New Delhi.

CGWB West Central Region. (2018). *Ground water year book - 2016-17*. Faridabad: CGWB, Ministry of Water Resources, River Development and & Ganga Rejuvenation, GOI.

Cosgrove, W. J., & Loucks, D. P. (2015). Water management: Current and future challenges and research directions. *Water Resources Research, 51*, 4823–4839. https://doi.org/10.1002/2014WR016869.

Davis, A. A., Hunt, W. F., Traver, R. G., & Clar, M. (2009). Bioretention technology: Overview of current practice and future needs. *Journal of Environmental Engineering, 135*(3) March, 109–117.

Dehais, M. (2011). *Bioretention: Evaluating their effectiveness for improving water quality in New England urban environments*. Masters Theses 1911 in Master of Landscape Architecture submitted to Department Landscape Architecture and Regional Planning, University of Massachusetts Amherst.

FAO. (2003). *Ground water management: The search for practical approaches*. World Bank Reports.

GOI. (2005). *Dynamic ground water resources of India*. Jaipur: Central Ground Water Board, Ministry of Water Resources, Government of India.

Irrigation Association of India (IAI) & Federation of Indian Chambers of Commerce & Industry (FICCI) & Grant Thornton India LLP. (2016). *Accelerating growth of Indian agriculture: Micro-irrigation an efficient solution. Strategy paper – Future prospects of micro irrigation in India*.

Keller, A., Keller, J., & Seckler, D. (1996). *Integrated water resources systems: Theory and policy implications, Research report 3*. Colombo: International Irrigation Management Institute (IIMI).

Khadri, S. F. R., & Moharir, K. (2016). Characterization of aquifer parameter in basaltic hard rock region through pumping test methods: a case study of Man River basin in Akola and Buldhana Districts Maharashtra India. *Modeling Earth System and Environment, 33*, 2.

Khadri, S. F. R., & Pande, C. (2015). Remote sensing based hydro-geomorphological mapping of Mahesh River Basin, Akola, and Buldhana Districts, Maharashtra, india-effects for water resource evaluation and management. *International Journal of Geology, Earth and Environmental Sciences, 5*(2), 178–187.

Khadri, S. F. R., & Pande, C. (2016a). GIS-based analysis of groundwater variation in Mahesh River Basin, Akola and Buldhana Districts, Maharashtra, India. *IJPRET, 4*(9), 127–136.

Khadri, S. F. R., & Pande, C. (2016b). Ground water flow modeling for calibrating steady state using MODFLOW software: A case study of Mahesh River basin, India. *Modeling Earth Systems and Environment, 2*, 39. https://doi.org/10.1007/s40808-015-0049-7.

Khadri, S. F. R., Pande, C., & Moharir, K. (2013). Geomorphological investigation of WRV-1 watershed management in Wardha district of Maharashtra India; using remote sensing and geographic information system techniques. *International Journal of Pure and Applied Research in Engineering and Technology, 1*(10), 152–163.

Kumar, M. D. (2001). *Demand management in the face of growing water scarcity and competition in India: Future options*. Working paper 153. Gujarat, India: Institute of Rural Management Anand (IRMA).

Kumar, M. D., & Van Dam, J. C. (2013). Drivers of change in agricultural water productivity and its improvement at basin scale in developing economies. *Water International, 38*, 312–325.

Kumar, M. D., Sharma, T. H., B Amaasinghe, U., & Singh, O. P. (2008). Water saving and yield enhancing micro-irrigation technologies in India: When and where can they become best bet technologies? In M. D. Kumar (Ed.), *Managing water in the face of growing scarcity, inequity and declining returns: Exploring fresh approaches, Proceedings of the 7th Annual Partners Meet* (Vol. 1, pp. 1–36). Hyderabad: IWMI – Tata Water Policy Research Program, ICRISAT.

Kumar, M. D., Ratna Reddy, V., Narayanamoorthy, A., Bassy, N., & James, A. J. (2017). Rainfed areas: Poor definitions and flawed solutions. *International Journal of Water Resources Development, 34*, 278–291.

Meti, C. B. (2012). Studies on factors influencing the drip irrigation adoption, constraints and remedial measures to increase area under drip irrigation. *International Journal of Agricultural Engineering, 5*(2), 236–239.

Moharir, K., Pande, C., & Patil, S. (2017). Inverse modeling of Aquifer parameters in basaltic rock with the help of pumping test method using MODFLOW software. *Geoscience Frontiers, 8*, 1385–1395.

Moharir, K., Pande, C., Singh, S., Choudhari, P., Rawat, K., & Jeyakumar, L. (2019). Spatial interpolation approach-based appraisal of groundwater quality of arid regions. *Aqua Journal, 68* (6), 431–447.

Moharir, K. N., Pande, C. B., Singh, S. K., & Del Rio, R. A. (2020). Evaluation of analytical methods to study aquifer properties with pumping test in Deccan Basalt region of the Morna River Basin in Akola District of Maharashtra in India. In *Groundwater hydrology*. London, UK: Intec Open Publication. https://doi.org/10.5772/intechopen.84632.

Molden, D., Amarasinghe, U., & Hussain, I. (2001). *Water for rural development: Background Paper on water for rural development prepared for the World Bank*. Colombo, Sri Lanka: International Water Management Institute (IWMI).

National Water Policy. (2012). Ministry of Water Resources, Government of India, New Delhi.

Pande, C. B. (2020a). Introduction. In *Sustainable watershed development. Springer briefs in water science and technology*. Cham: Springer. https://doi.org/10.1007/978-3-030-47244-31.

Pande, C. B. (2020b). Watershed management and development. In *Sustainable watershed development. Springer briefs in water science and technology*. Cham: Springer. https://doi.org/10.1007/978-3-030-47244-3_2.

Pande, C. B. (2020c). Thematic mapping for watershed development. In *Sustainable watershed development. Springer briefs in water science and technology*. Cham: Springer. https://doi.org/10.1007/978-3-030-47244-3_3.

Pande, C. B. (2020d). Sustainable Watershed Development Planning. In *Sustainable watershed development. Springer briefs in water science and technology*. Cham: Springer. https://doi.org/10.1007/978-3-030-47244-3_4.

Pande, C. B., & Moharir, K. (2015). GIS-based quantitative morphometric analysis and its consequences: a case study from Shanur River Basin, Maharashtra India. *Applied Water Science, 7*(2), 2015.

Pande, C. B., & Moharir, K. (2018). Spatial analysis of groundwater quality mapping in hard rock area in the Akola and Buldhana districts of Maharashtra, India. *Applied Water Science, 8*(4), 1–17.

Pande, C. B., Khadri, S. F. R., Moharir, K. N., & Patode, R. S. (2017). Assessment of groundwater potential zonation of Mahesh River basin Akola and Buldhana districts, Maharashtra, India using remote sensing and GIS techniques. *Sustainable Water Resources Management*. https://doi.org/10.1007/s40899-017-0193-5. Published online 8 September-2017.

Pande, C. B., Moharir, K. N., & Pande, R. (2018a). Assessment of Morphometric and Hypsometric study for watershed development using spatial technology - A case study of Wardha river basin in the Maharashtra, India. *International Journal of River Basin Management*. https://doi.org/10.1080/15715124.2018.1505737.

Pande, C. B., Moharir, K. N., Khadri, S. F. R., & Patil, S. (2018b). Study of land use classification in the arid region using multispectral satellite images. *Applied Water Science, 8*(5), 1–11.

Pande, C. B., Moharir, K. N., Singh, S. K., & Dzwairo, B. (2019a). Groundwater evaluation for drinking purposes using statistical index: Study of Akola and Buldhana districts of Maharashtra, India. *Environment, Development and Sustainability (A Multidisciplinary Approach to the Theory and Practice of Sustainable Development)*. https://doi.org/10.1007/s10668-019-00531-0.

Pande, C. B., Moharir, K. N., Singh, S. K., & Varade, A. M. (2019b). An integrated approach to delineate the groundwater potential zones in Devdari watershed area of Akola district, Maharashtra, Central India. *Environment, Development, and Sustainability*. https://doi.org/10.1007/s10668-019-00409-1.

Patode, R. S., Nagdeve, M. B., & Pande, C. B. (2016). Groundwater Level Monitoring of Kajaleshwar-Warkhed Watershed, Tq. Barshitakli, Dist. Akola, India through GIS Approach. *Advances in Life Sciences, 5*(24), 11207–11210.

Patode, R. S., Pande, C. B., Nagdeve, M. B., Moharir, K. N., & Wankhade, R. M. (2017). Planning of conservation measures for watershed management and development by using geospatial technology-A case study of Patur Watershed in Akola District of Maharashtra. *Current World Environment, 12*(3), 2017.

Sahasranaman, M., & Arijit, G. (2018). *Waste water treatment for water security in India*. IRAP Occasional Paper No.13-0418.

Seckler, D., Amarasinghe, U., Molden, D., de Silva, R., & Barker, R. (1998). *World water demand and supply, 1990 to 2025: Scenarios and issues, Research report 19*. Colombo, SriLanka: International Water Management Institute (IWMI).

Tanji K. K., & Kielen N. C. (2002). *Agricultural drainage water management in arid and semi-arid areas*. FAO Irrigation and Drainage Paper 61.

Tiwari, K. N., Kumar, M., Santosh, D. T., Singh, V. K., Maji, M. K., et al. (2014). Influence of drip irrigation and plastic mulch on yield of sapota (Achraszapota) and soil nutrients. *Irrigation & Drainage Systems Engineering, 3*, 116. https://doi.org/10.4172/2168-9768.1000116.

Chapter 2
Review of GIS Multi-Criteria Decision Analysis for Managed Aquifer Recharge in Semi-Arid Regions

Sajad Fathi, Jenny Sjåstad Hagen, Alessia Matanó, and Guilherme E. H. Nogueira

Contents

2.1 Introduction 20
2.2 Managed Aquifer Recharge Techniques 20
2.3 Data from Remote Sensing 23
2.4 Managed Aquifer Recharge Suitability Mapping 23
2.5 Scope 25
2.6 Materials and Methods 27
2.7 Review Process 28
2.8 Results 28
2.9 Database 29
2.10 Paper Review 29
2.11 Discussion 40
2.12 Geographical Patterns 41
2.13 Criteria Selection and Weight Distribution 42
2.14 Weighting Methods and Decision Rules 43
2.15 Specific Challenges in Semi-Arid Regions 44

S. Fathi (✉)
Simona Stadpipe AS, R&D Department, Stadlandet, Norway
e-mail: behnood.sjaastad-fathi@simona-stadpipe.com

J. S. Hagen
University of Bergen, Geophysical Institute, Bergen, Norway

University of Bergen, Bjerknes Centre for Climate Research, Bergen, Norway
e-mail: Jenny.Hagen@uib.no

A. Matanó
CIMA Research Foundation - International Centre on Environmental Monitoring, Savona, Italy
e-mail: alessia.matano@cimafoundation.org

G. E. H. Nogueira
Department of Hydrogeology, Helmholtz-Zentrum für Umweltforschung, Leipzig, Germany
e-mail: guilherme.nogueira@ufz.de

C. B. Pande, K. N. Moharir (eds.), *Groundwater Resources Development and Planning in the Semi-Arid Region*, https://doi.org/10.1007/978-3-030-68124-1_2

2.16 Conclusion 46
References 47

2.1 Introduction

The Sustainable Development Goals (SDGs) encompass 17 interconnected global goals aimed at directing global development toward sustainability and equality by 2030 (UN 2019). Specifically addressing water, the sixth SDG states that the global population should have access to clean drinking water and sanitation by 2030 (Pande et al. 2019). It has long been known that water scarcity in semi-arid regions is a complex problem driven by climate change and population growth (Falkenmark et al. 1989). As the demand for water increases with a growing population, the need for sustainable water extraction becomes increasingly more important. Meanwhile, climate change is making dry areas dryer and wet areas wetter (IPCC 2014); this calls for flexible solutions in semi-arid regions, in which technology and data are used to balance water supply and demand for present and future generations in pace with climatic changes.

In semi-arid regions, groundwater is predominantly the source of freshwater during dry seasons and droughts (Moharir et al. 2019). Thus, people living in areas with semi-arid climate are more vulnerable to water insecurity. Viewing water shortage in the complimentary frameworks of integrated water resources management and the water-energy-food nexus aids understanding of how adverse ring effects are brought on to societies without reliable access to water. Currently, only an estimated 1% of annual freshwater extraction globally is recovered with managed aquifer recharge (MAR) techniques—despite the rate of MAR implementation increasing by 5% since the 1960s (Dillon et al. 2019). The use of MAR varies among and within countries due to aquifer availability, the level of confidence and awareness among involved stakeholders, financial resources, expertise, and existing strategic plans and policies (Agostinetto et al. 2013; Dillon et al. 2019). Regional differences are evermore distinct between areas located in semi-arid regions, as low precipitation and high evapotranspiration rates establish favorable preconditions for water scarcity.

2.2 Managed Aquifer Recharge Techniques

Managed aquifer recharge (MAR) is the purposeful recharge of water to targeted confined or unconfined aquifers for further use or environmental benefits (Dillon 2005). MAR is widely applied for various purposes, including: (1) improving both quantity and quality of groundwater resources, (2) recovering groundwater depletion, (3) hindering saltwater intrusion, (4) handling land subsidence, (5) mitigating

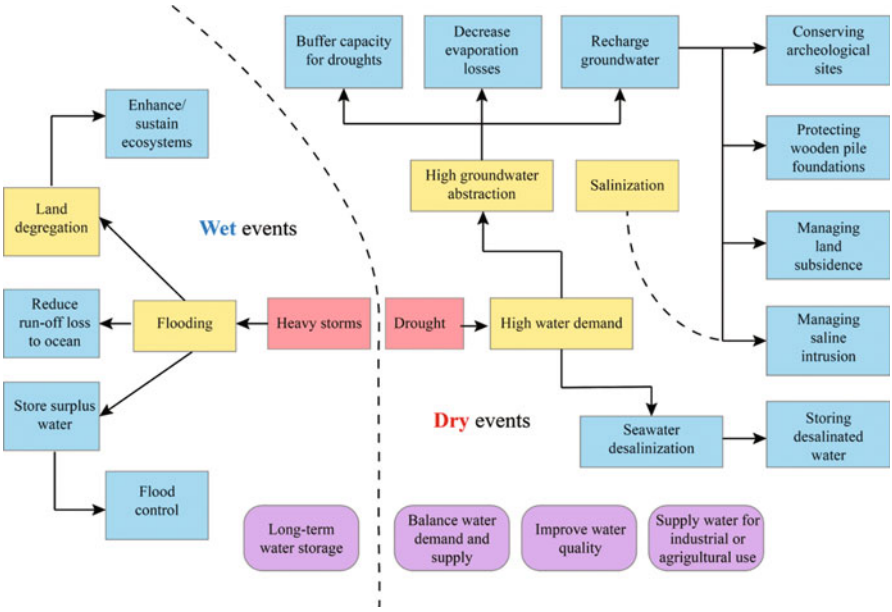

Fig. 2.1 Overview of common MAR objectives. Purple boxes refer to main MAR objectives; blue boxes refer to specific MAR objectives; red boxes refer to climate threats; and yellow boxes refer to secondary threats (modified from De Jeude (2016))

floods, and (6) gaining ecological benefits (see Fig. 2.1) (IGRAC 2007; Tuinhof et al. 2012). The various MAR objectives address either dry or wet events, with which different threats are associated. Although several classifications of MAR techniques exist in the literature (Tuinhof et al. 2012; Agostinetto et al. 2013; Casanova et al. 2016), this paper follows the classification proposed by IGRAC (2007). In this classification scheme, MAR techniques are grouped into five main categories: (1) spreading methods, (2) induced bank filtration, (3) well, shaft, and borehole recharge, (4) in-channel modification, and (5) rainfall and runoff harvesting; adhering subcategories, also referred to as specific MAR techniques, are shown in Table 2.1. A brief explanation of each main MAR technique follows below. In the remaining of this paper, the term "MAR techniques" refers to the five above-mentioned MAR techniques if otherwise not specified.

Spreading methods are used for unconfined shallow aquifers, where a vast surface of permeable soil is available for water to infiltrate. As such, spreading methods take advantage of the natural geo-purification capacity of the unsaturated zone. This MAR technique is suitable for small- to large-scale implementation at proportionally low costs. However, high sediment loads carried by the source water can reduce the infiltration rates and hence increase evaporation losses (Gale and Dillon 2005; Casanova et al. 2016; Escalante et al. 2016).

Table 2.1 Overview of MAR techniques

Function	Main MAR technique	Specific MAR technique	
Infiltration	Spreading methods	*Infiltration ponds*	
		Flooding	
		Ditch and furrow	
		Excess irrigation	
		Reverse drainage	
	Induced bank infiltration	*Galleries*	*Boreholes*
	Well, shaft, and borehole recharge	*Deep well injection*	*ASR*
			As(TR)
		Dug well/shaft/pit injection	
Interception	In-channel modification	*Recharge dams*	
		Subsurface dams	
		Sand dams	
		Channel spreading	
	Rainfall and runoff harvesting	*Barriers and bunds*	
		Trenches	
		Rooftop rainwater harvesting	

[a]*ASR* aquifer storage and recovery, *AS(TR)* aquifer storage (transfer and recovery)

Induced bank filtration involves structures located near perpetual surface bodies hydraulically conjoined with the adjacent aquifer. Declining water tables as a result of pumping lead to pressure head differences, creating suction into the aquifer. Induced bank filtration systems are conventionally practiced for enlarged drinking water abstraction due to the natural pollutant attenuation potential of riparian zones (Eckert et al. 2005; Dragoni and Sukhija 2008; Dillon et al. 2009; Lopez Mendez et al. 2016).

Well, shaft, and borehole recharge comprise injection systems for direct recharge to both shallow and deep aquifers. As opposed to spreading methods, this MAR technique does not require vast surface areas for implementation; rather, considerable volumes of water are kept underground, leading to minimal evaporation losses. For shallow aquifers, existing structures for freshwater extraction (wells, trenches, pits) that run dry can be exploited at relatively low costs, although high water quality is required to hinder contamination or clogging issues. Deep structures (borehole) are preferred where a thick, dense, and low permeable strata envelope the targeted aquifer. Well, shaft, and borehole recharge is used at medium- to large-scale for drinking water supply to communities and cities, since elaborate designs and frequent maintenance often are required (Gale and Dillon 2005; Dillon et al. 2012; Escalante et al. 2016; Lopez Mendez et al. 2016).

In-channel modification refers to structures for water streamflow interception, historically built in transient sandy rivers to increase groundwater recharge or retain floodwaters. Implementation varies from small-scale to large-scale at proportional costs without degrading surrounding landscapes. Small-scale structures can be

implemented in cascade at an assigned distance in one watercourse to enhance the infiltration rates (UNESCO 2005; IGRAC 2007; Lopez Mendez et al. 2016).

Rainfall and runoff harvesting involve diverting, collecting, and concentrating rainfall or runoff for increased infiltration or direct recharge to an aquifer. These techniques are mainly used at small-scale for domestic and agricultural purposes or at large-scale for recycling of water in urban regions (Gale and Dillon 2005; UNESCO 2005; Escalante et al. 2016; Lopez Mendez et al. 2016).

2.3 Data from Remote Sensing

With advances in remote sensing, data availability has increased globally over the last few decades. The distribution of in situ measurement stations is biased by both national and local decision-making as well as available human and financial resources. As a result, in situ monitoring tends to be sparse in developing countries as compared to developed countries. Likewise, locations that are difficult to reach or physically inaccessible with the necessary equipment, like high-altitude mountain ranges, are less monitored. Remote sensing, however, have unlocked unprecedented opportunities for data collection globally. Satellite data, in particular, is an important source for global data on atmospheric conditions—such as precipitation or cloud cover—and surface characteristics—such as land use or soil types (Pande et al. 2018). With spatial data available also in traditionally data-sparse regions, geographical information systems (GIS) may be used to carry out site selection for MAR implementation through MAR suitability mapping.

2.4 Managed Aquifer Recharge Suitability Mapping

Multi-criteria decision analysis with GIS (hereby referred to as GIS-MCDA) comprises a GIS-based methodology to evaluate alternative solutions to a problem given a specific goal (Malczewski 1999). GIS-MCDA has notably enhanced the conventional overlay mapping approaches for site suitability mapping and analysis. In short, GIS-MCDA is a decision-making tool to rank or rate entities composing the case study area, commonly referred to as criteria, in accordance with defined objectives (Malczewski and Rinner 2016). As such, a fundamental element of GIS-MCDA is the criteria selection (Adem Esmail and Geneletti, 2018). The criteria are needed to quantify the performance of the alternatives in achieving the identified objectives (Eisenführ et al. 2010; Gregory et al. 2012; Malczewski and Rinner 2016; Adem Esmail and Geneletti 2018) and should be complete, independent, non-redundant, and minimal (Malczewski 1999; Eisenführ et al. 2010; Valverde et al. 2016). The criteria should be normalized and transformed when skewed to distinctly distinguish value ranges while representing variability. The combination of GIS techniques with MCDA methods allows an efficient spatial analysis of the involved criteria.

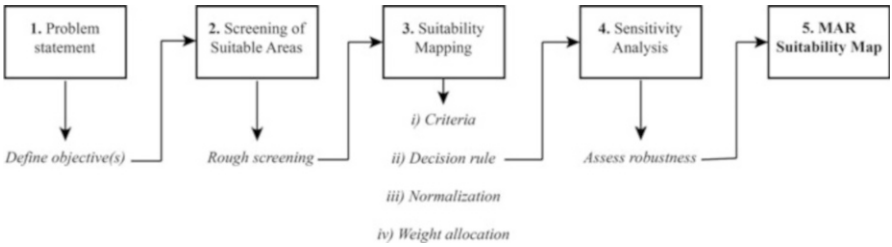

Fig. 2.2 Flowchart of GIS-MCDA methodology for MAR suitability mapping (Fathi et al. 2020)

GIS-MCDA for MAR suitability mapping as part of a decision-making process should pursue the scheme of: (1) problem definition, (2) screening of suitable areas, (3) suitability mapping including the classification of thematic layers or criteria, standardization, weighting of the criteria, and layers overlaying, and (4) sensitivity analysis (Rahman et al. 2012; Valverde et al. 2016; Sallwey et al. 2018; Fathi et al. 2020) (see Fig. 2.2).

The problem definition refers to the identification and formulation of the proper decision problem for analysis. This may include information on the purpose of MAR implementation and contingencies, such as source water and proposed MAR techniques. A clear understanding of the decision problem leads to the formulation of one or more MAR objectives. The MAR objective forms the basis for the identification of appropriate criteria (Eisenführ et al. 2010; Feizizadeh et al. 2014; Sallwey et al. 2018). Screening of suitable areas excludes parts of the case study that are not suitable for implementation of the relevant MAR technique. The reasons of non-suitability in an area can be polyvalent and are problem-conditional; constraint criteria and threshold values must therefore be specified accordingly. This rough screening is needed to remove strictly unsuitable areas by applying the Boolean logic before proceeding to MAR suitability mapping, in which areas are graded from low to high suitability.

Suitability mapping consists of assigning weights to the selected criteria and combining the weighted criteria by decision rules in GIS. The weights reflect the relative importance of each criterion (Van Berkum 2010). The most commonly applied weighting methods are rating methods, ranking methods, pairwise comparison, and multi-influencing factor (MIF). Boolean logic, fuzzy logic, or hybrid approaches combining elements from two or more weighting methods can also be used to assign weights (Sallwey et al. 2018). Rating and ranking methods involve weight allocation on a predesignated scale (Malczewski and Rinner 2016). In the MIF method, weights are extracted from a graphical interaction of the criteria calculated by the use of the number and the importance of relationships between each, as described in detail by Shaban et al. (2005) and Valverde et al. (2016). For pairwise comparison, a matrix proposed by Saaty (1987) is used to compare pairs of criteria in assigning weights. This method includes the computation of the consistency ratio, an indicator for the pairwise judgment consistency, and thus a reference factor for determining the goodness of judgment (Chandio et al. 2013; Sallwey et al.

2018). The decision rules manifest how weighted criteria are integrated to obtain the MAR suitability map (Malczewski 2000), and can be based on either threshold values (Boolean logic) or membership functions (fuzzy logic). Other commonly applied decision rules are weighted linear combination (WLC), weighted overlay combination (WOL), analytical hierarchy process (AHP), and ordered weighted averaging (OWA). Additionally, hybrid approaches consisting of two or more decision rules may also be utilized.

Criteria and weights are a reflection of subjective judgments and hence comprise central sources of uncertainty in the final MAR suitability map. Therefore, the final MAR suitability map should be accompanied by a sensitivity analysis. As a measure of robustness in the decision-making process, sensitivity analyses uncover the relative changes in the final MAR suitability map when changing criteria or weights. These relative changes can be displayed by changing one factor at the time or all factors simultaneously, depending on whether inter-factor influences are considered important or not. Various approaches to sensitivity analysis are summarized by Malczewski (1999, p. 260). Commonly applied techniques for sensitivity analysis include principal component analysis (PCA) (Andreo et al. 2008), scaling methods (Kattaa et al. 2010), re-assignation of criterion values (Fenta et al. 2015; Gdoura et al. 2015; Fathi et al. 2020), and combination of contrasting suitability classes using an area of interest technique (Fuentes and Vervoort 2020). It is beyond the scope of this review to provide an in-depth description of the various approaches to sensitivity analysis for MAR suitability mapping, and the reader is hence directed to the literature for a comprehensive overview (Malczewski 1999; Delgado and Sendra 2004; Ligmann-Zielinska and Jankowski 2008; Feizizadeh et al. 2015).

2.5 Scope

The objectives of this paper are to (1) present the state-of-the-art of multi-criteria decision analysis with GIS (GIS-MCDA) for MAR suitability mapping, (2) discuss the importance of coupling MAR technique with the method for GIS-MCDA, and highlight distinguishing features for semi-arid regions. Specifically, this chapter answers the following questions:

- *Are there challenges particular to MAR implementation in semi-arid regions?*
- *How has GIS-MCDA been used for MAR suitability mapping in semi-arid regions?*
- *Are there special considerations to be made for MAR suitability mapping in semi-arid regions—and, if so, what?*

While general reviews of MAR techniques (Steinel 2012; Casanova et al. 2016; Escalante et al. 2016) and GIS-MCDA for MAR suitability mapping (Sallwey et al. 2018) exist in the literature, a specific focus on semi-arid regions has not been undertaken prior to this paper. In an attempt to fill this gap, the aim of the current

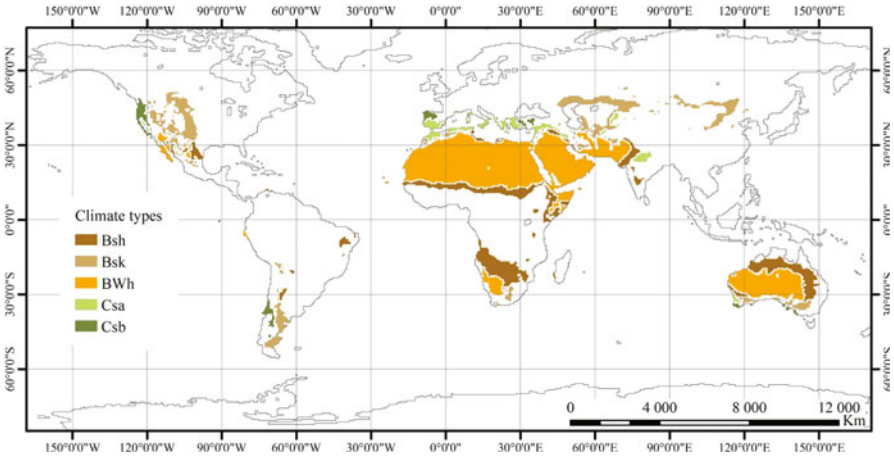

Fig. 2.3 Overview of geographical distribution of the relevant climate types considered in this review

paper is to provide a state-of-the-art overview of potential and limitations of MAR in semi-arid regions.

The Köppen-Geiger climate classification system is the most widely used system for classifying climates globally (Kottek et al. 2006). In this system, climates are grouped into five major climate types based on annual and monthly precipitation and temperature: tropical moist climates (A), dry climates (B), moist subtropical mid-latitude climates (C), moist continental mid-latitude climates (D), and polar climates (E). The five major climate types are further divided into subgroups based on precipitation and temperature patterns (Fig. 2.3). To limit the scope of this review to climates relevant to semi-arid regions in relation to present conditions and possible climatic changes, five climate types from the Köppen-Geiger climate classification system are considered with respect to MAR implementation: hot desert climate (BWh), hot semi-arid climate (BSh), cold semi-arid climate (BSk), hot-summer Mediterranean climate (Csa), and warm-summer Mediterranean climate (Csb) (see Fig. 2.1). These climate types comprise current semi-arid climates (Bsh, Bsk), similar climate types with respect to MAR implementation (Csa, Csb), and transient effects possibly brought on by climate change (BWh). Hence, this review encompasses a comprehensive overview of GIS-MCDA for MAR suitability mapping in semi-arid regions.

The remaining of this chapter is structured as follows. Section 2.6 outlines materials and methods. Section 2.7 describes the review process. Section 2.8 - Section 2.10 present the results from the review. Section 2.11 provides a discussion of the results relating to geographical patterns (Sect. 2.12), criteria selections and weight distributions (Sect. 2.13), weighting methods and decision rules (Sect. 2.14), and specific challenges for semi-arid regions (Sect. 2.15). Lastly, Section 2.16

summarizes the chapter, draws concluding remarks, and gives directions for future research.

2.6 Materials and Methods

The methodology followed in this review is described below. The first part presents the data used for statistical analyses and the second part describes the review process.

2.6.1 Data

Two distinct sources of information were utilized for this review: (1) selected papers on GIS-MCDA for MAR suitability mapping in semi-arid regions and (2) an existing database on MAR techniques used in various projects worldwide.

2.6.2 Database

To collect supplementary information to the paper review, the Global MAR Inventory Database (Stefan and Ansems 2018) was consulted. This database contains information on global MAR implementation in various climates and hydrological regimes, comprising a total of 1200 MAR schemes constructed worldwide. MAR studies carried out at sites with any of the five selected climate types (BWh, Bsh, Bsk, Csa, Csb) from the Köppen-Geiger climate classification system were extracted for a simple statistical analysis. Specifically, the following was investigated within the relevant climate types:

- Distribution of MAR techniques as a function of latitude
- Distribution of MAR techniques globally
- Distribution of MAR techniques per continent

2.6.3 Paper Selection

Papers were selected for review through online databases and search engines based on requirements fitting this review purpose as listed. Firstly, only peer-reviewed papers where GIS-MCDA for MAR suitability mapping is an integral part of the study are considered. Secondly, the paper must address one or more dry events MAR objectives (see Fig. 2.1, Sect. 2.2). Thirdly, the case studies must be located in relevant climate types for semi-arid regions, including any of the five selected

climate types (BWh, Bsh, Bsk, Csa, Csb) from the Köppen-Geiger climate classification system. Lastly, selected criteria and weights used for MAR suitability mapping must be reported.

This review only addresses literature that categorically elucidated the identification of suitable sites for implementation of MAR techniques. There is a vast literature on natural groundwater recharge in the area of potential recharge zones analysis. This analysis does not include peer-reviewed papers on the area of potential recharge zones, although natural recharge processes are, in some ways, analogous to MAR techniques.

2.7 Review Process

A systematic extraction of MAR objectives, criteria and weights was carried out on the selected papers. The MAR technique classification presented in Sect. 2.2 was followed to regroup specific MAR techniques into overarching main MAR techniques. Literature with no remark of a specific MAR technique was categorized as an "unspecified." When not explicitly mentioned, weights were recalculated using the cited methodology. In addition, information on weighting methods and decision rules was compiled. If screening of suitable areas or sensitivity analysis was excluded from a study, this information was also collected. The source water used for MAR was categorized into (1) rainfall/river/runoff and (2) reclaimed water. This separation was used to distinguish between naturally occurring water and humanly acquired and/or treated water.

The selected criteria were grouped into four overarching criterion classes, and the weights were recalculated as percentages when otherwise reported. The resulting classification consists of four main categories: (1) management, (2) physical geography, (3) surface water, and (4) groundwater criteria. The main categories are further divided into subcategories, where specific criteria are noted (see Fig. 2.1). A grouping of MAR techniques based on criteria weights, weighting methods, and decision rules was carried out using the *k*-means clustering algorithm based on Euclidean distance (Fig. 2.4). The maximum silhouette value was used to find the optimal number of clusters. After clustering, the relevant countries were paired with resulting cluster members.

2.8 Results

The following results are compartmentalized in two main sections, respectively addressing findings from the filtered database and the paper review.

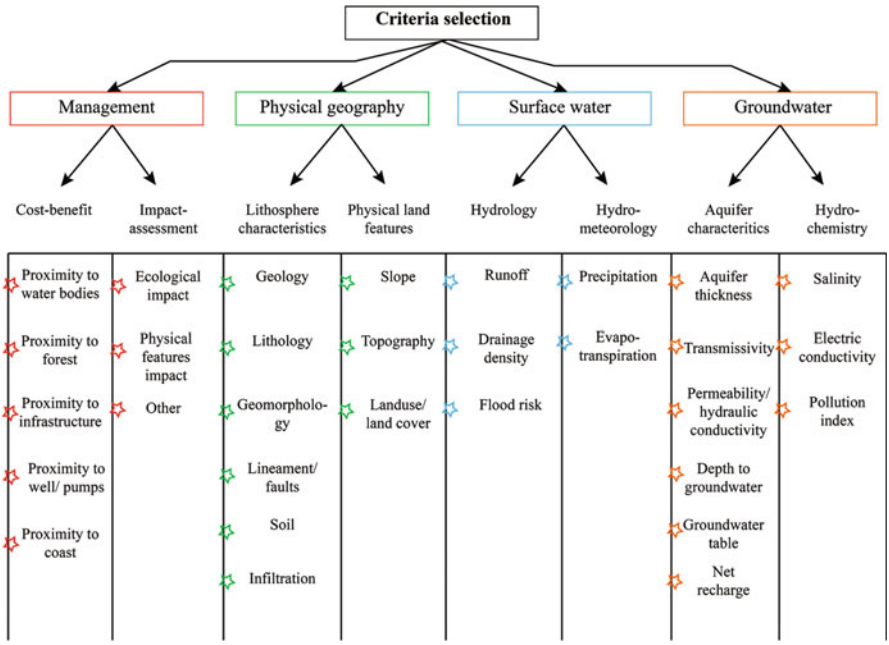

Fig. 2.4 Overview of criterion classification hierarchy

2.9 Database

Figure 2.5 shows the reported use of the five main MAR techniques, for semi-arid regions identified in this study, as a function of latitude with color-coded markers per country, ordered by continent and proportional to the number of studies found. Among the 297 MAR projects filtered from the database, the most frequently used MAR technique is well, shaft, and borehole recharge (43.8%), followed by spreading methods (35.4%) and in-channel modifications (16.8%) respectively (see Fig. 2.6). Use of well, shaft, and borehole recharge as well as spreading methods is reported in all continents, with the largest number of projects in North America. The distribution of MAR techniques and their respective number of studies identified per continent from the database are shown in Fig. 2.7. Europe has the least number of reported projects, but this may be partially biased by the few countries qualifying for the climate type filtering for semi-arid regions.

2.10 Paper Review

A total of 30 papers complying with the requirements delineated for this review were found. Figure 2.8 shows the countries in which case studies of papers reviewed in this chapter are located. As can be seen, no case studies in South America were

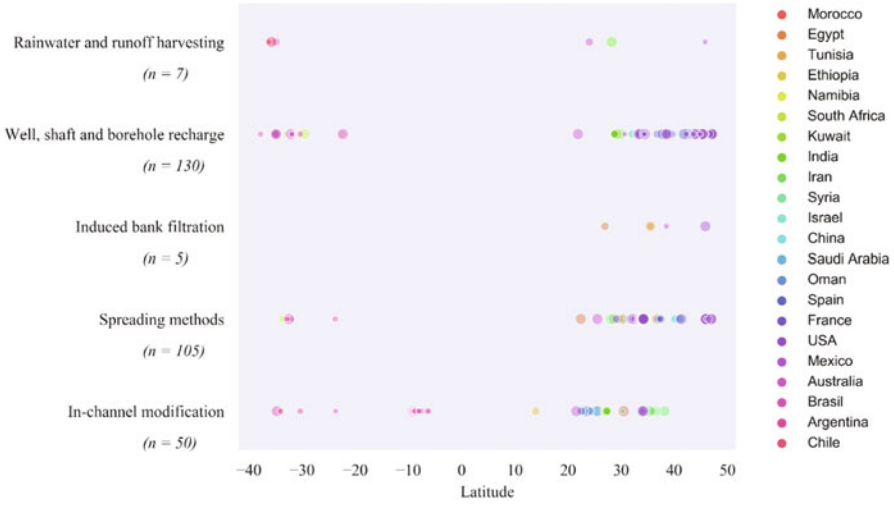

Fig. 2.5 MAR techniques as a function of latitude filtered by the relevant climates (Csa, Csb, Bsh, Bsk, Bwh) from the Köppen-Geiger climate classification. Data retrieved from Stefan and Ansems (2018)

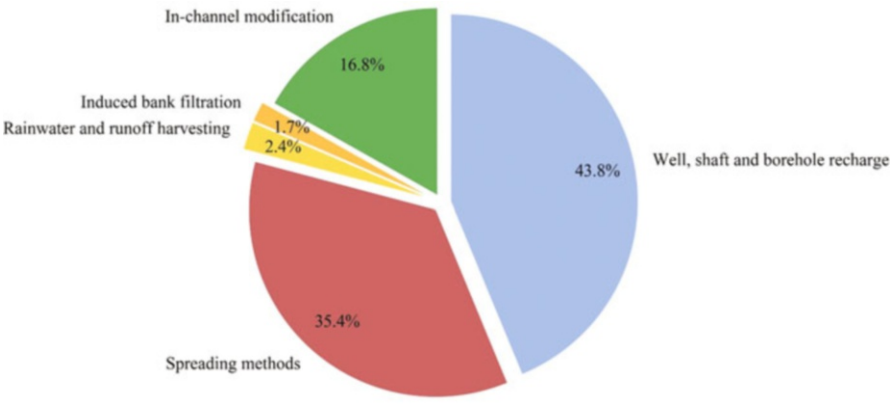

Fig. 2.6 Distribution of MAR techniques in semi-arid regions from 297 identified cases. Data retrieved from Stefan and Ansems (2018)

included. However, this relates partially to the few countries in South America with areas of relevant Köppen-Geiger climate types. The distribution of MAR techniques employed in the reviewed papers is shown in Fig. 2.9. Figure 2.10 shows the distribution of MAR techniques per continent as sampled from the current review. Note that the number of MAR techniques do not add up to the number of papers reviewed, as some studies reported more than one MAR technique.

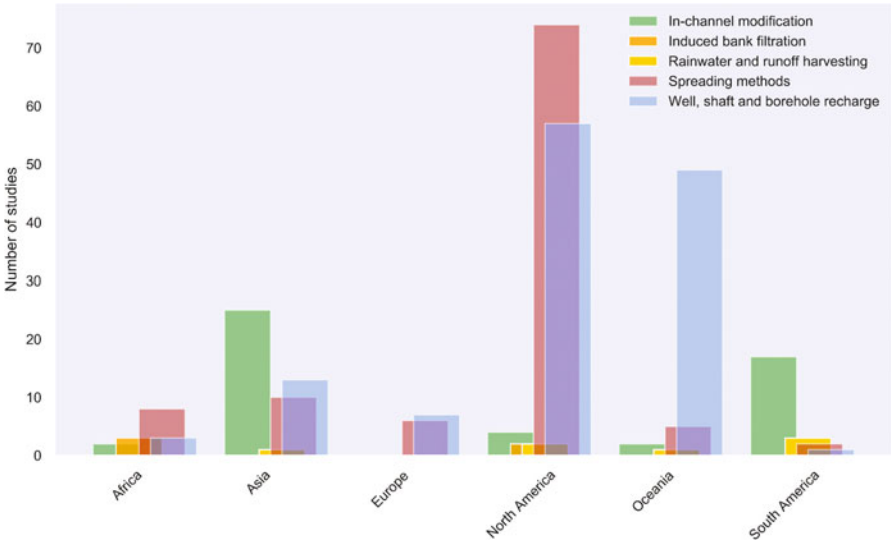

Fig. 2.7 Barplot displaying the distribution of main MAR techniques per continent. Data retrieved from Stefan and Ansems (2018)

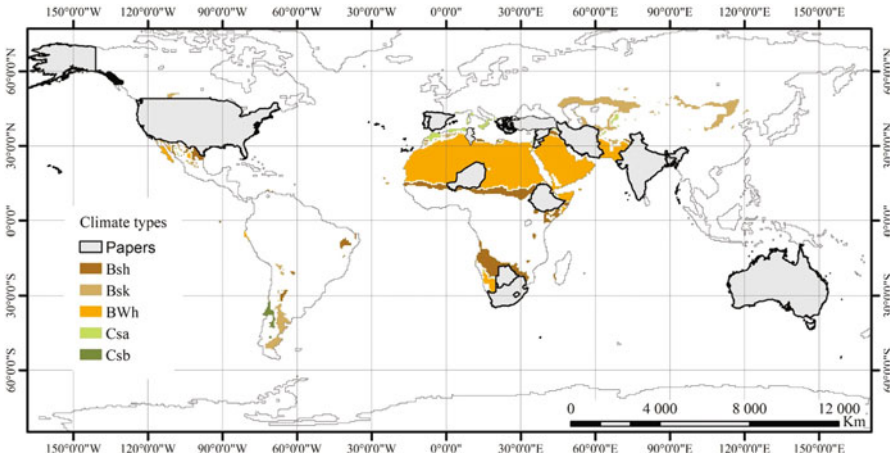

Fig. 2.8 Overview of countries included as case studies in this review

Table 2.2 summarizes the findings on MAR techniques and criteria selection. The weighting methods, decision rules, and MAR objectives for each paper are displayed in Table 2.3.

Figure 2.11 provides a stacked bar chart of the average number of criteria used for GIS-MCDA per MAR technique. Only the main MAR techniques with at least two case studies found in the review process are presented. While most studies used

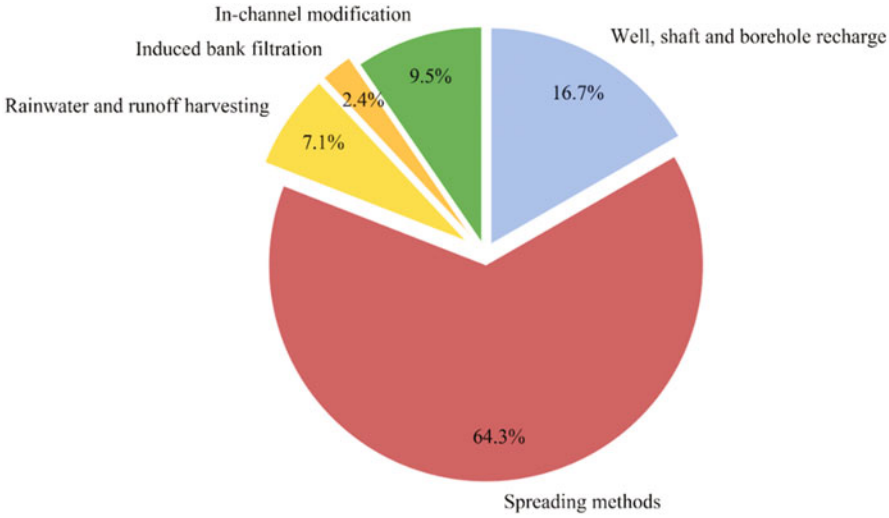

Fig. 2.9 Distribution of MAR techniques as reported in the 30 reviewed papers in semi-arid regions

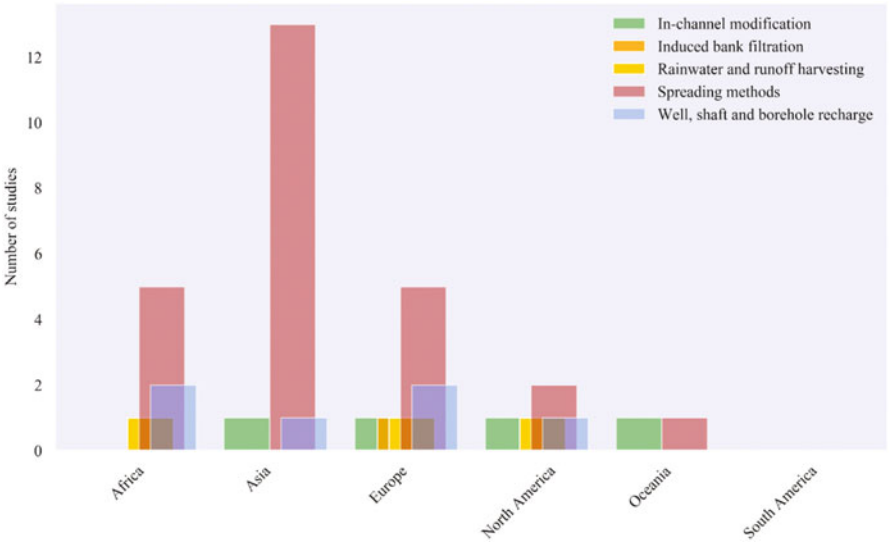

Fig. 2.10 Bar plot displaying the distribution of main MAR types per continent as identified in this review

about seven criteria, on average more than 50% of the criteria were related to the overarching criterion class *physical geography*. The overarching *surface water* criteria seem to be the least used. A boxplot of criterion classes in order of decreasing

Table 2.2 Summary of review: MAR techniques and criteria selection

	Article	Country	MAR techniques	Management									Physical geography										Surface water					Groundwater													
				Cost-benefit					Impact assessment				Lithosphere characteristics				Physical land features						Hydrology			Hydro-meteorology		Aquifer characteristics								Hydro-chemistry					
				Proximity to water bodies	Proximity to coast	Proximity to infrastructure	Proximity to forest	Proximity to wells/pumps	Ecological impacts	Agricultural impact	Physical features impact	Other	Geology	Lithology	Geomorphology	Faults/ lineament	Topography	Slope	Land use and land cover	Soil	Infiltration	Geophysics techniques	Runoff	Flood risk assessment	Drainage density	Precipitation	Evapotranspiration	Aquifer thickness	Transmissivity	Permeability	Depth to groundwater	Groundwater table	Hydraulic conductivity	Net recharge	Salinity	Electrical conductivity	Pollution index
1	(Karami *et al.*, 2016)	Iran	Spreading methods										30	10		13	10	17						5	15														
2	(Chenini *et al.*, 2010)	Tunisia	Spreading methods										16.67	16.67		16.67								16.67					16.66		16.66								
3	(Andreo *et al.*, 2008)	Spain	Spreading methods											37.5			12.5	12.5		12.5	25																		
4	(Oikonomidis *et al.*, 2015)	Greece	Spreading methods											30		4		14						4	30				4			14							
5	(Kattaa *et al.*, 2010)	Syria	Spreading methods										9.091	18.18	18.18					9.091	45.46																		
6	(Sener *et al.*, 2005)	Turkey	Spreading methods											14.29		14.29	14.29	14.29	14.29					14.29	14.29														
7	(Daher *et al.*, 2011)	Lebanon	Spreading methods										20	10	60						10																		
8	(Alraggad and Jasem, 2010)	Jordan	Spreading methods	25									25					25	25																				
9	(Mukherjee *et al.*, 2012)	India	Spreading methods											20	15	15	5	10	5	10				15	5														
10	(Fenta *et al.*, 2015)	Ethiopia	Well, shaft and borehole recharge											38	16	24		10	2					6	4														

(continued)

Table 2.2 (continued)

11	(Ghayoumian *et al.*, 2007)	Iran	Spreading methods															22.14			29.91							28.73							19.22					
12	(Machiwal *et al.*, 2011)	India	Spreading methods	6								14		17			13		13											16			21							
13	(Russo *et al.*, 2015)	USA	Spreading methods									20								25							25	20			10								
14	(Adham *et al.*, 2010)	Bangladesh	Spreading methods										47		13			18						22																
15	(Fashae *et al.*, 2014)	Nigeria	Well, shaft and borehole recharge	2.24								17.45		12.84	8.02		10.20	12.56	14.71					4.81	17.17															
16	(Dutta, 2015)	India	Spreading methods	20										20			20	20						20																
17	(Krishnamurthy *et al.*, 1996)	India	Spreading methods + in -channel modification									18.26	28.1		1.1		17.18	1.1	20.22					14.04																
18	(Ahani Amineh *et al.*, 2017)	Iran	Well, shaft and borehole recharge					7.4	22.2								1.8					5.1						3.5		15.5	2.5			10.8	31.2				
19	(Escalante *et al.*, 2014)	Spain	Spreading methods + well, shaft and borehole recharge + in -channel modification + rainwater and runoff harvesting + induced bank filtration	0.26	1.55	1.80	4.13	4.64	0.52			0.52	14.43	1.55	3.09		2.05	8.25	28.35				5.15	10.82	3.09					1.55	4.64			1.03	2.58				
20	(Tsangaratos *et al.*, 2017)	Greece	Spreading methods + well, shaft and borehole recharge			5.9		3.3						39.8				11.2										39.8												
21	(Kamangar *et al.*, 2019)	Iran	Spreading methods												11.41			16.12	8		7.1			27.45				12	16.95		0.06					0.94			
22	(Anane *et al.*, 2008)	Tunisia	Spreading methods			34.01		22.12				8.92				10.90	0.91		8.92									8.92						2.65		2.65			
23	(de Winnaar *et al.*, 2007)	South Africa	Rainfall and runoff harvesting				33.3										33.3					33.4																

24	(Fuentes and Vervoort, 2020)	Australia	Spreading methods + in -channel modification	9.26		10.74								14.60				18.12		6.35					8.11				4.65		7.70		5.21		15.26		
25	(Ahmadi *et al.* , 2017)	Iran	Spreading metho ds + Well, shaft and borehole recharge			25		12.5			12.5		5			12.5	12.5	5	5												5						5
26	(Gdoura *et al.*, 2015)	Tunisia	Spreading methods			27		19.80					9.60				11.32	1.69	0.54	9.85											9.87				3.13	1.60	5.60
27	(Beganskas and Fisher, 2017)	USA	Rainfall and runoff harvesting + spreading methods + In -channel modification								20												20			20		20					20				
28	(Masoud Saatsaz *et al.*, 2005)	USA	Well, shaft and borehole recharge			18.75		6.25	12.5		6.25	18.75																	6.25						6.25		25
29	(Fathi *et al.*, 2020)	South Africa and Botswana	Spreading methods											32		12		12	20	16					8												
30	(Rahman *et al.* , 2012)	Portugal	Spreading methods															10		30								5			20		25		5		5

Table 2.3 Summary of review: MAR objectives, weighting methods, decision rules

	Article	MAR type	Country	Water source	Weighting methods	Decision rule	Range	Sensitivity analysis	MAR objective
1	(Karami *et al.*, 2016)	Spreading method	Iran	Rainfall/ river/ runoff	Rating method	WOC	1 - 9	No	Agriculture, Recreation
2	(Chenini *et al.*, 2010)	Spreading method	Tunisia	Rainfall/ river/ runoff	Rating method	WLC	0 - 10	No	Agriculture
3	(Andreo *et al.*, 2008)	Spreading method	Spain	Rainfall/ river/ runoff	Rating method	WLC	1 - 10	Yes (PCA)	Recreation
4	(Oikonomidis *et al.*, 2015)	Spreading method	Greece	Rainfall/ river/ runoff	Pairwise comparison	AHP	1 - 9	No	Ecology, Domestic
5	(Kattaa *et al.*, 2010)	Spreading method	Syria	Rainfall/ river/ runoff	Rating method	AHP	0 - 4	Yes (Scaling method)	Ecology, Domestic
6	(Sener *et al.*, 2005)	Spreading method	Turkey	Rainfall/ river/ runoff	Ranking method	WLC	10 - 70	No	Domestic, Agriculture
7	(Daher *et al.*, 2011)	Spreading method	Lebanon	Rainfall/ river/ runoff	Ranking method	WLC	0 - 4	No	Ecology, Domestic
8	(Alraggad and Jasem, 2010)	Spreading method	Jordan	Rainfall/ river/ runoff	Boolean logic	Boolean logic	0 - 1	No	Domestic, Ecology
9	(Mukherjee *et al.*, 2012)	Spreading method	India	Rainfall/ river/ runoff	Ranking method	WOC	1 - 5	Yes	Agriculture, Recreation
10	(Fenta *et al.*, 2015)	Well, shaft and borehole recharge	Ethiopia	Rainfall/ river/ runoff	Pairwise comparison	WLC	0 - 1	Yes (re-assignation of criterion values)	Domestic, Recreation
11	(Ghayoumian *et al.*, 2007)	Spreading method	Iran	Rainfall/ river/ runoff	Fuzzy logic	Fuzzy logic	0 - 1	No	Agriculture, Domestic
12	(Machiwal *et al.*, 2011)	Spreading method	India	Rainfall/ river/ runoff	Pairwise comparison	Hybrid	0 - 1	Yes (PCA)	Domestic, Agriculture
13	(Russo *et al.*, 2015)	Spreading method	USA	Rainfall/ river/ runoff	Rating method	WLC	1 - 5	No (verification used)	Ecology, Recreation, Domestic
14	(Adham *et al.*, 2010)	Spreading method	Bangladesh	Rainfall/ river/ runoff	MIF	WLC	1 - 10	No	Domestic, Agriculture
15	(Fashae *et al.*, 2014)	Well, shaft and borehole recharge	Nigeria	Rainfall/ river/ runoff	Pairwise comparison	AHP	1 - 4	No	Agriculture, Recreation
16	(Dutta, 2015)	Spreading method	India	Rainfall/ river/ runoff	Boolean logic	WOC	0 - 1	No	Agriculture, Domestic
17	(Krishnamurthy *et al.*, 1996)	Spreading method + in-channel modification	India	Rainfall/ river/ runoff	Ranking method	WLC	10 - 50	No	Agriculture
18	(Ahani Amineh *et al.*, 2017)	Well, shaft and borehole recharge	Iran	Rainfall/ river/ runoff	Pairwise comparison	AHP	0 - 1	No	Ecology, Recreation

19	(Escalante *et al.*, 2014)	Spreading methods + well, shaft and borehole recharge + in-channel modification + rainwater and runoff harvesting + induced bank filtration	Spain	Rainfall/ river/ runoff + reclaimed water	Rating method	WLC	0 - 3	No	Industrial, Ecology, Domestic and Agriculture
20	(Tsangaratos *et al.*, 2017)	Spreading method + well, shaft and borehole recharge	Greece	Reclaimed water	Pairwise comparison	AHP	0 - 1	No	Ecology
21	(Kamangar *et al.*, 2019)	Spreading method	Iran	Rainfall/ river/ runoff	Hybrid	Hybrid	0 - 1	No	Ecology, Recreation
22	(Anane *et al.*, 2008)	Spreading method	Tunisia	Reclaimed water	Pairwise comparison	AHP	0 - 1	No	Agriculture, Domestic, Ecology
23	(de Winnaar *et al.*, 2007)	Rainwater harvesting	South Africa	Rainfall/ river/ runoff	Ranking method	WLC	1 - 5	No	Agriculture
24	(Fuentes and Vervoort, 2020)	Spreading method and in-channel modification	Australia	Rainfall/ river/ runoff	Pairwise comparison	AHP	1 - 5	Yes (the area of interest (AOI))	Agriculture, Ecology
25	(Ahmadi *et al.*, 2017)	Spreading method + well, shaft and borehole recharge	Iran	Reclaimed water	Rating method	WLC	0 -1	No	Agriculture, Domestic
26	(Gdoura *et al.*, 2015)	Spreading method	Tunisia	Reclaimed water	Hybrid	WLC	0 - 1	Yes (re-assignation of criterion values)	Agriculture; Domestic; Recreation
27	(Beganskas and Fisher, 2017)	Spreading method + rainwater harvesting + in-channel modification	USA	Rainfall/ river/ runoff	Boolean logic	Boolean logic	0 - 1	No	Agriculture, Domestic, Ecology
28	(Masoud Saatsaz *et al.*, 2005)	Well, shaft and borehole recharge	USA	Reclaimed water	Boolean logic	Boolean logic	0 - 2	No	Ecology, Domestic, Recreation
29	(Fathi *et al.*, 2020)	Spreading method	South Africa and Botswana	Rainfall/ river/ runoff	MIF	WLC and OWA	0 - 1	Yes (re-assignation of criterion values)	Agriculture, Domestic Recreation
30	(Rahman *et al.*, 2012)	Spreading method	Portugal	Rainfall/ river/ runoff	Pairwise comparison	WLC and OWA	0 - 1	Yes (the effect of the decision rules on OWA)	Domestic

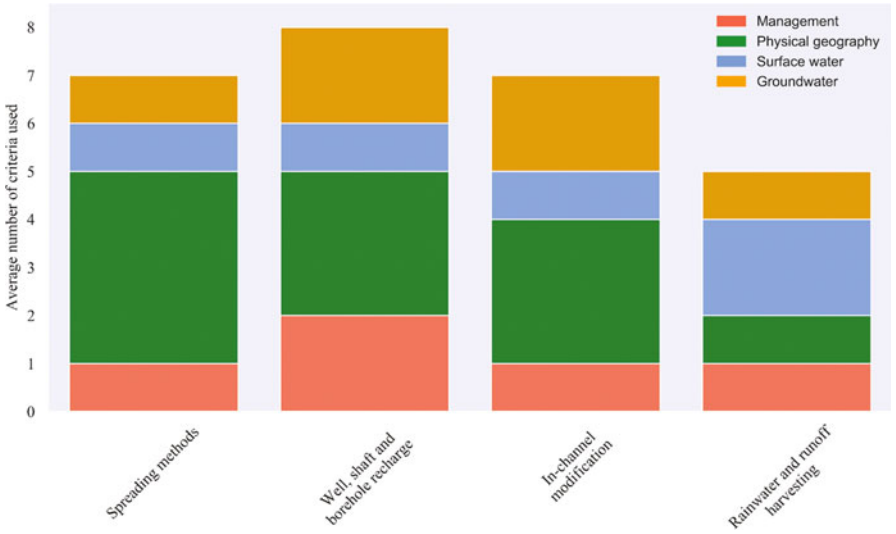

Fig. 2.11 Average number of criteria used in reviewed MAR studies based on main MAR techniques and overarching criteria Note: Induced bank filtration is not shown due to the limited number of studies found

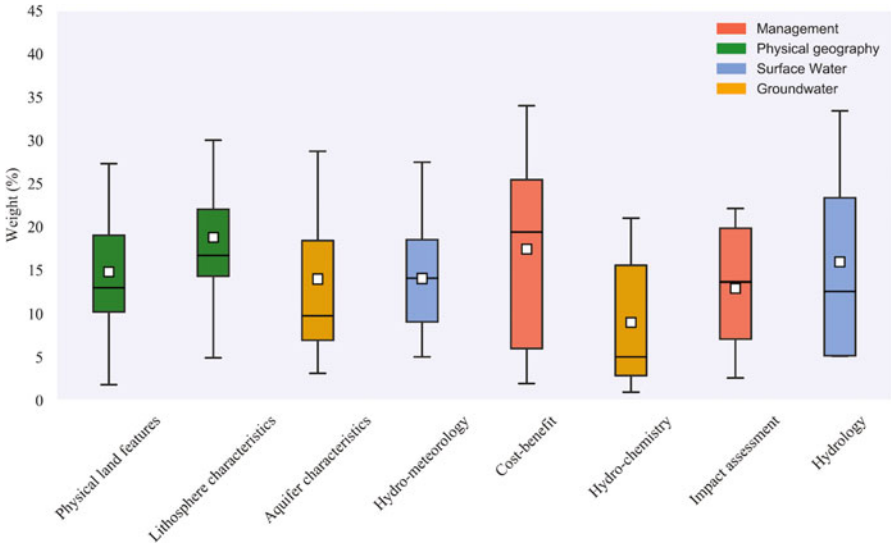

Fig. 2.12 Boxplot of weights (main categories) extracted from papers subject to this review sorted by number of times employed (from left to right). Arithmetic means are indicated by white markers

frequency is provided in Fig. 2.12. It is evident that criteria related to *physical geography* are consistently used, followed by *aquifer characteristics* and *hydro-meteorology*. A more detailed boxplot displaying the relative importance and weight ranges of individual criteria belonging to the four overarching criterion classes

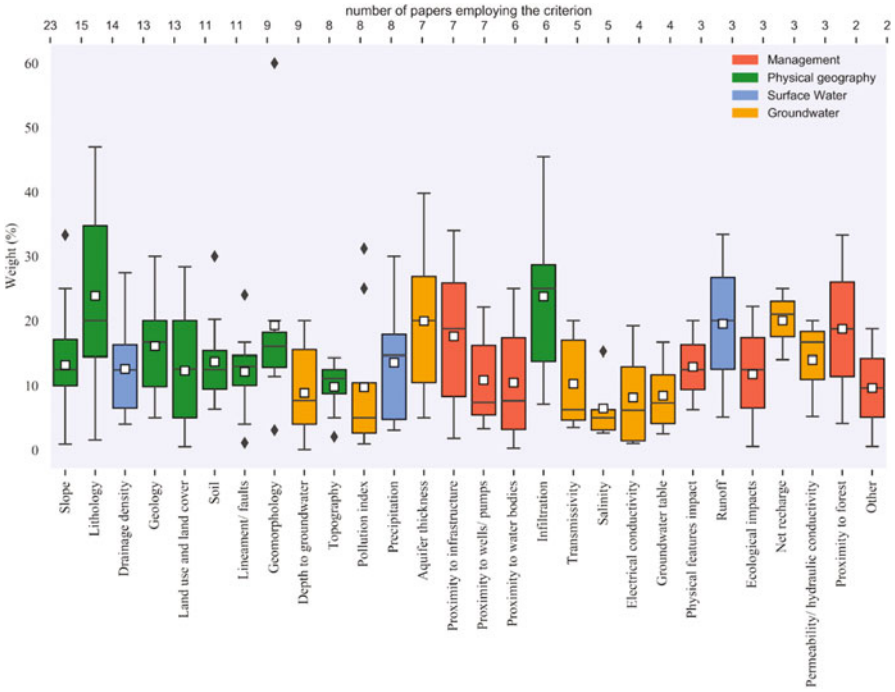

Fig. 2.13 Boxplot of weights (subcategories) extracted from papers subject to this review sorted by number of times employed (left to right). Arithmetic means are indicated by white markers

(*management*, *physical geography*, *surface water*, and *groundwater*) is shown in Fig. 2.13

The majority of the papers subject to this review included *slope* in the criteria selection, with a weighting between 10 and 20%. Furthermore, about half of the papers reviewed included *lithology*, *drainage density*, *geology,* and *land use/land cover*. Only one paper (Escalante et al. 2014) used *proximity to coast* and *flood risk*. Furthermore, three papers reported the use of *evaporation*, *geophysics*, and *agricultural impact*, respectively, without explicitly stating weights. Consequently, none of these criteria are displayed in the boxplots. About 20% of the papers reviewed used reclaimed water as source water for MAR; the remaining 80% used water from rainfall, river, or runoff.

A two-dimensional histogram displaying the relative frequency of various combinations of weighting methods and decision rules is provided in Fig. 2.14. The most frequent combination among the 30 papers reviewed is pairwise comparison for weight assignation and analytic hierarchy process (AHP) as decision rule (Fig. 2.4). Both ranking and rating methods are commonly applied with weighted linear combination (WLC). Interestingly, Boolean logic for weight assignment tends to be paired with Boolean logic decision rules; this pattern is also seen for fuzzy logic and the few numbers of hybrid approaches to weighting and integration.

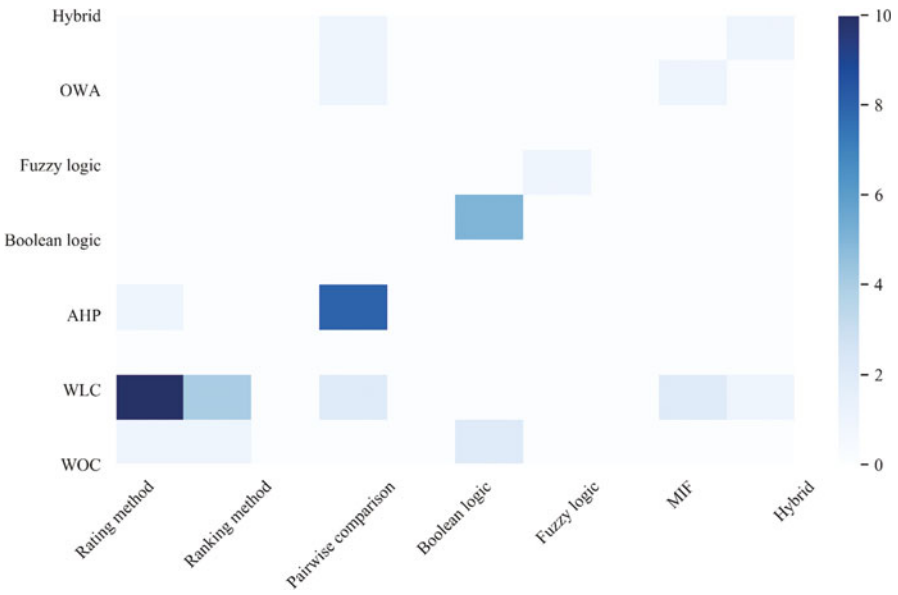

Fig. 2.14 Two-dimensional histogram showing weighting methods (x axis) and decision rules (y axis) as identified in this review (see Table 2.2 for abbreviations)

Figure 2.15 displays the resulting six clusters identified with *k*-means clustering of weights, weighting methods, and decision rules. After pairing the relevant countries with the identified cluster members, patterns of similarity for GIS-MCDA MAR suitability mapping criteria, weighting methods, and decision rules were found both within countries (Spain, USA, Australia, South Africa, and Iran) and across countries with similar characteristics like climate or development (Jordan, India, Nigeria, Spain, Iran). However, although the flexibility of spreading methods in various GIS-MCDA applications is illustrated, the limited data extracted in this review restricts further generalization on the sparse representation of other MAR techniques.

2.11 Discussion

This discussion consists of four subsections addressing (1) geographical patterns for MAR as identified from the paper review and the Global MAR Inventory Database, (2) criteria selection and weight distribution in the reviewed papers, (3) weighting methods and decision rules in the reviewed papers, and (4) a reflection on specific challenges for MAR implementation in semi-arid regions.

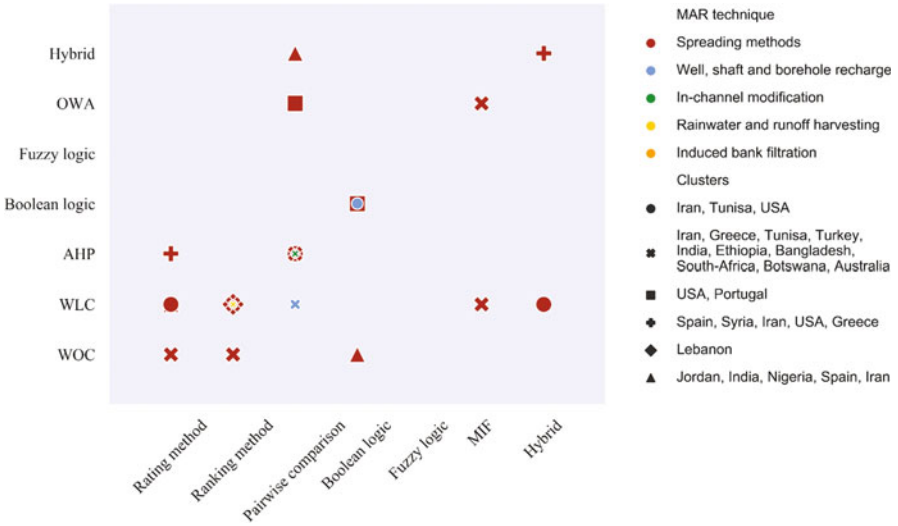

Fig. 2.15 Scatter plot showing clustered MAR techniques as function of weighting methods (x axis) and decision rules (y axis) as identified in this review (see Table 2.2 for abbreviations)

2.12 Geographical Patterns

The most commonly applied MAR techniques in semi-arid regions are spreading methods and well, shaft, and borehole recharge. This general pattern is consistent across the Global MAR Inventory Database and the paper review, providing a sampling of MAR studies in relevant climate types. While induced bank filtration was identified only in the Northern Hemisphere in the database, only one of the papers reviewed (Escalante et al. 2014) reported the use of this MAR technique. This paper, however, involved evaluations of 24 different specific MAR techniques and their applicability in Spain. Furthermore, no case studies in South America were included in the review; the limited samples of 30 papers cannot be considered representative for the vast northern Africa and Central Asia. Nevertheless, some interesting geographical patterns were found.

The frequent use of spreading methods may relate to the low costs and technical requirements for small- to large-scale implementation. Spreading method was addressed in 77% of the 30 studies included in the review (counting each MAR technique addressed per study lowers this percentage of coverage to 64%). Furthermore, some criteria and weight combinations were applied for two or more MAR techniques. In other words, specific consideration of the selected MAR techniques is not always consistent in the literature. Within MAR suitability mapping, criteria suitable for one MAR technique may not be suitable for another. This is particularly relevant when MAR techniques of contrasting costs and technical requirements are addressed (such as spreading methods and well, shaft, and borehole recharge). As such, complete, independent, non-redundant, and minimal criteria (Malczewski

1999; Eisenführ et al. 2010) for spreading methods may produce suboptimal results for well, shaft, and borehole recharge. As these two MAR techniques are the most frequently used techniques in semi-arid regions, consideration should be made when basing criteria selections on past studies for MAR suitability mapping.

2.13 Criteria Selection and Weight Distribution

Among the 30 papers reviewed, 28 different criteria relating to management, physical geography, surface water, and groundwater were explicitly employed for MAR suitability mapping. Additionally, three criteria were implicitly employed without weights (*evapotranspiration*, *physical features impact*, and *geophysics*). Despite the average number of criteria used per MAR technique ranging from five to eight, it is clear that the variability in criteria selections from the relatively small sample of 30 papers preclude robust statistical inferences. However, some patterns regarding criteria and weights could be identified.

More than half of the studies carried out screening of suitable areas by applying Boolean logic on one or more criteria (often *land use/land cover*, *soil,* or *geology*). Most studies (64% of the reviewed cases) used no more than seven criteria for MAR suitability mapping, with dominant focus on physical land features and lithosphere characteristics, leaving a less concentrated focus on aquifer characteristics. Most studies (77% of the reviewed cases) included slope in the set of criteria. A gentle slope enhances groundwater recharge by favoring infiltration. This criterion is mainly relevant for the use of spreading methods—the MAR technique most frequently addressed in the reviewed papers (64%). Only the work from Escalante et al. (2014) used the flood risk criterion for site selection since it was considered important for increasing the effectiveness of recharge rate in spreading methods.

The same tendency of GIS-MCDA application for assessing suitable areas mainly for spreading methods was observed by Sallwey et al. (2018). Indeed, MAR suitability mapping for spreading methods can be carried out with data from remote sensing. In particular, satellite data has the advantage of being available for all parts of the world with various spatiotemporal resolution and coverage, depending on the satellite orbits, putting aside constraints relating to financial and human resources within each country. In other words, dominant surface characteristics can be readily utilized for MAR suitability mapping for spreading methods. Other MAR techniques equally important for semi-arid regions, such as well, shaft, and borehole recharge, require direct field data on aquifer transmissivity, which is less accessible through remote sensing. Additionally, spreading methods present the lowest associated costs, favoring implementation when financial resources are limited.

Overall, the selection of criteria is intrinsic to both the MAR technique chosen in each study and to the water source planned to be used for recharge. Selection of additional criteria such as soil and groundwater salinities, as well as distance to pollution sources and water supply infrastructure, was mainly observed in studies where reclaimed water was used as a water source. Specifically, in semi-arid regions,

long dry periods that develop into hydrological droughts and high evapotranspiration rates limit the water sources available for MAR implementation. Therefore, the reuse of wastewater for MAR appears as an important component in semi-arid areas. Particularly in light of climate change and population growth, one may expect that the reuse of wastewater is likely to play a larger role in MAR implementation in the coming decades.

Based on the priority and preferences of decision-makers in the site selection process, different weight distributions were employed. Interestingly, slope, the criterion most frequently used in the reviewed studies, generally received a smaller weight compared to other criteria within the physical geography category, such as soil, geology, and geomorphology. For instance, soil and/or geology were considered more relevant for infiltration rates than slope itself . On average, slope weights also presented smaller values as compared to weights within the management category, especially in studies that used reclaimed water as the main water source for MAR (20% of the reviewed cases).

In cases where slope weights were smaller than either management criteria or other physical geography criteria, *cost-benefit* criteria in the site selection were preferred. Similarly, criteria such as soil and pollution index presented higher weights in these studies since authors considered *aquifer characteristics* (e.g., depth to groundwater, salinity, NO_3, and other solute concentrations) as important properties concerning improvement of the reclaimed water and to prevent water quality deterioration (Anane et al. 2008).

Overall, management criteria relating to *cost-benefit* and *impact assessment* (e.g., proximity to water bodies or infrastructure, and ecological or agricultural impacts) were not frequently used in the studies reviewed (less than 50% of the cases). However, the largest weight range and the highest mean value were found in these subcategories; studies that stated reclaimed water as the main water source for MAR systematically employed management criteria with higher weights. Indeed, as shown in the study by Gdoura et al. (2015), the environmental factors have greater impacts on the final site selection decision in comparison to other technical parameters.

2.14 Weighting Methods and Decision Rules

Among the reviewed papers, rating methods, ranking methods, and pairwise comparison were most frequently applied (by 87% of the reviewed cases). The widespread use of rating and ranking methods may be partially explained by their simplicity in basing scores on subjective judgments. As such, rating and ranking contrast pairwise comparison, which provides measures of consistency in pairwise subjective judgments (Hutton Barron 1992). Since pairwise comparison may reduce certain biases when applied to a limited number of criteria, the average number of criteria employed for the different MAR techniques substantiates recommendations in utilizing this weighting method. Indeed, the more recent publications among the

reviewed papers applied pairwise comparison as opposed to ranking or rating methods.

While Boolean was used as weighting method in four of the reviewed studies, only one study applied fuzzy logic. Furthermore, a few studies assigned weights by assessing the relative importance and influence of each criterion on the criteria selection in a graphical representation using multi-influencing factor (MIF) (7% of the reviewed cases). However, this low number may be biased by the late introduction of MIF to MAR suitability mapping, although MIF provides a better foundation for sensitivity analysis (Valverde et al. 2016).

Weighted linear combination (WLC) is the most frequently applied decision rule (by 47% of reviewed cases). WLC was introduced at first by Saraf and Choudhury (1998). A review study conducted by Sallwey et al. (2018) showed that WLC has been ubiquitous ever since its introduction, with increasing popularity in peer-reviewed studies from 2012; a statistic supported also by the findings of the current review paper. Furthermore, the subsequent use of certain weighting methods and decision rules confirmed patterns seen in the literature (Malczewski 2006; Malczewski and Rinner 2015; Sallwey et al. 2018).

Rating and ranking methods for weight allocation generally appears with WLC as decision rule. Likewise, pairwise comparison is often used in combination with analytical hierarchy process (AHP). However, AHP suffers from three important limitations, namely, the inability to consider threshold values, the lack of measures to assess the robustness of standardization, and the known rank-reversal issue (Schenkerman and Stan 1994; Wang and Elhag 2006). Although the rank-reversal issue may be solved by reducing the number of criteria, alternative decision rules such as the REMBRANDT (Lootsma 1992), MACBETH (Bana e Costa and Vansnick 1997), or Fuzzy TOPSIS (Wang and Elhag 2006) methods could provide more robust results. These methods were not included in the papers subject to this review, but may nevertheless be explored in future studies where the number of criteria precludes efficient use of AHP.

2.15 Specific Challenges in Semi-Arid Regions

Several areas located in semi-arid climates suffer from data sparsity; this makes the use of GIS-MCDA for MAR suitability mapping more challenging in cases where field measurements are needed. Furthermore, semi-arid regions located in developing countries may be subject to constrained financial resources, thereby limiting implementations to cheaper MAR techniques, such as spreading methods. This may be viewed also in light of the distribution of MAR objectives. The MAR objectives of the reviewed studies were distributed as following (not cumulative): (1) domestic (63%) (2) agricultural (60%), (3) ecological (43%), (4) recreational (37%), and (5) industrial (3%) purposes. As only one study addressed an industrial MAR objective, this may point to other challenges related to large-scale implementation of MAR in semi-arid regions. Requirements of technical expertise, field data, and

geophysical measurements, as well as high operational costs, may partially explain this deficit in the review. Agricultural MAR objectives, on the other hand, are consistently addressed with spreading methods in this review; agricultural fields are highly dependent on physical land features and hence suitable for spatial analysis with remotely sensed data in GIS. However, this pattern may also simply reflect a bias in the paper selection toward domestic and agricultural MAR objectives addressed with spreading methods.

Despite spreading methods being a frequently applied MAR technique in semi-arid regions, high evapotranspiration rates constitute a particular challenge. Interestingly, evapotranspiration was employed only once in the preparation process of the net recharge criterion (Oikonomidis et al. 2015) among the papers reviewed in this study. Indeed, in semi-arid regions, evapotranspiration is roughly equal to or larger than the precipitation on annual timescales (Kurc and Small 2004), and thus plays an essential role in water balance in such regions. It is not clear why evapotranspiration was excluded and left unconsidered among most of the reviewed papers—although part of the reason may be the lack of high-resolution evapotranspiration maps over the region and the fundamental challenges of deriving accurate estimates. Andreo et al. (2008) argued that aquifer recharge is more influenced by other factors than evapotranspiration based on results from PCA analysis—despite the case study being mainly formed by carbonate geological formations. Nevertheless, the inclusion of evapotranspiration for MAR suitability mapping in semi-arid regions may be investigated further in future studies.

Only nine studies (30% of the reviewed cases) applied sensitivity analysis to verify the robustness of achieved results. The consideration of a structured GIS-MCDA process followed by a sensitivity analysis can aid more robust site selection decisions. Smaller differences between the final map and maps resulted from varying weights (e.g., non-probabilistic sensitivity analysis) indicate more robust outcomes, as demonstrated by Fathi et al. (2020) and others. Despite this key role for verification in GIS-MCDA, sensitivity analysis was left unfocused in the majority of the reviewed papers. In the few studies reporting the use of sensitivity analysis, verification was mainly carried by comparing results to field data, such as natural recharge rates and well productivity values, or to actual MAR-sites. In a more advanced step, Russo et al. (2015) used a numerical model to validate the results, allowing for more detailed planning and assessment of the MAR effects. More recently, Fuentes and Vervoort (2020) proposed the use of natural recharge estimations through the water table fluctuation method in different monitoring wells located within selected sites for MAR implementation. With sensitivity analyses of the resulting MAR suitability maps, the site selection process of GIS-MCDA can be used as a guidance tool to focus on certain sites for further investigation, rather than final decisive operational strategies.

2.16 Conclusion

This chapter presented a sampled screening of GIS-MCDA in semi-arid regions. A collection of 30 peer-reviewed papers on GIS-MCDA for MAR suitability mapping were selected for this review based on requirements relating to MAR objectives and climate types. An existing database containing information on global MAR implementation was filtered by five Köppen-Geiger climate types deemed relevant for semi-arid regions and consulted for robust statistics on MAR techniques in semi-arid regions. To investigate patterns between MAR techniques and the use of GIS-MCDA for MAR suitability mapping, a *k*-means clustering of criteria, weights, weighting methods, and decision rules was performed, resulting in six clusters. Based on the statistical analyses carried out on data from the database and the paper review, the following was found:

1. Are there challenges particular to MAR implementation in semi-arid regions?

   The dominant MAR techniques in semi-arid regions are spreading methods and well, shaft, and borehole recharge. Due to high evapotranspiration rates and low precipitation, neither induced bank filtration nor rainfall and runoff harvesting is frequently used in semi-arid regions. As depicted in the database consulted, induced bank filtration has been implemented only in the Northern Hemisphere. While MAR implementation naturally preconditions on characteristics of the physical landscapes and the hydrological cycle on longer time scales through existing geological features, human and financial resources—or lack of thereof—may further bias the reported MAR techniques in the database. For instance, the frequently reported spreading methods are relatively cheap to implement as compared to other MAR techniques. Although MAR implementation also preconditions on financial and human resources, management criteria are less frequently applied. However, GIS-MCDA comprises a flexible methodology that allows for incorporation of local contingencies; hence, future applications of this tool for MAR suitability mapping may further strengthen the focus of MAR techniques in relation to criteria selection and weight assignation in semi-arid regions by including criteria relating to financial and human resources as a subcategory of management criteria.
2. How has GIS-MCDA been used for MAR suitability mapping in semi-arid regions?

   The findings of this review showed that GIS-MCDA has been used in various combinations of criteria selections, weights, weighting methods, and decision rules in semi-arid regions for dry events MAR objectives. For spreading methods, an average number of seven criteria were employed in the reviewed papers. Criteria relating to *physical geography*, such as lithology, geology, slope, soil and land use, and land cover, were consistently most frequently applied across well, shaft, and borehole recharge and in-channel modification. *Management* criteria seem to be more relevant and usually associated with MAR projects relying on the use of reclaimed water for aquifer recharge, taking into account safety, environmental impacts, and operational constraints. Moreover, drainage density was applied in 50% of the papers reviewed. Since neither rainwater and

runoff harvesting nor induced bank filtration is frequently applied in semi-arid regions as identified through this review, generalization cannot extend to cover these two MAR techniques.

3. Are there special considerations to be made for MAR suitability mapping in semi-arid regions—and, if so, what?

   The complex societal problem of water scarcity in semi-arid regions is accelerated by climate change and population growth. In striving to reach the sixth goal of the Sustainable Development Goals, namely, ensuring access to safe drinking water and sanitation for all by 2030, the reuse of wastewater for MAR implementation is a promising direction. In terms of data availability versus data requirements, costs, and findings from previous studies, spreading methods may seem the best choice of MAR technique in semi-arid regions. However, both well, shaft, and borehole recharge and in-channel modification should be considered viable options; especially in semi-arid regions, where evapotranspiration rates are high, and cities and communities to a large extent rely on groundwater for drinking water supply, well, shaft, and borehole recharge may be a better, if costlier, option. Also, given the popularity of the contrasting MAR techniques of spreading methods and well, shaft, and borehole recharge in semi-arid regions, consideration should be made and particular focus given to the coupling of criteria with the selected MAR technique.

Based on the findings from this review, the following recommendations are given. In applying GIS-MCDA for MAR suitability mapping concerning spreading methods in semi-arid regions, remotely sensed data on slope, geology/lithology, soil, land use/land cover, and drainage density may be used as baseline criteria. With this low number of criteria, pairwise comparison as weighting method in combination with analytical hierarchy process (AHP) as decision rule can readily be used for weighting and integration. Alternatively, for higher structural transparency, weighted linear combination may be used with either multi-influencing factor (MIF) or rating methods. From the baseline criteria, problem-specific criteria may be chosen based on the MAR objective and local contingencies. In applying GIS-MCDA for MAR suitability mapping concerning other MAR techniques in semi-arid regions, specific focus should be given to the linkages between criteria selections and technical requirements, costs, potential environmental degradation, and secondary effects of implementation of the chosen MAR technique.

References

Adem Esmail, B. and Geneletti, D. (2018) 'Multi-criteria decision analysis for nature conservation: A review of 20 years of applications', Methods in ecology and evolution. L. Dicks. British Ecological Society Cambridge, 9(1), pp. 42–53. doi: https://doi.org/10.1111/2041-210X.12899.

Adham, M. I., et al. (2010). Study on groundwater recharge potentiality of Barind tract, Rajshahi District, Bangladesh using GIS and remote sensing technique. *Journal of Geological Society of India, 75*, 432–438. https://doi.org/10.1007/s12594-010-0039-3.

Agostinetto, L., Dalla Venezia, F., & Gusmaroli, G. (2013). *Managed aquifer recharge (MAR) demonstrative techniques for the quantitative restoration of the groundwater balance in the Vicenza upper plain*. Veneto Agricoltura. Veneto Agricoltura Regional Agency for the Agriculture, Forestry and Agrifood Sectors. Retrieved from www.lifeaquor.org.

Ahani Amineh, Z. B., Hashemian, S. J. A. D., & Magholi, A. (2017). Integrating Spatial Multi Criteria Decision Making (SMCDM) with Geographic Information Systems (GIS) for delineation of the most suitable areas for aquifer storage and recovery (ASR). *Journal of Hydrology, 551*, 577–595. https://doi.org/10.1016/j.jhydrol.2017.05.031. Elsevier B.V.

Ahmadi, M. M., Mahdavirad, H. and Bakhtiari, B. (2017) 'Multi-criteria analysis of site selection for groundwater recharge with treated municipal wastewater', Water science and technology. IWA Publishing, London 76(4), pp. 909–919. doi: https://doi.org/10.2166/wst.2017.273.

Alraggad, M., & Jasem, H. (2010). Managed aquifer recharge (MAR) through surface infiltration in the Azraq Basin/Jordan. *Journal of Water Resource and Protection, 2*, 1057–1070. https://doi.org/10.4236/jwarp.2010.212125.

Anane, M., et al. (2008). Ranking suitable sites for soil aquifer treatment in Jerba Island (Tunisia) using remote sensing, GIS and AHP-multicriteria decision analysis. *International Journal of Water, 4*(1–2), 121–135. https://doi.org/10.1504/IJW.2008.018151. Inderscience Publishers.

Andreo, B., et al. (2008). Methodology for groundwater recharge assessment in carbonate aquifers: Application to pilot sites in southern Spain. *Hydrogeology Journal, 16*(5), 911–925. https://doi.org/10.1007/s10040-008-0274-5.

Bana e Costa, C. A., & Vansnick, J. C. (1997). Applications of the MACBETH approach in the framework of an additive aggregation model. *Journal of Multi-Criteria Decision Analysis, 6*(2), 107–114. https://doi.org/10.1002/(SICI)1099-1360(199703)6:2<107::AID-MCDA147>3.0.CO;2-1. John Wiley & Sons, Ltd.

Beganskas, S., & Fisher, A. T. (2017). Coupling distributed stormwater collection and managed aquifer recharge: Field application and implications. *Journal of Environmental Management, 200*, 366–379. https://doi.org/10.1016/j.jenvman.2017.05.058. Academic Press.

Casanova, J., Devau, N., & Pettenati, M. (2016). Managed aquifer recharge: An overview of issues and options. In A. J. Jakeman et al. (Eds.), *Integrated groundwater management: Concepts, approaches and challenges* (pp. 413–434). Cham, Switzerland: Springer. https://doi.org/10.1007/978-3-319-23576-9_16.

Chandio, I. A., et al. (2013). GIS-based analytic hierarchy process as a multicriteria decision analysis instrument: A review. *Arabian Journal of Geosciences, 6*, 3059–3066. https://doi.org/10.1007/s12517-012-0568-8. Springer.

Chenini, I., Mammou, A., & El May, M. (2010). Groundwater recharge zone mapping using GIS-based multi-criteria analysis: A case study in Central Tunisia (Maknassy Basin). *Water Resources Management., 24*, 921. https://doi.org/10.1007/s11269-009-9479-1.

Daher, W., et al. (2011). Karst and artificial recharge: Theoretical and practical problems. A preliminary approach to artificial recharge assessment. *Journal of Hydrology, 408*(3–4), 189–202. https://doi.org/10.1016/j.jhydrol.2011.07.017. Elsevier B.V.

de Winnaar, G., Jewitt, G. P. W., & Horan, M. (2007). A GIS-based approach for identifying potential runoff harvesting sites in the Thukela River basin, South Africa. *Physics and Chemistry of the Earth, 32*(15–18), 1058–1067. https://doi.org/10.1016/j.pce.2007.07.009. Pergamon.

Delgado, M. G., & Sendra, J. B. (2004). Sensitivity analysis in multicriteria spatial decision-making: A review. *Human and Ecological Risk Assessment, 10*, 1173–1187. https://doi.org/10.1080/10807030490887221. Taylor & Francis Group.

Dillon, P. (2005). Future management of aquifer recharge. *Hydrogeology Journal, 13*(1), 313–316. https://doi.org/10.1007/s10040-004-0413-6.

Dillon, P., et al. (2009). *Managed aquifer recharge : An introduction*. Waterlines Report Series No. 13.

Dillon, P., Escalante, E. F., & Tuinhof, A. (2012). *Management of aquifer recharge and discharge processes and aquifer storage equilibrium groundwater governance - A global framework for*

action - GEF-FAO Groundwater Governance Thematic Paper 4, 16-22. The Hague, Netherlands: FAO, GEF, IAH, IHP, and World Bank.

Dillon, P., et al. (2019). Sixty years of global progress in managed aquifer recharge. *Hydrogeology Journal, 27*(1), 1–30. https://doi.org/10.1007/s10040-018-1841-z. Springer.

Dragoni, W., & Sukhija, B. S. (2008). Climate change and groundwater. In W. Dragoni & B. S. Sukhija (Eds.), *Geological Society special publication*. London: The Geological Society. https://doi.org/10.1144/SP288.1.

Dutta, P. J. (2015). Assessment of groundwater potential in a part of the Vedganga watershed of Kolhapur District, Maharashtra, by a GIS-based bivariate statistical method. *International Journal of Advancement in Earth and Environmental Sciences, 3*(1), 22–29.

Eckert, P., Irmscher, R., & Rohns, H. P. (2005). Dynamic processes during bank filtration and their impact on raw water quality. 5th International Symposium on Managed Aquifer Recharge, ISMAR 5. Berlin, Germany: UNESCO.

Eisenführ, F., Weber, M., & Langer, T. (2010). *Rational decision making* (1st ed.). Berlin, Germany: Springer.

Escalante, E. F., et al. (2014). Economic assessment of opportunities for managed aquifer recharge techniques in Spain using an advanced geographic information system (GIS). *Water (Switzerland), 6*(7), 2021–2040. https://doi.org/10.3390/w6072021.

Escalante, E. F., et al. (2016). MARSOL, demonstrating managed aquifer recharge as a solution to water scarcity and drought. *European Union's Seventh Framework Programme for Research, Technological Development and Demonstration*.

Falkenmark, M., Lundqvist, J., & Widstrand, C. (1989). Macro-scale water scarcity requires micro-scale approaches: Aspects of vulnerability in semi-arid development. *Natural Resources Forum, 13*(4), 258–267. https://doi.org/10.1111/j.1477-8947.1989.tb00348.x. Wiley.

Fashae, O., et al. (2014). Delineation of groundwater potential zones in the crystalline basement terrain of SW-Nigeria: An integrated GIS and remote sensing approach. *Applied Water Science, 4*, 19–38. https://doi.org/10.1007/s13201-013-0127-9.

Fathi, S., Hagen, J. S., & Haidari, A. H. (2020). Synthesizing existing frameworks to identify the potential for managed aquifer recharge in a karstic and semi-arid region using GIS multi criteria decision analysis. *Groundwater for Sustainable Development, 11*, 100390. https://doi.org/10.1016/j.gsd.2020.100390. Elsevier BV.

Feizizadeh, B., et al. (2014). A GIS-based extended fuzzy multi-criteria evaluation for landslide susceptibility mapping. *Computers and Geosciences, 73*, 208–221. https://doi.org/10.1016/j.cageo.2014.08.001.

Feizizadeh, B., Kienberger, S., & Kamran, K. V. (2015). Sensitivity and uncertainty analysis approach for GIS-MCDA based economic vulnerability assessment. *Journal for Geographic Information Science, 1*, 81–89. https://doi.org/10.1553/giscience2015s81.

Fenta, A., et al. (2015). Spatial analysis of groundwater potential using remote sensing and GIS-based multi-criteria evaluation in Raya Valley, northern Ethiopia. *Hydrogeology Journal, 23*, 195–206. https://doi.org/10.1007/s10040-014-1198-x.

Fuentes, I., & Vervoort, R. W. (2020). Site suitability and water availability for a managed aquifer recharge project in the Namoi basin, Australia. *Journal of Hydrology: Regional Studies, 27*, 100657. https://doi.org/10.1016/j.ejrh.2019.100657. Elsevier B.V.

Gale, I., & Dillon, P. (Eds.). (2005). *Strategies for managed aquifer recharge (MAR) in semi-arid areas*. Paris: United Nations Educational, Scientific and Cultural Organization (UNESCO).

Gdoura, K., Anane, M., & Jellali, S. (2015). Geospatial and AHP-multicriteria analyses to locate and rank suitable sites for groundwater recharge with reclaimed water. *Resources, Conservation and Recycling, 104*, 19–30. https://doi.org/10.1016/j.resconrec.2015.09.003. Elsevier.

Ghayoumian, J., et al. (2007). Application of GIS techniques to determine areas most suitable for artificial groundwater recharge in a coastal aquifer in southern Iran. *Journal of Asian Earth Sciences, 30*(2), 364–374. https://doi.org/10.1016/j.jseaes.2006.11.002.

Gregory, R., et al. (2012). *Structured decision making: A practical guide to environmental management choices* (1st ed.). Hoboken, NJ: Wiley-Blackwell. https://doi.org/10.1002/9781444398557.

Hutton Barron, F. (1992). Selecting a best multiattribute alternative with partial information about attribute weights. *Acta Psychologica, 80*(1–3), 91–103. https://doi.org/10.1016/0001-6918(92)90042-C. Elsevier B.V.

IGRAC. (2007). *Artificial recharge of groundwater in the world report. Delft*. Retrieved August 4, 2017, from https://www.un-igrac.org/sites/default/files/resources/files/2008_IGRAC_GlobalMARInventory Report.pdf.

IPCC. (2014). In R. K. Pachauri & L. A. Meyer (Eds.), *IPCC, 2014: Climate change 2014: Synthesis report, contribution of working groups I, II and III to the fifth assessment report of the Intergovernmental Panel on Climate Change*. Geneva, Switzerland: IPCC. https://doi.org/10.1017/CBO9781139177245.003.

Jeude, E. V. L. De (2016) *Managed aquifer recharge : Opportunities and barriers*. Universiteit Utrecht, Deltares Company.

Kamangar, M. et al. (2019). A novel hybrid MCDM model to select a suitable location for implement groundwater recharge. Plant Archives 19(2):87–98.

Karami, G. H., Bagheri, R., & Rahimi, F. (2016). Determining the groundwater potential recharge zone and karst springs catchment area: Saldoran region, western Iran. *Hydrogeology Journal, 24*(8), 1981–1992. https://doi.org/10.1007/s10040-016-1458-z.

Kattaa, B., Al-Fares, W., & Al Charideh, A. R. (2010). Groundwater vulnerability assessment for the Banyas Catchment of the Syrian coastal area using GIS and the RISKE method. *Journal of Environmental Management, 91*(5), 1103–1110. https://doi.org/10.1016/j.jenvman.2009.12.008.

Kottek, M., et al. (2006). World map of the Köppen-Geiger climate classification updated. *Meteorologische Zeitschrift, 15*(3), 259–263. https://doi.org/10.1127/0941-2948/2006/0130. Schweizerbart'sche Verlagsbuchhandlung.

Krishnamurthy, J., et al. (1996). An approach to demarcate ground water potential zones through remote sensing and a geographical information system. *International Journal of Remote Sensing, 17*(10), 1867–1884. https://doi.org/10.1080/01431169608948744. Taylor & Francis Group.

Kurc, S. A., & Small, E. E. (2004). Dynamics of evapotranspiration in semiarid grassland and shrubland ecosystems during the summer monsoon season, Central New Mexico. *Water Resources and Research, 40*, 9305. https://doi.org/10.1029/2004WR003068.

Ligmann-Zielinska, A., & Jankowski, P. (2008). A framework for sensitivity analysis in spatial multiple criteria evaluation. In *Geographic information science* (pp. 217–233). Berlin: Springer. https://doi.org/10.1007/978-3-540-87473-7_14.

Lootsma, F. A. (1992). *The REMBRANDT system for multi-criteria decision analysis via pairwise comparisons or direct rating: Technical Report 92-05, Faculty of Technical Mathematics and Informatics, Delft University of Technology, Delft, Netherlands.*

Lopez Mendez, B., et al. (2016). *Aquifer Recharge*. Retrieved August 10, 2017, from https://www.ruvival.de/wp-content/uploads/2017/06/Literature-Review-Aquifer-Recharge.pdf.

Machiwal, D., Jha, M., & Mal, B. (2011). Assessment of groundwater potential in a semi-arid region of India using remote sensing, GIS and MCDM techniques. *Water Resources Management, 25*, 1359–1386. https://doi.org/10.1007/s11269-010-9749-y.

Malczewski, J. (1999). *GIS and multicriteria decision analysis*. Wiley. Retrieved November 16, 2018, from https://www.wiley.com/en-nl/GIS+and+Multicriteria+Decision+Analysis-p-9780471329442.

Malczewski, J. (2000). On the use of weighted linear combination method in GIS: Common and best practice approaches. *Transactions in GIS, 4*, 5–22. https://doi.org/10.1111/1467-9671.00035.

Malczewski, J. (2006). GIS-based multicriteria decision analysis: A survey of the literature. *International Journal of Geographical Information Science, 20*(7), 703–726. https://doi.org/10.1080/13658810600661508. Taylor & Francis.

Malczewski, J., & Rinner, C. (2015). Introduction to GIS-MCDA. In *Advances in geographic information science* (pp. 23–54). Heidelberg: Springer. https://doi.org/10.1007/978-3-540-74757-4_2.

Malczewski, J., & Rinner, C. (2016). *Multicriteria decision analysis in geographic information science* - Google Books. Retrieved August 27, 2017, from https://books.google.nl/books?id=1yl3BgAAQBAJ&pg=PA300&lpg=PA300&dq=Malczewski+and+Rinner+MCDA+sensitivity&source=bl&ots=p2nHzuXhBI&sig=0UDdBJffIqYhVfGPxkOIsU4Y18w&hl=en&sa=X&ved=0ahUKEwj76aK1sfjVAhWDaFAKHZ4rDscQ6AEIPTAC#v=onepage&q=MalczewskiandRin.

Moharir, K., Pande, C., Singh, S., Choudhari, P., Rawat, K., & Jeyakumar, L. (2019). Spatial interpolation approach-based appraisal of groundwater quality of arid regions. *Aqua Journal, 68* (6), 431–447.

Mukherjee, P., Singh, C., & Mukherjee, S. (2012). Delineation of groundwater potential zones in arid region of India—A remote sensing and GIS approach. *Water Resources Management, 26*, 2643–2672. https://doi.org/10.1007/s11269-012-0038-9.

Oikonomidis, D., Dimogianni, S., & Kazakis, N. (2015). A GIS/remote sensing-based methodology for groundwater potentiality assessment in Tirnavos area, Greece. *Journal of Hydrology, 525*, 197. https://doi.org/10.1016/j.jhydrol.2015.03.056.

Pande, C. B., Moharir, K. N., Khadri, S. F. R., & Patil, S. (2018). Study of land use classification in the arid region using multispectral satellite images. Applied Water Science, 8(5), 1–11. ISSN 2190–5487.

Pande, C. B., Moharir, K. N., Singh, S. K., & Varade, A. M. (2019). An integrated approach to delineate the groundwater potential zones in Devdari watershed area of Akola district, Maharashtra, Central India. *Environment, Development, and Sustainability, 22*, 4867. https://doi.org/10.1007/s10668-019-00409-1.

Rahman, M. A., et al. (2012). A new spatial multi-criteria decision support tool for site selection for implementation of managed aquifer recharge. *Journal of Environmental Management, 99*, 61–75. https://doi.org/10.1016/j.jenvman.2012.01.003. Elsevier Ltd.

Russo, T. A., Fisher, A. T., & Lockwood, B. S. (2015). Assessment of managed aquifer recharge site suitability using a GIS and modeling. *Groundwater, 53*, 389. https://doi.org/10.1111/gwat.12213.

Saatsaz, M., Sulaiman, W. N. A., & Shaharin Ebrahim, L. K. (2005). Development of an aquifer, storage and recovery (ASR) site selection suitability index in support of the Comprehensive Everglades restoration project. *Journal of Environmental Hydrology, 13*, 1–13.

Saaty, R. W. (1987). The analytic hierarchy process-what it is and how it is used. *Mathematical Modelling, 9*(3–5), 161–176. https://doi.org/10.1016/0270-0255(87)90473-8. Pergamon.

Sallwey, J., et al. (2018). Suitability maps for managed aquifer recharge: A review of multi-criteria decision analysis studies. *Environmental Reviews, 27*(2), 138–150. https://doi.org/10.1139/er-2018-0069. Canadian Science Publishing.

Saraf, A. K., & Choudhury, P. R. (1998). Integrated remote sensing and gis for groundwater exploration and identification of artificial recharge sites. *International Journal of Remote Sensing, 19*(10), 1825–1841. https://doi.org/10.1080/014311698215018. Taylor & Francis Group.

Schenkerman, & Stan. (1994). Avoiding rank reversal in AHP decision-support models. *European Journal of Operational Research, 74*(3), 407–419. Retrieved July 31, 2020, from https://ideas.repec.org/a/eee/ejores/v74y1994i3p407-419.html. Elsevier.

Sener, E., Davraz, A., & Ozcelik, M. (2005). An integration of GIS and remote sensing in groundwater investigations: A case study in Burdur, Turkey. *Hydrogeology Journal, 13*(5–6), 826–834. https://doi.org/10.1007/s10040-004-0378-5.

Shaban, A., Khawlie, M., & Abdallah, C. (2005). Use of remote sensing and GIS to determine recharge potential zones: The case of occidental Lebanon. *Hydrogeology Journal, 14*(4), 433–443. https://doi.org/10.1007/s10040-005-0437-6.

Stefan, C., & Ansems, N. (2018). Web-based global inventory of managed aquifer recharge applications. *Sustainable Water Resources Management, 4*(2), 153–162. https://doi.org/10.1007/s40899-017-0212-6. Springer.

Steinel, A. (2012). *Guideline for assessment and implementation of Managed Aquifer Recharge (MAR) in (semi-)arid regions Pre-feasibility study for infiltration of floodwater in the Amman-Zarqa and Azraq basins, Jordan, Bundesamt für Geowissenschaften und Rohstoffe*. Jordan. Retrieved from http://www.bgr.bund.de/EN/Themen/Zusammenarbeit/TechnZusammenarb/Downloads/jordanien_MAR.pdf?__blob=publicationFile&v=1%5Cn; http://www.bgr.bund.de/EN/Themen/Zusammenarbeit/TechnZusammenarb/Projekte/Abgeschlossen/Asien/1076_2002-3510-1-52_Jordanien_GWAnreic.

Tsangaratos, P., et al. (2017). Multi-criteria decision support system (DSS) for optimal locations of soil aquifer treatment (SAT) facilities. *Science of the Total Environment, 603–604*, 472–486. https://doi.org/10.1016/j.scitotenv.2017.05.238.

Tuinhof, A. et al. (2012) *Profit from storage the costs and benefits of water buffering*. BGR (Federal Institute for Geosciences and Natural Resources), IGRAC, ACACIA, META, RAIN, BMZ, IFAD.

UN. (2019). *The sustainable development goals report 2019*. New York: UN (The Sustainable Development Goals Report). https://doi.org/10.18356/55eb9109-en.

UNESCO. (2005). Recharge systems for protecting and enhancing groundwater resources. In F. Luck, M. Jekel, & I. Johnson (Eds.), *5th International Symposium on Management of Aquifer Recharge (ISMAR5)*. Berlin, Germany: UNESCO. Retrieved May 9, 2017, from http://unesdoc.unesco.org/images/0014/001492/149210e.pdf.

Valverde, J. P. B., et al. (2016). Application of a GIS multi-criteria decision analysis for the identification of intrinsic suitable sites in Costa Rica for the application of managed aquifer recharge (MAR) through spreading methods. *Water (Switzerland), 8*(9), 391. https://doi.org/10.3390/w8090391.

Van Berkum, S. W. (2010) *Assessing suitability for managed aquifer recharge by means of a GIS-application - case study for Kenya*. Utrecht. Retrieved from http://www.hwm.wur.nl/NR/rdonlyres/94013C92-71C5-4350-942F-6C26BA40E5DA/152154/berkum.pdf.

Wang, Y. M., & Elhag, T. M. S. (2006). An approach to avoiding rank reversal in AHP. *Decision Support Systems, 42*(3), 1474–1480. https://doi.org/10.1016/j.dss.2005.12.002. North-Holland.

Chapter 3
Robust Ensemble Modeling Paradigm for Groundwater Salinity Predictions in Complex Aquifer Systems

Alvin Lal and Bithin Datta

Contents

3.1 Introduction 53
3.2 Methodology 56
3.3 Prediction Model Development and Prediction Phases 58
3.4 Surrogate Model Performance Evaluation 59
3.5 Homogeneous Ensemble Model 60
3.6 Study Area 60
3.7 Results 63
3.8 Discussions 65
3.9 Conclusion 67
References 68

3.1 Introduction

Coastal aquifers are complex aquifer systems where continental fresh groundwater and saltwater meet (Post 2005). Coastal aquifers are important source of freshwater for millions of people worldwide, especially those residing near coastal areas (Costall et al. 2020). Saltwater intrusion is a major coastal aquifer management problem confronting the sustainability of coastal groundwater reserves in many parts

A. Lal (✉)
Discipline of Engineering & Physics, University of the South Pacific, Suva, Fiji
e-mail: alvin.lal@usp.ac.fj

B. Datta
Dicipline of Civil Engineering, College of Science and Engineering, James Cook University, Townsville, QLD, Australia
e-mail: bithin.datta@jcu.edu.au

C. B. Pande, K. N. Moharir (eds.), *Groundwater Resources Development and Planning in the Semi-Arid Region*, https://doi.org/10.1007/978-3-030-68124-1_3

of the world. Excessive and/or unplanned withdrawal of groundwater in coastal areas due to rapid population growth, agricultural needs, and industrial revolutions are the major causes of saltwater intrusion, which is posing a long-term threat to valuable and life sustaining coastal aquifer systems (Antonellini et al. 2008). Accurately predicting the extent of saltwater intrusion and adaptively developing management strategies are critical for future sustainability of fragile coastal groundwater resources. The present study demonstrates the application and evaluation of several machine learning-based prediction models and a homogeneous ensemble model for predicting groundwater salinity levels in a coastal aquifer system.

Saltwater intrusion is a highly complex and nonlinear process (Bhattacharjya and Datta 2005). Due to density differences, saltwater (denser then freshwater) intrudes beneath the freshwater systems, creating a saltwater "wedge" at the seawater-freshwater intersection (Mohsen et al. 1990). The resulting seawater-freshwater interface and its movement reflecting changes in salinity are keys to understanding saltwater intrusion processes in an aquifer. Both sharp interface and dispersive interface approaches have facilitated the understanding of relevant processes that cause saltwater intrusion into coastal aquifers. Sharp interface approach assumes that saltwater and freshwater are immiscible and therefore are separated by an abrupt interface (Bear and Verruijt 2012). The first attempt to model saltwater intrusion was made by Badon-Ghyben (1889) and Herzberg (1901) and consequently referred to as the Ghyben-Herzberg approach (Bobba 1993). Specifically, this approach treats the interface between saltwater and freshwater as sharp and well-defined. Conversely, the diffusive interface approach considers saltwater and fresh groundwater as miscible liquids separated by a transition zone (Voss and Souza 1987; Pande et al. 2019a, b). The transition zone has a finite thickness and the density of the water varies continuously. The diffusive interface approach contemplates the density dependence of the flow and transport processes. As a result, simultaneously solving flow and transport equations is essential. The mixing of the two fluids forming a transition zone at the interface is due to hydrodynamic dispersion and diffusion (Hussain et al. 2015). Modeling saltwater intrusion processes using the diffusive interface approach have given more realistic results for both homogeneous and heterogeneous aquifer systems (Nguyen 2016). Several numerical models based on the dispersive approach (SEAWAT, MODFLOW, FEMWATER, and SUTRA) have proven successful in modeling saltwater processes in coastal aquifers. Despite its usefulness, groundwater numerical simulation models are not always preferred in groundwater quality forecasting and management investigations because of its inherent complexities and due to computational power and time requirements. On the contrary, the use of prediction models in groundwater salinity forecasting and management has seen a significant rise in recent times.

Prediction models are developed to approximate the responses of a complex-coupled groundwater flow and transport numerical simulation models. Accurate training and testing is a key to developing a reliable and efficient prediction model. For this purpose, numerous patterns of input-output dataset are required. These datasets are obtained from a groundwater numerical simulation model, which

is to be approximated by the prediction model (Khadri and Moharir 2016; Khadri and Pande 2016; Moharir et al. 2017). This is because of several reasons. First, compared to the complex groundwater numerical simulation models, prediction models are computationally friendly, i.e., it requires lesser computational run time and CPU power. With the recent technological advancements, it is easier to develop and evaluate the performances of prediction models utilizing large datasets. Second, several studies have established that prediction models are capable of approximating coastal aquifer processes with reasonable accuracy and efficiency. Thirdly, several prediction models have the ability to identify the relative influence (impact) of each input variable on the outputs. For example, in a recent work, Lal and Datta (2020a) employed Group Method of Data Handling-models to identify the influence of individual pumping rates from groundwater pumping bores on the output groundwater salinity concentration at different aquifer locations (Pande et al. 2017; Moharir et al. 2020). These advantages have encouraged scientists and engineers to employ prediction models with little concern.

A range of machine learning-based prediction models have been used in saltwater intrusion modeling and prediction studies. These include artificial neural networks (ANN) (Bhattacharjya and Datta 2009; Bhattacharjya et al. 2009; Das and Datta 1999; Kourakos and Mantoglou 2009), modular neural networks (MNN) (Kourakos and Mantoglou 2013; Sreekanth and Datta 2010), genetic programming (GP) (Sreekanth and Datta 2011), Evolutionary Polynomial regression (EPR) (Hussain et al. 2015), radial basis function (RBF) (Christelis et al. 2019; Christelis and Mantoglou 2019; Papadopoulou et al. 2010), Fuzzy Inference System (FIS) (Roy and Datta 2017a), Extreme learning machine (ELM) (Yadav et al. 2018), Support Vector Machine Regression (SVMR) (Lal and Datta 2017, 2018a, c, 2019a), Kriging (Christelis et al. 2019), Multivariate Adaptive Regression Splines (MARS) (Roy and Datta 2018), and Gaussian Process regression (GPR) (Kopsiaftis et al. 2019; Lal and Datta 2018b, 2019b; Rajabi and Ketabchi 2017). All of these models have shown reasonable accuracy and efficiency. However, some models do possess several advantages over others. The selection of a specific prediction model type is dependent on the modeler and also sometimes depended on the modeling task at hand. In recent times, the use of ensemble prediction models has become more useful in groundwater modeling investigations. Ensemble modeling paradigm combines several individual predictive models into one ensemble (collective) model to give more robust and reliable prediction results. The application of ensemble models for saltwater intrusion modeling in complex aquifer systems is rare. Only recently, Sreekanth and Datta (2011), Roy and Datta (2017b), and Lal and Datta (2020b) have developed and applied ensemble models to predict groundwater salinity concentration in coastal aquifer systems. These studies have established that ensemble models have superior prediction powers and have the potential to provide improved prediction results when compared to individual predictive models.

The main objectives of this study are twofold. The first is to employ five different machine learning algorithms to develop groundwater salinity prediction tools. The second is to utilize the best performing predictive model out of the five models to develop a homogeneous ensemble prediction model capable of addressing

prediction uncertainties due to uncertain groundwater pumping rates. This study has, for the first time, developed groundwater salinity prediction models by training and testing ANN, GP, SVMR, GMDH, and GPR models using identical datasets obtained from an illustrative coastal aquifer system. The evaluation of the prediction accuracies of these machine learning-based models and the development of a robust homogeneous ensemble prediction model are presented in the chapter.

3.2 Methodology

3.2.1 Three-Dimensional Coastal Aquifer Numerical Simulation Model

The 3D numerical simulation FEMWATER (Lin et al. 1997) model was used for simulating pumping-induced saltwater intrusion phenomena into a costal aquifer system. The FEMWATER model allows simulation of density-dependent coupled groundwater flow and transport processes in an aquifer system. The coupled flow and transport equations can be found in (Lin et al. 1997). FEMWATER uses the Galerkin finite-element approximation and residual finite-element method for approximating flow and transport equations respectively and has been extensively used in various groundwater modeling applications (Carneiro et al. 2010; Kim et al. 2012; Koda and Wienclaw 2005).

3.2.2 Machine Learning Algorithms for Groundwater Salinity Predictions

Five machine learning algorithms were utilized to predict groundwater salinity concentrations at different monitoring wells in the aquifer. These individual machine learning algorithms are described below.

3.2.2.1 Artificial Neural Network (ANN)

ANN can be categorized as a group of machine learning model that originated from the desire of developing a system that makes decisions by following the working principles of the human brain (Oyebode and Stretch 2019). ANN encompasses a group of processors called neurons, which receives, evaluates, and exchanges information over a network of weighted connections. By mimicking the human brain, ANN is capable of representing an arbitrary, complex, and nonlinear process by correlating the input and output of a given system (Tanty and Desmukh 2015). The neurons in an ANN are structured in layers and neurons of each layer are connected to those of the neighboring layers. The strength of these connecting layers

is termed as the weights. During the training and testing process of an ANN model, the interconnecting weights are attuned until the inputs produce the preferred output. A more detailed structural description of the ANN models can be found in Ahmad and Simonovic (2005). Also, various applications of ANN in hydrological studies are reported in Tanty and Desmukh (2015), Govindaraju (2000), and Maier and Dandy (2000).

3.2.2.2 Genetic Programming (GP)

GP is categorized as an evolutionary approach based on the Darwinian principle of natural selection and survival of the fittest (Pandey et al. 2015). The GP algorithm is utilized to develop mathematical models based on the input-output (training and testing) data supplied. The GP algorithm itself develops computer programs to approximate the relationship between the input and output dataset without stipulating the structure of the solution in advance. GP adopts four key steps to approximate the relationship between the input-output dataset supplied. These steps include initialization, selection, reproduction, and termination (Niazkar and Niazkar 2020). In the first step, initial candidates describing the systems relationship are developed depending on the train and testing datasets. Second, the generated candidates are evaluated and subjected to genetic operators, which mainly favor the best candidate solution. These processes are reported in an iterative manner until the best candidate solution is chosen, which best describes the input-output dataset relationship. More detailed explanation on the structure and working principle of the GP models is reported in Mehr et al. (2018) and Banzhaf et al. (1998). Over the years, the GP-based models have been use in various hydrological prediction studies such as Sreekanth and Datta (2012), Fallah-Mehdipour et al. (2013), and Wang et al. (2009).

3.2.2.3 Support Vector Machine Regression (SVMR)

SVMR machine learning technique is based on the foundation of Support Vector Machine, which was introduced by Vapnik and Chervonenkis (Vapnik and Chervonenkis 1974). For a given set of input and output patterns, the objective of the SVMR model is to approximate a regression function $y = f(x)$, which can efficiently and accurately predict an output when a new set of input is fed to the model (Yang and Shieh 2010). SVMR algorithm begins by introducing a loss function that aims to minimize the regression error. Also, kernel functions are used to find the best regression hyperplane with the lowest structural risk in the high-dimensional feature space (Yeh et al. 2011). Detailed explanation on the SVMR technique can be found in Drucker et al. (1997), Smola and Schölkopf (2004), and Gunn (1998). The SVMR-based prediction models have been used in several groundwater modeling and management studies such as Al-Fugara et al. (2020), Yoon et al. (2011), and Lal and Datta (2018a).

3.2.2.4 Group Method of Data Handling (GMDH)

The GMDH machine learning algorithm was introduced by Ivakhnenko in 1968 (Farlow 1981). It is a heuristic self-organization process that approximates the relationship between the supplied input–output dataset obtained from a complex system (Tsai and Yen 2017). The GMDH algorithm is capable of automatically synthesizing adequate models that have the capability of replicating the inherent structure of highly complex and nonlinear systems. Specifically, in the GMDH networks, the important input variables, number of layers, neurons, and optimal model structure are automatically selected based on the input training dataset. This reduces the influence of user biasness and also lessens the burden on the analyst. The GMDH algorithm learns in an inductive way and builds predictive model (polynomial model), which can accurately determine input-output relationship and provide minimum error between the predicted and expected output value (Srinivasan 2008). A more complete description of the GMDH algorithm is reported in Farlow (1984) and Farlow (1981). GMDH algorithm has been widely applied in various groundwater modeling investigations including Barzegar et al. (2017), Zhu et al. (2010), and Khedri et al. (2020).

3.2.2.5 Gaussian Process Regression (GPR)

The GPR algorithm is categorized as a nonparametric probabilistic approach that is widely used in statistical modeling and forecasting tasks (Zhang et al. 2016). In principle, a GPR model defines prior probability distributions over latent functions directly. This is stated by its mean function and covariance function. The mean function encodes the central tendency of the function, and is often presumed to be zero. The covariance function on the other hand translates information about the shape and structure of the function. The relationship between a given input and output training dataset is descried as $=f(x) + \in$, where noise $\in$ is believed to be independent, owning Gaussian distribution with zero mean and variance. A more thorough explanation on the GPR working principle is presented in Vanhatalo et al. (2013) and Williams and Rasmussen (2006). The GPR-based models have been widely used in several groundwater forecasting studies such as Kopsiaftis et al. (2019), Raghavendra and Deka (2016), and Rajabi (2019).

3.3 Prediction Model Development and Prediction Phases

The basic aim of constructing the prediction models was to capture the functional relationship between the input (transient pumping patterns from each pumping wells) and output (salinity concentration at monitoring wells) datasets. For cross-validation purposes, generated datasets were partitioned randomly into development

and prediction datasets. For the construction of individual prediction models, N input-output datasets were generated. The inputs, i.e., the randomized input transient groundwater pumping patterns from pumping wells were generated using Latin Hypercube sampling strategy. Each set of these pumping patterns was fed to the 3D numerical simulation model and the resulting output salinity concentration datasets at different monitoring wells were recorded. These corresponding input-output datasets were used to construct the individual machine learning-based prediction models. The accumulated datasets were randomly divided into development and prediction sets. The development dataset was further divided into training and testing dataset. The training and testing sets were used to construct the prediction models, while the prediction set was used to independently evaluate its performance (Westerhuis et al. 2008). The input and output were both fed to the model during training and testing phase only. No output concentration was fed to the model during the final independent prediction phase. The prediction model itself predicted concentrations based on the specified pumping datasets, which were then compared with the output concentrations obtained from the numerical simulation model.

3.4 Surrogate Model Performance Evaluation

Evaluation of the predictive capabilities of individual machine learning models was an important step in this study. The predictive accuracy of the constructed five models was evaluated through calculation of various statistical indices such as root mean square error (RMSE), mean absolute error (MAE), Nash-Sutcliffe efficiency (NE), coefficient of determination (R^2), and correlation coefficient (r). Mathematical expressions of these statistical indices are presented in Eqs. (3.1)–(3.5).

$$\mathrm{RMSE} = \sqrt{\frac{1}{K}\sum_{k=1}^{K}\left(C_k^{\mathrm{o}} - C_k^{\mathrm{p}}\right)^2} \tag{3.1}$$

$$\mathrm{MAE} = \frac{1}{K}\sum_{k=1}^{K}\left|C_k^{\mathrm{p}} - C_k^{\mathrm{o}}\right| \tag{3.2}$$

$$\mathrm{NE} = 1 - \frac{\sum_{k=1}^{K}\left(C_k^{\mathrm{o}} - C_k^{\mathrm{p}}\right)^2}{\sum_{k=1}^{K}\left(C_k^{\mathrm{o}} - c^{\mathrm{o}}\right)^2} \tag{3.3}$$

$$R^2 = \frac{\sum_{k=1}^{K}\left(C_k^{\mathrm{p}} - c^{\mathrm{o}}\right)^2}{\sum_{k=1}^{K}\left(C_k^{\mathrm{o}} - c^{\mathrm{o}}\right)^2} \tag{3.4}$$

$$r = \frac{\sum_{k=1}^{K}\left(C_k^{\mathrm{o}} - c^{\mathrm{o}}\right)\left(C_k^{\mathrm{p}} - c^{\mathrm{p}}\right)}{\sqrt{\sum_{k=1}^{K}\left(C_k^{\mathrm{o}} - c^{\mathrm{o}}\right)^2}\sqrt{\sum_{k=1}^{K}\left(C_k^{\mathrm{p}} - c^{\mathrm{p}}\right)^2}} \tag{3.5}$$

where, C_k^{o} is observed (from 3D numerical simulation model) salinity concentration, C_k^{p} is predicted (from machine learning-based models) salinity concentration, c^{o} is mean observed salinity concentration, c^{p} is mean predicted salinity concentration, and K is the total number of data points.

3.5 Homogeneous Ensemble Model

The best performing individual model was statistically combined to form a homogeneous ensemble model. Each homogeneous model consisted of five individual models of the same machine learning algorithm. Each of these same machine learning models was developed using different realization of the original input-output datasets. Each realization of the original dataset was used to develop one individual model in the homogeneous ensemble model. The different realizations of the input-output datasets were generated using random sampling without replacement methodology (Horvitz and Thompson 1952). These different realizations of the data set provided a platform for incorporating input groundwater pumping uncertainties. The output of the homogeneous ensemble model is obtained by combining the outputs of the individual prediction models using the simple average methodology as expressed by Eq. 3.6.

$$E_n = \frac{1}{N}\sum_{n=1}^{N} P^n \quad n = 1, 2, \ldots, N \tag{3.6}$$

where, E_n is the homogeneous ensemble model prediction output, n represents each of the individual prediction model, and N is the total number of individual prediction models in the ensemble.

3.6 Study Area

For performance evaluation, an illustrative study area containing of a portion of a multilayered coastal aquifer was modeled using FEMWATER. The length of the coastline (Boundary A) was 2.13 km and the other two boundaries were 2.04 km (Boundary B) and 2.79 km (Boundary C), respectively. The study area was approximately 2.53 km^2. The sea-side boundary was a constant head and constant conc. Boundary having a concentration of 35 kg/m^3. The other two boundaries of the study area were taken as no-flow boundaries. The total aquifer depth was 60 m, divided equally into three layers. A constant groundwater recharge of 0.00054 m/day was

specified over the entire study area. The study area consisted of five barrier wells (B_1, B_2, ..., B_5), eight freshwater wells (F_1, F_2, ..., F_8), and three monitoring wells (M_1, M_2 and M_3). Freshwater wells were installed for withdrawing fresh groundwater for domestic consumption. On the other hand, barrier wells were installed near the shoreline for saltwater intrusion prevention (acted as hydraulic control). Pumping from barrier wells induced a steeper hydraulic gradient towards the sea, thus controlling/minimizing saltwater intrusion into the aquifer system (Dhar and Datta 2009). Monitoring wells were installed for groundwater salinity concentration monitoring purposes. The screening interval of all the wells was taken from the second and third layers of the aquifer. The study area with specific well locations is presented in Fig. 3.1. Some key coastal aquifer parameters used during the development of 3D numerical simulation model are listed in Table 3.1.

Establishing convergence of the 3D numerical simulation groundwater model was vital. First, the FEMWATER numerical code required the model domain to be converted into a finite element mesh that defines the location of nodes at which the head and the solute concentration values can be calculated. Deciding on the appropriate level of discretization of the model domain was a key challenge of the study. Utilizing a high-resolution discretization had some implications such as increased model run time and high memory requirements. Merz (2012) stated that some of the factors to consider while deciding element size when using finite element modeling methodology include: (1) the developed model should provide an adequate representation of the investigated problem, (2) the model should converge in an appropriate model run time, and (3) the model should have executable file sizes. A

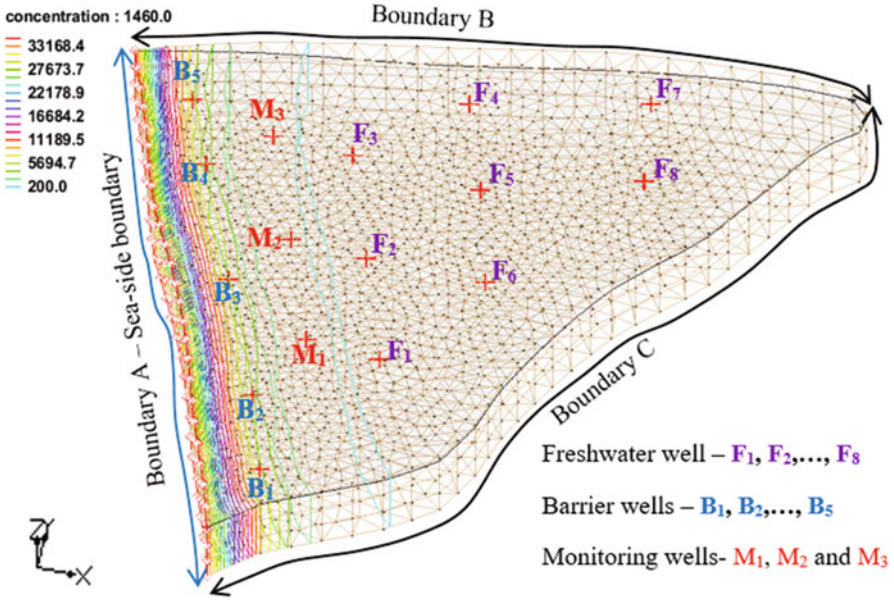

Fig. 3.1 3D study area with different well locations and aquifer boundaries

Table 3.1 Key coastal aquifer hydrological parameters

Aquifer parameters		Numerical values
Hydraulic conductivity	*x* direction	15 m/day
	y direction	7.5 m/day
	z direction	1.5 m/day
Bulk density		1600 kg/m^3
Longitudinal dispersivity		50 m
Lateral dispersivity		25 m
Molecular dispersion coefficient		0.69 m^2/day
Density reference ratio		7.14×10^{-7}
Soil porosity		0.46
Compressibility		8.5×10^{-15} md^2/kg

trade-off between these factors was used to decide on the number of elements needed for mesh construction. To achieve sufficiently accurate modeling results, the triangular elements were arranged in a specific way, so that it provides a relatively dense array of finer elements near well placements (area of interest), while upholding coarse elements in areas where wells were not installed (Merz 2012). After trial and error, the modeled aquifer study area was discretized into triangular finite elements having an average element size of 150 m. The element size near the wells was set to 75 m. Increasing element sizes beyond these specified numbers increased model convergence time without having much impact on the output results.

The 3D transient simulation was initiated from an initially steady state condition of the aquifer, achieved via constant pumping of 300 m^3/day from only three of the freshwater wells (F_2, F_5, and F_8) for a period of 20 years. The resulting heads and concentration after 20 years were used as initial conditions (initial head and concentration) for aquifer simulation for the specified period of 4 years (*1460 days*). This 4-year simulation considered pumping from all freshwater and barrier wells.

Randomized 700 input transient pumping patterns from both well types were obtained using the Latin Hypercube sampling strategy. These 700 input pumping patterns were fed to the 3D numerical simulation model each at a time to obtain the corresponding output groundwater salinity concentration at the three monitoring wells. These 700 input and output datasets were used for the construction of the machine learning-based prediction models. The accumulated 700 datasets were divided into development and prediction sets in the ratio of 6:1, i.e., 600 input-output patterns were used for prediction model development and 100 input-output patterns were used for independent prediction task. The development dataset was further divided into training and testing dataset in the ration of 2:1, i.e., 400 datasets were used for prediction model training and 200 datasets were used for testing. Three prediction models using a single machine learning algorithm were developed to predict groundwater salinity concertation at the corresponding three different

Table 3.2 Different prediction models developed

Monitoring wells	Prediction models developed
M_1	ANN_1, GP_1, $SVMR_1$, $GMDH_1$, and GPR_1
M_2	ANN_2, GP_2, $SVMR_2$, $GMDH_2$, and GPR_2
M_3	ANN_3, GP_3, $SVMR_3$, $GMDH_3$, and GPR_3

monitoring wells. In total, 15 prediction models were trained and tested. These prediction models are listed in Table 3.2.

The ANN-based prediction models were developed using the R2016a MATLAB platform. A feedforward neural network with the back propagation training algorithm was used to develop the three ANN-based prediction models. GP-based prediction models were developed using the Discipulus GP Software. Main GP modeling parameters such as the population size, crossover probability, and number of generations were obtained after conducting several trial and errors runs. For this specific prediction investigation, minimization of the RMSE was chosen as the fitness function. The SVMR-based models were developed using the R2016a MATLAB platform. For the present study, Gaussian kernel was used, with ε, C, and γ (Gaussian kernel parameter) having a value of 0.60, 10, and 0.001, respectively. The GMDH-based prediction models were developed using GMDH shell; forecasting software developed for regression prediction tasks. The RMSE was used as the external criterion while developing GMDH-based prediction models. Lastly, the GPR-based prediction models were developed using the R2016a MATLAB platform. The squared-exponential covariance function with automatic relevance determination was used as the covariance function with default MATLAB parameters used for all other related hyper-parameters of this covariance function.

3.7 Results

3.7.1 Performance Evaluation Results for Individual Machine Learning Models'

The performance evaluation results of the five data-driven machine learning algorithms are presented in the Tables 3.3, 3.4, 3.5, 3.6 and 3.7 below.

3.7.2 Future Groundwater Salinity Level in the Aquifer

The best performing GPR-based models were used to simulate groundwater salinity concentration for the next 3 years. The prediction results were compared with the results obtained by running the complex 3D groundwater flow and transport model. The results are presented below.

Table 3.3 GPR model performances evaluation results

Model	Stage	Performances indices				
		RMSE	MAE	NE	R^2 (%)	r
GPR1	Training	0.321	0.255	1	99.83	0.999
	Testing	0.326	0.258	1	99.81	0.999
	Prediction	0.329	0.250	1	99.79	0.998
GPR2	Training	0.273	0.251	1	99.72	0.998
	Testing	0.288	0.249	1	99.70	0.997
	Prediction	0.254	0.248	1	99.71	0.998
GPR3	Training	0.368	0.257	1	99.75	0.998
	Testing	0.377	0.261	1	99.86	0.999
	Prediction	0.372	0.264	1	99.85	0.999

Table 3.4 GMDH model performance evaluation results

Model	Stage	Performances indices				
		RMSE	MAE	NE	R^2 (%)	r
$GMDH_1$	Training	0.366	0.292	1	99.68	0.997
	Testing	0.358	0.289	1	99.72	0.997
	Prediction	0.379	0.299	1	99.61	0.996
$GMDH_2$	Training	0.281	0.175	1	99.67	0.998
	Testing	0.298	0.174	1	99.66	0.998
	Prediction	0.263	0.186	1	99.73	0.997
$GMDH_3$	Training	0.440	0.298	1	99.68	0.998
	Testing	0.368	0.293	1	99.69	0.998
	Prediction	0.458	0.306	1	99.66	0.996

Table 3.5 SVMR model performance evaluation results

Model	Stage	Performances indices				
		RMSE	MAE	NE	R^2 (%)	r
$SVMR_1$	Training	0.405	0.299	0.98	99.55	0.996
	Testing	0.449	0.295	0.99	99.46	0.994
	Prediction	0.394	0.301	0.99	99.58	0.995
$SVMR_2$	Training	0.323	0.212	1	99.61	0.997
	Testing	0.218	0.214	1	99.64	0.997
	Prediction	0.271	0.236	0.99	99.62	0.996
$SVMR_3$	Training	0.458	0.306	0.98	99.52	0.995
	Testing	0.452	0.303	0.98	99.49	0.995
	Prediction	0.485	0.307	0.99	99.53	0.994

Table 3.6 GP model performance evaluation results

Model	Stage	Performances indices				
		RMSE	MAE	NE	R^2 (%)	r
GP_1	Training	0.475	0.307	0.95	99.40	0.993
	Testing	0.416	0.308	0.94	99.41	0.992
	Prediction	0.449	0.304	0.94	99.46	0.992
GP_2	Training	0.355	0.238	0.97	99.49	0.996
	Testing	0.328	0.246	0.98	99.51	0.995
	Prediction	0.388	0.256	0.97	99.46	0.995
GP_3	Training	0.472	0.309	0.97	99.48	0.993
	Testing	0.456	0.312	0.97	99.45	0.992
	Prediction	0.506	0.313	0.95	99.49	0.991

Table 3.7 ANN model performance evaluation results (WRM paper)

Model	Stage	Performances indices				
		RMSE	MAE	NE	R^2 (%)	r
ANN1	Training	0.617	0.388	0.94	99.11	0.989
	Testing	0.608	0.381	0.93	99.10	0.990
	Prediction	0.602	0.376	0.94	99.06	0.989
ANN2	Training	0.508	0.301	0.95	99.15	0.992
	Testing	0.501	0.312	0.96	99.28	0.992
	Prediction	0.539	0.358	0.94	99.24	0.992
ANN3	Training	0.564	0.387	0.95	99.13	0.991
	Testing	0.702	0.409	0.96	99.16	0.989
	Prediction	0.713	0.402	0.96	99.24	0.988

3.8 Discussions

Out of all the five algorithms used for predicting groundwater salinity, the ANN-based models performed the worst. However, in this performance evaluation exercise, the errors in terms of accuracy in training, testing, and prediction modes were quite high irrespective of the models used. The ANN models had the highest RMSE and MAE vales and the lowest NE, R^2, and r values. The accuracy was the highest for the GPR-based models. Also, the GPR-based models seemed to exhibit very comparable, if not slightly better performance in the prediction mode. Therefore, GPR-based models were established to be most efficient groundwater salinity prediction model. In terms of the five statistical indices used, the GPR-based models had the lowest RMSE and MAE values and highest R^2 and r values. The NE values for the GPR and GMDH-based models were the same, i.e., 1. These results validate the accuracy of the GPR models and establish it as an effective and reliable tool for predicting and monitoring groundwater salinity levels in the coastal aquifer system.

To incorporate groundwater pumping uncertainties, different realization of the initial input-output dataset and the best performing GPR models were used to

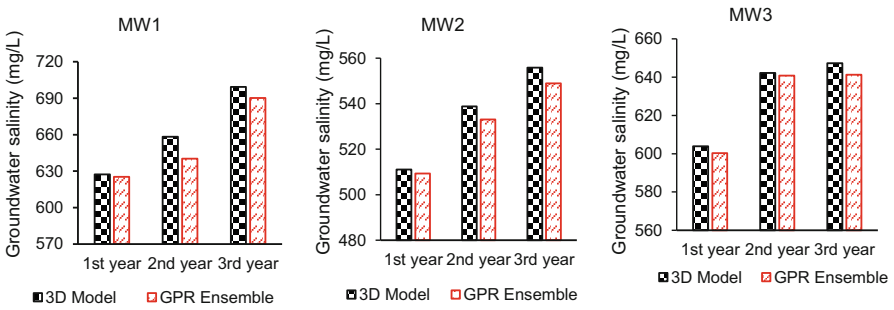

Fig. 3.2 Groundwater salinity level obtained from the 3D model and GPR homogeneous ensemble models at the end of first, second, and third year

construct GPR homogeneous ensemble models. These homogeneous ensemble models were then used to predict groundwater salinity levels in the aquifer for the next 3 years. The solution results are presented in Fig. 3.2. The results show that GPR ensemble model prediction results were almost similar to the responses of the 3D aquifer model. The results also provide insights into the ability of the GPR homogeneous ensembles to produce improved prediction performance with available data, and also allow incorporation of groundwater pumping uncertainty when developing prediction models. The use of homogeneous ensemble models is particularly important in hydrological studies where groundwater pumping patterns fluctuate due to water demand, and change in climatic conditions such as draught and flooding.

The machine learning-based groundwater salinity prediction tool cannot only be used to predict future groundwater conditions, but also be used for assessing the impacts of human activity on groundwater. Various changes in pumping patterns will have different salinity consequences at the monitoring locations. Evaluating these salinity data at respective monitoring wells will allow the user to access the impact of pumping. This can also enable decision-makers make reliable and robust groundwater pumping decisions and enact legislations. Also, the prediction models provide us with a tool that can be used to understand flow and pollutant patterns in the aquifer. For example, installing monitoring wells at different locations and collecting salinity data can display the different salinity patterns in the aquifer. This can be instrumental when deciding where to install pumping wells for extracting groundwater. In addition, the homogeneous GPR ensemble models can be used as emulators of the complex 3D groundwater flow and transport model and integrated into coupled simulation-optimization models for developing sustainable groundwater management strategies. Numerous studies have used data-driven machine learning algorithm as reliable emulators of complex groundwater systems. However, the use of ensemble models in linked S/O models is rare.

The conclusions drawn from this study are based on the limited performance evaluation calculations. However, the groundwater salinity prediction trend for the five machine learning algorithm used may be different for a different coastal

groundwater case study area. The predictive capabilities of each of the individual models are dependent on the training and validation datasets. These training datasets are extracted from the complex 3D aquifer models.

Hence, they are dependent on individual 3D models, groundwater pumping patterns and other hydrological parameters. Development of the 3D aquifer models for modeling complex groundwater flow and transport processes needs attention to detail and reliable groundwater data for 3D model calibration and validation. The 3D aquifer simulation model should accurately replicate the real aquifer processes and this can only be achieved by properly calibrating and validating the model with historical datasets. In this case, the machine leaning tools were used to simulate and predict saltwater intrusion in an illustrative aquifer system. The calibration and validation of the 3D numerical simulation model was not needed as the data used were synthetic. Also, synthetic simulated data facilitate evaluation of performances for various possible scenarios, not other possible to replicate in field for evaluation purpose. However, for a real aquifer system, calibration and validation of the numerical simulation model is utmost important.

3.9 Conclusion

In this study, five different machine learning algorithms (ANN, GP, SVMR, GMDH, and GPR) were used to predict groundwater salinity concentration in an illustrative coastal aquifers system. The performance evaluation results established GPR models as the most reliable groundwater salinity prediction tool. Out of the all the algorithm used, GPR models had the lowest RMSE and MAE values and highest NE, R^2, and r values. Later, to incorporate groundwater pumping uncertainties, five different realizations of the original training and testing dataset were used to train five different sets of GPR models. These five sets of GPR models were then used to construct homogeneous GPR ensemble models, which were used to predict future (for the next 3 years) groundwater salinity conditions in the aquifer. The prediction performance of the homogeneous ensemble models was compared with the simulated responses of the 3D groundwater flow and transport model and the results were found to be accurate and nearly the same. Overall, the findings of this study suggest that data-driven machine learning algorithms can be used for predicting future groundwater quality conditions in an aquifer. Also, ensemble models provide a platform for incorporating groundwater pumping uncertainties when predicting future groundwater conditions. This property of ensemble modeling has further applications in the field of hydrology as ensemble prediction models can be used to develop robust coastal aquifer monitoring and management strategies.

References

Ahmad, S., & Simonovic, S. P. (2005). An artificial neural network model for generating hydrograph from hydro-meteorological parameters. *Journal of Hydrology, 315*, 236–251.

Al-Fugara, A. K., Ahmadlou, M., Al-Shabeeb, A. R., Al Ayyash, S., Al-Amoush, H., & Al-Adamat, R. (2020). Spatial mapping of groundwater springs potentiality using grid search-based and genetic algorithm-based support vector regression. *Geocarto International, 1*, 1–20.

Antonellini, M., et al. (2008). Salt water intrusion in the coastal aquifer of the southern Po Plain, Italy. *Hydrogeology Journal, 16*, 1541–1556.

Badon–Ghyben, W. (1889). Nota in verband met de voorgenomen putboring nabil Amsterdam, report, 27 pp., Tijdschr. K. Inst. van Ing., Hague, Netherlands.

Banzhaf, W., Nordin, P., Keller, R. E., & Francone, F. D. (1998). *Genetic programming: An introduction: On the automatic evolution of computer programs and its applications*. San Francisco: Morgan Kaufmann.

Barzegar, R., Fijani, E., Moghaddam, A. A., & Tziritis, E. (2017). Forecasting of groundwater level fluctuations using ensemble hybrid multi-wavelet neural network-based models. *Science of the Total Environment, 599*, 20–31.

Bear, J., & Verruijt, A. (2012). *Modeling groundwater flow and pollution* (Vol. 2). Reidel, Dordrecht: Springer.

Bhattacharjya, R. K., & Datta, B. (2005). Optimal management of coastal aquifers using linked simulation optimization approach. *Water Resources Management, 19*, 295–320. https://doi.org/10.1007/s11269-005-3180-9.

Bhattacharjya, R. K., & Datta, B. (2009). ANN-GA-based model for multiple objective management of coastal aquifers. *Journal of Water Resources Planning and Management, 135*, 314–322.

Bhattacharjya, R. K., Datta, B., & Satish, M. G. (2009). Performance of an artificial neural network model for simulating saltwater intrusion process in coastal aquifers when training with noisy data. *KSCE Journal of Civil Engineering, 13*, 205–215.

Bobba, A. (1993). Mathematical models for saltwater intrusion in coastal aquifers. *Water Resources Management, 7*, 3–37.

Carneiro, J. F., Boughriba, M., Correia, A., Zarhloule, Y., Rimi, A., & El Houadi, B. (2010). Evaluation of climate change effects in a coastal aquifer in Morocco using a density-dependent numerical model. *Environmental Earth Sciences, 61*, 241–252.

Christelis, V., & Mantoglou, A. (2019). Pumping optimization of coastal aquifers using seawater intrusion models of variable-fidelity and evolutionary algorithms. *Water Resources Management, 33*, 555–568.

Christelis, V., Kopsiaftis, G., & Mantoglou, A. (2019). Performance comparison of multiple and single surrogate models for pumping optimization of coastal aquifers. *Hydrological Sciences Journal, 64*, 336.

Costall, A., Harris, B., Teo, B., Schaa, R., Wagner, F., & Pigois, J. (2020). Groundwater throughflow and seawater intrusion in high quality coastal aquifers. *Scientific Reports, 10*, 1–33.

Das, A., & Datta, B. (1999). Development of multiobjective management models for coastal aquifers. *Journal of Water Resources Planning and Management, 125*, 76–87.

Dhar, A., & Datta, B. (2009). Saltwater intrusion management of coastal aquifers. I: Linked simulation-optimization. *Journal of Hydrologic Engineering, 14*, 1263–1272.

Drucker, H., Burges, C. J., Kaufman, L., Smola, A. J., & Vapnik, V. (1997). Support vector regression machines. In *Advances in neural information processing systems* (pp. 155–161). Cambridge: MIT Press.

Fallah-Mehdipour, E., Haddad, O. B., & Mariño, M. (2013). Prediction and simulation of monthly groundwater levels by genetic programming. *Journal of Hydro-Environment Research, 7*, 253–260.

Farlow, S. J. (1981). The GMDH algorithm of Ivakhnenko. *The American Statistician, 35*, 210–215.

Farlow, S. J. (1984). *Self-organizing methods in modeling: GMDH type algorithms* (Vol. 54). Boca Raton: CRC Press.

Govindaraju, R. S. (2000). Artificial neural networks in hydrology. II: hydrologic applications. *Journal of Hydrologic Engineering, 5*, 124–137.

Gunn, S. R. (1998). *Support vector machines for classification and regression*. ISIS technical report 14, pp. 5–16.

Herzberg, A. (1901). Die Wasserversorgung einiger Nordseebader. *J. Gasbeleucht. Wasserversorg., 44*, 815–819, 842–844.

Horvitz, D. G., & Thompson, D. J. (1952). A generalization of sampling without replacement from a finite universe. *Journal of the American Statistical Association, 47*, 663–685.

Hussain, M. S., Javadi, A. A., Ahangar-Asr, A., & Farmani, R. (2015). A surrogate model for simulation–optimization of aquifer systems subjected to seawater intrusion. *Journal of Hydrology, 523*, 542–554.

Khadri, S. F. R., & Moharir, K. (2016). Characterization of aquifer parameter in basaltic hard rock region through pumping test methods: A case study of Man River basin in Akola and Buldhana districts Maharashtra India. *Modeling Earth Systems and Environment, 2*, 33.

Khadri, S. F. R., & Pande, C. (2016). Ground water flow modeling for calibrating steady state using MODFLOW software: A case study of Mahesh River basin, India. *Modeling Earth Systems and Environment, 2*, 39. https://doi.org/10.1007/s40808-015-0049-7.

Khedri, A., Kalantari, N., & Vadiati, M. (2020). Comparison study of artificial intelligence method for short term groundwater level prediction in the Northeast Gachsaran unconfined aquifer. *Water Supply, 20*, 909–921.

Kim, S.-D., Lee, H.-J., & Park, J.-S. (2012). Simulation of seawater intrusion range in coastal aquifer using the FEMWATER model for disaster information. *Marine Georesources and Geotechnology, 30*, 210–221.

Koda, E., & Wienclaw, E. (2005). Flow and transport modelling in old landfill subsoil with vertical barrier. In *Proceedings of the International Conference on Soil Mechanics and Geotechnical Engineering* (Vol. 2, p. 921). Accord, MA: AA Balkema Publishers.

Kopsiaftis, G., Protopapadakis, E., Voulodimos, A., Doulamis, N., & Mantoglou, A. (2019). Gaussian process regression tuned by bayesian optimization for seawater intrusion prediction. *Computational Intelligence and Neuroscience, 10*, 1–12.

Kourakos, G., & Mantoglou, A. (2009). Pumping optimization of coastal aquifers based on evolutionary algorithms and surrogate modular neural network models. *Advances in Water Resources, 32*, 507–521.

Kourakos, G., & Mantoglou, A. (2013). Development of a multi-objective optimization algorithm using surrogate models for coastal aquifer management. *Journal of Hydrology, 479*, 13–23.

Lal, A., & Datta, B. (2017). Modelling saltwater intrusion processes and development of a multi-objective strategy for management of coastal aquifers utilizing planned artificial freshwater recharge. *Modeling Earth Systems and Environment, 4*, 111–126.

Lal, A., & Datta, B. (2018a). Development and implementation of support vector machine regression surrogate models for predicting groundwater pumping-induced saltwater intrusion into coastal aquifers. *Water Resources Management, 32*, 2405–2419.

Lal, A., & Datta, B. (2018b). Genetic programming and Gaussian Process Regression Models for groundwater salinity prediction: machine learning for sustainable water resources management. In: *2018 IEEE Conference on Technologies for Sustainability (SusTech)* (pp 1–7). IEEE.

Lal, A., & Datta, B. (2018c). Multiple objective management strategies for coastal aquifers utilizing new surrogate models. *International Journal of Geomate, 15*, 79–85.

Lal, A., & Datta, B. (2019a). Multi-objective groundwater management strategy under uncertainties for sustainable control of saltwater intrusion: Solution for an island country in the South Pacific. *Journal of Environmental Management, 234*, 115–130.

Lal, A., & Datta, B. (2019b). Optimal pumping strategies for the management of coastal groundwater resources: Application of Gaussian Process Regression metamodel-based simulation-optimization methodology. *ISH Journal of Hydraulic Engineering, 1*, 1–10.

Lal, A., & Datta, B. (2020a). Application of the group method of data handling and variable importance analysis for prediction and modelling of saltwater intrusion processes in coastal aquifers. *Neural Computing and Applications, 1*, 1–12.

Lal, A., & Datta, B. (2020b). Performance evaluation of homogeneous and heterogeneous ensemble models for groundwater salinity predictions: A regional-scale comparison study. *Water, Air, & Soil Pollution, 231*, 1–21.

Lin, H-C. J., Richards, D. R., Yeh, G-T., Cheng, J-R., Cheng, H-P., & Jones, N. L. (1997). FEMWATER: A three-dimensional finite element computer model for simulating density-dependent flow and transport in variably saturated media. Army Engineer Waterways Experiment Station Vicksburg MS Coastal Hydraulics Lab. Technical Report CHl-97-12.

Maier, H. R., & Dandy, G. C. (2000). Neural networks for the prediction and forecasting of water resources variables: A review of modelling issues and applications. *Environmental Modelling and Software, 15*, 101–124.

Mehr, A. D., Nourani, V., Kahya, E., Hrnjica, B., Sattar, A. M., & Yaseen, Z. M. (2018). Genetic programming in water resources engineering: A state-of-the-art review. *Journal of Hydrology, 566*, 643–667.

Merz, S. K. (2012). *Australian groundwater modelling guidelines*. Waterlines Report Series.

Moharir, K., Pande, C., & Patil, S. (2017). Inverse modeling of aquifer parameters in basaltic rock with the help of pumping test method using MODFLOW software. *Geoscience Frontiers, 8*, 1385–1395.

Moharir, K. N., Pande, C. B., Singh, S. K., & Del Rio, R. A. (2020). Evaluation of analytical methods to study aquifer properties with pumping test in Deccan Basalt Region of the Morna River Basin in Akola district of Maharashtra in India. In *Groundwater hydrology*. London, UK: Intec Open Publication. https://doi.org/10.5772/intechopen.84632. (Web of Science Indexed).

Mohsen, M. S., Singh, V. P., & Amer, A. M. (1990). A note on saltwater intrusion in coastal aquifers. *Water Resources Management, 4*, 123–134.

Nguyen, B. T. (2016). *Coupling geophysical and isotopic approaches to better simulate saltwater intrusion into coastal aquifers: A case study in the Crau aquifer*. Université d'Avignon.

Niazkar, M., & Niazkar, H. R. (2020). COVID-19 outbreak: Application of multi-gene genetic programming to country-based prediction models. *Electronic Journal of General Medicine, 17*, em247.

Oyebode, O., & Stretch, D. (2019). Neural network modeling of hydrological systems: A review of implementation techniques. *Natural Resource Modeling, 32*, e12189.

Pande, C. B., Khadri, S. F. R., Moharir, K. N., & Patode, R. S. (2017). Assessment of groundwater potential zonation of Mahesh River basin Akola and Buldhana districts, Maharashtra, India using remote sensing and GIS techniques. *Sustainable Water Resources Management*. https://doi.org/10.1007/s40899-017-0193-5. ISSN 2363-5037. Published online 8 September-2017.

Pande, C. B., Moharir, K. N., Singh, S. K., & Dzwairo, B. (2019a). Groundwater evaluation for drinking purposes using statistical index: Study of Akola and Buldhana districts of Maharashtra, India. *Environment, Development and Sustainability (A Multidisciplinary Approach to the Theory and Practice of Sustainable Development), 22*, 7453. https://doi.org/10.1007/s10668-019-00531-0.

Pande, C. B., Moharir, K. N., Singh, S. K., & Varade, A. M. (2019b). An integrated approach to delineate the groundwater potential zones in Devdari watershed area of Akola district, Maharashtra, Central India. *Environment, Development, and Sustainability, 22*, 4867. https://doi.org/10.1007/s10668-019-00409-1.

Pandey, D. S., Pan, I., Das, S., Leahy, J. J., & Kwapinski, W. (2015). Multi-gene genetic programming based predictive models for municipal solid waste gasification in a fluidized bed gasifier. *Bioresource Technology, 179*, 524–533.

Papadopoulou, M. P., Nikolos, I. K., & Karatzas, G. P. (2010). Computational benefits using artificial intelligent methodologies for the solution of an environmental design problem: Saltwater intrusion. *Water Science and Technology, 62*, 1479–1490.

Post, V. (2005). Fresh and saline groundwater interaction in coastal aquifers: Is our technology ready for the problems ahead? *Hydrogeology Journal, 13*, 120–123.

Raghavendra, N. S., & Deka, P. C. (2016). Multistep ahead groundwater level time-series forecasting using gaussian process regression and ANFIS. In *Advanced computing and systems for security* (pp. 289–302). New York: Springer.

Rajabi, M. M. (2019). Review and comparison of two meta-model-based uncertainty propagation analysis methods in groundwater applications: Polynomial chaos expansion and Gaussian process emulation. *Stochastic Environmental Research and Risk Assessment, 33*, 607–631.

Rajabi, M. M., & Ketabchi, H. (2017). Uncertainty-based simulation-optimization using Gaussian process emulation: Application to coastal groundwater management. *Journal of Hydrology, 555*, 518–534.

Roy, D. K., & Datta, B. (2017a). Genetic algorithm tuned fuzzy inference system to evolve optimal groundwater extraction strategies to control saltwater intrusion in multi-layered coastal aquifers under parameter uncertainty. *Modeling Earth Systems and Environment, 3*, 1707–1725.

Roy, D. K., & Datta, B. (2017b). Multivariate adaptive regression spline ensembles for Management of Multilayered Coastal Aquifers. *Journal of Hydrologic Engineering, 22*, 04017031.

Roy, D. K., & Datta, B. (2018). A surrogate based multi-objective management model to control saltwater intrusion in multi-layered coastal aquifer systems. *Civil Engineering and Environmental Systems, 34*, 238–263.

Smola, A. J., & Schölkopf, B. (2004). A tutorial on support vector regression. *Statistics and Computing, 14*, 199–222.

Sreekanth, J., & Datta, B. (2010). Multi-objective management of saltwater intrusion in coastal aquifers using genetic programming and modular neural network-based surrogate models. *Journal of Hydrology, 393*, 245–256.

Sreekanth, J., & Datta, B. (2011). Coupled simulation-optimization model for coastal aquifer management using genetic programming-based ensemble surrogate models and multiple-realization optimization. *Water Resources Research, 47*, 1–17.

Sreekanth, J., & Datta, B. (2012). *Genetic programming: Efficient modeling tool in hydrology and groundwater management*. London: InTech.

Srinivasan, D. (2008). Energy demand prediction using GMDH networks. *Neurocomputing, 72*, 625–629.

Tanty, R., & Desmukh, T. S. (2015). Application of artificial neural network in hydrology-a review. *International Journal of Engineering Research & Technology, 4*, 184–188.

Tsai, T.-M., & Yen, P.-H. (2017). GMDH algorithms applied to turbidity forecasting. *Applied Water Science, 7*, 1151–1160.

Vanhatalo, J., Riihimäki, J., Hartikainen, J., Jylänki, P., Tolvanen, V., & Vehtari, A. (2013). GPstuff: Bayesian modeling with Gaussian processes. *Journal of Machine Learning Research, 14*, 1175–1179.

Vapnik, V., & Chervonenkis, A. (1974). *Theory of pattern recognition*. Moscow: Nauka.

Voss, C. I., & Souza, W. R. (1987). Variable density flow and solute transport simulation of regional aquifers containing a narrow freshwater-saltwater transition zone. *Water Resources Research, 23*, 1851–1866.

Wang, W., Xu, D., Qiu, L., & Ma, J. (2009). Genetic programming for modelling long-term hydrological time series. In: *2009 Fifth international conference on natural computation, 2009* (pp 265–269). IEEE.

Westerhuis, J. A., et al. (2008). Assessment of PLSDA cross validation. *Metabolomics, 4*, 81–89.

Williams, C. K., & Rasmussen, C. E. (2006). *Gaussian processes for machine learning* (Vol. 2 and 3). Cambridge, MA: MIT Press.

Yadav, B., Mathur, S., & Yadav, B. K. (2018). Data-based modelling approach for variable density flow and solute transport simulation in a coastal aquifer. *Hydrological Sciences Journal, 63*, 210–226.

Yang, C.-C., & Shieh, M.-D. J. C. (2010). A support vector regression-based prediction model of affective responses for product form design. *Computers & Industrial Engineering, 59*, 682–689.

Yeh, C.-Y., Huang, C.-W., & Lee, S.-J. (2011). A multiple-kernel support vector regression approach for stock market price forecasting. *Expert Systems and Applications, 38*, 2177–2186.

Yoon, H., Jun, S.-C., Hyun, Y., Bae, G.-O., & Lee, K.-K. (2011). A comparative study of artificial neural networks and support vector machines for predicting groundwater levels in a coastal aquifer. *Journal of Hydrology, 396*, 128–138.

Zhang, C., Wei, H., Zhao, X., Liu, T., & Zhang, K. (2016). A Gaussian process regression-based hybrid approach for short-term wind speed prediction. *Energy Conversion and Management, 126*, 1084–1092.

Zhu, X., Zhang, Z., & Liu, L. (2010). Prediction of groundwater levels in irrigation districts based on chaos optimization of GMDH neural network. *Journal of Hohai University: Natural Sciences, 38*, 317–321.

Chapter 4
Modeling Landscape Dynamics, Erosion Risk, and Annual Sediment Yield in Guna-tana Watershed: A Contribution for Microwatershed Level Conservation Priority Area Identification

Daniel Asfaw, Getachew Workineh Gella, and Mulualem Asfaw

Contents

4.1 Introduction 74
4.2 Materials and Methods 75
4.3 Data Source and Analytical Approach 76
4.4 Results and Discussion 80
4.5 Erosion Risk and Watershed Level Annual Sediment Yield 82
4.6 Sediment Yield 85
4.7 Prioritization of Watershed for Soil and Water Conservation 85
4.8 Validation 86
4.9 Discussion 86
4.10 Conclusion 88
References 88

D. Asfaw (✉)
Department of Geography and Environmental Studies, Bahir Dar University, Bahir Dar, Ethiopia

Geospatial Data and Technology Center (GDTC), Bair Dar University, Bahir Dar, Ethiopia

G. W. Gella · M. Asfaw
Department of Geography and Environmental Studies, Debre Tabor University, Debre Tabor, Ethiopia

C. B. Pande, K. N. Moharir (eds.), *Groundwater Resources Development and Planning in the Semi-Arid Region*, https://doi.org/10.1007/978-3-030-68124-1_4

4.1 Introduction

Though soil is an essential natural resource, it is being degraded at an unprecedented scale, both in the rate and geographical extent. Soil erosion by water is a widespread environmental problem of the twenty-first century especially in developing countries (Lal 2001; Kuo et al. 2016). Globally, about 80% of the agricultural land degradation is caused by soil erosion (Rodrigo Comino et al. 2015) and annually, it also causes to loss ten million hectares of cropland (Pimentel 2006) that cost $523.1 million per year with the assumption of farmers management practice is not changed (Biggelaar et al. 2004). This is also costing additional trade-off for conservation activities and the replacement of nutrient losses.

Africa is the worst erosion affected continent in the world, where 50% of the total erosion affected segment of population resides (FAO 2002; Pande et al. 2019). In the sub-Sahara Africa too, 77% of the region is affected by soil erosion (FAO 2015; Pande 2020a, b) triggered by population pressure, cultivation of fragile ecosystems, and overgrazing (Nkonya et al. 1999). Similar to sub-Saharan trend, Ethiopia is also quoted as a severely suffering nation for this perturbation. Estimates show that about 50% of its highland areas have significant soil erosion where 25% of its area was highly eroded and 4% of its area is seriously eroded beyond reclamation (Bewket and Sterk 2002; and Aklilu 2006). Though at a national scale, 23% of terrestrial land is identified as soil and water conservation priority area (Kirui and Mirzabaev 2015), intense rainfall coupled with improper land use management, poor farming practices, and removal of the natural vegetation worsened soil erosion problem, and reduced productivity (Adimassu et al. 2014; Angassa 2014), and costs 23% of national GDP (Kirui and Mirzabaev 2015).

In the Blue Nile River basin, soil erosion is a major problem and Lake Tana basin is identified as the most soil erosion affected area (Setegn et al. 2009). The high rate of surface erosion and sediment transport in the river system increased sedimentation problem in the Lake Tana and other water reservoirs found in the sub-basin. Lake Tana and Ribb irrigation dam are highly threatened by sedimentation. Many studies (Balabathina et al. 2019; Haregeweyn et al. 2017; Tadesse et al. 2017; and Zerihun et al. 2018) have been conducted in the basin to quantify soil loss and prioritize areas for conservation. However, limited studies (Estifanos 2014; Meseret and Gangadhara 2017) have been carried in the Guna-tana watershed, which is the major water contribute to Lake Tana and Bule Nile (Abay) River. Besides the estimated soil loss, reported findings were not consistent. For example, Estifanos (2014) and Meseret and Gangadhara (2017) have reported an annual soil loss rate of 39.8 and 40 t ha^{-1} $year^{-1}$, respectively. Thus, quantifying soil loss in the watershed provides comprehensive information at the whole watershed level (both Gumara and Ribb) and helps to substantiate investment in sustainable land management. Further investment on sustainable land management and soil conservation can be used to sustain the life of reservoirs (lakes, dams) by lessening the rate of sediment yield from the watershed and enhance land productivity. Therefore, the present study was dedicated to model watershed level landscape change and annual sediment yield from Guna-tana watershed to identify conservation priority areas.

4.2 Materials and Methods

4.2.1 Description of the Study Area

Guna-tana watershed is part of Lake Tana sub-basin located between 37°30′ to 38°30′E Latitude and 11°30′ to 12°30′ N Longitude (Fig. 4.1). The watershed is found in the South Gondar Zone, Amhara National Regional State (ANRS), which extends from the tip of Mount Guna towards Lake Tana including the Fogera plain. It consists of Farta, Fogera, Este, Libokemkem, and Ebnat districts. Its elevation ranges from 4108 to 1785 m above mean sea level and covers a total of 3522.25 km^2 area. The watershed was drained by two main tributaries of Lake Tana (Ribb and Gumara) rivers. These rivers have a pivotal role in the socio-economic life of the society in the basin.

The mean annual rainfall of the watershed is 1231 mm which is mainly precipitated in the summer season (June, July, and August). Mean annual maximum and the minimum temperature reached around 25.65 and 13.25 °C, respectively. Agro-ecological, the upper catchment of the watershed experiences *Wurch* (Afro-alpine), whereas *Woina-Dega* (Subhumid) is dominant in the lower part. *Dega* (Humid) and *Woina-Dega* (Subhumid) are dominant in the mid part of the watershed. Vertisols, Nitosols, Luvisols, and Cambisols are major types of soils found in the watershed.

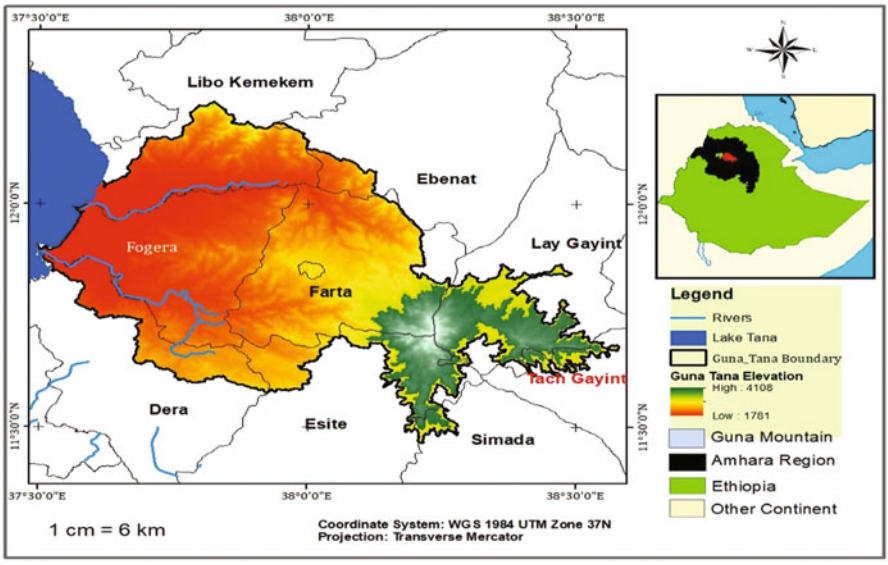

Fig. 4.1 Map of Guna-tana watershed

4.3 Data Source and Analytical Approach

To estimate water induced soil loss and to identify vulnerable parts of the Guna-tana watershed, six datasets from different sources were used (Table 4.1). Field data was collected using Global Positioning System (GPS), while ERDAS Imagine 2015 and ArcGIS 10.5.1 were used for processing the collected data (Pande et al. 2018a, b; Moharir et al. 2020). Land use land cover (LULC) change of the watershed was derived from time-series satellite image (Landsat TM, ETM+, and OLI, and Sentinel 2) of 1988, 2003, and 2019. A field survey was conducted to collect 150 sample points for training and 100 points for validation.These samples were collected using simple random sampling approach. Classification was done using the maximum likelihood algorithm (Andorson et al. 1983; Pande et al. 2017, 2018a, b). Before collection of the data and actual classification scheme, the operational definition of five dominant land use/cover classes was prepared to guide data collection and signature generation process (Table 4.2).

4.3.1 RUSLE Model Description

An attempt to develop an equation for soil loss was begun about 1940 in the Corn Belt (Wischmeier and Smith 1978). The original version of the model named Universal Soil Loss Equation (USLE) was designed to compute the average rate of soil loss from sheet and rill erosion. It was empirically derived from more than 10,000 plots and years of runoff and soil loss data contributed from 49 locations in

Table 4.1 Data types and sources

Data type	Resolution	Source
DEM	30 m	USGS (http://www.usgs.gov/)
Lansat	30 m	USGS (https://earthexplorer.usgs.gov/)
Soil type	1:50,000 scale	EMoA
Ground truth points	Points data	Field survey
Precipitation (1988–2019)	Station-based point data	NMSA

Table 4.2 Description of major land use land covers classes

LULC type	Description
Water body	Land area persistently covered by water
Forest and plantations	The land area covered by natural forest, plantation tree, shrubs with permanently green
Grazing land	The land area covered mainly by grass, small shrubs, and used for grazing purposes as communal land
Cultivated area	Land area cultivated and used for agricultural purpose and cultivation
Built-up area	Land covered with man-made features like building

the United States (Renard et al. 1997). In 1985, USLE was improved to the Revised Universal Soil Loss Equation (RUSLE) with the same formula but with improved procedure for computation of determinant factors (Renard et al. 1978). In this study, the RUSLE model which was developed by Wischmeier and Smith (1978) and modified by Hurni (1985) to the Ethiopian conditions was employed.

RUSLE model estimates soil loss by integrating rainfall erosivity (R), soil erodibility (K), slope length and steepness (LS), cover management (C), and conservation practices (P) parameters (Melesse 2011; Renard et al. 1978). The mathematical relationships of the parameters and factor generation flow chart of the model described in Eq. (4.1) and Fig. 4.2:

$$A_r = K * R * \mathrm{LS} * C * P \tag{4.1}$$

where A_r is annual average soil loss (t $ha^{-1}y^{-1}$), K is rainfall erosivity (MJ mm $h^{-1}ha^{-1}y^{-1}$), R is soil erodibility (t ha^{-1} MJ^{-1} mm^{-1}), P is land management factor, C is LULC factor, and LS is terrain parameter. Rainfall erosivity factor (R) is a climate factor that contributes to soil erosion via the detaching power of raindrop and transporting via runoff (Morgan 1995). It is computed by using Eq. (4.2):

$$R = \mathrm{EI}_{30}/100 \tag{4.2}$$

where R is erosivity power of rainfall and EI is kinetic energy (30 min rainfall intensity) of rain drops (Morgan 2005). Though EI data is not available for the study area, erosivity power of rainfall was derived from mean annual precipitation which

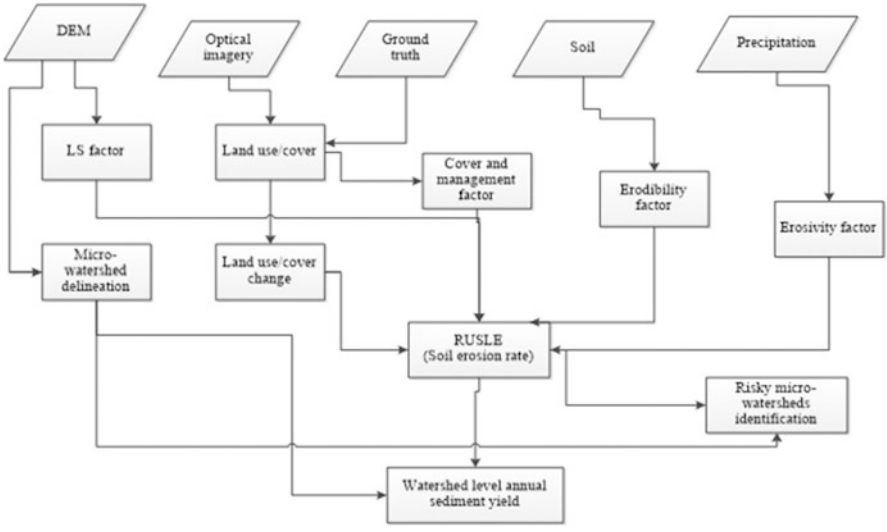

Fig. 4.2 RUSLE model analytical flow chart

Table 4.3 Summary of meteorological stations in and around Guna-tana watershed (1988–2019)

Station	Lat	Long	Altitude (m)	Mean rainfall (mm)
Debre Tabor	11.87	38.00	2612	1437.90
Gasay	11.79	38.14	2787	1442.00
Ebnat	12.12	38.05	2212	869.20
Hamusit Dera	11.79	37.56	1930	1533.20
K/Dngay	11.81	38.12	2980	1309.60
M/Eyesus	11.61	38.05	2337	1293.30
Alem ber	11.91	37.88	2043	1301.00
Woreta	11.92	37.7	1819	946.60

was adapted to Ethiopian case by Hurni (1985) and which further was implemented in many research works (Melesse 2011; Haregeweyn et al. 2017; Meseret and Gangadhara 2017). It was provided in Eq. (4.3) as

$$R = -8.12 + (0.562 * p) \tag{4.3}$$

where p is mean annual precipitation in millimeters. Thus, the mean annual rainfall of eight meteorological stations for the period of 1988–2019 was used to drive the R-factor of Guna-tana watershed (Table 4.3). A layer for the R-factor was created by using ordinary kriging interpolation method in ArcGIS environment.

Soil erodibility factor (K) is the rate of soil loss per unit of R-factor on a unit plot. It measures the soil resistance to detachment and transportation by raindrop and surface runoff (Wischmeier and Smith 1978). Soil texture, organic matter, and permeability of the soil profile are the main physical properties of a soil that affect the K-factor of the soil (Kouli et al. 2008). However, in the conditions where there is unavailability of detail data about soil properties, the K-factor was determined based on the soil color property as described in Hurni (1985). Similar to studies (Gemechu 2016; Haregeweyn et al. 2017; Meseret and Gangadhara 2017; Tadesse et al. 2017; Tamene et al. 2017; Zerihun et al. 2018), the K-factor was derived from soil color. Thus, in the present study, a systematic field observation on the soil color was carried and integrated with FAO soil property description to determine the K-factor of the study watershed (Table 4.4).

The topographic effect on soil erosion is represented by the slope length and slope steepness (LS-factors). In RUSLE model, the LS factor is relative to the site conditions with the "standard" slope steepness of 9% and slope length of 22 m plot (Wischmeier and Smith 1978; Renard et al. 1997). An increase in the slope length and slope steepness produces higher overland flow velocities and correspondingly higher erosion (Kouli et al. 2008). In the present study, LS factor was derived from DEM (SRTM) with 30 m spatial resolution. The equation developed by Moore and Burch (1986) was used to calculate the LS factor (Eq. 4.4) as:

Table 4.4 Soil erodibility factor and associated *K*-value

Soil color	Black	Brown	Red
K-factor (t ha^{-1} MJ^{-1} mm^{-1})	0.15	0.2	0.25
Soil type	Vertisols	Lithosols, Cambisols, Luvisols	Nitosols

Table 4.5 Land use land cover and *C*-factor value of Guna-tana watershed

Land cover	Area (ha)	*C*-value	% (Area)
Cultivated land	329,248	0.15	93.47
Forest	14,003	0.001	3.97
Grazing land	6364.04	0.08	1.80
Built-up areas	1305.88	0.09	0.37
Water body	1304.03	0	0.37

$$\mathrm{LS} = \left(\frac{A}{22.13}\right)^{0.4}\left(\frac{\sin\theta}{0.0896}\right)^{1.3} \tag{4.4}$$

where LS *is the slope length and steepens, A* is the product of flow accumulation and cell size (30 m by 30 m), and θ is the slope in degrees.

Vegetation cover and management factor (*C*-factor) is the ratio of soil loss from vegetated plots versus bare soil plots with values between 0 and 1 (Wischmeier and Smith 1978; Robert and Hilborn 2000).

C-factor represents the effect of cropping and management practices in agricultural management, and the effect of ground, tree, and grass covers on reducing soil loss in noncultivated area (Kouli et al. 2008). It was derived from the land use and land cover map of the watershed (Table 4.5).

The support practice factor (*P*-factor) is the ratio of soil loss with a support practice (contouring, stripcropping, or terracing) in tilling up and down the slope (Wischmeier and Smith 1978). It reflects the impact of specific erosion management practices on erosion rate with a value that ranges between 0 and 1 where the highest values correspond to a bare land without any support practices (Blanco and Lal 2008). As there is no well-organized data and consistent soil and water conservation (SWC) practice in the study area, *P*-value was determined by integrating LULC and slope category (Wischmeier and Smith 1978). Thus, the LULC grouped as cultivated land and others. Cultivated land was categorized into six slope classes. Each slope class was assigned a *P*-value which is adopted in most studies (Haregeweyn et al. 2017; Meseret and Gangadhara 2017; Molla and Sisheber 2017; Zerihun et al. 2018) (Table 4.6).

Finally, watershed level annual sediment yield and sediment delivery ratio were quantified. Sediment yield is the sediment load at the end of the slope length or the channel outlet of the watershed. It is the sediment load normalized for the drainage area (the net result of erosion and deposition processes) within the watershed (Kouli and Soupios 2008; Vemu and Pinnamaneni 2012; Pande 2020c, d).

Table 4.6 *P*-value of Guna-tana watershed based on the LULC and slope category

LULC	Slope	*P*-value
Cultivated land	0–2	0.12
	2–5	0.12
	5–8	0.4
	8–15	0.19
	15–30	0.25
	>30	0.33
Others	–	1

The amount of sediment yield from the watershed was estimated from sediment delivery ratio (SDR) of the watershed. Even though there are different models used to estimate SDR at the outlet of the watershed, a model suggested by Williams and Berndt (1972) was used in this study (Eq. 4.6) as

$$S_y = (A) * (\text{SDR}) \tag{4.5}$$

where S_y is annual sediment yield tones per year, A is total gross erosion computed from RUSLE, and SDR is sediment delivery ratio, which is the ratio between sediment delivered to the stream and gross sediment produced at the catchment. It was calculated as:

$$\text{SDR} = 0.627 * \text{SLP}^{0.403} \tag{4.6}$$

where SLP is percentage mean slope of main channel stream.

4.4 Results and Discussion

4.4.1 Trends of Land Use Land Cover Change

Land use and land cover change is a proxy for dynamics of the earth surface caused by diverse drivers and factors (Pande and Moharir 2014; Hailemariam et al. 2016; Mahender Reddy et al. 2017). Thereby indicates level of human interventions and contribution for soil erosion. Guna-tana watershed was classified into five major classes, such as cultivated land, forest and plantations, grazing land, and built-up area with high classification accuracy (overall classification accuracy 85% and kappa coefficient 82%) for each period (1988, 2003, and 2019). Land use land cover classification maps for the years 1988 and 2015 are given in Fig. 4.3. The spatial distribution of land use land cover classes of the watershed in the year 1988, 2003, and 2019 shows that cultivated land and built-up area have increased, while the extent of forest and plantation, and grazing land declined continuously from 1988 till 2019. By the year 1988, forest and plantation, and grazing land have covered

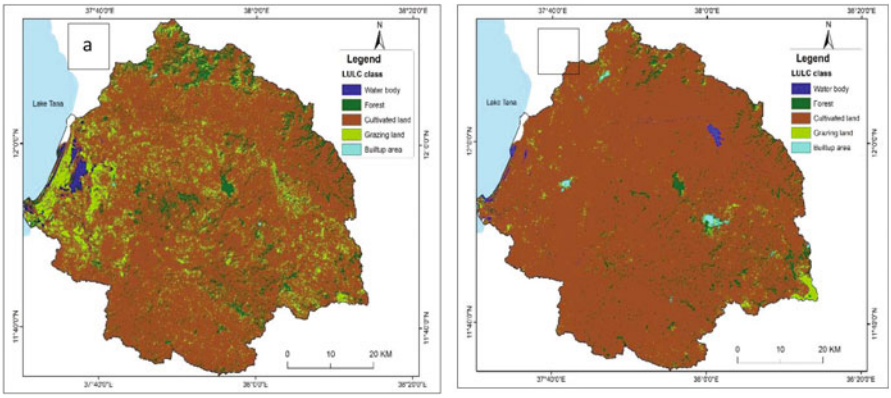

Fig. 4.3 LULC map of Guna-tana watershed (**a**) 1988, and (**b**) 2019

Table 4.7 LULC change and rate of change (1988, 2003, and 2019)

	1988		2003		2019		Annual rate of change (1988–2019)
LULC type	Area (km^2)	%	Area (km^2)	%	Area (km^2)	%	$km^2 year^{-1}$
Water body	27.19	0.77	25.65	0.72	13.04	0.37	−1.67
Forest	272.54	7.74	232.89	6.61	130.03	3.97	−1.5
Cultivated land	2886.32	81.95	3029.83	86.01	3282.48	93.47	0.45
Grazing land	324.9	9.51	202.90	6.31	43.64	1.81	−2.59
Built-up area	11.32	0.04	31.04	0.32	53.06	0.37	2.8
Total	3522.25	100	3522.25	100	3522.25	100	

272.54 km^2 (7.74%), 324.9 km^2 (951%), respectively, and their coverage was declined to 130 and 4.64 km^2 in the year 2019 by −1.5 and −2.59 km^2 $year^{-1}$ rate of change, respectively. On the other hand, coverage of cultivated land and built-up area have increased by the rate of 0.45 and 2.8 $km^2 year^{-1}$, respectively and by 2019 more than 90% of the watershed was covered by cultivated land and built-up areas (Table 4.7 and Fig. 4.3).

According to Yang et al. (2017), cultivated and built-up area have high probability to expand to grazing land and forest area. Accordingly, in the watershed cultivated land and built-up area have highly expanded to other land use classes which imply degradation of natural environment and soil erosion.

4.5 Erosion Risk and Watershed Level Annual Sediment Yield

4.5.1 Erosion Risk Mapping

The spatial distribution of erosion risk of Guna-tana watershed was modeled using RUSLE erosion model. The model integrates five important bio-physical (*R, K,* LS*, C, and P*) factors. The *R*-factor was computed from the mean annual rainfall data of the entire watershed using Eq. (4.3). The mean annual rainfall ranges from 869.2 to 1437.9 mm and subsequently, the estimated rainfall erosivity ranges from 510 to 782.37 MJ mm ha^{-1} h^{-1}year^{-1} with average value of 646.5 MJ mm ha^{-1} year^{-1}. Spatially, erosive power of *R*-factor is higher in the southeastern and southern (Gumara subwatershed) and decreased to the northernpart of the watershed (Fig. 4.4a, b). The soil erodibility (*K*) factor, which was derived from major soil types of the watershed, ranges from 0.15 to 0.25 t ha^{-1} MJ^{-1} mm^{-1}(Table 4.6). In the watershed, nearly 62% of the areas have high (>0.2 t ha^{-1} MJ^{-1} mm^{-1}) soil erodibility value and were less resistance to detachment and transportation from raindrop and surface runoff, respectively (Fig. 4.4c). The lower *K*-value coincided with the lower slope areas, whereas highest erodibility of the soil occurred at high elevation with steep slope areas of the watershed (Fig. 4.4d).

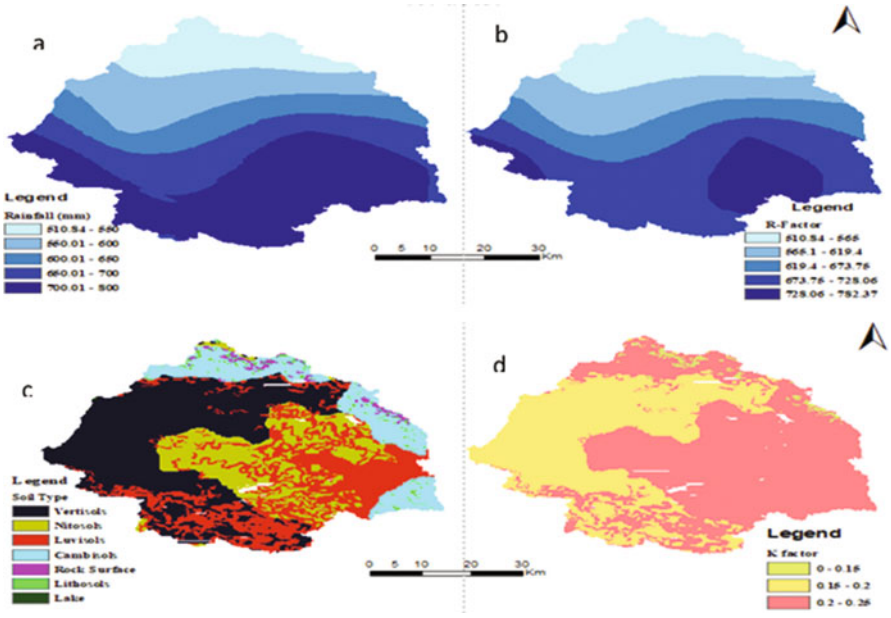

Fig. 4.4 Maps of (**a**) rainfall distribution, (**b**) *R*-factor, (**c**) major soil, and (**d**) *K*-factor

4.5.2 Slope Length and Steepness Factor (LS)

In RUSLE, topographic factor (LS-factor) represents the influence of slope length and slope steepness on erosion process. Flow accumulation and the slope condition of the watershed were considered for computing the LS factor (Jain et al. 2001). From the analysis, it was observed that the topographic factor increases from 0 up to 68 as flow accumulation and slope increase. According to Haan et al. (1994), when the slope length and steepness increases, the velocity of overland flow becomes higher which subsequently results in higher rate of erosion. Thus, higher LS value implies higher erosion probability.

4.5.3 Cover and Management (C) Factor and Support (P) Factor

In present study, the *C* and *P* factors derived from the land use land cover type. Thus, the *C* factor ranges from 0 to 0.15, where 0 (lower value) for waterbody and 0.15 (higher value) for cultivated land were assigned (Fig. 4.5). The value of *P* factor ranges from 0.12 to 1.0. The lower the *P* value coincides in the cultivated area with lower slope and deemed to be at lower soil erosion problem.

4.5.4 Soil Loss

The estimated quantity of soil loss in Guna-tana watershed was identified and mapped into five soil erosion risk levels, viz, low, moderate, high, very high, and severe with the consideration of the country's tolerable soil loss rate

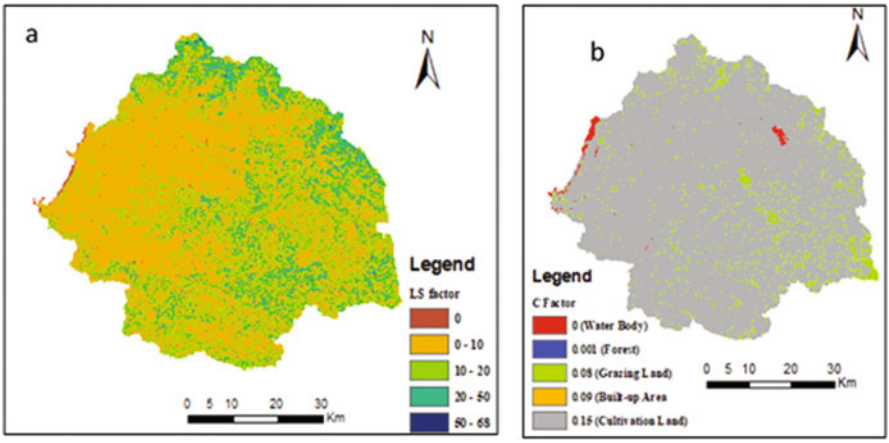

Fig. 4.5 Map of (**a**) LS factor, and (**b**) *C*-factor of RUSLE model

(5–12 t $ha^{-1}y^{-1}$) and rate of soil formation (Hurni 1988). In the study watershed, nearly 39% (1351.7 km^2), 24.95% (879.22 km^2), and 25.1% (884.41km^2) fall under severe, very high, and high soil erosion classes, respectively (Table 4.8).

Guna-tana watershed annually losses with an average soil loss rate of 50.29 t $ha^{-1}y^{-1}$. High to severe soil erosion class contributed much because the area is intensively cultivated and experiences relatively high rainfall, and steep slope (Fig. 4.6 and Table 4.8). In the same vein, south western, northwestern, and some part of north and northeastern part of the watershed fall under high and very high soil erosion class.

Table 4.8 Soil loss and soil erosion class of Guna-tana watershed

Soil loss (t ha^{-1} $year^{-1}$)	Mean soil loss (t ha^{-1} $year^{-1}$)	Soil erosion class	Area (km^2)	Area (%)	Total soil loss (t ha^{-1} $year^{-1}$)
0–5	50.29	Low	113.87	3.24	65,033
5–10		Moderate	293.12	8.30	325,689
10–20		High	884.41	25.1	982,669
20–40		Very high	879.22	24.95	976,902
40–180		Severe	1351.69	38.40	1,501,872

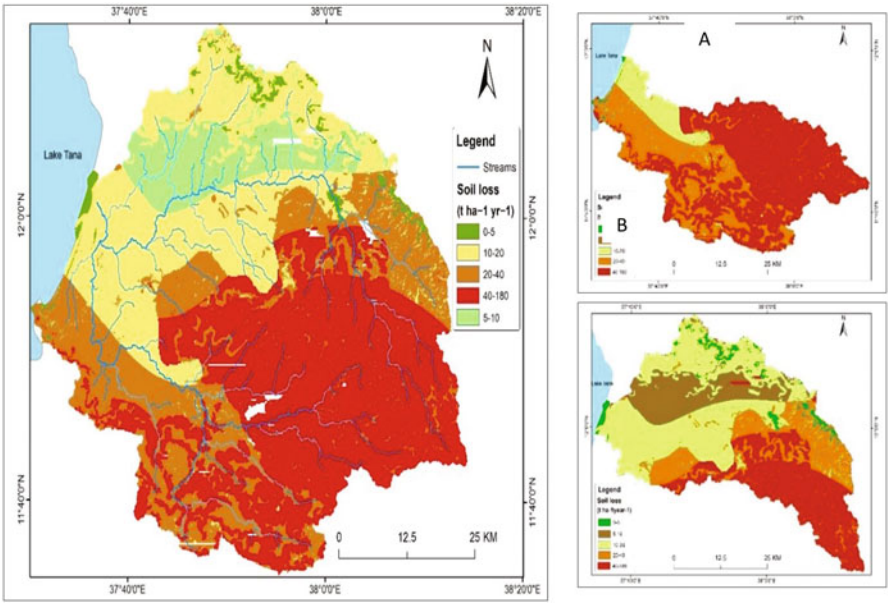

Fig. 4.6 RUSLE model estimated soil loss (**a**) Gumara, and (**b**) Ribb subwatersheds

4.6 Sediment Yield

The amount of sediment load at the outlet of Guna-tana watershed was estimated from sediment delivery ratio (SDR) of the watershed. SDR is a measure of sediment transport efficiency which accounts for the amount of sediment actually transported from the eroding sources to a catchment outlet compared to the total amount of soil detached over the same area (Habtamu 2016). It is well suited to estimate current sediment yield and predicting the effect of land treatment and land use changes on the future sediment yield (USAD-SCS 1972; Pande and Moharir 2014).

The simulated SDR of Guna-tana watershed varies from 0.0 to 1.0 with an overall watershed level average of 0.5. Accordingly, the amount of sediment yield in the watershed varies from 0 to 108 t ha^{-1} year^{-1} with an average of 33 t ha^{-1} year^{-1} which has a similar spatial pattern with the gross soil loss. The estimated sediment yield from the watershed categorized from low (0–5 t ha^{-1} year^{-1}) to very high sediment delivery class (>20 t ha^{-1} year^{-1}). The lower sediment yield capacity class (0–5 t ha^{-1} year^{-1}) contributes about 92% (2.5 t ha^{-1} year^{-1}) total annual S_y and nearly 7% (64 t ha^{-1} year^{-1}) total annual sediment delivered from high to very high soil erosion class (Table 4.9).

4.7 Prioritization of Watershed for Soil and Water Conservation

The severity of erosion risk differs across the watershed with the spatial distribution of variables (slope, soil type, vegetation covers, and rainfall) and practices of soil conservation measures (Pande and Moharir 2015; Gashaw et al. 2017; Patode et al. 2017; Pande et al. 2018a, b). Thus, identifying soil erosion risk areas and prioritizing areas according to erosion severity level is imperative.

Therefore, in the watershed areas were identified and prioritized on the basis of average soil loss rate estimated using the RUSLE model and sediment yield. Guna-tana watershed has two major subwatersheds named as: Gumara and Ribb subwatershed (Fig. 4.6). In Gumara sub watershed, nearly 53% of the area losses >40 t ha^{-1} year^{-1} soil which was above the tolerance level of soil loss and categorized as severely affected area, whereas in Ribb subwatershed 23.99% of

Table 4.9 Sediment delivery capacity class and total annual sediment yield

Range of S_y (t ha^{-1} year^{-1})	Mean S_y	Sediment yield capacity class	Area (ha)	% of total area	Total annual S_y (t ha^{-1} year^{-1})	% of total annual S_y
0–5	2.5	Low	3488.94	99.26	8722.35	92.03
5.01–10.	7.5	Moderate	3.87	0.11	29.025	0.306
10.01–20	15	High	13.86	0.39	207.9	2.19
>20	64	Very high	8.1	0.23	518.4	5.47

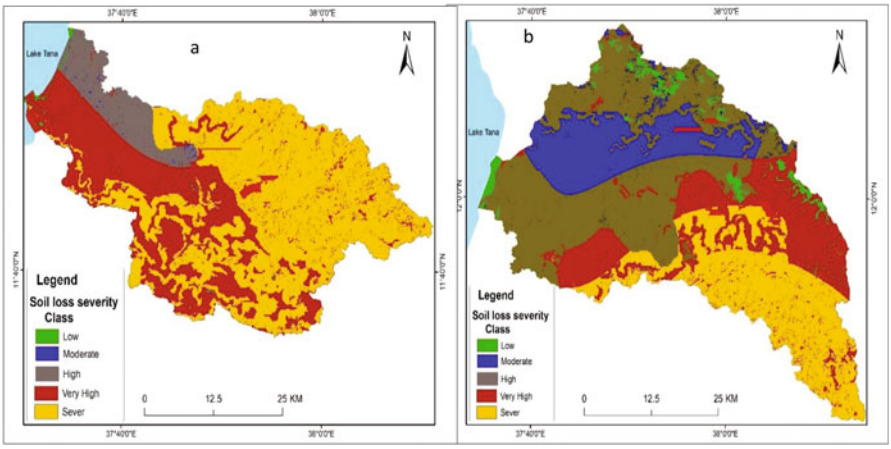

Fig. 4.7 Prioritized subwatersheds of Guna-tana watershed (**a**) Gumara, (**b**) Ribb subwatershed

the area losses >40 t ha^{-1} $year^{-1}$. On the other hand, about 10% of Gumara subwatershed losses the range of the national tolerable soil loss rate but in Ribb subwatershed, more than 55% of the area losses to the level of tolerable soil loss rate. Thus, Gumara subwatershed (more specifically Farta, Fogera, and Este *woredas)* losses much soil and requires immediate intervention. Northeastern and southeastern (Ebinat and Farta districts) parts of Ribb subwatershed were also fall under severe and very high soil loss classes which demand interventions (Fig. 4.7).

4.8 Validation

Validating RUSLE is very essential to confirm the validity of the result and compatibility of the model. However, absence of measured soil loss and sediment yield data in the study area inhibited validating the estimated soil loss with in-situ based values. Thus, field observations and previous studies conducted in the Upper Blue Nile basin were used to validate the estimated result and effectiveness of the model. Therefore, the estimated soil loss rate and the spatial distribution of erosion classes in the study watershed were consistent when compared with the results of field observation and previous studies (Setegn et al. 2009; Haregeweyn et al. 2017; Meseret and Gangadhara 2017; Gashaw et al. 2018; and Balabathina et al. 2019).

4.9 Discussion

In the present study, Guna-tana watershed has experienced a significant LULC change, where forest and grazing land use types were changed to cultivated and built-up with the rate of −2.59 and − 1.67 $km^2 year^{-1}$, respectively between 1988

and 2019. As Setegn et al. (2009) stated, a change in LULC increases the detachability and transport of soil particles, and subsequently mount surface runoff, and soil erosion. Accordingly, the watershed experienced 50.29 t ha^{-1} $year^{-1}$ mean gross soil loss rate which exceeds the soil loss tolerance rate (5–12 t ha^{-1} $year^{-1}$) estimated for Ethiopia by Hurni (1985). The amount of sediment yield was also higher (33 t ha^{-1} $year^{-1}$) in the watershed. The problem of soil erosion is more severe in Gumara subwatershed where more than 70% of its part was suffered from very high to severe soil loss which was higher than the Ribb subwatershed (nearly 40%). In 2014, average soil loss estimated for Ribb subwatershed was 39.8 t ha^{-1} $year^{-1}$ (Estifanos 2014), which was increased to 40 t ha^{-1} $year^{-1}$ in 2016 (Meseret and Gangadhara 2017) and in the present study, the estimated soil loss rate for Ribb subwatershed was 43.07 t ha^{-1} $year^{-1}$. Currently, about 95% of the subwatershed suffered from moderate to severe soil loss rate, however, it was 70% in 2016 (Meseret and Gangadhara 2017). In this subwatershed, the rate of soil loss and the area suffered from soil loss showed an increment. This could be due to prevailing changes in land use and intensive cultivation without proper conservation practices especially at hill slopes. Similarly, in the Lake Tana basin, Balabathina et al. (2019) have reported 41.54 t ha^{-1} $year^{-1}$ soil loss from Megech river basin, while Gelagay and Minale (2016) have also estimated 47.4 t ha^{-1} $year^{-1}$ loss of soil from Koga watershed in 2016, which is lower than the estimated soil loss rate (50.29 t ha^{-1} $year^{-1}$) for Guna-tana watershed. In the Blue Nile basin, Gashaw et al. (2018) estimated 23.7 t ha^{-1} $year^{-1}$ average soil loss rate and Haregeweyn et al. (2017) also estimated 27.5 t ha^{-1} $year^{-1}$ average soil loss rate with a gross loss of 473 Mt. $year^{-1}$. Zerihun et al. (2018) have also reported 49 t ha^{-1} $year^{-1}$ loss of soil from Dembecha district. The estimated soil loss rate in Guna-tana watershed was also within the range of results presented from site-specific tests (between 0.04 and 212 t ha^{-1} $year^{-1}$) conducted in 1987 and 1988 in Amhara region (Desta et al. 2000) and estimated soil loss for the general Ethiopian highlands (0–300 t ha^{-1} $year^{-1}$) (Hurni 1985). Similarly, Setegn et al. (2009) have confirmed that the two main streams of the study watershed (Ribb and Gumara rivers) contribute large amount of sediment yield production to the Lake Tana. This could be attributed to steeper and longer slope land configuration, and continuous plow of the same land without fallowing and proper conservation. Besides, change in land use from natural cover to cultivation and built-up plays a significant role for intensifying the rate of soil erosion and land degradation. Most studies (Mutua et al. 2006; Melesse 2011; Meseret and Gangadhara 2017; Molla and Sisheber 2017; Balabathina et al. 2019) confirmed that land use and land cover change and improper soil and water management practices worsen problem of soil erosion.

4.10 Conclusion

Existing change in LULC and the subsequent high rate of soil loss and sediment yield from Guna-tana watershed calls for intensive sustainable soil and water conservation practices. Unless the existing erosion rate and sediment load are not curved back, Lake Tana and recently constructed Ribb irrigation dam would be at risk of sedimentation, nutrient pollution, and loss of water quality. Though large amount soil is currently leaving from the watershed, prioritizing areas according to the level of soil erosion severity will ease to address the problem properly. Thus, Gumara subwatershed particularly the upper part of the watershed where Farta, Fogera, and Este districts required intensive soil and water conservation practices and steeper part of Ribb subwatershed is also under consideration. This is very important to save Lake Tana, Ribb irrigation dam, and Grand Ethiopian Renaissance Dam from siltation. More importantly, appropriate conservation practiced should be placed to enhance soil productivity and respective food security of local smallholder farmers.

Acknowledgments The Authors greatly acknowledge Debre Tabor University for financial support, and ANRS BoFED and MOA for providing soil data; Ethiopian Metrological Agency for providing metrological data and South Gonder Zone Agricultural office for their cooperation in collecting field data. We would also like to express our deepest gratitude to anonymous editors and reviewers for their invitation and valuable comments for the betterment of the paper.

References

Adimassu, Z., Mekonnen, K., Yirga, C., & Kessler, A. (2014). Effect of soil bunds on runoff, soil and nutrient losses, and crop yield in the central highlands of Ethiopia. *Land Degradation and Development, 25*, 554–564. https://doi.org/10.1002/ldr.2182.

Aklilu, A. (2006). *Best practices in soil and water conservation in Beressa watershed, highland of Ethiopia*. Tropical Resource Management paper. Number 36. Netherlands: Wageningen University.

Andorson, J. R., Hardy, E. E., Roach, J. T., & Witmeer, R. E. (1983). *A land use and land cover classification system for use with remote sensor data*. Washington, DC: USGS.

Angassa, A. (2014). Effects of grazing intensity and bush encroachment on herbaceous species and rangeland condition in southern Ethiopia. *Land Degradation and Development, 25*, 438–451. https://doi.org/10.1002/ldr.2160.

Balabathina, V., Raju, R. P., & Mulualem, W. (2019). Integrated remote sensing and GIS-based universal soil loss equation for soil erosion estimation in the Megech River Catchment, Tana Lake Sub-basin, Northwestern. *American Journal of Geographic Information System 2019, 8* (4), 141–157. https://doi.org/10.5923/j.ajgis.20190804.01.

Bewket, W., & Sterk, G. (2002). Farmers' perception in the soil and water conservation activities in Chemoga watershed, Blue Nile Basin. *Journal of Ethiopia Land Degradation Development, 13*, 189–200.

Biggelaar, Lal, R., Wiebe, K. & Breneman, B. (2004). Theglobal impact of soil erosion on productivity. I: absolute andrelative erosion-induced yield losses. *Advances in Agronomy, 81*, 1–48.

Blanco, H., & Lal, R. (2008). *Principles of soil conservation and management*. Columbus, OH: The Ohio State University.

Desta, H., Kassie, M., Benin, S., & Pender, J. (2000). Land degradation in the high lands of the Amhara region and strategies for sustainable land management. In: *ILRI*, Nairobi, Kenya, vol II, 114P. ISBAN 92-9146-090-7.

Estifanos, A. (2014). *Assessment of micro-watershed vulnerability for soil erosion in Ribb watershed using GIS and remote sensing*. MSc Thesis, Mekelle University, Ethiopia.

FAO. (2002). *Reducing poverty and hunger: The critical role of financing for food, agriculture, and rural development*. Paper presented at International Conference on Financing for Development, Monterrey, Mexico, 18–22 March 2002.

FAO. (2015). *Status of the World's soil resources: Regional assessment of soil changes in Africa South of the Sahara*. Rome, Italy: FAO and ITPS.

Gashaw, T., Tulu, T., & Argaw, M. (2017). Erosion risk assessment for prioritization of conservation measures in Geleda watershed, Blue Nile basin, Ethiopia. *Environmental Systems Research, 6*(1), 1–14. https://doi.org/10.1186/s40068-016-0078-x.

Gashaw, T., Tulu, T., & Argaw, M. (2018). Erosion risk assessment for prioritization of conservation measures in Geleda watershed, Blue Nile basin, Ethiopia. *Environmental Systems Research, 6*(1), 1–14. https://doi.org/10.1186/s40068-016-0078-x.

Gelagay, H. S., & Minale, A. S. (2016). Soil loss estimation using GIS and remote sensing techniques: A case of Koga watershed, northwestern Ethiopia. *International Soil and Water Conservation Research, 4*(2), 126–136.

Gemechu, A. (2016). Estimation of soil loss using revised universal soil loss equation and determinants of soil loss in Tiro Afeta and Dedo Districts of Jimma Zone, Oromiya National Regional State, Ethiopia. *Trends in Agricultural Economics, 9*(1), 1–12. https://doi.org/10.3923/tae.2016.1.12.

Haan, C. T., Barfield, B. J., & Hayes, J. C. (1994). *Design hydrology and sedimentology for small catchments*. San Diego, CA: Academic Press.

Habtamu, S. G. (2016). RUSLE and SDR Model Based Sediment Yield Assessment in a GIS andRemote Sensing Environment; A Case Study of Koga Watershed, UpperBlue Nile Basin, Ethiopia. *Hydrology Current Research, 7*(2). https://doi.org/10.4172/2157-7587.1000239.

Hailemariam, S. N., Soromessa, T., & Teketay, D. (2016). Land use and land cover change in the Bale. *Land, 5*(41), 1–22. https://doi.org/10.3390/land5040041.

Haregeweyn, N., Tsunekawa, A., Poesen, J., Tsubo, M., Tsegaye, D., Almaw, A., & Adgo, E. (2017). Comprehensive assessment of soil erosion risk for better land use planning in river basins: Case study of the Upper Blue Nile River. *Science of the Total Environment, 574*, 95–108. https://doi.org/10.1016/j.scitotenv.2016.09.019.

Hurni, H. (1985). Erosion productivity conservation system in Ethiopia. IV. *International Conference on Soil Conservation*, Mercacy, Venezuela

Hurni, H. (1988). Degradation and conservation of the resources in the Ethiopian Highlands Hans Hurni. *Mountain Research and Development, 8*(2), 123–130.

Jain, S. K., Kumar, S., & Varghese, J. (2001). Estimation of soil erosion for a Himalayan watershed using GIS technique. *Water Resources Management, 15*, 41–54.

Kirui, K. O., & Mirzabaev, A. (2015). Costs of land degradation in Eastern Africa. In *International Conference of Agricultural Economists*, Milan, Italy, August 8–12.

Kouli, M., Soupios, P., & Vallianatos, F. (2008). Soil erosion prediction using the Revised Universal Soil Loss Equation (RUSLE) in a GIS framework, Chania, Northwestern Crete, Greece. *Environmental Geology, 5*(2), 23–34. https://doi.org/10.1007/s00254-008-1318-9.

Kuo, K. T., Sekiyama, A., & Mihara, M. (2016). Determining C factor of universal soil loss equation (USLE) based on remote sensing. *International Journal of Environmental and Rural Development, 7*(2), 154–161. https://doi.org/10.32115/ijerd.7.2_154.

Lal, R. (2001). Soil degradation by erosion. *Land degradation and Development, 12*(6). https://doi.org/10.1002/ldr.472.

Mahender Reddy, D., Patode, R. S., Nagdeve, M. B., Satpute, G. U., & Pande, C. B. (2017). Land use mapping of The Warkhed Micro-watershed with geo-spatial technology. *Contemporary Research in India, 7*(3). ISSN 2231-2137.

Melesse, A. M. (Ed.). (2011). *Nile river basin: hydrology, cliamet and water use*. New York: Springer.

Meseret, D., & Gangadhara, M. H. (2017). Integration of geospatial technologies with RUSLE for analysis of land use/cover change impact on soil erosion: Case study in Rib watershed, north-western highland Ethiopia. *Environmental Earth Sciences, 76*, 765. https://doi.org/10.1007/s12665-017-7109-4.

Moharir, K. N., Pande, C. B., Singh, S. K., & Del Rio, R. A. (2020). Evaluation of analytical methods to study aquifer properties with pumping test in Deccan Basalt region of the Morna River Basin in Akola District of Maharashtra in India. In *Groundwater hydrology*. London, UK: Intec Open Publication. https://doi.org/10.5772/intechopen.84632. (Web of Science Indexed).

Molla, T., & Sisheber, B. (2017). Estimating soil erosion risk and evaluating erosion control measures for soil conservation planning at Koga watershed in the highlands of Ethiopia. *Solid Earth, 8*(1), 13–25. https://doi.org/10.5194/se-8-13-2017.

Moore, I., & Burch, G. (1986). Physical basis of the length-slope factor in the Universal Sol Loss Equation. *Soil Society of America Journal, 50*, 194–1298.

Morgan, R. P. C. (1995). *Soil erosion and conservation* (2nd ed.). Essex: Longman.

Morgan, R. P. C. (2005). *Soil erosion and conservation* (3rd ed.). New York: Blackwell Publishing.

Mutua, B. M., Klik, A., & Loiskandl, W. (2006). Modelling soil erosion and sediment yield at a catchment scale: The case of Masinga catchment, Kenya. *Land Degradation and Development, 17*(5), 557–570. https://doi.org/10.1002/ldr.753.

Nkonya, E., Barkley, A., Hamilton, S. & Burnardo, D. (1999). *Environmental and economic impacts of soil erosion and fertility mining in Northern Tanzania*. Paper presented at American Agricultural Economics Association Annual Meeting, Nashvilee, TN, August 9–11.

Pande, C. B. (2020a). Introduction. In *Sustainable watershed development. Springer briefs in water science and technology*. Cham: Springer. https://doi.org/10.1007/978-3-030-47244-3_1.

Pande, C. B. (2020b). Watershed management and development. In *Sustainable watershed development. Springer briefs in water science and technology*. Cham: Springer. https://doi.org/10.1007/978-3-030-47244-3_2.

Pande, C. B. (2020c). Thematic mapping for watershed development. In *Sustainable watershed development. Springer briefs in water science and technology*. Cham: Springer. https://doi.org/10.1007/978-3-030-47244-3_3.

Pande, C. B. (2020d). Sustainable watershed development planning. In *Sustainable watershed development. Springer briefs in water science and technology*. Cham: Springer. https://doi.org/10.1007/978-3-030-47244-3_4.

Pande, C., & Moharir, K. (2014). Analysis of land use/land cover changes using remote sensing data and GIS Techniques of Patur Taluka, Maharashtra, India. *International Journal of Pure and Applied Research in Engineering and Technology, 2*(12), 85–92.

Pande, C. B., & Moharir, K. (2015). GIS-based quantitative morphometric analysis and its consequences: a case study from Shanur River Basin, Maharashtra India. *Applied Water Science, 7*(2). Published online 23 June 2015.

Pande, C. B., Khadri, S. F. R., Moharir, K. N., & Patode, R. S. (2017). Assessment of groundwater potential zonation of Mahesh River basin Akola and Buldhana districts, Maharashtra, India using remote sensing and GIS techniques. *Sustainable Water Resources Management*. https://doi.org/10.1007/s40899-017-0193-5. ISSN 2363-5037. Published online 8 September-2017.

Pande, C. B., Moharir, K. N., & Pande, R. (2018a). Assessment of Morphometric and Hypsometric study for watershed development using spatial technology - A case study of Wardha river basin in the Maharashtra, India. *International Journal of River Basin Management*. https://doi.org/10.1080/15715124.2018.1505737.

Pande, C. B., Moharir, K. N., Khadri, S. F. R., & Patil, S. (2018b). Study of land use classification in the arid region using multispectral satellite images. *Applied Water Science, 8*(5), 1–11. ISSN 2190-5487.

Pande, C. B., Moharir, K. N., Singh, S. K., & Varade, A. M. (2019). An integrated approach to delineate the groundwater potential zones in Devdari watershed area of Akola district, Maharashtra, Central India. *Environment, Development, and Sustainability*. https://doi.org/10.1007/s10668-019-00409-1.

Patode, R. S., Pande, C. B., Nagdeve, M. B., Moharir, K. N., & Wankhade, R. M. (2017). Planning of conservation measures for watershed management and development by using geospatial technology – A case study of Patur Watershed in Akola District of Maharashtra. *Current World Environment, 12*(3), 706–714.

Pimentel, D. (2006). Soil erosion: A food and environmental threat. *Environment, Development and Sustainability, 8*, 119–137.

Renard, K., Yoder, D. C., Lightle, D. T., & Dabney, S. M. (1978). Universal soil loss equation and revised universal soil loss equation. In *Predicting soil erosion by water: Guide to conservation planning with RUSEL model.pdf* (pp. 137–167). Washington, DC: USAID.

Renard, K. G., Foster, G. R., Weesies, McCool, D. K., & Yoder, D. C. (1997). *Predicting soil erosion by water: Guide to conservation planning with RUSEL model*. Washington, DC: USAID.

Robert, P. S., & Hilborn, D. (2000). *Factsheet: Universal soil loss equation (USLE), index no-572/751*. Toronto, Canada: Queen's Printer for Ontario.

Rodrigo Comino, J., Brings, C., Lassu, T., Iserloh, T., Senciales, J. M., Martínez Murillo, J. F., Ruiz Sinoga, J. D., Seeger, M., & Ries, J. B. (2015). Rainfall and human activity impacts on soil losses and rill erosion in vineyards (Ruwer Valley, Germany). *Solid Earth, 6*, 823–837. https://doi.org/10.5194/se-6-823.

Setegn, S. G., Srinivasan, R., Dargahi, B., & Melesse, A. M. (2009). Spatial delineation of soil erosion vulnerability in the Lake Tana Basin, Ethiopia. *Hydrological Processes, 3750*, 3738–3750. https://doi.org/10.1002/hyp.

Tadesse, L., Suryabhagavan, K. V., Sridhar, G., & Legesse, G. (2017). Land use and land cover changes and Soil erosion in Yezat Watershed, North Western Ethiopia. *International Soil and Water Conservation Research, 5*(2), 85–94. https://doi.org/10.1016/j.iswcr.2017.05.004.

Tamene, L., Adimassu, Z., Aynekulu, E., & Yaekob, T. (2017). Estimating landscape susceptibility to soil erosion using a GIS-based approach in Northern Ethiopia. *International Soil and Water Conservation Research, 5*(3), 221–230. https://doi.org/10.1016/j.iswcr.2017.05.002.

USAD-SCS. (1972). Sediment sources, yields, and delivery ratios. In *National engineering handbook, section 3, sedimentation* (pp. 5–6). Washington, DC: United States Department of Agriculture.

Vemu, S., & Pinnamaneni, U. B. (2012). Sediment yield estimation and prioritization of watershed using remote sensing and GIS. *International Archives of the Photogrammetry, XXXIX*, 529–533.

Williams, J. R., & Berndt, H. D. (1972). Sediment yield computed with universal equation. *Journal of the Hydraulics Division, 98*(12), 2087–2098.

Wischmeier, W. H., & Smith, D. (1978). *Predicting Rainfall Erosion Losses: A guide to conservation planning*. Washington, DC: USAID.

Yang, H., Li, S., Chen, J., Zhang, X., & Xu, S. (2017). The standardization and harmonization of land cover classification systems towards harmonized datasets: A review. *International Journal of Geo-Information, 6*(154), 1–16. https://doi.org/10.3390/ijgi6050154.

Zerihun, M., Mohammedyasin, M. S., Sewnet, D., Adem, A. A., & Lakew, M. (2018). Assessment of soil erosion using RUSLE, GIS and remote sensing in NW Ethiopia. *Geoderma Regional*. https://doi.org/10.1016/j.geodrs.2018.01.002.

Chapter 5
Evaluation of Multiwell Pumping Aquifer Tests in Unconfined Aquifer System by Neuman (1975) Method with Numerical Modeling

Nitin Rane and Geetha K. Jayaraj

Contents

5.1 Introduction 93
5.2 Materials and Methods 96
5.3 Results 99
5.4 Discussion 101
5.5 Conclusions 104
References 105

5.1 Introduction

The Neuman (1975) method used to interpret hydraulic parameters using pumping aquifer tests and that are essential inputs to groundwater modeling of unconfined aquifers used for simulation of various scenarios for sustainable groundwater management. The analysis involves matching the Neuman $W(\mu_A, \mu_B, \beta)$ well function for unconfined aquifers to time-drawdown data obtained during pumping aquifer test. The solution is said to be valid when $S_y/S > 10$, for observation wells near the pumping wells where the drawdown observations made after adequate long pumping time. When analyzing the pumping test data that is conducted for unconfined

N. Rane (✉)
Department of Civil Engineering, Pillai HOC College Of Engineering and Technology, Navi Mumbai, India

G. K. Jayaraj
Shivajirao S Jondhle College of Engineering and Technology, Thane, India

C. B. Pande, K. N. Moharir (eds.), *Groundwater Resources Development and Planning in the Semi-Arid Region*, https://doi.org/10.1007/978-3-030-68124-1_5

aquifers, it is found that the response of the drawdown does not follow the traditional Theis (1935) method. When time-drawdown relation plotted on, semi log graph tends to represent a steeper segment curve at an initial time, a flat segment in central time, and steep segment in ending time. The initial segment represents some water that released from the storage of the aquifer as an increase in drawdown. The central segment shows that there is an addition in water source released from the storage with certain slowdown time. While most of the flow comes from this additional source, the drawdown time graph turns into comparatively steeper (Neuman 1979).

The response to the delayed yield reported by the Neuman model (1975) presupposes instant drainage in groundwater level and shows three different segments of drawdown. Initial time response is controlled by the transmissivity, and elastic storage coefficient is similar to the confined aquifer response. In the central time, the response is controlled by the vertical hydraulic conductivity of the aquifer. End time response is a function of specific yield and transmissivity. Traditionally, two sets of curves have been used, one matching the Type A curve to initial time-drawdown data and Type B curves matching to end time response (Neuman 1975). Type A curves are used for early time-drawdown data during the water released from elastic storage. When the influence of gravity drainage becomes more important, the Type B-curve is useful to the ending water level drawdown data.

Transmissivity and specific yield of the aquifer of the unconfined aquifer interpreted from the Neuman (1975) method based on Eqs. (5.1)–(5.3a) as follows.

The equation of drawdown from Neuman (1975) method for the unconfined aquifer is

$$S = \frac{Q}{4\pi T} W\left(\mu_{A,}\mu_{B,}\beta\right) \tag{5.1}$$

$W(\mu_{A,}\mu_{B,}\beta)$ is known as the unconfined well function.

In the initial time conditions, Eq. (5.1) shows the first segment of time-drawdown curve and then reduces to

$$S = \frac{Q}{4\pi T} W\left(\mu_{A,}\beta\right) \tag{5.2}$$

where

$$\mu_A = \frac{r^2 S}{4Tt} \tag{5.2a}$$

$S =$ elastic storage coefficient

Under ending time conditions, shows the third segment of time-drawdown curve and then reduces to

$$S = \frac{Q}{4\pi T} W(\mu_{B,}\beta) \tag{5.3}$$

where

$$\mu_A = \frac{r^2 S_Y}{4Tt} \tag{5.3a}$$

where

S_y = Specific yield

Neuman β parameter is described as,

$$\beta = \frac{r^2 K_v}{D^2 K_h} \tag{5.4}$$

where

K_v, K_h = vertical and horizontal hydraulic conductivity

There should be rule for determining how far the observation well distance located from source pumping well and the duration of pumping, which is long enough. In the case of isotropic and homogeneous aquifer, transmissivity and specific yield must remain unchanged during the period of pumping regardless observation well distance from the source of pumping well and the direction of observation well. The pumping test duration is to be chosen in such a way that, the steady state condition is to be attained (Kruseman and Ridder 1990; Khadri and Moharir 2016, Khadri and Pande 2016; Moharir et al. 2017). Therefore, the selection of observation distance from pumping well is still a real challenge. Literature suggestions on observation distance from the source pumping well are relatively subjective. Kruseman and Ridder (1990) recommended that the observation wells are required to be placed on moderate distance from the source pumping well; however, due to lack of clear standard criteria, the moderate distance cannot be calculated. In theory, there is also a narrow understanding of the possible practical problems and the effect of time-drawdown data analysis if observation distance is not small or reasonable enough.

For a long time, groundwater numerical modeling has been used to assess the function of analytical solutions to analyze the pumping aquifer test data (Halford et al. 2006; Osiensky et al. 2000; Trinchero et al. 2008; Cardiff et al. 2013; Lin and Der Yeh 2008; Louwyck et al. 2014; Llopis-Albert and Pulido-Velazquez 2015; Shapoori et al. 2015; Calvache et al. 2015; Khadri and Moharir 2016; Khadri and Pande 2016; Moharir et al. 2020). Although several studies have previously evaluated the application of pumping aquifer test method, the influence of the observation well distance from the pumping well on the interpretation of multiwell aquifers in an isotropic, and homogeneous aquifers using the Neuman (1975) solution is not discussed. A study to evaluate and represent the effect of how the interpretation of

multiwell pumping aquifer tests in the homogeneous and isotropic aquifer using the Neuman (1975) solution impacts the transmissivity, and specific yield analysis. In the present study, MODFLOW numerical groundwater models are developed to simulate multiwell pumping aquifer tests data and interpreted using the Neuman (1975) solution to find the aquifer parameters. The benefit of multiple observation well is the drawdowns observed in the observation well used in two approaches, to determine the time-drawdown relationship and the determination of distance drawdown. This study helps in improving the practical insights for the groundwater modelers and hydrogeologist for applying the Neuman (1975) solution to analyze multiwell pumping aquifer tests.

5.2 Materials and Methods

5.2.1 Groundwater Flow Model Development

Two groundwater flow models of multiwell pumping aquifer tests have been simulated in single layer isotropic, and homogeneous unconfined aquifer models using Visual MODFLOW flex 6.1 (WHI 2019; Moharir et al. 2017) for testing the performance of Neuman (1975) solution on hydraulic properties of the aquifer. Models include a hypothetical pumping well that is assumed at a central cell location and extracts the groundwater at a specific pumping rate and time and observed at observation wells which are placed at different radial distances. The temporal distribution of hydraulic heads at each observation wells is observed for real problems. In exclusion to the infinite areal extent assumption, other assumptions are used to interpret pumping aquifer test data in unconfined aquifers for unsteady and steady state flow condition and evaluated in a MODFLOW groundwater numerical model. Kruseman and Ridder (1990) have stated the assumptions and situations under which pumping test solutions for unsteady and steady flow can be used for an unconfined aquifer. These assumptions and situations should be satisfied to analyze the time-drawdown data to use Neuman (1975) solution for unsteady flow in an unconfined aquifer.

These models are all isotropic and homogeneous unconfined aquifers, and pumping wells and observation wells completely penetrated, in order to make sure horizontal well flow takes place. The lower and upper boundary specified as no flux boundary. Fixed constant head boundary conditions are used at all the model boundary to ensure that each boundary has equal to the amount of water. In order to provide generalization for the aquifer, infinite areal extent assumption boundaries are set as far as possible. In Models 1, aquifer length and width are 5000 m $\times$ 5000 m and aquifer thickness is assumed as 13 m. MODFLOW finite difference grids are centered on the block and are associated with boundary conditions of the aquifers. The boundaries are located at distance of 2500 m from central source pumping well. In Models 2, aquifer length and width are considered as 8000 m $\times$ 8000 m and aquifer thickness is taken as 17 m. The boundaries located at distance of 4000 m

from central source pumping well. The grid width and length for both models are considered as 50 m each side; therefore, the number of MODFLOW finite differences grid is 100 × 100 for Model 1 and 160 × 160 for Model 2, respectively. To provide generalization for the aquifer, infinite areal extent assumption with boundaries, drawdown at model boundaries are considered as negligible. The groundwater flow model parameters are selected arbitrarily to remove the possible deviations in the results. The central cell is used as the pumping well source, with a pumping rate of 665.28 m^3/day for Model 1 whereas, in Model 2, pumping rate is considered as 967.68 m^3/day keeping the pumping period 121 days, in both the Models. The observation wells are positioned randomly in a radial direction. A summary of groundwater flow models' properties and parameters used is summarized in Table 5.1. In order to improve the simulation of time-drawdown, subgrid has been used by refining grids at and near the cells of observation and pumping wells.

5.2.2 *Aquifer Test Data Analysis*

In order to confirm the model validity to meet the assumptions that ensure the analytical solutions used to analyze pumping aquifer tests for homogeneous and isotropic unconfined aquifer, simulated drawdown of different observation wells are analyzed using Neuman (1975) curve fitting method in Aquifer Test software (WHI 2016). The observation data, transmissivity, and specific yield in models 1 and 2 data interpreted are presented in Tables 5.1, 5.2, 5.3, and 5.4.

Table 5.1 Summary of groundwater flow models properties and parameters

Model features	Model 1	Model 2
Model dimensions (m)	5000 × 5000	8000 × 8000
Cell size (m)	50 × 50	50 × 50
Aquifer thickness (m)	13	17
Pumping rate (m^3/day)	665.28	967.68
Duration of pumping (days)	121	121
Initial head (m)	4	8
Transmissivity (m^2/day)	287	128
Specific yield (S_y)	0.0270	0.0403

Table 5.2 Distance of the observation well from pumping source well explained in the results and discussion section

Serial number	Observation well number	Observation distance in m
Model 1	OW-1	50.22
	OW-16	721.77
Model 2	OW-1	50.22
	OW-16	721.77

Table 5.3 Transmissivity and specific yield interpreted from observation well time-drawdown using and the Neuman (1975) solutions for pumping aquifer tests simulated in model 1

Observation well number	Observation well distance in m	Transmissivity in m^2/day	Specific yield
OW-1	50.22	287.06	0.0265
OW-2	68.68	287.30	0.0261
OW-3	89.18	287.61	0.0258
OW-4	123.99	288.09	0.0251
OW-5	165.91	288.71	0.0248
OW-6	215.66	289.35	0.0242
OW-7	252.13	289.95	0.0238
OW-8	295.23	290.55	0.0235
OW-9	333.98	290.98	0.0233
OW-10	377.52	291.65	0.0229
OW-11	439.42	292.46	0.0226
OW-12	497.33	293.32	0.0225
OW-13	570.25	294.30	0.0222
OW-14	628.88	295.20	0.0221
OW-15	678.34	295.98	0.0219
OW-16	721.77	296.61	0.0218
OW-17	788.45	297.41	0.0216
OW-18	892.45	298.86	0.0213

Table 5.4 Transmissivity and specific yield interpreted from observation well time-drawdown using and the Neuman (1975) solutions for pumping aquifer tests simulated in model 2

Observation well number	Observation well distance (m)	Transmissivity (m^2/day)	Specific yield
OW-1	50.22	128.05	0.0401
OW-2	68.68	128.57	0.0395
OW-3	89.18	129.12	0.0388
OW-4	123.99	129.95	0.0379
OW-5	165.91	130.95	0.0375
OW-6	215.66	131.99	0.0371
OW-7	252.13	132.58	0.0365
OW-8	295.23	133.72	0.0355
OW-9	333.98	134.45	0.0351
OW-10	377.52	135.51	0.0348
OW-11	439.42	136.85	0.0339
OW-12	497.33	138.15	0.0331
OW-13	570.25	139.89	0.0328
OW-14	628.88	141.35	0.0326
OW-15	678.34	142.35	0.0321
OW-16	721.77	143.21	0.0313
OW-17	788.45	144.68	0.0310
OW-18	892.45	147.12	0.0305

5.3 Results

Time-drawdown data results of the two observation wells from Model 1 and Model 2 are discussed for illustration purpose. One observation well from each model located nearest to pumping well and the second far away at radial distances from the pumping well. Table 5.2 represents the distance of observation well from the source pumping well explained in the results and discussion. For the illustration purpose, the analysis of two observation wells from each Model is discussed in the following sections.

5.3.1 Model 1

The Neuman (1975) solution is used to analyze the pumping aquifer test data of observation wells which are located at different radial distances (OW-1, Fig. 5.1 and OW-16, Fig. 5.2). Using the Neuman (1975) solution, the transmissivity values are found to be 287.06 and 296.61 m^2/day, respectively and specific yield estimates are obtained as 0.0265 and 0.0218, respectively which are interpreted from the time-drawdown data of OW-1 and OW-16. Specific yield values of 0.0265 and 0.0218 are interpreted from the time-drawdown data of OW-1 and OW-16 observation wells. It is apparent that the transmissivity computed from the observation well 1 at a radial distance 50.22 m is found to less than tranmissivity calculated for observation wells 16, which is located at a radial distance of 721.77 m. The specific yield estimated from the observation well No. 1 at a radial distance of 50.22 m is more than the specific yield computed at observation wells 16, which is located at a radial distance

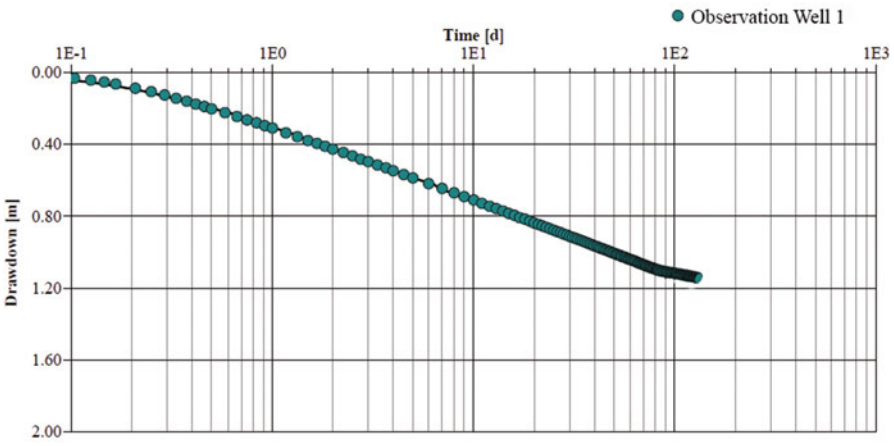

Fig. 5.1 Neuman solution fit of time-drawdown data of the observation well 1 (OW-1)

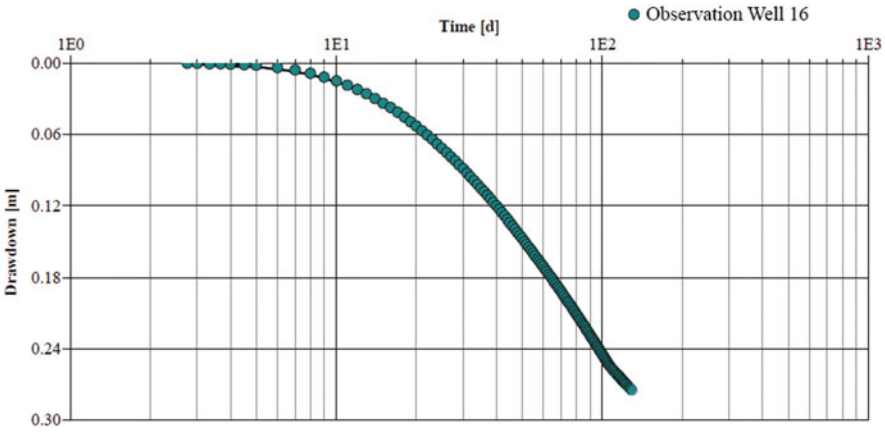

Fig. 5.2 Neuman solution fit of time-drawdown data of the observation well 16 (OW-16)

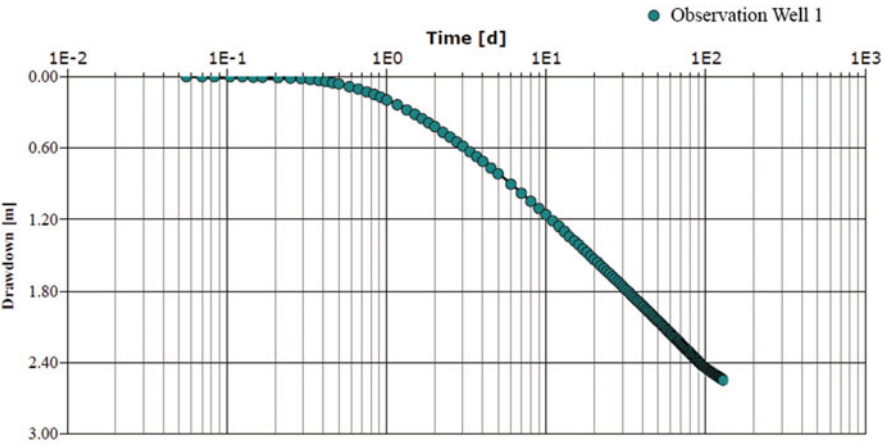

Fig. 5.3 Neuman solution fit of time-drawdown data of the observation well 1 (OW-1)

of 721.77 m. Transmissivity and specific yield interpreted from time-drawdown data of observation well at different radial distances using the Neuman (1975) solution and MODFLOW simulation for Model 1 are summarized in Table 5.3. Figures 5.1 and 5.2 show the graphical representation of Neuman solution fit with the time-drawndowns data observed at OW-1 and OW-16, respectively.

5.3.2 Model 2

Transmissivity and specific yield values estimated from observation wells (OW-1, Fig. 5.3 and OW-16, Fig. 5.4) located at different radial distances using the Neuman

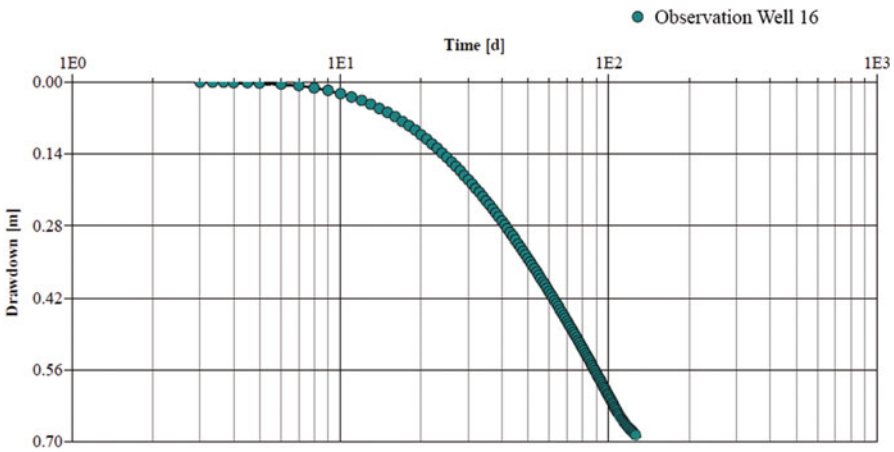

Fig. 5.4 Neuman solution fit of time-drawdown data of the observation well 16 (OW-16)

(1975) solution for pumping aquifer tests simulated in Model 2 are summarized in Table 5.4. Using the Neuman (1975) solution, transmissivity estimates of 128.05 and 143.21 m^2/day and specific yield estimates of 0.0401 and 0.0313 interpreted from drawdown data of OW-1 and OW-16 observation wells, respectively. In Model 2, it is found that the transmissivity calculated for observation OW-1 which is located at a radial ditance of 50.22 m is 128.05 m^2/day and specific yield is obtained as 0.0401, respectively whereas in the case of OW-16, which is located at a radial distance of 721.77 m, the the Transmissivity and Specific yield are obtained as 143.21 m^2/day and 0.0313, respectively. It is apparent from Tables 5.3 and 5.4 that the transmissivity increases with the increase in the radial distance, whereas the specific yield decreases with the radial distance. Figures 5.3 and 5.4 show the graphical representation of Neuman solution fit with the time-drawndowns data observed at OW-1 and OW-16, respectively.

The plot between transmissivity and radial distance of each observation well is shown in for Model 1 and Model 2 in Figs. 5.5 and 5.6, respectively.

5.4 Discussion

Although the Neuman (1975) solution has been used traditionally and may remain be used to analyze the time-drawdown data of multiwell pumping aquifer tests, the present study has made an attempt to evaluate the application of the Neuman (1975) solution using MODFLOW numerical modeling to analyze multiwell pumping aquifer tests and understand the effect of the radial distance of observation well on the hydraulic properties of an aquifer. This brings the practical significance of the application of this method. In an ideal isotropic porous and homogeneous aquifer, the effect of observation well distance on the interpreted parameters is noticeable,

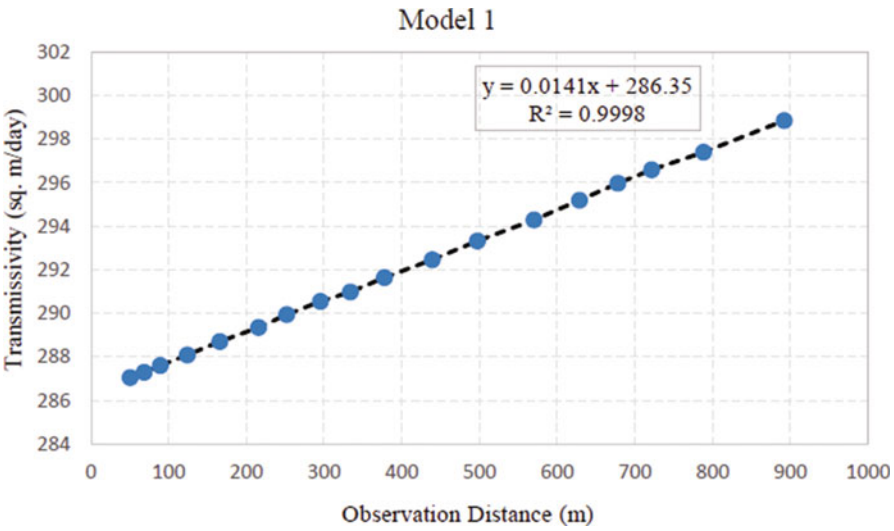

Fig. 5.5 The exponential correlation of the observation well distance and transmissivity interpreted using the Neuman (1975) solution for Model 1

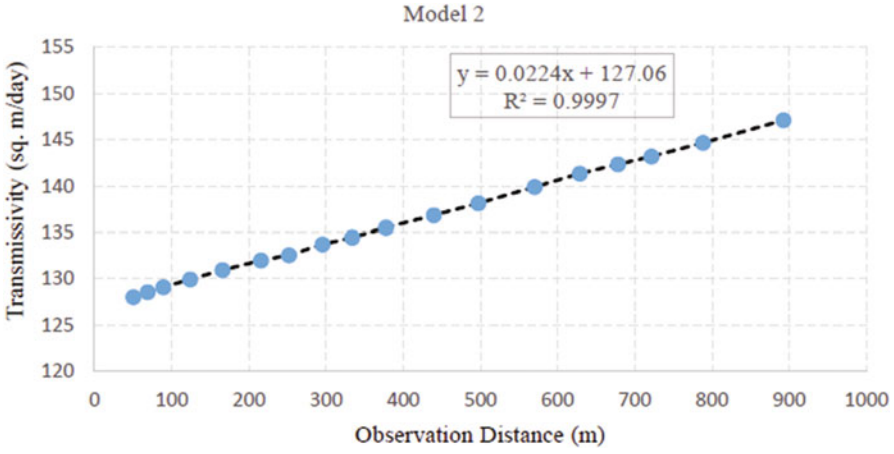

Fig. 5.6 The exponential correlation of the observation well distance and transmissivity interpreted using the Neuman (1975) solution for Model 2

which means that the observation well distance may be more complicated under heterogeneous condition. When the Neuman (1975) solution is used, it is acceptable to avoid the effect of observation well distance on hydraulic parameter interpretation. While the study considering an ideal isotropic and homogeneous porous unconfined aquifer, it provides an essential understanding for hydrogeologist and groundwater practitioners to improve the practical application of Neuman (1975) solution.

Although in this study, the results based on simulations of the model's development with ideal unconfined aquifer condition properties, and parameters, due to the same influence principle, the trend of increase of transmissivity with an increase in radial observation distance of observation wells and the trend of decreasing specific yield with respect to increase in radial distance of observation wells does not change. This indicates the study contributes towards the practical implications to different circumstances in which the Neuman (1975) solution can be used.

5.4.1 Effect of Different Radial Observation Distance on the Transmissivity Interpretation

The transmissivity results from an observation well time-drawdown data by applying Neuman (1975) solution are summarized in Tables 5.3 and 5.4, respectively and it is observed that the transmissivity interpreted usually increases with radial distance from the source of pumping well. A subsequent analysis with scatter plots represents an exponential relationship of observation distance and transmissivity interpreted from time-drawdown data using the Neuman (1975) solution. The favorable exponential correlation for both the models $r = 0.9998$, of the transmissivity interpreted from the observation well time-drawdown data and the observation well distance from source pumping well clearly indicated, as shown in Figs. 5.5 and 5.6. The transmissivity generally increases with increasing observation distance, can be because of the fact of decrease in the hydraulic head as the expand in aquifer area influences with the increasing in the observation distance from the source pumping well used to interpret transmissivity in the Neuman (1975) solution (Eq. 5.1). The overall influence of reduction of the drawdown in Neuman's solution (1975) is that the transmissivity interpreted increases with observed distance. However, it is not easy to analyze in the heterogeneous condition since the transmissivity everywhere can differ naturally with the location of the aquifer. The results of this evaluation and its possible significance are limited in the literature, so the problem of information gap needs to be addressed.

It must be noted that the results of the exponential correlations, as represented in Figs. 5.5 and 5.6 are not unique; it can be varying with model characteristics and the boundary conditions used. The overall tendency of increasing transmissivity interpreted from the increase in distance cannot change since it is primarily a working of Neuman's (1975) transmissivity method (Eq. 5.1). It is clear from Neuman's (1975) method that the transmissivity is inversely proportional to the change in the drawdown from the increasing observation distance. This effect leads to higher transmissivity with the increase in observation distance. Therefore, a significant practical challenge to put forward, that is, the proper observation distance of observation wells, so that the transmissivity interpreted by using observation well data is acceptable.

5.4.2 *Effect of Different Radial Observation Distance on the Specific Yield Interpretation*

The specific yield interpretation from observation well data seems to be decreasing with increasing the observation well distance (Fig. 5.7). This tendency is consistent with the Neuman (1975) solution for estimating specific yield. This may recommend; the specific yield is lesser responsive to the influence of increasing the observation well distance.

5.5 Conclusions

In this study, the MODFLOW groundwater numerical model is used to simulate time- drawdown data and to assess the application of Neuman (1975) solution to evaluate multiwell pumping aquifer tests in an isotropic and homogeneous unconfined aquifer. The advantage of multiple observation well is drawdowns observed in the observation well used in two approaches, to determine the time-drawdown relationship and second, the determination of distance-drawdown relationship. Results illustrate that the transmissivity interpreted from observation well drawdown data by applying Neuman (1975) solution increases exponentially with observation well distance from the source pumping well. The transmissivity generally increases with increasing the observation distance, can be because of the fact of decrease in the hydraulic head as the expand in aquifer area influences with the increase of the observation distance from the source pumping well used to interpret transmissivity in the Neuman (1975) solution. Specific yield interpreted from

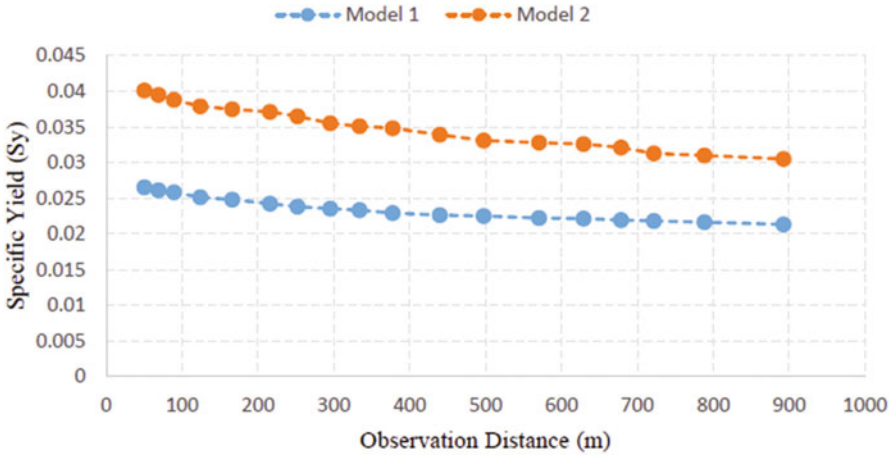

Fig. 5.7 Scatter plots of Specific yield interpreted using Neuman (1975) solution and the observation well distance from the source pumping well

time-drawdown data decreases with increasing the observation well distance as control by the Neuman (1975) solution. The transmissivity and specific yield interpreted from different radial drawdown data using the Neuman (1975) solution always differ from the exact transmissivity. The study results contribute to improve practical consideration of the effect of different radial observation well distance on specific yield and transmissivity interpreted from the observation well time-drawdown data by applying the Neuman solution (1975) as well as the overall application of the Neuman (1975) method in the analysis of multiwell pumping aquifer tests.

References

Calvache, M. L., Sánchez-Ubeda, J. P., Duque, C., Lopez-Chicano, M., & De La Torre, B. (2015). Evaluation of analytical methods to study aquifer properties with pumping tests in coastal aquifers with numerical modelling (Motril-salobreña aquifer). *Water Resources Management, 30*, 559. https://doi.org/10.1007/s11269-015-1177-6.

Cardiff, M., Barrash, W., & Kitanidis, P. K. (2013). Hydraulic conductivity imaging from 3-D transient hydraulic tomography at several pumping/observation densities. *Water Resources Research, 49*, 7311. https://doi.org/10.1002/wrcr.20519.

Halford, K. J., Weight, W. D., & Schreiber, R. P. (2006). Interpretation of transmissivity estimates from single-well pumping aquifer tests. *Ground Water, 44*, 467. https://doi.org/10.1111/j.1745-6584.2005.00151.x.

Khadri, S. F. R., & Moharir, K. (2016). Characterization of aquifer parameter in basaltic hard rock region through pumping test methods: A case study of Man River basin in Akola and Buldhana districts, Maharashtra, India. *Modeling Earth Systems and Environment, 2*, 33.

Khadri, S. F. R., & Pande, C. (2016). Ground water flow modeling for calibrating steady state using MODFLOW software: A case study of Mahesh River basin, India. *Modeling Earth Systems and Environment, 2*, 39. https://doi.org/10.1007/s40808-015-0049-7.

Kruseman, G. P., & De Ridder, N. A. (1990). *Analysis and evaluation of pumping test data, ILRI publication 47*. The Netherlands: International Institute for Land Reclamation and Improvement.

Lin, Y. C., & Der Yeh, H. (2008). Identifying groundwater pumping source information using simulated annealing. *Hydrological Processes, 22*, 3010. https://doi.org/10.1002/hyp.6875.

Llopis-Albert, C., & Pulido-Velazquez, D. (2015). Using MODFLOW code to approach transient hydraulic head with a sharp-interface solution. *Hydrological Processes, 29*, 2052. https://doi.org/10.1002/hyp.10354.

Louwyck, A., Vandenbohede, A., Bakker, M., & Lebbe, L. (2014). MODFLOW procedure to simulate axisymmetric flow in radially heterogeneous and layered aquifer systems. *Hydrogeology Journal, 22*, 1217. https://doi.org/10.1007/s10040-014-1150-0.

Moharir, K., Pande, C., & Patil, S. (2017). Inverse modeling of aquifer parameters in basaltic rock with the help of pumping test method using MODFLOW software. *Geoscience Frontiers, 8*, 1385–1395.

Moharir, K. N., Pande, C. B., Singh, S. K., & Del Rio, R. A. (2020). Evaluation of analytical methods to study aquifer properties with pumping test in Deccan Basalt Region of the Morna River Basin in Akola District of Maharashtra in India. In *Groundwater hydrology*. London, UK: Intec Open Publication. https://doi.org/10.5772/intechopen.84632. (Web of Science Indexed).

Neuman, S. P. (1975). Analysis of pumping test data from anisotropic unconfined aquifers considering delayed gravity response. *Water Resources Research, 11*, 329. https://doi.org/10.1029/WR011i002p00329.

Neuman, S. P. (1979). Perspective on 'delayed yield. *Water Resources Research, 15*, 899. https://doi.org/10.1029/WR015i004p00899.

Osiensky, J. L., Williams, R. E., Williams, B., & Johnson, G. (2000). Evaluation of drawdown curves derived from multiple well aquifer tests in heterogeneous environments. *Mine Water and the Environment, 19*, 30. https://doi.org/10.1007/bf02687263.

Shapoori, V., Peterson, T. J., Western, A. W., & Costelloe, J. F. (2015). Decomposing groundwater head variations into meteorological and pumping components: A synthetic study. *Hydrogeology Journal, 23*, 1431. https://doi.org/10.1007/s10040-015-1269-7.

Theis, C. V. (1935). The relation between the lowering of the Piezometric surface and the rate and duration of discharge of a well using ground-water storage. *EOS, Transactions American Geophysical Union, 16*, 519. https://doi.org/10.1029/TR016i002p00519.

Trinchero, P., Sanchez-Vila, X., Copty, N., & Findikakis, A. (2008). A new method for the interpretation of pumping tests in leaky aquifers. *Ground Water, 46*, 133. https://doi.org/10.1111/j.1745-6584.2007.00384.x.

WHI. (2016). *Aquifer test pumping & slug test analysis, interpretation & visualization software user's manual*. Waterloo, Canada: Waterloo Hydrogeologic.

WHI. (2019). *Visual Modflow flex 6.1 Integrated conceptual & numerical groundwater modeling software user's manual*. Waterloo, Canada: Waterloo Hydrogeologic.

Chapter 6
Groundwater Remediation Design Strategies Using Finite Element Model

S. M. V. Sharief and Mohammad Zakwan

Contents

6.1 Introduction 107
6.2 Governing Equations for Groundwater Flow and Contaminant Transport 109
6.3 Materials and Methods 111
6.4 Strategies of Aquifer Remediation 114
6.5 Results and Discussion 115
6.6 Conclusion 122
References 124

6.1 Introduction

In many countries of the world including India, groundwater constitutes the main source of drinking water. Moreover, groundwater is the major source of water supply for domestic, industrial, and agricultural purposes (Psilovikos 1999; Li et al. 2013; Muzzammil et al. 2015; Zakwan 2018; Pande and Moharir 2018). But in recent decades, the groundwater quality has very much deteriorated due to rapid industrialization and human mismanagement (Pandey et al. 2018). The increasing trends of industrial effluents including municipal sewage are the main sources for contaminants in groundwater (Chang et al. 1992; Ara and Zakwan 2018; Pande and Moharir 2018; Pande et al. 2019a, b; Moharir et al. 2019; Stoppiello et al. 2020).

S. M. V. Sharief
Department of Civil Engineering, Maulana Azad National Urdu University, Hyderabad, Telangana, India

M. Zakwan (✉)
Civil Engineering Department, IIT Roorkee, Roorkee, Uttarakhand, India

C. B. Pande, K. N. Moharir (eds.), *Groundwater Resources Development and Planning in the Semi-Arid Region*, https://doi.org/10.1007/978-3-030-68124-1_6

Contaminants must often be removed from groundwater before it reaches wells used by agriculture and municipal water supplies (Muzzammil et al. 2018). Decline in rainfall in many parts of the world has also led to reduction in natural recharge of groundwater (Pande et al. 2017, 2019a, b; Kalimeris and Kolios 2019; Shrestha et al. 2019; Zakwan 2020). Recently, Zakwan and Ara (2019) analyzed the rainfall pattern of Bihar, India and reported a noticeable decline in rainfall in post monsoon and monsoon season. Similarly, Khozeymehnezhad and Tahroudi (2019) reported decline in rainfall has reported in Arabian countries.

The removal of contaminants or pollutants has called groundwater remediation. Groundwater remediation has required when concentrations of contaminants exceed or have expected to exceed predetermined levels for the type of resource that has impacted (Ahlfeld et al. 1988; Rajanayaka and Kulasiri 2001; Moharir et al. 2017). The groundwater environment is being assaulted with an ever-increasing number of soluble chemicals, industrial wastes which are let out on to the surface without treatment (Birkinshaw et al. 2008; Li et al. 2015). Recently, the increase in number of incidents of groundwater pollution due to waste disposal activities has given a way to growing need for the development of effective management strategies for the contaminated aquifers (Alexander et al. 2018; Pande 2020a, b). Due to the complexity of the problem, to solve flow and solute transport problem in aquifers, numerical models have generally used (Zakwan et al. 2018; Khadri and Pande 2016; Moharir et al. 2020).

Over the years, application of optimization techniques and numerical modeling has increased (Rogers et al. 1995; Prommer et al. 2000; Das 2002; Maqsood et al. 2005; Birkinshaw et al. 2008; Haimes et al. 2011; Zakwan 2019; Matiatos et al. 2019; Chenini et al. 2019; Egbueri and Unigwe 2019; Tikhamarine et al. 2020). Finite Element Method (FEM) is one of the most commonly used numerical method in aquifer modeling, due to its flexibility in choosing elements and in dealing with irregular boundaries and complex boundary conditions. A large number of studies are available in the literature on the flow and contaminant transport modeling. Bredehoeft and Pinder (1973) investigated salt water contamination of the groundwater system. Marino (1974) developed one- and two-dimensional analytical solutions for contaminant transport in porous media. Hunt (1978) studied the dispersive phenomena of contaminants in porous media. Sykes et al. (1982) examined the leachate migration from the landfill using a finite-difference model. Zheng and Andrews (1991) developed a methodology for the problem of evaluating groundwater remedial alternatives for a waste disposal site. Liji et al. (1991) presented several analytical solutions for three-dimensional solute transport in semiinfinite porous media with simplified boundary conditions. Rogers et al. (1995) used ANN and GA to design groundwater remediation strategy. Yu and Singh (1995) modified the Galerkin's finite element formulation for solute transport. Charles and Karen (1998) presented a modeling approach to compare the effectiveness of horizontal and vertical well scenarios for remediation of an aquifer. Before the remediation strategies for an aquifer were initiated, the flow and transport phenomena in the system are to be studied in-detail to understand the movement of the plume.

Psilovikos and Tzimopoulos (2004) tested the performance of quadratic and nonlinear computing techniques for optimal groundwater management and reported the performance of nonlinear computing approach superior. Khelifi et al. (2006) developed a framework to assess the various aspects of groundwater remediation. Mondal et al. (2010) applied Simulation tools such as the finite element method (FEM) coupled with optimization tools such as the genetic algorithm (GA) for aquifer remediation and has found to be an efficient and easy to use methodology to solve such arduous problems. A simulation model using the FEM for groundwater flow and contaminant transport has developed and coupled with a multiobjective optimization model based on the nondominated sorting genetic algorithm II (NSGA II). Three alternative remediation design scenarios with different pumping well locations have compared and the best remediation design scenario has identified to be the one that gives the best Pareto-optimal front. Meenal and Eldho (2012) applied Particle Swarm Optimization (PSO) technique for groundwater remediation. Satavalekar and Sawant (2014) developed a finite element model to solve the advection-dispersion equation for layered soil system. FEM and Meshfree method (Element-free Galerkin Method) have used to simulate phenomenon of contaminant transport in one dimension. Parametric study has done by changing the dispersion coefficient, average velocity, geochemical reactions, height of leachate, and height of liner for obtaining suitability. Kazemzadeh-Parsi et al. (2015) analyzed the performance of firefly optimization technique for groundwater remediation. Hosseini (2017) applied PSO and GA for calculating aquifer parameter and reported that PSO blend with kriging can be potential competitor for groundwater remediation. Alexander et al. (2018) applied constraint integer program for groundwater remediation. Yin et al. (2020) proposed the use Multiobjective spatial pumping optimization for groundwater remediation. In this paper, aquifer remediation strategies have investigated using a coupled finite element model for flow and contaminant transport.

In general, the selection of a particular aquifer cleanup strategy has decided based upon the local hydrogeological conditions of the contaminated aquifer, scale of contamination, and its nature. Equally important are the resources available to the regulating authorities and the time frame within which aquifer restoration has to be completed. Groundwater remediation is the process that has used to treat groundwater by removing the pollutants. There are many different groundwater remediation methods, but they all have the same goal, i.e., clean polluted water.

6.2 Governing Equations for Groundwater Flow and Contaminant Transport

The governing equation describing the flow in an inhomogeneous confined aquifer in two dimensions is given by (Bear 1979)

$$\frac{\partial}{\partial x}\left[T_x\frac{\partial h}{\partial x}\right]+\frac{\partial}{\partial y}\left[T_y\frac{\partial h}{\partial y}\right]=S\frac{\partial h}{\partial t}+Q_w\delta(x-x_i)(y-y_i)-q \tag{6.1}$$

The Eq. (6.1) is solved by using the initial condition

$$h(x,y,0)=h_0(x,y)\quad x,y\in\Omega$$

and the boundary conditions

$$h(x,y,t)=H(x,y,t)\quad x,y\in\partial\Omega_1$$

$$T\frac{\partial h}{\partial n}=q(x,y,t)\quad x,y\in\partial\Omega_2$$

where $h(x,y,t)$ = piezometric head (m); $T(x,y)$= transimissivity (m^2/day); S= storage coefficient; x, y = horizontal space variables (m); Q_w = source or sink function ($-Q_w$ source, Q_w= Sink) (m^3/day/m^2); t = time in days; Ω = the flow region; $\partial\Omega$= boundary region ($\partial\Omega_1\cup\partial\Omega_2=\partial\Omega$); $\frac{\partial}{\partial n}$ = normal derivative; $h_0(x,y)$ = initial head in the flow domain (m); $H(x,y,t)$ = known head value of the boundary head (m); and $q(x,y,t)$ = known inflow rate (m^3/day/m).

The governing partial differential equation describing the physical processes of convection and hydrodynamic dispersion is basically obtained from the principle of conservation of mass (Freeze and Cherry 1979). The derived partial differential equation for transport of a single chemical constituent in groundwater, considering advection-dispersion, fluid sources/sinks can be given (Wang and Anderson 1982; Sun 1996) as follows.

$$R\frac{\partial C}{\partial t}=\frac{\partial}{\partial x}\left(D_{xx}\frac{\partial C}{\partial x}\right)+\frac{\partial}{\partial x}\left(D_{xy}\frac{\partial C}{\partial y}\right)+\frac{\partial}{\partial y}\left(D_{yx}\frac{\partial C}{\partial x}\right)+\frac{\partial}{\partial x}\left(D_{yy}\frac{\partial C}{\partial y}\right)-\frac{\partial}{\partial x}(V_xC)$$
$$-\frac{\partial}{\partial y}(V_yC)-\frac{c'w}{nb}+\frac{W}{\theta}C_0-\frac{Q}{\theta}C \tag{6.2}$$

where V_x and V_y= seepage velocity in x and $y$direction; D_{xx},D_{yy}, D_{xy}, D_{yx}= Components of dispersion coefficient tensor [L^2T^{-1}]; C= Dissolved concentration [ML^{-3}]; θ = Porosity (dimensionless); w = elemental recharge rate with solute concentration c'; n = elemental porosity; b = aquifer thickness under the element; R= Retardation factor; C_0= water with concentration injected into an aquifer; W= water injected per unit time per unit aquifer volume (T^{-1}); Q = volume of water extracted away from per unit aquifer volume per unit time.

The initial condition for the problem is

$$C(x, y, 0) = f \quad (x, y) \in \Omega \tag{6.3}$$

and the boundary conditions are

$$\begin{aligned} C(x, y, t) &= g_1 \qquad (x, y) \in \Gamma_1 \\ \frac{\partial C}{\partial n}(x, y, t) &= g_2 \quad (x, y) \in \Gamma_2 \end{aligned} \tag{6.4}$$

where Γ_1= boundary sections of Ω; f= a given function in Ω; g_1= given function along Γ_1, which is known solute concentration from the present study. g_2 = concentration gradient normal to the boundary Γ_2; n= unit normal vector.

6.3 Materials and Methods

6.3.1 Finite Element Formulation for Groundwater Flow and Transport

6.3.1.1 Finite Element Formulation for Groundwater Flow

For numerical analysis, the finite element method is selected because of its relative flexibility to discretize a prototype system and representation boundaries accurately. FEM approximates the governing partial differential equation by integral approach (Pathania et al. 2019; Hao et al. 2019; Zeinali et al. 2020). In the present study, two-dimensional linear triangular elements are used for spatial discritization and Galerkin approach (Reddy 1993) is used for finite element approximation. In the FEM, the head variable in Eq. (6.1) is initially approximated as

$$\widehat{h}(x, y, t) = \sum_{L=1}^{\mathrm{NP}} h_L(t) N_L(x, y) \tag{6.5}$$

where h_L = unknown head; N_L= known basis function at node$L$; $\widehat{h}(x, y, t)$= trial solution; NP= total number of nodes in the problem domain. A set of simultaneous equations is obtained when residuals weighted by each of the basis function are forced to be zero and integrated over the entire domain. Applying the Galerkin's finite element method (Istok 1989).

$$\begin{aligned} &[[P] + \omega \Delta t[G]] = \\ &[[P] - (1 - \omega)\Delta t[G]]\{h\}_t + \Delta t(1 - \omega)\{F\}_t + \omega\{F\}_{t+\Delta t}\{h\}_{t+\Delta t} \end{aligned} \tag{6.6}$$

where $[G]$ = conductance matrix containing transmissivity terms; $[P]$ = storage matrix containing storage coefficient terms; Δt= time step size; $\{h\}$= groundwater

head; {F} = nodal recharge or discharge vector; $h_{t+\Delta t}$= unknown head vector; h_t= known head vector at time t. The subscripts t and $t + \Delta t$ represent the groundwater head values at previous and present time steps. By rearranging the terms of equation, all these are global matrices. ω= Relaxation factor which depends on the type of finite difference scheme used. In the present study, Crank-Nicolson scheme with $\omega = 0.5$ is used. These global matrices can be constructed using the element matrices of different shapes based on discretization of the domain. The linear simultaneous equations derived above are solved to obtain the head distribution at nodal points using Cholesky's method for the given initial and boundary conditions, recharge, pumping, transmissivity, and storage coefficient values. After getting the nodal head values, the time step is incremented and the solution proceeds in the same manner by updating the time matrices and recomputing the nodal head values. From the obtained nodal head values, the velocity vectors in x and $y$directions can be calculated using the Darcy's law.

6.3.1.2 Finite Element Formulation for Contaminant Transport

Applying Galerkin's FEM to solve partial differential equation (6.2), similar to the groundwater flow equation, final form of equation in implicit form that is used in the contaminant transport model is given as follows.

$$[[S] + \omega\Delta t[D]]\{C\}_{t+\Delta t} = [[S] - (1-\omega)\Delta t[D]]\{C\}_t + \Delta t(1-\omega)\{F\}_t + \omega\{F\}_{t+\Delta t} \tag{6.7}$$

where $[S]$ = element sorption matrix; $[D]$ = element advection–dispersion matrix; $[F]$ = flux matrix; $\{C\}$ = nodal concentration column matrix; the subscripts t and Δt indicate the concentration at previous time step and current time step. As in the case of groundwater flow, Eq. (6.7) is applied to all elements and assembled to form system of equations. The system of equations are solved, similar to the groundwater flow, after the application of initial and boundary conditions to get the unknown concentration distribution in the aquifer region.

6.3.1.3 Two-Dimensional Coupled Flow and Transport Model

Based on the Galerkin's finite element formulation, one-dimensional and two-dimensional flow and transport models have been developed using C programing. The code is applied for steady and transient groundwater flow and solute transport problems in confined aquifer including the discharge term. The model uses linear triangular elements. The aquifer parameters can vary from element to element, but assumed constant over an element. The head distribution in the aquifer domain is calculated from the flow model and these head values are used to calculate the flow velocities. The resulting velocity vectors are used for the transport model to find the

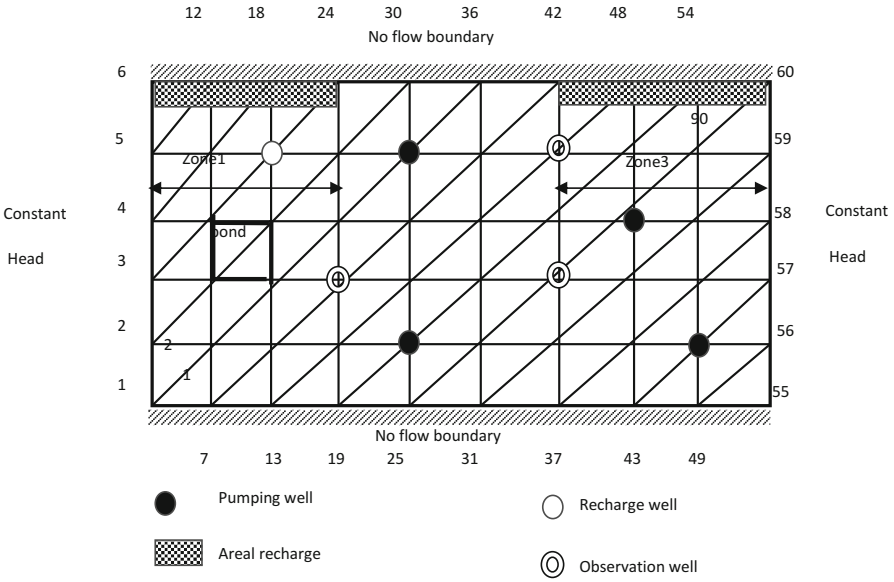

Fig. 6.1 Finite element discretization

concentration distribution in the aquifer region. In the present study, a hypothetical two-dimensional coupled flow and solute transport problem were investigated. The confined aquifer (Fig. 6.1) is assumed to be heterogeneous, anisotropic, and having three zonal pattern. The boundary conditions for the flow model are constant head on east (95 m) and west sides (100 m) and no flow on the north and south sides. For transport model, the boundary conditions are no-mass flux on all the sides other than east. The aquifer is discretized into finite element mesh with a grid spacing of 200 m $\times$ 200 m (Fig. 6.1). Four production wells extracting water at the rate of 600, 800, 1500, and 700 m^3/day, respectively are considered in the flow region. These wells are located at nodes 26, 29, 46, and 50, respectively. A recharge well with inflow rate of 500 m^3/day is located at node 17. Three observation wells are located at node 21, 39, and 41.

The problem involves seepage from a polluted pond into the underlying aquifer (Fig. 6.1). The bottom of the pond is assumed to be sufficiently close to the groundwater surface so that the flow in the unsaturated region is neglected. The recharge rate from the pond controls the amount of solute introduced into the system and contributes the defining velocity in the field. The aquifer is assumed initially uncontaminated. In this problem, the contaminant is entering into the flow field through seepage from the polluted pond having 3500 ppm and a polluted recharge well having concentration 1500 ppm (total dissolved solids). For the first case, pollution is caused in the system due to polluted pond. For second case, the system is polluted by polluted pond and a polluted recharge well. The present study examines the coupled flow and solute transport problem for three different scenarios. For the first and second scenarios, pumping was not involved during the simulation

Table 6.1 Hydrogeological parameters of various zones

Properties	Zone 1	Zone 2	Zone 3
Transmissivity T_x (m^2/day)	1200	900	600
Transmissivity T_y (m^2/day)	1100	800	500
Porosity	0.2	0.25	0.15
Longitudinal dispersivity (m)	125	75	40
Transverse dispersivity (m)	12.5	7.5	4.0

period. In the third scenario, the system was affected along with the two input sources by pumping wells for the existing simulation period of 10,000 days. The following data is used for finding the head and concentration distribution for steady and unsteady state conditions for coupled flow and contaminant transport problem. Thickness of the confined aquifer = 50 m; Size of the confined aquifer = 1800 m × 1000 m; storativity = 0.0002; aquifer is recharged through some aquitard in between node numbers 1–24 and 37–60 at the rate of 0.00024 and 0.00012 m/day; rate of seepage from the pond = 0.04 m/day. Table 6.1 summarizes the hydrogeological parameters for the selected problem.

6.4 Strategies of Aquifer Remediation

In this study, the decontamination process in the aquifer is analyzed by two different strategies that are remediation by pumping wells and flushing through a recharge pit. In the first strategy, four potential abstraction wells extract the contaminant from the system. During this process contaminant from the pond is inactive. Whereas, in case of second strategy, the cleanup of the aquifer takes due to flushing through the recharge pond. No pumping operation is involved in this process. Three scenarios have been considered for each remediation strategy, i.e., case 1(a, b, & c) and case 2 (a, b, & c). In an aquifer contaminated by pollutants, if the sources of the pollutants are removed or the entry of the pollutants to the aquifer is stopped by some means, then the pollutants move away and the decontamination process takes place in the aquifer. It is assumed that from the beginning to a specified period, the contamination process is going on. At a particular time, the contamination source is removed and the resulting concentration movement is analyzed. For case 1(a), initially the system was affected by seepage at the rate of 0.04 m/day, from the polluted pond with solute concentration of 3500 ppm. For case 1(b), the input sources are seepage from the polluted pond and a contaminated recharge well. Considering these as input sources, pumping wells in the flow domain are treated as inactive and the system was simulated for a period of 10,000 days for case 1(a) and 1(b). For the case 1(c) apart from these input sources, pumping wells are active during the simulation period. The obtained simulated plume is considered as initial conditions for remediation strategies.

In the first remediation strategy, the input sources are cutoff; four pumping wells are extracting water at the rate of 600, 800, 1500, and 750 m^3/day, respectively from the system involved during the remediation period. The movement of the plume is due to the existing hydraulic gradient in the system by higher and lower head boundaries. In the second strategy, the aquifer is flushed from the seepage of the polluted pond having concentration of 50 ppm at the same rate (0.04 m/day), also before the remediation process starts, the input sources are arrested, and hence the flow in the system is due to constant head boundary conditions.

6.5 Results and Discussion

6.5.1 Case 1(a)

A 500 ppm concentration contour is considered for this analysis to study the movement and the influencing area of this contour for a particular period. The behavior of this contour is analyzed for a period of 1000 and 2000 days after the decontamination begins. Initially this contour is distributed for a length of 1750 m, influencing an area of 1.1375 km^2. Once the decontamination is initiated, the reduction in length of this contour is very significant. The length of this plume is reduced to 1350 m and area is reduced to 0.77 km^2 after 1000 days. When this period is doubled to 2000 days, the concentration is found moving far away from the pond, the length of this plume is reduced to 850 m, and area is reduced to 0.47 km^2. The progress of the aquifer decontamination for this alternative is shown in Fig. 6.2a–c).

6.5.2 Case 1(b)

The length and area under 500 ppm contour are 1775 m and 1.3 km^2, which are larger, compared to case 1(a) as the system was affected by a polluted recharge well in addition to the seepage from the contaminated pond. Once the decontamination process started, the influence of this contour is reduced to a length of 1400 m and the area is reduced to 0.84 km^2 after a period of 1000 days. Further the concentration for the chosen contour is showing a considerable decrease in its shape and size in terms of length (950 m) and area (0.625 km^2) after 2000 days. The concentration distribution for this scenario is shown in Fig. 6.3a–c. Therefore after this period, the aquifer can be considered as partially cleaned-up for practical purpose.

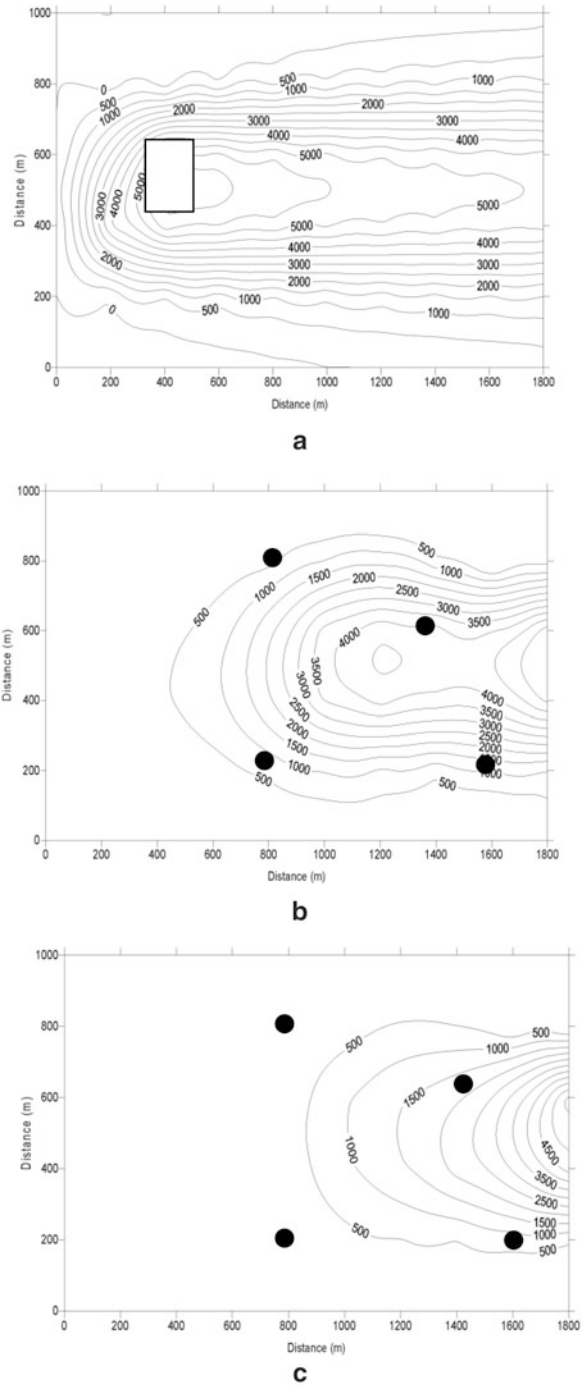

Fig. 6.2 (**a**) Concentration distribution after 10,000 days of simulation for case 1 (a). (**b**) Remediation by pumping after 1000 days for case 1(a). (**c**) Remediation by pumping after 2000 days for case 1(a)

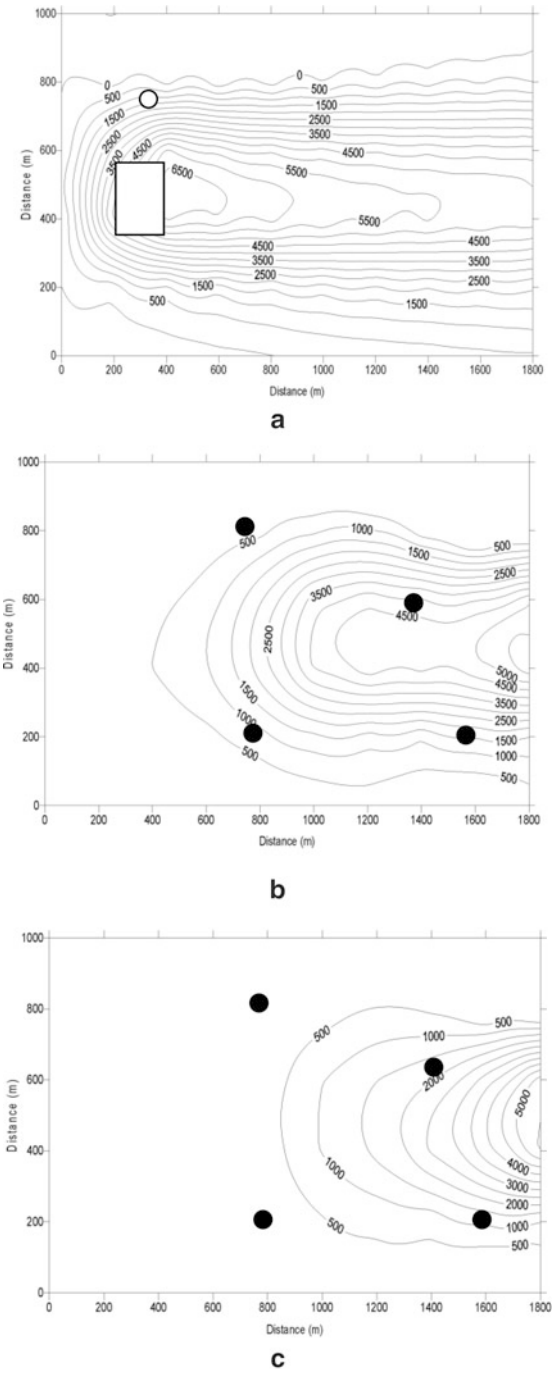

Fig. 6.3 (**a**) Concentration distribution after 10,000 days of simulation for case 1 (b). (**b**) Remediation by pumping after 1000 days for case 1(b). (**c**) Remediation by pumping after 2000 days for case 1(b)

6.5.3 Case 1(c)

The same contour (500 ppm) is studied for the case 1(c) in this decontamination alternative. For this scenario, the system was affected by seepage from the contaminated pond, recharge well, and additionally four pumping wells were also in operation during the simulation period. Before the remediation, the concentration distribution for the 500 ppm contour is 1750 × 600 m, which is influencing an area of 1.018 km^2. The length of this contour is reduced to 1250 m after 1000 days; the reduction in the area of this contour is 0.835 km^2. After a period of 2000 days, the concentration distribution is reduced to a length to 850 m, and area is reduced to 0.47 km^2. Concentration distribution for different times has shown in Fig. 6.4a–c.

From the above three cases for this remediation strategy, it has been found that the effectiveness of this strategy mainly depends upon severity of the initial concentration conditions in the system. Results have shown that when the pollution from the source is ceased, the remediation by abstraction wells takes less time. The cleanup time for the contaminated aquifer can be reduced further by increasing the number of pumping wells with more pumping capacity located near the maximum polluted regions. As expected the cleaning process is expedited, when pumping wells are also operated.

6.5.4 Case 2(a)

The initial conditions for this remediation strategy (flushing through a recharge pit) are same as for case 1(a). Once the decontamination is initiated, the length of this plume is reduced to 1400 m and the area under this contour is reduced to 0.83 km^2 after a period of 1000 days. Further when this period is doubled to 2000 days, the concentration is found moving far away from the pond showing a considerable decrease in its shape and size in terms of length of 950 m and area of 0.577 km^2. The progress of the aquifer decontamination for this alternative is shown in Fig. 6.5a–c.

6.5.5 Case 2(b)

The initial conditions for this strategy are same as case 1(b). After the decontamination process starts, the influence of this contour is reduced to a length of 1400 m and area is reduced to 0.84 km^2 after 1000 days. The reduction in length of 950 m and area of 0.53 km^2 is found after 2000 days. The Fig. 6.6a–c illustrates, the state of contamination of the aquifer after 1000 and 2000 days in this strategy.

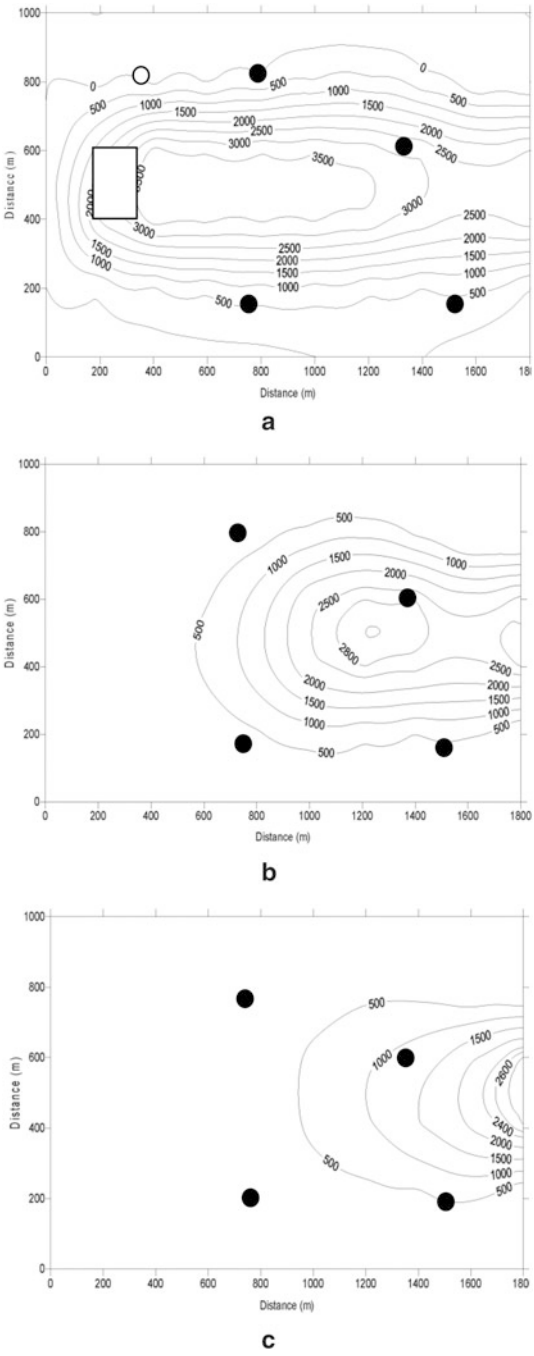

Fig. 6.4 (**a**) Concentration distribution after 10,000 days of simulation for case 1 (c). (**b**) Remediation by pumping after 1000 days for case 1(c). (**c**) Remediation by pumping after 2000 days for case 1(c)

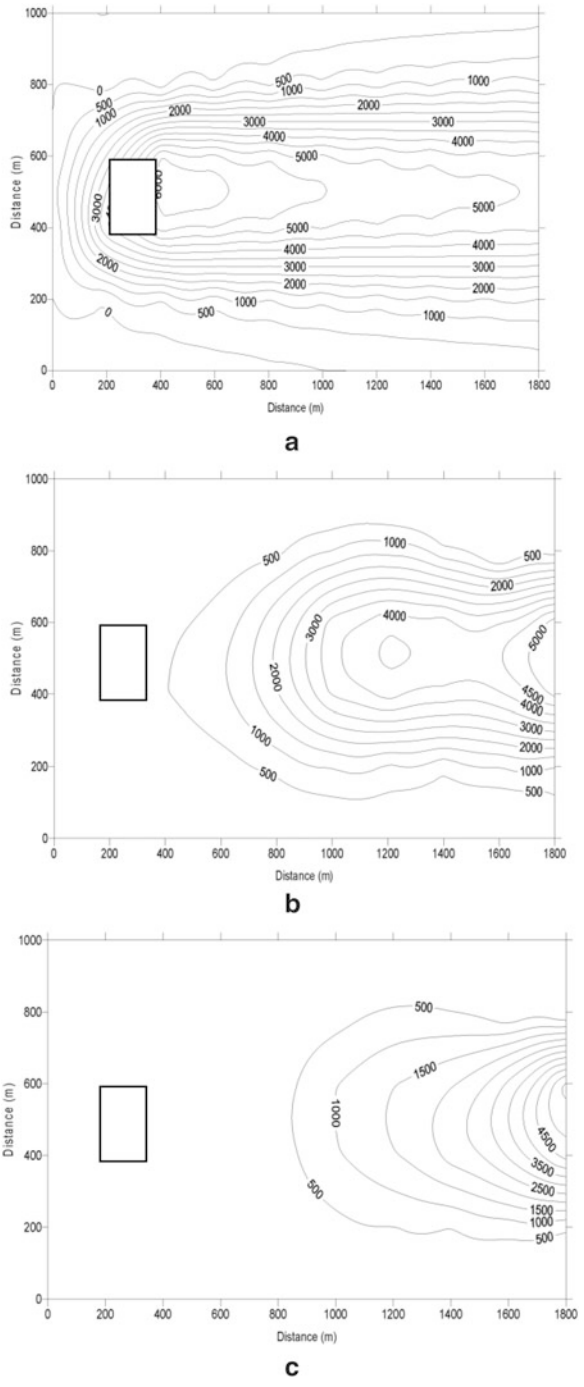

Fig. 6.5 (**a**) Concentration distribution after 10,000 days of simulation for case 2 (a). (**b**) Remediation by flushing after 1000 days for case 2(a). (**c**) Remediation by flushing after 2000 days for case 2(a)

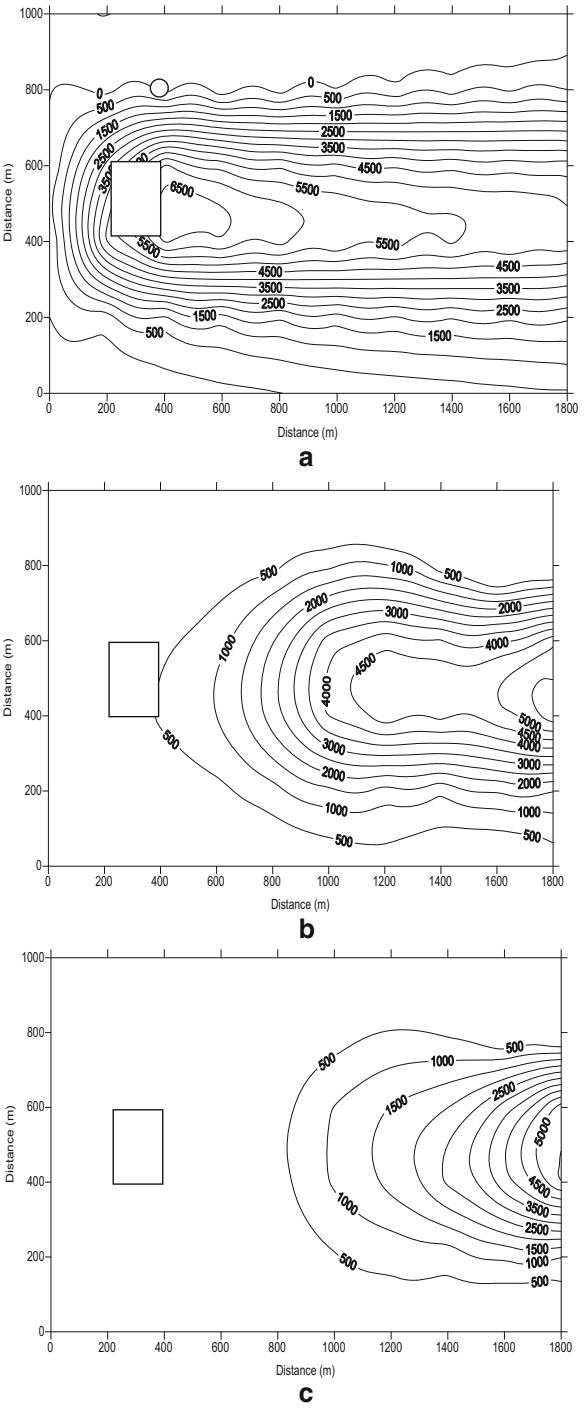

Fig. 6.6 (**a**). Concentration distribution after 10000 days of simulation for case 2 (b) (**b**). Remediation by flushing after 1000 days for case 2 (b) (**c**). Remediation by flushing after 2000 days for case 2 (b)

6.5.6 Case 2(c)

The initial conditions for this strategy are similar to case 1(c). After 1000 days, the spreading of this contour is reduced to 1250 m and the area is reduced to 0.835 km^2 in this decontamination process. The effect of this contour on the system in terms of length and area is found as 900 m and 0.50 km^2, respectively. The distribution of concentration contours is presented in Fig. 6.7a–c.

Based on the results obtained from the second remediation strategy, it could be concluded that with the increase of remediation time, the influence of the chosen contour is reduced on the system. This happens because of the seepage from the pond pushes forward the concentration plume. The cleanup time for the contaminated aquifer can be reduced further by increasing the rate of fresh water recharge from the pond.

6.6 Conclusion

Contamination of groundwater is a wide spread problem and remediation process is very complex. In this study, the contaminated aquifer remediation is investigated using a coupled flow and transport modeling with two different strategies, i.e., remediation by abstraction wells and flushing through a recharge pond. From the results, it is observed that the chosen initial concentration contour in the aquifer is reduced to a reasonable extent within 1000 days and further reduced by 2000 days in the abstraction wells alternative. Hence, it is understood that when the pollution from the source is ceased, remediation by abstraction wells takes less time. The area of the plume is significantly reduced in this strategy as the contaminant mass is extracted out of the aquifer through pumping wells. The cleanup time in this alternative mainly depends on the rate of pumping and also the number of pumping wells in the contaminated area. In case of second decontamination strategy, the cleanup time is more as compared to the first strategy, since it depends upon small natural groundwater flow velocities and recharge from the pond. Favorable hydraulic gradients are produced due to fresh water flushing from the seepage pond causing contaminated plume move away from the pond. Many such strategies therefore can be examined by the coupled FEM model which can eventually help to pickup the most economically viable method (or least time taking) from practical consideration.

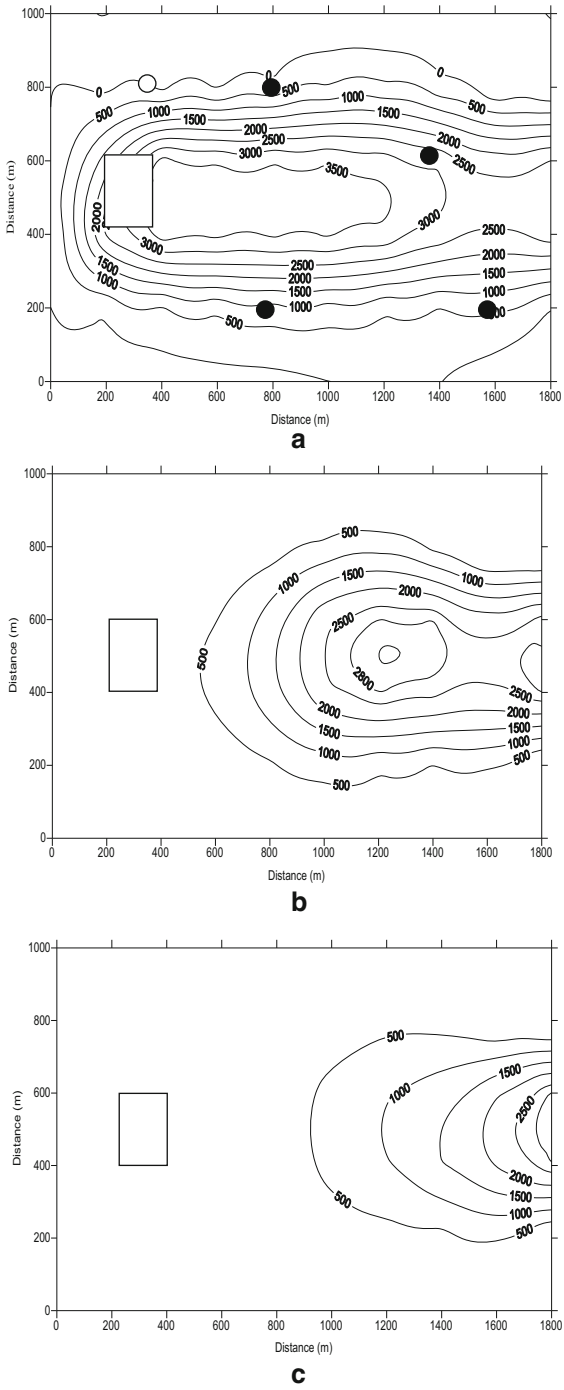

Fig. 6.7 (**a**). Concentration distribution after 10000 days of simulation for case 2 (c) (**b**). Remediation by flushing after 1000 days for case 2 (c) (**c**). Remediation by flushing after 2000 days for case 2 (c)

References

Ahlfeld, D. P., Mulvey, J. M., Pinder, G. F., & Wood, E. F. (1988). Contaminated groundwater remediation design using simulation, optimization, and sensitivity theory: 1. Model development. *Water Resources Research, 24*(3), 431–441.

Alexander, A. C., Ndambuki, J. M., Salim, R. W., & Manda, A. K. (2018). Groundwater remediation optimization using Solving Constraint Integer Program (SCIP). *Groundwater for Sustainable Development, 7*, 176–184.

Ara, Z., & Zakwan, M. (2018). Estimating runoff using SCS curve number method. *International Journal of Emerging Technology and Advanced Engineering, 8*, 195–200.

Bear, J. (1979). *Hydraulics of groundwater*. New York: McGra-Hill Publishing.

Birkinshaw, S. J., Parkin, G., & Rao, Z. (2008). A hybrid neural networks and numerical models approach for predicting groundwater abstraction impacts. *Journal of Hydroinformatics, 10*(2), 127–137.

Bredehoeft, J. D., & Pinder, G. F. (1973). Mass transport in flowing groundwater. *Water Resources Research, 9*(1), 194–210.

Chang, L. C., Shoemaker, C. A., & Liu, P. L. F. (1992). Optimal time-varying pumping rates for groundwater remediation: Application of a constrained optimal control algorithm. *Water Resources Research, 28*(12), 3157–3173.

Charles, S. S., & Karen, K. L. (1998). Productivity comparison of horizontal and vertical groundwater remediation well scenarios. *Groundwater, 36*(1), 98–103.

Chenini, I., Msaddek, M. H., & Dlala, M. (2019). Hydrogeological characterization and aquifer recharge mapping for groundwater resources management using multicriteria analysis and numerical modeling: A case study from Tunisia. *Journal of African Earth Sciences, 154*, 59–69.

Das, D. B. (2002). Hydrodynamic modelling for groundwater flows through permeable reactive barriers. *Hydrological Processes, 16*(17), 3393–3418.

Egbueri, J. C., & Unigwe, C. O. (2019). An integrated indexical investigation of selected heavy metals in drinking water resources from a coastal plain aquifer in Nigeria. *SN Applied Sciences, 1*(11), 1422.

Freeze, R. A., & Cherry, J. A. (1979). *Groundwater*. New York: Englewood Cliffs.

Haimes, Y. Y., Hall, W. A., & Freedman, H. T. (2011). *Multiobjective optimization in water resources systems: The surrogate worth trade-off method*. Amsterdam: Elsevier.

Hao, Z., Park, M., Lin, G., & Cai, Z. (2019). Finite element method for two-sided fractional differential equations with variable coefficients: Galerkin approach. *Journal of Scientific Computing, 79*(2), 700–717.

Hosseini, S. M. (2017). Parameter estimation of aquifer transmissivity variogram using WLS, GA and PSO algorithms. *International Journal of Hydrology Science and Technology, 7*(2), 103–123.

Hunt, B. (1978). Dispersive sources in uniform groundwater flow. *Journal of Hydraulics Division, 104*(HY1), 75–85.

Istok, J. (1989). *Groundwater modeling by the finite element method*. Washington: American Geophysical union.

Kalimeris, A., & Kolios, S. (2019). TRMM-based rainfall variability over the Central Mediterranean and its relationships with atmospheric and oceanic climatic modes. *Atmospheric Research, 230*, 104649.

Kazemzadeh-Parsi, M. J., Daneshmand, F., Ahmadfard, M. A., Adamowski, J., & Martel, R. (2015). Optimal groundwater remediation design of pump and treat systems via a simulation–optimization approach and firefly algorithm. *Engineering Optimization, 47*(1), 1–17.

Khadri, S. F. R., & Pande, C. (2016). Groundwater flow modeling for calibrating steady state using MODFLOW software: a case study of Mahesh River basin, India. *Modeling Earth Systems and Environment, 2*, 39. https://doi.org/10.1007/s40808-015-0049-7.

Khelifi, O., Lodolo, A., Vranes, S., Centi, G., & Miertus, S. (2006). A web-based decision support tool for groundwater remediation technologies selection. *Journal of Hydroinformatics, 8*(2), 91–100.

Khozeymehnezhad, H., & Tahroudi, M. N. (2019). Annual and seasonal distribution pattern of rainfall in Iran and neighboring regions. *Arabian Journal of Geosciences, 12*(8), 271.

Li, P., Wu, J., & Qian, H. (2013). Assessment of groundwater quality for irrigation purposes and identification of hydrogeochemical evolution mechanisms in Pengyang County, China. *Environmental Earth Sciences, 69*(7), 2211–2225.

Li, J., He, L., Lu, H., & Xu, M. (2015). A simulation-based nonlinear goal programming model for groundwater remediation systems design. *Polish Journal of Environmental Studies, 24*(2), 563–574.

Liji, F. J., Skaggs, T. H., & Genuchten, V. (1991). Analytical solutions for solute transport in three dimensional semi-infinite porous media. *Water Resource Research, 27*(10), 2719–2733.

Maqsood, I., Huang, G., Huang, Y., & Chen, B. (2005). ITOM: An interval-parameter two-stage optimization model for stochastic planning of water resources systems. *Stochastic Environmental Research and Risk Assessment, 19*(2), 125–133.

Marino, M. A. (1974). Longitudinal dispersion in saturated porous media. *Journal of Hydraulics Division, 100*(HY1), 151–157.

Matiatos, I., Varouchakis, E. A., & Papadopoulou, M. P. (2019). Performance evaluation of multiple groundwater flow and nitrate mass transport numerical models. *Environmental Modeling & Assessment, 24*(6), 659–675.

Meenal, M., & Eldho, T. I. (2012). Simulation–optimization model for groundwater contamination remediation using meshfree point collocation method and particle swarm optimization. *Sadhana, 37*(3), 351–369.

Moharir, K., Pande, C., & Patil, S. (2017). Inverse modeling of aquifer parameters in basaltic rock with the help of pumping test method using MODFLOW software. *Geoscience Frontiers, 8*, 1385–1395.

Moharir, K., Pande, C., Singh, S., Choudhari, P., Rawat, K., & Jeyakumar, L. (2019). Spatial interpolation approach-based appraisal of groundwater quality of arid regions in. *Aqua Journal, 68*(6), 431–447.

Moharir, K. N., Pande, C. B., Singh, S. K., & Del Rio, R. A. (2020). *Evaluation of analytical methods to study aquifer properties with pumping test in Deccan basalt region of the Morna River basin in Akola District of Maharashtra in India, groundwater hydrology*. London, UK: Intec Open Publication. https://doi.org/10.5772/intechopen.84632.

Mondal, A., Eldho, T. I., & Rao, V. G. (2010). Multiobjective groundwater remediation system design using coupled finite element model and nondominated sorting genetic algorithm II. *Journal of Hydrologic Engineering, 15*(5), 350–359.

Muzzammil, M., Alam, J., & Zakwan, M. (2015). An optimization technique for estimation of rating curve parameters. In *National Symposium on Hydrology*, New Delhi (pp. 234–240).

Muzzammil, M., Alam, J., & Zakwan, M. (2018). A spreadsheet approach for prediction of rating curve parameters. In *Hydrologic modeling* (pp. 525–533). Singapore: Springer.

Pande, C. B. (2020a). Watershed management and development. In *Sustainable watershed development. Springer briefs in water science and technology*. Cham: Springer. https://doi.org/10.1007/978-3-030-47244-3_2.

Pande, C. B. (2020b). Sustainable watershed development planning. In *Sustainable watershed development. Springer briefs in water science and technology*. Cham: Springer. https://doi.org/10.1007/978-3-030-47244-3_4.

Pande, C. B., & Moharir, K. (2018). Spatial analysis of groundwater quality mapping in hard rock area in the Akola and Buldhana districts of Maharashtra, India. *Applied Water Science, 8*(4), 1–17.

Pande, C. B., Khadri, S. F. R., Moharir, K. N., & Patode, R. S. (2017). Assessment of groundwater potential zonation of Mahesh River basin Akola and Buldhana districts, Maharashtra, India using remote sensing and GIS techniques. *Sustainable Water Resources Management*. https://doi.org/10.1007/s40899-017-0193-5. Published online 8 September-2017.

Pande, C. B., Moharir, K. N., Singh, S. K., & Dzwairo, B. (2019a). Groundwater evaluation for drinking purposes using statistical index: Study of Akola and Buldhana districts of Maharashtra, India, environment. *Development and Sustainability (A Multidisciplinary Approach to the*

Theory and Practice of Sustainable Development), 22, 7453. https://doi.org/10.1007/s10668-019-00531-0.

Pande, C. B., Moharir, K. N., Singh, S. K., & Varade, A. M. (2019b). An integrated approach to delineate the groundwater potential zones in Devdari watershed area of Akola district. *Maharashtra, Central India in Environment, Development, and Sustainability, 22*, 4867. https://doi.org/10.1007/s10668-019-00409-1.

Pandey, M., Zakwan, M., Sharma, P. K., & Ahmad, Z. (2018). Multiple linear regression and genetic algorithm approaches to predict temporal scour depth near circular pier in non-cohesive sediment. *ISH Journal of Hydraulic Engineering, 26*, 96–103.

Pathania, T., Bottacin-Busolin, A., Rastogi, A. K., & Eldho, T. I. (2019). Simulation of groundwater flow in an unconfined sloping aquifer using the element-free Galerkin method. *Water Resources Management, 33*(8), 2827–2845.

Prommer, H., Barry, D. A., & Davis, G. B. (2000). Numerical modelling for design and evaluation of groundwater remediation schemes. *Ecological Modelling, 128*(2–3), 181–195.

Psilovikos, A. (1999). Optimization models in groundwater management, based on linear and mixed integer programming. An application to a Greek hydrogeological basin. *Physics and Chemistry of the Earth (B), 24*(1–2), 139–144.

Psilovikos, A., & Tzimopoulos, C. (2004). Comparison of quadratic and non-linear programming (QP and NLP) optimization models in groundwater management. *Journal of Hydroinformatics, 6*(3), 175–185.

Rajanayaka, C., & Kulasiri, D. (2001). Investigation of a parameter estimation method for contaminant transport in aquifers. *Journal of Hydroinformatics, 3*(4), 203–213.

Reddy, J. N. (1993). *An introduction to the finite element method*. New York: McGraw-Hill.

Rogers, L. L., Dowla, F. U., & Johnson, V. M. (1995). Optimal field-scale groundwater remediation using neural networks and the genetic algorithm. *Environmental Science & Technology, 29*(5), 1145–1155.

Satavalekar, R. S., & Sawant, V. A. (2014). Numerical modelling of contaminant transport using FEM and meshfree method. *Advances in Environmental Research, 3*(2), 117–129.

Shrestha, S., Yao, T., & Adhikari, T. R. (2019). Analysis of rainfall trends of two complex mountain river basins on the southern slopes of the Central Himalayas. *Atmospheric Research, 215*, 99–115.

Stoppiello, M., Lofrano, G., Carotenuto, M., Viccione, G., Guarnaccia, C., & Cascini, L. (2020). A comparative assessment of analytical fate and transport models of organic contaminants in unsaturated soils. *Sustainability, 12*(7), 2949.

Sun, N. (1996). *Mathematical modeling of groundwater pollution*. New York: Springer.

Sykes, J., Pahwa, F., Lantz, S. B., & R. B. & Ward, D.S. (1982). Numerical simulation of flow and contaminant migration at an extensively monitored landfill. *Water Resource Research, 18*(6), 1687–1704.

Tikhamarine, Y., Souag-Gamane, D., Ahmed, A. N., Kisi, O., & El-Shafie, A. (2020). Improving artificial intelligence models accuracy for monthly streamflow forecasting using grey Wolf optimization (GWO) algorithm. *Journal of Hydrology, 582*, 124435.

Wang, H., & Anderson, M. P. (1982). *Introduction to groundwater modeling finite difference and finite element methods*. New York: W. H. Freeman.

Yin, J., Pham, H. V., & Tsai, F. T. C. (2020). Multiobjective spatial pumping optimization for groundwater management in a multiaquifer system. *Journal of Water Resources Planning and Management, 146*(4), 04020013.

Yu, F. X., & Singh, V. P. (1995). Improved finite element method for solute transport. *Journal of Hydraulic Engineering, 121*(2), 145–158.

Zakwan, M. (2018). Spreadsheet-based modelling of hysteresis-affected curves. *Applied Water Science, 8*(4), 101–105. https://doi.org/10.1007/s13201-018-0745-3.

Zakwan, M. (2019). Comparative analysis of the novel infiltration model with other infiltration models. *Water and Environment Journal, 33*(4), 620–632.

Zakwan, M. (2020). Revisiting maximum observed precipitation and discharge envelope curves. *International Journal of Hydrology Science and Technology, 10*(3), 221–229. https://doi.org/10.1504/IJHST.2020.107215.

Zakwan, M., & Ara, Z. (2019). Statistical analysis of rainfall in Bihar. *Sustainable Water Resources Management, 5*(4), 1781–1789.

Zakwan, M., Ahmad, Z., & Sharief, S. M. V. (2018). Magnitude-frequency analysis for suspended sediment transport in the Ganga River. *Journal of Hydrologic Engineering, 23*(7), 05018013.

Zeinali, M., Azari, A., & Heidari, M. M. (2020). Simulating unsaturated zone of soil for estimating the recharge rate and flow exchange between a river and an aquifer. *Water Resources Management, 34*(1), 425–443.

Zheng, G. D. B., & Andrews, C. B. (1991). Analysis of groundwater remedial alternatives at a superfund site. *Groundwater, 29*(6), 838–848.

Chapter 7
Modeling of Groundwater Level Using Artificial Neural Network Algorithm and WA-SVR Model

Shishir Gaur, Anne Johannet, Didier Graillot, and Padam Jee Omar

Contents

7.1 Introduction 129
7.2 Methodology 131
7.3 Gradient Descent with Momentum (GDM) 136
7.4 Performance Measures 137
7.5 Model Development 139
7.6 SVR-WA Model 139
7.7 Result and Discussion 141
7.8 Conclusion 143
References 149

7.1 Introduction

Water is an important natural resource without which life cannot imagine on the Earth (Shivhare et al. 2018). Groundwater has found beneath the Earth's surface in soil pores and fractures of the rocks (Moharir et al. 2017). It is one of the most important water resources. Groundwater is used in many purposes such as domestic, agricultural, and industrial (Omar et al. 2021). Depletion in the groundwater level is

S. Gaur · P. J. Omar (✉)
Department of Civil Engineering, Indian Institute of Technology (BHU), Varanasi, India

A. Johannet
École des mines d'Alès, Alès Cedex, France
e-mail: anne.johannet@mines-les.fr

D. Graillot
CNRS, Ecole Nationale Supérieure des Mines de Saint-Etienne, Saint-Etienne, France
e-mail: graillot@emse.fr

C. B. Pande, K. N. Moharir (eds.), *Groundwater Resources Development and Planning in the Semi-Arid Region*, https://doi.org/10.1007/978-3-030-68124-1_7

a significant engineering problem due to excess extraction of the groundwater (Omar et al. 2020). Therefore, proper and sustainable management of groundwater is tremendously important for current scenario and for future generation (Omar et al. 2019). To estimate the groundwater head accurately, groundwater modeling is needed. In the earlier studies, an Artificial Neural Network (ANN) was applied in the modeling of the groundwater as a strong tool (Coulibaly et al. 2001; Daliakopoulos et al. 2005). At present, ANNs have been very useful in an extensive range of applications/fields. The ANN model is capable to learn and answer the problem by pursuing several hypotheses in the parallel (Ahmad and Simonovic 2005; Anmala et al. 2000; Aitkenhead and Cooper 2008). It develops a memory which is able to associate a great number of input datasets which results a set of outputs. ANN can provide the accurate solutions to many of the complex models, which can be treated as a global approximation model (Cancelliere et al. 2002; Dogan et al. 2007; Karunanithi et al. 1994; Raman and Sunilkumar 1995). ANN model is the most excellent for the dynamic nonlinear modeling system (Sajikumar and Thandaveswara 1999). Advancement in the field of Artificial Intelligence (AI) provides the capability to fill the gaps of the water head measurements and prediction of the water heads. In hydrology and water science field, idea and useful applications of ANN model have been talked about by many scientist, researchers, and water resources engineers. Now-a-days, ANN technique is widely used in simulation of precipitation, forecasting of river flow (Thirumalaiah and Deo 1998; Kumar et al. 2004), prediction of the water quality parameters, and flood routing (Peters et al. 2006). ANN technique has been used in many areas of the water resources such as water quality, identification of groundwater contamination sources, simulation of the chemical oxygen demand (COD) reduction, groundwater potential zone (GPZ) mapping, etc.

This paper focuses a new technique for the management of groundwater by establishing a new computational approach for the optimization which utilizes artificial neural networks (ANNs). Performance of ANN was checked and prediction of groundwater head in the given terrain using precipitation data was done. In this method, artificial neural network has trained to predict the certain outcome of the groundwater head. In the training, precipitation data has been provided as an input, and using Levenberg–Marquardt (LM) algorithm, a training pattern was developed**.** As ANN is not a program, it learns to solve the problem by examples. Under supervised learning method, the ANN has "trained" on the datasets (input) having the known relationships.

The results suggest that the ANN approach is far better than traditional approaches in many means. A precise study was done to get the most favorable network of the model. Performance of all the cases has been studied and taken into the consideration while deciding the best network for the model.

7.2 Methodology

In this study, two models, i.e., feedforward neural network (FFNN) and support vector regression (SVR) have used for the comparative analysis. In the primarily work, one networks with various algorithms were analyzed and compared to find out the finest performing algorithms that can simulate and predict the groundwater head under acceptable limits. In all the cases, random iteration method has used in optimizing network structure. The wavelet support vector regression (WA-SVR) model has developed to find out the river water head. Results from both the models have been compared. Analysis by FFNN using various algorithms is shown by SVR. Brief description about FFNN, different algorithms, and WA-SVR is presented in following sections.

7.2.1 Feedforward Neural Networks (FFNN)

In the feedforward neural network, the network was structured in the form of layers. In this, dataset passes on from the initial layer (input) to the final layer (output) without using any feedback mechanism. FFNN has utilized in various issues as it is based on the error back propagation learning algorithm. This backpropagation algorithm adjusts the weights subjected to the Mean Square Error (MSE). The main benefit of FFNNs is that it is easy to deal, which permits it to approximate any kind of input and output model parameters (Hornik 1991; Hornik et al. 1989).

7.2.2 Artificial Neural Networks (ANNs)

Artificial Neural Network is a combination of three different layers. First one has input layer, second is hidden layer which can be more than one, and last one is output layer (Sudheer and Jain 2004). A schematic diagram representing the ANN model system has shown in Fig. 7.1. Main advantage of ANN is that without having any prior information of actual condition of the system, training has provided to the network (Cross et al. 1995). This training helps the network to find out the relationship between input and output. In this study, different ANN algorithms techniques have studied, which can be found here.

1. Levenberg-Marquardt (LM) training algorithm
2. The Resilient backpropagation Algorithm
3. Scaled conjugate gradient (SCG) backpropagation Algorithm
4. The Fletcher-Reeves Conjugate gradient backpropagation Algorithm
5. One-step secant (OSS) backpropagation
6. Conjugate gradient backpropagation Algorithm by Polak-Ribiere (CGP)
7. Gradient descent with momentum (GDM) backpropagation
8. Gradient descent with adaptive learning rate backpropagation (GDA)

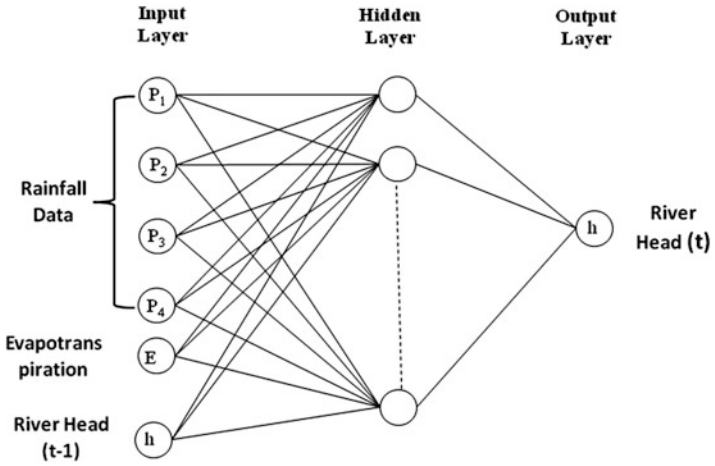

Fig. 7.1 Schematic diagram of ANN showing three layers

Proper selection of number of hidden layers is very significant step of ANN. Performance of ANN depends on the selection of ANN parameters and their precision. In the hidden layers (one or more than one), number of neurons affect the model computation time, accuracy, and learning rate of the model. If adequate neurons are available in the hidden layer, ANN network with one hidden layer may be used to approximate any function. Due to this feature of ANN, one hidden layer was used in this study. In hidden layer, total five neurons were used (Fig. 7.1).

At the start of iterations, initial weights were randomly allotted to the ANN model. Sigmoidal activation function is used for the computations, in order for an ANN to generate an output vector $Y = (y_1, y_2 \ldots y_p)$ that is as close as possible to the target vector $T = (t_1, t_2 \ldots t_p)$, a training process, also called learning. Training of the network is very important as it helps in finding out the best possible weight matrix and bias vectors for the network. This optimal weight matrix minimizes a predetermined error function that usually has the form

$$E = \sum\nolimits_p \sum\nolimits_p (y_i - t_i)^2$$

Training process of ANN requires active modification of the matrices (weight) and the bias vectors in such a way that the main function of minimizing the error can be achieved.

Training process will stop based on the particular maximum number of epochs or if the model performance gradient falls below the set minimum gradient.The training exercise of the model network will terminate when the least performance gradient falls below 10^{-10}, because the backpropagation Neural Network (BPNN) performance did not improve even if further training continues (Ghose et al. 2010; Hagan et al. 1996).

7.2.3 Algorithms

The training of a network is usually a minimization problem, the objective function being to obtain minimum mean square error. Hence, the training algorithms are an optimization technique, which help in fulfilling the objective function. For the present study, the supervised type of training has used. There are various algorithms for training the neural networks that are present in the literature, out of which few techniques have presented here.

7.2.4 The Levenberg-Marquardt Training Algorithm

The Levenberg-Marquardt (LM) training algorithm is a neural network program that has mostly used to revise the multilayer perceptron (MLP) weights and vector biases (Hagan and Menhaj 1994). The LM algorithm has developed for achieving the best solution to minimizing the problem. It is an optimization technique based on the classic Newton algorithm. In the algorithm learning process, it decreases the volume of oscillation. LM employs a rough calculation to the Hessian matrix within the following Newton such as weight update (Eq. 7.1):

$$z_{n+1} = z_n + \left[J^T J + \mu I\right]^{-1} J^T e \tag{7.1}$$

where,

z: Neural network weight;
J: Jacobian matrix;
μ: Scalar value that controls the learning exercise;
e: Residual error vector.

7.2.5 The Resilient BackPropagation Algorithm

The resilient backpropagation algorithm works as a local adaptive learning scheme. It fulfills the interesting batch learning in feedforward neural networks (FFNNs). The fundamental principle of this algorithm is the elimination of the detrimental effect of the size of the partial derivative on the weight step (Riedmiller and Braun 1993). Multilayer networks typically use sigmoidal activation function in the hidden layer. This function is a quashing function and should reach zero for larger input values. This causes a problem when using a steepest gradient algorithm to train the network, as it results in small weight changes even though they are far from the optimal values. To overcome these problems of small magnitude of partial derivatives, the

Resilient Backpropagation (RP) training algorithm is used. The application and uses of resilient back propagation to train neural networks applied to hydrological problems are notable (Cannon and Whitefield 2002).

7.2.6 The Scaled Conjugate Gradient Algorithm (SCG)

The standard SCG backpropagation algorithm modifies the weights in the steepest descent direction, the direction in which the performance function was decreasing more quickly. Performance function may not be necessarily provide the fastest convergence and often behaves badly on large-scale problems. The scaled conjugate gradient (SCG) algorithm defines the quadratic estimation to the error in the neighborhood of a point (Moller 1993). SCG is a second-order fast algorithm, which utilizes a step size scaling mechanism which evades time-consuming line search per learning iteration. SCG algorithm also helps in minimizing the multidimensional target function (Karmokar et al. 2012). The conjugate gradient method overcomes this problem by conducting a search along conjugate directions, which usually provides faster convergence than the steepest descent gradients.

7.2.7 The Fletcher-Reeves Conjugate Gradient Algorithm

Fletcher and Reeves (1964) develop this algorithm to achieve faster search which is a modification of standard conjugate gradient algorithm. Like the conjugate gradient algorithm, this algorithm starts out by searching in the steepest descent direction (negative of the gradient) on the first iteration (Eq. 7.2).

$$p_o = -g_o \tag{7.2}$$

where,

- g_o is the gradient,
- p_o is the initial search direction.

To find out the most favorable distance to move along the current search direction, a line search technique has performed (Eq. 7.3).

$$x_{k+1} = x_k + \alpha_k p_k \tag{7.3}$$

Here α_k is calculated by the equation given by (Eq. 7.4).

$$\alpha_k = \frac{g_k^T g_k}{p_k^T A p_k} \tag{7.4}$$

where,

g_k: The gradient,

$p_{k:}$ Search direction in the kth step;

A: The position matrix.

Gradient in the next step g_{k+1} is calculated using (Eq. 7.5).

$$g_{k+1} = g_k - \alpha_k A p_k \tag{7.5}$$

The next search direction was found out in such a way that it was conjugate to the earlier search directions. The common method for deciding the new search direction is to merge the new steepest descent direction with the earlier search direction (Eq. 7.6).

$$p_k = -g_k + \beta_k p_{k-1} \tag{7.6}$$

The procedure by which constant β_k was computed determines the method of conjugate gradient algorithm. For the Fletcher-Reeves Algorithm, the formula for β_k computation was (Eq. 7.7).

$$\beta_k = \frac{g_k^T g_k}{g_{k-1}^T g_{k-1}} \tag{7.7}$$

This is the ratio of the norm squared of the current gradient to the norm squared of the previous gradient. After calculation of new search direction, whole iteration starts from Eq. (7.4) and continues till optimum solution is obtained.

7.2.8 The One Step Secant (OSS) Backpropagation

OSS technique is an endeavor to overcome any barrier between the conjugate gradient algorithms and the Quasi Newton (secant) algorithms. This calculation does not store the entire Hessian matrix. It supposes that in every iteration, the earlier Hessian was the identity matrix [I]. This has an extra benefit that the new search direction can be determined without computing inverse matrices.

7.2.9 Conjugate Gradient Algorithm by Polak and Ribiere

Polak and Ribiere presented the conjugate gradient algorithm in another form. They proposed a new technique for the computation of β_k which was used in the equation number 6 (Fletcher-Reeves algorithm for search direction in each iteration).

$$\beta_k = \Delta g T_k - 1 g_k g T_k - 1 g_k - 1 \tag{7.8}$$

This can be explained as the inner product of the previous change in the gradient with the existing gradient divided by the norm squared of the earlier gradient.

7.3 Gradient Descent with Momentum (GDM)

Gradient descent with momentum, executed via traingdm, permits the set-up to react not only to the local gradient, but also to recent trends in the error surface. The mechanism of GDM acts like a low-pass filter, in which momentum permits the set-up to overlook the minute features in the error surface. Without momentum, the set-up can get stuck in a shallow local minimum while with momentum the system can slide through such a minimum.

7.3.1 Gradient Descent with Adaptive Learning Rate Backpropagation

In general, the learning rate remains constant during the training in typical steepest descent. Appropriate setting of the learning rate is very important as the performance of the algorithm is depending on the learning rate. Depending on the learning rate algorithm behaves, for example in case of small learning rate, the algorithm takes time to converge while in case of high learning rate, the algorithm may oscillate and became unstable. However, it is very tough to fix the most favorable learning rate before the training. The optimal learning rate varies during the training exercise, as the algorithm progresses across the performance surface. Thus, a versatile learning rate endeavors to keep the learning step size as extensive as possible while maintaining stable learning. The learning rate was made receptive to the multifaceted nature of the neighborhood error surface. Adaptive learning rates have need of a few modifications in the training method adopted by the trained. In the first step, output of the initial network and error was computed. At each epoch, new weights and vector biases were calculated using the present learning rate. This way, new outputs and errors have been came out and incorporated in the next iterations to get the optimal solution.

7.4 Performance Measures

To find out the most favorable network structure, performance of the calibrated network model has assessed. This model performance evaluation has done using the quantitative error metric. To assess the efficiency of the network, the following performance measures have used.

1. Nash–Sutcliffe Efficiency Index (E_f)
2. Correlation Coefficient (R)

7.4.1 Nash–Sutcliffe Efficiency Index (E_f)

Before using any neural network technique in the hydrologic model, calibration of the model is essential. Conventionally, various methods are available to measure the residual error of the model. Root Mean Square Error (RMSE), correlation coefficient, and Standard Error of Estimate (SEE) are the most widely used to measure the goodness of fit on the model calibration and the error of a model in predicting the quantitative data (Eq. 7.9). The correlation coefficient is theoretically valid only to the linear models that include an intercept. This method is based on certain assumptions as it supposes that the model tested is being unbiased. Here, unbiasing means summation of the errors in the model is zero.

Due to this limitation of the correlation coefficient, in 1971, Nash and Sutcliffe suggested another goodness of fit index. This index is commonly known as the *efficiency index*. The Nash–Sutcliffe Efficiency Index (also called Coefficient of Efficiency) gives a suggestion of how fine a model is at predicting the values away from the mean. This criterion can give some sign of how fine the model will act in either high or low magnitudes of the observed

event. E_f value closer to 1, the modeled network has better fit. Nash–Sutcliffe Efficiency Index is given by

$$E_f = 1 - \frac{\sum_{i=1}^{n} (y_i - x_i)^2}{\sum_{i=1}^{n} (y_i - \overline{x})^2} \tag{7.9}$$

where,

y_i and x_i are the actual and obtained values of the output,
$\overline{y}$ is the mean of actual output values.

Coefficient of Efficiency may vary from $-\infty$ to 1. Efficiency equal to one ($E_f = 1$) indicates an ideal match between the modeled parameter to the observed dataset of the same parameter. In the same manner, efficiency equal to zero ($E_f = 0$)

represents that the model forecasts are accurate as the average value of the observed data. Efficiency below zero ($E_f < 0$) corresponds the observed average value is a better predictor than the model computed. For the better prediction of the model output, the model efficiency must be close to 1 (as possible), this represents that the model is accurate.

7.4.2 *Coefficient of Determination* ($\mathbf{R^2}$)

The coefficient of determination, r^2, is another method to assess the performance of the predictive models (Kendall 1938). It is own advantage as it gives the proportion of the fluctuation of one parameter that is predictable from the other parameter. Coefficient of determination helps in finding out the certainty in the parameter. It suggests and helps in the predictions of the network values from a certain pattern. The coefficient of determination corresponds to the percent of the dataset that is very close to the best fit line. For better understanding, let us take $r = 0.95$ then $r^2 = 0.90$, it suggests that 90% of the total variation in y can be explained by the linear relationship between x and y (as expressed by the regression equation). The remaining 10% of the total variation in y remains unexplained.

The correlation coefficient (R) between the model outputs and the targets are a measure of the variations in the target outputs. The equation of correlation coefficient is presented in following (Eq. 7.10).

$$R = \frac{\sum_{i=1}^{N} (x_i - \bar{x})(y_i - \bar{y})}{\sqrt{\sum_{i=1}^{N} (x_i - \bar{x})^2} \sqrt{\sum_{i=1}^{N} \left((y_i - \bar{y})^2 \right.}} \tag{7.10}$$

where,

y_i and x_i are actual and obtained values of output,
$\bar{y}$ is the mean of actual output values.

The value of correlation coefficient varies from -1 to $+1$. Highest value ($+1$) indicates a linear equation that depicts the direct relationship between X and Y. In this linear equation, all the data points lying on a straight line for which Y changes as X changes (Proportionally). Lowest value (-1) represents that all the data points also lie on the straight line for which Y changes as X changes but inversely proportional. A zero value indicates that there is no linear relationship between both the variables X and Y. Coefficient of determination can be determined by squaring the correlation coefficient.

7.5 Model Development

In the model development, the available dataset were separated into two subsets. One dataset were used in the training of the model and the other data set kept separately for testing purposes. When the data (number of patterns) available are more, another subset may be taken as a validation subset. The training set provided to the network decides the performance of the network. Larger the distribution of parameters in the training set, better will it help in generalizing the process. As there is no pattern was observed in the data set, validation part cannot be done separately.

7.5.1 Dataset

In the present work, one case has analyzed with five inputs including one input related to previous river head data. For the input data, daily observations data were available from 1st January 1992 to 31st December 2013. Dataset was divided into two separate parts, in the ratio of 70:30. Major part of the dataset was used for training purposes and the minor was used in the model testing. The distribution of the dataset is presented below.

- Dataset used for model training: 1st January 1992 to 1st August 2007.
- Dataset used for model testing Set: 2nd August 2007 to 31st December 2013.

7.6 SVR-WA Model

The wavelet support vector machine (WA-SVR) model has conceptualized for forecasting the river water level at the desire location. The details of the wavelet decomposition time series and details regarding the input parameters have been presented in the following sections. Structure of the WA-SVR model is presented in the Fig. 7.2.

WA-SVR models have created by uniting the decomposing capacity of the wavelet with support vector machines (SVM). For this, wavelet toolbox of MATLAB has used. The input data of daily rainfall (P) and evapotranspiration (E) in WA-SVR models have decomposed into subseries component using the Harr transform (D's and A's symbolize details and approximations of the subseries, respectively). D's correspond to the detailed frequency series and time series of the input dataset. The original time series has decomposed into lower resolution components by iterating the decomposition of successive approximation signals. In the present study, total eight resolution levels were used. All the subseries coefficients contain the data about the original time-series of the particular model param-

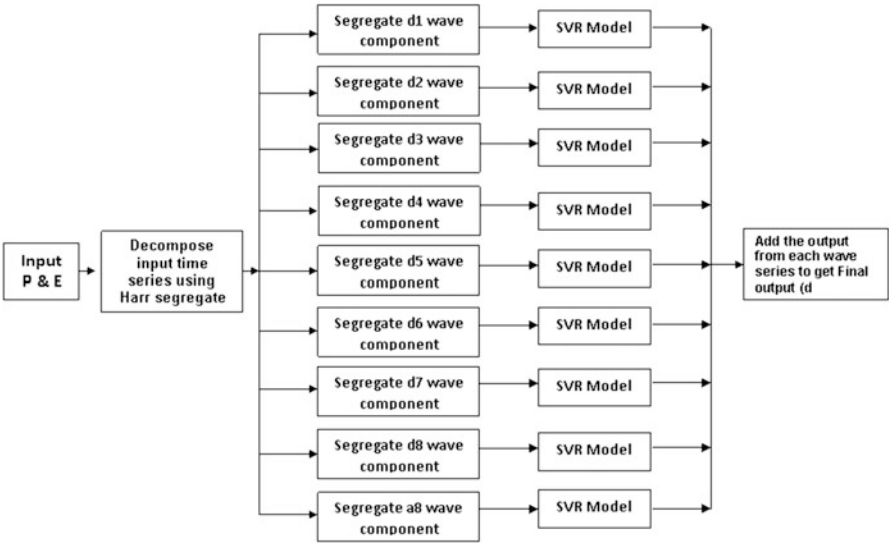

Fig. 7.2 Structure of WA-SVR model

eter. Therefore, all the parameters of the subseries were used to give input to the SVR model. Figure 7.3 shows the wavelet decomposition series of daily rainfall (P) and evapotranspiration (E) data of the study area. Here, $A8$ subseries represents the low-frequency dataset and $D1$, $D2$, $D3$, $D4$, $D5$, $D6$, $D7$, and $D8$ were the eight level decomposed subseries in sequence when the data continuously pass four times through the high-pass filters. Similarly, the data at other stations have decomposed using Harr wavelet transform as shown in Figs. 7.4 and 7.5. All figures show that precipitation variation has been varying at all the stations. Figure 7.2 shows the input and output structure of the proposed WA-SVR model. The subseries $A8$, $D1$, $D2$, $D3$, $D4$, $D5$, $D6$, $D7$, and $D8$ of rainfall (P) and evapotranspiration (E) were set apart for each well and standardized to given as input to the SVR models as shown in Fig. 7.5. The proposed WA-SVR model has tested for different input combinations of the standardized dataset of the decomposed time series separately. The output (predicted river water head) was the summation of the outputs from each decomposed time series. It has compared with the observed river water level at different locations. The optimum values of the SVR parameters C and γ has selected by a trial and error procedure. The best WA-SVR model was the one, which has the best performance criteria. It has chosen by training and testing the SVR model with different input data time series to all the parameters. The best performing WA-SVR model has chosen among the different input combinations which provide the best performance criteria.

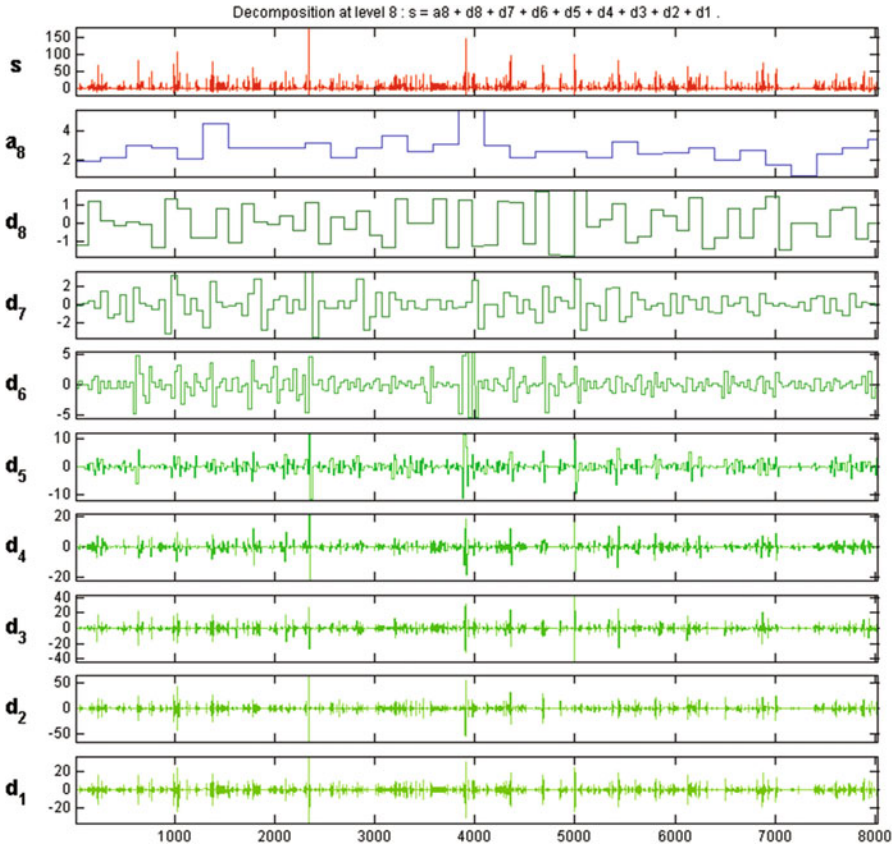

Fig. 7.3 Wavelet decomposition series of precipitation at study area Tharaux

7.7 Result and Discussion

From the results, it has observed that the Artificial Neural Networks (ANNs) were simulated the river water head and also predicted the water heads in the river with reasonable accuracy, whereas WA-SVR model's results were more accurate. On comparison of the predicted river water heads with input data, FFNN trained with Gradient descent with momentum backpropagation and Gradient descent with adaptive learning rate backpropagation taken five inputs has formed well above all other algorithms. It was observed that all the networks have converged at respective same points in order to achieve corresponding best error measures. Figures 7.6, 7.7, 7.8, 7.9, 7.10, 7.11, 7.12, and 7.13 show the correlation graph for various algorithms. Figure 7.13 shows the correlation coefficient values for various algorithms.

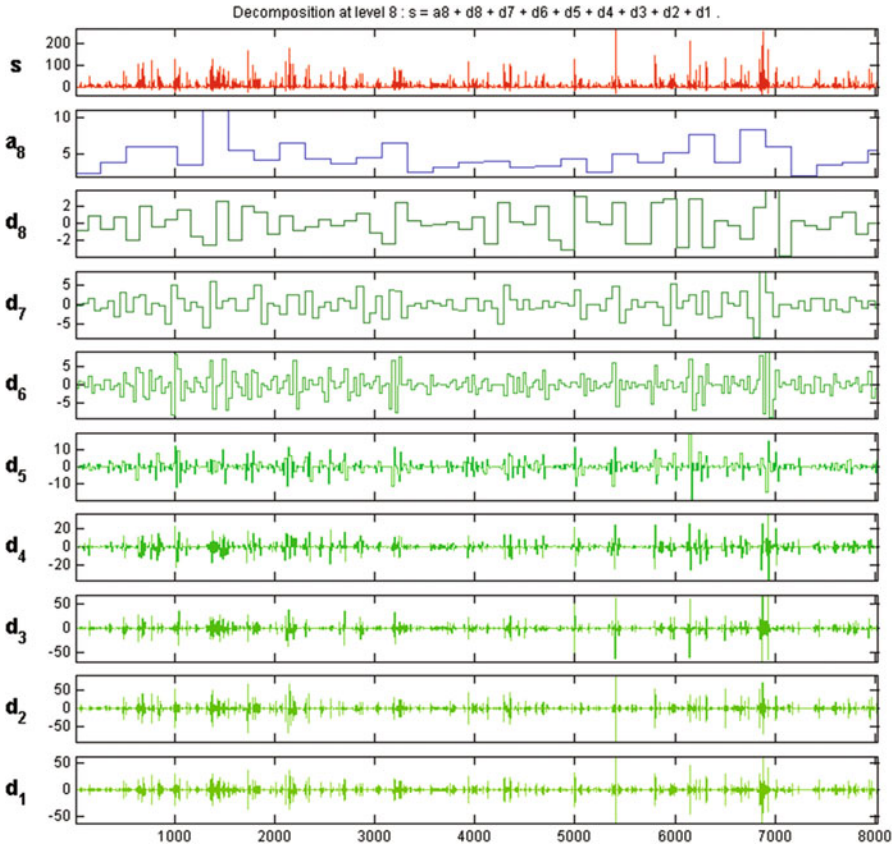

Fig. 7.4 Wavelet decomposition series of precipitation at study area SénéEhas

It has observed that momentum backpropagation and gradient descent with adaptive learning rate backpropagation have found well above all other algorithms. Figures 7.14 and 7.15 show the comparison between actual and simulated values by all the algorithms of FFNN. It has also observed that Scaled conjugate gradient backpropagation and One-step secant back propagation (OSS) performed less efficiently. Figure 7.16 shows the performance measures (corrleation) for FFNN and WA-SVR. From the study, it has also concluded that in case of FFNN, optimal number of neurons range may be fixed in and around the number of inputs being fed to the neural network that each neuron dominantly influences a particular input in the network. The study shows the efficiency of ANNs and WA-SVR in modeling the daily water level in the river. The main part of the modeling is the selection of parameters, as inputs for the network, and it must be done very carefully. The network inputs must be significant to the physical independent influence of each

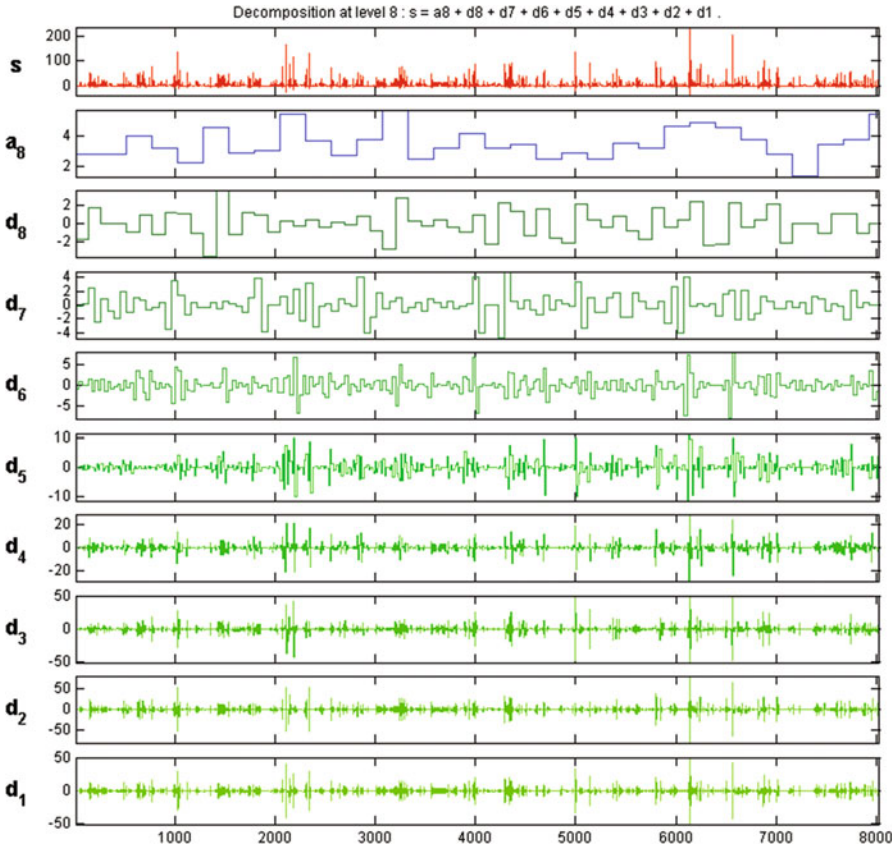

Fig. 7.5 Wavelet decomposition series of precipitation at study area Croix

parameter over the output. Study concludes that wavelet decomposition-based SVR has found superior in comparison of ANN model. Performance measures, which are presented in Fig. 7.16, show that WA-SVR model is very efficient for the prediction of the river water level.

7.8 Conclusion

In this work, the ability of the Artificial Neural Network models with different networks to simulate water head fluctuations has been studied and analyzed. Furthermore, the results of different algorithms were also analyzed. Therefore, Artificial Neural Network (ANNs) computing has been considered as a successful technique

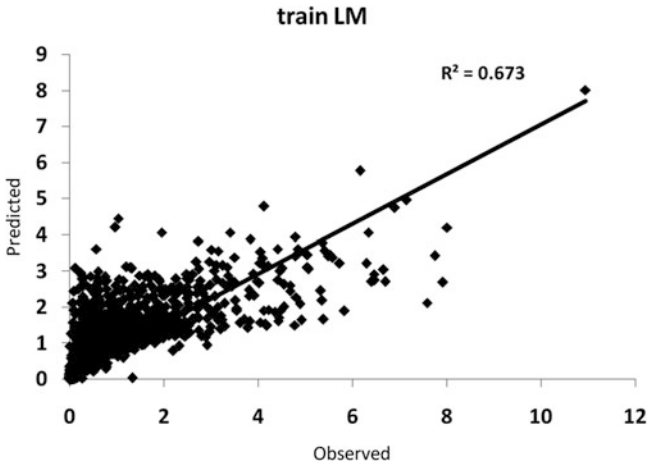

Fig. 7.6 Showing the performance measures for L-M backpropagation algorithm

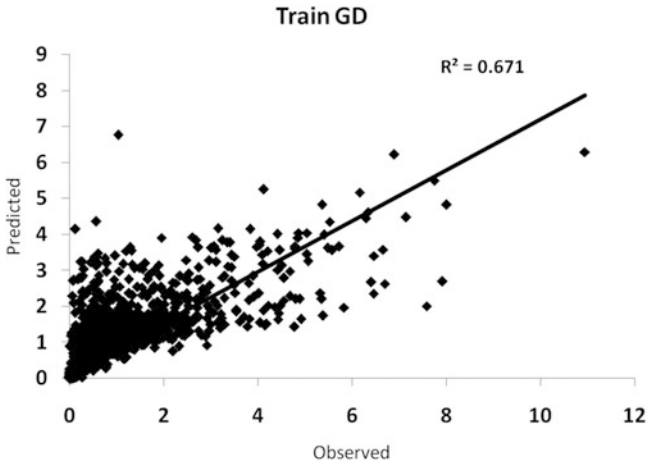

Fig. 7.7 Showing the performance measures for Gradient descent algorithm

to apply for the monthly groundwater head simulation from the available groundwater data. On comparison of river water levels predicted with input data, FFNN trained with Gradient descent with momentum backpropagation and Gradient descent with adaptive learning rate backpropagation taken five inputs has formed well above all other algorithms. It has been also observed that the Scaled conjugate gradient backpropagation and One-step secant backpropagation performed less efficiently. The most appropriate method for the networks trained with the Levenberg-Marquardt (LM) approach as it demonstrated the most precise

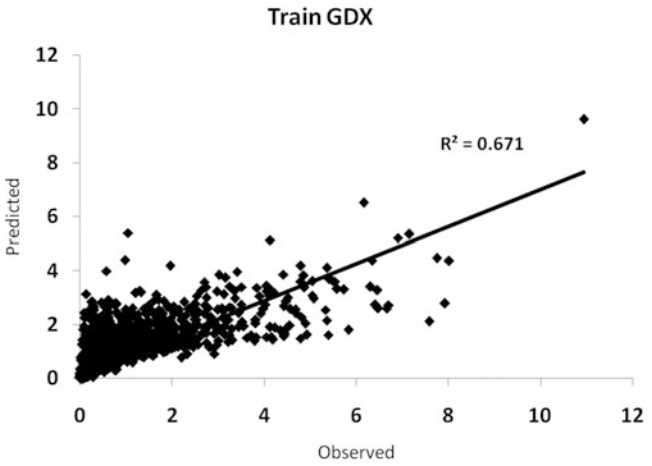

Fig. 7.8 Showing the performance measures for Gradient descent with momentum and adaptive learning rate backpropagation algorithm

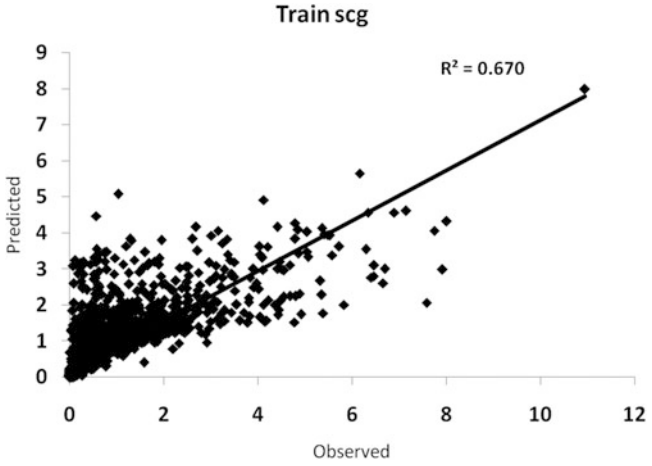

Fig. 7.9 Showing the performance measures for Scaled conjugate gradient backpropagation algorithm

simulations of the groundwater heads. From the results, it can be concluded that, once the network model satisfactorily trained and calibrated that wavelet decomposition-based SVR is found superior in comparison of the ANN models. Performance measures, which are presented in Fig. 7.16, show that WA-SVR model is very efficient for the precise prediction of the river water head. It was also observed from the results that the ANNs can simulate and predict the water heads

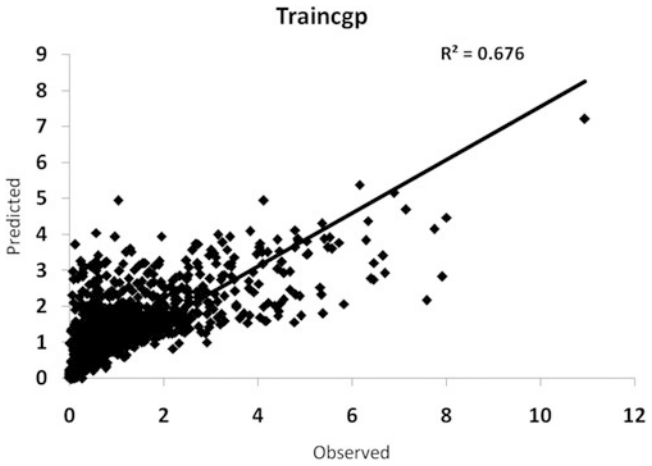

Fig. 7.10 Showing the performance measures for Conjugate gradient backpropagation with Polak-Ribiére update algorithm

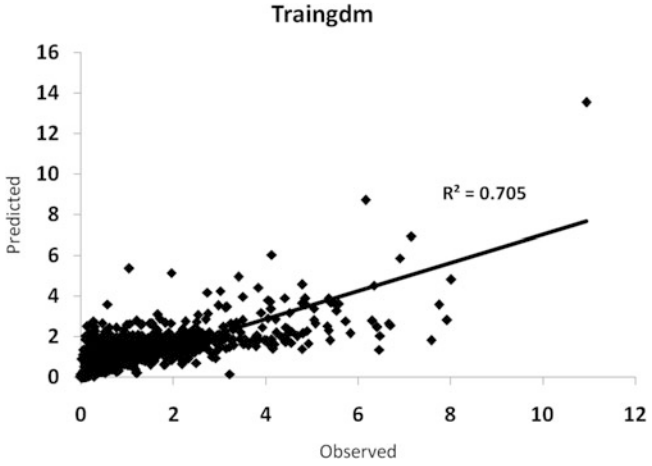

Fig. 7.11 Showing the performance measures for Gradient descent with momentum backpropagation algorithm

in the river with reasonable accuracy, whereas WA-SVR model's results are more accurate. The results derived from the study were quite satisfactory and justified that artificial neural networks (ANNs) can be an advantageous simulation technique to utilize in the field of groundwater hydrology.

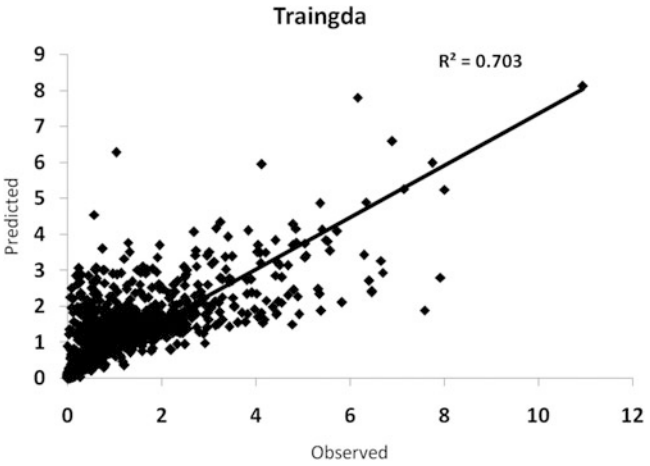

Fig. 7.12 Showing the performance measures for Gradient descent with adaptive learning rate backpropagation algorithm

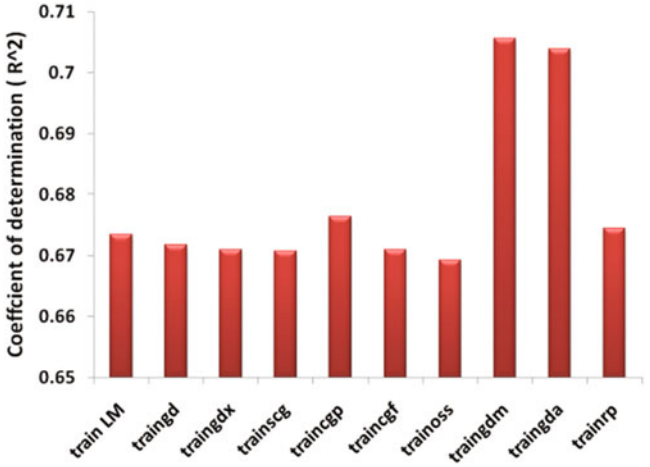

Fig. 7.13 Showing the performance measures (correlation) for different methods

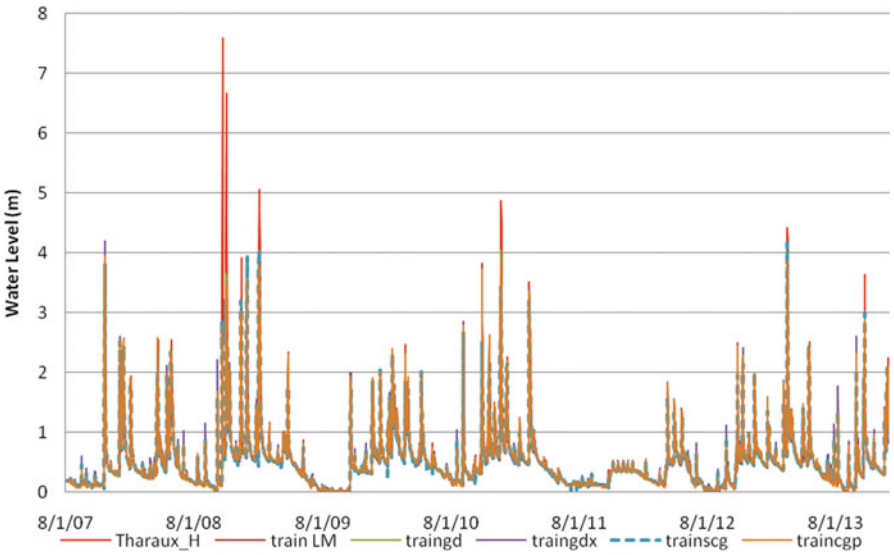

Fig. 7.14 Showing the performance measures (correlation) for different methods

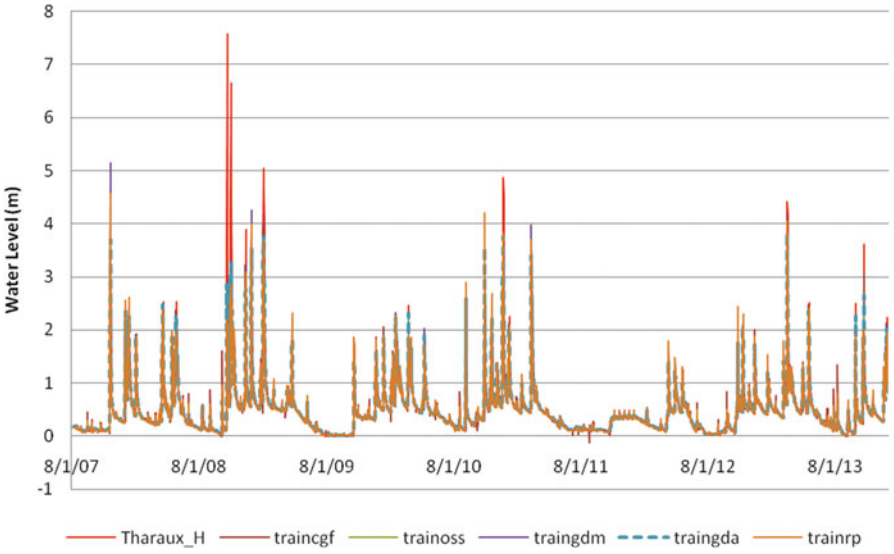

Fig. 7.15 Showing the performance measures (correlation) for different methods

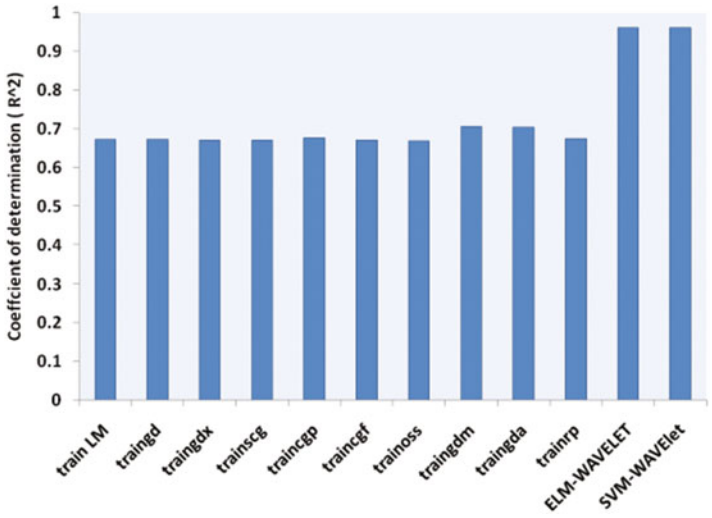

Fig. 7.16 Showing the performance measures (correlation) for different methods

References

Ahmad, S., & Simonovic, S. P. (2005). An artificial neural network model for generating hydrograph from hydro-meteorological parameters. *Journal of Hydrology, 315*(1–4), 236–251.

Aitkenhead, M. J., & Cooper, R. J. (2008). Neural network time series prediction of environmental variables in a small upland headwater in NE Scotland. *Hydrological Processes: An International Journal, 22*(16), 3091–3101.

Anmala, J., Zhang, B., & Govindaraju, R. S. (2000). Comparison of ANNs and empirical approaches for predicting watershed runoff. *Journal of Water Resources Planning and Management, 126*(3), 156–166.

Cancelliere, A., Giuliano, G., Ancarani, A., & Rossi, G. (2002). A neural networks approach for deriving irrigation reservoir operating rules. *Water Resources Management, 16*(1), 71–88.

Cannon, A. J., & Whitfield, P. H. (2002). Downscaling recent streamflow conditions in British Columbia, Canada using ensemble neural network models. *Journal of Hydrology, 259*(1–4), 136–151.

Coulibaly, P., Anctil, F., Aravena, R., & Bobée, B. (2001). Artificial neural network modeling of water table depth fluctuations. *Water Resources Research, 37*(4), 885–896.

Cross, S. S., Harrison, R. F., & Kennedy, R. L. (1995). Introduction to neural networks. *The Lancet, 346*(8982), 1075–1079.

Daliakopoulos, I. N., Coulibaly, P., & Tsanis, I. K. (2005). Groundwater level forecasting using artificial neural networks. *Journal of Hydrology, 309*(1–4), 229–240.

Dogan, D., Isik, S., Toluk, T., & Sandalci, M. (2007). Daily streamflow forecasting using artificial neural networks. In *International Congress on River Basin Management, River Basin Flood Management* (Chap. IV, pp. 448–459).

Fletcher, R., & Reeves, C. M. (1964). Function minimization by conjugate gradients. *Computer Journal, 7*, 149–154.

Ghose, D. K., Panda, S. S., & Swain, P. C. (2010). Prediction of water table depth in western region, Orissa using BPNN and RBFN neural networks. *Journal of Hydrology, 394*(3-4), 296–304.

Hagan, M. T., & Menhaj, M. B. (1994). Training feedforward networks with the Marquardt algorithm. *IEEE Transactions on Neural Networks, 5*(6), 989–993.

Hagan, M. T., Demuth, H. B., & Beale, M. (1996). *Neural network design, Thomson learning*. Noida: Vikas Publishing House.

Hornik, K. (1991). Approximation capabilities of multilayer feedforward networks. *Neural Networks, 4*(2), 251–257.

Hornik, K., Stinchcombe, M., & White, H. (1989). Multilayer feedforward networks are universal approximators. *Neural Networks, 2*(5), 359–366.

Karmokar, B. C., Mahmud, M. P., Siddiquee, M. K., Nafi, K. W., & Kar, T. S. (2012). Touchless written English characters recognition using neural network. *International Journal of Computer & Organization Trends, 2*(3), 80–84.

Karunanithi, N., Grenney, W. J., Whitley, D., & Bovee, K. (1994). Neural networks for river flow prediction. *Journal of Computing in Civil Engineering, 8*(2), 201–220.

Kendall, M. G. (1938). A new measure of rank correlation. *Biometrika, 30*(1/2), 81–93.

Kumar, D. N., Raju, K. S., & Sathish, T. (2004). River flow forecasting using recurrent neural networks. *Water Resources Management, 18*(2), 143–161.

Moharir, K., Pande, C., & Patil, S. (2017). Inverse modeling of Aquifer parameters in basaltic rock with the help of pumping test method using MODFLOW software. *Geoscience Frontiers, 8*, 1385–1395.

Moller, H. (1993). A scaled conjugate gradient algorithm for fast supervised learning. *Neural Networks, 6*(4), 525–533.

Nash, J. E., & Sutcliffe, J. V. (1971). River flow forecasting through conceptual models. Part 1: A discussion of principles. *Journal of Hydrology, 10*(3), 282–290.

Omar, P. J., Gaur, S., Dwivedi, S. B., & Dikshit, P. K. S. (2019). Groundwater modelling using an analytic element method and finite difference method: an insight into lower ganga river basin. *Journal of Earth System Science 128*(7), 195

Omar, P. J., Gaur, S., Dwivedi, S. B., & Dikshit, P. K. S. (2020). A modular three-dimensional scenario-based numerical modelling of groundwater flow. *Water Resources Management 34*(6), 1913–1932.

Omar P.J., Gaur S., Dwivedi S.B., & Dikshit P.K.S. (2021) Development and Application of the Integrated GIS-MODFLOW Model. In: Gupta P.K., Bharagava R.N. (eds) Fate and Transport of Subsurface Pollutants. *Microorganisms for Sustainability*, vol 24. Springer, Singapore. https://doi.org/10.1007/978-981-15-6564-9_16

Peters, R., Schmitz, G., & Cullmann, J. (2006). Flood routing modelling with artificial neural networks. *Advances in Geosciences, 9*, 131–136.

Raman, H., & Sunilkumar, N. (1995). Multivariate modelling of water resources time series using artificial neural networks. *Hydrological Sciences Journal, 40*(2), 145–163.

Riedmiller, M., & Braun, H. (1993). A direct adaptive method for faster backpropagation learning: The RPROP algorithm. In *IEEE International Conference on Neural Networks* (pp. 586-591).

Sajikumar, N., & Thandaveswara, B. S. (1999). A non-linear rainfall–runoff model using an artificial neural network. *Journal of Hydrology, 216*(1–2), 32–55.

Shivhare, N., Rahul, A. K., Omar, P. J., Chauhan, M. S., Gaur, S., Dikshit, P. K. S., & Dwivedi, S. B. (2018). Identification of critical soil erosion prone areas and prioritization of micro-watersheds using geoinformatics techniques. *Ecological engineering, 121*, 26–34.

Sudheer, K. P., & Jain, A. (2004). Explaining the internal behaviour of artificial neural network river flow models. *Hydrological Processes, 18*(4), 833–844.

Thirumalaiah, K., & Deo, M. C. (1998). River stage forecasting using artificial neural networks. *Journal of Hydrologic Engineering, 3*(1), 26–32.

Chapter 8
Development of Conceptual Model and Groundwater Flow Modeling Using GMS Software: A Case Study for Dharsiwa Block, Chhattisgarh, India

Aman Kumar Bohidar and Ishtiyaq Ahmad

Contents

8.1 Introduction 151
8.2 Materials and Methodology 153
8.3 Results and Discussion 158
8.4 Conclusion 161
References 163

8.1 Introduction

Development of a conceptual model gives an insight to the field problem and also acts as a bridge between modeler, end user, code developer, and domain experts. It tells the details about the facets of the model and its usage in different areas of interest. Diligent work can give more precise results and can depict the field conditions in a more accurate way. Cognizance of the boundary conditions with proper literature review helps in getting an easier way of simulation. According to Zhou and Herath (2017), single layer model is enough for determining the water balance, for practical applications three-layer model and five-layer model for aquitards representation. Commendable work has been done by Enemark et al. (2019), where authors have compared alternative multiple models in various scenarios and pertaining hindrances. Different authors have taken different parameters

A. K. Bohidar · I. Ahmad (✉)
Department of Civil Engineering, National Institute of Technology Raipur, Raipur, Chhattisgarh, India
e-mail: iahmad.ce@nitrr.ac.in

C. B. Pande, K. N. Moharir (eds.), *Groundwater Resources Development and Planning in the Semi-Arid Region*, https://doi.org/10.1007/978-3-030-68124-1_8

for the development of the conceptual model, Keupers and Willems (2017) took biological oxygen demand (BOD), dissolved oxygen (DO), nitrate, ammonia, and temperature as main parameters. Groundwater flow is affected by the head of groundwater and also by the type of pores in the media. In case there are pores but the pores are not interconnected, then it may cause hindrance in groundwater flow. Whereas effective porosity helps in easy flow of fluid and transmits contaminant with ease (Ginting 2005). When contaminants get infiltrated into the ground because of fractures, faults, or pores, then it causes multiphase flow to occur (Fumagalli et al. 2016; Moharir et al. 2017). Multiphase flow occurs because of anthropogenic activities, effluent discharged from industries into low-lying areas or landfill areas which percolate down to groundwater, or because of the fertilizers used in crop fields. Groundwater is a vital resource and judicious use of groundwater can help us improve this resource both qualitatively and quantitatively. Conceptual model helps in the determination of the future conditions and unknown parameters which are difficult to measure in the field (Almasri and Kaluarachchi 2007; Khadri and Pande 2016).

Many factors make detection of groundwater movement study a tedious job because of the heterogeneity involved and multiphase flow. A Conceptual model is the nitty-gritty for the study of a field problem and is prerequisite in most cases for further research work. Many authors have approached with different techniques for different purposes of making conceptual model (Gelhar et al. 1992). Conceptual model is also used for the transport modeling and it was found that dispersity increases with scale, accounting for nonuniform flow effects and without the arbitrary assumption of geological layers. In this particular paper by Gelhar et al. (1992), they provided with various values for dispersity for different field scales. In other findings, Robinson et al. (2015) did a study to carry out benefits, purpose, and definition of the conceptual model by the experts in that domain. The zest of the paper was that conceptual model is the simulation of the real-world problem which can be studied and proper solutions can be derived. Conceptual model can be developed using isotopic, hydrochemical, and hydrogeological approach (Kpegli et al. 2018). Stable isotopes can be used to detect the recharge zones in the ground. For simulating, the movement of nitrate in groundwater method of characteristics was used in one previous study (Molnar and Viraraghavan 1990). In this particular paper, it was assumed that the hydraulic gradient is the only driving mechanism for the fluid flow. The calculated concentration of nitrate form simulation is used for future prediction of nitrate concentration. After the development of conceptual model, upscaling can be performed. Various authors have used different methods for upscaling. Adaptive numerical homogenization was used by Singh et al. (2017). JHomogenizer is a computational tool developed by Amaziane and Koebbe (2006) for upscaling of permeability of both heterogeneous and porous media. Upscaling is substituting a fine scale region to a coarse scale region by applying a suitable technique (Eichel et al. 2005; Pande et al. 2018, 2019; Moharir et al. 2020). A Numerical method like finite element method for conceptual model development and upscaling can also be used (Ma and Zabaras 2011). Singhal and Goyal (2011) in

their analysis used spatial distribution of recharge rather than the average value of recharge which is normally obtained from the water budget.

In this study, conceptual model has been developed using GMS and future works that can be done on that model have been shown. The inputs given to the model have been tried to make it more realistic to get exact field conditions. The layer thickness has taken from Central groundwater Board and a few data have been taken from Groundwater year book of Chhattisgarh, (2015). For validation purpose, wells water head has been used for the estimation of groundwater flow modeling.

8.2 Materials and Methodology

8.2.1 Study Area

Instead of taking whole Dharsiwa block which is of 650 km^2 for study purpose, we took a square grid of 2 km size in the North Dharsiwa which contains industries, paddy fields, and small villages. Hence all aspects for the chances of nitrate contamination are covered in this grid. The study area is located in between latitude of 21°27′25″N to 21°22′0″N and longitude of 81°37′12″E to 81°44′24″E. The total area of the study site is 100 Km^2. The case study area is shown in Fig. 8.1. During a visit to the case study area, some questions were asked to local farmers and residents of the area. Nearby industries included steel industry, rubber industries, sponge iron industries, and power plants. In some places, food processing industries were also there. All these industries contaminate the water bodies by their industrial sewage and hence chemical gets discharged into the water, causing eutrophication and algae formation.

Dharsiwa block is surrounded by paddy field from all sides and the use of pesticides and anthropogenic activities are the main reasons for the nitrate contamination (Yadav 2012). In an important study done by Yao et al. (2015), tracers were used to get actual information about the recharge sources. However, the geology of the area consists of Chandi formation (limestone and dolomite), which has effective porosities and can transmit contaminants easily. This is the main cause of the easy transport of contaminant throughout the area (Chen 2006). The local farmers added that they use pesticides in their fields namely, Urea, Potash, Gromor, Rakha (Quizalofop ethyl 5%), Superphosphates, Zinc, etc. These chemicals during the farming process infiltrate into the ground through the transplanting method employed during rice planting. Locations of wells were determined and their depths were also measured during the visit to the area. Lakes/ponds had eutrophication as a common scenario there. Kharun River flows in the Dharsiwa block and it is one of the major rivers of Chhattisgarh. Industries have polluted the river nonchalantly and no remedial measures are being taken by concerned persons. Hence, nitrate has many sources and its transport becomes easy because of the sedimentary rocks present there. Although dispersion is one of the important parameters taken by many authors for groundwater modeling (Eberhard 2004; Le Borgne et al. 2011),

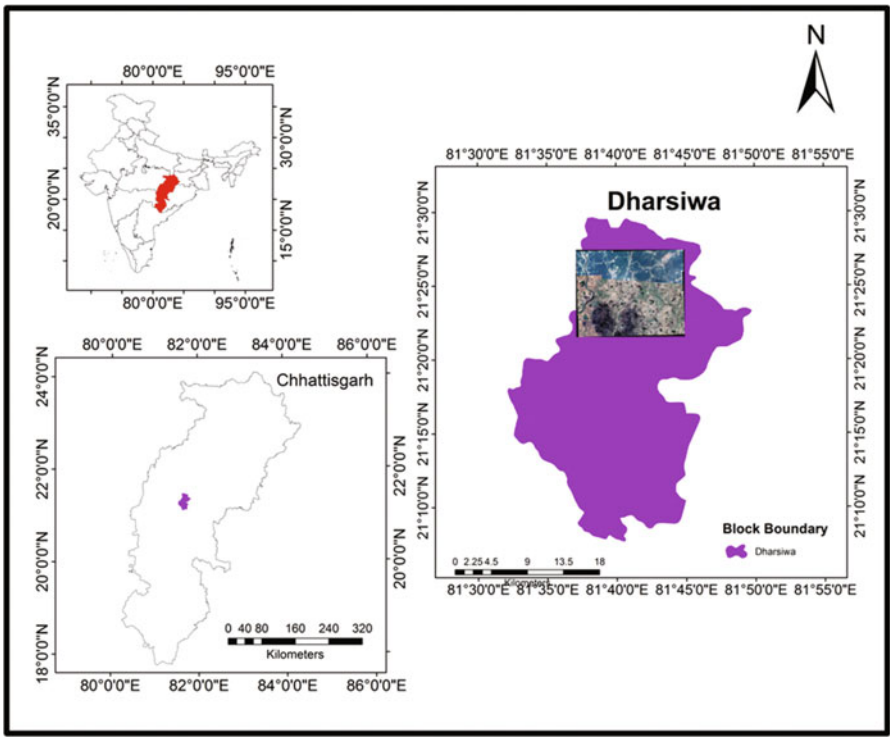

Fig. 8.1 Location map of study area

however, Vermeulen et al. (2006) in their research showed the importance of hydraulic head and conservation of continuity. Hence, in this study also more importance is given to the hydraulic head.

8.2.2 Digitization and Boundary Conditions

The first step for the development of conceptual model is the digitization of study area. Google earth images of the study area were taken. Small images were taken to bring each and every detail in the image and then mosaicked, after Georeferencing, to cover the whole area of 100 km^2 in the ArcGIS software. The concerned area was digitized in the ArcGIS.

Also, grids were created in ArcGIS to distribute the whole area in small areas of 2 km^2. The map with grids is shown in Fig. 8.2. The gridded map was then analyzed with proper latitude and longitude. During site visit of the area, exact well locations were noted and water levels were measured for future validation purpose.

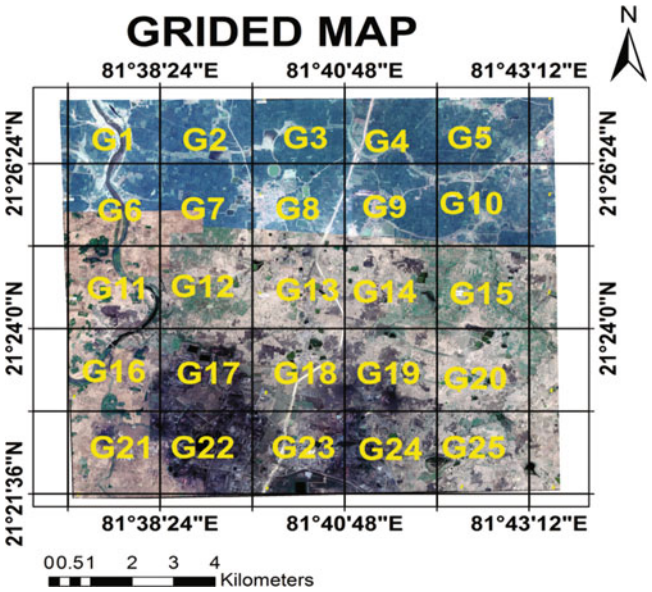

Fig. 8.2 2 × 2 km grids created in ArcGIS for study area

The digitized shape files which include river, drains, wells, ponds, and boundary of Dharsiwa were then imported to GMS. After importing the shape files, boundary of the model is created with proper boundary condition. In the selected study area, Kharun River was considered as a specific head.

8.2.3 Sources and Sinks Description

In the model under the source and sinks coverage, all the drains, specific head, ponds, and wells were defined. The bottom elevation of the drains is taken from Google earth pro. The flow rate of the wells is taken from Central ground water board (2016). The average river depth was taken as 1 m and an average depth of pond was assumed to be 0.6 m. These depths were assumed after the site visit and doing a survey around the area. The well flow rate is taken as 17.28 m^3/day. These data were provided from CGWB for Dharsiwa block. All the ten wells in the study area have been assumed to have the same flow rate. All the major ponds in the area have been given a general head value.The head stage value in ponds has been taken after adding the elevation value from google earth which gives the bottom surface elevation and then 0.6 m has been added in each pond to get head stage.

Calculation of conductance in the ponds and drains has been done using the following formula given in the GMS manual:

$$\text{For drains} : \frac{K \times w}{t} \tag{8.1}$$

$$\text{For ponds} : \frac{K}{t} \tag{8.2}$$

where K is hydraulic conductivity, w is the width of drains, and t is the thickness of the bed material. In our case, limestone and dolomite have been considered as the bed material.

From Darcy's law, we know.

$$Q = K \times i \times A = \frac{K \times \Delta H \times A}{L} = C \times \Delta H \tag{8.3}$$

Here C is conductance and in GMS for arcs, it is provided per unit length and for polygons (ponds), it is provided per unit area. Q is discharge.

The exact location of wells was verified from Google earth pro and location was taken from site.

8.2.4 Delineating Recharge Zone

In our study, it has been assumed that overall recharge is uniform in the whole area. Rainfall is the major source of recharge in the study area according to the report of Groundwater Estimation Committee (GEC) (1997). All the rain gauge stations were located around the study area in ArcGIS software and Thiessen polygons were created.

In the study area, there were two rain gauge stations whose Thiessen polygons were overlapping with the case study area, namely Pirda and Pindrawan. Area of Thiessen polygons was calculated in ArcGIS software and average yearly rainfall was taken to calculate average rainfall in the selected study area. Thiessen polygon for rain gauge stations is shown in Fig. 8.3 and rainfall details are shown in Table 8.1.

In the report of GEC (1997), recharge percentage for various ground conditions was given, out of which we selected the type of ground conditions that persist in our study area.

$$\begin{aligned}\text{Average rainfall} &= \frac{A_1P_1 + A_2P_2}{A_1 + A_2} \\ &= \frac{8.653 \times 920.54 + 100.321 \times 792.261}{8.654 + 100.321} \\ &= 802.67 \text{ mm}\end{aligned}$$

In Dharsiwa block of Raipur district, rainfall is the major source of recharge. Here, we have assumed that other sources of recharge in the groundwater are negligible.

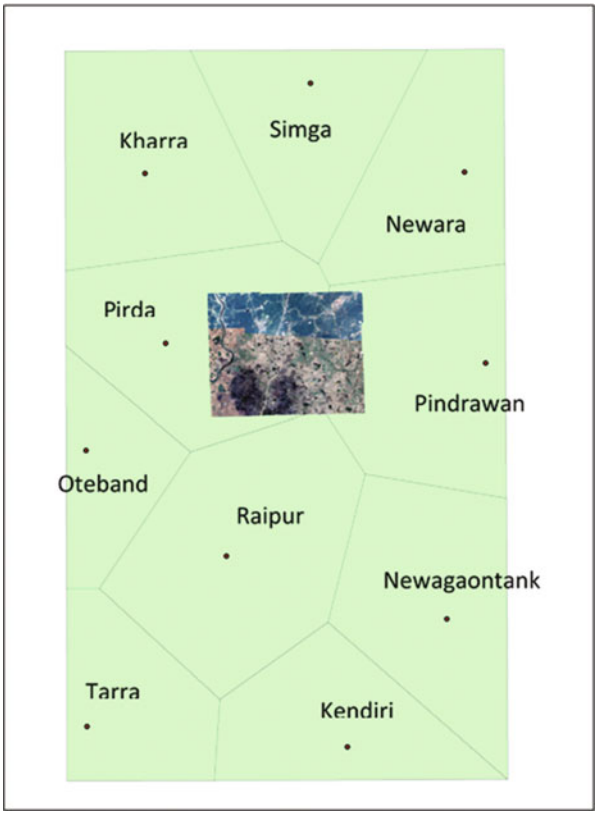

Fig. 8.3 Thiessen polygon for rain gauge stations

Table 8.1 Rainfall details of the study area

Station name	Rainfall (P_i)	Area of overlapping polygon (km^2) (A_i)
1. Pindrawan	920.54	8.653
2. Pirda	792.261	100.321

From the report of Groundwater estimation committee, it was found that in case of limestone, 6% of total rainfall infiltrates into the ground as groundwater.

$$\text{Recharge (m/day)} = \{(\text{average Rainfall} \times 6\%)/365\} \tag{8.4}$$

8.2.5 *Defining the Hydraulic Conductivity and Layer Elevation*

In the case of Chandi formation, the main constituents are limestone and dolomite. In the process of development of conceptual model, hydraulic conductivity is required for the kind of formation. The value for hydraulic conductivity has been taken from

Domenico and Schwartz (1998). In this model, we have assumed that hydraulic conductivity is same throughout the boundary of the study area. They provided a list of hydraulic conductivity ranges for different types of material. An average value was chosen from that range. The range was 1×10^{-9} to 6×10^{-6} m/s.

For defining layer of the conceptual model, data given by Central ground water board were analyzed. The thickness of the first layer, i.e., Chandi formation given in the study area location was 205 m. The second layer being Gunderdehi formation (shale) is ignored, because it has very low porosity and low hydraulic conductivity, so chances of having groundwater in such layer are very rare. Hence it has been ignored.

8.2.6 Running the Modflow

Grids were created around the defined boundary using a 3D grid tool of GMS and the starting head for the model was kept same as the top elevation of the layer. After checking for simulation error, Modflow was run. Color coded grid is formed where groundwater head contour is depicted at eachgrid. The color code range is shown in the legend bar.

8.3 Results and Discussion

8.3.1 Developed Conceptual Model

The final result for the developed conceptual model is in the form of color-coded contours. The gridded model consists of grids. Each grid has some specific values regarding head value. Near the wells, the grids come closer and that is why dark color is shown near wells.

The color contour formed shows the total head values at every point. Also, the specific points if selected, then we can get the flow budget for that section. If required, the flow budget for the whole model can be studied. In the case of river, the flow budget shows the points where the river is effluent and where it is influent. From Fig. 8.4, we can infer that direction of groundwater flow is from SE toNW. Also, another direction of flow is from NE to NW to the middle of Kharun River.

The flow budget of the model is shown in Table 8.2 for various sources and sinks. From flow budget, it is clear that the major source of groundwater is recharge. Drains are contributing negligible amount in groundwater.

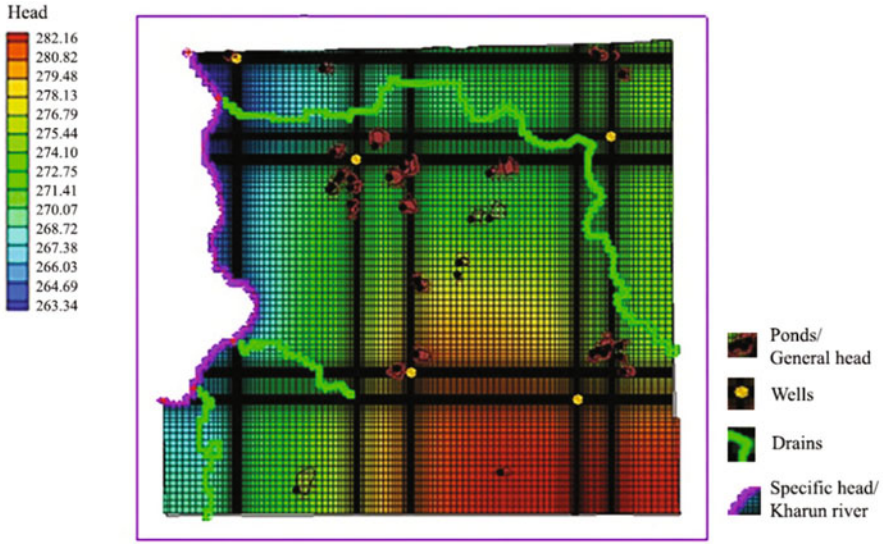

Fig. 8.4 Conceptual model with grids of different head values

Table 8.2 Flow budget for conceptual model

Sources and sinks	Flow in (m^3/day)	Flow out (m^3/day)
Constant heads	33.48	−3299.06
Drains	0.0	−5692.47
General heads	1585.36	−4073.78
Wells	0.0	−86.40
Recharge	11532.84	0.0
Total source/sink	13151.68	−13151.72

8.3.2 Calibration

After trying with different values of hydraulic conductivity and using the observation wells head value for comparison between simulated and observed head, we finally arrived at a calibrated model. The Calibration target is set up with a 95% confidence interval. The interval for calibrated head error value is set as 5 m. Out of five observation wells, four show well head within the interval, thus show green color, and one well shows yellow color which shows error being less than 200% in that particular well. The calibrated model is shown in Fig. 8.5.

For measuring observed head in the field, well head was measured in the field. For measurement of the head, ground elevation was considered from Google earth pro and the static water level was measured manually. Following formula was used

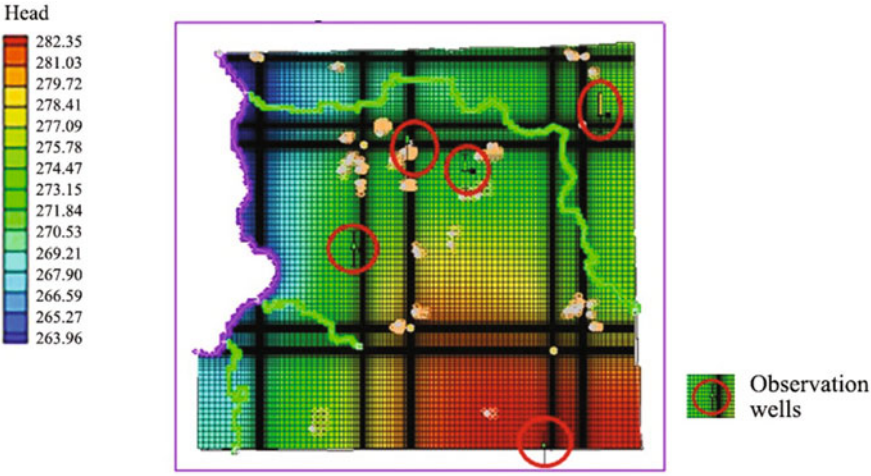

Fig. 8.5 Calibrated model

$$H_i = \text{Elevation of the ground surface} - \text{static water level}$$

Here H_i is the total head value of water in well considering mean sea level as the datum.

For measurement of the head value for different wells, a rope and measuring tape were used. A heavy object was tied at the end of the rope and allowed to drop in the well up to the point where there is no tension in the rope. In this way, the actual depth of the well was measured. The length of the rope up to the hard surface was measured to get the total depth of well. Similarly, static water level from the top of the parapet wall was measured and the length of the parapet wall was also measured for calculation of head.

For calibration after trying with different hydraulic conductivity values, one giving best result was chosen. The Basic assumption that is assumed here is that for whole area, hydraulic conductivity is considered to be same. Although, in real condition, different portions of the area have different values of hydraulic conductivity, but as the geology is not changing drastically anywhere, hence values do not differ much.

8.3.3 Validation

The observed and the computed head values are shown in Table 8.3. The difference in computed and simulated values can be because of various reasons. Foremost reason can be assumption taken during simulation that the whole area has the same hydraulic conductivity. Secondly, wells taken into account were provided with the same yield value, however, in the real condition, they may vary. Thirdly, only major

Table 8.3 Observed and computed head

Observed well	Observed head (m)	Computed head (m)
Well 1	272.9	274.46
Well 2	268.82	271.47
Well 3	268.65	271.03
Well 4	268.05	274.69
Well 5	282.1	283.48

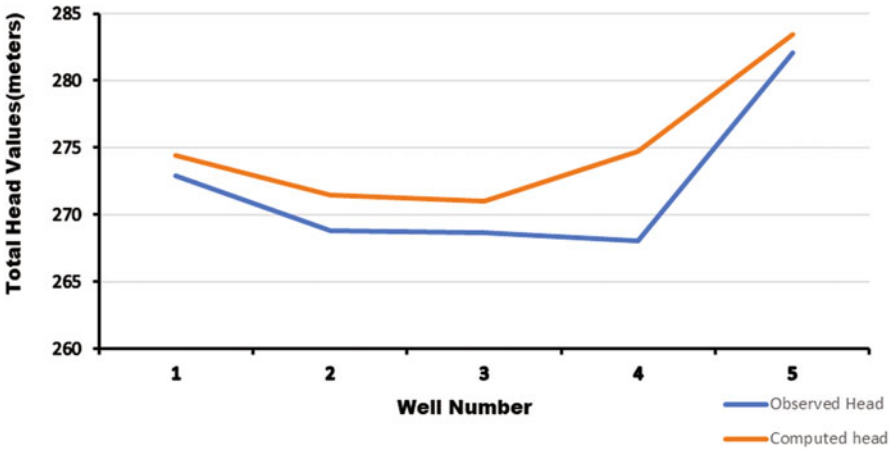

Fig. 8.6 Graph comparing observed and simulated head for validation purpose

drains were plotted in the conceptual model and minor drains were neglected for maintaining the simplicity of work. Another assumption that has been taken is related to pond and river depth. With the help of local people during the site visit, a rough estimation of depth was done. Hence, an average depth was allotted to pond and river.

The graph in Fig. 8.6 shows that the head value obtained in conceptual model for the observation wells and the measured head values of the field is near about the same. Also, the error percentage for the above data is less than 5%.

The error in the observed and simulated head values is zero for mean error, 3.7% in case of root mean squared error, and 3.1% in case of mean absolute error.

8.4 Conclusion

The developed conceptual model for the Dharsiwa area shows the head value within the range and flow budget can be used to know the contributors for inflow and how much water is outflowing. Benefits of developing a conceptual model are:

- It helps to predict the aquifer conditions and tells about the *flow budget of the system.*
- To investigate *real world problems*, e.g., nitrate mixing and its transportation, which can be simulated and research questions related to that domain can be investigated.
- Build a means of communication between modeler, coder, end user, and domain experts.
- Understand the nature of the model and nature of groundwater flow.
- The Conceptual Model is an asset that can be *re-used for making different solution designs* for a variety of research queries either in the same or another simulation work.

The conclusions that can be drawn from this research work are as discussed below:

1. The error percentage is below 5% and the observed and the computed heads were well within the range. Hence the developed conceptual model is a usable model for future use.
2. The head values obtained from the conceptual model help us understand the groundwater flow direction as it is dependent upon head value.
3. Unknowns can be generated from conceptual model which are a little bit cumbersome to measure on the field.
4. The efficiency of the developed conceptual model depends upon various factors like recharge rate, hydraulic conductivity, layers elevation, well flow rate, and conductance value.
5. From the flow budget of the conceptual model, we can infer that river leakage is contributing less to the groundwater but the river is taking water from groundwater which shows effluent nature of the river.

This study can be carried forward with many important applications as shown in Fig. 8.7. A few major applications include:

- Contaminant transport modeling.
- Upscaling of model.

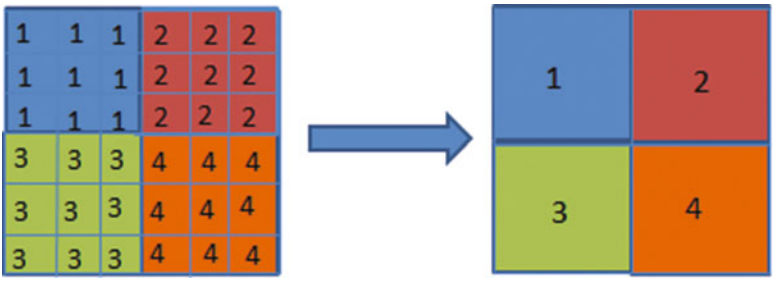

Fig. 8.7 Conceptual view of upscaling

Acknowledgments We are grateful to our institute, NIT Raipur, for providing the essential Institutional facilities during the research work. We wish our sincere thanks to "Central Ground Water Board, Raipur", and "Water Resources Department, Chhattisgarh" for providing various data for this study. We indebt our thanks to faculty members of our Institute for constant support and encouragement.

References

Almasri, M. N., & Kaluarachchi, J. J. (2007). Modeling nitrate contamination of groundwater in agricultural watersheds. *Journal of Hydrology, 343*(3–4), 211–229.

Amaziane, B., & Koebbe, J. (2006). JHomogenizer: A computational tool for upscaling permeability for flow in heterogeneous porous media. *Computational Geosciences, 10*(4), 343–359.

Central Ground Water Board. (2015). *Central Ground Water Board*. Chhattisgarh: Ministry of Water Resources Government of India.

Chen, Z. (2006). Recent advances of upscaling methods for the simulation of flow transport through heterogeneous porous media. *Journal of Computational Mathematics, 24*, 393–400.

Domenico, P. A., & Schwartz, F. W. (1998). *Physical and chemical hydrogeology* (Vol. 506). New York: Wiley.

Eberhard, J. (2004). Upscaling and dispersion for transport in heterogeneous media. *Journal of Physics A: Mathematical and General, 37*(40), 9587.

Eichel, H., Helmig, R., Neuweiler, I., & Cirpka, O. A. (2005). Upscaling of two-phase flow processes in porous media. In *Upscaling multiphase flow in porous media* (pp. 237–257). Dordrecht: Springer.

Enemark, T., Peeters, L. J., Mallants, D., & Batelaan, O. (2019). Hydrogeological conceptual model building and testing: A review. *Journal of Hydrology, 569*, 310–329.

Fumagalli, A., Pasquale, L., Zonca, S., & Micheletti, S. (2016). An upscaling procedure for fractured reservoirs with embedded grids. *Water Resources Research, 52*(8), 6506–6525.

Gelhar, L. W., Welty, C., & Rehfeldt, K. R. (1992). A critical review of data on field-scale dispersion in aquifers. *Water Resources Research, 28*(7), 1955–1974.

Ginting, V. E. (2005). *Computational upscaled modeling of heterogeneous porous media flow utilizing finite volume method*. Doctoral Dissertation, Texas A&M University.

Groundwater Resource Estimation Committee. (1997). *Report of the Groundwater Resource Estimation Committee*.

Keupers, I., & Willems, P. (2017). Development and testing of a fast conceptual river water quality model. *Water Research, 113*, 62–71.

Khadri, S. F. R., & Pande, C. (2016). Ground water flow modeling for calibrating steady state using MODFLOW software: A case study of Mahesh River basin, India. *Modeling Earth Systems and Environment, 2*, 39. https://doi.org/10.1007/s40808-015-0049-7.

Kpegli, K. A. R., Alassane, A., van der Zee, S. E., Boukari, M., & Mama, D. (2018). Development of a conceptual groundwater flow model using a combined hydrogeological, hydrochemical and isotopic approach: A case study from southern Benin. *Journal of Hydrology: Regional Studies, 18*, 50–67.

Le Borgne, T., Bolster, D., Dentz, M., Anna, P., & Tartakovsky, A. (2011). Effective pore-scale dispersion upscaling with a correlated continuous time random walk approach. *Water Resources Research, 47*(12), 12538.

Ma, X., & Zabaras, N. (2011). A stochastic mixed finite element heterogeneous multiscale method for flow in porous media. *Journal of Computational Physics, 230*(12), 4696–4722.

Moharir, K., Pande, C., & Patil, S. (2017). Inverse modeling of aquifer parameters in basaltic rock with the help of pumping test method using MODFLOW software. *Geoscience Frontiers, 8*, 1385–1395.

Moharir, K. N., Pande, C. B., Singh, S. K., & Del Rio, R. A. (2020). Evaluation of analytical methods to study aquifer properties with pumping test in Deccan basalt region of the Morna River basin in Akola District of Maharashtra in India. In *Groundwater hydrology*. London, UK: Intec Open Publication. https://doi.org/10.5772/intechopen.84632.

Molnar, G. S., & Viraraghavan, T. (1990). Modelling of nitrate movement in groundwater: A case study. *Canadian Water Resources Journal, 15*(1), 12–23.

Pande, C. B., Moharir, K. N., & Pande, R. (2018). Assessment of morphometric and hypsometric study for watershed development using spatial technology – a case study of Wardha river basin in the Maharashtra, India. *International Journal of River Basin Management*, Taylors & Francis Journal, https://doi.org/10.1080/15715124.2018.1505737.

Pande, C. B., Moharir, K. N., & Pande, R. (2019). An integrated approach to delineate the groundwater potential zones in Devdari watershed area of Akola district, Maharashtra, Central India. *Environment, Development, and Sustainability Springer Journal*. https://doi.org/10.1007/s10668-019-00409-1.

Robinson, S., Arbez, G., Birta, L. G., Tolk, A., & Wagner, G. (2015). Conceptual modeling: definition, purpose and benefits. In *Proceedings of the 2015 Winter Simulation Conference* (pp. 2812–2826). IEEE Press.

Singh, G., Amanbek, Y., & Wheeler, M. F. (2017). Adaptive homogenization for upscaling heterogeneous porous medium. In *SPE Annual Technical Conference and Exhibition*. Society of Petroleum Engineers.

Singhal, V., & Goyal, R. (2011). Development of conceptual groundwater flow model for Pali area, India. *African Journal of Environmental Science and Technology, 5*(12), 1085–1092.

Vermeulen, et al. (2006). Limitations to upscaling of groundwater flow models dominated by surface water interaction. *Water Resources Research, 42*(10), 1–32.

Yadav, P. K. (2012). Analytical models for plume length estimations, 1-88, http://nbn-resolving.de/urn:nbn:de:bsz:14-qucosa-99399.

Yao, Y., Zheng, C., Liu, J., Cao, G., Xiao, H., Li, H., & Li, W. (2015). Conceptual and numerical models for groundwater flow in an arid inland river basin. *Hydrological Processes, 29*(6), 1480–1492.

Zhou, Y., & Herath, H. M. P. S. D. (2017). Evaluation of alternative conceptual models for groundwater modelling. *Geoscience Frontiers, 8*(3), 437–443.

Chapter 9
Numerical Modeling for Groundwater Recharge

Marykutty Abraham, Priyadarshini, and Kavisri Manikannan

Contents

9.1 Introduction 165
9.2 Study Area 167
9.3 Methodology 167
9.4 Results and Discussion 170
9.5 Transport Model 173
9.6 Conclusions 174
References 175

9.1 Introduction

Excessive resource utilization, uncontrolled urban and industrial discharges, and agricultural intensification are causing increasingly widespread degradation of aquifers. Conserving water by recharge and managing the natural resource by artificial recharge are very important for meeting the challenges of twenty-first century (Pande and Moharir 2015; Pande et al. 2018; Pande and Moharir 2018; Pande 2020a, b, c, d). The frequent occurrence of water crisis in many regions of the world is not due to scarcity alone, but it is mainly due to the poor water management practices (Pande et al. 2017, 2019a, b). Groundwater levels continue to fall beyond

M. Abraham (✉)
Centre for Remote Sensing and Geoinformatics, Sathyabama Institute of Science and Technology, Chennai, Tamil Nadu, India

Priyadarshini · K. Manikannan
Department of Civil Engineering, Sathyabama Institute of Science and Technology, Chennai, Tamil Nadu, India

C. B. Pande, K. N. Moharir (eds.), *Groundwater Resources Development and Planning in the Semi-Arid Region*, https://doi.org/10.1007/978-3-030-68124-1_9

acceptable levels, and this clearly indicates an unsustainable situation. The availability of water is very much restricted with respect to quantity and quality and varies considerably on spatial and temporal scale that leads to a situation where about one third of the country is drought prone. Hence, the development of suitable means of augmenting groundwater levels (Patode et al. 2016, 2017) and an appropriate method for precise estimation of effectiveness of artificial recharge are prerequisites for planning groundwater systems. Artificial recharge is essential for the sustainable groundwater development in the light of increasing water demand. In artificial recharge, excess surface water is sent into underground formations through appropriate structures to supplement groundwater at a rate much higher than the natural rates. Artificial recharge was defined by Todd (1959) as the practice of increasing groundwater level of a groundwater reservoir by artificial means. Due to highly complicated hydrogeological conditions, the modeling studies on groundwater recharge in aquifers are necessary to develop guidelines for optimum operation (Khadri and Pande 2016; Khadri and Moharir 2016; Moharir et al. 2017). Recent advances in the development of three-dimensional groundwater flow and contaminant transport models made it possible to simulate the effects due to artificial recharge arrangements. Such models are being successfully applied to develop spatially and temporally varying head and concentration contours.

A model can be viewed as an approximation and not as an exact duplication of field conditions. By mathematically representing a simplified version of a hydrogeological system, reasonable alternative scenarios can be predicted, tested, and compared. The equations that describe the groundwater flow and transport processes may be solved using different types of models. Some models such as analytical models may result in exact solutions to equations, which describe very simple flow, or transport conditions and others such as numerical models can be approximations of equations, which describe very complex conditions. The simplifications inherent with analytical models make it impossible to account for field conditions that change spatially in different time periods. Models for groundwater flow and transport vary from analytical solutions for one-dimensional flow in a homogeneous aquifer to complex numerical codes developed to simulate multiphase transport of reactive species in heterogeneous, three-dimensional porous media (Moharir et al. 2020).

Several researchers developed numerical models to simulate aquifer response for various hydrogeological scenarios using MODFLOW (Lubczynski and Gurwin 2005; Aish and Smedt 2006; Wang et al. 2008; Szucs et al. 2009; Chenini et al. 2010; Panagopoulos 2012; Chitsazan and Movahedian 2015; Abraham and Mohan 2019). Groundwater recharge in India ranged from 5 to 20% for hard rock to alluvial areas (Athavale et al. 1992). Recharge in coastal Cuddalore area was estimated to be 19% of rainfall (Mohan and Abraham 2010). Favorable groundwater recharge zones and potential recharge were assessed using GIS technology by few researchers (Yeh et al. 2016; Bhanja et al. 2019; Senthilkumar et al. 2019). Groundwater modeling can be integrated with geographic information system for better resource management (Khadri and Pande 2016; Sudhakar et al. 2016). Vulnerable zones for groundwater

contamination were mapped along flow paths using GIS interpretation by William (2001). Few researchers conducted geochemical studies and groundwater quality modeling with options of pumping and recharge (Johnson et al. 1998; Schijven et al. 2000; Saaltink et al. 2003). Numerical models for groundwater flow and transport were developed by various researchers to study the contaminant movement (Wang et al. 2005; Mohrlok et al. 2010; Ghoraba et al. 2013a; Sevinç Şengör and Ünlü 2013; Abraham and Mohan 2017; Sundararajan and Sankaran 2020).

9.2 Study Area

The study area is part of Cuddalore aquifer in Tamil Nadu, India, between 11°15′ to 11°45' N latitudes and 79° 15′ to 79° 45′ E longitudes in Survey of India toposheet 58 M/6. A large amount of groundwater is being extracted from Cuddalore aquifer for industrial and domestic, water supply, irrigation, and mining purposes. To avoid adverse consequences due to large-scale pumping and for sustainable management of this aquifer, artificial recharge is necessary. The recharge occurring in this area due to rainfall is directly feeding the deep-water table in this region, thus augmenting the confined aquifer in the Cuddalore groundwater basin. The area with an extent of 420 km^2 has been demarcated as recharge area by a study conducted by Geological Survey of India (11). In order to find out the favorable recharge zone, a geoelectrical resistivity survey was carried out in the area and the geological section was interpreted (Mohan 2003) for identifying suitable locations for recharge structures. A village named Nadiyapattu within the area was identified as the suitable location for creating artificial recharge structures and to study their effectiveness. The various structural arrangements were Check dams with one recharge well, Pond with three percolation wells, and an area consisting of pond with three percolation wells, check dam, and one recharge well, which will be referred to as combined structure.

9.3 Methodology

9.3.1 General

Numerical models consist of mathematical equations that describe groundwater flow or transport and solution techniques to solve the governing flow equation for field conditions. Model needs selection of the appropriate model design and solution methodology. Valid field data are necessary in the model construction. The simulation of groundwater flow requires a thorough understanding of the hydrogeologic characteristics of the site. Through the process of model calibration and verification, the values of the hydrogeologic conditions are varied to reduce any disparity between the model simulations and field data and to improve the accuracy of the model. The model can also be used to simulate possible future changes to hydraulic

head or groundwater flow rates as a result of future changes in stresses on the aquifer system.

9.3.2 MODFLOW (MODular FLOW) Model

The groundwater flow model, MODFLOW, uses finite-difference approximation for simulations in porous medium (Harbaugh et al. 2000) with GMS as graphical user interface (EMRL 2002) to study the effectiveness of individual and combinations of artificial recharge structures. In the finite-difference approximation, a grid is superimposed over the model domain, and hydraulic properties of the aquifer are averaged over each cell. The entire flow domain represented by equations as the number of cells is solved numerically, by an iterative process. Finite differences compute the average head value for a cell at the node. The model is based on a governing equation that represents the physical processes in the system (Fig. 9.1),

$$\frac{\partial}{\partial x}\left(k_{xx}\frac{\partial h}{\partial x}\right)+\frac{\partial}{\partial y}\left(k_{yy}\frac{\partial h}{\partial y}\right)+\frac{\partial}{\partial z}\left(k_{zz}\frac{\partial h}{\partial z}\right)\pm w=S_{\mathrm{s}}\frac{\partial h}{\partial t}$$

where

h is the hydraulic head in the aquifer [L],
x, y, and z are the cartesian coordinates associated with hydraulic conductivity tensor K_{xx}, K_{yy}, and K_{zz} [1/T],
w is the Recharge/pumping per unit volume,
K_{xx}, K_{yy}, and K_{zz} are the hydraulic conductivities expressed in the principal directions of anisotropy [L/t],
S_{s} is the specific storage [1/L].

Development of numerical groundwater models needs incorporation of model domain, boundary conditions, model parameters, and calibration and validation of the model. Model construction consists of design of conceptual model, creation of 3D finite difference grids, and running the simulation.

9.3.3 MT3D (Modular Transport 3D) Model

Groundwater quality improvement due to artificial recharge can be studied using transport models to simulate the primary transport processes such as advection and hydrodynamic dispersion. Consequent to continuous pumping and improper management, many aquifers are facing severe threat of being depleted and contaminated. Improvement of water quality of an aquifer is one of the main concerns for an artificial recharge project**.** Due to dilution, natural degradation, and other

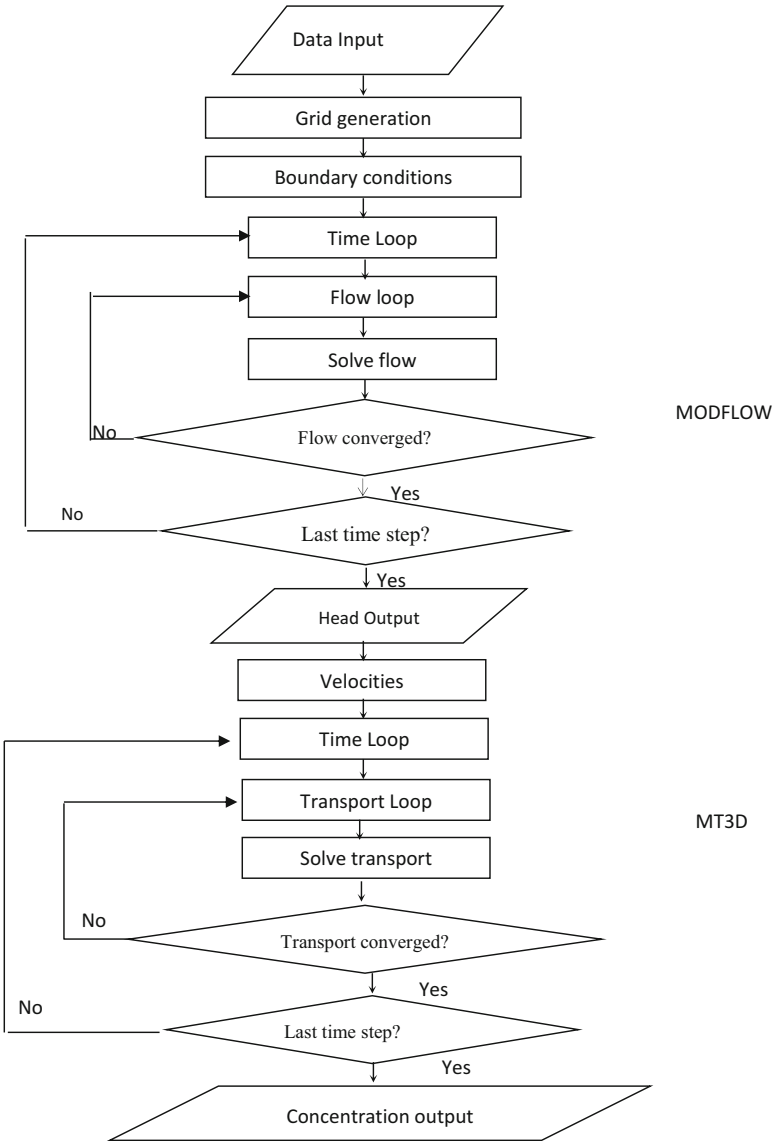

Fig. 9.1 Flowchart showing the steps involved in the flow and transport modeling

transformation processes, artificial recharge can reduce the concentration of contaminant along the flow direction (Fig. 9.1).

Transport study can be carried out using Modular Three-Dimensional Transport Model (MT 3D) (Zheng 1990) with Groundwater Modeling Systems (GMS) as graphical user interface (EMRL 2002). The model can simulate the primary transport processes of advection and hydrodynamic dispersion. Transport models require the

development of a calibrated groundwater flow model or, at a minimum, an accurate determination of the velocity and direction of groundwater flow, which has been based on field data. Contaminant transport occurs due to mass transport processes, such as advection, mechanical dispersion, and diffusion. The development of differential equations to describe the transport of solutes in porous medium is to consider the flux of solute into and out of a fixed elemental volume within the flow domain.

The general form of the advection dispersion equation for solute transport in three-dimensional flow through an aquifer was described by Freeze and Cherry (1979),

$$\frac{\partial}{\partial x}\left(D_x\frac{\partial c}{\partial x}\right)+\frac{\partial}{\partial y}\left(D_y\frac{\partial c}{\partial y}\right)+\frac{\partial}{\partial z}\left(D_z\frac{\partial c}{\partial z}\right)-\left(\frac{\partial}{\partial x}(V_xC)\right) -\left(\frac{\partial}{\partial y}(V_yC)\right)-\left(\frac{\partial}{\partial z}(V_zC)\right)=\frac{\partial c}{\partial t},$$

where

x, y, and z are the cartesian coordinate directions,
V_x, V_y, and V_z are the seepage velocities in the respective directions [LT^{-1}],
D_x, D_y, and D_z are the dispersion coefficients in the respective directions [L^2T^{-1}],
C is the solute concentration ML^{-3}, and
T is the time [T]

9.4 Results and Discussion

Numerical modeling of the hydrogeological regime could be applied on the basis of the known water balance components. Hydrological parameters, aquifer parameters, initial conditions, and boundary conditions were given as input to enable the model to simulate groundwater heads. The model was calibrated and verified by comparing the computed water levels with observed levels and then used to study the performance of individual structural arrangements. Borehole locations are shown in Fig. 9.2. For the present study, six percolation wells, one recharge well, and 15 observation wells were considered in the study area.

9.4.1 Flow Model

A finite-difference model was developed using MODFLOW software package by incorporating the measured and inferred hydrologic data for 30 months. Input parameters included hydraulic conductivity of the aquifers, hydraulic head, pumping values, recharge values, evapotranspiration values, aquifer thickness, etc.

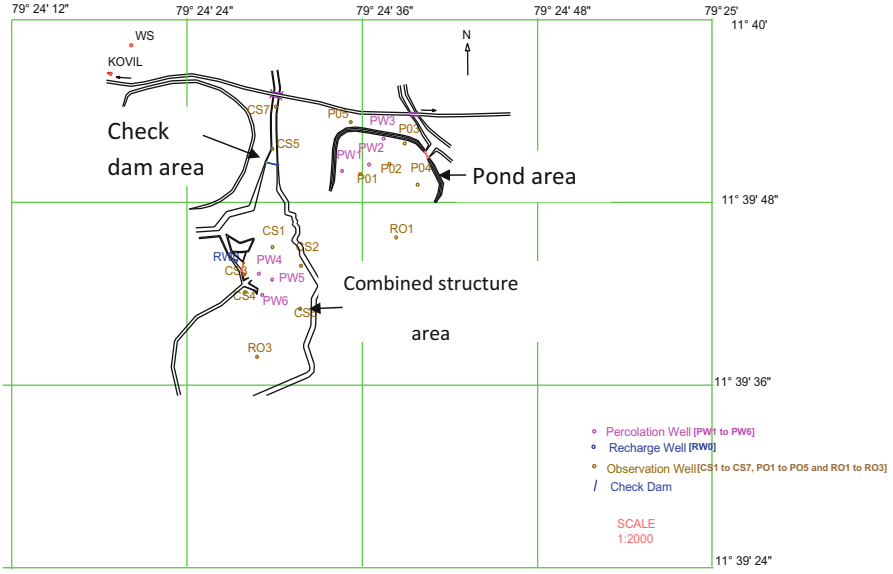

Fig. 9.2 Borehole locations in Nadiyapattu Artificial Recharge Site

9.4.2 Model Construction

For conceptual model design, the base map of the model domain was imported, then the system boundaries were defined, and the boundary conditions were assigned. The outer boundaries were treated as head-dependent boundaries, and a constant head boundary was given. Finally, the inputs and outputs to the system were defined. Input parameters included hydraulic conductivity of the aquifers, measured head, estimated recharge values, evapotranspiration values, pumping data, and aquifer thickness. Outputs include hydraulic heads and groundwater flow and transport rates.

9.4.3 Model Discretization

The modeling domain consisted of an area of 1450 m × 1100 m. The study area was discretized into 32 rows and 39 columns with 1248 cells. Twenty-two bore holes were used to identify the layer elevations. The modeling domain extended vertically 80 m above mean sea level (msl) to 45 m below msl.

9.4.4 Initial Conditions and Boundary Conditions

Average water levels in the observation wells during the first month were taken as the initial condition. Boundary conditions were specified for all the modeled area. Constant head boundaries (i.e., Dirichlet boundaries) were given for all the sides of the model. Constant head cells varying from 69 m at the north side to 68 m at the south side were considered as the eastern boundary. Constant head cells varying from 58 m at the northern side to 54 m at the southern side were considered as the western boundary. The top boundary was assumed as a recharge boundary, and the natural recharge rate was taken as 19% of rainfall based on the natural recharge study (Abraham and Mohan 2019). Evapotranspiration values were calculated for the region according to Penman-Monteith method.

9.4.5 Model Parameters and Stresses

Hydraulic conductivity values were allocated based on an infiltration study directed in the area. Hydraulic conductivity in the vertical direction was set to 1 m/day, which is 1/tenth of the horizontal conductivity. Specific yield of the aquifer was assumed to be 0.2.

There was only one agricultural pumping well near the boundary of the area.

9.4.6 Temporal Conditions and Solver

The numerical model was run in transient state. The total time period of 30 months was divided into 30 stress periods. Preconditioned Conjugate Gradient procedure (PCG) was selected as the solver.

9.4.7 Model Calibration and Validation

Average monthly data for 16 months were used for calibration, and the average monthly data for 14 months were used for validation of the model. The hydraulic conductivity was varied within reasonable limit during calibration and found to be 12 m/day. Fifteen observation wells were considered for calibration. Observed and simulated heads matched well (Fig. 9.3).

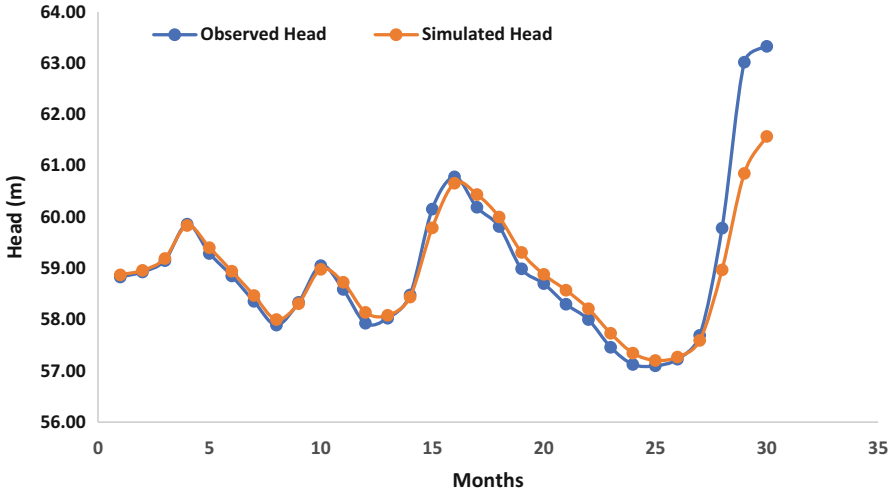

Fig. 9.3 Observed head and modeled head for a representative observation well

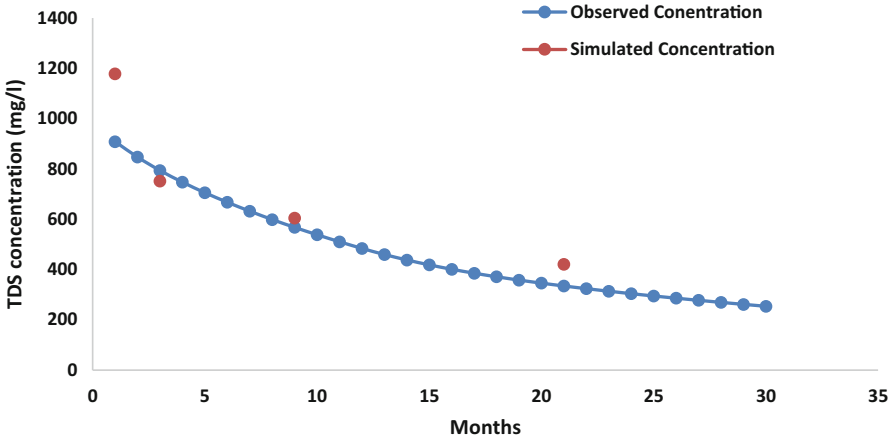

Fig. 9.4 Observed and modeled concentration for a representative observation well

9.5 Transport Model

The solute-transport modeling was initiated using the calibrated MODFLOW model constructed to simulate water quality variation due to artificial recharge. The model simulated the primary transport processes of advection and hydrodynamic dispersion. Concentration of TDS was analyzed before and after artificial recharge. All the boundaries were assigned as constant concentration boundaries based on the existing water quality data. Dispersivity was varied during calibration, and the value was found to be 1 m. Figure 9.4 shows the comparison of observed and modeled

concentration values. From the calibration charts, it was observed that there is concordance in the model output and the observed TDS values.

It was observed that concentration levels did not rise after the monsoon as the recharge structures helped in diluting the native water by the huge volume of surface water collected in them. From the model, it was clear that artificial recharge structures could maintain the TDS concentration even after the rainy season, which wouldn't have been possible by natural recharge alone. The TDS concentration near the structures was very less compared to other places in the study area. From the results of the transport model simulation, it is found that TDS concentration has decreased from 1000 mg/l to around 200 mg/l and the decrease is mainly attributed due to artificial recharge.

9.5.1 Performance of Individual Structures

Spatial distribution in head due to individual structures was assessed from the calibrated flow model. After 2 years of artificial recharge, groundwater levels increased by 3.46, 2.54, and 4.7 m, and the zone of influence was 400, 600, and 500 respectively, for check dam, pond, and combined structure area. The error statistics such as mean error, root mean square error, and mean absolute error for the observation wells during calibration period was −0.13, 0.87, and 0.71 m, respectively, indicating acceptable level of calibration.

9.6 Conclusions

The two components of a groundwater model are conceptual model, representing the hydrogeological processes in the system, and a mathematical model, represented by differential equations with certain assumptions to quantify the processes. A model mimics the system to an acceptable level and offers a predictive logical tool to assess the impacts of various stresses on the system.

The developed models provide a consistent regional representation of the overall groundwater flow and transport. Models are useful tools in assessing recharge pattern in aquifers and supportive for planning artificial recharge schemes. The modeled head contours from the numerical model can be used to compare the recharge pattern with and without structures to assess the recharge pattern under various scenarios to draw useful conclusions. From the field study of artificial recharge for 2 years, around 2 m increase in head was observed in the study area along with considerable increase in groundwater quality. From the transport model results, it can be inferred that water quality has improved considerably after artificial recharge.

References

Abraham, M., & Mohan, S. (2017). Role of artificial recharge structures in enhancing groundwater quality – A modeling study. *International Journal of Earth and Atmospheric Science, 4*(2), 107–116.

Abraham, M., & Mohan, S. (2019). Effectiveness of check dam and pond with percolation wells for artificial groundwater recharge using groundwater models. *Water Science and Technology-Water Supply, 19*(7), 2107–2115.

Aish, A., & Smedt, F. (2006). Modeling of a groundwater mound resulting from artificial recharge in the Gaza strip, Palestine. *Water for Life in the Middle East, 2*, 779–787.

Athavale, R. N., Rangarajan, R., & Muralitharan, D. (1992). Measurement of natural recharge in India. *Journal of Geological Society of India., 39*(3), 235–244.

Bhanja, S. N., Mukherjee, A., Rangarajan, R., Scanlon, B. R., Malakar, P., & Verma, S. (2019). Long-term groundwater recharge rates across India by in situ measurements. *Hydrology and Earth System Sciences, 23*, 711–722.

Chenini, I., Mammou, A. B., & El May, M. (2010). Groundwater recharge zone mapping using GIS-based multi-criteria analysis: A case study in Central Tunisia (Maknassy Basin). *Water Resources Management, 24*(5), 921–939.

Chitsazan, M., & Movahedian, A. (2015). Evaluation of artificial recharge on groundwater using MODFLOW model (case study: Gotvand plain-Iran). *Journal of Geoscience and Environment Protection, 3*(5), 122–132.

Environmental Modeling Research Laboratory [EMRL]. (2002). *Groundwater Modeling System (GMS) version 4.0 Tutorial Documents* (Vols. 1–4, Environmental Modeling Research Laboratory). Provo, UT: Brigham Young University.

Freeze, R. A., & Cherry, J. A. (1979). Groundwater. Englewood Cliffs, New Jersey, USA: Prentice-Hall, Inc.

Ghoraba, S. M., Zyedan, B. A., & Rashwan, I. M. H. (2013a). Solute transport modeling of the groundwater for quaternary aquifer quality management in Middle Delta, Egypt. *Alexandria Engineering Journal, 52*(2), 197–207.

Ghoraba, S. M., Zyedan, B. A., & Rashwan, I. M. H. (2013b). Solute transport modeling of the groundwater for quaternary aquifer quality management in Middle Delta, Egypt. *Alexandria Engineering Journal, 52*(2), 197–207.

Harbaugh, A. W., Banta, E. R., Hill, M. C., & McDonald, M. G. (2000). *MODFLOW-2000, the U.S. Geological Survey modular ground-water model – User guide to modularization concepts and the groundwater flow process*. U.S. Geological Survey Open-File Report 00-92, 121.

Johnson, S. J., Baker, L. A., & Fox, P. (1998). Geochemical transformations during artificial ground water recharge: Soil water interactions of inorganic constituents. *Water Research, 34*(7), 2110–2118.

Khadri, S. F. R., & Moharir, K. (2016). Characterization of aquifer parameter in basaltic hard rock region through pumping test methods: A case study of Man River basin in Akola and Buldhana districts Maharashtra India. *Modeling Earth Systems and Environment, 2*, 33.

Khadri, S. F. R., & Pande, C. (2016). Ground water flow modeling for calibrating steady state using MODFLOW software: A case study of Mahesh River basin, India. *Modeling Earth Systems and Environment, 2*, 39.

Lubczynski, M. W., & Gurwin, J. (2005). Integration of various data sources for transient groundwater modeling with spatio-temporally variable fluxes-Sardon study case, Spain. *Journal of Hydrology, 306*(1–4), 71–96.

Mohan, S. (2003). Study on enhancement of recharge potential in the recharge area of the Neyveli deep seated aquifers. Interim Report submitted to Neyveli Lignite Corporation, Neyveli, Tamil Nadu, India.

Mohan, S., & Abraham, M. (2010). Derivations of simple site-specific recharge-precipitation relationships: A case study from the Cuddalore Basin, India. *Environmental Geoscience, 17*(1), 37–44.

Moharir, K., Pande, C., & Patil, S. (2017). Inverse modeling of aquifer parameters in basaltic rock with the help of pumping test method using MODFLOW software. *Geoscience Frontiers., 8*(6), 1385–1395.

Moharir, K. N., Pande, C. B., Singh, S. K., & Del Rio, R. A. (2020). Evaluation of analytical methods to study aquifer properties with pumping test in Deccan basalt region of the Morna River basin in Akola District of Maharashtra in India. In *Groundwater hydrology*. London: Intech Open Publication. https://doi.org/10.5772/intechopen.84632.

Mohrlok, C., Kirubaharan, S., & Eldho, T. I. (2010). Transport characteristics in a 3D groundwater circulation flow field by experimental and numerical investigations, practice periodical of hazardous. *Toxic Radioactive Waste Manage, 14*, 185.

Panagopoulos, G. (2012). Application of MODFLOW for simulating groundwater flow in the Trifilia karst aquifer, Greece. *Environmental Earth Sciences, 67*, 1877–1889.

Pande, C. B. (2020a). Introduction. In *Sustainable watershed development. Springer briefs in water science and technology*. Cham, Switzerland: Springer. https://doi.org/10.1007/978-3-030-47244-3_1.

Pande, C. B. (2020b). Watershed management and development. In *Sustainable watershed development. Springer briefs in water science and technology*. Cham, Switzerland: Springer. https://doi.org/10.1007/978-3-030-47244-3_2.

Pande, C. B. (2020c). Thematic mapping for watershed development. In *Sustainable watershed development. Springer briefs in water science and technology*. Cham, Switzerland: Springer. https://doi.org/10.1007/978-3-030-47244-3_3.

Pande, C. B. (2020d). Sustainable watershed development planning. In *Sustainable watershed development. Springer briefs in water science and technology*. Cham, Switzerland: Springer.

Pande, C. B., & Moharir, K. (2015). GIS-based quantitative morphometric analysis and its consequences: A case study from Shanur River Basin, Maharashtra India. *Applied Water Science, 7*(2), 1–11.

Pande, C. B., & Moharir, K. (2018). Spatial analysis of groundwater quality mapping in hard rock area in the Akola and Buldhana districts of Maharashtra, India. *Applied Water Science, 8*(4), 1–17.

Pande, C. B., Khadri, S. F. R., Moharir, K. N., & Patode, R. S. (2017). Assessment of groundwater potential zonation of Mahesh River basin Akola and Buldhana districts, Maharashtra, India using remote sensing and GIS techniques. *Sustainable Water Resources Management*. https://doi.org/10.1007/s40899-017-0193-5. ISSN 2363-5037. Published online 8 September-2017.

Pande, C. B., Moharir, K. N., & Pande, R. (2018). Assessment of morphometric and hypsometric study for watershed development using spatial technology - a case study of Wardha river basin in the Maharashtra, India. *International Journal of River Basin Management*. https://doi.org/10.1080/15715124.2018.1505737.

Pande, C. B., Moharir, K. N., Singh, S. K., & Dzwairo, B. (2019a). Groundwater evaluation for drinking purposes using statistical index: Study of Akola and Buldhana districts of Maharashtra, India, environment. *Development and Sustainability (A Multidisciplinary Approach to the Theory and Practice of Sustainable Development), 22*, 7453. https://doi.org/10.1007/s10668-019-00531-0.

Pande, C. B., Moharir, K. N., Singh, S. K., & Varade, A. M. (2019b). An integrated approach to delineate the groundwater potential zones in Devdari watershed area of Akola district. *Maharashtra, Central India in Environment, Development, and Sustainability, 22*, 4867. https://doi.org/10.1007/s10668-019-00409-1.

Patode, R. S., Nagdeve, M. B., & Pande, C. B. (2016). Groundwater level monitoring of Kajaleshwar-Warkhed watershed, Tq. Barshitakli, Dist. Akola, India through GIS approach. *Advances in Life Sciences, 5*(24), 11207–11210.

Patode, R. S., Pande, C. B., Nagdeve, M. B., Moharir, K. N., & Wankhade, R. M. (2017). Planning of conservation measures for watershed management and development by using geospatial technology – A case study of Patur watershed in Akola District of Maharashtra. *Current World Environment, 12*(3), 2017.

Saaltink, M. W., Ayora, C., Stuyfzand, P. J., & Timmer, H. (2003). Analysis of a deep well recharge experiment by calibrating a reactive transport model with field data. *Journal of Contaminant Hydrology, 65*(1–2), 1–18.

Schijven, J. F., Medema, G., Vogelaar, A. J., & Hassanizadeh, S. M. (2000). Removal of micro-organisms by deep well injection. *Journal of Contaminant Hydrology, 44*(3–4), 301–327.

Senthilkumar, M., Gnanasundar, D., & Arumugam, R. (2019). Identifying groundwater recharge zones using remote sensing & GIS techniques in Amaravathi aquifer system, Tamil Nadu, South India. *Sustainable Environmental Research, 29*, 15. https://doi.org/10.1186/s42834-019-0014-7.

Sevinç Şengör, S., & Ünlü, K. (2013). Modeling contaminant transport and remediation at an acrylonitrile spill site in Turkey. *Journal of Contaminant Hydrology, 50*, 77–92.

Sudhakar, S., Verma, M. K., & Soumya, S. (2016). Application of GIS and MODFLOW to ground water hydrology-a review. *International Journal of Engineering Research and Applications, 6* (1), 36–42.

Sundararajan, N., & Sankaran, S. (2020). Groundwater modeling of Musi basin Hyderabad, India: A case study. *Applied Water Science, 10*, 14. https://doi.org/10.1007/s13201-019-1048-z.

Szucs, P., Madarasz, T., & Civan, F. (2009). Remediating over-produced and contaminated aquifers by artificial recharge from surface waters. *Environmental Modeling & Assessment, 14*(4), 511–520.

Todd, D. K. (1959). *Annotated bibliography on artificial recharge of ground water through 1954: U.S. Geological Survey Water-Supply Paper 1477*, p. 115.

Wang, P., Zheng, C., & Gorelick, M. S. (2005). A general approach to advective–dispersive transport with multi-rate mass transfer. *Advances in Water Resources, 28*, 33–42.

Wang, S., Shao, J., Song, X., Zhang, Y., Huo, Z., & Zhou, X. (2008). Application of MODFLOW and geographic information system to groundwater flow simulation in North China plain, China. *Environmental Geology, 55*, 1449–1462.

William, B. (2001). *Characterizing the water quality and contamination level of groundwater along the Ceil Zarqa River using the Fuzzy Logic Approach in GIS Environment, 2001*. Retrieved from http://www.medaqua.org/Conf2001/abstracts/7.htm.

Yeh, H. F., Cheng, Y. S., Lin, H. I., & Lee, C. H. (2016). Mapping groundwater recharge potential zone using a GIS approach in Hualian River, Taiwan. *Sustainable Environment Research, 26* (1), 33–43.

Zheng, C. (1990). *MT3D, a modular three-dimensional transport model*. Rockville, MD: S.S. United States Environmental Protection Agency and Papadopulos and Associates.

Chapter 10
Assessment of Aquifer Vulnerability for Sea-Water Intrusion in Nagapattinam Coast, Tamil Nadu, Using Geospatial Techniques

Rajesh Jayaraman and Lakshumanan Chokkalingam

Contents

10.1 Introduction 179
10.2 Study Area Description 180
10.3 Methodology 181
10.4 GALDIT: An Open-Ended Model 181
10.5 Decision Criteria 190
10.6 Application of the GALDIT Method to a Case Study in Nagapattinam Taluk 190
10.7 Conclusion 196
References 196

10.1 Introduction

The abuse of groundwater along parts of the beach front belts of India for different purposes has influenced groundwater quality and amount. It has prompted a fast decrease in groundwater levels (Khadri and Pande 2016b, c; Patode et al. 2016), prompting salt water interruptions and water quality crumbling especially in parts of Gujarat, Tamil Nadu, Andhra Pradesh, Orissa, and West Bengal. The geospatial methods are very powerful for estimation of the aquifer vulnerability and sea water intrusion. Nowadays, aquifer vulnerability is very important for the balance of the

R. Jayaraman (✉)
Mahatma Phule Krishi Vidyapeeth, Ahmednagar, Maharashtra, India

L. Chokkalingam
Department of Remote Sensing, Bharathidasan University, Tiruchirapalli, Tamil Nadu, India
e-mail: drlaks@bdu.ac.in

C. B. Pande, K. N. Moharir (eds.), *Groundwater Resources Development and Planning in the Semi-Arid Region*, https://doi.org/10.1007/978-3-030-68124-1_10

groundwater and sea water interruption. The coastal zone has very serious problems for drinking and irrigation purposes due to sea water interruption. By and large, the term of weakness alludes to the potential level of harm that can be normal, relying upon the qualities of a component in danger concerning a specific peril (Georgescu et al. 1993). Identifying with groundwater, the defenselessness was characterized by Lobo-Ferreira and Cabral (1991) as "the affectability of groundwater quality to a forced contaminant load, which is determined by the inborn attributes of the spring" (Khadri et al. 2013; Khadri and Pande 2015a, b). In this manner, the weakness of groundwater to various contaminations or to seawater interruption comprises a subject of examination in a few investigations (Chachadi and Lobo-Ferreira 2001; Lobo-Ferreira et al. 2005; Pande and Moharir 2018; Pande et al. 2019; Moharir et al. 2019). Likewise, the powerlessness of soil to salinization has been shown in numerous investigations (Aller et al. 1987; Chachadi and Lobo-Ferreira 2001; Honnanagoudar et al. 2012; Ferreira and Chachadi 2005). The fundamental motivation behind the examination is to decide the weakness of the groundwater in the south western piece of the Dakshina Kannada coast against seawater interruption to the ebb and flow ocean level.

10.2 Study Area Description

Nagapattinam Taluk is a seaside area of Tamil Nadu, 326 km, from south of Chennai and lies between Northern Latitude 10.46"16' and 79.50"50′ Eastern Longitude. A District is known for its Rich Religious Heritage and Communal Harmony. The absolute populace is 282,784 according to 2011 statistics; male populace is around 139,917, and female populace is 142,867. The quantity of household in this Taluk is 70,683. The region gets precipitation affected by both southwest and upper east storm. A decent piece of the precipitation happens during serious tempests coming about fundamentally from violent winds created in the Bay of Bengal particularly during the upper east storm. The precipitation design in the locale shows fascinating highlights. Yearly precipitation, which is 1500 mm in Vedaranyam, the southeast corner of the Taluk, quickly diminishes to about 1100 mm toward the west of the area. The territory appreciates damp and tropical atmosphere with blistering summers, noteworthy to mellow winters and moderate to overwhelming precipitation. The temperatures are different from 40.6 to 19.3 °C with sharp fall in night temperatures during storm period. The relative stickiness ranges from 70 to 77%, and it is high during the period from October to November (Fig. 10.1).

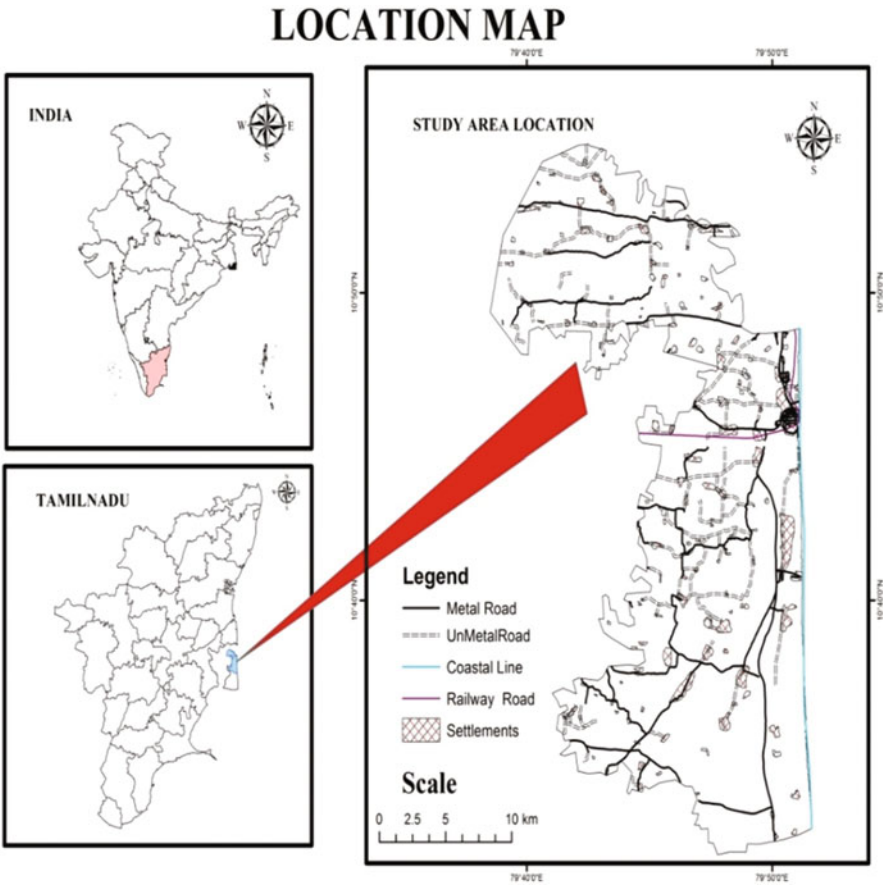

Fig. 10.1 Study area location map

10.3 Methodology

The philosophy utilized in the examination comprises an appraisal of powerlessness to groundwater sullying utilizing GALDIT technique, recognizable proof of saltwater encroached zone utilizing markers of saltwater interruption like $Cl/(HCO_3 + CO_3)$ proportion.

10.4 GALDIT: An Open-Ended Model

The framework exhibited hereinafter enables the client to decide a numerical incentive for any hydrogeophysical setting by utilizing an added substance model. This model is an open-finished model taking into consideration the expansion and

Table 10.1 Assessing aquifer vulnerability variables

Sr. no.	Factors	Weights
1.	Groundwater occurrence (aquifer type)	1
2.	Aquifer hydraulic conductivity	3
3.	Height of groundwater level above sea level	4
4.	Distance from the shore	2
5.	Impact of the existing status of seawater intrusion	1
6.	The thickness of aquifer being mapped	2

erasure of at least one marker. In any case, under ordinary conditions, presented arrangement of pointers ought not to be erased and any expansion of the marker would require Reinferring of the loads and grouping of Table 10.1.

10.4.1 Groundwater Occurrence or Aquifer Type (G)

In nature, groundwater by and large happens in the land layers and these layers might be kept, unconfined, broken restricted, or constrained by at least one limit (Moharir et al. 2017; Khadri and Pande 2016a; Khadri and Moharir 2016; Moharir et al. 2020). The degree of seawater interruption is subject to this essential nature of groundwater event. For instance, an unconfined spring under characteristic conditions would be increasingly influenced via seawater interruption contrasted with limited spring as the kept spring is feeling the squeeze. Thus, a limited spring might be increasingly inclined to seawater interruption contrasted with cracked restricted spring as the broken kept spring keeps up least water powered weight by method for spillages from connecting springs. Along these lines, in allocating the relative loads to Galdit parameter G, one ought to deliberately contemplate the demeanor and kind of the springs in the examination zone. The kept spring is increasingly powerless because of the bigger cone of sorrow and prompt arrival of water to wells during siphoning and subsequently scores the high evaluation. On account of different spring frameworks in a region, the most elevated rating might be received. For instance, on the off chance that a region has all the three springs, at that point, the rating of 10 of a kept spring might be picked. The accompanying gives the appraisals for various hydrogeological conditions: For instance, if a region has all the three springs, the rating of 10 for an unconfined spring might be picked. Nagapattinam zone falls under various spring type (Dhinagaran 2008), and in this way, the given rating is 10. Table 10.2 gives the ratings for different hydrogeological conditions.

Table 10.2 Ratings for parameter groundwater occurrence/aquifer type

Indicator	Weight	Indicator variables	Importance rating
Groundwater occurrence/aquifer type	1	Confined aquifer	10
		Unconfined aquifer	7.5
		Leaky confined aquifer	5
		Bound aquifer (recharge and/or impervious boundary aligned parallel to the coast)	2.5

Table 10.3 Ratings for parameter aquifer hydraulic conductivity

Indicator	Weight	Indicator variables		Importance rating
		Class	Range	
Aquifer hydraulic conductivity (m/day)	3	High	>81	10
		Medium	41–81	7.5
		Low	12–28	5
		Very low	<12	2.5

10.4.2 Aquifer Hydraulic Conductivity (A)

The parameter spring pressure-driven conductivity is utilized to gauge the pace of stream of water in the spring and consequently to the ocean. By definition, the spring water-driven conductivity is the capacity of the spring to transmit water. The water-driven conductivity is the consequence of the interconnected pores (also called successful porosity) inside the residue and a crack in united rocks. The greatness of the seawater front development is impacted by the pressure-driven conductivity of the spring. The higher the conductivity, the higher the inland development of the seawater fronts. The high conductivity additionally brings about more extensive cone of misery during siphoning. For this situation, the client should consider the pressure-driven obstructions like mud layers and impenetrable dykes parallel to the coast, which may go about as dividers to seawater interruption. Based on Table 10.3, the springs in Nagapattinam seaside territory have a water-driven conductivity that falls in the range from 0 to 4 m/day and 4 to 12 m/day depending on the neighborhood springs.

10.4.3 Depth to Groundwater Level above Mean Sea Level (L)

The degree of groundwater regarding mean ocean height is a significant factor in the assessment of the seawater interruption in a zone essentially in light of the fact that it decides the water-powered constrained accessibility to push back the seawater front. As observed from the Ghyben-Herzberg connection, for each meter of crisp water

Table 10.4 Ratings for parameter height of groundwater level above sea level

Indicator	Weight	Indicator variables		Importance rating
		Class	Range	
Height of ground water level above msl (m)	4	High	<3.9	10
		Medium	4.4–4.8	7.5
		Low	4.5–5.4	5
		Very low	>5.4	2.5

put away above mean ocean height, 40 m of new water put away beneath it down to the interface. In doling out the rating to L, one should investigate the fleeting variety of groundwater levels in the regions. The groundwater table changes because of the consolidated impact of penetration and with drawl occasions. During the pouring season in the rainstorm time frame, penetration is more and that builds groundwater table. During summer season periods, withdrawal of groundwater is relatively higher than the invasion and that will in general lower the groundwater table. The time incorporated amount of penetration and withdrawal, yielding the net consequence of the groundwater table. The GALDIT modeler remarks utilization of normal groundwater table during the prestorm period that was seen over quite a while. The rationale behind such a methodology is that just during the storm time frame, the seawater can possibly enter the ground spring. During rainstorm period, the freshwater front applies water-driven weight on the seawater front and drives it back toward the ocean. Doling out the normal prestorm groundwater level into the GALDIT model likewise guarantees that the evaluated saline water interruption defenselessness is the most extreme, and this gives a well-being edge. In this study, the premonsoon groundwater table for 20 years (1996–2015) was collected for the 07 coastal observation wells and monitored by the public work department (PWD) of the state Government of Tamil Nadu. The average groundwater table was computed for each observation well. The average of groundwater table for the seven observation wells ranged from 3.30 to 5.22 and is depicted in Table 10.4 and Fig. 10.2.

The groundwater level information as for mean ocean rise can be acquired by building up the perception wells in the zone.

10.4.4 Distance from the Shore (D)

The effect of seawater interruption by and large declines as one moves inland at right edges to the shore and the rivulet. This basically speaks to the angle accessible for saline water interruption. According to the GALDIT model, the most extreme rating is 10, which can be received for separation under 100 m from the coast. The rating worth can be diminished. Each 100 m increment out yonder from the coast till 800 m. A rating of 2 is appropriate for separation scope of 801–1000 m, and a rating

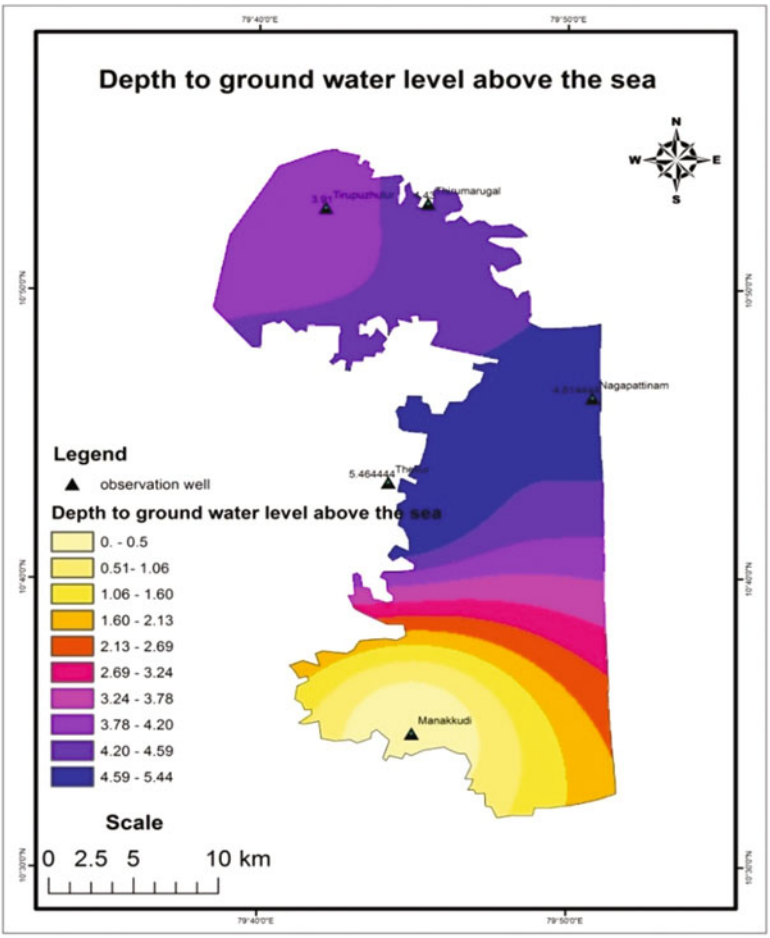

Fig. 10.2 Depth to groundwater level above the sea

is 1 is received for all the separation more noteworthy than 1001 m. In the present examination, boundaries of beach front regions inside 100, 200, 300, 400, 500, 600, 700, 800, 900, 1000, and >1000 m from the coastline are recognized and delineated (Fig. 10.3 and Table 10.5).

10.4.5 Impact of the Existing Status of Seawater Intrusion (I)

At the point when the zone under mapping is under saline pressure, this pressure might have just adjusted the characteristic water-powered harmony among seawater and new ground waterfronts. The examination territory is as of now under pressure

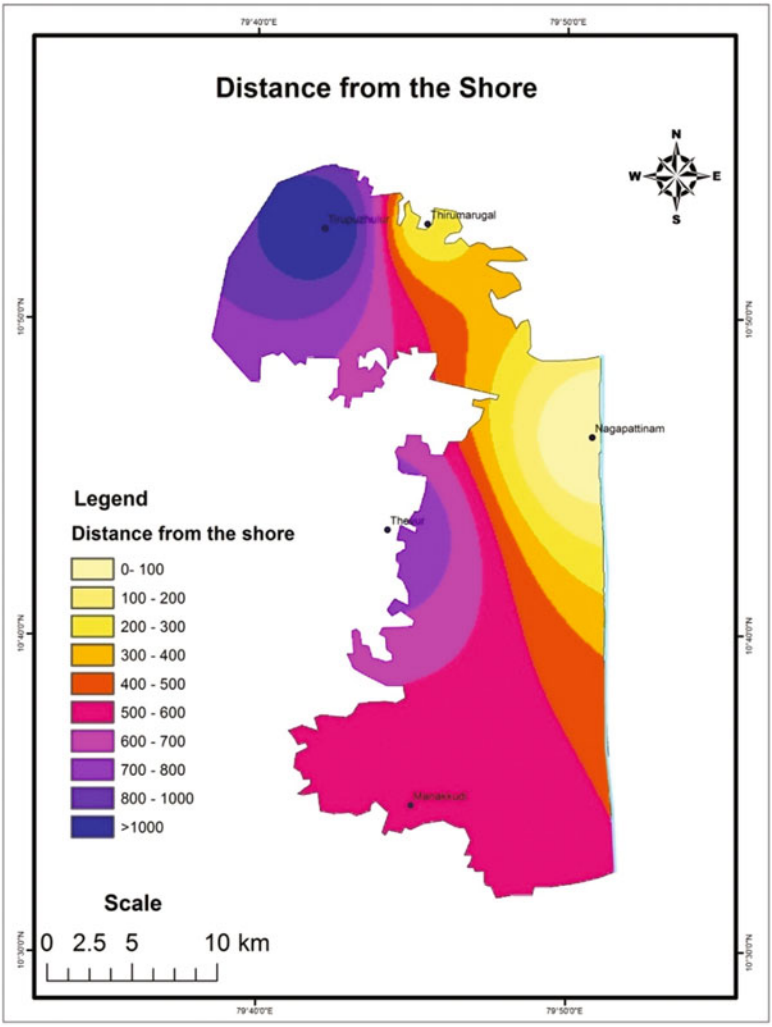

Fig. 10.3 Distance from the sea

Table 10.5 Ratings for parameter distance from shore/high tide

Indicator	Weight	Indicator variables		Importance rating
		Class	Range	
Distance from shore/high tide (m)	2	Very small	<500	10
		Small	500–750	7.5
		Medium	750–1000	5
		Far	>1000	2.5

Table 10.6 Ratings for parameter impact status of existing seawater intrusion

Indicator	Weight	Indicator variables		
		Class	Range of Cl^{-}/ $[HCO_3^{-1} + co_3^{2-}]$, the ratio in epm in groundwater	Importance rating CI^{-1}/ $[HCO_3^{-1} + CO_3^{2-}]$, ratio of ground water
Impact status of existing seawater intrusion	1	High	>2	10
		Medium	1.5–2.0	7.5
		Low	1–1.5	05
		Very low	<1	2.5

(Dhinagaran 2008), and along these lines such saline pressure should to be considered in surveying the defenselessness of the waterfront springs for saline water interruption. The particular appraisals were distinguished by the GALDIT model (Table 10.6)

1. Areas previously interfered by the seawater in all seasons or groundwater tests demonstrating the proportion of $Cl/(HCO_3 + CO_3)$ >2 epm.
2. Areas where occasional seawater interruption wins or groundwater tests having a proportion of $1.5 < Cl/(HCO_3 + CO_3) < 2$ epm.
3. Areas where seawater interruption was seen previously or groundwater tests show a proportion of $Cl/(HCO_3 + CO_3)$ <1.5 epm.

The data for the above rating were assembled from verifiable reports, a request from the neighborhood individuals, and compound examination of groundwater information. For this investigation, the groundwater quality information checked over time of 10 years (1996–2015) at the 07 perception wells by the general population work division (PWD) of the state Government was used. It ought to be noted here that these 04 perception wells are similar wells from where the groundwater level was watched. The Cl/ $(HCO + CO_3)$ for each observation well of all 07 observation well data was calculated. Then, the average of ratio was calculated. The calculated average of $Cl/(HCO + CO_3)$ ratio in the study area was found to be in the range of 0.56–2.82 and is depicted in Table 10.6 and Fig. 10.4.

10.4.6 The Thickness of the Aquifer Mapped (T)

Spring thickness or immersed thickness of an unconfined spring assumes a significant job in deciding the degree and greatness of seawater interruption in seaside territories. It is settled that the bigger the spring thickness, the bigger the degree of seawater interruption and the other way around. Keeping this as a rule, a rating of 1 is given for springs with a thickness under 1 m, and this rating increments by a factor of 1 for each 1 m increment in spring till 8 m. For springs between 8.1 and 10 m thickness, a rating of 9 is allocated. Past 10.1 m, a consistent rating of 10 is utilized.

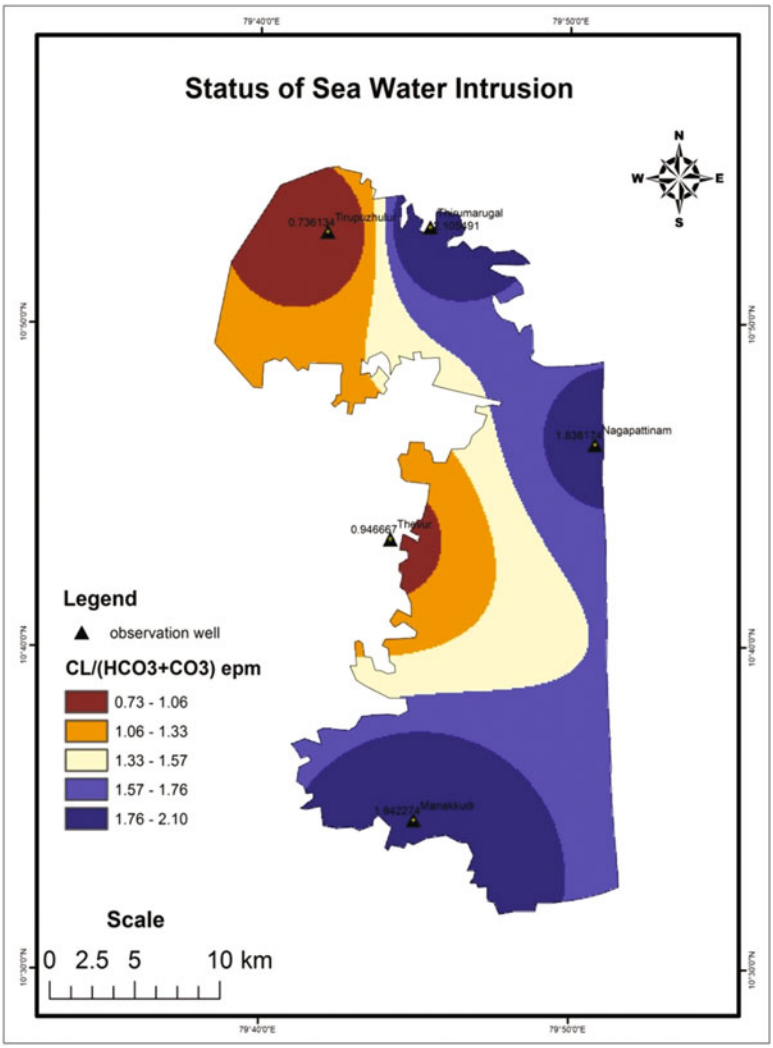

Fig. 10.4 Status of sea water intrusion

The thickness of springs in Nagapattinam beach front zone territory is from 30 to 70 m (Dhinagaran 2008). A rating of 10 is given for this parameter in the whole examination region of the coast according to Table 10.7.

The spring thickness in a given zone can be gotten from lithological logs and can be reasoned from deliberately led vertical electrical sounding information.

Table 10.7 Ratings for parameter aquifer thickness (saturated)

Indicator	Weight	Indicator variables		Importance rating based on the saturated aquifer thickness
		Class	Range	
Aquifer thickness (saturated) in meters	2	Large	>10	10
		Medium	7.5–10	7.5
		Small	5–7.5	5
		Very small	<5	2.5

10.4.7 Computing the GALDIT Index

Every one of the six pointers has a predecided fixed weight that mirrors its relative significance to seawater interruption. The GALDIT Index is then gotten by figuring the individual pointer scores and adding them according to the accompanying articulation,

$$\text{GALDIT-index} = \sum_{i=1}^{6} \{(W_i)R_i\} / \sum_{i=1}^{6} W_i \tag{10.1}$$

where W_i is the weight of the ith indicator and R_i is the importance rating of the ith Indicator.

In this manner, the client can utilize hydrogeologic and land data from the region of intrigue and pick factors to reflect explicit conditions inside that region to pick comparing significance evaluations and process the marker score. This framework enables the client to decide a numerical incentive for any hydrotopographical setting by utilizing this added substance model. The "most extreme GALDIT-Index" is gotten by subbing the greatest significance evaluations of the pointers as shown below.

Similarly,

$$\begin{aligned} \max &= \{(1)*R1+(3)*R2+(4)*R3+(2)*R4+(1)*R5+(2)*R6\} / \sum_{i=1}^{6} W_i \\ &= \{(1)*10+(3)*10+(4)*10+(2)*10+(1)*10+(2)*10\}/13 = 10 \end{aligned} \tag{10.2}$$

The "minimum GALDIT-Index" is obtained by substituting the minimum importance ratings of the indicators as shown below:

$$\text{in} = \{(1)*R_1 + (3)*R_2 + (4)*R_3 + (2)*R_4 + (1)*R_5 + (2)*R6\} / \sum_{i=1}^{M} W_i$$
$$= \{(1)*2.5 + (3)*2.5 + (4)*2.5 + (2)*2.5 + (1)*2.5 + (2)*2.5\}/13 = 2.5 \quad (10.3)$$

Along these lines, the base and most extreme GALDIT-Index changes between 2.5 and 10. The powerlessness of the region to seawater interruption is surveyed dependent on the greatness of the GALDIT Index. In a general manner, bring down the file less helpless against seawater interruption.

10.5 Decision Criteria

When the GALDIT-Index has been registered, it is, accordingly, conceivable to group the beach front regions into different classifications of seawater interruption weakness. The scope of least and greatest GALDIT-Index scores (for example, 2.5–10) is separated into three gatherings as shown in Table 10.8. All the six markers have 2.5, 5, 7.5, and 10 as their significance evaluations. Table 10.9 shows a nitty gritty grouping as obtained from Table 10.5.

10.6 Application of the GALDIT Method to a Case Study in Nagapattinam Taluk

The above strategy was approved utilizing a contextual analysis in the beach front territory of Nagapattinam coast. The GALDIT scores at each of the 04-PWD groundwater checking wells were figured for the Nagapattinam study region Taluk for ordinary existing ocean level (Tables 10.9 and 10.10). These GALDIT esteems alongside the *x* and *y* coordinates were utilized in the Arc GIS 10.1 bundle to draw the weakness map. The guide inferred for this examination territory is given in Fig. 10.5.

A rundown of spots powerless for saline water interruption along the waterfront Nagapattinam is shown in Table 10.11. The outcomes demonstrate that the seaside springs Nagapattinam and Thirumarugal are profoundly defenseless. Different spots fall under defenseless and decently and low classes.

Table 10.8 GALDIT vulnerability classes

Sr. no.	GALDIT-Index range	Vulnerability classes
1	≥7.5	Highly vulnerability
2	5–7.5	Moderately vulnerability
3	<5	Low vulnerability

Table 10.9 Application of the GALDIT method to a case study in Nagapattinam Taluk

S. no.	Indicator	Weight	Range of importance ratings				Range of scores (weight*importance rating)			
			Minimum	In between		Maximum	Min	In between		Max
1	Groundwater occurrence (aquifer type)	1	2.5	5	7.5	10	2.5	5	7.5	10
2	Aquifer hydraulic conductivity	3	2.5	5	7.5	10	7.5	15	22.5	30
3	Depth to groundwater level above sea	4	2.5	5	7.5	10	10	20	30	40
4	Distance from the shore	2	2.5	5	7.5	10	10	20	30	20
5	Impact of the existing status of seawater intrusion	1	2.5	5	7.5	10	2.5	5	7.5	10
6	The thickness of aquifer being mapped	2	2.5	5	7.5	10	5	10	15	20
Total score (T.S)							37.5	75	112.5	130
GALDIT-							2.5	5	7.5	10
Index = T.S/13										

Table 10.10 Classification of Nagapattinam coastal area using GALDIT model

S. no	Vulnerability classification	Affected areas (km^2)	Percentage of affected areas
1	Highly vulnerable	58.63	11.08
2	Vulnerable	174.86	33.07
3	Moderately vulnerable	192.07	36.32
4	Low vulnerable	103.15	19.50

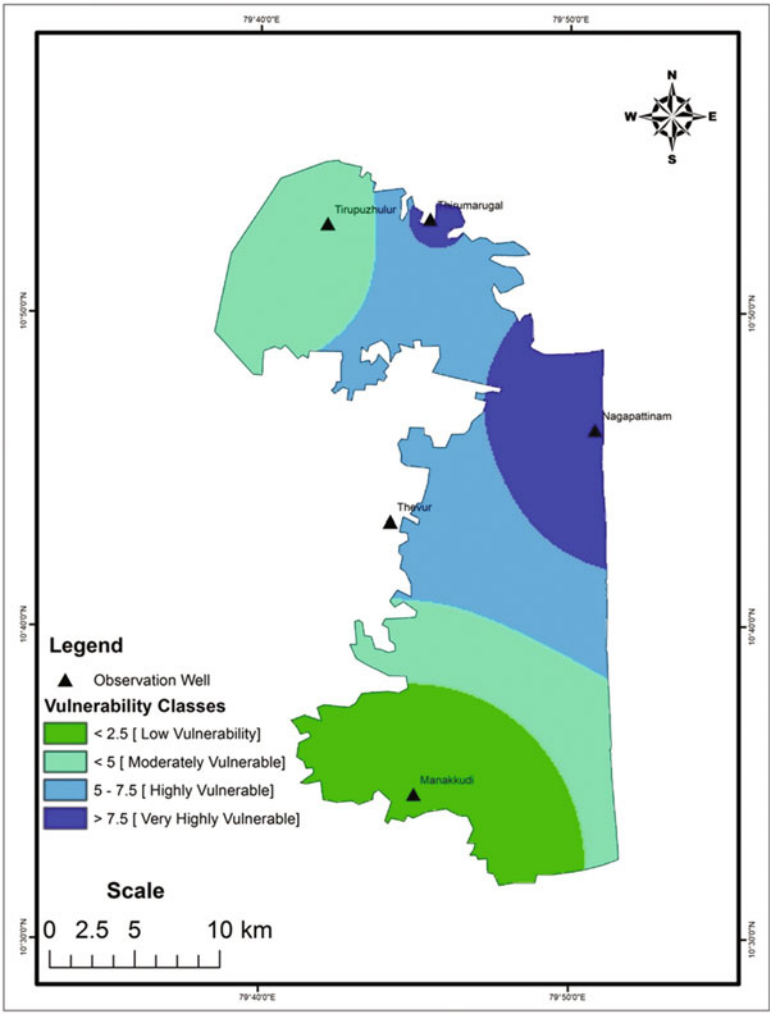

Fig. 10.5 Groundwater vulnerability map

Table 10.11 Level of aquifer vulnerability along the coast belt on Nagapattinam Taluk

Nagapattinam (M)	Highly Vulnerable	Anakkudi	Vulnerable	Mohanur	Moderate
Vadakudi	Highly vulnerable	Radhamangalam	Vulnerable	Thannilappadi	Moderate
Perungandambanur	Highly vulnerable	Thurukkanangudi	Vulnerable	Vappanchery	Moderate
Palaiyur and Sellur	Highly vulnerable	Themangalam	Vulnerable	Palakurichi	Moderate
Nagapattinam	Highly vulnerable	Themangalam	Vulnerable	Ottathattai	Moderate
Sengamangalam	Highly vulnerable	Kohur	Vulnerable	Thalayamazhai	Moderate
Ivanallur	Highly vulnerable	Okkur	Vulnerable	Vadakkupanaiyur	Moderate
Poravacheri	Highly vulnerable	Kottarakkudi	Vulnerable	Anakkudi	Moderate
Andanapettai	Highly vulnerable	Amoor	Vulnerable	Cholavidyapuram	Moderate
Vadakkupoigainallur	Highly vulnerable	Anaimangalam	Vulnerable	Madapuram	Moderate
Pappakovil	Highly vulnerable	Panangudi	Vulnerable	Thiruppoondi (west)	Moderate
Karuvalangadai	Highly vulnerable	Gopurajapuram	Vulnerable	Malavelakarai	Moderate
Panangudi	Highly vulnerable	Kattumavadi	Vulnerable	Karunguni	Moderate
Nagore (Kottagam) and Thethi	Highly vulnerable	Kattumavadi	Vulnerable	Thiruppoondi (east)	Moderate

(continued)

Table 10.11 (continued)

Alathur	Vulnerable	Kurichi	Vulnerable	Kilapidagai	Moderate
Pandaravadai	Vulnerable	Narimanam	Vulnerable	Vizhunthamavadi	Moderate
Siyathanmangai	Vulnerable	Ambal	Moderate	Vettaikkaraniruppu	Moderate
Tirumarugal	Vulnerable	Porakudi	Moderate	Kovilpathu	Moderate
Thittacheri (TP)	Vulnerable	Kongaryanallur	Moderate	Therkupanaiyur	Moderate
Segal	Vulnerable	Kidamangalam	Moderate	Erayankudy	Moderate
Iravancheri	Vulnerable	Polagam	Moderate	Kangalancheri	Moderate
Marungur	Vulnerable	Kayattur	Moderate	Enangudi	Moderate
Turaiyur	Vulnerable	Puttagaram	Moderate	Thirukuvalai	Moderate
Neykuppai	Vulnerable	Tirupugalur	Moderate	Meenamanallur	Low
Kuttalam	Vulnerable	Kuruvadi	Moderate	Valakarai	Low
Periyakannamangalam	Vulnerable	Adalaiyur	Moderate	Keeramber	Low
Vengidangal	Vulnerable	Pudukkadai	Moderate	Keelaiyur	Low
Uttamacholapuram	Vulnerable	Tirukkannapuram	Moderate	Vallam	Low
Vadagarai	Vulnerable	Tiruchengathangudi	Moderate	Karappidagai (north)	Low
Kilvelur (TP)	Vulnerable	Vadagarai	Moderate	Esanur	Low
Sikkal	Vulnerable	Kottur	Moderate	Ettugudi	Low
Abaranadari	Vulnerable	Magilancheri and Visalur	Moderate	Sithamoor	Low
Ponveli	Vulnerable	Kilabudanur	Moderate	Thiruvaimur	Low
Agaraorathur	Vulnerable	Pillali	Moderate	Venmanacheri	Low
Puduchery	Vulnerable	Rarantimangalam	Moderate	Puthur	Low
Orauthur	Vulnerable	Tenkarai	Moderate	Nathapalam	Low
Vadakkalathur	Vulnerable	Melabudanur	Moderate	Karappidagai (south)	Low
Alangudi	Vulnerable	Tiruppayathangudi	Moderate	Manakkudi	Low
Irukkai	Vulnerable	Virukudi	Moderate	Kadanthethi	Low
Vadugachery	Vulnerable	Karaiyur	Moderate	Neermulai	Low
Vadavoor	Vulnerable	Kilathanjavur	Moderate	Pirinjimulai	Low

Mahadanam	Vulnerable	Surakkudi	Moderate	Vadugoor	Low
Therkupoigainallur	Vulnerable	Vaipur	Moderate	Tirumalam	Low
Sembiyamahadevi	Vulnerable	Thiruvathivaimangalam, Kurumberi, and Cholanganallur	Moderate	Muthurasapuram	Low
Chinathumboor	Vulnerable	Vazhkkudi	Moderate	Thalainayar (TP)	Low
Agalangam	Vulnerable	Karaiyur	Moderate	Thalainayar Agraharam	Low
Vandalur	Vulnerable	Serugudi	Moderate	–	–
Velankanni (TP)	Vulnerable	Nadappur	Moderate	–	–
Prathabaramapuram	Vulnerable	Vandampalai,Tiruppallimukkoodal	Moderate	–	–

10.7 Conclusion

A numerical positioning framework to evaluate seawater interruption potential in hydrogeologic settings has concocted utilizing GALDIT factors. The framework contains three critical parts: loads and going from 1 to 4 (1: least noteworthy to 4: generally huge), and a rating an incentive between 1 and 10 relies on the nearby conditions. Each GALDIT factor has been assessed concerning the other to decide the overall significance of each factor. The outcome demonstrates that 58.62 km^2 is highly powerless for saline water intrusion. 174.86 km^2 is defenseless, 192.07 km^2 moderately, and 103.15 km^2 low helpless for Nagapattinam spring to seaside saline water interruption. The perception that the whole examination zone is 534 km^2 might get influenced by the saline water interruption ± to various degrees.

Acknowledgement We thank *Dr.D. Ramesh,* Associate Professor, Department of Remote Sensing, Bharathidasan University, Tiruchirappalli 620 024, India, for assistance with provided laboratory facilities and data products to carried out the research, and *Dr. R.Jegankumar*, Associate Professor and Head, Department of Geography, School of Earth Sciences, Bharathidasan University, Tiruchirappalli 620 024, for comments that greatly improved this manuscript. We would also like to show our gratitude to the *Mr. P.Karthick,* Reseach Scholar, Department of Remote Sensing, Bharathidasan University, Tiruchirappalli 620 024, for sharing their pearls of wisdom with us during this research. Finally, I would like to express my sincere thanks to *Bharathidasan University, Tiruchirappalli*, for providing considerable support and laboratory facilities during the course of this research work.

References

Aller, L., Bennett, T., Lehr, J. H., & Petty, R. J. (1987). *DRASTIC: A standardized system for evaluating groundwater pollution potential using hydrogeologic settings*. U.S. EPA report 600/2-85/018.

Chachadi A. G., & Lobo-Ferreira, J. P. (2001). Sea water intrusion vulnerability mapping of aquifers is using GALDIT method. In *Proceedings of Workshop on Modeling in Hydrogeology* (pp.143–156). Chennai: Anna University and in *COASTIN A Coastal Policy Research Newsletter*, No. 4, March 2001, pp. 7–9. New Delhi: TERI (cf. http://www.teriin.org/teri-wr/coastin/newslett/coastin4.pdf.)

Dhinagaran, V. (2008). *District groundwater brochure Nagapattinam District, Tamil Nadu*. Central Ground Water Board, Government of India.

Ferreira, L., & Chachadi, A. G. (2005). Assessing aquifer vulnerability to saltwater intrusion using GALDIT method: Part 1 – Application to the Portuguese aquifer to Monte Gordo. In *Proceedings of this 4th Interseltic Colloquim on Hydrology, Mangement of Water Resources*, Portugal, pp. 1–12.

Georgescu, P., Dinu, C., Niculescu, V., & Ion, D. (1993). Some applications of VES to groundwater exploration in the vicinity of Romanian coast of the black sea. *Revue Roumaine de Geophysique, 37*, 113–121.

Honnanagoudar, S. S., Venkata Reddy, D., & Mahesha, A. (2012). Aquifer characterization and water quality investigations of tropical aquifer of west coast of India. *International Journal of Earth Sciences and Engineering, 5*(6), 1619–1629.

Khadri, S. F. R., & Moharir, K. (2016). Characterization of aquifer parameter in basaltic hard rock region through pumping test methods: A case study of Man River basin in Akola and Buldhana districts Maharashtra India. *Model Earth System Environment, 2*, 33.

Khadri, S. F. R., & Pande, C. (2015a). Groundwater quality mapping using hydrogen chemistry and Geostatistical analyst of Mahesh River basin, Akola and Buldhana District, Maharashtra, India. *International Journal of Research (IJR), 2*(10), 1–13.

Khadri, S. F. R., & Pande, C. (2015b). Analysis of hydro-geochemical characteristics of groundwater quality parameters in hard rocks of Mahesh River Basin, Akola, and Buldhana Dist. Maharashtra, India using geo-informatics techniques. *American Journal of Geophysics, Geochemistry and Geosystems, 1*(3), 105–114.

Khadri, S. F. R., & Pande, C. (2016a). Ground water flow modeling for calibrating steady state using MODFLOW software: A case study of Mahesh River basin, India. *Model Earth System Environment, 2*, 39. https://doi.org/10.1007/s40808-015-0049-7.

Khadri, S. F. R., & Pande, C. (2016b). GIS-based analysis of groundwater variation in Mahesh River Basin, Akola and Buldhana Districts, Maharashtra, India. *IJPRET, 4*(9), 127–136.

Khadri, S. F. R., & Pande, C. (2016c). Geo-environmental resource management in Mahesh River Basin in Akola and Buldhana Districts, Maharashtra using remote sensing and GIS techniques. *IJPRET, 4*(9), 151–163.

Khadri, S. F. R., Pande, C., & Moharir, K. (2013). Groundwater quality mapping of PTU-1 Watershed in Akola district of Maharashtra India using geographic information system techniques. *International Journal of Scientific & Engineering Research, 4*(9), 832–854.

Lobo-Ferreira, J. P., & Cabral, M. (1991). Proposal for an operational definition of vulnerability for the European Community's Atlas of groundwater resources. In: Meeting of the European Institute for Water, Groundwater Work Group Brussels, Feb. 1991.

Lobo-Ferreira, J. P, Chachadi, A. G., Diamantino, C., & Henriques, M. J. (2005). Assessing aquifer vulnerability to sea-water intrusion using GALDIT method: Part 1 – Application to the Portuguese aquifer of Monte Gordo. IAHS and LNEC. in *Proceedings of the 4th the Fourth Inter Celtic Colloquium on Hydrology and Management of Water Resources*, held at niversidade do Minho, Guimarães, Portugal, July 11–13, 2005.

Moharir, K., Pande, C., & Patil, S. (2017). Inverse modeling of aquifer parameters in basaltic rock with the help of pumping test method using MODFLOW software. *Geoscience Frontiers, 8*, 1385–1395.

Moharir, K., Pande, C., Singh, S., Choudhari, P., Rawat, K., & Jeyakumar, L. (2019). Spatial interpolation approach-based appraisal of groundwater quality of arid regions in aqua. *Journal of Water Supply: Research and Technology-Aqua, 68*(6), 431–447.

Moharir, K. N., Pande, C. B., Singh, S. K., & Del Rio, R. A. (2020). *Evaluation of analytical methods to study aquifer properties with pumping test in Deccan basalt region of the Morna River basin in Akola District of Maharashtra in India, groundwater hydrology*. London, UK: Intec Open Publication. https://doi.org/10.5772/intechopen.84632.

Pande, C. B., & Moharir, K. (2018). Spatial analysis of groundwater quality mapping in hard rock area in the Akola and Buldhana districts of Maharashtra, India. *Applied Water Science, 8*(4), 1–17.

Pande, C. B., Moharir, K. N., Singh, S. K., & Dzwairo, B. (2019). Groundwater evaluation for drinking purposes using statistical index: Study of Akola and Buldhana districts of Maharashtra, India. *Environment, Development and Sustainability (A Multidisciplinary Approach to the Theory and Practice of Sustainable Development), 22*, 7453. https://doi.org/10.1007/s10668-019-00531-0.

Patode, R. S., Nagdeve, M. B., & Pande, C. B. (2016). Groundwater level monitoring of Kajaleshwar-Warkhed watershed, Tq. Barshitakli, Dist. Akola, India through GIS approach. *Advances in Life Sciences, 5*(24), 11207–11210.

Chapter 11
Watershed Planning and Development Based on Morphometric Analysis and Remote Sensing and GIS Techniques: A Case Study of Semi-Arid Watershed in Maharashtra, India

Chaitanya B. Pande, Kanak N. Moharir, and SFR. Khadri

Contents

11.1 Introduction 199
11.2 Study Area 201
11.3 Methodology 202
11.4 Computation of Morphometric Parameters 202
11.5 Usefulness of Morphometric Parameters 204
11.6 Watershed Planning Method 209
11.7 Results and Discussion 209
11.8 Drainage Network and Basin Geometry Parameters of Watershed Area 211
11.9 Land Use and Land Cover 213
11.10 Soil Slope 216
11.11 Conclusion 216
References 217

11.1 Introduction

Nowadays conservation of water and soil resource management are major problems around the globe, but India faces particular challenges with respect to ecosystem and natural resource management. Many advanced technologies are available, but

C. B. Pande (✉) · K. N. Moharir
Sant Gadge Baba Amravati University, Amravati, Maharashtra, India

All India Coordinated Research Project for Dryland Agriculture, Akola, Maharashtra, India

S. Khadri
Sant Gadge Baba Amravati University, Amravati, Maharashtra, India

C. B. Pande, K. N. Moharir (eds.), *Groundwater Resources Development and Planning in the Semi-Arid Region*, https://doi.org/10.1007/978-3-030-68124-1_11

policymakers need to adopt them. Novel technology introduced in this paper, while currently so many researchers focused on the morphometric parameters analysis studied of stream through mathematical equations and which outcomes shown the direction which important part influence on the hydrogeological system, geomorphology, groundwater, geology, and water harvesting (Khadri and Moharir 2016; Khadri and Pande 2016). Drainage parameters provided helpful information on watersheds (Horton 1945; Strahler 1957; Melton 1958; Pakhmode et al. 2003; Gangalakunta 2004; Asfaw and Workineh 2019). Morphometric parameter analysis was conducted to obtain more useful information about landforms and hydrological processes (Srivastava 1997; Agarwal 1998; Nag 1998; Das and Mukhrjee 2005). Currently many researchers and scientists are working on the computing drainage and geomorphic parameters using advanced tools and mathematical formulas (Horton 1932; Clarke 1966).

Majumdar (1982) explained that large drainage networks indicate a linear related with minimum deviation into a direct line ensuing for number of drainages against with drainage orders through logarithm graph. Strahler (1964) described morphometric characteristics to provide information for the known starting surface slope and uncertain rock formations, structural controls, and lithological data on basin areas. Eze and Joel (2010) stated that large volumes of ground runoff are stored using geomorphological structures; surface runoff is a very complex issue in watersheds, while morphometric characteristics should play the main role in controlling and understanding surface runoff in watersheds. Nautiyal (1994) calculated the types of morphometric characteristics, viz. linear features, and earth slope (Nag and Chakraborty 2003; Magesh et al. 2011). Linear and aerial factors such as basin perimeter, slope, soil erosion, stream length, drainage density, stream patterns, and other parameters related to drainage, geology, and erosion were calculated by remote sensing techniques (Kale et al. 1990; Malur and Nagendra 1994; Mesa 2006).

A study of total stream flow intensity was conducted using morphological parameters with associated geographical features. Precise morphometric parameter analysis results indicated that lower-order streams make the main contribution to discharge in watershed areas (Gregory and Walling 1973; Ozdemir and Bird 2009; Srinivasa et al. 2004). The land use variations have been identified as challenging factors related to the planning of watershed activities, and it can be determined through multispectral satellite images which land use types are responsible for environmental modification and damage (Sarangi et al. 2003; Grohmann et al. 2007; Kaliraj and Chandrasekar 2012). From GIS methods are created digital data such as drainage network, slope, geology, and geomorphology maps, and these data can be utilized for conservation planning, i.e. rainwater storage and existing drainage lines for the development of groundwater in rainfed areas. Even though this is a recognized authenticity, currently an insufficient number of studies describe morphometric parameters that can be utilized in watershed areas. Therefore, the aim must be to calculate hydro-morphometric parameters which are suitable for

rainwater collection structures to contribute to rainwater collection preparations related to the watershed growth.

11.2 Study Area

The watershed area is situated in between latitude and long in between 76°46′11″ E and longitude 20°40′ 36″ N latitude . In the study area the annual rainfall is 750–850 mm in the rainfed area. The maximum study area is under older and younger alluvium. The watershed area is a main branch of the Man River basin, which runs west to south in the Akola and Buldhana districts (Fig. 11.1) (Kanak Moharir et al. 2017). In the study area, most farmers sows various crops, such as cotton, soybeans, and chickpeas under dryland conditions. The dryland condition

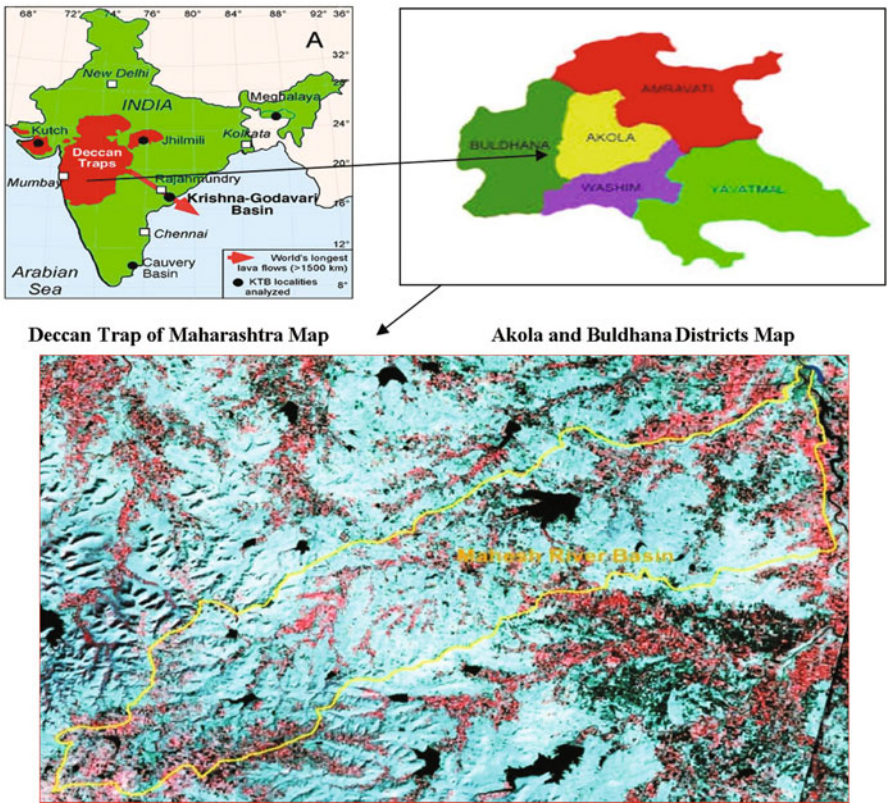

Fig. 11.1 Location map of arid watershed area

causes various problems related to sustainable agriculture production, namely poor yield production and climate change factors, and the watershed area shows problems in terms of groundwater shortages and loses groundwater daily in the aquifer zones. The total basin area is 328.25 km^2. The watershed area has a dry and tropical climate with very warm summers and mild winters. The annual temperature fluctuates from 10.3 °C in winter to 48.7 °C in summer. The basaltic rock formation in the area is thick and includes lava flows between 4.5 and 30 m thick. The Ajanta valley ranges are adjoining both the districts. (Pande et al. 2017b).

11.3 Methodology

This study was conducted using the 35 most important morphometric parameters for watershed management planning purposes in the watershed area. These parameters were taken from DEM data and vector database. Drainage network, basin geometry, stream segments, stream order, drainage pattern, bifurcation ratio, stream density, stream frequency, form factor, relief ratio, overland flow, sub-basin length, perimeter, circularity ratio (Rcn), and drainage texture (Dt) were calculated by mathematical equations and GIS software. (Pareta and Pareta 2011; Magesh et al. 2013). These morphometric characteristics can be play significant roles in the growth of the watershed area. Thematic layers viz. soil slope, flow direction, and viewsheds maps etc. were generated by satellite images and ground truth data. These maps and morphometric parameters are more important for soil and water conservation planning in the area. (Pande and Moharir 2015; Pande et al. 2017a, b). The stream order map was made using a drainage basin network. The soil slope values were generated through satellite data with field data integrated in ArcGIS software; these values indicate soil erosion and provide useful information for water management planning in the area. Land use features were identified through supervised classification techniques and satellite data with ground data. These categories play a major role in land and water planning. Morphometric characteristic analysis easily identified features of the behaviour of the watershed and hydrological systems in the area.

11.4 Computation of Morphometric Parameters

Calculations for the morphometric parameter analysis were performed for two aspects: (1) Drainage Network (2) Basin geometry using defined mathematical equations (Table 11.1). The linear elements were computed such as length of river channel, elongated length, stream hierarchical orders, bifurcation ratio, and stream length ratio were measured for increasing and maintain the watershed natural resources management. In the area aspect of analysis, watershed area, stream density and frequency, circulatory ratio, elongation ratio, and formfactor were measured. Drainage texture, valley index, Texture ratio, and area etc. were estimated under the

Table 11.1 Quantitative characteristics of morphometric parameters with respect to area

S. N	Morphometric parameter	Formula	Reference	Results
A	*Drainage network*			
1	Stream order (S_u)	Hierarchical Rank	Strahler (1957)	1–5
2	First-order stream (S_{uf})	$S_{uf} = N_1$	Strahler (1957)	696.00
3	Stream number (N_u)	$N_u = N_1 + N_2 + \cdots N_n$	Horton (1945)	931.00
4	Stream length (L_u) (km)	$L_u = L_1 + L_2 + \cdots L_n$	Strahler (1964)	761.98
5	Stream length ratio (L_{ur})	GIS Software Analysis	Strahler (1964)	1.34–11.71
6	Mean stream length ratio (L_{urm})	GIS Software Analysis	Horton (1945)	4.33
7	Weighted mean stream length ratio (L_{uwm})	GIS Software Analysis	Horton (1945)	2.97
8	Bifurcation ratio (R_b)	GIS Software Analysis	Strahler (1964)	3.15–13.00
9	Mean bifurcation ratio (R_b)	GIS Software Analysis	Strahler (1964)	6.1
10	Weighted mean bifurcation ratio (R_b)	GIS Software Analysis	Strahler (1953)	4.04
11	Main channel length (C_1) (km)	GIS Software Analysis	–	65.17
12	Valley length (V_1) (km)	GIS Software Analysis	–	48.70
13	Minimum aerial distance (A_{dm}) (km)	GIS Software Analysis	–	46.56
14	Channel index (C_i)	$C_i = C_l/A_{dm}$ (H & TS)	–	1.40
15	Valley index (V_i)	$V_i = V_l/A_{dm}$ (T_S)	–	1.05
16	Rho coefficient (ρ)	$\rho = L_{ur}/R_b$	Horton (1945)	1.94
B	*Basic geometry*			
17	Length from *W* center to mouth of *W* (L_{cm}) (km)	GIS Software Analysis	–	32.98
18	Width of *W* at center of mass (W_{cm}) (km)	GIS Software Analysis	–	13.84
19	Basin length (L_b) (km)	GIS Software Analysis	Schumm (1956)	48.70
20	Mean basin width (W_b)	$W_b = A/L_b$	Horton (1932)	6.74
21	Basin area (A) (km^2)	GIS Software Analysis	Schumm (1956)	328.25
22	Mean area ratio (A_{rm})	GIS Software Analysis	–	4.95
23	Weighted mean ratio (A_{rwm})	GIS Software Analysis	–	2.82

(continued)

Table 11.1 (continued)

S. N	Morphometric parameter	Formula	Reference	Results
24	Basin perimeter (P) (km)	GIS Software Analysis	Schumm (1956)	119.77
25	Relative perimeter (P_r)	$P_r = A/P$	Schumm (1956)	2.74
26	Length area relation (L_{ar})	$L_{ar} = 1.4 * A^6$	Hack (1957)	45.27
27	Lemniscate (k)	$k = L_b^2/A$	–	7.22
28	Form factor ratio (F_f)	$F_f = A/L_b^2$	Horton (1932)	0.14
29	Shape factor ratio (R_s)	$S_f = L_b^2/A$	–	7.22
30	Elongation ratio (R_e)	$R_e = 2/L_b*(A/\pi)^{0.5}$	Schumm (1956)	0.42
31	Ellipticity index (I_e)	$I_e = \pi * V_1^2/4A$		5.67
32	Texture ratio (R_t)	$R_t = N_1/P$	Schumm (1956)	5.81
33	Circularity ratio (R_c)	$R_c = 12.57 * (A/P^2)$	–	0.29
34	Circularity ration (R_{cn})	$R_{cn} = A/P$	Strahler (1964)	2.74
35	Drainage texture (D_t)	$D_t = N_u/P$	Horton (1945)	7.77

basin geometry. All geomorphic parameters were calculated by Arc GIS 10.3 software (Fig. 11.2). These morphometric parameters may effectively use for river basin management (Pande and Moharir 2015).

11.5 Usefulness of Morphometric Parameters

The outcomes of watershed morphometric feature analysis can be valuable information in terms of watershed management planning and ecosystem management. These morphometric parameter values can be important in the preparation of flood zonation maps. The results may be useful for overexploited watershed area. This planning is very helpful for controlling of soil erosion with developed the groundwater recharge structures for overcome of decreasing groundwater level in the futures as well as created some conserved rainwater through soil and water conservation activates and this stored rainwater can be protected crops and maintain the soil moisture in the agriculture field during dry spells and winter seasons.

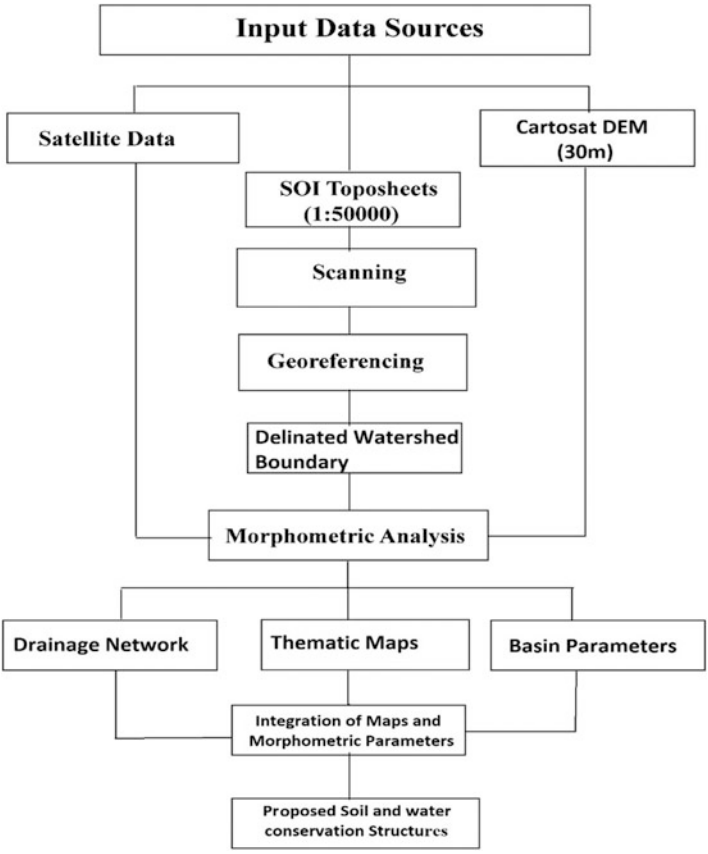

Fig. 11.2 Flow chart of morphometric analysis and soil and water conservation planning

11.5.1 Stream Order

The stream order describes the origin of streams and interconnections among them. Stream order results proved to be helpful for the understanding of stream shape, size, length, width, and discharge amount of the stream system. In this paper, the stream order was classified according to Strahler's ordering system (Strahler 1964). According, to Strahler (1964) the minimum fingertip branches are chosen as stream order 1. Suppose in the drainage network two first-order streams are connected; then a third stream will be denoted as stream order 3.

11.5.2 Stream Number (N_u)

a stream number. Horton (1945) suggested a condition whereby the names of stream parts of respective orders form a geometric arrangement opposite to the stream order number.

11.5.3 Bifurcation Ratio (R_b)

N_u ($N_u + 1$) (Table 11.1) Horton (1945). For different watersheds and basin regions, bifurcation ratio (R_b) has a slight variance value (1957).. The R_b is not similar from one stream order to the following order. Such irregularity is required for geological and hydrological management and the progress of stream basins (Strahler 1964).

11.5.4 Weighted Mean Bifurcation Ratio (R_{bwm})

The bifurcation ratio has been utilized. Bifurcation ratio is every successive couple of stream orders by whole numbers the of drainage and addition of those values of ratio.

11.5.5 Stream Length (L_u)

The stream length values are among the important factors during planning of watershed development. The goal of the construction of any existing drainage is to make it possible to draw on time stream length parameters during the budgeting of soil and water management activities. (Horton 1945).

11.5.6 Mean Stream Length (L_{um})

This parameter is related to the stream line components of a drainage network and their contribution to watershed area water surfaces. L_{um} was calculated using a mathematical equation and standard methods were identified by various scientists and researchers with modern techniques (Strahler 1964).

11.5.7 Stream Length Ratio (L_{urm})

The stream length ratio is an essential parameter for controlling soil erosion, groundwater level, and in situ area planning. Examination of the drainage length ratio between drainage of multiple orders reveals a change in the watershed. This variation is attributed to differences in Mean Sea Level (MSL) and surface slope, representative of the late-young stage of geomorphometric development in the drainage. Horton (1945) has stated that L_{urm} is the ratio of the mean (L_{u}) of the parts of the drainage order (S_{o}) to the mean length of parts of the following lesser stream order ($L_{\mathrm{u}-1}$), which tends to be continuous during successive drainage orders. His law of the stream length ratio states that the mean drainage lengths of stream parts of every consecutive order of a watershed tend to indicate a straight geometric parameter sequence in which the first defined (stream length) is the average length of parts of the first order (Table 11.1). In this analysis, some variations in the stream length ratio for groundwater planning and growth from one law to another indicates their young stages (Kokate et al. 2014).

11.5.8 Channel Index (C_i) and Valley Index (V_i)

The index of river channels was separated into parts (Mueller (1968)) of sinuosity parameter. The analysis of channel length, valley length, and the direct distance between the source and mouth of the river (A_{dm}), i.e., air lengths, is used during the estimation of the channel index and valley index (Table 11.1).

11.5.9 Rho Coefficient (ρ)

The rho coefficient is a significant factor connecting stream density to physiographic and drainage line treatment development of drainage and watershed areas, which simplifies the assessment of the storage volume of a stream network and hence serves as a basis of the final degree of stream improvement (Horton 1945). The watershed development factors has been changed due to climatic, geologic, biological, and geomorphological changes in this parameter.

11.5.10 Length of Basin (L_b)

The basin length and dimension of a basin were estimated by various ways (Schumm (1956)). Similar to the mainstream line. Gregory and Walling (1973) discussed the basin length as being extended in the area in which are finish being the opening of basin. The watershed is measured the distance of the stream network by watershed

inlet to a point on the perimeter intermediate from the watershed or any basin mouth in also way whole the perimeter (Gardiner 1975).

11.5.11 Basin Area (A)

The basin area is a vital parameter like drainage length. Schumm (1956) documented a notable construction in between the total basin area and the entire stream length, which are maintained by sharing watershed or basin areas.

11.5.12 Basin Perimeter (P)

The river basin perimeter is a boundary outside of the basin and watershed area in the surrounding area. This factor is computed along the divisions within the basin, and this parameter may be used as a symbol of watershed size and shape.

11.5.13 Length Area Relation (L_{ar})

Hack (1957) was the first to introduce a large number of watersheds and basins, and the drainage length and basin area are connected by an easy power function as follows:

$$L_{\mathrm{ar}} = 1.4 * A^{0.6}$$

11.5.14 Elongation Ratio (R_e)

It is an important parameter for understanding of the hydrological character system in the stream basin area. Values near 1.0 are characteristic of regions of shallow relief (Strahler 1964).

11.5.15 Digital Elevation Model

Cartosat data with (30 m) were collected from Bhuvan web portal. In this study, various thematic maps were obtained by satellite data to understand the watershed area's situation. They are used to develop the elevation model usually used to describe a topographic surface in three dimensions using geographic information system software. DEM data are handy in terrain analysis, and the different terrain features, including the slope, aspect, relief, watershed hill shade, and flow direction,

were derived using the Arc hydro tool, and these terrain factors are displayed as a form of maps. These data are important for obtaining valuable information on morphometric parameters to allow for enhanced natural resource management (Khadri et al. 2013; Khadri and Pande 2015a, b).

11.5.16 Land Use and Land Cover

The classes of land use were derived using a supervised image classification technique and ArcGIS 10.3 software (Pande and Moharir 2014)). The results demonstrated that the most of the land under in the kharif crops . Land use defines how a portion of land is used, for example, agriculture, settlements, or industry, whereas land cover denotes physical classes such as vegetation, rocks, or water bodies that are present on the Earth's surface. A land use map is important during the planning of watershed development as well as potential ecological development for the watershed area (Pande 2014).

11.6 Watershed Planning Method

In this paper, the results of morphometric analysis are helpful in the preparation of planning for suitable soil and water conservation sites in the watershed. Remote sensing and GIS technologies have been given suitable sites for groundwater recharge planning in the semi-arid region. The preparation of soil and water conservation site maps was done based on digital data. The results can be used for groundwater exploration, cropping systems, and drainage line treatments with the planning of water resource development. Subsequently, all important morphometric parameters were integrated into thematic maps, viz., land use/cover, landforms, drainage, and soil slope, through remote sensing and GIS methods. Thematic maps may be helpful when proposing suitable sites, and these activities are related to rainwater harvesting structures like Nala bund, check dams, percolation tanks, and recharge shafts within the study area (Fig. 11.3).

11.7 Results and Discussion

In a morphometric study, various aspects like drainage and network basin parameters are measured for further planning in the area. Theses parameters are helpful for understanding basic fundamental hydrological system processes and geomorphic landforms through remote sensing and GIS techniques. It is also connected to climate and surface roughness and runoff (Moharir and Pande 2014). In the watershed area, the stream patterns observed are dendritic and sub-dendritic patterns,

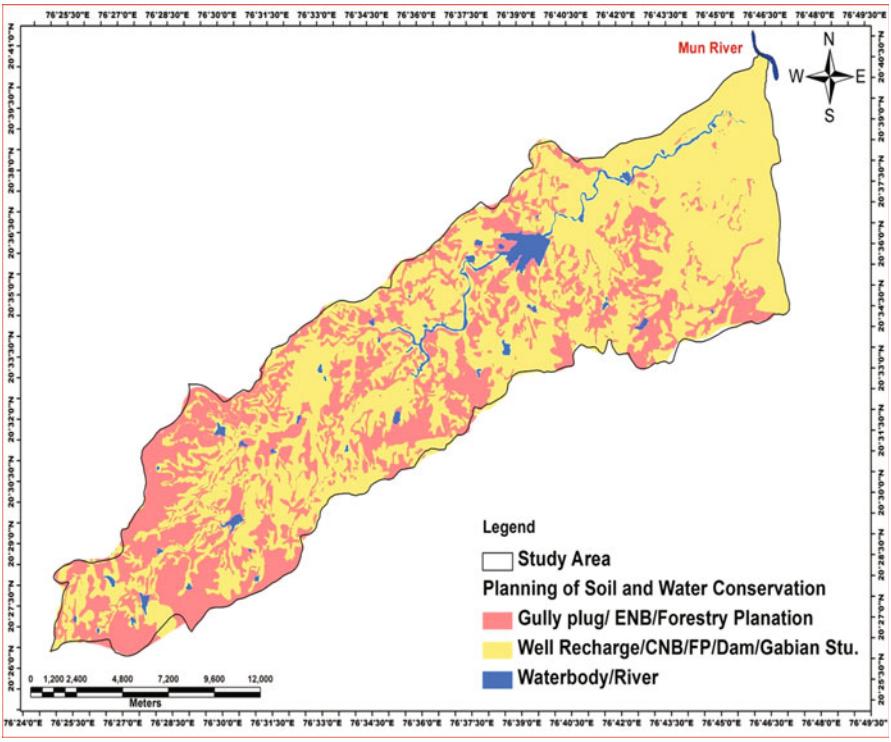

Fig. 11.3 Planning of land and water resources in semi-arid area

which are the more common types formed in drainage networks and are composed the homogeneous rock without control. The dendritic and sub-dendritic system contains large shared drainages, which join into the rivers of the main river network. The longer the period of creation of a stream basin, the more easily dendritic and sub-dendritic patterns form. Arid areas have low values of stream intensity, which implies that the stream density and stream frequency are little impacted on the extent due to denudation lowered surfacestream density. The morphometric parameters are most important in formulating plans related to land and water resource use at the micro-watershed level through RS and GIS techniques. The different parameters are presented in Table 11.1.

11.8 Drainage Network and Basin Geometry Parameters of Watershed Area

Innovative techniques are important in order to obtain accurate information about various aspects to evaluate numerous morphometric characteristics for watershed management. In the observed watershed, the streams were between first and fifth orders. The area showed the large frequency of first-order streams. Drainage network analysis revealed a higher lower frequency of streaming and other stream order on the side. The stream-order maps of the watershed were created using ArcGIS 10.3 software along with the attribute data of the drainage network (Fig. 11.4 and Table 11.1). Stream number were calculated using GIS techniques. In this watershed, the stream numbers 696, 180, 41, 13, and 1 were observed. Total number of the stream by 931 (Fig. 11.4 and Table 11.1). The bifurcation ratio values was found by 3.86–13.00 (Table 11.1). The resulting values or ranges of the ratio R_b are helpful for understanding the watershed area, which have survived small structural disorders (Strahler 1964; Nag 1998). Mean Bifurcation ration was 6.1 by remote sensing and GIS techniques (Schumm 1956). From the study area, the values of R_{bwm} are very close to each other (4.04).

The stream length was examined in ArcGIS 10.3. Generally, the stream length decreases as the stream number increases. Usually, the length of drainage line is large first-order drainage with and order increases. In this paper, the drainage length values were observed to be 433.65, 149.24, 93.76, 44.60, and 40.70, and the total drainage length value was 761.98, as calculated by ArcGIS 10.3. The first-order stream's length was shown to have increased and the fifth-order stream to have

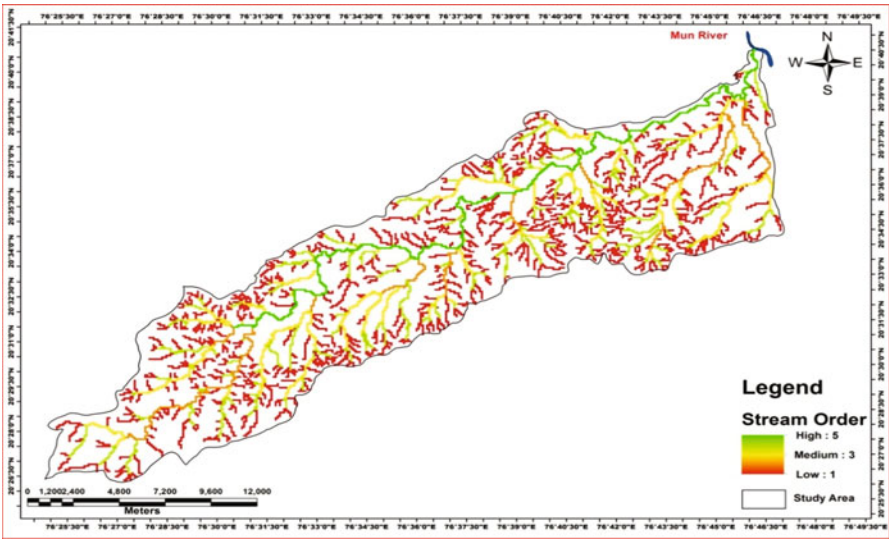

Fig. 11.4 Automatic stream ordering using spatial analysis tools

decreased in the watershed area. The mean stream length ratio was 4.33. Values such as 1.34, 2.75, 1.50, and 11.71 were found, a range of 1.34–11.71. All of this parameter's values were measured from Cartosat-2 data in GIS. The main channel length values computed by 65.17 km (Table 11.1). Rho value is 1.94. These values have shown that the hydrological system increased during flooding. The 48.70 km value was obtained by stream network line (Table 11.1). The obtained values showed 48.70 km through stream network line (Table 11.1). As per Miller (1968) the investigation of valley index value is 1.05 by ArcGIS 10.3 software. This value is more accurate in relation to a valley or watershed area.

An elongated ratio as the thickness of a round is large basin length by Schumm (1956). It is calculated of the shape of watershed and it depend on the associated to the hydrological process, climatic, and geologic formation types. The elongated ratio is 0.42 (Table 11.1). A spherical watershed area or basin is large an effective in the surface runoff discharge than an elongated watershed or basin. The different slopes were obtained using index of elongation ratio, i.e., circular (0.9–0.10), oval (0.8–0.9), less elongated (0.7–0.8), elongated (0.5–0.7), and more elongated (<0.5). That ratio is 0.42, which is denoted the study area is large elongated shape. As Strahler (1964) indicate, the elongation ratio commonly fluctuates in a ratio 0.6–1.0 of the hydrological process system, climatic factors, and geologic structure. The basin area in ArcGIS 10.3 was calculated and observed to be 328.25 km^2 (Table 11.1). The basin perimeter was calculated afnd found to be 119.77 km in the arid area. These parameters are important for natural resource conservation planning (Table 11.1). Therefore, five stream orders were found in the present area.

The maps of the five stream orders were created using GIS software (Fig. 11.5). Two types of techniques were used for the estimation of stream orders. The conventional and automatic techniques are computed (Fig. 11.4). A stream network is very complex in terms of planning drainage line treatment activities and rainwater harvesting structures.

Elevation values were observed by Cartosat-2 DEM data. elevation values. The maximum elevation indicates high runoff and the lowest values show low runoff within Deccan basaltic rocks (Fig. 11.6). The lowest and highest flow direction values of 1–228 were taken by ArcGIS 10.3 in the study area (Fig. 11.7). The flow direction map is important for watershed planning. Water and geological conditions are shown for planning of soil and water activities on the current drainage line and necessary areas within the region under research. Salt water and other water supplies may be decreased with the goal of improving groundwater and surface water resources.

Large part is under in low flow direction hence the water conservation planning is needed for future plan of watershed by data integration in GIS software. Many researchers have conducted drainage and linear parameter analysis but in the ground area, watershed planning has not been conducted using RS and GIS methods. That is why many projects have failed due to irrational planning and system management. Suppose all policymakers related departments and implementing agencies can be implementing of same planning any watershed area that time it can develop more

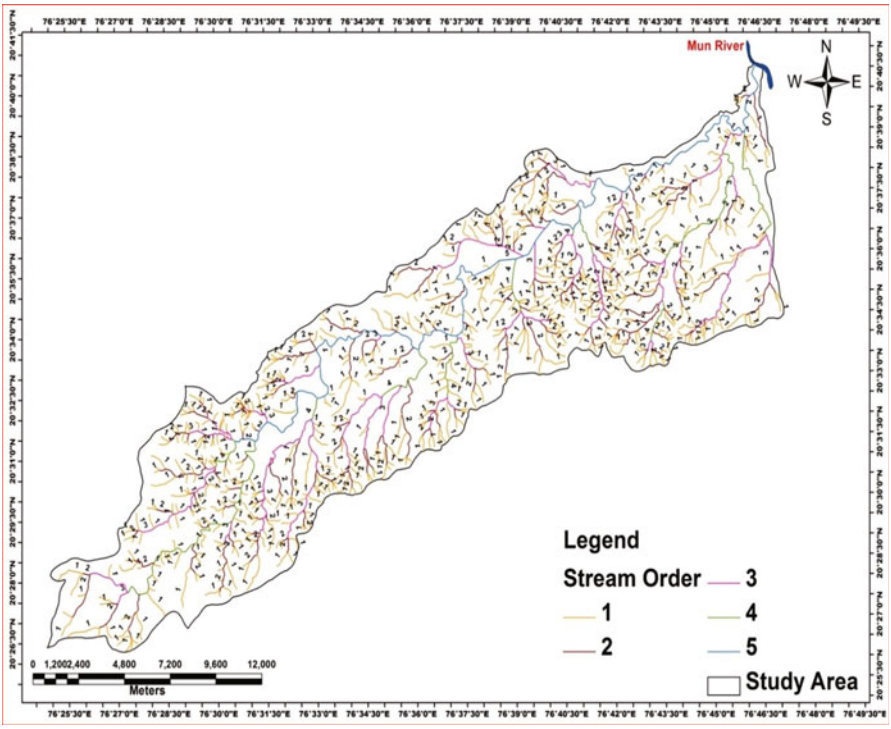

Fig. 11.5 Stream order map

effective on the groundwater and agriculture development area. The viewshed map is made by RS and GIS systems (Fig. 11.8).

11.9 Land Use and Land Cover

Thus, the results show that the area mainly consists of 17 types of land use such as deciduous forest cover, tree plantation, agriculture, water bodies, and settlements (Patode et al. 2017a). These land use map classes play a more prominent role in the planning of watershed development and groundwater improvement recharge structures in Deccan basaltic area (Pande and Moharir 2014; Pande et al. 2018, 2019). The various types of water bodies found are rivers, canals, tanks, ponds, and reservoirs, as seen in satellite images, and these data showed directly the land classification in the area (Fig. 11.9).

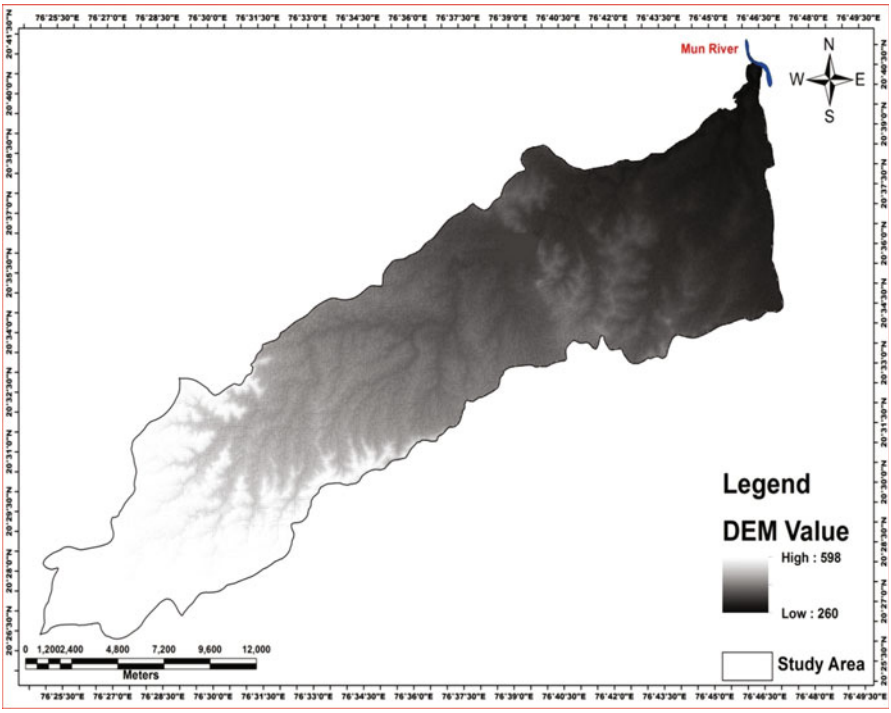

Fig. 11.6 DEM values

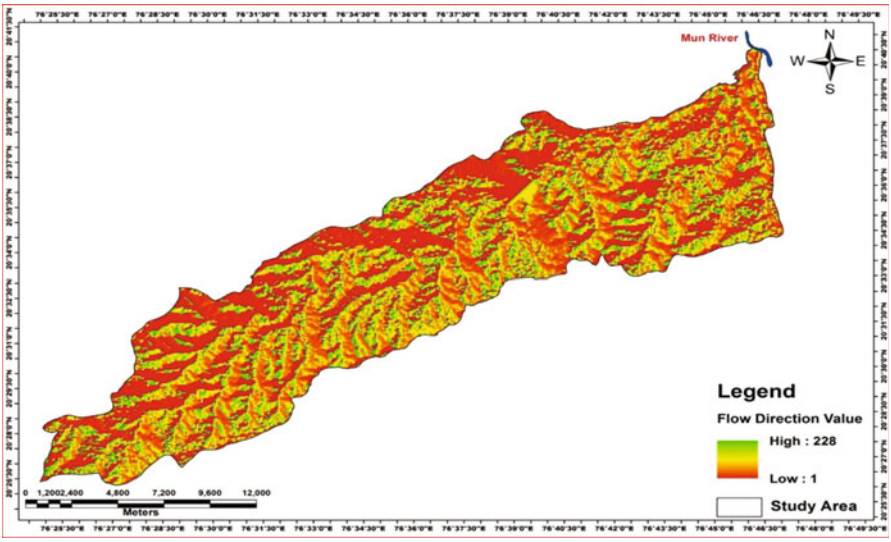

Fig. 11.7 Flow direction

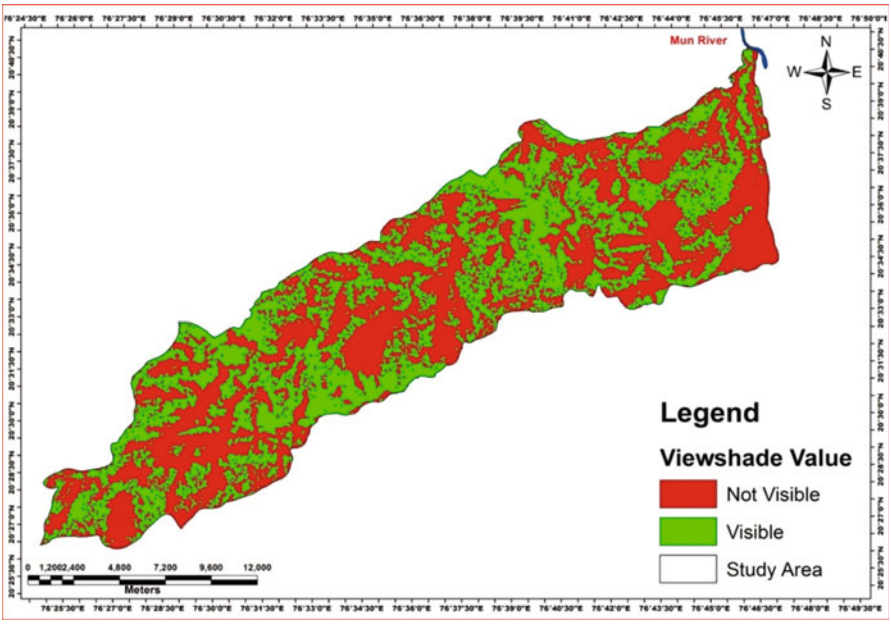

Fig. 11.8 Viewshed map of arid area

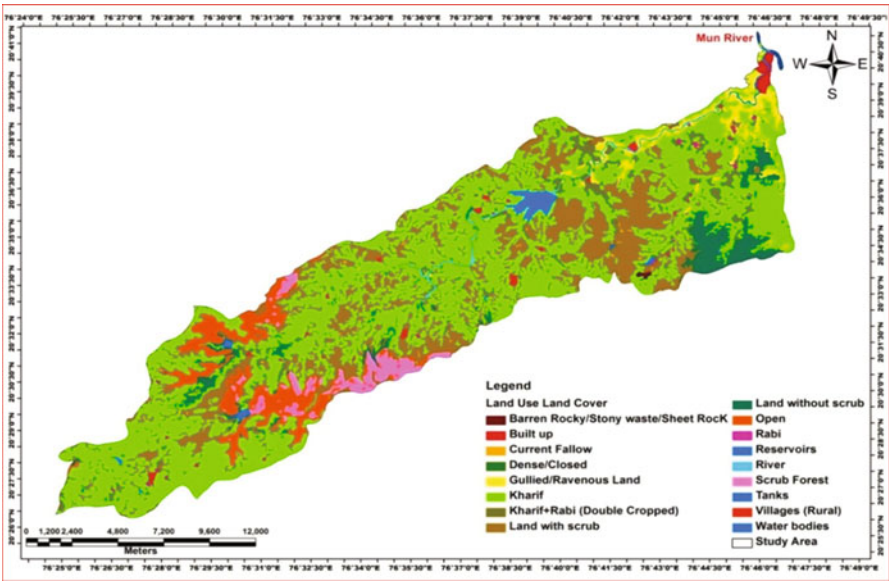

Fig. 11.9 Land use and land cover map (Level III)

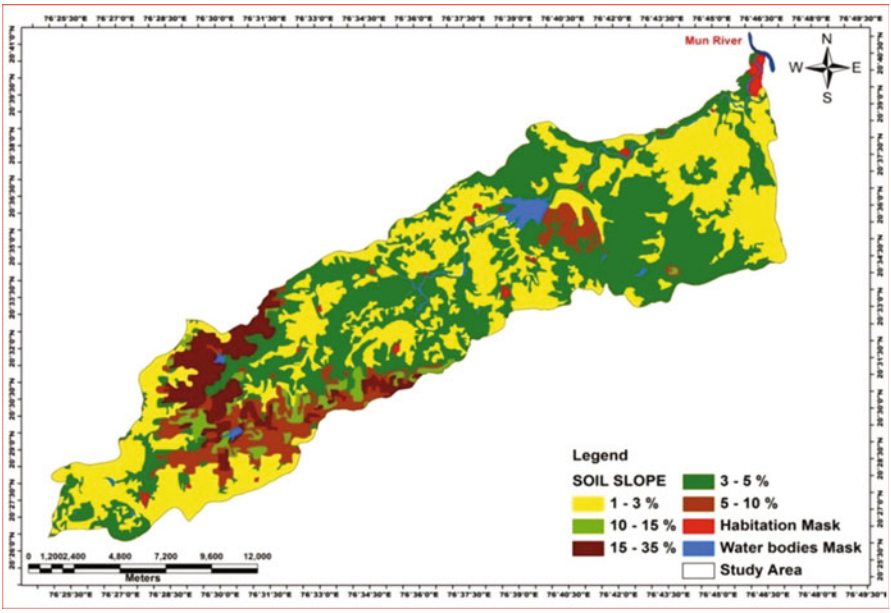

Fig. 11.10 Soil slope map

11.10 Soil Slope

Slope is considered an essential factor in soil genesis and land use. The region of soil slope values have useful for the overall runoff of rainwater and soil erosion groups. A hill is generally defined based on slope percentage. A 10% slope is 10 m in vertical drop per 100 m horizontal distance. Soil management measures become essential in land with a hill as slight as 1–2% to avoid erosion difficulties. The slope map values were estimated from satellite data and field verification information in the area. The soil slope class may be measured during the field investigations. The slope classes are presented in Fig. 11.10 and Table 11.2.

11.11 Conclusion

Basic information was obtained from remote sensing and GIS techniques. The quantitative analysis related to the calculation of the watershed or drainage parameters is more accurate.Various studies have been carried out on the hydrological system mechanism, the drainage network and the management of the basin. Remote Sensing and GIS methods are being given easy platform for computing the various geo-processing functionalities. The analysis of drainage and basin characteristics such as stream length, basin width, basin area, and perimeter may

Table 11.2 Details of soil slope classes

Slope class	Slope (%)
Level to nearly level	0–1
Very gently sloping	1–3
Gently sloping	3–8
Moderately sloping	8–15
Moderately steeply sloping	15–30
Steeply sloping	30–50
Very steeply sloping	>50

be helpful for sustainable and water resources management entire area and existing drainage line. The morphometric parameters were measured by GIS system. It is used for the hydrological systems and morphological land forms. The surface and hydrological system interaction was determined through various morphometric parameters, viz. the stream order, stream length, stream flow direction, catchment area, elongated distance, and morphological landforms for watershed development and management. The different maps was created by Cartosat-2 DEM such as land use, soil slope, and digital elevation can be very helpful for estimating surface runoff and planning of water resources. The land and water planning maps are suggested the soil and water conservation activities such as gully plug/Earthen Nala Bund (ENB)/Planation, well recharge/Cement Nala Bund (CNB)/Farm Pond (FP)/Dam for growth of watershed area (Patode et al. 2017b; Pande 2020a, b, c, d). The proposed soil and water suitable activities are verified with field data and this planning may be very beneficial for agriculture crops, groundwater, and drainage line management.

References

Agarwal, C. S. (1998). Study of drainage pattern through high data in Nahargarh area of Varansi district, U.P. Jour. Indian Soc. *Remote Sensing, 26*(4), 169–175.

Asfaw, D., & Workineh, G. (2019). Quantitative analysis of morphometry on Ribb and Gumara watersheds: Implications for soil and water conservation. *International Soil and Water Conservation Research*. https://doi.org/10.1016/j.iswcr.2019.02.003.

Clarke, J. I. (1966). *Morphometry from maps, Essays in geomorphology* (pp. 235–274). New York: Elsevier.

Das, A. K., & Mukhrjee, S. (2005). Drainage morphometry using satellite data and GIS in Raigad district, Maharashtra. *Journal of Geological Society of India, 65*, 577–586.

Eze, E. B., & Joel, E. (2010). Morphometric parameters of the Calabar river basin: implication for hydrologic processes. *Journal of Geography and Geology, 2*(1), 19–26.

Gangalakunta, P. (2004). Drainage morphometry and its influence on landform characteristics in a basaltic terrain, Central India-A remote sensing and GIS approach. *International Journal of Applied Earth observation and Geo-Information, 6*, 1–16.

Gardiner, V. (1975). *Drainage basin morphometry*. British Geomorphology Group Technical Bulletin No 14, 48p.

Gregory, K. J., & Walling, D. E. (1973). *Drainage basin form and process: A geomorphological approach* (pp. 456–457). New York: Wiley.

Grohmann, C. H., Riccomini, C., & Alves, F. M. (2007). SRTM-based morphotectonic analysis of the Pocos de Caldas alkaline Massif, south eastern Brazil. *Computers and Geosciences, 33*, 10–19.

Hack, J. T. (1957). *Studies of longitudinal stream profiles in Virginia and Maryland*. USGS Professional Paper, 294B.

Horton, R. E. (1932). Drainage basin characteristics. *Transactions of the American Geophysical Union, 13*, 350–361.

Horton, R. E. (1945). Erosional development of streams and their drainage basins: The hydrophysical approach to quantitative morphology. *Bulletin of Geological Society of America, 56*, 275–370.

Kale, V. S., Mudholkar, A. V., Phansalkar, V. G., & Peshwa, V. V. (1990). Stratigraphy of the Bhima group. *J. Palaeontological Society of India, 35*, 91–103.

Kaliraj, S., & Chandrasekar, N. (2012). Geo-processing model on the coastal vulnerability index to explore risk zone along the south-west coast of Tamilnadu, India. *International Journal Earth Science and Engineering, 5*(5), 1138–1147.

Khadri, S. F. R., & Moharir, K. (2016). Characterization of aquifer parameter in basaltic hard rock region through pumping test methods: A case study of Man River basin in Akola and Buldhana Districts Maharashtra India. *Modeling Earth Systems and Environment, 2*, 33.

Khadri, S. F. R., & Pande, C. (2015a). Remote sensing based hydro-geomorphological mapping of Mahesh River Basin, Akola, and Buldhana Districts, Maharashtra, India-effects for water resource evaluation and management. *International Journal of Geology, Earth and Environmental Sciences, 5*(2), 178–187.

Khadri, S. F. R., & Pande, C. (2015b). Analysis of hydro-geochemical characteristics of groundwater quality parameters in hard rocks of Mahesh River Basin, Akola, and Buldhana Dist. Maharashtra, India using geo-informatics techniques. *American Journal of Geophysics, Geochemistry and Geosystems, 1*(3), 105–114.

Khadri, S. F. R., & Pande, C. (2016). Ground water flow modeling for calibrating steady state using MODFLOW software: A case study of Mahesh River basin, India. *Modeling Earth Systems and Environment, 2*, 39. https://doi.org/10.1007/s40808-015-0049-7.

Khadri, S. F. R., Pande, C., & Moharir, K. (2013). Geomorphological investigation of WRV-1 Watershed management in Wardha district of Maharashtra India; using Remote sensing and Geographic Information System techniques. *International Journal of Pure and Applied Research in Engineering and Technology, 1*(10), 151–163.

Kokate, N. R., Moharir, K. N., & Pande, C. B. (2014). Morphometric analysis of Ural Khurd Nala watershed in Akola District of Maharashtra, India: Using remote sensing and geographic information system (GIS) techniques. *International Journal of Research (IJR), 1*(11), 387–397.

Magesh, N. S., Chandrasekar, N., & Soundranayagam, J. P. (2011). Morphometric evaluation of Papanasam and Mani muthar watersheds, parts of Western Ghats, Tirunelveli district, Tamil Nadu, India: A GIS approach. *Environmental Earth Sciences, 64*, 373–381.

Magesh, N. S., Jitheshlal, K. V., & Chandrasekar, N. (2013). Geographical information system-based morphometric analysis of Bharathapuzha river basin, Kerala, India. *Applied Water Science, 3*, 467–477. https://doi.org/10.1007/s13201-013-0095-0.

Majumdar, J. P. (1982). Morphometric analyses of the 4th order drainage watersheds of the Khowai river basin, Tripura, India-some preliminary results and observations. *J Indian Society of Remote Sensing, 10*(3), 49–53.

Malur, M. N., & Nagendra, R. (1994). Litho-stratigraphy of the Bhima Basin, India (Central part), Karnataka, Southern India. *Journal of Palaeontological Society of India, 39*, 55–60.

Melton, M. A. (1958). Geometric properties of mature drainage systems and their representation in E4 Phase Space. *Journal of Geology, 66*, 35–54.

Mesa, L. M. (2006). Morphometric analysis of a subtropical Andean basin (Tucuman, Argentina). *Environment Geology, 50*, 1235–1242.

Moharir, K. N., & Pande, C. B. (2014). Analysis of morphometric parameters using remote-sensing and GIS techniques in The Lonar Nala in Akola District, Maharashtra, India. *International Journal for Technological Research in Engineering, 1*(10), 1034–1040.

Moharir, K., Pande, C., & Patil, S. (2017). Inverse modeling of Aquifer parameters in basaltic rock with the help of pumping test method using MODFLOW software. *Geoscience Frontiers, 2017*, 1–13.

Mueller, J. E. (1968). An introduction to the hydraulic and topographic sinuosity indexes. *Annals of the Association of American Geographers, 58*(2), 371–385.

Nag, S. K. (1998). Morphometric analysis using remote sensing techniques in the Chaka sub-basin, Purulia district, West Bengal. *Journal of Indian Society of Remote Sensing, 26*(2), 69–76.

Nag, S. K., & Chakraborty, S. (2003). Influence of rock types and structures in the development of drainage network in hard rock area. *Journal of Indian Society of Remote Sensing, 31*(1), 25–35.

Nautiyal, M. D. (1994). Morphometric analysis of a drainage basin, district Dehradun, Uttar Pradesh. *Journal of Indian Society of Remote Sensing, 22*(4), 251–261.

Ozdemir, H., & Bird, D. (2009). Evaluation of morphometric parameters of drainage networks derived from topographic maps and DEM in point of floods. *Environmental Geology, 56*, 1405–1415.

Pakhmode, V., Kulkarni, H., & Deolankar, S. B. (2003). Hydrological drainage analysis in watershedprogrammeplanning: A case study from the Deccan basalt. *India Hydrogeology Journal, 11*, 595–604.

Pande, C. (2014). Change detection in land use/land cover in Akola Taluka using remote sensing and GIS technique. *International Journal of Research (IJR), 1*(8), 1–11.

Pande, C. B. (2020a). Introduction. In *Sustainable watershed development. Springer briefs in water science and technology*. Cham: Springer. https://doi.org/10.1007/978-3-030-47244-3_1.

Pande, C. B. (2020b). Watershed management and development. In *Sustainable watershed development. Springer briefs in water science and technology*. Cham: Springer. https://doi.org/10.1007/978-3-030-47244-3_2.

Pande, C. B. (2020c). Thematic mapping for watershed development. In *Sustainable watershed development. Springer briefs in water science and technology*. Cham: Springer. https://doi.org/10.1007/978-3-030-47244-3_3.

Pande, C. B. (2020d). Sustainable watershed development planning. In *Sustainable watershed development. Springer briefs in water science and technology*. Cham: Springer. https://doi.org/10.1007/978-3-030-47244-3_4.

Pande, C., & Moharir, K. (2014). Analysis of land use/land cover changes using remote sensing data and GIS techniques of Patur Taluka, Maharashtra, India. *International Journal of Pure and Applied Research in Engineering and Technology, 2*(12), 85–92.

Pande, C. B., & Moharir, K. (2015). GIS-based quantitative morphometric analysis and its consequences: a case study from Shanur River Basin, Maharashtra India. *Applied Water Science, 7*(2). ISSN 2190-5487. Published online 23 June 2015.

Pande, C. B., Patode, R. S., & Moharir, K. N. (2017a). Morphometric analysis using remote sensing and GIS techniques (a case study of Devdari Watershed, Patur Tq., Akola District, Maharashtra). *Trends in Biosciences, 10*(1), 219–223. ISSN 0974-8431.

Pande, C. B., Khadri, S. F. R., Moharir, K. N., & Patode, R. S. (2017b). Assessment of potential groundwater zonation of Mahesh River basin Akola and Buldhana districts, Maharashtra, India using remote sensing and GIS techniques. *Sustainable Water Resources Management*. https://doi.org/10.1007/s40899-017-0193-5. Published online 8 September-2017.

Pande, C. B., Moharir, K. N., Khadri, S. F. R., & Patil, S. (2018). Study of land use classification in the arid region using multispectral satellite images. *Applied Water Science, 8*(5), 1–11.

Pande, C. B., Moharir, K. N., Singh, S. K., & Varade, A. M. (2019). An integrated approach to delineate the groundwater potential zones in Devdari watershed area of Akola district, Maharashtra, Central India. *Environment, Development, and Sustainability*. https://doi.org/10.1007/s10668-019-00409-1.

Pareta, K., & Pareta, U. (2011). Quantitative morphometric analysis of a watershed of Yamuna Basin, India using ASTER (DEM) data and GIS. *International Journal of Geomatics and Geosciences, 2*(1), 248–269.

Patode, R. S., Nagdeve, M. B., Pande, C. B., & Moharir, K. N. (2017a). Land use and land cover changes in Devdari Watershed Tq. Patur, Distt. Akola, of Vidarbha Region in Maharashtra. Trends in Biosciences, 10(8), 1622–1627.

Patode, R. S., Pande, C. B., Nagdeve, M. B., Moharir, K. N., & Wankhade, R. M. (2017b). Planning of conservation measures for watershed management and development by using Geospatial Technology – A case study of Patur watershed in Akola District of Maharashtra. *Current World Environment, 12*(3), 708–716.

Sarangi, A., Madramootoo, C. A., & Enright, P. (2003). Development of user interface in ArcGIS for estimation of watershed geomorphology. In *CSAE/SCGR 2003 Meeting*, pp. 120–130

Schumm, S. A. (1956). Evolution of drainage systems and slopes in badlands at Perth, Amboy, New Jersey. *Geological Society of American Bulletin, 67*, 597–646.

Srinivasa, V. S., Govindainah, S., & Honne Gowda, H. (2004). Morphometric analysis of sub-watersheds in the Pawagada area of Tumkur district South India using remote sensing and GIS techniques. *Journal of Indian Society of Remote Sensing, 32*(4), 351–362.

Srivastava, V. K. (1997). Study of drainage pattern of Jharia Coalfield (Bihar), India, through remote sensing technology. *Journal of Indian Society of Remote Sensing, 25*(1), 41–46.

Strahler, A. N. (1957). Quantitative analysis of watershed geomorphology. *Transactions of American Geophysical Union, 38*, 913–920.

Strahler, A. N. (1964). Quantitative geomorphology of drainage basins and channel networks. In V. T. Chow (Ed.), *Handbook of applied hydrology*. New York: McGraw Hill Book.

Chapter 12
Correlation Between Land Surface Temperature and Vegetation Cover of Nagapattinam Coastal Zone, Tamil Nadu, Using Geospatial Techniques

Rajesh Jayaraman and Lakshumanan Chokkalingam

Contents

12.1 Introduction 221
12.2 Study Area Description 222
12.3 Land Surface Temperature Mapping 224
12.4 Results and Discussion 226
12.5 Conclusion 233
References 237

12.1 Introduction

Land surface temperature (LST) is a significant factor in global environmental change studies in valuing radiation budgets in heat balance measurements and as a regulator for climate models. Thermal infrared radiation (TIR) remote sensing data can offer significant information on land surface heat changes and surface temperature that is essential when considering landscape processes and reactions. Many satellite sensors are able to sense thermal infrared radiation (TIR) with dissimilar spectral and spatial resolutions. The use of satellite thermal remote sensing in the valuation of surface physical properties and other related variables is explored by

R. Jayaraman (✉)
Mahatma Phule Krishi Vidyapeeth, Ahmednagar, Maharashtra, India

L. Chokkalingam
Department of Remote Sensing, Bharathidasan University, Tiruchirapalli, Tamil Nadu, India
e-mail: drlaks@bdu.ac.in

C. B. Pande, K. N. Moharir (eds.), *Groundwater Resources Development and Planning in the Semi-Arid Region*, https://doi.org/10.1007/978-3-030-68124-1_12

Bayarjargal et al. (2002), Belda & Melia (2000), Cane (1997), Cui and Shi (2012), Ferguson & Woodbury (2007), Gupta (1997), Javari (2001), Khosravi et al. (2017), Kulawardhana (1999), Lai et al. (2012), Li et al. (2002). Satellites with medium spatial resolutions are used predominantly at the regional scale. For this purpose, medium-resolution thermal infrared imagery or data, Landsat thematic mapper (TM)/ETM+, and ASTER have been widely used to read surface temperature (*Ts*) deviations and to relate them to land cover appearances. Emissivity and surface temperature provide greater insight into the overall urban land use/land cover classes and in turn help in considering energy budget issues (Myneni et al. (1996), Yang et al. (1998), Pande et al. (2018)). Guo et al. (2008) applied Landsat ETM+ image 60 m thermal infrared data to observe the connection between LST and vegetation richness in Indianapolis.

Assessing vegetation conditions using satellite imagery requires the development of relevant indices. The normalized difference vegetation index (NDVI) has been recognized as the most useful tool not only in the monitoring of vegetation changes but also in ecosystem assessment in general. Vegetation is directly affected by climatic conditions, mainly in arid and semi-arid areas, and spatio-temporal analysis of the NDVI can enable the assessment of climate changes at local and regional scales. Numerous researchers have also observed the effects of climatic variables on the NDVI (Gao et al. 2012; Wang et al. 2003a, b). In a study on the effects of human activities on the northern lands of South Africa, Wessels et al. (2004) successfully identified degraded lands by assessing advanced very-high-resolution radiometer (AVHRR) NDVI time series. Gao et al. (2012) used a moderate-resolution imaging spectroradiometer (MODIS)-derived NDVI to monitor the impact of forests in north-eastern (N-E) China on climate change.

12.2 Study Area Description

Nagapattinam is a taluk (administrative district) of the Nagapattinam Coastal District of Tamil Nadu located 326 km from southern Chennai; it lies between 10.7906° northern latitude and 79.8428° eastern longitude. The district is famous for its rich religious heritage and communal harmony. In Nagapattinam Taluk, the total population in 2011 was 282,784, with 139,917 males and 142,867 females. The number of households in Nagapattinam Taluk is 50,793. The taluk receives rainfall under the influence of both south-west (S-W) and north-east monsoons. A good amount of rainfall comes as part of very intensive storms resulting mainly from cyclones in the Bay of Bengal, particularly during north-east monsoons. The rainfall pattern in the district shows exciting features. Annual rainfall, 1500 mm at Vedaranyam in the south-east corner of the taluk, quickly decreases to about 1100 mm near the western part of the district. The district enjoys a humid and tropical climate with hot summers, significant to mild winters, and moderate to heavy rainfall. Temperatures

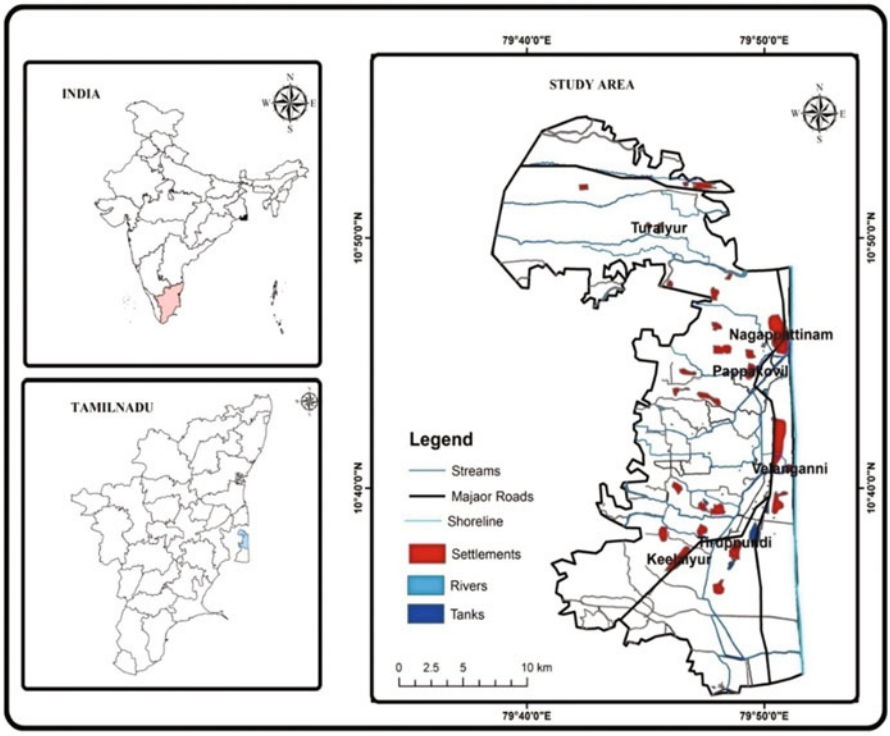

Fig. 12.1 Study area map

vary from 40.6 to 19.3 °C, with sharp declines at night during the monsoon period. The relative humidity ranges from 70% to 77% and is high during the October–November period (Fig. 12.1).

12.2.1 Objectives

The purpose of this study is to correlate the LST and normalized difference vegetation index (NDVI) through the following objectives:

1. Calculate the LST and NDVI.
2. Convert TIRS band data to TOA spectral radiance.
3. Calculate atmospheric brightness temperature.
4. Estimate the LST and NDVI.
5. Determine correlation between LST and NDVI using scatterplot.

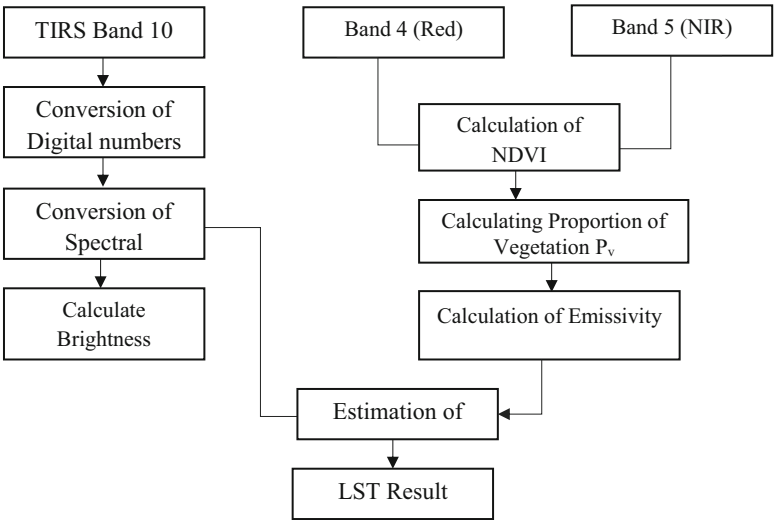

Fig. 12.2 Flow chart of research methodology

12.2.1.1 Methodology

See Fig. 12.2.

12.3 Land Surface Temperature Mapping

The LST maps were prepared using Landsat TM and Landsat OLI for the period of 20 years from 1995 to 2015 using the band math option in the ENVI image processing software package. Following the methodology, measures were adopted to prepare the land surface temperature distribution maps (Fig. 12.2).

12.3.1 Conversion of DN Value to Spatial Radiance

Radiance ($W/m^2 \cdot sr \cdot \mu m$) in TIRS band 10 was calculated from its digital numbers (DNs) using standard NASA calculations by taking the required information from the MTL files given for Landsat 8. It was derived using band math techniques in ENVI. However, TM band 6 (thermal infrared) with a radiant thermal energy between 10.40 and 12.50 was incorporated into ENVI directly to evaluate temperature using the Landsat calibration function to convert DN values into radiance. Additionally, the band math was used to transform the temperature in Kelvin to Celsius. The spectral radiance (L_λ) is considered using the following equation;

however, L_{MAX} and L_{MIN} were replaced by R_{MAX} and R_{MIN}, which are taken from the Landsat 8 MTL file (Eq. 12.1):

$$L_\lambda = \frac{(R_{MAX} - R_{MIN})}{QCALMAX - QCALMIN} \times (DN - QCALMIN) + R_{MIN} \quad (12.1)$$

where

- L_λ = spectral radiance at sensor's aperture (w/m^2 · sr · μm).
- DN = quantized calibrated pixel value (Q cal).
- QCALMIN = minimum quantized calibrated pixel value corresponding to LMINλ [DN] = 1.
- QCALMAX = maximum quantized calibrated pixel value corresponding to LMAXλ [DN] = 255.
- However, QCALMAX for Landsat 8 is 65,535.
- RMIN = spectral at-sensor radiance scaled to QCALMIN (W/m^2 · sr · μm).
- RMAX = spectral at-sensor radiance scaled to QCALMAX (W/m^2 · sr · μm).

12.3.2 Spatial Radiance into Temperature in Kelvin

TM thermal and TIRS band data were converted to spatial radiance, which is a more physically useful variable (Table 12.1). Assuming surface emissivity = 1, the following equation is used to convert radiance to temperature in Kelvin (Eq. 12.2):

$$T = \frac{k_2}{[k_1 \div L_\lambda] + 1} \quad (12.2)$$

where T = temperature in Kelvin, and L_λ = spectral radiance.

12.3.3 Kelvin in Temperature to Celsius

The temperature in Celsius was calculated using the following equation:

$$T\,(^{\circ}\mathrm{C}) = T - 273.13$$

Table 12.1 Spatial radiance into temperature in Kelvin

Constants (units)	K1 (W/m^2 · sr · μm)	K2 (Kelvin)
L5TM	607.76	1260.56
L8 TIRS	774.89	1321.08

where

T (°C) = temperature in Celsius, T = temperature in Kelvin, and 273.13 = zero temperature Kelvin.

Then, with the identification of temperature, temperature difference maps were prepared using ArcGIS.

12.3.4 Normalized Difference Vegetation Index

The NDVI was prepared using Landsat TM and Landsat OLI data for the period of 20 years from 1995 to 2015 using ENVI and ArcGIS software for vegetation changes and correlation studies.

The NDVI is a vegetation index used for deriving vegetation thickness from remotely sensed data. In essence, the algorithm separates the dramatic increase in reflectance over the visible red to near-infrared (NIR) wavelengths and regulates it by isolating the overall brightness of each pixel at those wavelengths as shown in the equation.

$$\mathrm{NDVI} = \frac{\mathrm{NIR} - \mathrm{RED}}{\mathrm{NIR} + \mathrm{RED}}$$

The values in each band were converted from raw DN values to the reflectance of solar electromagnetic radiation. The result of this algorithm is a single band data, and the values range from −1 to +1, where values close to +1 signify larger vegetation cover and negative values represent water bodies.

12.4 Results and Discussion

12.4.1 Correlation Between NDVI and LST (1995)

It is observed that areas like Nagapattinam, Velankkanni, Akkaraipettai, Tirupugalur, and Karapidagai show very low vegetation density with high LST.

The 2D scatterplot of the NDVI and LST (Fig. 12.3) shows a positive correlation, which specifies that the areas with greater vegetation have a lower range of LST. In 1995, the NDVI values ranged from −0.35 to +0.54 and LST varied from 12.58 to 25.61 °C.

The N-S and E-W profiles of the region for LST and NDVI (Fig. 12.4) show significant vegetation and lower LST. The N-S profile has a high value of NDVI with low LST. From the E-W profile, one can observe areas with high temperature values of LST with high NDVI. The E-W area is mostly covered by coastal plain and land-

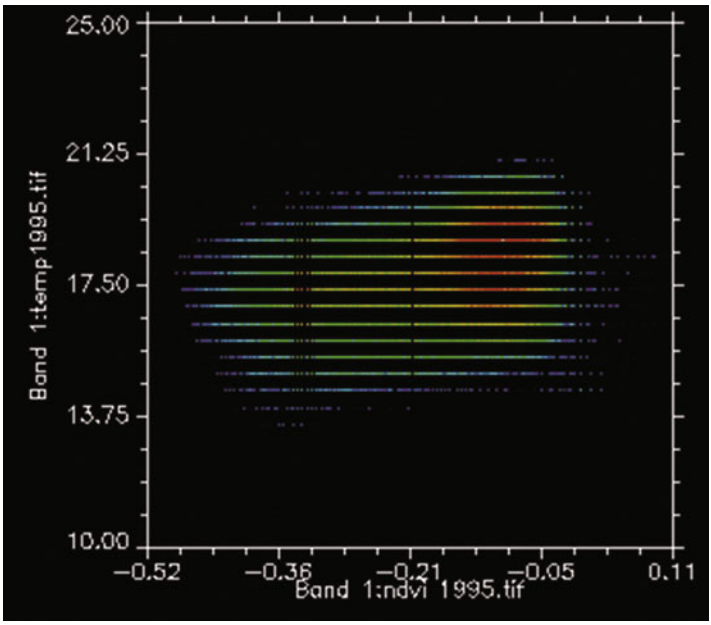

Fig. 12.3 Scatterplot for NDVI and LST (1995)

use categories, viz. most of the terrestrial area is barren land and cropland due to a lack of water and mudflat areas converted into aquaculture ponds, and plantation areas have encroached on aquaculture activity, which is the main reason for the vegetation loss of high LST.

12.4.2 Correlation of NDVI and LST (2000)

LST and NDVI data have shown that areas such as Thalainayar Agragharam, Nagapattinam, Velankkanni, and Thirupundi have very low vegetation density with high LST.

The 2D scatterplots of NDVI and LST (Fig. 12.5) show a positive correlation, which indicates that areas with larger vegetation have a lower range of LST. In 2000, the NDVI values ranged from −0.55 to +0.41 and the LST varied from 16.79 to 28.38 °C.

The N-S and E-W profiles of the LST and NDVI (Fig. 12.6) show a clear negative correlation. The N-S profile shows a high value of LST with low NDVI. From the E-W profile, high values of LST with a low NDVI are observed. The areas mostly occupied by coastal plains and deltaic plains in most regions are barren land and cropland due to a lack of rainfall and water. Most lands are currently fallow and

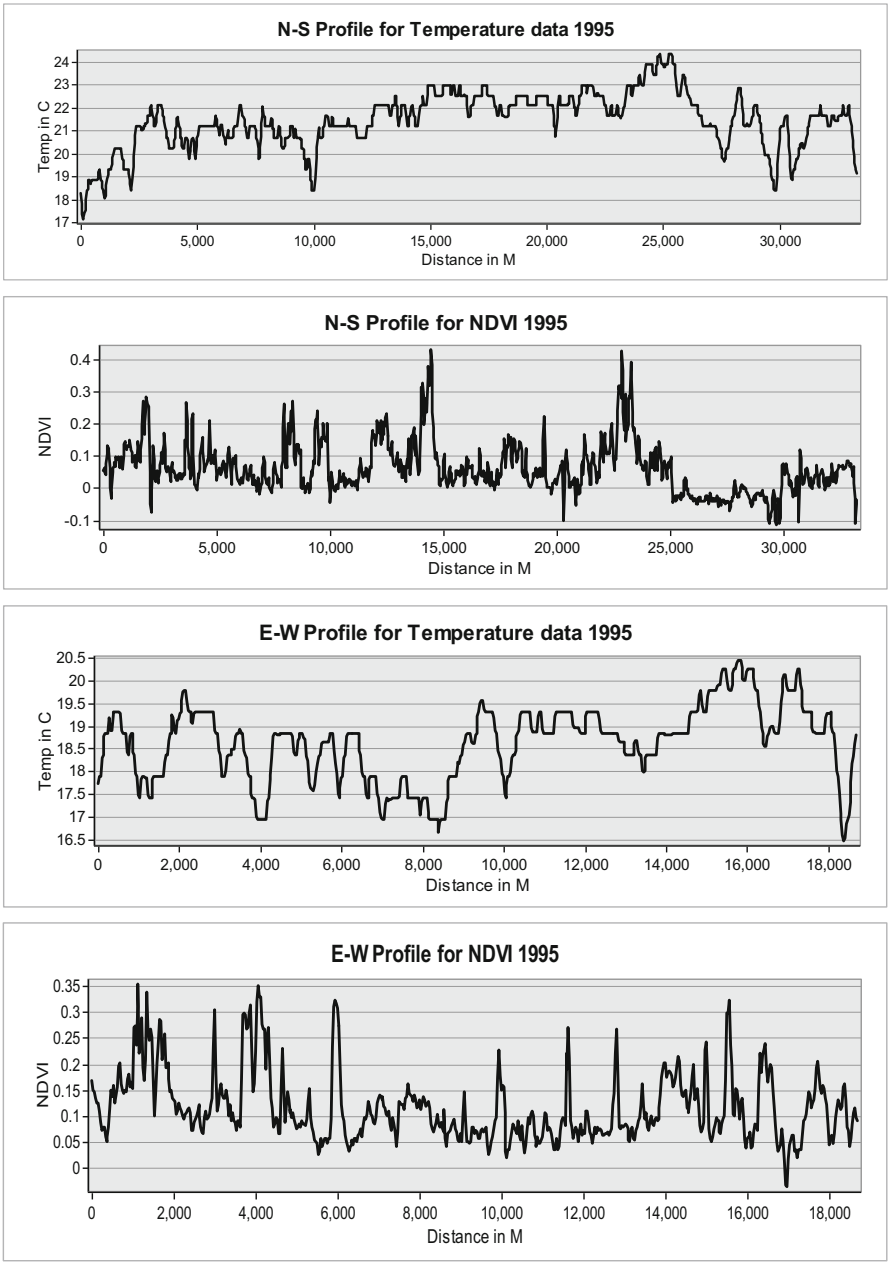

Fig. 12.4 N-S and E-W Profiles of NDVI and LST (1995)

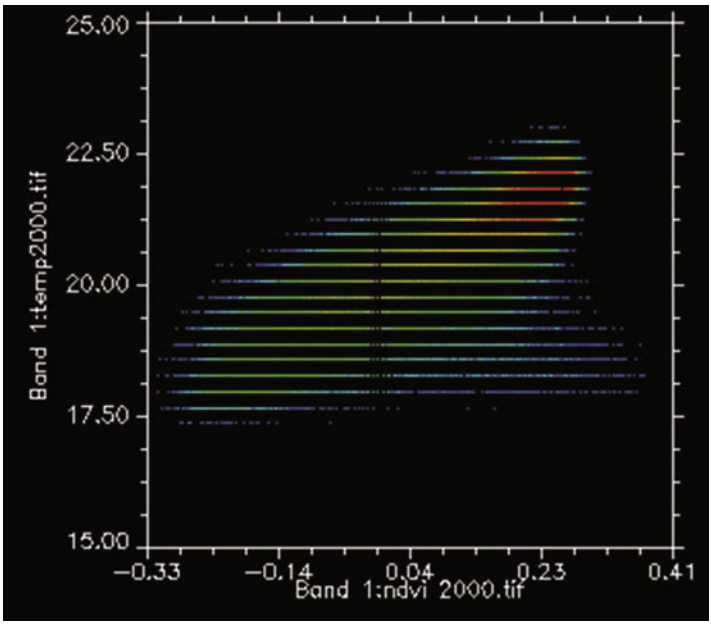

Fig. 12.5 Scatterplot for NDVI and LST (2000)

croplands have been developed, which is the main reason for the loss of vegetation cover.

12.4.3 Correlation of NDVI and LST (2005)

Areas such as Nagapattinam, Velankkanni, Tirupugalur, Kilapidagai, and Therkupoigainallur show very low vegetation cover with high LST. The 2D scatterplot of the NDVI and LST (Fig. 12.7) show a positive correlation, indicating areas with high temperature and a lower range of NDVI. In 2005, the NDVI values ranged from −0.51 to +0.70 and LST varied from 08.55 to 32.14 °C.

The N-S and E-W profiles of LST and NDVI (Fig. 12.8) show a clear positive correlation. The areas in the N-S profile have a peak value of LST with low NDVI. The E-W profile shows that areas between distances of 8000 and 16,000 m show peak values of LST with high NDVI. The areas are mostly barren land, and most of the areas are cropland due to monsoon failure and a lack of water in the river, and most are currently fallow and have been converted for aquaculture purposes, and the vegetation cover decreased and became desertified in the last decade.

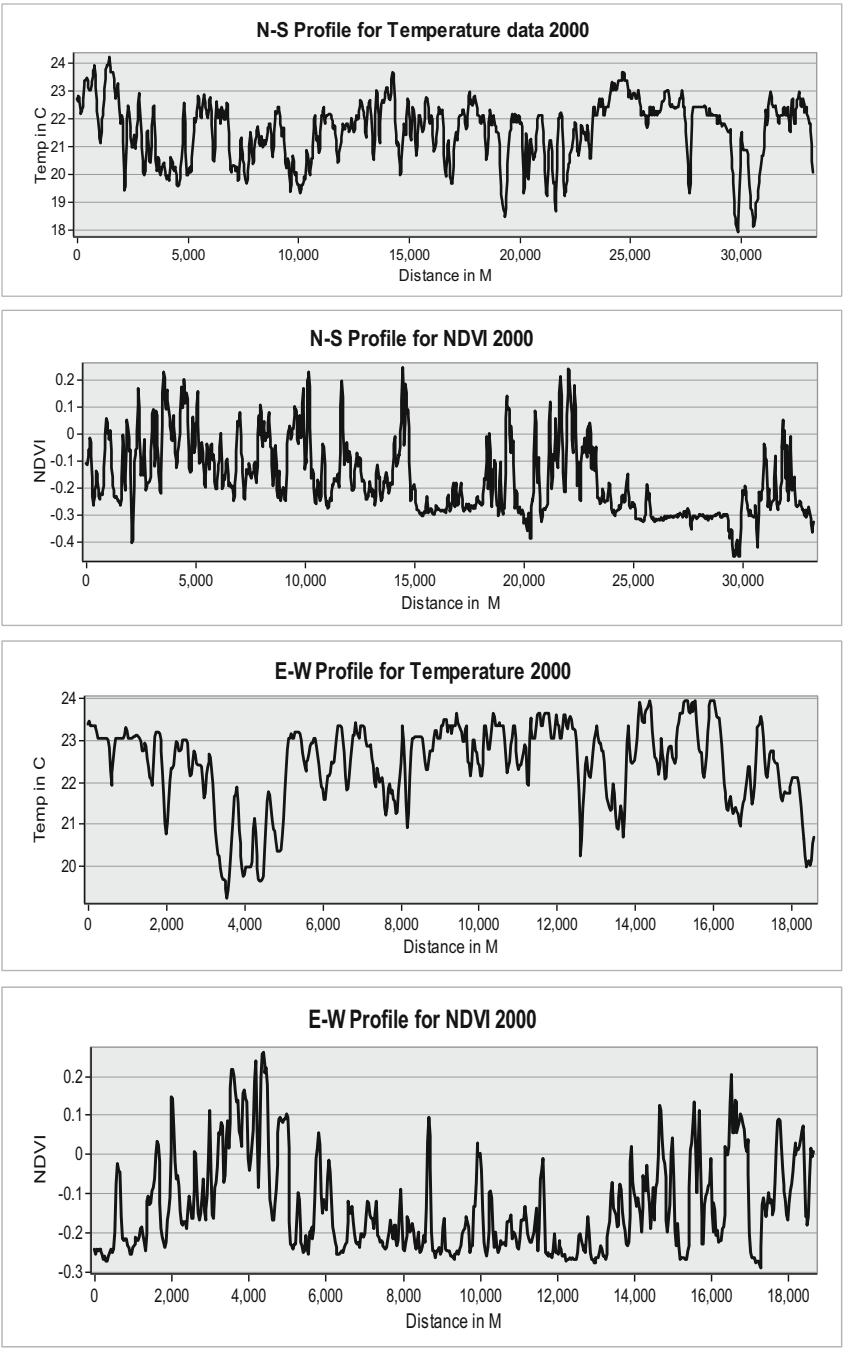

Fig. 12.6 N-S and E-W Profiles for NDVI and LST (2000)

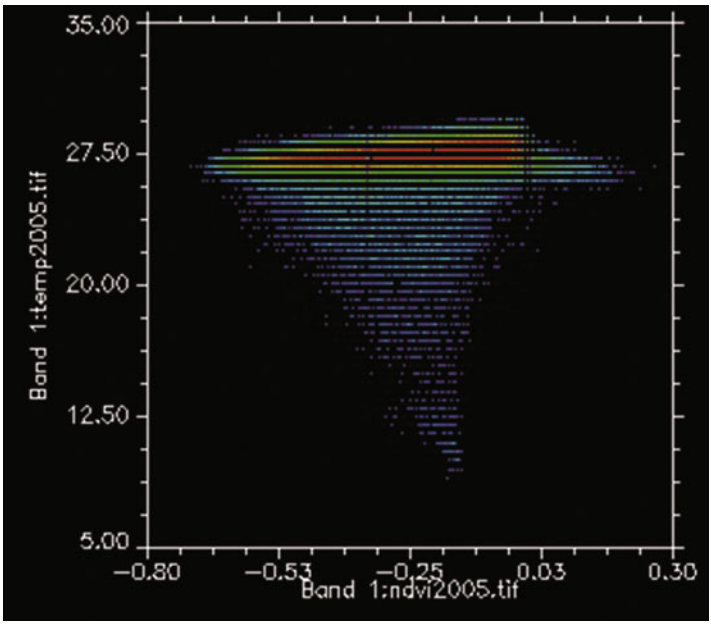

Fig. 12.7 Scatterplot for NDVI and LST (2005)

12.4.4 Correlation of NDVI and LST (2010)

Areas such as Nagapattinam, Velankkanni, Vilunthamavadi, and Tirupundi have very low vegetation with high LST.

The 2D scatterplots of NDVI and LST (Fig. 12.9) display an inverse correlation, which indicates that areas with greater vegetation cover have a lower range of LST. In 2010, the NDVI values range from −0.46 to +0.70 and LST varies from 21.52 to 31.66 °C.

The N-S and E-W profiles of LST and NDVI (Fig. 12.10) display a clear negative correlation. The N-S profile has a maximum value of LST with high NDVI. The E-W profile show high values of LST with high NDVI. The area is mostly cropland and barren land and the land temperature shows expanding low vegetation cover.

12.4.5 Correlation of NDVI and LST (2015)

Areas such as Nagapattinam, Velankkanni, chinathumpoor, Thalayamazhai, Karapidagai, and Cholavidyapuram have very low vegetation with high LST.

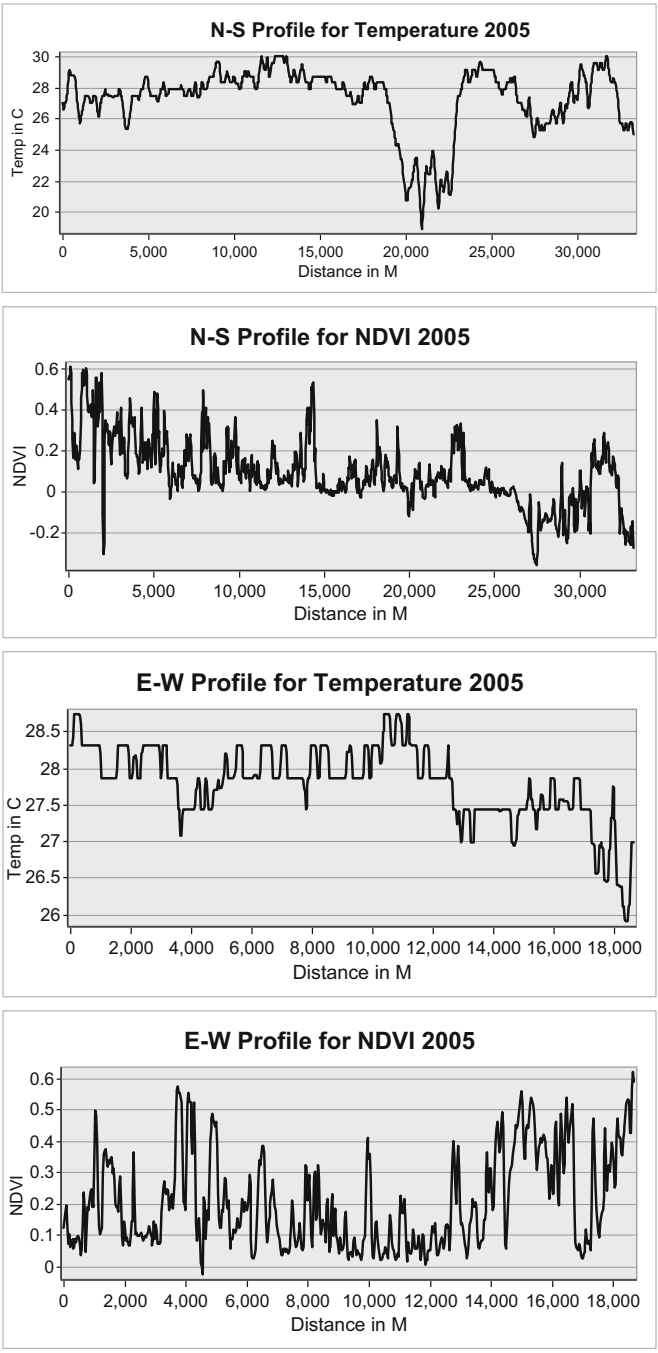

Fig. 12.8 N-S and E-W Profiles for NDVI and LST (2005)

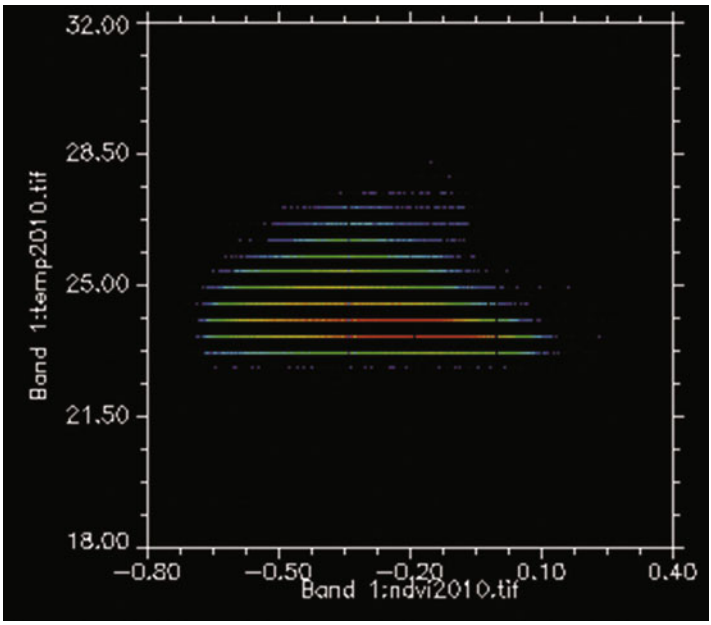

Fig. 12.9 Scatterplot for NDVI and LST (2010)

The 2D scatterplot of NDVI against LST (Fig. 12.11) shows an inverse correlation, which indicates that areas with high LST have a lower range of NDVI. In 2015, the NDVI values ranged from −0.17 to +0.57 and the LST varied from 23.43 to 33.63 °C.

The N-S and E-W profiles of LST and NDVI (Fig. 12.12) display a negative correlation, which is clearly shown in the peaks and valleys. The areas between 20,000 and 30,000 m in the N-S profile has a peak value of LST with low NDVI. The E-W profile shows areas with high values of LST have high NDVI. But in recent times, since June 2015, vegetation cover has increased slightly.

12.5 Conclusion

Areas such as Nagapattinam, Nagore Kottagam Thethi, Velankkani, Vizunthamavadi, Vettaikaraniruppu, Thirupundi, Thalainayar, Tirupundi, Karapidagai, Kovilpathu, Thirukuvalai, Manakkudi, and Keeramber have undergone high land surface temperature changes. The increasing trend in temperature is attributed to a huge lack of aquaculture activities, changes in land cover, especially

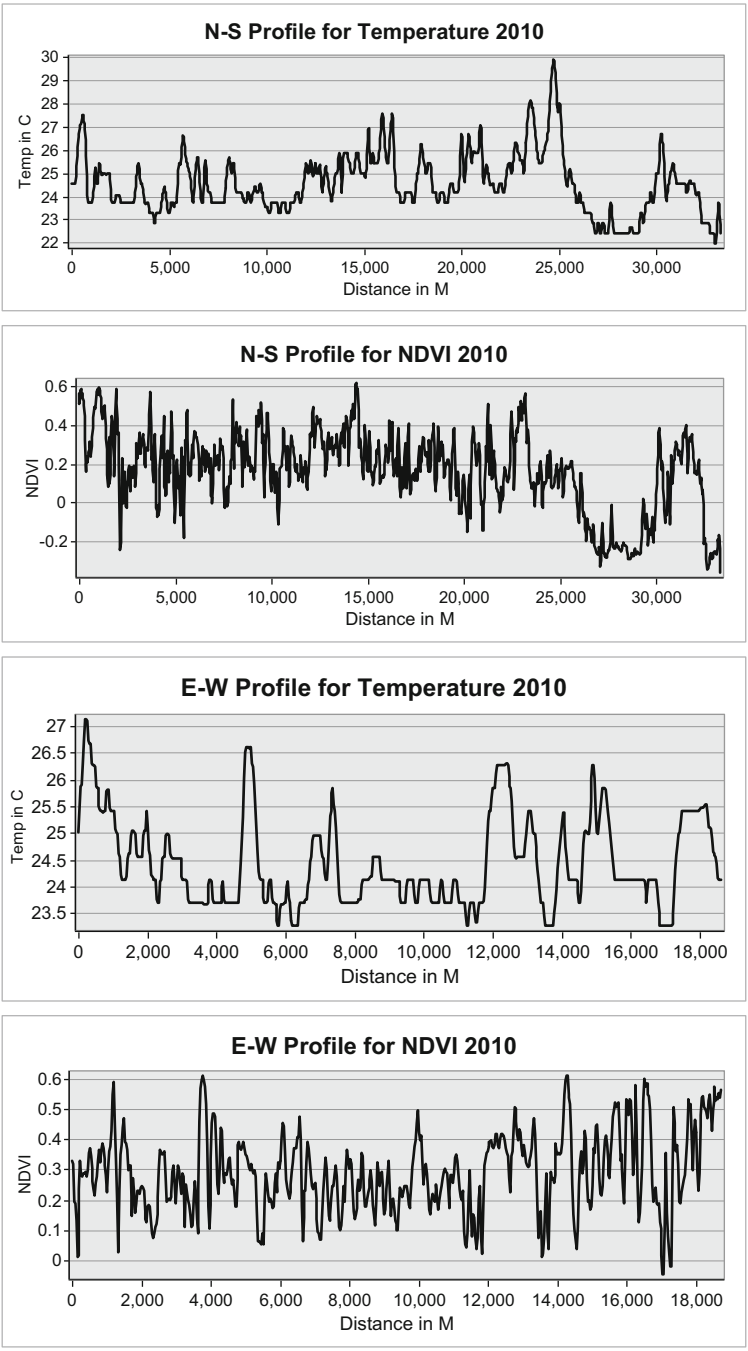

Fig. 12.10 N-S and E-W Profile for NDVI and LST (2010)

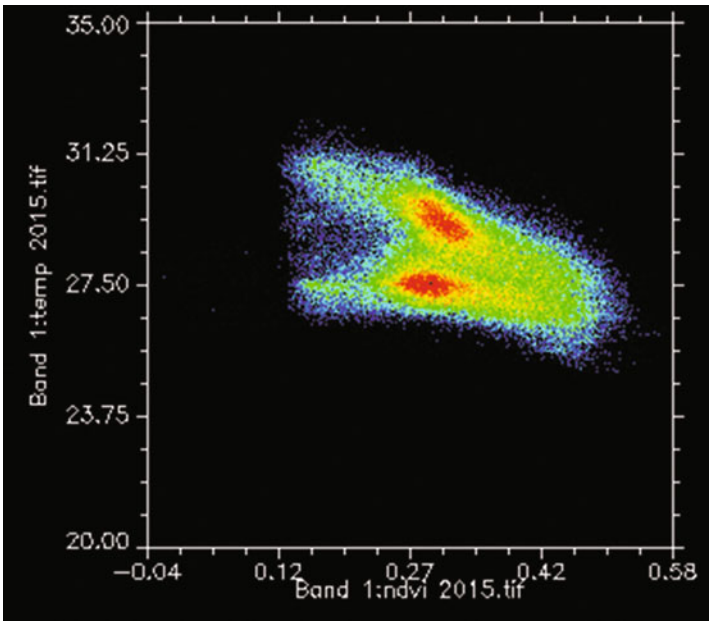

Fig. 12.11 Scatterplot for NDVI and LST (2015)

vegetation cover, and population pressure on the coastal environment in Nagapattinam. The NDVI maps indicate that the vegetation of the Nagapattinam region significantly decreased in the August 1995 to September 2000 period. But compared with previous year, vegetation cover suddenly improved in September 2005, varying from −0.51 to 0.70. The results of NDVI for Nagapattinam, Velankkani, Nagore, Segal, Enangudi, Pandaravadai, Pappakovil, Karuguni, Keelaiyur, and Vallam show vegetation cover decreasing in the 1995–2010 period, slightly increasing later, in 2015, in areas like Ambal, Nagapattinam, Velankanni, Panakkudi, Puthagaram, Palaiyur, Tirupundi, Vilunthamavadi, and Vettaikaraniruppu.

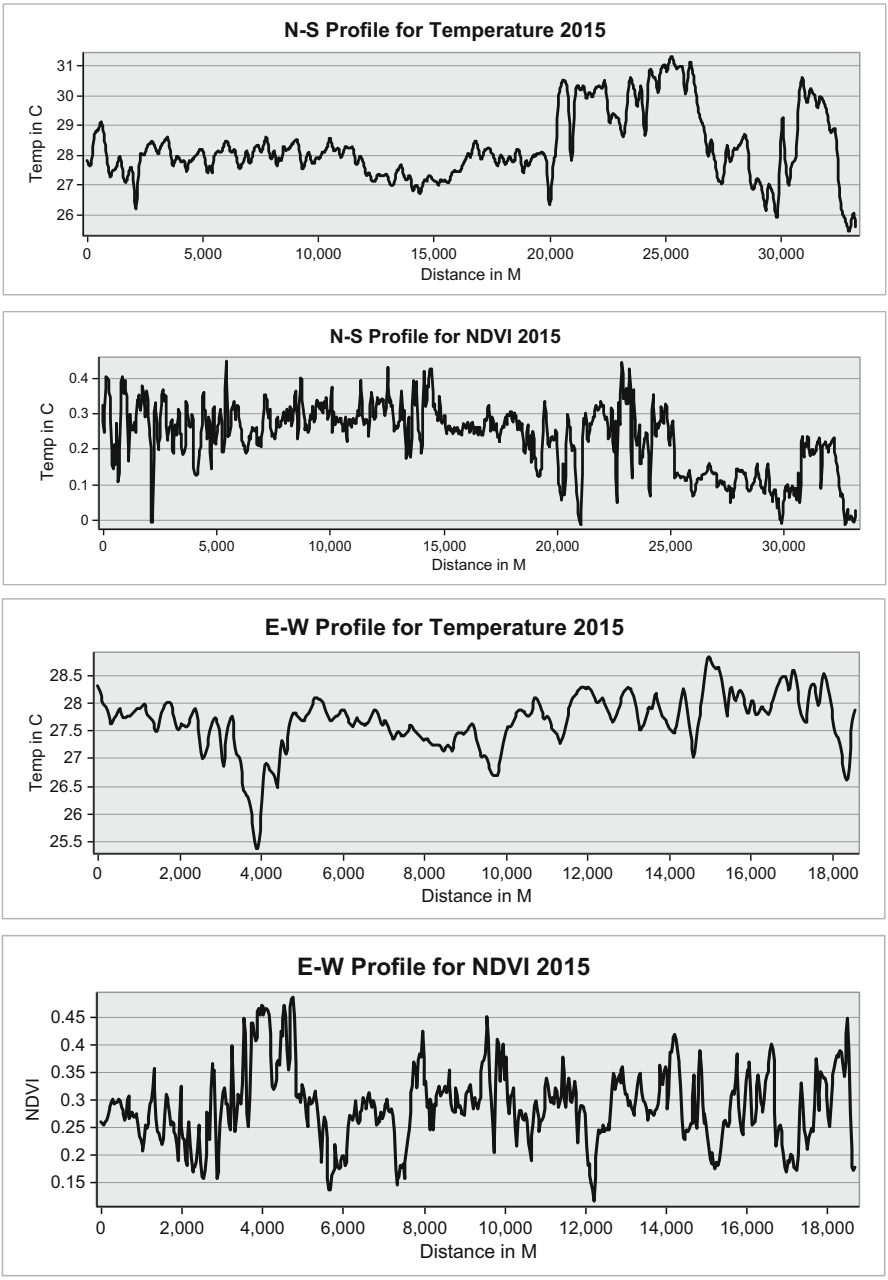

Fig. 12.12 N-S and E-W Profiles for NDVI and LST (2015)

References

Bayarjargal, Yu., Adyasuren, Ts., & Munkhtuya, Sh. (2002). *Drought and vegetation monitoring in the arid and semi-arid regions of Mongolia using remote sensing and ground data [online] GIS development*. Retrieved from http://www.gisdevelopment.net/aars/acrs/2000/ts8/hami0004a.shtml

Belda, F., & Melia, J. (2000). Relationships between climatic parameters and forest vegetation: Application to a burned area in Alicante (Spain). *Forest Ecology and Management, 135*, 195–204.

Cane, M. A. (1997). Twentieth-century sea surface temperature trends. *Science, 275*(5302), 957–960.

Cui, L., & Shi, J. (2012). *Urbanization and its environmental effects in Shanghai, China* (Vol. 3, pp. 123–132). Amsterdam: Elsevier.

Ferguson, G., & Woodbury, A. D. (2007). Urban heat island in the subsurface. *Geophysical Research Letters, 34*, L23713. https://doi.org/10.1029/2007GL032324.

Gao, Y., Huang, J., Li, S., & Li, S. (2012). The spatial pattern of non-stationarity and scale-dependent relationships between NDVI and a climatic factors-a case study in Qinghai-Tibet Plateau, China. *Ecological Indicators, 20*, 170–176.

Guo, N., Zhu, Y., Wang, J., & Deng, C. (2008). The relationship between NDVI and climate elements for 22 years in different vegetation areas of northwest China. *Journal of Plant Ecology, 32*, 319–327.

Gupta, R. K. (1997). The estimation of surface temperature over an agricultural area in the state of Haryana and Punjab, India, and its Relationship with Normalised Difference Vegetation Index (NDVI) using NOAA-AVHRR data. *International Journal of Remote Sensing, 18*(18), 3729–3741.

Javari, M. (2001). *Temperature and precipitation changes in Iran* (pp. 132–138). Tehran: Ph.D. thesis, Tehran University.

Khosravi, H., Azareh, A., Dameneh, H. E., Sardoii, E. R., & Dameneh, H. E. (2017). Assessing the effects of the climate change on land cover changes in different time periods. *Arabian Journal of Geosciences, 3*, 286–294. https://doi.org/10.1007/s12517-017-2837-z.

Kulawardhana, R. W. (1999). *Determination of spatio-temporal variations of vegetation cover, land surface temperature, and rainfall and their relationships over Sri Lanka using NOAA AVHRR data* (pp. 1–67). Kandy: Thesis for the degree of Masters of Philosophy in Integrated Water Resources Management, Institute of Agriculture University of Peradeniya in Sri Lanka.

Lai, Y.-J., Li, C.-F., Lin, P.-H., Wey, T.-H., & Chang, C.-S. (2012). Comparison of MODIS land surface temperature and ground-based observed air temperature in complex topography. *International Journal of Remote Sensing, 33*(24), 17–24.

Li, B., Tao, S., & Dawson, R. W. (2002). Relations between AVHRR NDVI and eco climatic parameters in China. *International Journal of Remote Sensing, 23*(5), 989–999.

Myneni, R. B., Los, S. O., & Tucker, C. J. (1996). Satellite-based identification of linked vegetation index and sea surface temperature anomaly areas from 1982–1990 for Africa, Australia, and South America. *Geophysical Research Letters, 23*, 729–732.

Pande, C. B., Moharir, K. N., Khadri, S. F. R., & Patil, S. (2018). Study of land use classification in an arid region using multispectral satellite images. *Applied Water Science, 8*(5).

Wang, J., Price, K. P., & Rich, P. M. (2003b). Temporal responses of NDVI to precipitation and temperature in the central Great Plains, USA. *International Journal of Remote Sensing, 24*(11), 2345–2364.

Wang, J., Rich, P., & Price, K. (2003a). Temporal responses of NDVI to precipitation and temperature in the central Great Plains, USA. *International Journal of Remote Sensing, 24*, 2345–2364.

Wessels, K. J., Prince, S. D., Frost, P. E., & Van Zyl, D. (2004). Assessing the effects of human-induced land degradation in the former homelands of northern South Africa with a 1 km AVHRR NDVI time-series. *Remote Sensing Environmental Science, 91*, 47–67.

Yang, L., Wylie, B., Tieszen, L. L., & Reed, B. C. (1998). An analysis of relationships among climate forcing and time-integrated NDVI of grasslands over the U.S. Northern and Central Great Plains. *Remote Sensing of Environment, 65*, 25–37.

Chapter 13
GIS-Based Legitimatic Evaluation of Groundwater's Health Risk and Irrigation Susceptibility Using Water Quality Index, Pollution Index, and Irrigation Indexes in Semiarid Region

Balamurugan Panneerselvam, Kirubakaran Muniraj, Maciej Thomas, and Nagavinothini Ravichandran

Contents

13.1 Introduction 240
13.2 Background of the Study 240
13.3 Objective of the Study 241
13.4 Materials and Methods 241
13.5 Results and Discussion 248
13.6 Major Anions 250
13.7 Major Cations 252
13.8 WQI 254
13.9 NPI 254
13.10 FPI 255
13.11 HHRA 256
13.12 Irrigation Indexes 257
13.13 Conclusion 262
References 263

B. Panneerselvam (✉)
Department of Civil Engineering, M. Kumarasamy College of Engineering, Karur, Tamilnadu, India
e-mail: balamuruganp.civil@mkce.ac.in

K. Muniraj
Srii Vickiy and Co., Erode, Tamilnadu, India

M. Thomas
Chemiqua Water & Wastewater Company, Kraków, Poland

N. Ravichandran
Department of Structures for Engineering and Architecture, University of Naples Federico II, Naples, Italy

C. B. Pande, K. N. Moharir (eds.), *Groundwater Resources Development and Planning in the Semi-Arid Region*, https://doi.org/10.1007/978-3-030-68124-1_13

13.1 Introduction

A rapid increase in population density, industrial activities, urbanization, and inappropriate planning of waste management creates more stress on quality of freshwater all over the world. Approximately two third of the world population is depending on groundwater source for their daily needs (Nag and Das 2014; Rawat et al. 2018; Radfarda et al. 2019; Pande and Moharir 2018). Groundwater is one of the most extensive natural sources for domestic, irrigation, and industrial activities and energy generation process (Rufino et al. 2019). In the past two decades, inadequate rainfall, climatic changes, global warming, and contamination of surface water sources due to waste disposal from industries are the major reason for deterioration of groundwater quality in arid and semiarid region of India and all over the world (Solangi et al. 2019; Pande et al. 2019; Khadri et al. 2013; Khadri and Pande 2015a, b). Groundwater contamination is a serious issue related to human health, and it causes 80% of the health risk problems such as diarrhea, anemia, oral hygiene degradation, dental caries, and hepatitis on human being in developing and developed countries (UNESCO 2007).

The nature of groundwater quality is highly depending on the chemical composition, types of aquifer, earth metals, human activities, and minerals present in the soil and rocks (Moharir et al. 2017). The excess concentration of chemical composition in groundwater results the dangerous effects on drinking and irrigation purposes (Moharir et al. 2019, 2020). However, it is critical and major challenge for the researcher works on groundwater chemistry (Aravindan et al. 2010; Shankar et al. 2011b). Numerous researchers across the world have adopted the various techniques along with indexes are water quality index (WQI), nitrate pollution index (NPI), fluoride pollution index (FPI), and irrigation water quality indexes (IWQI) to understand the process of groundwater mechanisms, quality, and hydrogeochemical process, which are associated with lithological effects (Patil et al. 2020; Udeshani et al. 2020; Verma et al. 2020a; Bahir et al. 2020; Zhang et al. 2020a).

13.2 Background of the Study

Narsimha Adimalla (2019) investigated the groundwater quality for drinking, irrigation purpose, and human health risk assessment in semiarid region and stated that geogenic sources such as rock water interaction and infiltrate of leachate from dumping yards are the major factors that influence the nature of groundwater. Aravinthasamy et al. (2019a) carried out the fluoride contamination in groundwater of the shanmuganadhi river basin using multivariate statistics techniques and found that utilization of synthetic fertilizers and modern agricultural activities affect the groundwater quality. They recommended to follow the managed aquifer recharge (MAR) techniques to control the groundwater contamination. Kumari et al. (2019) classified the groundwater suitability for irrigation uses in ulagalla tank cascade

landscape using geographical information system (GIS) and culminated that fluctuation of rainfall intensity, anthropogenic activities, and characteristics of lithological condition deteriorate the good quality of water.

13.3 Objective of the Study

Nilakottai taluk in Dindigul is one of the well-developing regions in Tamil Nadu. However, groundwater is an only source of water for drinking and irrigation uses in the study region. Previous study around the Dindigul district has focused on groundwater contamination due to anthropogenic activities (Selvam et al. 2016; Johnny and Sashikkumar 2014; Sashikkumar et al. 2017). No actions have been carried out to elaborate the nature of groundwater and to identify the source of contamination in the agricultural field of Nilakottai region, Tamil Nadu. The main objectives of the present study are (a) to evaluate the hydrogeochemical properties of groundwater for drinking uses (b) to identify the NPI and FPI of groundwater, and (c) to assess the suitability of groundwater for irrigation uses. The expected outcomes of the present study are going to give detailed knowledge of current status of groundwater and helpful in making an operative waste disposal measure for people in the study region.

13.4 Materials and Methods

13.4.1 Study Area

Nilakottai taluk in dindigul district is located in the south western part of Tamil Nadu, India. It lies in the latitude between 10°0′00″ N and 10°15′00″ N and longitude between 77°40′00″ E and 77°55′00″ E. It has a total surface area of 481.73 km^2. A semi- and tropical monsoon type of climate is predominant in the study area. The average temperature was recorded as 28.6 °C, and minimum of 19.7 °C was recorded during the post monsoon season. The cumulative rainfall of four-monsoon period is 836 mm, and 417.9 mm was recorded during the northeast monsoon. The study area is famous for flowers and grapes compared to other taluks in the district. The most cultivable crops in the study area are vegetables, rice, sugarcane, and cotton. Most of the people depend on groundwater for their daily uses such as drinking and agricultural activities.

13.4.2 Geology Settings

Crystalline groups of rocks occupy over 75% of the area in study region. The study area is essentially covered by Quartzite, which is an important member of group of lithological formation, and a high-grade gneissic terrain characterized by highly deformed rocks was observed in the study area (Fig. 13.1). The linear bands of quartz ranged between 5 and 50 m thick, interlocking with garnet, biotite, diopside, sillimanite, and magnetite minerals. It has a dark gray color, which typically weathers and results in various proportions of quartz and garnet. Action of weathering decreases the silicate minerals and increases carbonate content in aquifers. A few part of the study area covered by quartz k-feldspar rich layers in sandaiyur, kombaipatti, and musuvanooth locations.

13.4.3 Sampling and Analysis

Thirty-six groundwater samples were collected throughout the study region based on the population density, modern agricultural activities, and dumping yards from the bore wells. However, more than 70% of the bore wells were less than 95 m in depth, which are used for domestic and agricultural activities. The samples were collected in prewashed acid leached polyethylene bottles during the premonsoon period and

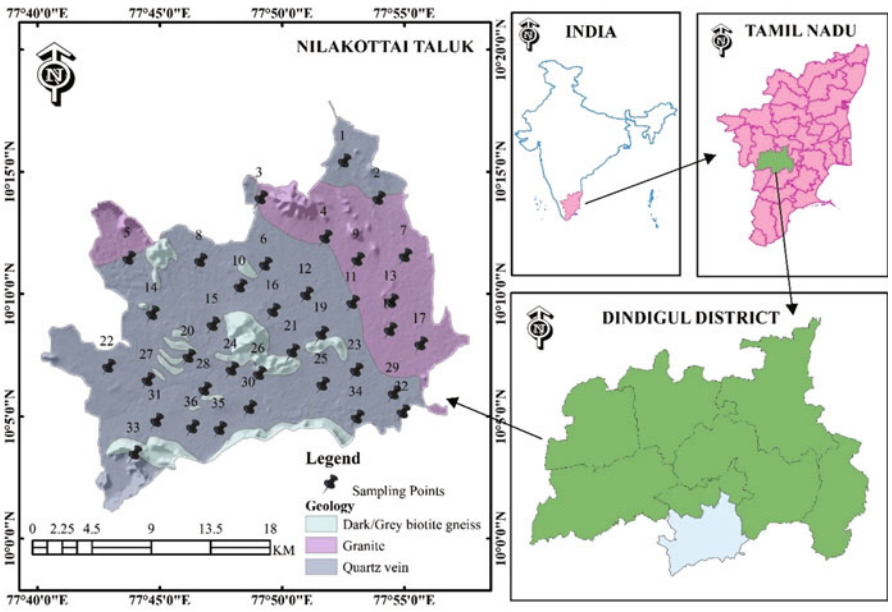

Fig. 13.1 Sample Locations in the study area

stored by adding 5 ml/L of HNO_3. The samples were collected for 10–15 min of purging in order to remove stagnant water from a bore well. It helps to represent the actual nature of aquifer conditions and to obtain more accuracy of geochemical properties. pH and electrical conductivity (EC) of the groundwater were tested during the sampling using hand-type pH, EC, and TDS meter (Hanna, HI-98129). A chemical composition of groundwater was analyzed using standard procedure recommended by American Public Health Association (APHA 2005). In the laboratory, Ca^{2+} and Mg^{2+} were estimated using 0.05 mol L^{-1} of ethylenediaminetetraacetic acid (EDTA) solution by following complexometric titration method. Na^+ and K^+ ions were estimated using flame photometer (S-931). SO_4^{2-} and NO_3^- were determined by UV-visible spectroscopy (LMSP UV1000B). Cl^-, CO_3^{2-}, and HCO_3^- were measured by the titration methods. F^- was estimated using potentiometric ion selective electrode at a temperature of 25 °C. Moreover, in order to avoid the standard error of chemical characterization using Ionic Balance Error (IBE) formula, Eq. 13.1 was used for all the groundwater samples and it was recorded with in the acceptance limit of IBE in the range of ±10%,

$$\text{IBE} = \frac{\sum \text{Cations} - \sum \text{Anions}}{\sum \text{Cations} - \sum \text{Anions}} \times 100. \tag{13.1}$$

13.4.4 Water Quality Index (WQI)

The weighted arithmetic WQI method was used to assess the suitability of groundwater for drinking purpose, and it was developed by Horton (1965) using ten basic water quality parameters (Seifi et al. 2020; Verma et al. 2020b; Bawoke and Anteneh 2020). It helps to communicate the present nature of water to the general public or to the decision makers in water management (Alghamdi et al. 2020; Alam et al. 2020; Badeenezhad et al. 2020). For calculation, WQI has three steps, which are as follows: first step, weightage (w_i) was assigned to each parameter based on the importance of overall water quality for drinking uses and the range of weightage given to each parameter in the present study from 5 to 2 (Table 13.1); second step, relative weight has been calculated for each parameter (Eq. 13.2); and in third step, quality rating (Q_i) was computed for each parameter (Eq. 13.3); finally, water quality index was computed to summation of sub index(SI_i) of each parameter (Eqs. 13.4 and 13.5),

$$W_i = \frac{w_i}{\sum_{i=1}^{n} w_i}, \tag{13.2}$$

Table 13.1 Relative weight of each parameter

Parameters	Weight (w_i)	Relative weight (W_i)
pH	4	0.108
TDS	4	0.108
TH	2	0.054
Ca^{2+}	2	0.054
Mg^{2+}	2	0.054
Na^{+}	2	0.054
K^{+}	2	0.054
Cl^{2-}	3	0.081
$SO_4{}^{2-}$	4	0.108
$HCO_3{}^{2-}$	3	0.081
$NO_3{}^{-}$	5	0.135
F^{-}	4	0.108
	$\sum w_i = 37$	$\sum W_i = 1.000$

$$Q_i = \frac{C_i}{S_i} \times 100, \tag{13.3}$$

$$\mathrm{SI}_i = W_i \times Q_i, \tag{13.4}$$

$$\mathrm{WQI} = \sum \mathrm{SI}_i. \tag{13.5}$$

13.4.5 Nitrate Pollution Index (NPI)

The major reasons for nitrate contamination in groundwater are anthropogenic activities such as waste disposal, sewage intrusion, and synthetic fertilizers for high crop yield and disposal from industries (Shukla and Saxena 2020; Egbi et al. 2020; Suvarna et al. 2020). The threshold and maximum permissible limits for nitrate in groundwater are 20 and 45 mg/L, respectively (WHO 2011; BIS 2012). A continuous consumption of elevated concentration of nitrate in groundwater causes severe effects on human health such as rectum cancers and blue baby syndrome (methemoglobinemia) for infants and children (Wagh et al. 2020; Juntakut et al. 2020; Gao et al. 2020). The main intension of the NPI is to evaluate the nitrate contamination in groundwater, and it was classified into five classes, which are as follows: less than zero is clean water, 0–1 is light pollution, 1–2 is moderate pollution, 2–3 is significant pollution, and greater than 3 is very significant pollution for drinking uses (Bahrami et al. 2020). The following formula was used to compute the NPI of groundwater sample,

$$\mathrm{NPI} = \frac{C_S - \mathrm{HAV}}{\mathrm{HAV}}, \tag{13.6}$$

where C_s is the concentration of nitrate in groundwater sample and HAV is the threshold limit of the nitrate in groundwater.

13.4.6 Fluoride Pollution Index (FPI)

Fluoride is an essential mineral for both animal and human being (Adimalla and Qian 2019a; Younas et al. 2019; Elumalai et al. 2019; Aravinthasamy et al. 2019b). An insufficient and excess concentration of fluoride ion in drinking water causes skeletal and dental problem on human health (Balamurugan et al. 2020b; Singh et al. 2020; Dehghani et al. 2019; Sunkari and Abu 2019). The maximum permissible limit of fluoride in drinking is 1.5 mg/L (WHO 2011; BIS 2012). The main goal of FPI is to assess the level of contamination due to elevated concentration of fluoride ion in groundwater. FPI can be calculated in two steps: (1) to assign weightage for different concentration of fluoride, bicarbonate, sodium/calcium ratio, and pH of groundwater and (2) to calculate average of all parameters using following formula:

$$\mathrm{FPI} = \frac{W_f + W_{\mathrm{HCO3}} + W_{\mathrm{Na/Ca}} + W_{\mathrm{pH}}}{N}, \tag{13.7}$$

where,

W_f is the weight of fluoride, W_{HCO3} is the weight of bicarbonate, $W_{\mathrm{Na/Ca}}$ is the weight of Na/Ca, W_{pH} is the weight of pH, shown in Table 13.2, and N is the total

Table 13.2 Weightage of each water quality parameter

Parameter	Concentration (mg/L)	Weight
F^-	Less than 0.6	1
	0.6–1.2	2
	1.2–1.5	3
	Greater than 1.5	4
HCO_3^-	Less than 100	1
	100–200	2
	200–300	3
	Greater than 300	4
Na^+/Ca^{2+}	Less than 1	1
	1–2	2
	2–3	3
	Greater than 3	4
pH	Less than 6.5	1
	6.5–7.5	2
	7.5–8.5	3
	Greater than 8.5	4

number of parameters. The value of FPI ranging from 1 to 2 is low pollution, 2 to 3 is medium pollution, and 3 to 4 is high pollution due to the presence of fluoride ions in groundwater.

13.4.7 Irrigation Water Quality Indexes (IWQI)

Agriculture is a major source of income for the rural-based people in South India. Highly contaminated groundwater utilized for irrigation uses causes the severe effects on soil structure and crop yield (Adimalla and Qian 2019b). Use of polluted water affects the permeability problem and high salinity and reduces the naturally available minerals in soil (Ravindra et al. 2019). To evaluate the appropriateness of groundwater for irrigation purpose based on the irrigation water quality, indexes are sodium absorption ratio (SAR), residual sodium carbonate (RSC), percentage sodium (%Na), magnesium hazards (MH), permeability index (PI), potential salinity (PS), residual sodium bicarbonate (RBSC), kelly ratio (KR), synthetic harmful coefficient (K), and exchangeable sodium percentage (ESP), which are calculated using the following formulas:

Sodium Absorption Ratio:

$$\mathrm{SAR} = \frac{\mathrm{Na}}{\sqrt{(\mathrm{Ca} + \mathrm{Mg})/2}}; \tag{13.8}$$

Residual Sodium Carbonate:

$$\mathrm{RSC} = [\mathrm{HCO_3} + \mathrm{CO_3}] - [\mathrm{Ca} + \mathrm{Mg}]; \tag{13.9}$$

Percentage Sodium:

$$\%\mathrm{Na} = \frac{(\mathrm{Na} + \mathrm{K}) \times 100}{\mathrm{Ca} + \mathrm{Mg} + \mathrm{Na} + \mathrm{K}}; \tag{13.10}$$

Magnesium Hazards:

$$\mathrm{MH} = \frac{\mathrm{Mg} \times 100}{\mathrm{Ca} + \mathrm{Mg}}; \tag{13.11}$$

Permeability Index:

$$\mathrm{PI} = \frac{\sqrt{\mathrm{HCO_3}} + \mathrm{Na}}{\sqrt{(\mathrm{Na} + \mathrm{Mg} + \mathrm{Ca};}} \tag{13.12}$$

Potential salinity:

$$\mathrm{PS} = \mathrm{Cl}^{-} + \frac{1}{2} \times \mathrm{SO}_4^{2-}; \tag{13.13}$$

Residual sodium bicarbonate:

$$\mathrm{RBSC} = \mathrm{HCO}_3^{-} - \mathrm{Ca}^{2+}; \tag{13.14}$$

Kelly ratio:

$$\mathrm{KR} = \frac{\mathrm{Na}^{+}}{\mathrm{Ca}^{2+} + \mathrm{Mg}^{2+}}; \tag{13.15}$$

Synthetic harmful coefficient:

$$K = 12.4\,\mathrm{M} + \mathrm{SAR}; \tag{13.16}$$

Exchangeable sodium percentage:

$$\mathrm{ESP} = \frac{100\,(-0.0126 + 0.01475SAR)}{1 + (-0.0126 + 0.01475\,SAR)}. \tag{13.17}$$

13.4.8 Human Health Risk Assessment (HHRA)

Human health risk assessment model is an evaluation method, revealing the impact of consumption of high-contaminated groundwater on human health (Dehghani et al. 2019; Panneerselvam et al. 2020a; Rezaei et al. 2019; Zhang et al. 2020b; Asgari et al. 2019). It describes the harmful impact of human exposure to environmental hazards. The results describe the degree of harmful to the human health under various environmental conditions. Various contaminants enter the human body in different ways and more importantly via drinking water (Yadav et al. 2019;, Kaur et al. 2020; Adimalla 2020; Zango et al. 2019; Karunanidhi et al. 2019; Ganyaglo et al. 2019; Radfarda et al. 2019). The effects are categorized as two different types: carcinogenic and noncarcinogenic risks (Panneerselvam et al. 2020b). The risk model was used to assess three age (Children, Men and Women) groups of people in the study area, who are consuming elevated concentration of fluoride in groundwater. The main objective of this study is to evaluate the health impact of drinking water on the people surviving in the study area,

$$E = \frac{\text{CPW} \times \text{IR} \times \text{ED} \times \text{EF}}{\text{ABW} \times \text{AET}}, \tag{13.18}$$

$$\text{HQ} = \frac{E}{\text{RfD}}, \tag{13.19}$$

where,

E is the Chronic daily intake and is expressed in mg per kg/day, CPW is the Concentration of specific pollutant in groundwater in mg per day, IR is the Rate of human ingestion in Liters per day, ED is the Duration of exposure and is expressed in years, EF is the Frequency of exposure and is expressed in no. of days per year, and ABW is the Average body weight in kilogram. AET is the Average time in days, HQ is the Noncarcinogenic for Hazard Quotient, and RfD is the Reference dose of nitrate and expressed in mg/kg/day.

13.4.9 GIS Analysis

GIS is an efficient tool to assess and represent the impact of environmental issue on the public people and decision makers in relevant field. Inverse distance weighted (IDW) interpolation of water quality data was performed to represent the highly contaminated zone in the research area (Tiwari et al. 2017; El-Zeiny and Elbeih 2019). An IDW helps to predict a value for any unmeasured location and gives greater weights to points closest to the prediction locations in the study area. In the present study, IDW interpolation method was carried out to identify the highly contaminated locations using Arc GIS 10.2.

13.5 Results and Discussion

13.5.1 Physical Characteristics of Groundwater

The minimum, maximum, mean, and standards recommended by WHO (2011) and BIS (2012) of groundwater parameters are given in Table 13.3.

13.5.1.1 pH

The physical characteristics of the groundwater are pH, EC, TDS, and TH. The hydrogen ion concentration in groundwater was presented by pH value (Abbasnia et al. 2019). In the study area, the range of pH is from 7.30 to 8.6 with an average of 8.08. About 8.33% of the sample locations exceed the permissible limit for drinking purpose. The pH concentration map reveals that Kunnuvarankottai, Jambuthuraikottai, and Gullalagundu locations were recorded as slightly contaminated zones.

Table 13.3 Descriptive analysis of groundwater parameters

Parameter	Min	Max	Avg.	SD	Kurtosis
pH	7.30	8.60	8.08	0.31	−0.26
EC	298.08	3316.00	1783.66	892.64	−1.17
TH	35.00	390.00	154.22	76.03	1.46
TDS	172.08	1977.92	1004.12	505.71	−1.06
Ca	7.00	198.00	56.27	37.63	4.77
Mg	9.77	128.36	47.32	28.53	0.37
Na	0.00	411.00	171.00	104.46	−0.45
K	0.00	25.00	8.98	7.51	−0.58
Cl	28.00	709.00	286.47	194.51	−0.77
SO_4	2.00	420.00	79.55	78.96	9.57
CO_3	0.00	18.00	2.20	4.06	6.02
HCO_3	100.46	802.73	415.38	192.20	−0.71
F	0.26	1.92	0.93	0.40	−0.34
NO_3	1.00	67.00	15.96	16.79	2.05

Table 13.4 Handa classification of EC in the study area

EC (μS/cm)	Water type	Classification	No. of samples	% of Samples
0–250	Low	Excellent	–	–
251–750	Medium	Good	5	13.88
751–2250	High	Permissible	19	52.77
2251–6000	Very high	Doubtful	12	33.33
6001 – 10,000	Extensively high	Poor	–	–
10,0001 – 20,000	Brines weakly conc.	Very poor	–	–

13.5.1.2 EC

Electrical conductivity (EC) is the most important parameter to evaluate the suitability of groundwater for both drinking and irrigation uses (Alam et al. 2020). An elevated concentration of EC may contribute to the salinity and total dissolved solid concentration in groundwater (Chaudhary 2020). In the study area, EC concentration varies from 298.08 to 3316 μS/cm with an average of 1783.66 μS/cm. In addition, Handa classification has been performed in the study area and revealed that 13.88% of the sample locations are medium salinity, 25.77% of the sample locations are high salinity, and 33.33% of the sample locations are very high salinity type of water (Table 13.4). About 12 sample locations are highly affected due to action of anthropogenic and geochemical process predominant for excess concentration of EC in the study area.

13.5.1.3 TDS

TDS includes the sum of the cations and anions dissolved in the water. TDS in drinking water originates from the natural sources such as mineral present in the springs, carbonate deposits and salt deposits, and other sources such as sewage disposal, urban runoff, industrial wastewater, and agriculture runoff (Eslami et al. 2019). In the study area, TDS ranges between 172.08 and 1977.92 mg/L with a mean of 4001.12 mg/L. As per WHO and BIS standards, the allowable limit of TDS is 500 mg/L and most permissible limit is 1500 mg/L. In the study area, 22.22% of the sample locations are unfit for drinking purpose. A man-made source of pollutants such as uncovered septic tanks, sewage intrusion, and modern agriculture activities may affect the nature of groundwater in the study region.

13.5.1.4 TH

TH is another important parameter to evaluate the groundwater for drinking purpose. It is caused mainly due to the action of polyvalent cations such as calcium and magnesium present in the groundwater (Johnny et al. 2018; Kirubakaran et al. 2015; Kumar and Balamurugan 2018). Sawyer and McCarthy classification reveals that 13.88% of the sample locations are soft, 30.55% of the sample locations are moderately hard, 52.77% of the sample locations are hard, and 2.77% of the sample locations are very hard type of groundwater in the study area. As per WHO and BIS standards, all the sample locations are coming under the most desirable limit for drinking purpose. An elevated concentration of TH in groundwater is due to weathering of sedimentary, limestone, calcium rich minerals, and utilization of lime to the soil for high crop yield in agricultural field in study area.

13.6 Major Anions

13.6.1 Calcium

Calcium is an essential mineral to maintain the stable equilibrium in groundwater chemistry. It is a key mineral for functioning of the structural element in the human body. The major reason for excess concentration of groundwater is nature of earth metal (Aravindan and Shankar 2011; Balamurugan et al. 2020a). Excess and lack of calcium causes hypertension, kidney stones, and colorectal cancer in human health. In the study area, calcium concentration varies from 7 to 198 mg/L with an average of 56.27 mg/L. About 25% of the sample locations exceed the permissible limit of calcium concentration recommended by WHO (2011). Figure 13.2a shows that 430.46 km^2 area was fall in the acceptable limit and 51.27 km^2 area is desirable limit of calcium concentration in groundwater.

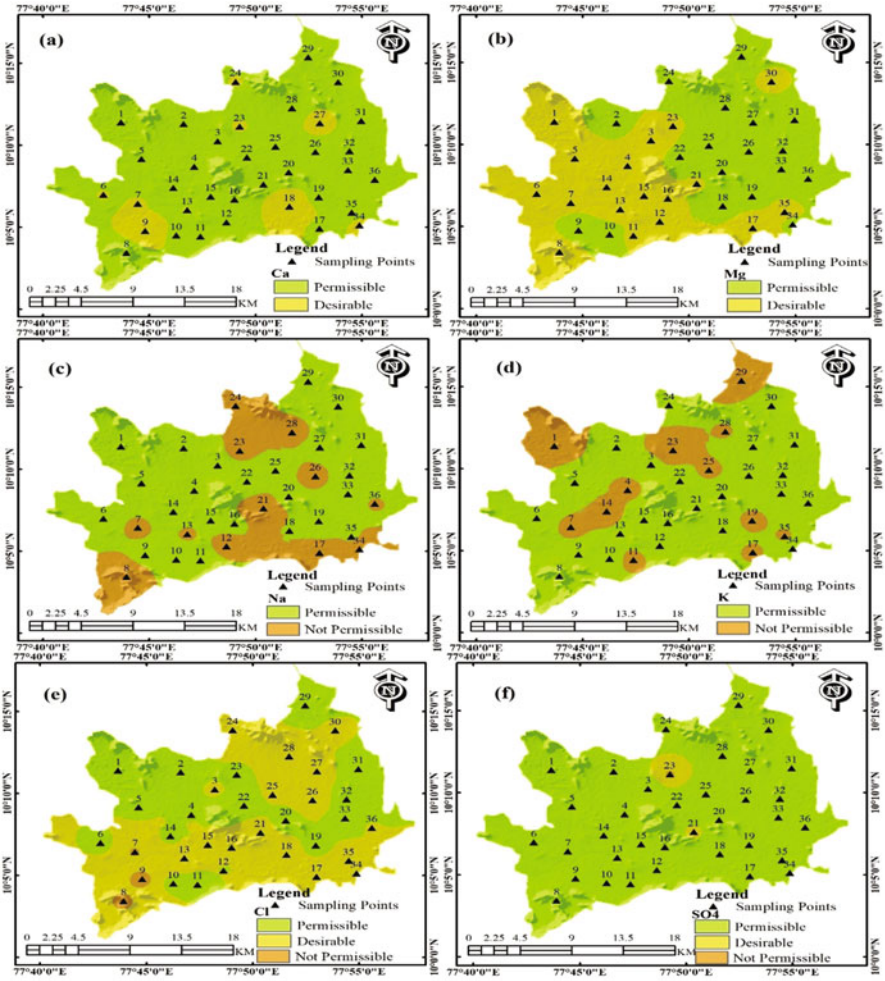

Fig. 13.2 Spatial distribution of (**a**) Ca^{2+}, (**b**) Mg^{2+}, (**c**) Na^{+}, (**d**) K^{+}, (**e**) Cl^{-}, and (**f**) $SO_4{}^{2-}$

13.6.2 Magnesium

Magnesium and other alkali earth metals are the major reason for water hardness. The nature of the aquifer contains higher amount of alkali matter, which causes the unbalance of chemical composition of groundwater. In the study area, concentration of magnesium ranges from 9.77 to 128.36 mg/L with an average of 47.32 mg/L. More than 50% of the sample locations are affected by excess concentration of magnesium in groundwater. Figure 13.2b shows that 234.22 km^2 area was recorded as desirable limit for drinking purpose in the study area. The continuous

consumption of magnesium causes muscle slackening, nerve problems, depression, and personality changes (Shankar et al. 2011a; Shankar and Kawo 2019).

13.6.3 Sodium

Sodium is the most imperious nutrient for human and abundant in groundwater. The essential limit of sodium in human blood is 20 mg/L (Kumar and Balamurugan 2019; Mohanakavitha et al. 2019a). As per WHO 2011, the maximum allowable limit of sodium in groundwater is 200 mg/L. In the study area, sodium concentration varies between 15 and 411 mg/L with an average of 171 mg/L. About 33.33% of the sample locations have excess concentration of sodium in groundwater. Figure 13.2c represents that 130.97 km^2 area is not permissible for drinking uses in the study region. The mineral deposit, rock water interaction, weathering of rocks, and ion exchange process are the major reason for elevated concentration of sodium in the study area.

13.6.4 Potassium

A source of potassium in groundwater is due to the action of weathering of rich potassium bearing minerals. Higher concentration of potassium causes hypertension, diabetes, heart diseases, and artery diseases on human health. In the study area, potassium concentration varies from 0 to 25 mg/L with a mean of 8.98 mg/L. Figure 13.2d shows that 33.33% of the sample locations are highly affected due to excess concentration of potassium in groundwater.

13.7 Major Cations

13.7.1 Chloride

Chloride is a naturally occurring mineral in both surface and groundwater. In more cases, chloride was found with the combination of sodium, calcium, and potassium. In the study area, concentration of chloride ions varies from 28 to 708 mg/L with an average of 286.47 mg/L. About 50% of the sample locations were within the desirable limits (WHO 2011). Figure 13.2e shows that 259.34 km^2 area is desirable limit for drinking uses. In the study area, weathering of rocks, salt bearing aquifers, and anthropogenic sources such as runoff from agricultural field, sewage intrusion, and animal feed are the major reason for elevated concentration of chloride ions in groundwater.

13.7.2 Sulfate

Sulfate is the combination of sulfur and oxygen ions, and it is naturally present in the soil and rock. Sulfate easily gets dissolved in the groundwater (Mohanakavitha et al. 2019b). The sulfate concentration in the study area varies from 2 to 420 mg/L with an average of 79.55 mg/L. Figure 13.2f shows that 469.29 km^2 area fall under the acceptable limit for drinking uses and few locations fall in desirable limit of sulfate concentration in groundwater recommended by WHO (2011).

13.7.3 Fluoride

Fluoride is a most essential mineral for dental and bone growth in human body. An excess concentration of fluoride in groundwater causes server diseases, namely, fluorosis (Gunaalan et al. 2018). Fluorosis is a very serious disease affecting more than millions of peoples all around the world. In the study area, concentration of fluoride ions varies from 0.26 to 1.92 mg/L with an average of 0.93 mg/L. About 33.33% of the sample locations exceed the desirable limit of fluoride recommended by WHO (2011).

13.7.4 Nitrate

In general, nitrate concentration in groundwater is low compared with chloride and sulfate ions. The source of nitrate in groundwater is mainly due to anthropogenic activities (Dhanasekarapandian et al. 2016). In the study area, nitrate concentration varies from 1 to 67 mg/L with an average of 15.96 mg/L. The higher concentration of nitrate was recorded in the three-sample location, namely, Mallanampatti, Musuvanoothu, and Sengattampatti.

13.7.5 Carbonate and Bicarbonate

Carbonate and bicarbonate ions mostly have combined with calcium and magnesium in chemical composition of groundwater. Carbonate-rich minerals such as sedimentary and limestone are the major source of carbonate and bicarbonate in groundwater (Duraisamy et al. 2019). In the study area, carbonate and bicarbonate varied from 0 to 18 mg/L with an average of 2.2 mg/L and 400.46 to 802.73 mg/L with an average of 415.38 mg/L, respectively. Due to the action of carbonate weathering and carbonic acid dissolution are the major the source of elevated concentration of bicarbonate in the study area.

13.8 WQI

Water quality index (WQI) was carried to assess the nature of groundwater for drinking purpose in the study region. The classification of water type based on WQI is represented in Table 13.5. In the study area, 25% of the sample locations were good, 36.11% of the sample locations were moderate, 27.78% of the sample locations were doubtful, and 11.11% of the sample locations are unsuitable nature of water for drinking purpose in study area. The sample locations, namely, Kombaipatti, Sandaiyur, Kunnuvarankottai, and Musuvanoothu, are found to be highly affected due to excess concentration of sodium, magnesium, and fluoride ion in groundwater. Spatial analysis revealed that 31.56 km^2 area is good, 334.13 km^2 area is moderate, 112.39 km^2 area is doubtful, and 3.66 km^2 area is recorded as unsuitable for drinking uses (Fig. 13.3a).

13.9 NPI

The value of NPI indicates the status of nitrate contamination in the study region. The value of NPI is zero, which indicates the clean, and greater than 3, which indicates very significant level of pollution in groundwater. In the study area, NPI ranged between −0.95 and 2.35 with an average of −0.20. About 66.67% of the sample locations are clean, 22.22% of the sample locations are light pollution, 8.33% of the samples are moderate pollution, and 2.77% of the sample locations are significant pollution based on the nitrate contamination (Table 13.6). The NPI value indicate that anthropogenic activities such as uncovered septic tank, modern agriculture activities, and synthetic fertilizers used for high crop yield are the major source for nitrate contamination in the study area. Spatial analysis shows that 20.14 and 0.63 km^2 areas were moderate and significant pollution, respectively (Fig. 13.3b).

Table 13.5 Classification of groundwater based on WQI value

Range	Water type	No. of samples	% of the samples
0–25	Excellent	0	0.00
25–50	Good	9	25.00
50–75	Moderate	13	36.11
75–100	Doubtful	10	27.78
> 100	Unsuitable	4	11.11

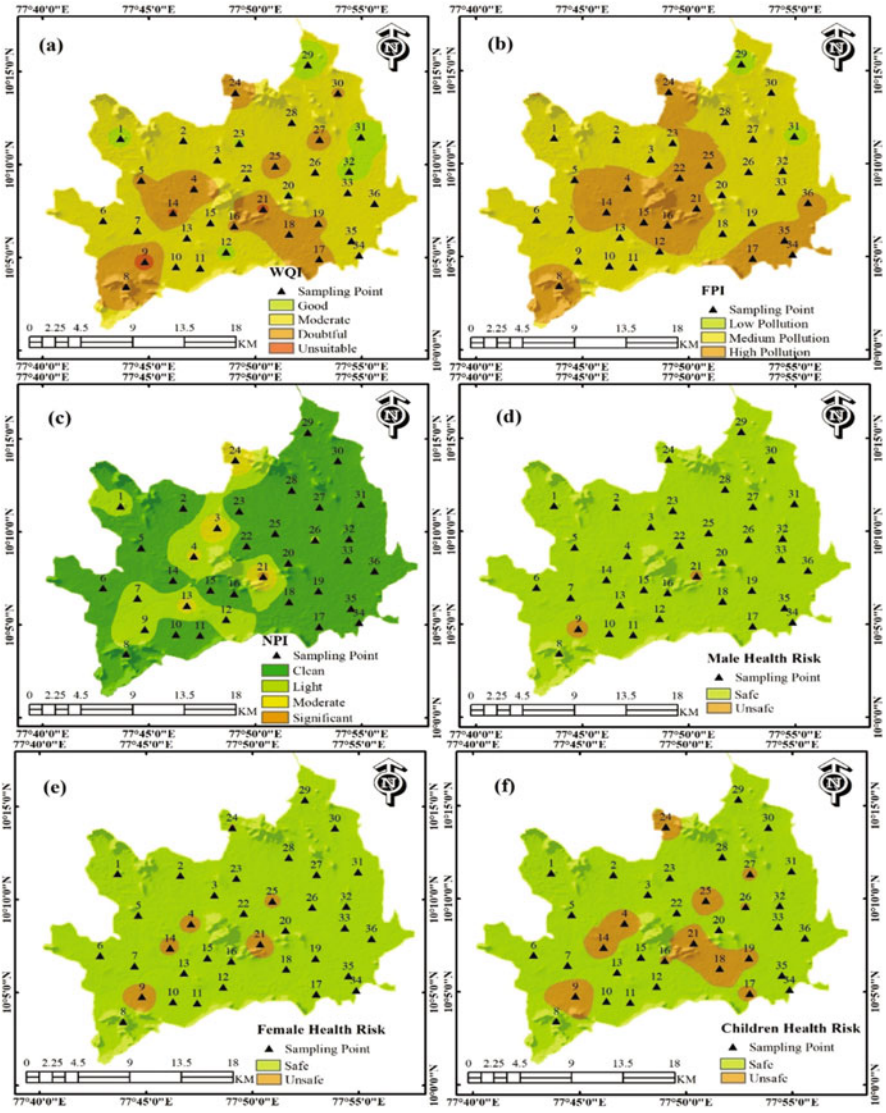

Fig. 13.3 Spatial distribution of (**a**)WQI (**b**) FPI, (**c**) NPI, (**d**) HHRA Male, and (**e**) HHRA female

13.10 FPI

FPI of the groundwater indicates the three major types are low, medium, and high level of fluoride contamination. In the study area, FPI varies from 1.75 to 3.5 with an average of 2.89. FPI classified that more than 50% of the sample locations fell in the high level of pollution type (Table 13.7). It indicates rock geochemistry such as

Table 13.6 NPI classification of groundwater

Range	Class of water	No. of samples	% of the samples
Less than 0	Clean	24	66.66
0–1	Light pollution	8	22.22
1–2	Moderate pollution	3	8.33
2–3	Significant pollution	1	2.77
Greater than 3	Very significant pollution	0	0

Table 13.7 FPI value of groundwater in study area

Range	Class of water	No. of samples	% of the samples
1–2	Low pollution	2	5.55
2–3	Medium pollution	11	30.55
3–4	High pollution	23	63.90

decomposition or weathering of rocks, dissociation, and consequent dissolution along with long residence time may be responsible for fluoride leaching in the study area. In Fig. 13.3c shows that 163.24 km^2 area is highly polluted due to excess concentration of fluoride in groundwater.

13.11 HHRA

The above discussion on WQI, NPI, and FPI divulged the nature of groundwater and source of contamination in the study area. In addition, it is necessary to evaluate the human health risk assessment, since the most of the people depend on groundwater for drinking and results also disclosed that fluoride concentration was much higher than the desirable limit in greater part of the study region. In the present study, health risk assessment model was introduced to evaluate the impact of continuous consumption of elevated concentration fluoride on human health. The HHRA in study area, for male, varies from 1.67E−01 to 1.*23E*+00 with an average of 5.98E−01, for female, it varies from 1.97E−01 to 1.45E+00 with a mean of 7.06E−01, and for children, it varies from 2.25E−01 to 1.66E+00 with a mean of 8.08E−01. About 33.33%, 16.67%, and 5.56% of the sample locations exceed the acceptable limit for noncarcinogenic risk (greater than 1.00E+00) of children, female, and male, respectively. The continuous consumption of fluoride-contaminated water causes fluorosis, teeth and bone disease, and skeletal problems. In spatial analysis, 3.59, 17.72, and 68.84 km^2 areas were recorded as risk zone for male, female, and children, respectively (Fig. 13.3d–f). The results of the health risk model reveal that children are at high risk than male and female.

13.12 Irrigation Indexes

13.12.1 Sodium Absorption Ratio (SAR)

SAR is a most efficient tool to evaluate the suitability of groundwater for irrigation uses based on the concentration of sodium, calcium, and magnesium ions (Khadri and Pande 2015c; Esmeray and Gökcekli 2020; Yang et al. 2020; Zhou et al. 2020). The value of SAR less than 10 is excellent, 10–18 is good, 18–26 is doubtful, and greater than 26 is unsuitable for irrigation uses. In the study area, SAR varies from 0 to 10.83 with an average of 4.22. Around 98% of the sample locations are fit, and one sample location is good for irrigation uses. In addition, US salinity laboratory diagram (USSL 1954) helps to identify the salinity influence of groundwater in agriculture field. Figure 13.4 shows that 61.11% of the sample locations fell under high salinity-low sodium (C3-S1), 8.33% of the samples fell under very high salinity-high sodium (C4-S3), very high salinity-medium sodium (C4-S2) and medium salinity-low sodium (C2-S1), 5.55% of the sample locations fell under very high salinity-low sodium (C4-S1), and high salinity-medium sodium (C3-S2) 2.77% of the sample locations fell under high salinity-high sodium(C3-S3). It revealed that salinity of the groundwater influences the suitability and degrades the quality of water in the study region for irrigation uses.

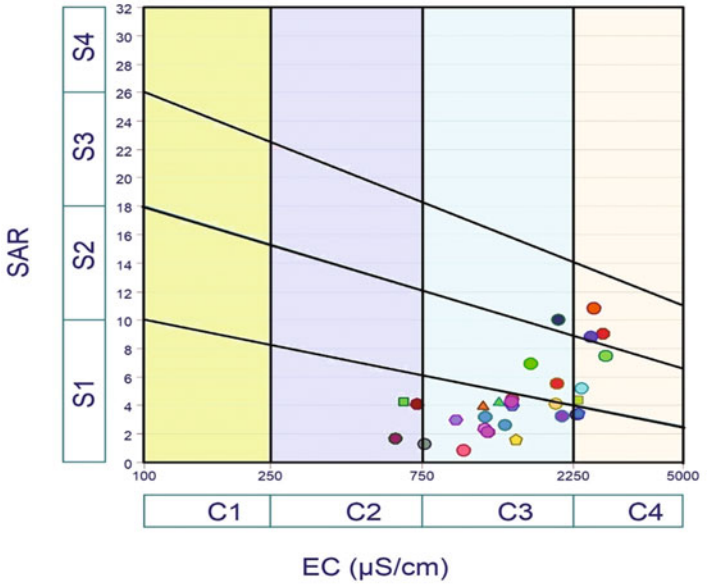

Fig. 13.4 USSL classification of groundwater in the study region

13.12.2 Residual Sodium Carbonate (RSC)

RSC shows the relationship between the weak acids and alkaline earth metals influencing the nature of groundwater. The RSC classifies the water into three classes, which are less than 1.25 meq/L is satisfactory, 1.25–2.5 meq/L is marginal, and greater than 2.5 meq/L is unsatisfactory for irrigation uses (Adimalla et al. 2020; Balamurugan et al. 2020c; Ding et al. 2020). The value of RSC in the study area ranged between −9.36 and 10.38 meq/L with a mean of 0.18 meq/L. 72.22% of the samples were satisfactory, 5.56% of the samples were marginal, and 22.22% of the samples were unsatisfactory for irrigation uses. Figure 13.5a shows that 63.91 km^2 area is highly affected due to higher concentration of residual sodium ions in groundwater.

13.12.3 Magnesium Hazards

An excess concentration of magnesium in groundwater causes adverse effect on irrigation water quality. The continuous irrigation of higher magnesium water leads to infertility of soil and affects the physical properties of the soil structure (Barbieri et al. 2019; Carasek et al. 2020). Therefore, it is necessary to evaluate the magnesium hazards of groundwater for irrigation purpose. In the study area, 19.11 to 86.97% with an average of 56.76% and 22 sample locations are highly affected due to excess magnesium concentration. Figure 13.5b shows that 332.12 km^2 area is unsuitable of irrigation purpose.

13.12.4 Permeability Index

PI is another important parameter to assess the fitness of groundwater for irrigation uses. It represents the relation between major cations with bicarbonate in hydrochemistry (Balamurugan et al. 2020d; Khawla and Mohamed 2020; Gopinathan et al. 2020). The PI value classifies the groundwater into three classes, which are greater than 75% is Class I, 25–75% is Class II, and less than 25% is Class III. In the study area, PI varies from 34.83 to 105.78% with an average of 69.9%. It shows that all the groundwater samples fell under Classes I & II and indicate that fit for irrigation uses (Fig. 13.5c).

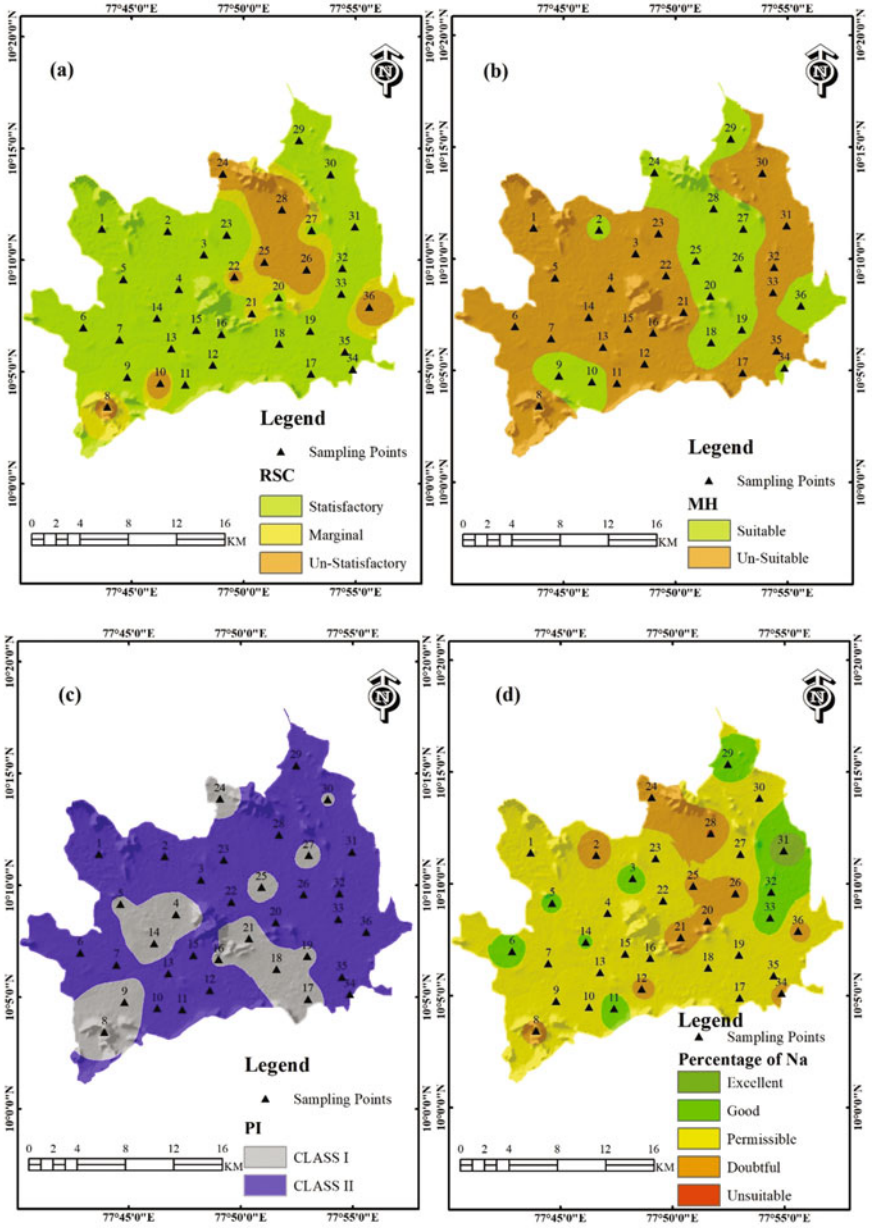

Fig. 13.5 Spatial distribution of (**a**) RSC, (**b**) MH, (**c**) PI, and (**d**) %Na

13.12.5 Percentage Sodium

Percentage sodium (%Na) is a very important index value to evaluate the suitability of groundwater for irrigation uses. It indicates the impact of sodium hazards for irrigation water quality. Based on the %Na, groundwater classified into five classes are 0–20% is excellent, 20–40% is good, 40–60% is permissible, 60–80% is doubtful, and greater than 80% is unsuitable of irrigation uses (Liu et al. 2019; Khalid 2019). In the study area, totally 69.44% of the sample locations fell under the permissible, 25% of the sample locations are doubtful, and 5.64% of the sample locations are unsuitable for irrigation uses. In spatial analysis, 345.81 km^2 area is permissible, 68.59 km^2 area is doubtful, and 0.42 km^2 area is unsuitable for irrigation uses in the study region (Fig. 13.5d).

13.12.6 Residual Sodium Bicarbonate

RBSC represents the excess sodium carbonate and bicarbonate, which are considered to be harmful to the physical properties of soil and increase the dissolution of organic matter in the soil layers (Zhou et al. 2020). In the study area, RBSC ranged between −0.73 and 11.72 with a mean of 4.00, around 25% of the samples were marginally affected, and 5.56% of the sample locations were greater than 10 of RBSC value. While 103.25 km^2 area is marginally affected, 2.5 km^2 area is unsuitable for irrigation uses in the study area (Fig. 13.6a).

13.12.7 Potential Salinity

PS is calculated using chloride concentration and half of the sulfate ion concentration (meq/L) in groundwater. It classifies the groundwater into three classes, which are less than 5 is satisfactory, 5–10 is marginal, and greater than 10 is unsatisfactory (Xu et al. 2019). In the study area, PS varies from 0.82 to 20.79 with an average of 8.91 and 38.89% of the sample locations has PS above 10, suggesting that water is unsuitable for irrigation uses. In spatial analysis, 148.70 km^2 area was recorded as highly affected zone in the study area (Fig. 13.6b).

13.12.8 Synthetic Harmful Coefficient (K)

K can be broadly reflecting the salt and alkali hazards present in the groundwater. The groundwater categorized into four classes based on *K* value, which are less than 25 is excellent, 25–36 is good, 36–44 is injurious, and greater than 44 is unsuitable

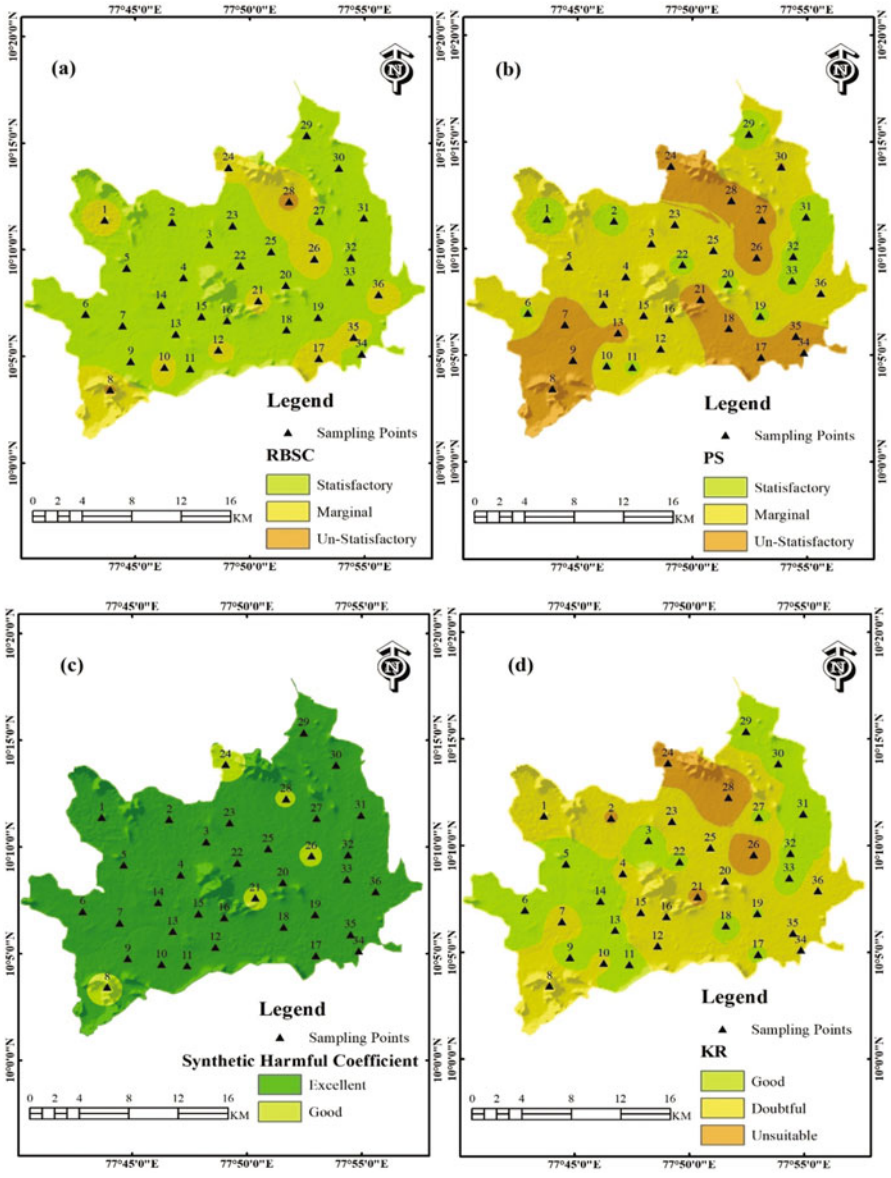

Fig. 13.6 Spatial distribution of (**a**) RBSC, (**b**) PS, (**c**) K, and (**d**) KR

for irrigation uses. In the study area, *K* ranged between 2.06 and 32.92 with an average of 16.27 and 86.11% of the samples had *K* value below 25, suggesting that water is excellent for irrigation uses. It covers an area of 461.65 km^2 in the study region (Fig. 13.6c).

13.12.9 Kelly Ratio

KR is very significant index value to evaluate the groundwater for irrigation uses. It classifies the groundwater into two major classes, less than 1 is suitable, and greater than 1 is unsuitable (Kelley 1963; Khawla and Mohamed 2020). In the study area, KR varies from 0 to 4.23 with an average of 1.26 and 52.78% of the samples have KR value above 1, suggesting that unsuitable for irrigation. Figure 13.6d shows that 271.26 km^2 area is doubtful and 43.74 km^2 area is unsuitable for irrigation uses in the study area.

13.12.10 Exchangeable Sodium Percentage

Saline soils are highly affecting the growth of crops and crop yield in the agriculture field. Excess salinity of groundwater supplied to agriculture field causes an issue when adequate salts are deposited in the root zone to negatively affect plant growth (Cemek et al. 2007; Emadi et al. 2008; Bouksila et al. 2013). The value of ESP is less than 15 is sodic soil and greater than 15 is nonsodic soil. In the study area, ESP varies from −1.28 to 12.82 with a mean of 4.6 and 100% of the samples had ESP value less than 15, indicating that sodic soil is present in the study region.

13.13 Conclusion

In arid and semiarid regions of Tamil Nadu, India, a larger number of people's primary depend on groundwater for their daily needs and agricultural activities. Moreover, groundwater is the widely available source in the study area compared with surface water. In the present study, 36 samples were collected and analyzed for various physiochemical parameter of groundwater. The results of the present study are following: The pH of the studied groundwater is about 8.33% of the sample locations exceed the permissible limit for drinking purpose. EC, TDS, TH, Ca, Mg, Na, K, Cl, SO_4, NO_3, F, CO_3, and HCO_3 of a groundwater in few locations exceed the acceptable limit recommended by WHO (2011). WQI shows that 31.56 km^2 area is good, 334.13 km^2 area is moderate, 112.39 km^2 area is doubtful, and 3.66 km^2 area was recorded as unsuitable for drinking uses. NPI reveals that 20.14 and 0.63 km^2 area were moderate and significant pollution, respectively. FPI shows that 163.24 km^2 area is highly polluted due to excess concentration of fluoride in groundwater. Based on HHRA, 33.33%, 16.67%, and 5.56% of the sample locations exceed the acceptable limit for noncarcinogenic risk (THI > 1) of children, female, and male, respectively. The continuous consumption of fluoride contaminated water causes fluorosis, teeth and bone disease, and skeletal problems. The Irrigation indexes show that majority of groundwater sample were fit for irrigation uses. The

study found that rock water interaction, weathering of rocks, anthropogenic activities such as sewage intrusion, uncovered septic tank, synthetic fertilizers, and waste disposal from resident are the major factors that deteriorate the nature of groundwater in the study area.

References

Abbasnia, A., Yousefi, N., Mahvi, A. H., Nabizadeh, R., Radfard, M., Yousefi, M., & Alimohammadi, M. (2019). Evaluation of groundwater quality using water quality index and its suitability for assessing water for drinking and irrigation purposes: Case study of Sistan and Baluchistan province (Iran). *Human and Ecological Risk Assessment: An International Journal, 25*(4), 988–1005.

Adimalla, N. (2019). Groundwater quality for drinking and irrigation purposes and potential health risks assessment: A case study from semi-arid region of South India. *Exposure and Health, 11* (2), 109–123.

Adimalla, N. (2020). Spatial distribution, exposure, and potential health risk assessment from nitrate in drinking water from semi-arid region of South India. *Human and Ecological Risk Assessment: An International Journal, 26*(2), 310–334.

Adimalla, N., Dhakate, R., Kasarla, A., & Taloor, A. K. (2020). Appraisal of groundwater quality for drinking and irrigation purposes in Central Telangana, India. *Groundwater for Sustainable Development, 10*, 100334.

Adimalla, N., & Qian, H. (2019a). Groundwater quality evaluation using water quality index (WQI) for drinking purposes and human health risk (HHR) assessment in an agricultural region of Nanganur, South India. *Ecotoxicology and Environmental Safety, 176*, 153–161.

Adimalla, N., & Qian, H. (2019b). Spatial distribution and health risk assessment of fluoride contamination in groundwater of Telangana: A state-of-the-art. *Geochemistry, 80*(4), 125548.

Alam, W., Singh, K. S., Gyanendra, Y., Laishram, R. J., & Nesa, N. (2020). Hydrogeochemical assessment of groundwater quality for few habitations of Chandel District, Manipur (India). *Applied Water Science, 10*(5), 1–13.

Alghamdi, A. G., Aly, A. A., Aldhumri, S. A., & Al-Barakaha, F. N. (2020). Hydrochemical and quality assessment of groundwater resources in Al-Madinah City, Western Saudi Arabia. *Sustainability, 12*(8), 3106.

American Public Health. APHA. (2005). *Standard methods for the examination of water and wastewater* (21st ed.). Washington, DC: American Public Health Association.

Aravindan, S., & Shankar, K. (2011). Ground water quality maps of Paravanar River Sub Basin, Cuddalore District, Tamil Nadu, India. *Journal of Indian Society of Remote Sensing, 39*(4), 565–585.

Aravindan, S., Shankar, K., Ganesh, P., & Rajan, K. D. (2010). Groundwater geochemical mapping in hard rock area of Gadilam river basin using GIS technique, Tamil Nadu, India. *Journal of Applied Geochemists, 12*(2), 209–216.

Aravinthasamy, P., Karunanidhi, D., Subramani, T., Anand, B., Roy, P. D., & Srinivasamoorthy, K. (2019a). Fluoride contamination in groundwater of the Shanmuganadhi River basin (South India) and its association with other chemical constituents using geographical information system and multivariate statistics. *Geochemistry, 80*(4), 125555.

Aravinthasamy, P., Karunanidhi, D., Subramani, T., Srinivasamoorthy, K., & Anand, B. (2019b). Geochemical evaluation of fluoride contamination in groundwater from Shanmuganadhi River basin, South India: implication on human health. *Environmental Geochemistry and Health, 42*, 1937–1963.

Asgari, G., Ghalehaskar, S., Moghaddam, V. K., Radfard, M., Heidarinejad, Z., Mohammadi, A. A., & Faraji, H. (2019). Monitoring and health risk assessment of fluoride in drinking water in Babol, Mazandaran Province, Iran. *Desalination and Water Treatment, 165*, 141–147.

Badeenezhad, A., Tabatabaee, H., Nikbakht, H. A., Radfard, M., Abbasnia, A., Baghapour, M. A., & Alhamd, M. (2020). Estimation of the groundwater quality index and investigation of the affecting factors their changes in shiraz drinking groundwater, Iran. *Groundwater for Sustainable Development, 11*, 100435.

Bahir, M., Ouhamdouch, S., Ouazar, D., & Chehbouni, A. (2020). Assessment of groundwater quality from semi-arid area for drinking purpose using statistical, water quality index (WQI) and GIS technique. *Carbonates and Evaporites, 35*(1), 1–24.

Bahrami, M., Zarei, A. R., & Rostami, F. (2020). Temporal and spatial assessment of groundwater contamination with nitrate by nitrate pollution index (NPI) and GIS (case study: Fasarud plain, southern Iran). *Environmental Geochemistry and Health, 42*, 3119–3130.

Balamurugan, P., Kumar, P. S., Shankar, K., Nagavinothini, R., & Vijayasurya, K. (2020a). Non-carcinogenic risk assessment of groundwater in southern part of Salem district in Tamil Nadu, India. *Journal of the Chilean Chemical Society, 65*(1), 4697–4707.

Balamurugan, P., Kumar, P. S., & Shankar, K. (2020b). Dataset on the suitability of groundwater for drinking and irrigation purposes in the Sarabanga River region, Tamil Nadu, India. *Data in Brief, 29*, 105255.

Balamurugan. P., Kumar. P.S., Shankar. K., & Sajil Kumar, PJ. (2020c). Impact of climate and anthropogenic activities on groundwater quality for domestic and irrigation purposes in Attur region, Tamilnadu, India. *Desalination and Water Treatment, 208*, 172–195.

Balamurugan, P., Shunmugapriya, G., & Vanitha, R. (2020d). GIS based assessment of ground water for domestic and irrigation purpose in Vazhapadi Taluk, Salem, Tamil Nadu, India. *Taiwan Water Conservancy, 68*(2), 1–10.

Barbieri, M., Ricolfi, L., Vitale, S., Muteto, P. V., Nigro, A., & Sappa, G. (2019). Assessment of groundwater quality in the buffer zone of Limpopo National Park, Gaza Province, southern Mozambique. *Environmental Science and Pollution Research, 26*(1), 62–77.

Bawoke, G. T., & Anteneh, Z. L. (2020). Spatial assessment and appraisal of groundwater suitability for drinking consumption in Andasa watershed using water quality index (WQI) and GIS techniques: Blue Nile Basin, northwestern Ethiopia. *Cogent Engineering, 7*(1), 1748950.

BIS (Bureau of Indian Standards) 10500 (2012) Indian Standard Drinking Water Specification.

Bouksila, F., Bahri, A., Berndtsson, R., Persson, M., Rozema, J., & Van der Zee, S. E. (2013). Assessment of soil salinization risks under irrigation with brackish water in semiarid Tunisia. *Environmental and Experimental Botany, 92*, 176–185.

Carasek, F. L., Baldissera, R., Oliveira, J. V., Scheibe, L. F., & Dal Magro, J. (2020). Quality of the groundwater of the Serra Geral aquifer system of Santa Catarina west region, Brazil. *Groundwater for Sustainable Development, 10*, 100346.

Cemek, B., Güler, M., Kiliç, K., Demir, Y., & Arslan, H. (2007). Assessment of spatial variability in some soil properties as related to soil salinity and alkalinity in Bafra plain in northern Turkey. *Environmental Monitoring and Assessment, 124*(1–3), 223–234.

Chaudhary, J. K. (2020). A comparative study of fuzzy logic and WQI for groundwater quality assessment. *Procedia Computer Science, 171*, 1194–1203.

Dehghani, M. H., Zarei, A., Yousefi, M., Asghari, F. B., & Haghighat, G. A. (2019). Fluoride contamination in groundwater resources in the southern Iran and its related human health risks. *Desalination and Water Treatment, 153*, 95–104.

Dhanasekarapandian, M., Chandran, S., Devi, D. S., & Kumar, V. (2016). Spatial and temporal variation of groundwater quality and its suitability for irrigation and drinking purpose using GIS and WQI in an urban fringe. *Journal of African Earth Sciences, 124*, 270–288.

Ding, L., Yang, Q., Yang, Y., Ma, H., & Martin, J. D. (2020). Potential risk assessment of groundwater to address the agricultural and domestic challenges in Ordos Basin. *Environmental Geochemistry and Health, 2020*, 1–16.

Duraisamy, S., Govindhaswamy, V., Duraisamy, K., Krishinaraj, S., Balasubramanian, A., & Thirumalaisamy, S. (2019). Hydrogeochemical characterization and evaluation of groundwater quality in Kangayam taluk, Tirupur district, Tamil Nadu, India, using GIS techniques. *Environmental Geochemistry and Health, 41*(2), 851–873.

Egbi, C. D., Anornu, G. K., Ganyaglo, S. Y., Appiah-Adjei, E. K., Li, S. L., & Dampare, S. B. (2020). Nitrate contamination of groundwater in the lower Volta River basin of Ghana: Sources and related human health risks. *Ecotoxicology and Environmental Safety, 191*, 110227.

Elumalai, V., Nwabisa, D. P., & Rajmohan, N. (2019). Evaluation of high fluoride contaminated fractured rock aquifer in South Africa–geochemical and chemometric approaches. *Chemosphere, 235*, 1–11.

El-Zeiny, A. M., & Elbeih, S. F. (2019). GIS-based evaluation of groundwater quality and suitability in Dakhla oases, Egypt. *Earth Systems and Environment, 3*(3), 507–523.

Emadi, M., Baghernejad, M., & Maftoun, M. (2008). Assessment of some soil properties by spatial variability in saline and sodic soils in Arsanjan plain, southern Iran. *Pakistan Journal of Biological Sciences: PJBS, 11*(2), 238–243.

Eslami, F., Yaghmaeian, K., Mohammadi, A., Salari, M., & Faraji, M. (2019). An integrated evaluation of groundwater quality using drinking water quality indices and hydrochemical characteristics: A case study in Jiroft, Iran. *Environmental Earth Sciences, 78*(10), 314.

Esmeray, E., & Gökcekli, C. (2020). Assessment of groundwater quality for drinking and irrigation purposes in Karabuk province, Turkey. *Environmental Earth Sciences, 79*(13), 1–17.

Ganyaglo, S. Y., Gibrilla, A., Teye, E. M., Owusu-Ansah, E. D. G. J., Tettey, S., Diabene, P. Y., & Asimah, S. (2019). Groundwater fluoride contamination and probabilistic health risk assessment in fluoride endemic areas of the upper east region, Ghana. *Chemosphere, 233*, 862–872.

Gao, S., Li, C., Jia, C., Zhang, H., Guan, Q., Wu, X., et al. (2020). Health risk assessment of groundwater nitrate contamination: A case study of a typical karst hydrogeological unit in East China. *Environmental Science and Pollution Research, 27*, 9274–9287.

Gopinathan, P., Nandini, C. V., Parthiban, S., Sathish, S., Singh, A. K., & Singh, P. K. (2020). A geo-spatial approach to perceive the groundwater regime of hard rock terrain-a case study from Morappur area, Dharmapuri district, South India. *Groundwater for Sustainable Development, 10*, 100316.

Gunaalan, K., Ranagalage, M., Gunarathna, M. H. J. P., Kumari, M. K. N., Vithanage, M., Srivaratharasan, T., et al. (2018). Application of geospatial techniques for groundwater quality and availability assessment: A case study in Jaffna peninsula, Sri Lanka. *ISPRS International Journal of Geo-Information, 7*(1), 20.

Horton, R. K. (1965). An index number system for rating water quality. *Journal of Water Pollution Control Federation, 37*(3), 300–306.

Johnny, J. C., & Sashikkumar, M. C. (2014). Groundwater quality assessment in Dindigul District, Tamil Nadu using GIS. *Nature Environment and Pollution Technology, 13*(1), 49.

Johnny, J. C., Sashikkumar, M. C., Kirubakaran, M., & Mathi, L. M. (2018). GIS-based assessment of groundwater quality and its suitability for drinking and irrigation purpose in a hard rock terrain: A case study in the upper Kodaganar basin, Dindigul district, Tamil Nadu, India. *Desalination and Water Treatment, 102*, 49–60.

Juntakut, P., Haacker, E. M., & Snow, D. D. (2020). Risk and cost assessment of nitrate contamination in domestic wells. *Water, 12*(2), 428.

Karunanidhi, D., Aravinthasamy, P., Subramani, T., Wu, J., & Srinivasamoorthy, K. (2019). Potential health risk assessment for fluoride and nitrate contamination in hard rock aquifers of Shanmuganadhi River basin, South India. *Human and Ecological Risk Assessment: An International Journal, 25*(1–2), 250–270.

Kaur, L., Rishi, M. S., & Siddiqui, A. U. (2020). Deterministic and probabilistic health risk assessment techniques to evaluate non-carcinogenic human health risk (NHHR) due to fluoride and nitrate in groundwater of Panipat, Haryana, India. *Environmental Pollution, 259*, 113711.

Kelley, W. P. (1963). Use of saline irrigation water. *Soil Science, 95*(6), 385–391.

Khadri, S. F. R., & Pande, C. (2015a). Groundwater quality mapping using hydrogen chemistry and Geostatistical Analyst of Mahesh River Basin, Akola and Buldhana District, Maharashtra, India. *International Journal of Research (IJR), 2*(10), October-2015.

Khadri, S. F. R., & Pande, C. (2015b). Analysis of hydro-geochemical characteristics of groundwater quality parameters in hard rocks of Mahesh River Basin, Akola, and Buldhana Dist.

Maharashtra, India using geo-informatics techniques. *American Journal of Geophysics, Geochemistry and Geosystems, 1*(3), 105–114.

Khadri, S. F. R., & Pande, C. (2015c). Ground water quality mapping for Mahesh River Basin in Akola and Buldhana Districts of (MS) India using interpolation methods. *International Journal on Recent and Innovation Trends in Computing and Communication, 3*(2), 113–117.

Khadri, S. F. R., Pande, C., & Moharir, K. (2013). Groundwater quality mapping of PTU-1 Watershed in Akola district of Maharashtra India using geographic information system techniques. *International Journal of Scientific & Engineering Research, 4*(9), September-2013.

Khalid, S. (2019). An assessment of groundwater quality for irrigation and drinking purposes around brick kilns in three districts of Balochistan province, Pakistan, through water quality index and multivariate statistical approaches. *Journal of Geochemical Exploration, 197*, 14–26.

Khawla, K., & Mohamed, H. (2020). Hydrogeochemical assessment of groundwater quality in greenhouse intensive agricultural areas in coastal zone of Tunisia: Case of Teboulba region. *Groundwater for Sustainable Development, 10*, 100335.

Kirubakaran, M., Ashokraj, C., Colins Johnny, J., & Anjali, R. (2015). Groundwater quality analysis using WQI and GIS techniques: A case study of Manavalakurichi in Kanyakumari District, Tamilnadu, India. *International Journal of Innovative Science Engineering and Technology, 2*(11), 341–347.

Kumar, P. S., & Balamurugan, P. (2018). Evaluation of groundwater quality for irrigation purpose in attur taluk, Salem, Tamilnadu, India. *Water and Energy International, 61*(4), 59–64.

Kumar, P. S., & Balamurugan, P. (2019). Suitability of ground water for irrigation purpose in. Omalur Taluk, Salem, Tamil Nadu, India. *Indian Journal of Ecology, 46*(1), 1–6.

Kumari, M. K. N., Sakai, K., Kimura, S., Yuge, K., & Gunarathna, M. H. J. P. (2019). Classification of groundwater suitability for irrigation in the Ulagalla tank Cascade landscape by GIS and the analytic hierarchy process. *Agronomy, 9*(7), 351.

Liu, J., Feng, J., Gao, Z., Wang, M., Li, G., Shi, M., & Zhang, H. (2019). Hydrochemical characteristics and quality assessment of groundwater for drinking and irrigation purposes in the Futuan River basin, China. *Arabian Journal of Geosciences, 12*(18), 560.

Mohanakavitha, T., Divahar, R., Meenambal, T., Shankar, K., Rawat, V. S., Haile, T. D., & Gadafa, C. (2019b). Dataset on the assessment of water quality of surface water in Kalingarayan Canal for heavy metal pollution, Tamil Nadu. *Data in Brief, 22*, 878–884.

Mohanakavitha, T., Shankar, K., Divahar, R., Meenambal, T., & Saravanan, R. (2019a). Impact of industrial wastewater disposal on surface water bodies in Kalingarayan canal, Erode district, Tamil Nadu, India. *Archives of Agriculture and Environmental Science, 4*(4), 379–387.

Moharir, K. N., Pande, C. B., Singh, S. K., & Del Rio, R. A. (2020). Evaluation of analytical methods to study aquifer properties with pumping test in Deccan basalt region of the Morna River basin in Akola District of Maharashtra in India. *Groundwater Hydrology*. https://doi.org/10.5772/intechopen.84632.

Moharir, K., Pande, C., & Patil, S. (2017). Inverse modeling of aquifer parameters in basaltic rock with the help of pumping test method using MODFLOW software. *Geoscience Frontiers, 8*(6), 1385–1395.

Moharir, K., Pande, C., Singh, S., Choudhari, P., Rawat, K., & Jeyakumar, L. (2019). Spatial interpolation approach-based appraisal of groundwater quality of arid regions. *Aqua Journal, 68*(6), 431–447.

Nag, S. K., & Das, S. (2014). Quality assessment of groundwater with special emphasis on irrigation and domestic suitability in Suri I & II blocks, Birbhum District, West Bengal, India. *American Journal of Water Resources, 2*(4), 81–98.

Pande, C. B., & Moharir, K. (2018). Spatial analysis of groundwater quality mapping in hard rock area in the Akola and Buldhana districts of Maharashtra, India. *Applied Water Science, 8*(4), 1–17.

Pande, C. B., Moharir, K. N., Singh, S. K., & Dzwairo, B. (2019). Groundwater evaluation for drinking purposes using statistical index: Study of Akola and Buldhana districts of Maharashtra, India, environment. *Development and Sustainability (A Multidisciplinary Approach to the*

Theory and Practice of Sustainable Development) Springer Journal, 22, 7453. https://doi.org/10.1007/s10668-019-00531-0.

Panneerselvam, B., Karuppannan, S., & Muniraj, K. (2020a). Evaluation of drinking and irrigation suitability of groundwater with special emphasizing the health risk posed by nitrate contamination using nitrate pollution index (NPI) and human health risk assessment (HHRA). *Human and Ecological Risk Assessment: An International Journal*, 1–25.

Panneerselvam, B., Paramasivam, S. K., Karuppannan, S., Ravichandran, N., & Selvaraj, P. (2020b). A GIS-based evaluation of hydrochemical characterisation of groundwater in hard rock region, South Tamil Nadu, India. *Arabian Journal of Geosciences, 13*(17), 1–22.

Patil, V. B. B., Pinto, S. M., Govindaraju, T., Hebbalu, V. S., Bhat, V., & Kannanur, L. N. (2020). Multivariate statistics and water quality index (WQI) approach for geochemical assessment of groundwater quality—A case study of Kanavi Halla Sub-Basin, Belagavi, India. *Environmental Geochemistry and Health, 42*(9), 2667–2684.

Radfarda, M., Gholizadehc, A., Azhdarpoorb, A., Badeenezhada, A., Mohammadid, A. A., & Yousefie, M. (2019). Health risk assessment to fluoride and nitrate in drinking water of rural residents living in the Bardaskan city, arid region, southeastern Iran. *Water Treat, 145*, 249–256.

Ravindra, K., Mor, S., Singh, A., Singh, V. J., Dhanda, N., Rani, P., & Mor, S. (2019). Hydrochemistry of groundwater in a north Indian city and its suitability assessment for drinking and irrigation purposes. *Journal of Environmental Biology, 40*(2), 200–210.

Rawat, K. S., Singh, S. K., & Gautam, S. K. (2018). Assessment of groundwater quality for irrigation use: A peninsular case study. *Applied Water Science, 8*(8), 233.

Rezaei, H., Jafari, A., Kamarehie, B., Fakhri, Y., Ghaderpoury, A., Karami, M. A., et al. (2019). Health-risk assessment related to the fluoride, nitrate, and nitrite in the drinking water in the Sanandaj, Kurdistan County, Iran. *Human and Ecological Risk Assessment: An International Journal, 25*(5), 1242–1250.

Rufino, F., Busico, G., Cuoco, E., Darrah, T. H., & Tedesco, D. (2019). Evaluating the suitability of urban groundwater resources for drinking water and irrigation purposes: An integrated approach in the agro-Aversano area of southern Italy. *Environmental Monitoring and Assessment, 191*(12), 768.

Sashikkumar, M. C., Selvam, S., Kalyanasundaram, V. L., & Johnny, J. C. (2017). GIS based groundwater modeling study to assess the effect of artificial recharge: A case study from Kodaganar river basin, Dindigul district, Tamil Nadu. *Journal of the Geological Society of India, 89*(1), 57–64.

Seifi, A., Dehghani, M., & Singh, V. P. (2020). Uncertainty analysis of water quality index (WQI) for groundwater quality evaluation: Application of Monte-Carlo method for weight allocation. *Ecological Indicators, 117*, 106653.

Selvam, S., Venkatramanan, S., Chung, S. Y., & Singaraja, C. (2016). Identification of groundwater contamination sources in Dindugal district of Tamil Nadu, India using GIS and multivariate statistical analyses. *Arabian Journal of Geosciences, 9*(5), 407.

Shankar, K., Aravindan, S., & Rajendran, S. (2011a). Hydro geochemistry of the Paravanar River Sub-Basin, Cuddalore District, Tamilnadu, India. *Journal of Chemistry, 8*(2), 835–845.

Shankar, K., Aravindan, S., & Rajendran, S. (2011b). Hydrochemical profile for assessing the groundwater quality of Paravanar River Sub-Basin, Cuddalore District, Tamil Nadu, India. *Current World Environment, 6*(1), 45.

Shankar, K., & Kawo, N. S. (2019). Groundwater quality assessment using geospatial techniques and WQI in north east of Adama town, Oromia region, Ethiopia. *Hydrospatial Analysis, 3*(1), 22–36.

Shukla, S., & Saxena, A. (2020). Sources and leaching of nitrate contamination in groundwater. *Current Science, 118*(6), 00113891.

Singh, A., Patel, A. K., & Kumar, M. (2020). *Mitigating the risk of arsenic and fluoride contamination of groundwater through a multi-model framework of statistical assessment and natural remediation techniques* (In emerging issues in the water environment during Anthropocene) (pp. 285–300). Singapore: Springer.

Solangi, G. S., Siyal, A. A., Babar, M. M., & Siyal, P. (2019). Application of water quality index, synthetic pollution index, and geospatial tools for the assessment of drinking water quality in the Indus Delta, Pakistan. *Environmental Monitoring and Assessment, 191*(12), 731.

Sunkari, E. D., & Abu, M. (2019). Hydrochemistry with special reference to fluoride contamination in groundwater of the Bongo District, upper east region, Ghana. *Sustainable Water Resources Management, 5*(4), 1803–1814.

Suvarna, B., Sunitha, V., Reddy, Y. S., & Reddy, N. R. (2020). Data health risk assessment of nitrate contamination in groundwater of rural region in the Yerraguntla Mandal, South India. *Data in Brief, 30*, 105374.

Tiwari, K., Goyal, R., & Sarkar, A. (2017). GIS-based spatial distribution of groundwater quality and regional suitability evaluation for drinking water. *Environmental Processes, 4*(3), 645–662.

U. S. Salinity Laboratory (USSL). (1954). *Diagnosis and improvement of saline and alkaline soil; USSA handbook No. 60* (p. 71). Riverside, CA: USSL.

Udeshani, W. A. C., Dissanayake, H. M. K. P., Gunatilake, S. K., & Chandrajith, R. (2020). Assessment of groundwater quality using water quality index (WQI): A case study of a hard rock terrain in Sri Lanka. *Groundwater for Sustainable Development, 11*, 100421.

UNESCO. (2007). *Water Portal newsletter no. 161: water-related diseases*. Paris: UNESCO.

Verma, A., Yadav, B. K., & Singh, N. B. (2020a). Data on the assessment of groundwater quality in Gomti-ganga alluvial plain of northern India. *Data in Brief, 30*, 105660.

Verma, P., Singh, P. K., Sinha, R. R., & Tiwari, A. K. (2020b). Assessment of groundwater quality status by using water quality index (WQI) and geographic information system (GIS) approaches: A case study of the Bokaro district, India. *Applied Water Science, 10*(1), 27.

Wagh, V. M., Panaskar, D. B., Mukate, S. V., Aamalawar, M. L., & Laxman Sahu, U. (2020). Nitrate associated health risks from groundwater of Kadava river basin Nashik, Maharashtra, India. *Human and Ecological Risk Assessment: An International Journal, 26*(3), 654–672.

WHO. (2011). *Guidelines for drinking-water quality* (Vol. 216, pp. 303–304). Geneva: World Health Organization.

Xu, P., Feng, W., Qian, H., & Zhang, Q. (2019). Hydrogeochemical characterization and irrigation quality assessment of shallow groundwater in the central-western Guanzhong basin, China. *International Journal of Environmental Research and Public Health, 16*(9), 1492.

Yadav, K. K., Kumar, V., Gupta, N., Kumar, S., Rezania, S., & Singh, N. (2019). Human health risk assessment: Study of a population exposed to fluoride through groundwater of Agra city, India. *Regulatory Toxicology and Pharmacology, 106*, 68–80.

Yang, Q., Li, Z., Xie, C., Liang, J., & Ma, H. (2020). Risk assessment of groundwater hydrochemistry for irrigation suitability in Ordos Basin, China. *Natural Hazards, 101*, 301–325.

Younas, A., Mushtaq, N., Khattak, J. A., Javed, T., Rehman, H. U., & Farooqi, A. (2019). High levels of fluoride contamination in groundwater of the semi-arid alluvial aquifers, Pakistan: Evaluating the recharge sources and geochemical identification via stable isotopes and other major elemental data. *Environmental Science and Pollution Research, 26*(35), 35728–35741.

Zango, M. S., Sunkari, E. D., Abu, M., & Lermi, A. (2019). Hydrogeochemical controls and human health risk assessment of groundwater fluoride and boron in the semi-arid north east region of Ghana. *Journal of Geochemical Exploration, 207*, 106363.

Zhang, L., Zhao, L., Zeng, Q., Fu, G., Feng, B., Lin, X., et al. (2020a). Spatial distribution of fluoride in drinking water and health risk assessment of children in typical fluorosis areas in North China. *Chemosphere, 239*, 124811.

Zhang, Q., Xu, P., & Qian, H. (2020b). Groundwater quality assessment using improved water quality index (WQI) and human health risk (HHR) evaluation in a semi-arid region of Northwest China. *Exposure and Health, 12*, 487–500.

Zhou, Y., Li, P., Xue, L., Dong, Z., & Li, D. (2020). Solute geochemistry and groundwater quality for drinking and irrigation purposes: A case study in Xinle City, North China. *Geochemistry, 80*(4), 125609.

Chapter 14
Hydrogeochemistry of Groundwater Quality in Amaravathi River Basin of Karur District (Tamilnadu) Using Graphical and Multivariate Statistical Methods

Jafar Ahamed A and Loganathan K

Contents

14.1 Introduction 269
14.2 Study Area Description 271
14.3 Materials and Methods 275
14.4 Results and Discussion 277
14.5 Conclusions 288
References 289

14.1 Introduction

Groundwater is an important source of water supply next to river water used for domestic, industrial, agricultural, and recreational activities in both urban and rural places. One-third of the world's population is using groundwater for drinking and agricultural purpose (Selvakumar et al. 2017; Pande et al. 2018a; Paul et al. 2019). Meanwhile, the groundwater quality is controlled by various factors, such as, soil characteristics, topography of the region, mode of flow of groundwater through the rock types, and saline water interference in coastal areas and human activities on the

Jafar Ahamed A
PG and Research Department of Chemistry, Jamal Mohamed College (Autonomous), Bharathidasan University, Tiruchirappalli, Tamilnadu, India

Loganathan K (✉)
Department of Chemistry, Vivekanandha College of Arts and Sciences for Women (Autonomous), Periyar University, Elayampalayam, Tamilnadu, India
e-mail: drkloganathan@vicas.org

C. B. Pande, K. N. Moharir (eds.), *Groundwater Resources Development and Planning in the Semi-Arid Region*, https://doi.org/10.1007/978-3-030-68124-1_14

earth (Arslan 2013; Pande et al. 2019a, b). Among the various reasons, the most important are nonavailability of potable surface water and general belief that groundwater is purer and safer than surface water due to the protective qualities of the soil cover (Arumugam and Elangovan 2009; Pande 2020a, d; Pande et al. 2018b).

Recently, water demand of the river basin has been raised rapidly by increasing population and industrial activities and it has led to heavy exploitation of the available water resources. At the same time, the unplanned disposal of the anthropogenic wastes has resulted in an excessive addition of pollutants into river and land surface and the subsequent leaching of the pollutants have caused the notable degradation of water quality of surface and shallow groundwater of the river basin (Chapagain et al. 2010; Jafar Ahamed et al. 2014; Khadri and Pande 2015a, b). On the other hand, regular use of poor quality water gives rise to various waterborne diseases. So, there has been increased awareness in public about the safe drinking water in view of its health effect. The occurrence of pollution in groundwater dependent on many external physical factors such as, pit-latrines, animal waste, organic manure, sewerage, and fertilizers (Verma et al. 2020; Guo et al. 2019).

Karur is a major textile center and has five major product groups, namely bed linens, kitchen linens, toilet linens, table linens, and wall hangings. An earlier survey in 2011 says, the total number of factories located on the banks of the Amaravathi River is about 515. The dyeing industry consumes totally 3225 L/day for dyeing process; they took water from the river. About 14,600 m^3 of colored effluent with TDS 5000–10,000 mg/L is let into the river Amaravathi River daily. Big factories had even dug tube wells to a depth of 275 m and discharged effluents into these wells leads to contamination of groundwater in the area. Soil turned infertile, the yield of the crops came down, slowly the farmlands became barren and 250 open wells get contaminated. Kidney disorders, cancer, and abortion are high in the affected villages saying by local natives. Owing to zero discharge of effluents, in 2011, 459 dyeing units were closed and only 54 factories were given permission after they installed ETP (Suchitra 2014).

Sivakumar et al. (2011) quantified that groundwater quality parameters of the Amaravathi River basin were crossing the permissible limits due to industrial and textile industrial activities. Similar results were reported by Raja and Venkatesan (2010), the groundwater in Punnam village of Karur district is highly polluted due to the release of textile industries effluent, same observation was also obtained by Rajamanickam and Nagan (2010), the groundwater quality in the Amaravathi River basin was severely affected by the discharge of untreated or partially treated effluent from the bleaching and dyeing units in Karur. The aim of the study is to investigate the effects of the industrial activities and increase of human population on groundwater quality in the Amaravathi River basin of Karur region since groundwater resources are widely used for drinking, agricultural and industrial purposes. Hence, in the present work the following was planned to (1) examine the physicochemical parameters, (2) estimate the drinking suitability of water samples using water quality index, (3) discriminate the relationship between the arrangement, the samples and

the parameters using principal component analysis, (4) identify the spatial variability (Dendogram Q & R mode) by means of cluster analysis, and (5) find out the spatial distribution pattern (ordinary kriging) of different water quality parameters using ArcGIS 9.3.

14.2 Study Area Description

14.2.1 Location

Amaravathi River originates from Naimakad at an elevation of 2300 m above mean sea level in the Western Ghats in Idukki region of state Kerala (Fig. 14.1). The total length of the river is about 282 km and it covers a total area of 8280 km^2 mainly constituting five districts in Tamilnadu namely Coimbatore, Tirupur, Erode, Karur, and Dindigul. Amaravathi River in Karur lies between north latitudes 11.20° and 12.00° and east longitudes 77.28° and 78.50°. Amaravathi is a tributary of river Shanmuganadhi, Nanganji, and Kodaganar, which joins at 60, 40, and 20 km upstream of Karur city (Fig. 14.2a), respectively. Amaravathi river reach Karur district near Aravakurichi and joins with Cauvery River near Thirumakudalur

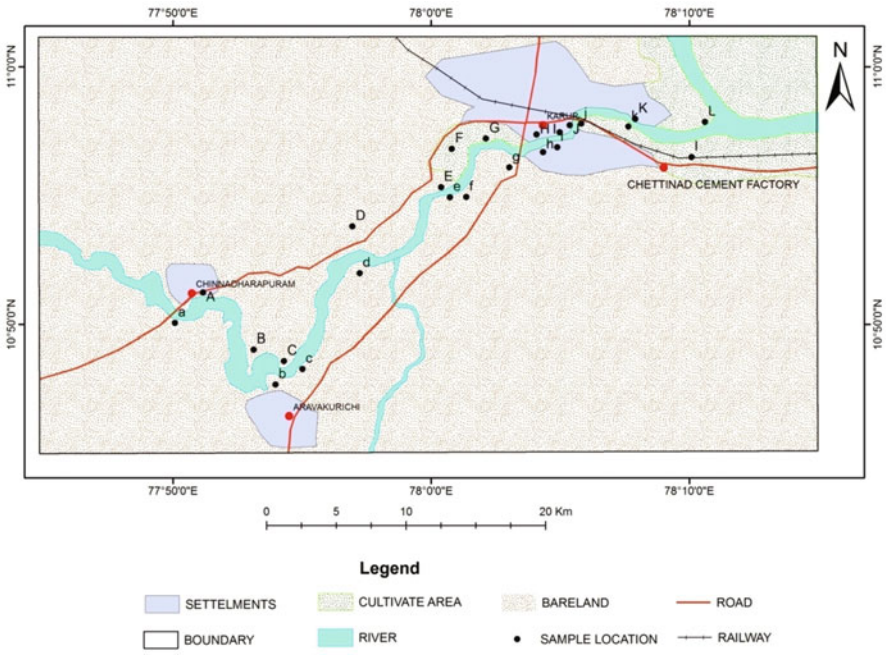

Fig. 14.1 Study area map of the Amaravathi River basin showing sampling sites

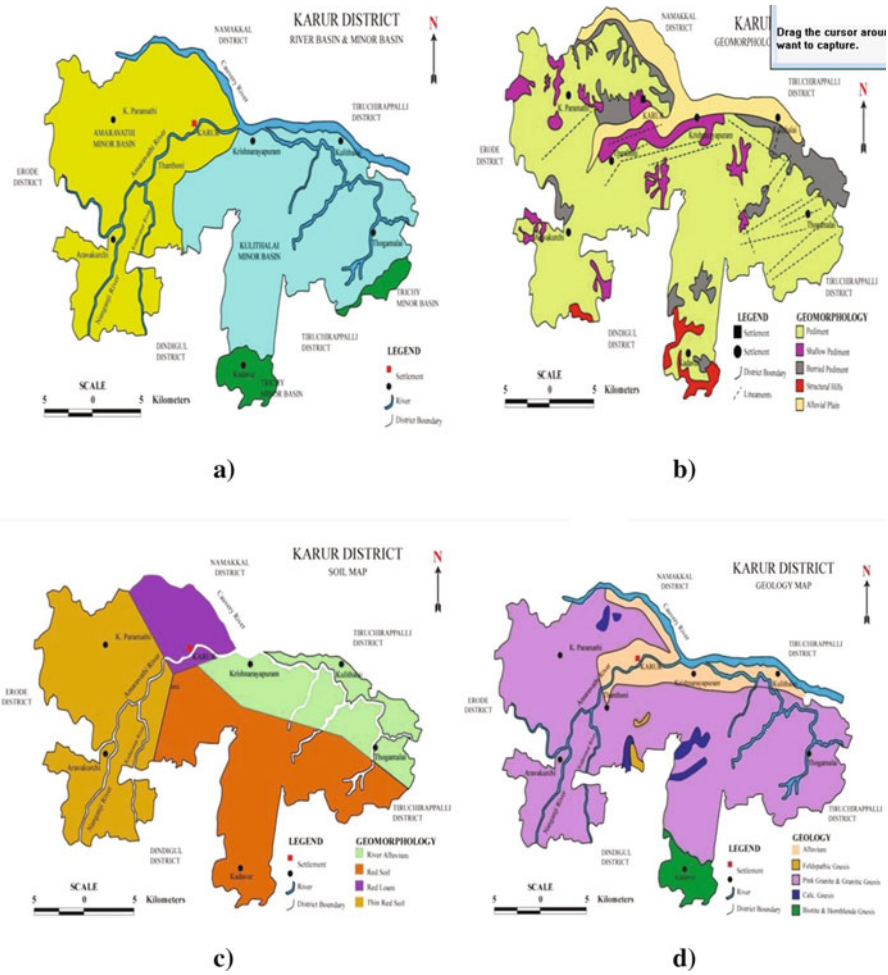

Fig. 14.2 Map showing the (**a**) River, (**b**) Geomorphology, (**c**) Soil, and (**d**) Geology of the Karur district

village, and the water flow in the river is seasonal from late October to early February.

14.2.2 Drainage

Cauvery River drained the major parts of the Karur district. Amaravathi, Kodavanar, and Nanganji are the chief rivers draining the western region of the district and Pungar River drains in the eastern region of the district. The drainage pattern

generally, is dendritic. Except river Cauvery, all the rivers are seasonal and bring substantial flows during the monsoon time (Jafar and Loganathan 2012; Pande and Moharir 2015; Loganathan and Jafar Ahamed 2017; Pande et al. 2018b).

14.2.3 Geomorphology

The entire area of the Karur district is a pediplain. Kadavur and Rangamalai hills occurring in the southern part of the district comprise the loose ends of the much denuded Eastern Ghats and rise to heights of over 1031 m above mean sea level. District possesses several small residual hills represented by Ayyarmalai, Thanthonimalai, and Velayuthampalayam hills. General altitude of the area is ranging between 100 and 200 m above mean sea level. The well-known geomorphic units (Fig. 14.2b) known in the district are pediments, shallow pediments, buried pediments, structural hill and alluvial plain (Khadri et al. 2013a, b; Khadri and Pande 2015a, b; Ahamed and Loganathan 2017; Pande et al. 2017; Pande & Moharir 2018; Khadri & Moharir 2016).

14.2.4 Soil and Vegetation Area

Major part of the district has been covered with red soil is the predominant one followed by red loam and thin red soil. Red soil is mostly seen in Kulithalai, Kadavur, Krishnarayapuram, Thogamalai, and Thanthoni blocks. Karur block is generally covered by red loam. The thin red soils have been seen in K. Paramathy and Aravakurichi blocks (Fig. 14.2c). The major economic crops cultivated in this area are jowar (22.60%), paddy (16.30%), groundnut (6.90%), sugar cane (6.40%), and banana (5.30%). The total geographical area is 2,89,557 ha of which vicinity

Table 14.1 The ninefold land-use/land-cover statistics for the district (CGWB 2008)

S. no.	Classification	Area (ha)
1	Forests	6187
2	Barren and uncultivable lands	2901
3	Land put to nonagricultural uses	37,264
4	Cultivable waste	67,831
5	Permanent pastures and other grazing lands	10,801
6	Groves not included in the area sown	1278
7	Current fallows	4774
8	Other fallow lands	46,802
9	Net area sown	111,719
Total		289,557

employed in cultivation is 1,14,554 ha, 37,264 ha land put into nonagricultural uses and remaining are engaged in other activities (Table 14.1).

14.2.5 Irrigation Practices

The available data indicates that an area of about 54,709 ha, which is about 18.90% of the total geographical area of the district is in irrigated agriculture. Dug wells accounting for about 59.97% of the total area irrigated in the district was the major source of water for irrigation. Tube wells account for about 9.48% of the total area irrigated in the district, while tank irrigation accounts only for 1.10%. Comparing the entire irrigation type, the canal irrigates only 29.45% area (Khadri et al. 2013a, b; Jafar Ahamed et al. 2015; Moharir et al. 2019).

14.2.6 Rainfall and Climate

Amaravathi River basin and subbasin has four different seasons, namely summer season from March to May, southwest monsoon commencing from June to early September, northeast monsoon beginning of October to December and winter season starting from January to February. The district receives the rain from both northeast and southwest monsoons. The northeast monsoon primarily contributes to the rainfall in the district. Precipitation habitually occurs in the form of cyclonic storms is due to the effect of depressions in Bay of Bengal. The southwest monsoon rainfall is highly inconsistent whereas summer rains are negligible (Jafar Ahamed et al. 2016). The average annual rainfall over the district from 1901 to 2011 varies between 620 and 745 mm, and in 2012, it was founded as 527.6 mm, much less than the states normal average rainfall of 652.20 mm (Renganathan 2014), and it is the least around Aravakurichi (622.7 mm) in the western region of the district. It progressively increases toward eastern parts and reach a maximum around Kulithalai (744.6 mm). The district enjoys a subtropical climate, and the relative humidities generally range from 40% to 80%. The average maximum temperature ranges from 26.7 to 38.56 °C, and the average minimum temperature ranged between 18.7 and 29.3 °C. The daylight heat is oppressive and the temperature attains high as 43.9 °C and the lowest temperature observed is 13.9 °C (CGWB 2008).

14.2.7 Geology and Hydrogeology

The district is underlained entirely by Archaean Crystalline formations with fresh alluvial deposits taking place along the river and stream courses (Fig. 14.2d). The rigid consolidated crystalline rocks of Archaean age symbolize weathered, fractured

and fissured formations of gneisses, granites, charnockites, and additional related rocks. Deep groundwater occurs beneath phreatic conditions, and the most saturated thickness of the aquifer in rigid rock creation varied between 15 and 35 m depending upon the topographic circumstances (Jafar Ahamed et al. 2015). Thickness of the alluvial deposit is estimated to be approximately 10–12 m. The specific capacity of large diameter wells tested in crystalline rocks from 31 to 200 lpm/m of drawdown. The yield characteristics of wells vary considerably depending on the topographic setup, lithology, and the degree of weathering. The seasonal fluctuation shows a rise in water level, which ranges from 0.46 to 1.98 m. The piezometric head varied between 3.53–5.34 m bgl during pre-monsoon and 2.04–7.59 m bgl during post-monsoon. The specific capacity in the weathered, partly weathered and jointed rocks varies from 31 to 240.5 lpm/m/dd and the transmissivity values in weathered, partly weathered and jointed rocks vary from 15.5 to 154 m^2/day. The optimum yield varied from 45.40 to 441.60 m^3/day. The specific capacity in the fissured and fractured formation ranges from 6.89 to 117.92 lpm/m/dd and the transmissivity values ranges from 11.42 to 669.12 m^2/day. The specific capacity values in the porous formation vary from 135 to 958 lpm/m.dd and the transmissivity values ranged from 67.5 to 264.5 m^2/day. The optimum yield varied from 232.8 to 549.6 m^3/day (Liu et al. 2003; Khadri & Pande 2016; Loganathan and Jafar Ahamed 2017; Pande 2020b; Pande 2020c).

14.3 Materials and Methods

14.3.1 Sampling

Totally 24 groundwater samples were collected from bore and hand pumps during May (2019) representing the summer season. Groundwater samples were collected along the banks of River Amaravathi from Chinnadharapuram (Upstream of Karur) to Thirumakudalur (downstream of Karur) from different locations. Simultaneously, two samples were collected from each site, i.e., from left and right side of the Amaravathi River. The bore wells and hand pumps location for sampling were chosen on the base of an industrial unit in addition to diverse land use patterns. Figure 14.1 demonstrates the GIS map of the study area showing sampling locations. During sample collection high density white polyethylene bottles were used. The samples were filled up to the rim and were instantly preserved to avoid exposure to air and were labeled scientifically and stored at 4 °C. The labeled water samples were analyzed for their physicochemical parameters in the laboratory. At sample collection for handling and preservation the American Public Health Association (APHA 2005) standard procedures were followed to promise data quality and consistency.

14.3.2 Analytical Procedure

Temperature and dissolved oxygen (DO) were examined at the time of sampling using 110 °C thermometer and Winkler's method respectively. The total dissolved solids (TDS), hydrogen ion concentration (pH) and electrical conductivity (EC) were also determined immediately on location by using water quality multi-tester probe (Eutech PC Tester 35), and the major ions were examined using the standard procedure suggested by the APHA (2005). Turbidity was determined using Nephelometric turbidity meter with sample cells. Sodium (Na^+) and potassium (K^+) were determined by Flame photometer using Systronics make 128. Total hardness (TH), calcium (Ca^{2+}), magnesium (Mg^{2+}), bicarbonate (HCO_3^-), and chloride (Cl^-) were analyzed by volumetric methods following Trivedy and Goel (1986) methods and sulfates (SO_4^{2-}) were estimated by precipitation method using spectrophotometer. Fluoride ion concentration was estimated by ion selective electrode (Thermo scientific Orion 4 star). Phosphate and Nitrate were examined by stannous chloride and brucine method using a spectrophotometer. Biochemical Oxygen Demand (BOD) and Chemical Oxygen Demand (COD) were calculated using Winkler's Iodometric method and $K_2Cr_2O_7$ method respectively. The accuracy of the results was checked by calculating the ionic balance errors and it was generally within ±5%, and the analytical precision for ions was determined by using this formula,

$$\text{Ionic Balance} = 100 \times (\text{cations} - \text{anions})/(\text{cations} + \text{anions}). \tag{14.1}$$

14.3.3 Water Quality Index

Water quality index (WQI) provides the overall water quality at a certain location and time, based on several water quality parameters. A water quality index based on some very important parameters can provide a simple indicator of water quality. To determine the suitability of the groundwater for drinking purposes, Water Quality Index (Tiwari and Mishra 1985; Pande et al. 2019a) is computed by adopting the method which is formulated as $\text{WQI} = \sum Q_i W_i / \sum W_i$, where, W_n, weightage $= K/S_n$ and K, constant $= 1/[1/s_1 + 1/s_2 + \ldots 0.1/S_n]$ and S_n correspond to the WHO/ICMR standard value of the parameters. Quality rating (Q_i) is calculated as $Q_{ni} = [(V_{\text{actual}} - V_{\text{ideal}})/(V_{\text{standard}} - V_{\text{ideal}})] \times 100$ where Q_{ni} = quality rating of "i"th parameter for a total of "n" water samples V_{actual} = value of the water quality parameter obtained from the analysis. V_{standard} = value of the water quality parameters obtained from the standard tables. V_{ideal} for pH = 7 and for the other parameters it is equal to zero (Reza and Sing 2010).

14.3.4 Statistical Analysis

SPSS software version 16.0 was used for statistical analysis. Karl Pearson correlation matrix analysis is a useful tool in hydrogeochemical studies that can indicate the associations between individual parameters and thus revealing the overall rationality of data set and enlightening the links between individual parameters and various controlling factors (Ahamed et al. 2017; Wang and Jiao 2012). A correlation coefficient of <0.5 exhibit poor correlation, 0.5 represent the good correlation and >0.5 highlight the excellent correlation. Pearson's correlation coefficient provides the elemental relationships between the original variables, are presented in nonparametric form (Vasanthavigar et al. 2013). Two multivariate statistical techniques were employed, the PCA and the HCA. PCA is used for data reduction and for deciphering patterns within large sets of data. PCs provide information on the most meaningful parameters, which describes a whole dataset affording data reduction with minimum loss of original information (Helena 2000). PCs were extracted on the symmetrical correlation matrix which consists of interrelations between variables; these PCs were subjected to varimax rotation (raw) generating. The HCA is a group of data classification technique, there are different clustering techniques; however, the hierarchical clustering is the one most widely useful in earth sciences (Davis 2002). Both Q-mode and R-mode were performed on the hydrochemical parameters. The Q-mode HCA was used to classify the samples into distinct hydrochemical groups while the R-mode HCA is linking variables. To perform CA, an agglomerative hierarchical clustering was developed using a combination of the ward's linkage method and squared Euclidean distances as a measure of similarity. GIS has emerged as a powerful tool for creating spatial distribution maps. The spatial analysis of various physicochemical parameters were carried out using the ArcGIS v.9.3 software. In order to interpolate the data spatially and to estimate values between measurements, an inverse distance weighed (IDW) raster interpolation technique was used (Srinivas et al. 2013). An analyzed result of May 2019 was presented in Table 14.2.

14.4 Results and Discussion

14.4.1 Physicochemical Parameters

Temperature is one of the important parameters which judge the range of pH and dissolved oxygen content in water samples. Samples with temperature >32 °C make water unsuitable for drinking purposes. An increase in temperature leads to the reduced dissolution of ambient oxygen into water samples. The mean temperature in groundwater samples ranges from 30.8 to 31.6 °C. The reasonably higher temperature at places could be attributed to the decreased flow rate or very shallow rock in river bed exposed to direct sunlight raising the temperature of water flowing

Table 14.2 Physicochemical characteristics of the groundwater samples

Stations	Temp	Turb	pH	EC	TDS	TH	Ca	Mg	Na	K	HCO_3	Cl	F	SO_4	PO_4	NO_3	DO	BOD	COD
A	31.3	0.3	7.48	3384	2345	760	214	48	506.82	60.56	515	738	0.7	261	0.1	1.45	5.32	1.80	94
B	31.4	0.2	6.76	3276	2270	995	278	62	440.45	22.61	392	841	0.5	233	0.2	1.02	4.53	2.40	71
C	31.2	0.1	7.13	2080	1441	590	64	104	225.00	17.87	515	340	0.6	174	0.0	1.15	4.33	2.30	79
D	31.0	0.4	7.03	2483	1721	725	118	105	282.93	18.36	393	528	0.3	273	0.2	2.27	4.92	2.60	64
E	31.2	0.3	6.85	2430	1684	525	173	22	318.49	46.06	484	404	0.7	235	0.4	0.95	3.74	2.90	61
F	31.3	0.6	6.81	1509	1045	630	96	89	65.36	18.34	306	315	0.5	154	0.5	1.16	3.94	3.00	64
G	31.1	1.0	6.7	2173	1506	290	98	11	372.78	12.77	515	305	0.8	189	0.1	1.77	4.33	2.20	77
H	31.2	1.2	7.66	3152	2184	520	173	21	566.43	15.45	448	635	1.1	323	0.1	1.43	3.34	3.20	71
I	31.3	0.2	7.57	2736	1896	470	134	27	408.54	59.63	757	336	0.3	172	0.2	1.62	3.74	2.80	106
J	31.3	0.9	7.45	4974	3447	684	215	35	882.45	63.88	999	1124	0.8	126	0.3	0.74	6.11	1.20	29
K	31.5	0.4	6.76	6207	4302	2020	709	60	707.11	21.42	545	1989	0.5	269	0.1	0.93	4.13	2.50	43
L	31.4	0.7	6.68	2274	1576	510	188	9	310.23	61.02	368	467	0.7	171	0.4	1.03	5.32	1.80	64
a	31.2	0.3	7.33	1459	1011	365	40	64	182.00	11.73	424	189	0.8	99	0.1	0.92	6.90	0.80	65
b	31.4	0.2	7.5	2816	1951	710	213	37	396.24	11.58	333	383	0.9	576	0.1	1.1	4.93	2.60	101
c	31.6	0.4	7.34	5476	3795	1190	423	56	743.18	19.15	454	1661	2.2	435	0.3	1.25	5.12	1.90	79
d	31.5	0.1	7.58	2261	1567	930	187	98	204.56	18.69	367	543	1.9	145	0.2	2.02	4.73	2.40	87
e	31.4	0.5	7.34	1901	1317	455	67	52	280.68	19.36	484	273	1.8	138	0.1	1.73	6.11	1.30	93
f	31.3	0.2	6.98	2055	1424	590	129	65	192.32	16.42	575	284	2.0	160	0.1	0.94	6.50	0.90	106
g	31.2	0.9	7.39	5310	3680	785	277	22	922.64	103.4	727	1338	4.1	285	0.3	0.93	5.91	1.10	59
h	31.1	0.4	7.36	3586	2485	845	212	77	519.23	68.85	424	994	0.7	188	0.1	1.22	6.10	0.90	87
i	30.8	0.5	8.01	5380	3728	2900	336	46	1000.5	14.71	434	1608	1.8	286	0.9	1.35	5.52	1.20	97
j	30.9	0.7	7.40	4382	3037	925	293	47	672.66	11.45	333	1453	1.3	225	0.2	0.63	5.12	1.90	101
k	30.9	0.6	7.42	4493	3114	925	316	64	675.94	13.26	323	1523	0.8	218	0.2	1.56	6.02	1.60	91
l	31.0	0.5	7.36	5259	3644	1070	294	81	728.84	21.06	424	1693	0.7	401	0.1	1.10	6.70	0.70	82

All the values are expressed in mg/L, except turbidity (NTU), pH, and electrical conductivity in μS/cm.

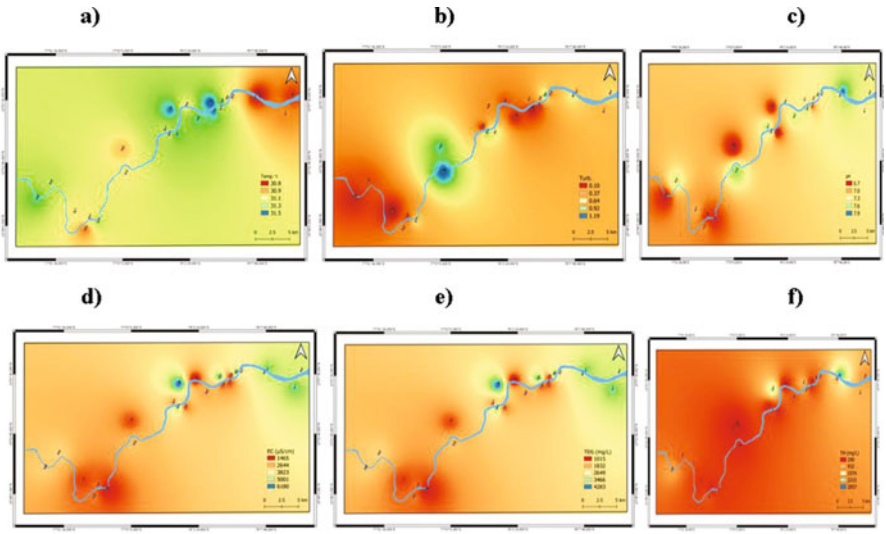

Fig. 14.3 Spatial distribution pattern of (**a**) Temperature (**b**) Turbidity (**c**) pH (**d**) EC (**e**) TDS and (**f**) TH

through/over. The spatial distribution of temperature in all the groundwater samples is shown in Fig. 14.3a. Turbidity in water is caused by suspending particles or colloidal matter that obstructs light transmission through the water (Kim et al. 2013). From the Table 14.2 all the groundwater samples fall within the limit of 5 NTU prescribed by WHO (2005) and BIS (2003), another fact, most of the samples fall within 1 NTU, they do not make any infection to consumers (Fig. 14.3b). pH in the groundwater samples ranges from 6.68 to 8.01 indicates that samples are slightly alkaline in nature, due to the collective effect of the high concentration of dissolved ions, variation in soil types, various aquifer system and anthropogenic activities, especially agricultural activities in the study area and its spatial distribution was shown in Fig. 14.3c. The pH value of groundwater is mainly controlled by the amount of dissolved carbon dioxide, carbonate and bicarbonate concentration (Zhou et al. 2013).

According to Langenegger (1990) classification, electrical conductivity value >1500 μS/cm is considered as saline, 95.83% of the groundwater samples falls under saline category. In general, EC depends upon temperature, concentration, and types of ions present (Hem 1985). Relatively higher EC values were recorded in the study area (Fig. 14.3d) indicating the enrichments of salts in groundwater; pH may also increase the dissolution process which ultimately increases the EC value. TDS is regarded as one of the main factors which determine the use of groundwater for any purpose (Maiti et al. 2013). Davis and De Wiest (1966) proposed four classes of waters based on TDS for drinking and irrigation purposes. No one sample fall under desirable for drinking (<500 mg/L) category, while 75% in samples are suitable for irrigation, and the remaining are unfit for drinking and irrigation

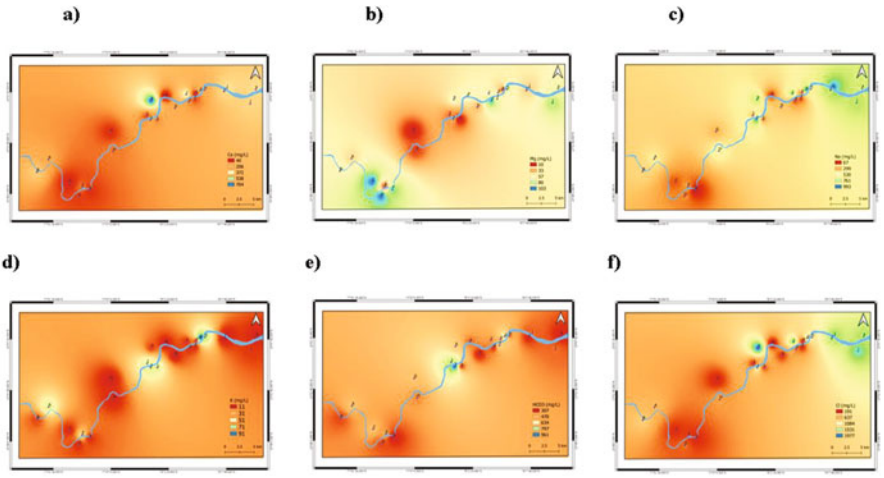

Fig. 14.4 Spatial distribution pattern of (**a**) Ca^{2+} (**b**) Mg^{2+} (**c**) Na^{+} (**d**) K^{+} (**e**) HCO_3^{-} and (**f**) Cl^{-}

purposes. At the lower basin of the study area contains a high TDS value may due to saline water intrusion and nutrient enrichment due to fertilizers could enhance TDS and, in turn, increases the EC in the lower basin. This was clearly shown in the spatial distribution map (Fig. 14.3e). Water can be classified into four categories by Sawyer and McCarthy (1967): soft (<75 mg/L), moderately hard (75–150 mg/L), hard (150–300 mg/L), and very hard (>300 mg/L) based on the total hardness. None of the samples belongs to soft and moderately hard; only 4% sample belong to hard type and remaining 96% samples in comprised of very hard water. From the results, groundwater in the study area is hard to very hard type. The spatial distribution of TH in the study region is illustrated in Fig. 14.3f. Higher TH value is due to the presence of cation like Ca^{2+}, Mg^{2+} and anion Cl^{-} and SO_4^{2-} ion released from rocks, industrial discharge, and sewage effluent.

The range of Ca^{2+} in groundwater was between 40 and 701 mg/L. Except three samples (C, a and e) all other samples exceeded the maximum allowable limit of 75 mg/L (WHO 2005). Majority of the samples (90%) exposed higher concentration, comparing the upper and lower basin of the Amaravathi River; lower basin was mainly controlled by both weathering and anthropogenic activities to increase the concentration. The spatial distribution map of Ca^{2+} (Fig. 14.4a) clearly shows that, samples from right side of the river basin exhibit higher value were highly influenced by dissolution process. The possible dissolution reaction of calcite and dolomite can be written as follows:

$$CaCO_3 + H_2CO_3 \rightarrow Ca^{2+} + 2HCO_3^{-}. \tag{14.2}$$

$$Ca \cdot Mg(CO_3)_2 + 2H_2CO_3 \rightarrow Ca^{2+} + Mg^{2+} + 4HCO_3^{-}. \tag{14.3}$$

The high level of calcium, magnesium, chlorides, and bicarbonates in several cases is probably due to their low rate of removal of soil (Jafar Ahamed et al. 2015).

The Mg^{2+} concentration in the groundwater samples ranged between 9 and 105 mg/L. About 54% samples experienced higher value and only 46% samples possess value <50 mg/L. Magnesium usually occurs in lesser concentration than calcium due to the fact that the dissolution of magnesium rich minerals is a slow process and that of calcium is more abundant in the earth's crust. If it is more than 30 mg/L, it causes an unpleasant taste to the water. Continuous usage of hard water may spoil the kidney and resulted in defunctioning (Ramesh and Thirumangai 2014). Spatial distribution map shows that Mg^{2+} is highly found in right side of the river basin covering upper and middle basin (Fig. 14.4b). The maximum permissible limit for Na^+ in drinking water is 200 mg/L, and it reveals that 88% of the samples exceeded the permissible limit of WHO (2005) and BIS (2003) and 12% samples are in a safe range. Excess concentration could be from natural sources like feldspar and also from cation exchange process. It is evident from the spatial distribution diagram (Fig. 14.4c) that the rock type and weathering were important in the upper region, but the anthropogenic activities played more significant role in downstream regions. K^+ concentration ranges between 11.45 and 103.40 mg/L, about 83% samples exceeded the maximum permissible limit of 12 mg/L given by WHO (2005) and BIS (2003). Weathering of Feldspar and presence of clay minerals in the aquifer matrix generates water soluble K^+ ions. Figure 14.4d obviously shows that K^+ concentration is uniformly distributed right through the entire study area with even difference. HCO_3^- concentration in all the groundwater samples exceeded the allowable limit of 200 and100 mg/L according to WHO (2005) and BIS (2003) guideline value. It may be due to action of carbon dioxide upon the basic mineral of soil and lithology. The spatial distribution map (Fig. 14.4e) shows the higher HCO_3^- concentration is observed in downstream of Amaravathi River basin mainly due to mixing of municipal sewage.

In fact, Cl^- concentration in groundwater samples ranged between 273 and 1989 mg/L, potable water should not exceed 200 and 250 mg/L suggested by WHO (2005) and BIS (2003), here all the samples exceeded the guideline value. The reason for that higher concentration observed in the downstream of the Amaravathi River Basin (Fig. 14.4f) is mainly from non-lithological sources and its solubility to water is high. Atmospheric deposits and chemical fertilizer is also another reason it leaching from upper soil layer. WHO (2005) and BIS (2003) described the drinking water quality; the permissible limit for F^- is 1 mg/L, where in the study area 33% of samples exceeding the guideline value (Fig.14.5a). The reason observed that higher Na^+ activates the dissolution of fluoride bearing minerals at higher pH in the groundwater (Srinivasamoorthy et al. 2012; Saxena and Ahmed 2003). The concentration of SO_4^{2-} in groundwater samples varied between 99 and 576 mg/L and the most admirable limit for SO_4^{2-} concentration in drinking water is 200 mg/L. The higher concentration (Fig. 14.5b) is due to chemical or physical reaction of gypsum with water and also enhanced by urban utilities. PO_4^{3-} and NO_3^- concentration in all water samples fall within the tolerable limit of 1 and 45 mg/L respectively. The spatial distribution pattern of PO_4^{3-} and NO_3^-

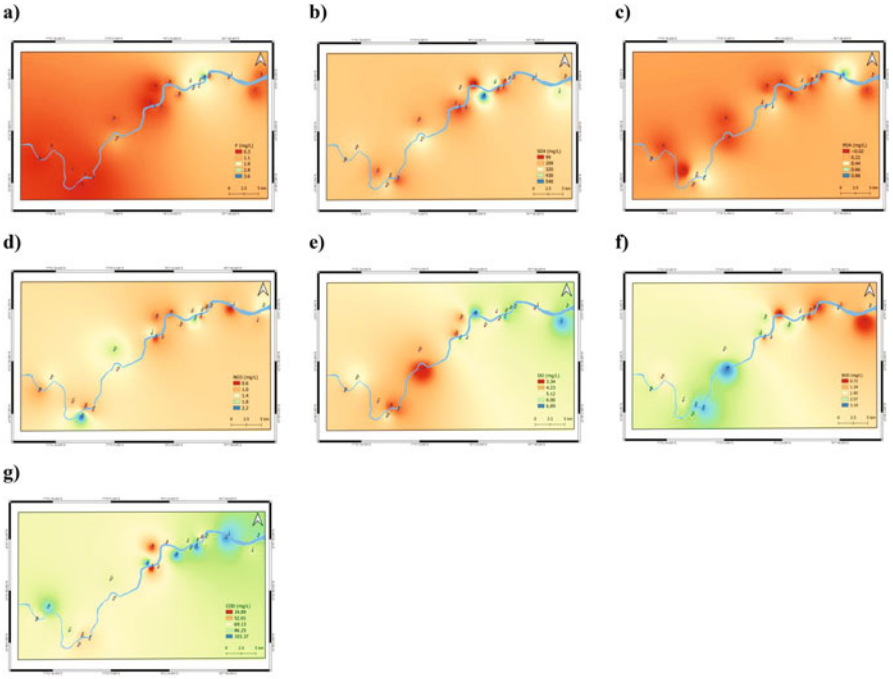

Fig. 14.5 Spatial distribution pattern of (**a**) F^- (**b**) SO_4^{2-} (**c**) PO_4^{3-} (**d**) NO_3^- (**e**) DO (**f**) BOD and (**g**) COD

(Fig. 14.5c and d) indicates that, the samples are evenly distributed throughout the study area.

Dissolved oxygen is the basic requirement for the preservation of life of all living organisms in water. A water body is said to be polluted when DO level falls below a certain minimal concentration (<5 mg/L) necessary for sustaining a normal biota for that water. Oxygen demanding substances can remove large amounts of DO from water, causes changing in their flora and fauna (Prabakaran and Poorna 2012). The DO concentration varied between 3.34 and 6.90 mg/L, the sample collected during summer season experienced low DO value, directly dependent on temperature, and its distribution is shown in Fig. 14.5e. The biochemical oxygen demand concentration varied between 0.70 and 3.20 mg/L and al the samples are within the recommended limit 5 mg/L for BOD given by WHO (2005) and BIS (2003). The spatial distribution of BOD in the study region is illustrated in Fig. 14.5f. COD of greater than 1.0 mg/L is assumed to be caused by anthropogenic influence. Drinking water supply should not exceed COD of 2.5 mg/L and potable water of COD content greater than 7.5 mg/L is regarded as poor. High COD interferes with oxygen transfer to the soil, thus affecting plant growth. The COD values of groundwater samples were not within the permissible limit of 10–40 mg/L. The high COD values may be due to the discharge of untreated or incompletely treated industrial effluents into the

sewage from the various manufacturing plants during past years (2000–2011), which affects the status of groundwater. Every so often high COD is emerged due to higher Cl^- content. COD cannot be accurately measured if the samples having Cl^- content greater than 500 mg/L, in the present study 96% samples experienced higher chloride value. The spatial distribution pattern (Fig. 14.5g) show except sample J, all other samples have high COD value. The most abundant important cation and anion in the water samples are in the following order: $Na^+ > Ca^{2+} > Mg^{2+} > K^+$ and $Cl^- > HCO_3^- > SO_4^{2-}$.

14.4.2 Water Quality Index (WQI)

For computing WQI values, each of the 19 parameters has been assigned a weight (W_i) and water quality rating (Q_i) according to the guidelines laid down by the WHO (1989). WQI can be categorized into five types; they are "Excellent" (0–24), "Good" (25–49), "Poor" (50–74), "Very poor" (75–100), and "Unfit for drinking" (>100). Depend upon these types, the groundwater is classified and to find its suitability for drinking purposes. The computed WQI percentage of water samples are graphically exposed in Fig. 14.6. About one-third (33.34%) of the samples fall in "Unfit for drinking" category (Samples: c, d, e, f, g, i, j and k). None of the samples constitute "Excellent" and "Good" category (Fig. 14.6). "Poor" category was represented by samples a, B, C, D and K, accounted for 20.83%. Nearly, 45.83% samples represent "Very poor" quality of groundwater comprised by samples A, b, E, F, G, H, h, I, J, L, and l. From the present WQI quality ratings, it was found that the groundwater within the study area is non-potable because most of the physicochemical parameters exceeded the desirable limit.

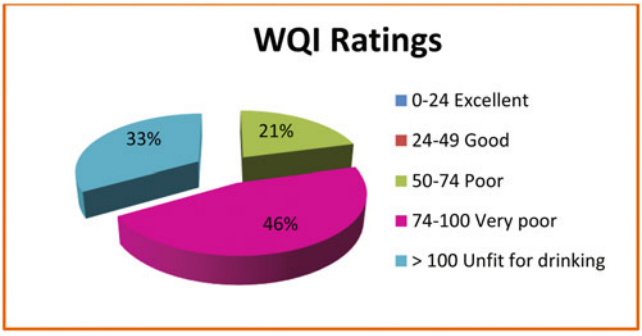

Fig. 14.6 Water quality index for groundwater samples

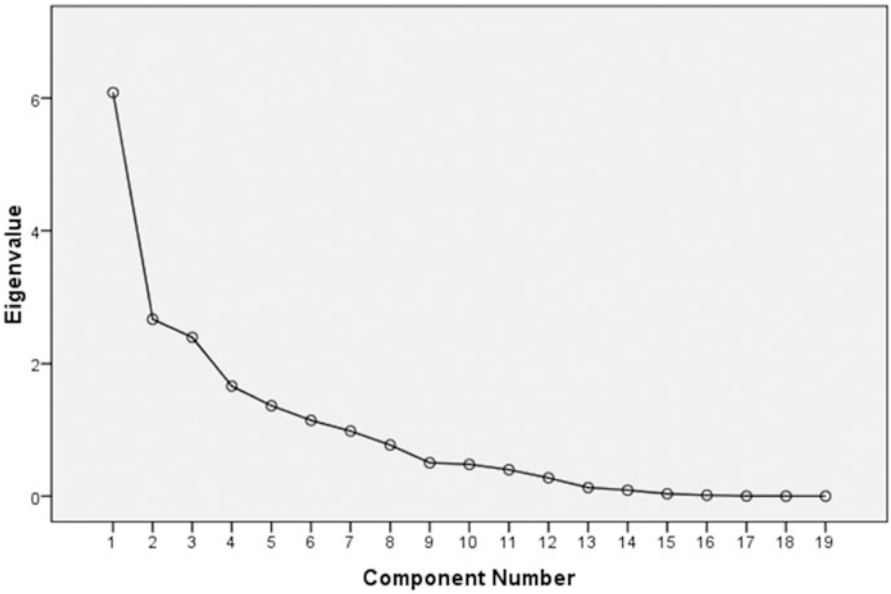

Fig. 14.7 Scree plot of the eigen values of PCs

14.4.3 Principle Component Analysis

Principle component analysis is carried out to identify major variables affecting on water quality of deep groundwater. In PCA, numbers of PCs equals to the number of unique variables and each PC includes the entire measured water quality variables. On the other hand, several criteria are used to identify the number of PCs to be retained in order to know the underlying data structure. PCs, having the eigen value greater than unity, are retained during the analysis, which has expressed that the selected PCs are able to carry more information than a single unique variable (Chapagain et al. 2010). In this study, six PCs reported 80.643% of the variance of the original data matrix, having eigen value of more than unity (Fig. 14.7). The results of six PCs are summarized in Table 14.3. The best positive and highly negative loadings of each variable in PCs 1–6 were as Factor 1 include EC, TDS, TH, Ca^{2+}, Na^{+}, and Cl^{-}, Factor 2 with TH, Mg^{2+}, $SO_4{}^{2-}$, COD and negatively by K^{+}, $HCO_3{}^{-}$, Factor 3 consists of pH, DO, COD and negatively by temperature, Factor 4 with $PO_4{}^{3-}$, turbidity, Factor 5 contains temperature and $SO_4{}^{2-}$, and Factor 6 comprised of $PO_4{}^{3-}$. Component 1 accounts for 32.020% of the total variance of the data matrix and appears to characterize the water–rock interaction processes, responsible for the high loadings in Ca^{2+}, Mg^{2+}, and Cl^{-}. The high contribution of Cl^{-} in this component could be attributed from atmospheric precipitation (by evaporation). The equal weightage of Na^{+} and Cl^{-} seems to be presence of Na^{+} in local halite rocks. The second component represents 14.056% of the total

Table 14.3 Varimax-rotated factor loadings of groundwater quality parameters

	Varimax-rotated components					
Variables	PC1	PC2	PC3	PC4	PC5	PC6
Temp	−0.055	−0.396	0.437	−0.178	−0.534	−0.408
Turbidity	0.123	−0.010	0.159	−0.132	0.884	0.037
pH	0.221	0.194	0.112	0.761	0.091	0.197
EC	0.956	0.131	0.163	0.025	0.129	0.061
TDS	0.956	0.131	0.163	0.025	0.129	0.061
TH	0.754	0.008	−0.156	0.137	−0.196	0.517
Ca^{2+}	0.936	−0.130	0.004	−0.151	−0.127	−0.032
Mg^{2+}	−0.047	0.251	−0.495	−0.060	−0.623	0.093
Na^{+}	0.828	0.181	0.266	0.162	0.358	0.164
K^{+}	0.023	0.105	0.800	−0.087	0.121	0.063
HCO_3^{-}	0.057	0.115	0.784	−0.156	0.119	0.029
Cl^{-}	0.951	0.190	−0.037	−0.022	0.077	0.098
F^{-}	0.205	0.228	0.517	0.432	0.013	0.042
SO_4^{2-}	0.553	−0.294	−0.160	0.415	0.065	−0.379
PO_4^{3-}	0.183	−0.117	0.101	0.078	0.067	0.864
NO_3^{-}	−0.318	−0.253	−0.252	0.390	−0.086	0.134
DO	0.074	0.938	0.076	0.109	−0.064	−0.088
BOD	−0.148	−0.940	−0.180	−0.092	0.005	−0.007
COD	−0.169	0.095	−0.288	0.778	−0.146	−0.090
Eigen values	5.474	2.391	2.367	1.876	1.756	1.458
Variance %	28.811	12.583	12.455	9.876	9.243	7.674
Cumulative %	28.811	41.394	53.849	63.725	72.968	**80.643**

variance, standing for the moderate loadings in TH, Mg^{2+}, SO_4^{2-}, and COD and negatively by K^{+}, HCO_3^{-}. This factor could be ascribed to the influence of anthropogenic inputs (by the use of chemical fertilizers and insecticides associated with SO_4^{2-} and Mg^{2+}). The PC3 is dominated by the inverse relation between the original rock matrix and external contribution associated with the proximity of the river basin. PO_4^{3-} explained with 10.511% of total variance. While, PC4, PC5, and PC6 explained 8.741%, 7.184% and 6.021% of the total variance of data set respectively. These factors explain their loadings are by man-made activities. Loadings of the first three components are represented by Fig. 14.8.

14.4.4 Cluster Analysis (CA)

Cluster analysis is a method for placing objects into more or less homogeneous groups so that the relation between the groups is revealed. It is also possible to evaluate whether water quality samples at various locations can be combined into homogeneous regions (Nagaraju et al. 2014). Q-mode cluster analysis of the summer

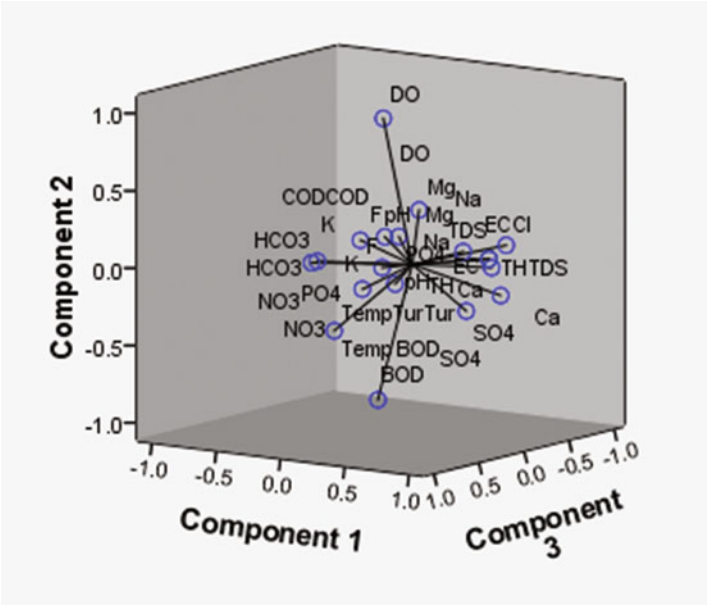

Fig. 14.8 Rotated loadings for components 1, 2, and 3

season dendrogram shows a variety of groups (Fig. 14.9). Group A consists of 8 components (sample no. 5, 12, 10, 13, 9, 23, 7, and 8) having equal linkage distance emerged from common sources. Group B & C has 2 samples each (sample no. 4, 17: 2, 11) and Group D contain four samples (1, 3, 16, and 15) has increased in linkage distance influenced by dissolution of minerals, weathering of silicate minerals and fracture of other secondary minerals contributes the geochemical evolution of groundwater. Two samples (sample no. 6 and 24) are in Group E and four samples comprise (sample no. 6, 24, 14, and 19) Group F. These group samples belonged from right side of the Amaravathi River basin affected by both point and non-point sources. Samples 18 and 21 makes Group G, regarded as high pollution loading, from both geogenic and anthropogenic origins.

Figure 14.10 shows the dendrogram of R-mode cluster analysis. From the figure, three clusters can be recognized in the physicochemical variables. The first cluster includes of EC and TDS and the second cluster contain TH and Cl^- make the third consists of HCO_3^-, Na^+, SO_4^{2-}, Ca^{2+} in addition to Mg^{2+}, COD, K^+, temperature, DO, pH, F^-, BOD, NO_3^-, PO_4^{3-} and turbidity. The first cluster is dominated by the effect of mineral dissolution and weathering processes. The Cl^- in second cluster is attributed by impurities, whereas chloride replaces hydroxide in biotite and hornblende (Kuroda and Sandell 1953). The third cluster is likely from natural processes, such as weathering of anhydrite, calcite and halite, strong evaporation, anthropogenic sources such as agricultural practices, sewage activities and wastewater from bleaching industries.

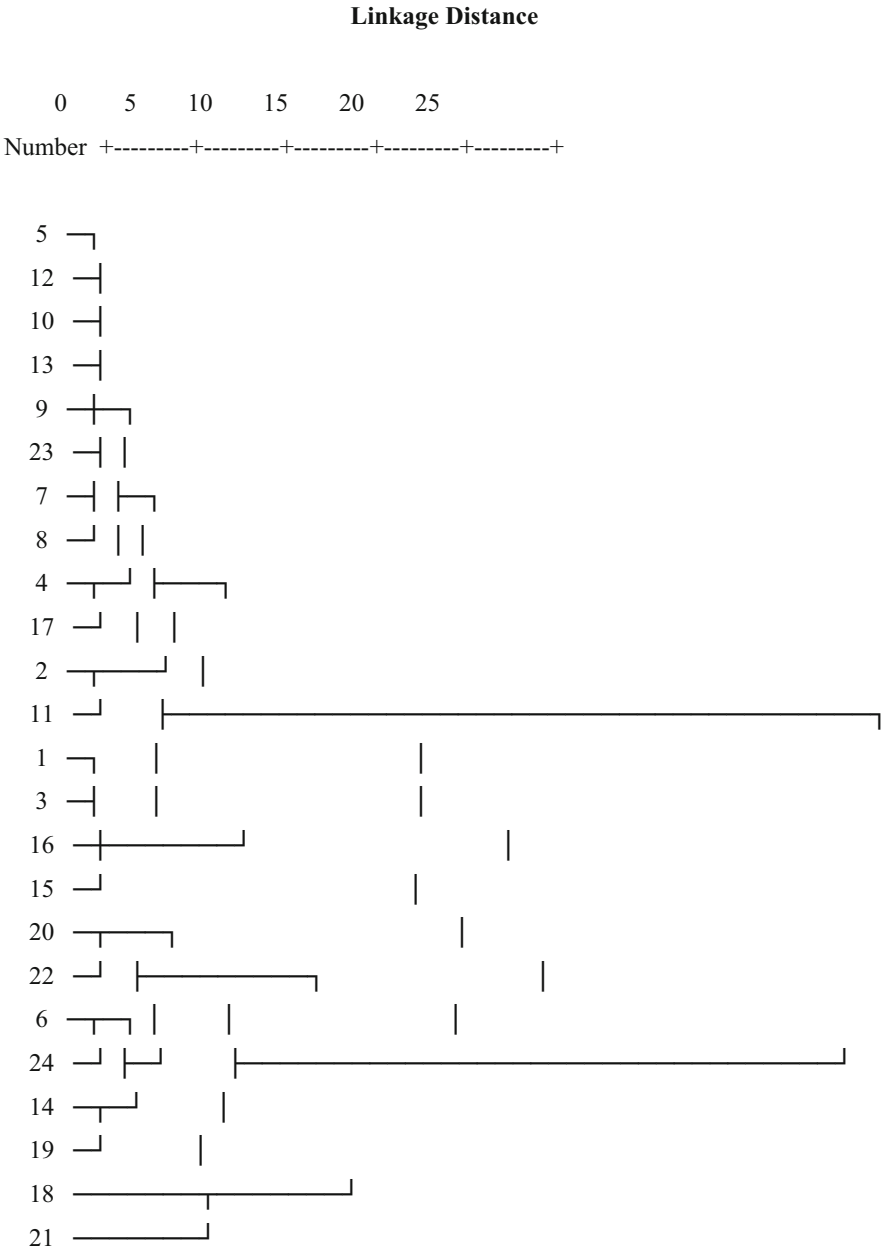

Fig. 14.9 Dendrogram of the Q-mode hierarchical cluster analysis

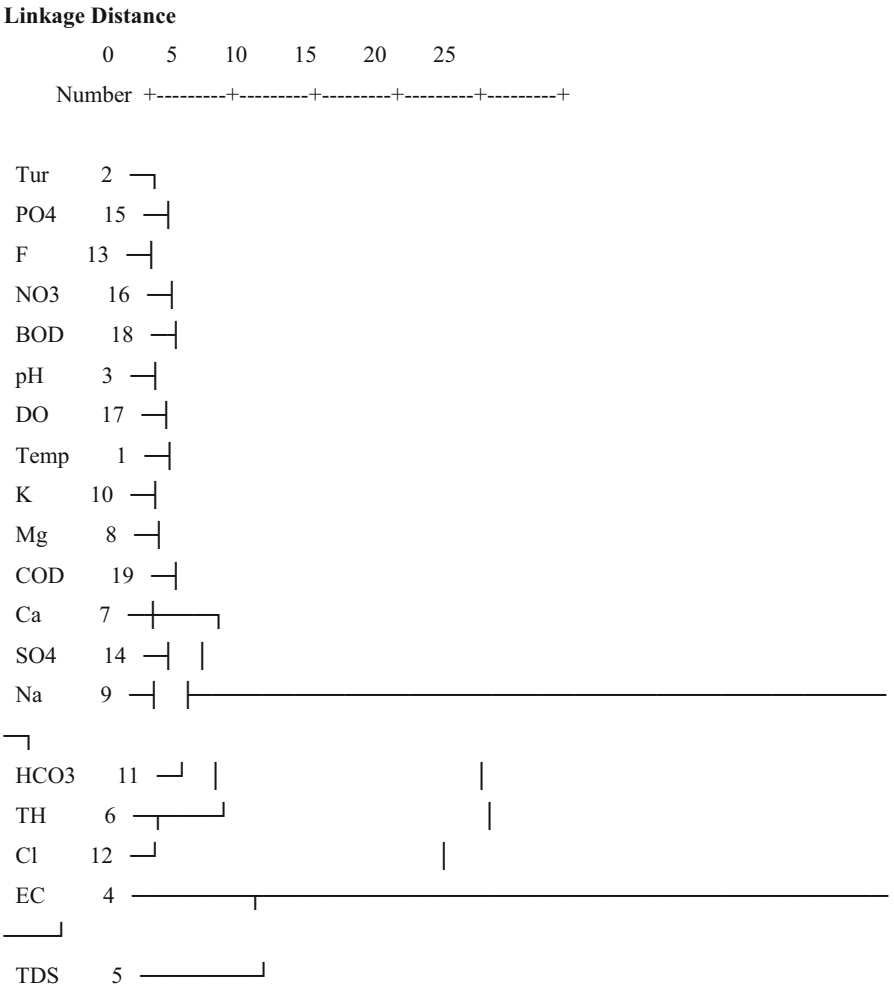

Fig. 14.10 Dendrogram of the R-mode hierarchical cluster analysis

14.5 Conclusions

The hydrogeochemistry of groundwater around Amaravathi River basin of Karur region indicates that most of the parameters exceeded the guideline value. Without prior treatment the water is not fit for drinking purpose according to WQI values. Five PCs were extracted which explains 81% of the total variance of the original data matrix. A first PC is loaded heavily by EC, TDS, TH, Ca^{2+}, Mg^{2+}, Na^{+}, and Cl^{-}. Other components are moderately accounted for the total variance. The parameters responsible for groundwater quality variations are mainly related to water–rock

interaction and anthropogenic sources. Q-mode CA consists of four main groups, in which Group D (samples 6, 18 and 19) has a high pollution loading. R-mode CA consists of two clusters, first cluster consists of EC and TDS, and the second cluster consists of all other 17 variables, mainly by Na^+, HCO_3^-, TH, SO_4^{2-}, Ca^{2+} in addition to COD, Mg^{2+}, K^+, temperature, DO, pH, F^-, BOD, NO_3^-, PO_4^{3-} and turbidity. The above results can be used for future sustainable development of the basin.

Acknowledgments The one of the author Dr. A. Jafar Ahamed is thankful to the University Grants Commission (UGC), New Delhi for providing Major Research Fund (F. No. 41-337/2012) and the Members of the Management Committee and the Principal of Jamal Mohamed College for providing necessary facilities. The authors also thank the anonymous reviewers for their valuable comments to improve the manuscript.

References

Ahamed, A. J., & Loganathan, K. (2017). Water quality concern in the Amaravathi River basin of Karur District: A view at heavy metal concentration and their interrelationships using geostatistical and multivariate analysis. *Geology, Ecology, and Landscapes, 1*, 19–36.

Ahamed, A. J., Loganathan, K., Ananthakrishnan, S., Ahmed, J. K. C., & Ashraf, M. A. (2017). Evaluation of graphical and multivariate statistical methods for classification and evaluation of groundwater in Alathur block, Perambalur District. *Applied Ecology and Environmental Research, 15*, 105–116.

APHA. (2005). *Standard methods for the examination of water and wastewater* (21st ed.). Washington, DC: American Public Health Association.

Arslan, H. (2013). Application of multivariate statistical techniques in the assessment of groundwater quality in seawater intrusion area in Bafra plain, Turkey. *Environmental Monitoring and Assessment, 185*, 2439–2452.

Arumugam, K., & Elangovan, K. (2009). Hydrochemical characteristics and groundwater quality assessment in Tirupur region, Coimbatore District, Tamil Nadu, India. *Environmental Geology, 58*, 1509–1520.

BIS. (2003). *Indian standards specification for drinking water 15:10500*. New Delhi: Bureau of Indian Standards.

CGWB. (2008). *District groundwater brochure Karur district, Tamil Nadu*. Chennai: Central Ground Water Board.

Chapagain, S. K., Pandey, V. P., Shrestha, S., Nakamura, T., & Kazama, F. (2010). Assessment of deep groundwater quality in Kathmandu Valley using multivariate statistical techniques. *Water, Air, and Soil Pollution, 210*, 277–288.

Davis, J. (2002). *Statistics and data analysis in geology* (3rd ed.). New York, NY: Wiley.

Davis, S. N., & De Wiest, R. J. M. (1966). *Hydrogeology* (Vol. 463). New York, NY: Wiley.

Guo, Q., Zhou, Z., Huang, G., & Dou, Z. (2019). Variations of groundwater quality in the multi-layered aquifer system near the Luanhe River, China. *Sustainability, 11*(4), 994. https://doi.org/10.3390/su11040994.

Helena, B. (2000). Temporal evolution of groundwater composition in an alluvial (Pisuerga river, Spain) by principal component analysis. *Water Research, 34*, 807–816.

Hem, J. D. (1985). Study and interpretation of the chemical characteristics of natural water. *USGS Water Supply Paper, 2254*, 117–120.

Jafar, A. A., & Loganathan, K. (2012). Assessment and correlation analysis of surface and groundwater of Amaravathi River basin – Karur, Tamilnadu, India. *Journal of Chemical and Pharmaceutical Research, 4*, 3972–3983.

Jafar Ahamed, A., Loganathan, K., Ananthakrishnan, S., & Manikandan, K. (2016). Physico-chemical and microbiological studies of soils in Amaravathi River bed area, Karur District, Tamil Nadu, India. In P. Ramasami, M. Gupta Bhowon, S. Jhaumeer Laulloo, & H. Li Kam Wah (Eds.), *Crystallizing ideas—The role of chemistry* (pp. 181–199). Cham: Springer.

Jafar Ahamed, A., Loganathan, K., & Jayakumar, R. (2015). Hydrochemical characteristics and quality assessment of groundwater in Amaravathi river basin of Karur district, Tamil Nadu, South India. *Sustainable Water Resources Management, 1*, 273–291.

Jafar Ahamed, A., Loganathan, K., Vijaya Kumar, P., & Ananthakrishnan, S. (2014). Suitability of groundwater for domestic use-a case study on Alathur block, Perambalur District, Tamil Nadu. *Proceedings of the International Symposium on Integrated Water Resources Management, 1*(p), 483–490. ISBN:978-81-8424-906-4.

Khadri, S. F. R., & Moharir, K. (2016). Characterization of aquifer parameter in basaltic hard rock region through pumping test methods: A case study of Man River basin in Akola and Buldhana districts Maharashtra India. *Modeling Earth Systems and Environment, 2*, 33.

Khadri, S. F. R., & Pande, C. (2015a). Remote sensing based hydro-geomorphological mapping of Mahesh River Basin, Akola, and Buldhana Districts, Maharashtra, india-effects for water resource evaluation and management. *International Journal of Geology, Earth and Environmental Sciences, 5*(2), 178–187.

Khadri, S. F. R., & Pande, C. (2015b). Ground water quality mapping for Mahesh River Basin in Akola and Buldhana Districts of (MS) India using interpolation methods. *International Journal on Recent and Innovation Trends in Computing and Communication, 3*(2), 113–117.

Khadri, S. F. R., & Pande, C. (2016). Ground water flow modeling for calibrating steady state using MODFLOW software: A case study of Mahesh River basin, India. *Model Earth System Environment, 2*, 39. https://doi.org/10.1007/s40808-015-0049-7.

Khadri, S. F. R., Pande, C., & Moharir, K. (2013a). Geomorphological investigation of WRV-1 watershed management in Wardha district of Maharashtra India; using remote sensing and geographic information system techniques. *International Journal of Pure and Applied Research in Engineering and Technology, 1*(10), 23.

Khadri, S. F. R., Pande, C., & Moharir, K. (2013b). Groundwater quality mapping of PTU-1 Watershed in Akola district of Maharashtra India using geographic information system techniques. *International Journal of Scientific & Engineering Research, 4*(9), September-2013.

Kim, K.-H., Susaya, J. P., Park, C. G., Uhm, J.-H., & Hur, J. (2013). Comprehensive monitoring of drinking well water quality in Seoul metropolitan city, Korea. *Environmental Monitoring and Assessment, 185*, 6353–6378.

Kuroda, P. K., & Sandell, E. B. (1953). Chlorine in igneous rocks. *Geological Society of America Bulletin, 64*, 879–896.

Langenegger O. (1990). Ground water quality in rural areas of western Africa, UNDP project INT/81/026:10.

Liu, W. X., Li, X. D., Shen, Z. G., Wang, D. C., Wai, O. W. H., & Li, S. Y. (2003). Multivariate statistical study of heavy metal enrichment in sediments of the Pearl River estuary. *Environmental Pollution, 121*, 377–388.

Loganathan, K., & Jafar Ahamed, A. (2017). Multivariate statistical techniques for the evaluation of groundwater quality of Amaravathi River basin: South India. *Applied Water Science, 7*(8), 4633–4649.

Maiti, S., Erram, V. C., Gupta, G., Tiwari, R. K., Kulkarni, U. D., & Sangpal, R. R. (2013). Assessment of groundwater quality: A fusion of geochemical and geophysical information via Bayesian neural networks. *Environmental Monitoring and Assessment, 185*, 3445–3465.

Moharir, K., Pande, C., Singh, S., Choudhari, P., Rawat, K., & Jeyakumar, L. (2019). Spatial interpolation approach-based appraisal of groundwater quality of arid regions. *Aqua Journal, 68* (6), 431–447.

Nagaraju, A., Sunil Kumar, K., Thejaswi, A., & Sharifi, Z. (2014). Statistical analysis of the hydrogeochemical evolution of groundwater in the Rangampeta area, Chittoor District, Andhra Pradesh, South India. *American Journal of Water Resources, 2*, 63–70.

Pande, C. B. (2020a). Introduction. In *Sustainable watershed development. Springer briefs in water science and technology*. Cham: Springer. https://doi.org/10.1007/978-3-030-47244-3_1.

Pande, C. B. (2020b). Watershed management and development. In *Sustainable watershed development. Springer briefs in water science and technology*. Cham: Springer. https://doi.org/10.1007/978-3-030-47244-3_2.

Pande, C. B. (2020c). Thematic mapping for watershed development. In *Sustainable watershed development. Springer briefs in water science and technology*. Cham: Springer. https://doi.org/10.1007/978-3-030-47244-3_3.

Pande, C. B. (2020d). Sustainable watershed development planning. In *Springer briefs in water science and technology*. Cham: Springer. https://doi.org/10.1007/978-3-030-47244-3_4.

Pande, C. B., Khadri, S. F. R., Moharir, K. N., & Patode, R. S. (2017). Assessment of groundwater potential zonation of Mahesh River basin Akola and Buldhana districts, Maharashtra, India using remote sensing and GIS techniques. *Sustainable Water Resources Management, 4*, 965–979. https://doi.org/10.1007/s40899-017-0193-5.

Pande, C. B., & Moharir, K. (2015). GIS-based quantitative morphometric analysis and its consequences: A case study from Shanur River basin, Maharashtra India. *Applied Water Science, 7*(2), 23.

Pande, C. B., & Moharir, K. (2018). Spatial analysis of groundwater quality mapping in hard rock area in the Akola and Buldhana districts of Maharashtra, India. *Applied Water Science, 8*(4), 1–17.

Pande, C. B., Moharir, K. N., Khadri, S. F. R., & Patil, S. (2018b). Study of land use classification in the arid region using multispectral satellite images. *Applied Water Science, 8*(5), 1–11.

Pande, C. B., Moharir, K. N., & Pande, R. (2018a). Assessment of morphometric and hypsometric study for watershed development using spatial technology – A case study of Wardha river basin in the Maharashtra. *India in International Journal of River Basin Management, 2018*, 1. https://doi.org/10.1080/15715124.2018.1505737.

Pande, C. B., Moharir, K. N., Singh, S. K., & Dzwairo, B. (2019a). Groundwater evaluation for drinking purposes using statistical index: Study of Akola and Buldhana districts of Maharashtra, India, environment. *Development and Sustainability (A Multidisciplinary Approach to the Theory and Practice of Sustainable Development), 22*, 7453. https://doi.org/10.1007/s10668-019-00531-0.

Pande, C. B., Moharir, K. N., Singh, S. K., & Varade, A. M. (2019b). An integrated approach to delineate the groundwater potential zones in Devdari watershed area of Akola district. *Maharashtra, Central India in Environment, Development, and Sustainability, 22*, 4867. https://doi.org/10.1007/s10668-019-00409-1.

Paul, R., Prasanna, M. V., Gantayat, R. R., & Singh, M. K. (2019). Groundwater quality assessment in Jirania block, west district of Tripura, India, using hydrogeochemical fingerprints. *SN Applied Science, 1*, 1055. https://doi.org/10.1007/s42452-019-1092-1.

Prabakaran, A., & Poorna, B. (2012). Computaional complexity analysis on water quality index. *International Journal of Advanced Research in Computer Engineering & Technology, 2*, 95–102.

Raja, G., & Venkatesan, P. (2010). Assessment of groundwater pollution and its impact in and around Punnam area of Karur District, Tamilnadu, India. *E-Journal of Chemistry, 7*, 473–478.

Rajamanickam, R., & Nagan, S. (2010). Groundwater quality modeling of Amaravathi River basin of Karur District, Tamilnadu, using visual mudflow. *International Journal of Environmental Science and Technology, 2*, 91–108.

Ramesh, K., & Thirumangai, V. (2014). Impacts of tanneries on quality of groundwater in Pallavaram, Chennai Metropolitan City. *International Journal of Engineering Research and Applications, 4*, 63–70.

Renganathan, L. (2014). Water table plummets to new low in Karur. *The Hindu*. Retrieved January 13, 2014, from http://www.thehindu.com.

Reza, R., & Sing, G. (2010). Assessment of groundwater quality status by using water quality index method in Orissa, India. *World Applied Sciences Journal, 9*(12), 1392–1397.

Sawyer, G. N., & McCarthy, D. L. (1967). *Chemistry of sanitary engineers* (2nd ed., p. 518). New York, NY: McGraw Hill.

Saxena, V., & Ahmed, S. (2003). Inferring chemical parameters for the dissolution of fluoride in groundwater. *Environmental Geology, 43*(6), 731–736.

Selvakumar, S., Chandrasekar, N., & Kumar, G. (2017). Hydrogeochemical characteristics and groundwater contamination in the rapid urban development areas of Coimbatore, India. *Water Resources and Industry, 17*, 26–33.

Sivakumar, K. K., Balamurugan, C., Ramakrishnan, D., & Leena Hebsibai, L. (2011). Studies on physicochemical analysis of groundwater in Amaravathi River basin at Karur (Tamil Nadu), India. *Water Rearch & Development, 1*, 36–39.

Srinivas, Y., Hudson Oliver, D., Stanley Raj, A., & Chandrasekar, N. (2013). Evaluation of groundwater quality in and around Nagercoil town, Tamilnadu, India: An integrated geochemical and GIS approach. *Applied Water Science, 3*, 631–651.

Srinivasamoorthy, K., Vijayaraghavan, K., Vasanthavigar, M., et al. (2012). Assessment of groundwater quality with special emphasis on fluoride contamination in crystalline bed rock aquifers of Mettur region, Tamilnadu, India. *Arabian Journal of Geosciences, 5*, 83–94.

Suchitra, M. (2014). Farmers affected by Karur's dye industry to exercise NOTA. *News-Down to Earth*. Retrieved November 28, 2014, from http://www.downtoearth.org.in/content.

Tiwari, T. N., & Mishra, M. A. (1985). A preliminary assignment of water quality index of major Indian rivers. *Indian Journal of Environmental Protection, 5*, 276–279.

Trivedy, R. K., & Goel, P. K. (1986). *Chemical and biological methods for water pollution studies*. Karad: Environmental Publication.

Vasanthavigar, M., Srinivasamoorthy, K., & Prasanna, M. V. (2013). Identification of groundwater contamination zones and its sources by using multivariate statistical approach in Thirumanimuthar sub-basin, Tamil Nadu, India. *Environment and Earth Science, 68*, 1783–1795.

Verma, A., Yadav, B. K., & Singh, N. B. (2020). Hydrochemical monitoring of groundwater quality for drinking and irrigation use in Rapti Basin. *SN Applied Sciences, 2*, 460.

Wang, Y., & Jiao, J. J. (2012). Origin of groundwater salinity and hydrogeochemical processes in the confined quaternary aquifer of the Pearl River Delta, China. *Journal of Hydrology, 438-439*, 112–124.

WHO. (1989). *Health guidelines for the use of wastewater in agriculture and aquaculture* (Vol. 778, p. 74). Geneva: World Health Organization.

WHO. (2005). *International standards for drinking water*. Geneva: World Health Organization.

Zhou, Y., Wang, Y., Li, Y., Zwahlen, F., & Boillat, J. (2013). Hydrogeochemical characteristics of central Jianghan plain, China. *Environment and Earth Science, 68*, 765–778.

Chapter 15
GIS-Based Assessment of Urban Groundwater Pollution Potential Using Water Quality Indices

Manish Kumar Sinha, Preeti Rajput, Klaus Baier, and Rafig Azzam

Contents

15.1 Introduction 293
15.2 Study Area 294
15.3 Materials and Methods 295
15.4 Results and Discussion 301
15.5 Conclusion 311
References 312

15.1 Introduction

The interaction of urbanization and water quality is considerably controlled by the city's land use structure as different types of land use labor various sources of contaminants and hazards which influence both water quality and quantity (Baier et al. 2014, 2015; Pande and Moharir 2018). Urbanization refers to a process in which an increasing proportion of an entire population lives in cities and the suburbs of cities and change of land use from agriculture to human settlements, commercial sectors, and industries (Putra and Baier 2008). The growing human population and development activities, increased human access to environmental resources, and the

M. K. Sinha (✉) · K. Baier · R. Azzam
Department of Engineering Geology and Hydrogeology, RWTH Aachen University, Aachen, Germany
e-mail: sinha@lih.rwth-aachen.de; baier@lih.rwth-aachen.de; azzam@lih.rwth-aachen.de

P. Rajput
Department of Civil Engineering, Government Engineering College Bilaspur, Koni, Chhattisgarh, India

C. B. Pande, K. N. Moharir (eds.), *Groundwater Resources Development and Planning in the Semi-Arid Region*, https://doi.org/10.1007/978-3-030-68124-1_15

exploitation of renewable or nonrenewable resources of land have led to changes in water quality (Ghorbani et al. 2014). The issue of water contamination and wastewater disposal is an intense problem in cities of developing countries where, generally, densely populated and inadequate managed sewer drains areas created by high rates of population migration into cities (Sinha et al. 2019a, b). These areas are unplanned and located in the outskirts of the cities forming shanty towns (typically between 30% and 60% of the overall urban population) where pit latrines or septic tanks are common. In some cities, septic tanks and pit latrines are the only way to dispose of sewage (Putra and Baier 2008). The consumption of these different contaminants through biodegradation or toxicity resistance to these pollutants by the microbial communities can provide information about pollutant exposure, metabolic diversity and the potential source of contamination and the potential for the ecosystem natural attenuation, thus may be a practical indicator of the water quality (Karbassi et al. 2011; Pande et al. 2018).

Water quality index was first introduced in 1848 about 168 years ago in Germany where the presence or absence of certain organism in water was used as fitness indicator of a water source. The use of numerical scale to represent gradation in water quality levels is a recent phenomenon, beginning with Horton index in 1965 (Mustapha and Aris 2011; Moharir et al. 2019). The concept also aims at eliminating the subjective assessment of water quality and the individual biases of water resource managers (Sarkar and Abbasi 2006). Water quality is the function of anything and everything the water might have picked up during its journey to the water body in dissolved, colloidal and suspended form. Water quality may be assessed in terms of: Quality for life (e.g., the quality of water needed for human consumption), Quality for food (e.g., the quality of water needed to sustain agricultural activities), Quality for nature (e.g., the quality of water needed to support a thriving and diverse fauna and flora in a region), and the selection of parameters used to assess the quality of water depends largely on the intended use of the body of water (Poonam et al. 2013; Nikoo et al. 2011; Khadri et al. 2013; Khadri and Pande 2015a, b).

15.2 Study Area

Raipur city is located between 21°12′N–21°18′N latitude and 81°33′–81°41′E longitude depicted in Fig. 15.1. The climate of the study area is subtropical with three different seasons. Temperature is moderate and May is the hottest month and December is the coldest month. The Kharun River flows to the west of the city of Raipur, which is also a source of domestic water supply to the city (RMC 2010; Sinha et al. 2016). The city has a population of 11,46,383 and experienced a growth rate of 51.06% during decade 2001–2011. Present study is focused on the groundwater condition in the municipal boundaries of Raipur City, Chhattisgarh, India (Sinha et al. 2019a, b). The sanitation ratings conducted as per national urban sanitation policy, Raipur ranked 274 out of 423 cities with a score of 30.8/100 and

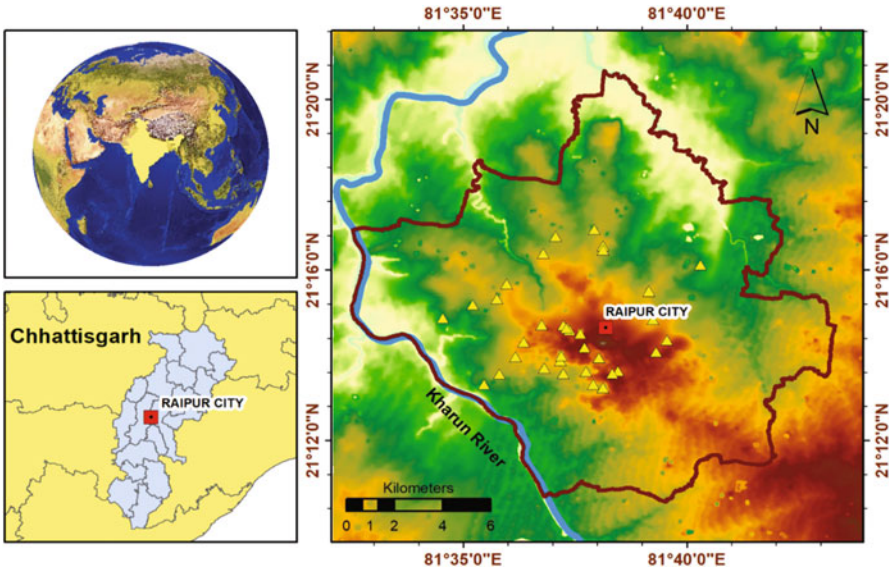

Fig. 15.1 Location map of the study area

falls in the red category. Raipur was blessed with 154 Talabs, which had either been built by nature or by human intervention, has presently only 85 Talabs survived. These 85 surface water bodies of varying sizes (2800–402,000 m^2) occupying a total surface area of 2.83 km^2, which is about 2% of the city's area. These lakes were one of most prominent sources to recharge the groundwater in Raipur, as the aquifer is shallow in the region. Due to human interference since long back the lakes were severely contaminated, which was also connected to groundwater and open wells. Thus, the pollutants get easily transferred from surface water to groundwater. Thirty-four prominent open wells near to lakes were selected for groundwater quality assessments (GIZ 2010, 2011).

15.3 Materials and Methods

The procedure adopted in this study was graphically shown in Fig. 15.2. This study aims to assess the groundwater quality of the Raipur city. The most prominent locations were selected on the basis of susceptibility toward polluted recharging zone in the city area to check the samples of groundwater. The distribution of selected parameters is geostatistical interpolated over the Raipur city area. These thematic maps of all the selected parameters are used for the spatial computation of National Sanitation Foundation Water Quality Index (NSFWQI). The resultant NSFWQI Map demarcates the safe groundwater withdrawal zone in the city area. Apart from that on the other hand Canadian Council of Ministers of the Environment

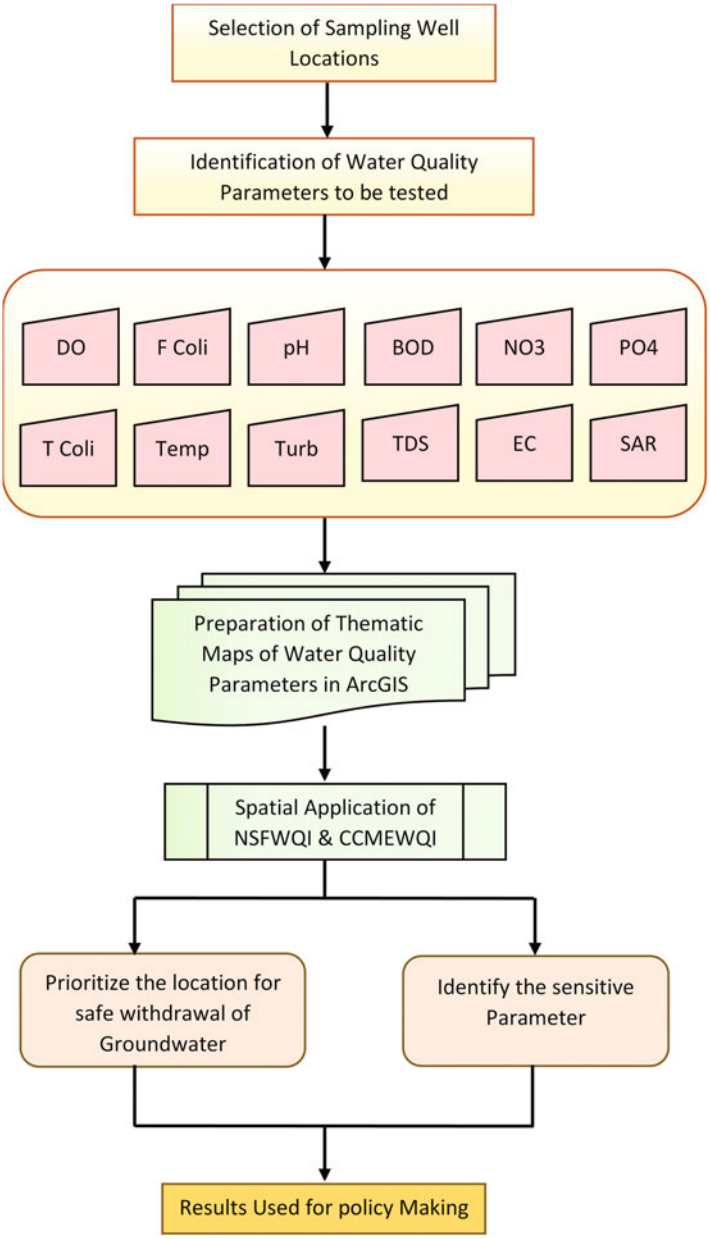

Fig. 15.2 Flow diagram of working procedure

Water quality Index (CCMEWQI) were computed over all 34 sampling locations and the most sensitive parameter affected due to urban pollution was identified. On the basis of these outcomes, groundwater use policy was suggested for the Raipur city.

15.3.1 Selection of Water Quality Parameters and Laboratory Analysis

Water quality parameters dissolved oxygen (DO), biochemical oxygen demand (BOD), electrical conductivity (EC), pH, sodium adsorption ratio (SAR), total coliforms (Tcoli), total hardness (TH), total dissolved solids (TDS), temperature (Temp), phosphate (PO_4), nitrate (NO_3), and turbidity (Turb) were selected to identify the most affected parameter due to pollution load on the water body. The statistical behavior of these parameters was shown in Fig. 15.3. And its statistical properties were listed in Table 15.1. These parameters were selected on the basis of:

- How strong is the influence of urban area on the parameter?
- Do the data values show anomalies as compared to expected values?
- Pollution intimation property for the different types of uses of groundwater.

Groundwater samples were collected in the second week of every 3 months gap from July 2018 to April 2019 at selected sites. The water samples were analyzed to study the physiochemical parameters by following the standard methods of American Public Health Association (Apha 2005; RMC 2011; Pande et al. 2019). The physical parameters were examined at the spot, and chemical parameters like DO were also carried out near the spot. Other chemical parameters like BOD, NO_3, PO_4, and TH were analyzed at the laboratory. The pH and DO of water samples were measured immediately after sampling at the field itself. Samples were subjected to filtration before chemical analysis. The determination of TDS was done by gravimetric process while the TH was carried out by EDTA complex metric titration method. The Winkler's alkali iodide-azide method was followed for the estimation of DO and BOD. NO_3 was determined colorimetric procedure. Fecal coliform population was analyzed by MPN/100 ml method by growing on M-FC medium at temperature 44.5 °C and counted after 48 h.

15.3.2 National Sanitation Foundation Water Quality Index

Brown, McClelland (Brown et al. 1970) developed a common scale and assigning weights to the selected parameters for which elaborate Delphic exercises were performed. The field data is transformed into *Q*-value which is nothing but the rating curve or sub-indices. Sub-indices transform to nondimensional scale values from the

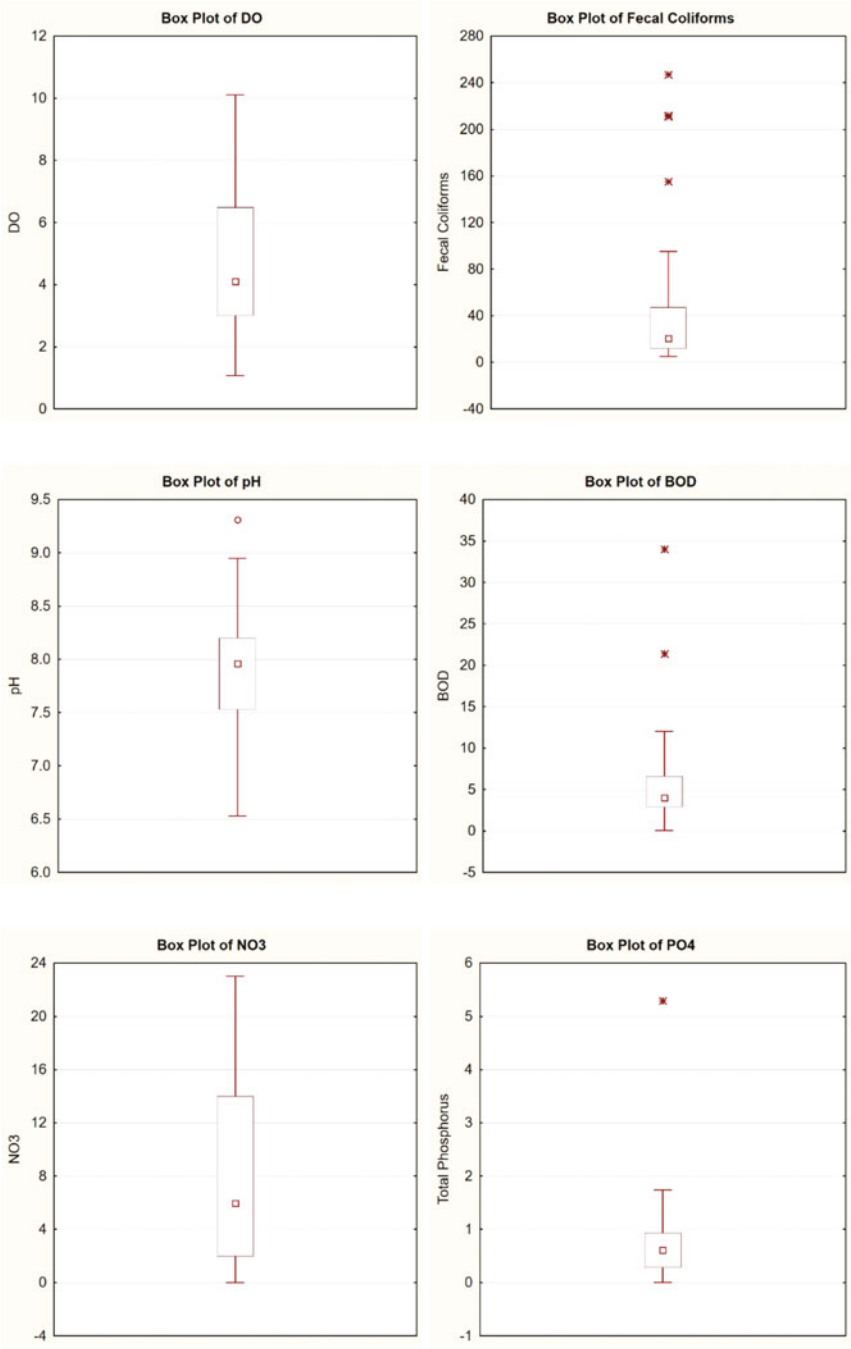

Fig. 15.3 Box plots of water quality parameters used to calculate water quality index

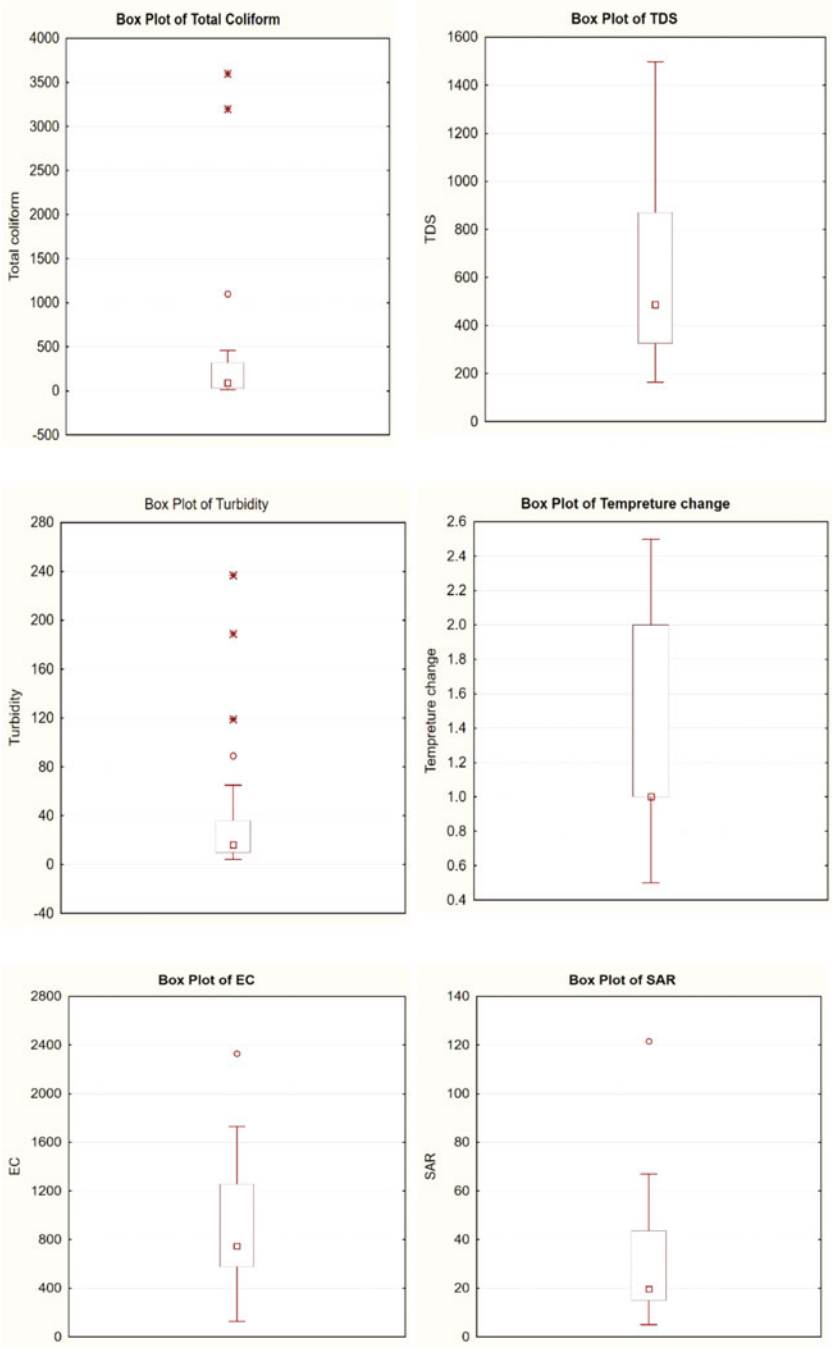

Fig. 15.3 (continued)

Table 15.1 Statistics of groundwater quality parameters used in the study

Parameters	Median	Outlier		Non-outlier range	
		25%	75%	Lowest	Highest
pH	7.96	7.53	8.2	6.53	8.95
EC	747	578	1255	130	1732
TDS	487	326	870	164	149
Turb	16.27	9.9	36	4.23	65
NO_3	5.95	2	14	0	23
PO_4	0.61	0.29	0.93	0.005	1.74
DO	4.1	3.01	6.49	1.07	10.11
BOD	4.005	2.89	6.6	0.05	12
T.coli.	93	28	320	15	320
F.coli.	20.5	12	47	5	95
SAR	19.64	14.96	43.56	5.04	66.97
Temp	1	1	2	0.5	2.5

Table 15.2 Categorical ranking of CCMEWQI and NSFWQI used after Poonam et al. (2013)

Category	NSFWQI	CCMEWQI	Description
Excellent	91–100	95–100	Water quality is protected with a virtual absence of threat or impairment; conditions very close to natural or pristine levels
Good	71–90	80–94	Water quality is protected with only a minor degree of threat or impairment; conditions rarely depart from natural or desirable levels
Medium	51–70	65–79	Water quality is usually protected but occasionally threatened or impaired; conditions sometimes depart from natural or desirable levels
Bad	26–50	45–64	Water quality is frequently threatened or impaired; conditions often depart from natural or desirable levels
Very bad	0–25	0–44	Water quality is almost always threatened or impaired; conditions usually depart from natural or desirable levels

variables of its different units and weighting factor W sets the relative importance of a particular parameter to overall water quality. The standard weight for the water quality parameters is DO (0.17), FColi (0.16), pH (0.11), BOD (0.11), NO_3 (0.1), PO_4 (0.1), Temp (0.1), Turb (0.08), and TDS (0.07). The standard formula to calculate water quality index is:

$$\mathrm{WQI} = \sum_{0}^{\mathrm{X}} W \times Q$$

Based upon the weight factor and *Q*-values the water quality rankings for NSFWQI are tabulated in Table 15.2.

15.3.3 Canadian Council of Ministers of the Environment Water Quality Index

Water quality parameters are compared to water quality guidelines or site-specific objectives. The index is based on three attributes of water quality that relate to water quality objectives: Scope F1—How many? The number of water quality variables that do not meet objectives in at least one sample during the time period under consideration, relative to the total number of variables measured. Frequency F2—How often? The number of individual measurements that do not meet objectives, relative to the total number of measurements made in all samples for the time period of interest. Amplitude F3—How much? The amount by which measurements which did not meet the objectives depart from those objectives.

$$\text{CCMEWQI} = 100 - [({F_1}^2 + {F_2}^2 + {F_3}^2)/1.732]^{1/2}.$$

The constant, 1.732, is a scaling factor (square root of three) to ensure the index varies between 0 and 100. The result is further simplified by assigning it to a descriptive category. Table 15.2 describes the assigned category.

15.4 Results and Discussion

The pollution load on the groundwater has been analyzed by calculating two water quality indices namely NSFWQI and CCMEWQI. To protect the groundwater by degradation and maintain its respective uses water quality index calculated for the standards of the parameters provided by the Central pollution control board (Govt. of India). The spatial variation of water quality parameters was by the geostatistical interpolation technique in GIS platform as depicted in Fig. 15.4, 15.5, 15.6, 15.7, and 15.8. There are many water quality parameters that indicate the pollution by their aberrant concentration. According to the computation of NSFWQI Table 15.3 reveals the present condition of groundwater in the selected location. Figure 15.9 shows the NSFWQI Map of Raipur city. After analysis of the data it is found that according to BIS (ISO: 10500) desirable limits of drinking water for the parameters chosen in NSFWQI computation deviate from its standard. In any of the 34 locations turbidity and fecal coliform does not meet the drinking water quality standard. Also, there are some locations at which pH, DO, BOD, PO4 and TDS violates the objective. It is revealed that only the NO_3 is in under desirable limit of 45 mg/l. The collective effect of these parameters by the NSFWQI computation represents that six sampling locations (W12L02, W14L01, W62L03, W65L03, W65L04, W68L01) are in BAD condition and only one sampling location (W16L04) is in GOOD condition. The remaining 28 sampling locations are in MEDIUM condition.

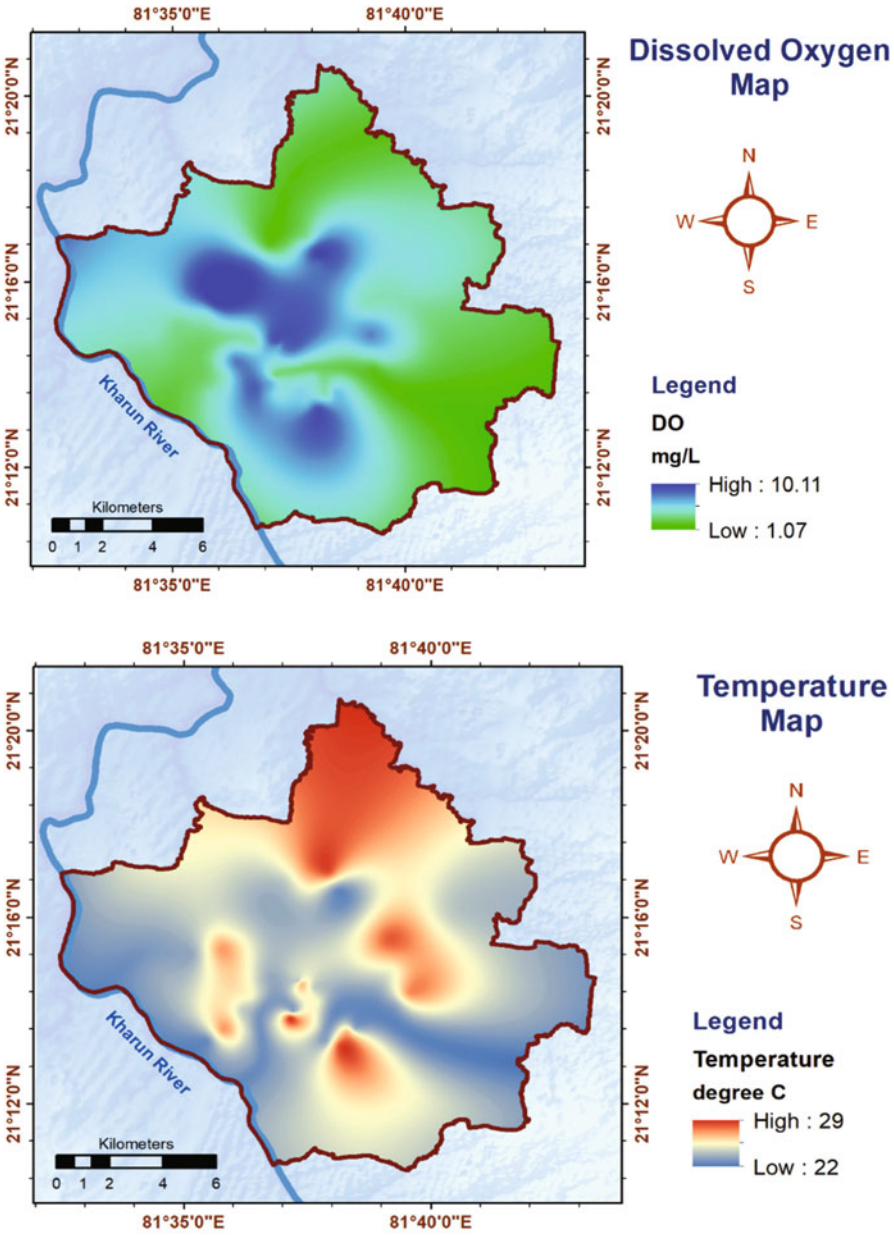

Fig. 15.4 Spatial distribution of dissolved oxygen and temperature in the study area

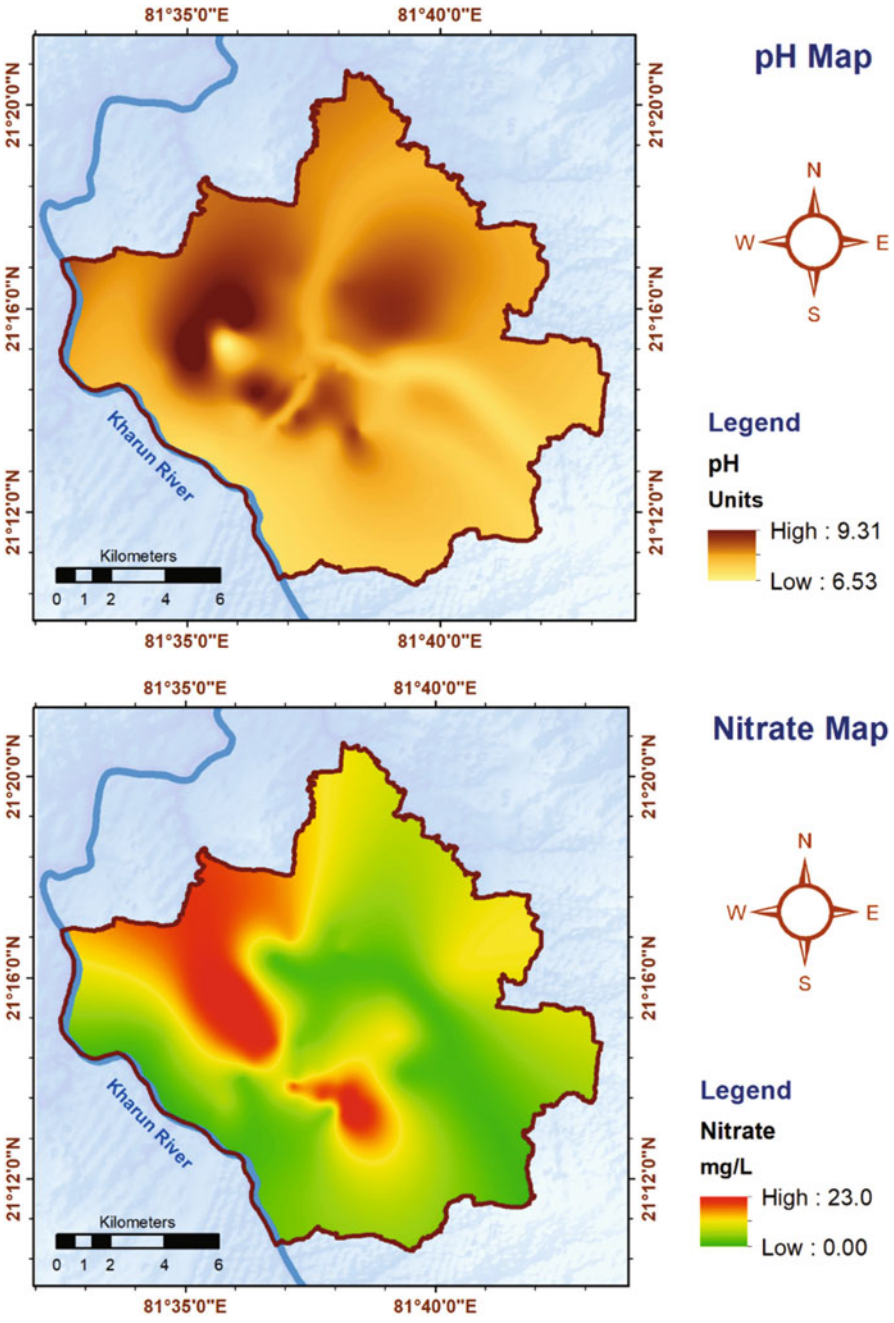

Fig. 15.5 Spatial distribution of pH and nitrate in the study area

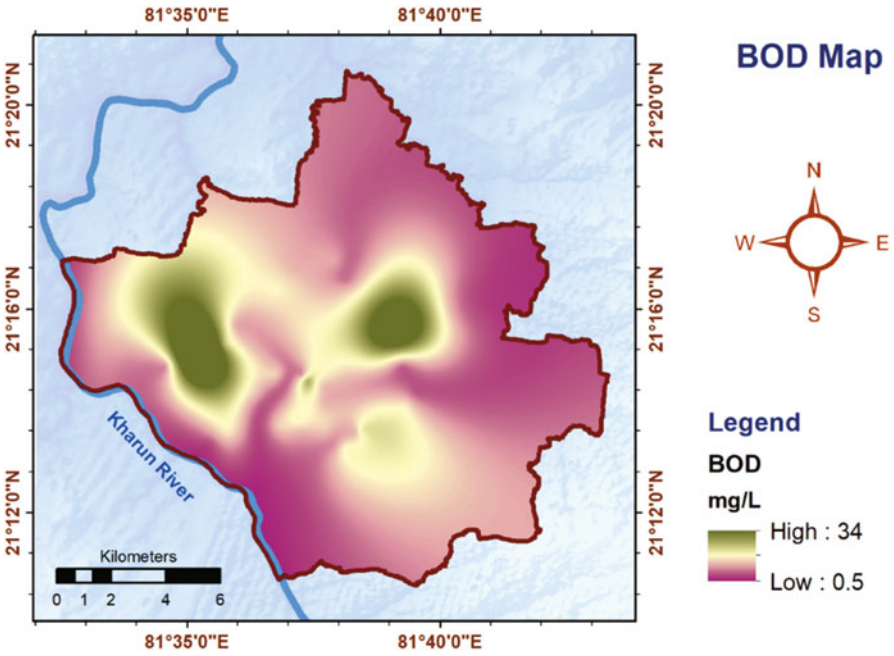

Fig. 15.6 Spatial distribution of BOD in the study area

15.4.1 NSFWQI Result

The spatial variation NSFWQI around the Raipur municipal boundary is shown in Fig. 15.9. Results of NSFWQI map reveals that the 79.41% of area of groundwater comes under the medium quality and 17.64% of area showing bed groundwater quality status. The only 2.94% is safe and suggest the good groundwater quality which can be used for drinking directly without any water treatment. A matrix of linear regression analysis has been drawn for all the parameters used in computation of NSFWQI. The linear regression between the parameters for the sample set is shown in Fig. 15.10. On the observation it is clear that there is strong positive correlation exist between BOD and pH, NO_3 and pH, PO4 and TDS, PO4 and DO, TDS and BOD. And on the other hand, strong negation correlation between, PO4 and pH, TDS and pH, TDS and NO_3, FColi and NO_3, DO and BOD, and NSFWQI and NO_3. The existence of these correlation matches well with the physical correlation of the parameters.

To identify the prominent parameter that affected seriously by pollution, CCMEWQI applied location wise. Central pollution control board, Ministry of Environment and Forests (Govt. of India) guidelines are considered for maintaining the respective use without degrading its life span and quality. Table 15.4 reveals the CCMEWQI result. From the result BOD is that parameter which is particularly more affected by the urban pollution. It categorized under poor condition according to

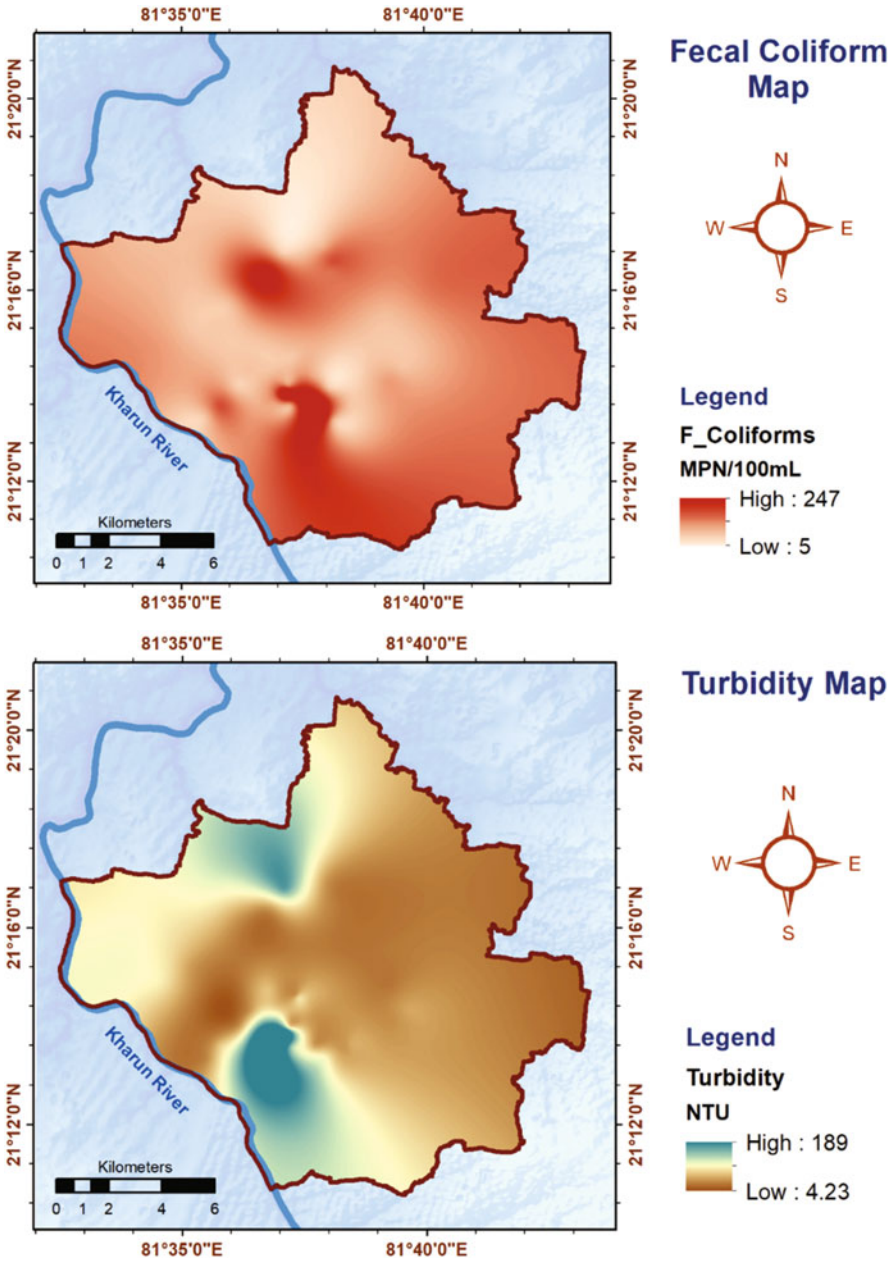

Fig. 15.7 Spatial distribution of fecal coliform and turbidity in the study area

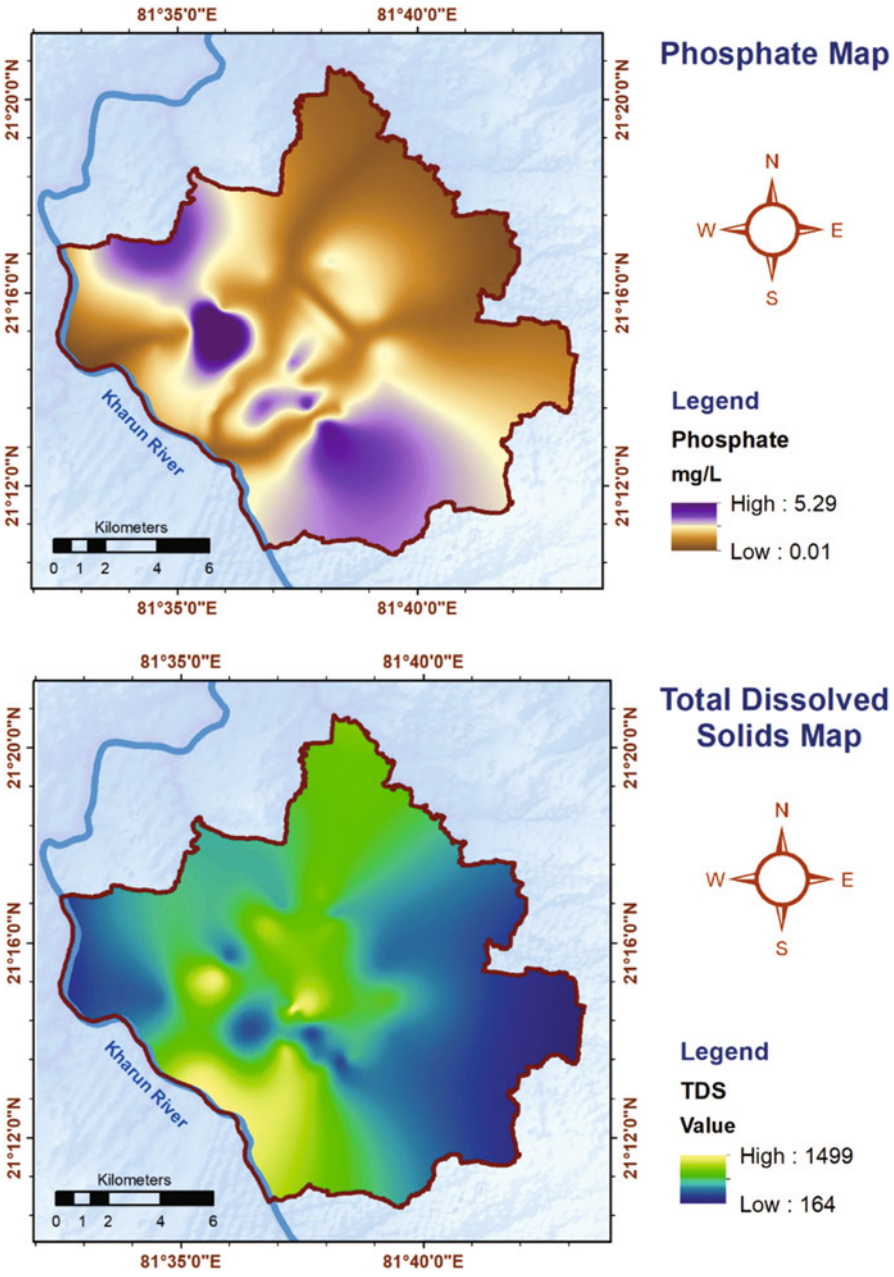

Fig. 15.8 Spatial distribution of total phosphate and TDS in the study area

Table 15.3 Water quality index and the parameters; violating standards based on present criteria

No.	Location_ID	NSFWQI	Category	DO	BOD	SAR	Total coli	pH	EC
1	W02L06	69.40	Medium		•			•	
2	W03L01	62.34	Medium		•	•	•		
3	W04L03	50.29	Medium	•	•				
4	W04L05	56.20	Medium	•		•			
5	W07L01	68.19	Medium				•		
6	W07L02	68.42	Medium						
7	W12L02	47.99	Bad		•				
8	W14L01	42.88	Bad	•	•			•	
9	W15L02	52.33	Medium	•	•				
10	W16L02	55.39	Medium		•	•			
11	W16L03	61.39	Medium			•			•
12	W16L04	71.27	Good						
13	W24L01	65.90	Medium						
14	W25L02	51.12	Medium	•	•				
15	W26L12	64.01	Medium	•					
16	W38L02	57.55	Medium		•	•			
17	W42L01	54.34	Medium	•	•				
18	W43L01	63.55	Medium	•					
19	W49L03	53.10	Medium		•				
20	W49L04	53.73	Medium	•	•				
21	W54L01	57.23	Medium		•	•			
22	W56L01	53.45	Medium			•	•		
23	W57L01	53.06	Medium	•	•				
24	W58L01	55.90	Medium	•	•				
25	W62L03	49.87	Bad		•		•		
26	W64L04	50.64	Medium		•	•			
27	W65L03	41.08	Bad		•	•	•		
28	W65L04	49.53	Bad	•	•				
29	W66L01	54.58	Medium		•				
30	W68L01	48.06	Bad	•	•	•			
31	W68L04	61.23	Medium	•		•			
32	W69L01	63.79	Medium	•	•				
33	W69L02	61.23	Medium		•			•	
34	W70L01	56.23	Medium	•					

CCMEWQI criteria. DO is marginal and SAR and TColi is in fair condition. Table 15.3 displays the sampling location IDs that violates the standard based on present criteria of CCMEWQI.

It was observed in the Table 15.3 that there are 24 sampling locations in which BOD violates the standard of pollution control board. After that DO and SAR violates the standard at 16 and 11 locations respectively. TColi, pH, and EC are violating standard at 5, 3, and 1 location respectively. As all these parameters were

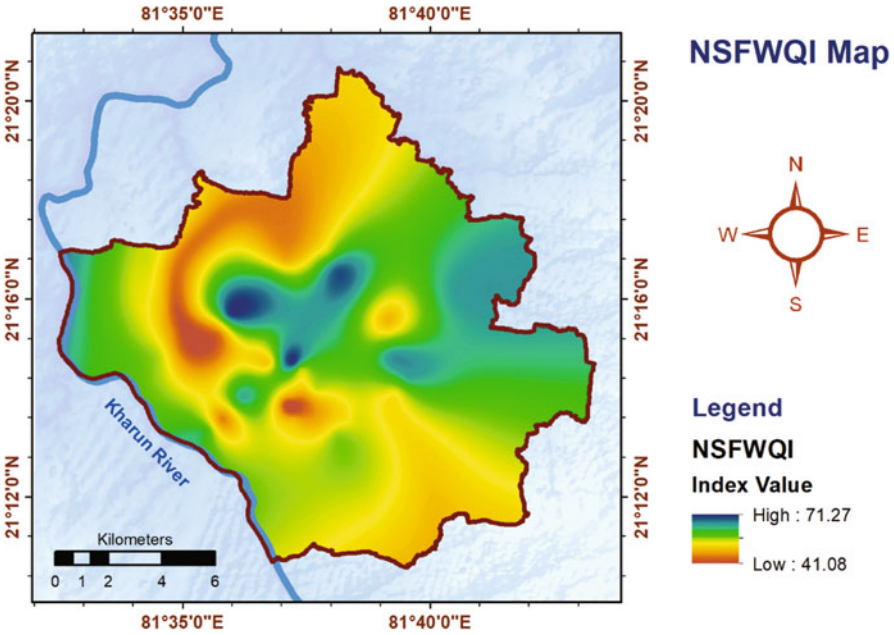

Fig. 15.9 Spatial variation of NSFWQI in Raipur City area

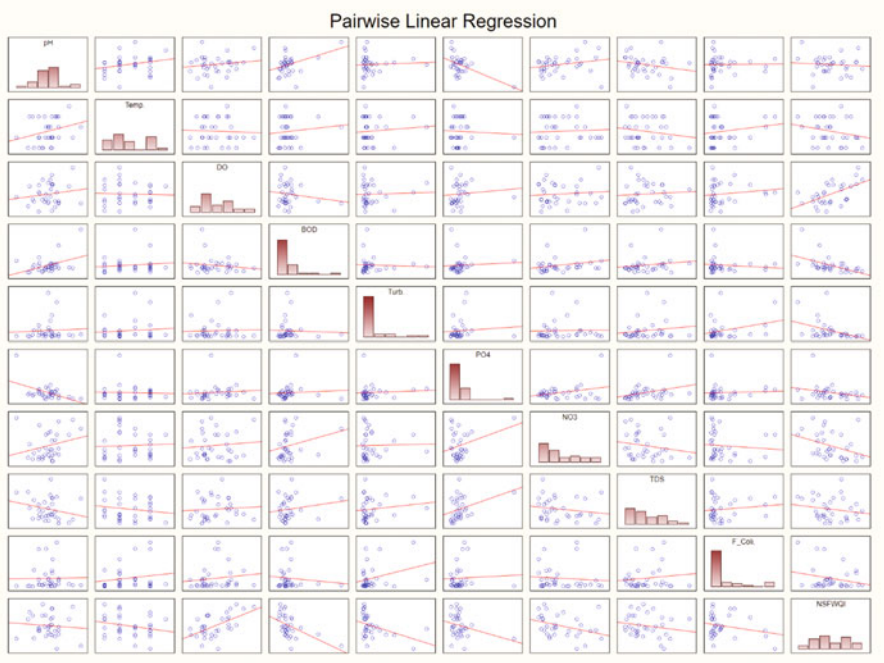

Fig. 15.10 Matrix plots of all water quality parameters used to calculate water quality index

Table 15.4 CCMEWQI analysis for 34 groundwater locations in Raipur city

Parameters	pH	EC	SAR	DO	BOD	Total coli.	NO_3
Total no. of locations	34	34	34	34	34	34	34
Number of failed locations	3	1	11	16	24	5	0
Total no. of tests	136	136	136	136	136	136	136
Number of failed tests	12	4	44	64	96	20	0
F1	8.82	2.94	32.35	47.06	70.59	14.71	0
F2	8.82	2.94	32.35	47.06	70.59	14.71	0
Excursion	0.18	0.04	11.51	10.37	35.25	19.40	0
Nse	0.01	0.00	0.34	0.31	1.04	0.57	0
F3	0.54	0.10	25.29	23.38	50.90	36.33	0
CWQI	92.79	97.60	69.82	59.27	35.30	66.27	100
Category	Good	Excellent	Medium	Bad	Very bad	Medium	Excellent

indicating their functions to make the water suitable for the use of humans, it's important to be on a prescribed limit.

15.4.2 Dissolve Oxygen (DO)

An important variable that shows significant effect on the groundwater quality. DO concentration can be used for estimation of the valence state of trace metals. Dissolved oxygen stabilizes the biodegradable substances with the help of living organisms by which quantify the organic contamination in groundwater. In this study DO varies with minimum value of 1.07 mg/l to maximum value of 10.00 mg/l in Raipur city area.

15.4.3 Temperature (Temp)

It is required for the estimation of decay and growth rates. Therefore, it is necessary for water quality simulation, it also affects the solubility of DO and other parameters. Temperature is the parameter which affects the acceptability of inorganic and chemical contaminants in water. In this study its value varies from 22 °C to 29 °C. Temperature will alter the odor, color, and taste of water.

15.4.4 pH

The strength of acidity or alkalinity of any solution sample is represented by the pH. There is no health-based guideline for the pH value. It is required for evaluation of chemical and biological processes such as adsorption rate of heavy metals. It has range of 6.53–9.31.

15.4.5 Electrical Conductivity (EC)

It is directly related to TDS. Concentrations of TDS in water depend on different geological regions due to the differences in the solubilities of minerals. For domestic use it is recommended that water should have TDS less than 500 mg/l. If it is more than 1000 mg/l, it imparts unpleasant taste and makes inadequate for other uses. In this study area EC value varies with minimum of 130 to maximum of 1732μΩ/cm.

15.4.6 Nitrate Nitrogen (NO_3)

Naturally the nitrate concentration is low in groundwater but due to the humans it appears in the water body in considerable amount. Nitrate reaches the water body by leaching or runoff from agricultural land or contamination from human or animal wastes as a consequence of the oxidation of ammonia. As per WHO standard for drinking water it should not more than 10 mg/l. In this study nitrate varies from nil to 23 mg/l.

15.4.7 Biochemical Oxygen Demand (BOD)

An important variable which shows the immediate discharge of organic waste in the water. The landfill leachate is one of the major sources of contamination in groundwater. Organic matter mainly comes from the leachate in groundwater. But its composition depends on the age of landfill, composition of landfill waste, and climatic conditions. BOD value ranges from 0.5 to 34 mg/l over the Raipur city area.

15.4.8 Fecal Coliform (FColi)

The presence of fecal coliform indicates the pollution of animal or human waste as it is specifically found in these wastes only. It shows the recent pollution in groundwater system that may have other bacteria, viruses or disease-causing organisms. In this study its values vary from 5 MPN/100 ml to 247 MPN/100 ml.

15.4.9 Phosphate (PO_4)

It enters in the groundwater system from the industrial effluents, manure, laundry and human & animal waste (Khadri and Pande 2015a, b). Phosphate lowers down the DO concentration which causes increase in organic nutrients. It gets attached with the soil particle and thereby moves with groundwater. Phosphate is not toxic to humans or animals unless they are present in very high levels. Phosphate present in the range of 0.01–5.29 mg/l.

15.4.10 Turbidity (Turb)

It is caused due to the presence of suspended matters either chemical or biological, organic or inorganic particle. Turbidity does not cause any direct risk to public health. Sudden change in turbidity gives the idea of considerable pollution attack in the area. It varies from 4.23 to 189 NTU in Raipur city.

15.4.11 Total Dissolved Solid (TDS)

TDS involves both the inorganic salts as Cl, Mg, Na, HCO3, Ca, and S and some organic matter in dissolved state. The high value of TDS concentration does not indicate that the water is hazardous for consumption, but it indicates that the water has aesthetic problems. Groundwater contains mineral ions.

15.4.12 Total Coliform (TColi)

It represents the presence of bacteria. Groundwater mostly contaminated by bacterial load due to the runoff from forming fields, untreated sewage discharge and effluent from septic system. Well water supply affected due to deficit construction quality and maintenance practice. Infiltration of animal and house hold fecal matter increases the risk in the groundwater system. This study witnessed the value of 28 MPN/100 ml to 320 MPN/100 ml over the Raipur city area.

15.5 Conclusion

The contradictory research findings in relation to these measures clearly point to the significant role played by location specific factors influencing water quality rather than purely land use. The underlying processes and concepts relating to urban water

quality are well known in a qualitative sense. However, their quantification has proved to be extremely difficult. Chemical processes exert a strong influence on urban storm water quality characteristics. Rainfall and the resulting surface runoff transport a variety of materials of chemical and biological origin to the nearest receiving water body and subsequently recharged to groundwater. This results in the groundwater fundamentally changed from its natural state. Urban expansion transforms local environments and can dramatically alter local conditions and in particular the rate of movement of pollutants into waterways, thereby adversely changing the quality of water. The primary sources include lawn fertilizer, sewer overflows, animal waste, vegetation debris, industrial activities, vehicle exhausts, power generation, and atmospheric dry and wet deposition. Some of the atmospheric pollutants in the solute or gaseous phases will undergo further synthesis due to physical or chemical processes. Results show that the organic load is more, which could be due to inadequate and deficiently designed, operated, and managed individual and community toilets in the urban poor areas resulting in open defection. This leads to pollution and sever health impacts. The sewage management system is deficient in city of Raipur which is evident from the fact that roughly 54% of the properties are connected to unscientifically designed septic tanks, part of which overflows into the open drains/areas ultimately draining into the natural water bodies. The outcomes of the study are required put in front of public, local administrator and government to aware them the condition of groundwater in their area. It is the need of the hour to work on a scientific and feasible planning for efficient groundwater quality management policy implementation.

Acknowledgments The authors would like to thank the Deutscher Akademischer Austauschdienst- German Academic Exchange Service (DAAD), as the research material is based upon work within the program "A New Passage to India". One of the authors would like to acknowledge the help in field data collection provided by LIH workgroup.

References

Apha, A. (2005). Standard methods for the examination of water and wastewater. *WEF, 21*, 258–259.

Baier, K., et al. (2014). Management tools for sustainable ground water protection in mega urban areas–small scale land use and ground water vulnerability analyses in Guangzhou, China. *International Journal of Environmental Research, 8*(2), 249–262.

Baier, K., et al. (2015). Towards integrated intentional agent simulation and semantic geodata management in complex urban systems modeling. *Computers, Environment and Urban Systems, 51*, 47–58.

Brown, R. M., et al. (1970). A water quality index – Do we dare. *Sewage Works, 117*(10), 339–343.

Ghorbani, A., Mohammadi, M., & Mohammadi, Z. (2014). Water quality evaluation of Torghabeh River of Mashhad using combination of NSFWQI index and geographic information system. *International Journal of Advanced Biological and Biomedical Research, 2*(8), 2416–2430.

GIZ, ASEM, and RMC. (2010). *City sanitation plan for Raipur*. Bengaluru: Raipur Municipal Corporation: Alchemy Urban Systems (P) LTD.

GIZ, ASEM, and RMC. (2011). *City level strategy: city sanitation plan for Raipur, G. ASEM, editor*. Bengaluru: Raipur Municipal Corporation: Alchemy Urban Systems (P) LTD.

Karbassi, A., et al. (2011). Development of water quality index (WQI) for Gorganrood River. *International Journal of Environmental Research, 5*(4), 1041–1046.

Khadri, S. F. R., & Pande, C. (2015a). Ground water quality mapping for Mahesh River Basin in Akola and Buldhana Districts of (MS) India using interpolation methods. *International Journal on Recent and Innovation Trends in Computing and Communication, 3*(2), 113–117.

Khadri, S. F. R., & Pande, C. (2015b). Analysis of hydro-geochemical characteristics of groundwater quality parameters in hard rocks of Mahesh River Basin, Akola, and Buldhana Dist. Maharashtra, India using geo-informatics techniques. *American Journal of Geophysics, Geochemistry and Geosystems, 1*(3), 105–114.

Khadri, S. F. R., Pande, C., & Moharir, K. (2013). Groundwater quality mapping of PTU-1 Watershed in Akola district of Maharashtra India using geographic information system techniques. *International Journal of Scientific & Engineering Research, 4*(9), September-2013.

Moharir, K., Pande, C., Singh, S., Choudhari, P., Rawat, K., & Jeyakumar, L. (2019). Spatial interpolation approach-based appraisal of groundwater quality of arid regions. *Aqua Journal, 68*(6), 431–447.

Mustapha, A., & Aris, A. Z. (2011). Application of water quality index method in water quality assessment. *Elixir Pollution, 33*, 2264–2267.

Nikoo, M. R., et al. (2011). A probabilistic water quality index for river water quality assessment: A case study. *Environmental Monitoring and Assessment, 181*(1–4), 465–478.

Pande, C. B., & Moharir, K. (2018). Spatial analysis of groundwater quality mapping in hard rock area in the Akola and Buldhana districts of Maharashtra, India. *Applied Water Science, 8*(4), 1–17.

Pande, C. B., Moharir, K. N., Singh, S. K., & Dzwairo, B. (2019). Groundwater evaluation for drinking purposes using statistical index: Study of Akola and Buldhana districts of Maharashtra, India, environment. *Development and Sustainability (A Multidisciplinary Approach to the Theory and Practice of Sustainable Development), 22*, 7453. https://doi.org/10.1007/s10668-019-00531-0.

Pande, C. B., Moharir, K. N., Khadri, S. F. R., & Patil, S. (2018). Study of land use classification in the arid region using multispectral satellite images. *Applied Water Science, 8*(5), 1–11.

Poonam, T., Tanushree, B., & Sukalyan, C. (2013). Water quality indices—Important tools for water quality assessment: A review. *International Journal of Advances in Chemistry, 1*(1), 15–28.

Putra, D. P. E., & Baier, K. (2008). *Impact of urbanization on groundwater recharge–the example of the Indonesian Million City Yogyakarta, in UN habitat—United Nations settlement programs*. Nanjing: Fourth Session of the World Urban Forum.

RMC. (2010). *Detailed Project report, sewerage, storm, surface water drains and lake protection works for Raipur city*. Singapore: Meinhardt Pte. Ltd.

RMC. (2011). *Topographic survey plan for Raipur storm water drainage and sewerage system*. Singapore: Meinhardt Pte. Ltd.

Sarkar, C., & Abbasi, S. A. (2006). QUALIDEX–A new software for generating water quality indice. *Environmental Monitoring and Assessment, 119*(1–3), 201–231.

Sinha, M. K., et al. (2016). Assessment of groundwater vulnerability using modified DRASTIC model in Kharun Basin, Chhattisgarh, India. *Arabian Journal of Geosciences, 9*(2), 1–22.

Sinha, M. K., et al. (2019a). *Impact of urbanization on surface runoff characteristics at catchment scale*. Singapore: Springer.

Sinha, M. K., et al. (2019b). *Semi-distributed modelling of Stormwater drains using integrated hydrodynamic EPA-SWM model*. Singapore: Springer.

Chapter 16
Multivariate Statistical Tools in Assessing the Quality of Water Resources in Netravati River Basin, Karnataka, India

S. Gayathri, A. Krishnakumar, K. Devi Chandana, Sibin Antony, Vinu V. Dev, V. Arun, and K. Anoop Krishnan

Contents

16.1 Introduction 316
16.2 Description of the Study Area 317
16.3 Materials and Methods 318
16.4 Results and Discussion 319
16.5 Surface and Groundwater Quality Characteristics for Irrigation Purpose 328
16.6 Conclusion 331
References 332

S. Gayathri · V. V. Dev · V. Arun · K. A. Krishnan (✉)
Biogeochemistry Group, National Centre for Earth Science Studies (NCESS), Thiruvananthapuram, Kerala, India
e-mail: sree.anoop@ncess.gov.in

A. Krishnakumar
Hydrology Group, National Centre for Earth Science Studies (NCESS), Trivandrum, Kerala, India
e-mail: rishnakumar.a@ncess.gov.in

K. D. Chandana
Biogeochemistry Group, National Centre for Earth Science Studies (NCESS), Thiruvananthapuram, Kerala, India

School of Ocean Studies, Kerala University of Fisheries and Ocean Studies, Kochi, Kerala, India

S. Antony
University of Kerala, Thiruvananthapuram, Kerala, India

C. B. Pande, K. N. Moharir (eds.), *Groundwater Resources Development and Planning in the Semi-Arid Region*, https://doi.org/10.1007/978-3-030-68124-1_16

16.1 Introduction

In this twenty-first century, fresh water is a basic requirement for the economic development of nations and regions (Khadri and Pande 2016; Moharir et al. 2017). One of the major issues challenging humanity is the quality and quantity of water resources required to satisfy the needs of humans and ecosystem (Disli 2017; Pande and Moharir 2018). Alarming the growth rates of population, industrialization, extensive agricultural practises and rapid urbanization have not only increased the exploitation of water resources but have also contributed towards the deterioration of its quality. Overexploitation and unabated pollution are threatening our ecosystems and even the life of future generations (Pande et al. 2017).

Many research scholars have undertaken the studies on surface and groundwater quality evaluations and employed hydrogeochemical tools to evaluate its appropriateness for consumption and agricultural purpose in different parts of India and around the world (Gupta et al. 2012; Rao et al. 2012; Nganje et al. 2014; Tajabadi et al. 2018; Karthika et al. 2018; Berihu 2020; Pande et al. 2019; Mahadevan et al. 2020). Water quality is one of the sensitive issues worldwide, potentially influenced by many natural and anthropogenic factors. These include temperature, geological and geochemical processes, aquifer lithology, weathering, evaporation, and precipitation. Water quality standards such as World Health Organisation (WHO 2011) and Bureau of Indian Standards (BIS 2012) will help to ascertain the usability of water for various purposes. Apart from these studies, many researchers have carried out monitoring of sedimentological and biological aspects in the river basins and respective coastal ocean systems (Kumar et al. 2014, 2020; Udayakumar et al. 2014a, b).

Within the study area, the chemistry of surface water and groundwater constitute the major source of water supply for drinking, domestic and agricultural purposes (Khadri et al. 2013; Khadri and Pande 2015a, b). A river basin can be considered as a total hydrological system in which meteoric water, surface water and groundwater interchange to form a complete cycle. The occurrence and availability of groundwater is governed by the interactions of numerous environmental factors especially climate, topography, vegetation, soil and geology of an area (Singh et al. 2011; Rajesh et al. 2012). Several researchers evaluated the suitability of groundwater for irrigation using various parameters such as percent sodium (%Na), sodium adsorption ratio (SAR), residual sodium carbonate (RSC), magnesium hazard (MH) etc. These standards and classifications have been used widely to assess the quality of water for irrigation (Moharir et al. 2019).

In this study, major ions are determined so as to draw a conclusion on the source of origin of these ions whether it is natural or anthropogenic. The aim of the present study is to evaluate the hydrochemical characteristics and quality of surface and groundwater resources in Netravati River basin of Karnataka. The main objectives of this study are (a) to determine the surface and groundwater quality parameters for drinking purposes, (b) to evaluate the hydrochemical facies and its mechanism controlling using WQI, Piper and Gibbs plots and (c) to assess the suitability of

water for irrigational use. Therefore, assessment of water quality and the identification of hydrogeochemical processes are necessary for assuring environmental sustainability and development.

16.2 Description of the Study Area

The Netravati River originates at an elevation of nearly 1000 m above the mean sea-level (msl), in the densely forested Sahyadri hills (Western Ghats) near Samse of Chikkamangaluru district, Karnataka, India. Groundwater and surface water are important water resources for drinking, industrial and agricultural uses in the Netravati River Basin. Netravati River flows from its origin at 13°06′10″N 75°25′08″E and flowing along Dharmasthala, Uppinangadi, Bantwal, Thumbe, Mangalore to Arabian sea at 12°50′36″N 74°49′45″E about 107 km length through its path many tributaries joins to this river which increases its discharge capacity (16.1). The river basin covers an area of 3657 km^2. The coastal tract in the west is a highly dissected landmass and the midlands are a rolling terrain of mounds and hillocks. Large scale expansion of industries during last two decades and later such as fertilizers, chemicals, petrochemicals, etc., has increased the conflicts in water utilization.

The basin is composed of rocks belonging to Tertiary and Quaternary Eras in the lower catchment and peninsular gneissic complex in the upper catchment. The greenstone-amphibolitic facies, metamorphic rocks and granulites could be seen in patches (Rajesh et al. 2002). The gneissic rocks cover the major portion of the basin, with charnockites occurring locally as small linear patches. The basin is lithologically composed of about 83% migmatites and granodiorites, 6% metabasalts, 5% charnockites and 2% laterites and amphibolites (Gurumurthy et al. 2012). The fractures, joints, and weathered zone lying above the bedrock host the groundwater in its pore spaces. The natural recharge, direct or diffused, takes place between June and October (southwest monsoon), while an irrigational return flow could be another source of recharge water during the non-monsoon. The Netravati watershed is characterized by high humidity (>70%) and in summer season the mean temperature is around 28–30 °C (±5 °C) hence, suffers scarcity of water. About 90% of rainfall contribution from South west monsoon (June–September) alone and rest during pre- and post-monsoon and the rivers are flooded in monsoon season. The minor irrigation department is constructing vented dams for supplying water for agricultural lands. The farmers construct temporary mud-kattas (bund using soil) for storing water for their agricultural and other activities.

16.3 Materials and Methods

Based on the analysis of hydrogeological conditions, 24 samples of surface and groundwater were collected in the post-monsoon season, 2019. The location of sampling sites is shown in Fig. 16.1. The samples were collected in 500 ml polyethylene bottles. The bottles were rinsed before the samples are poured into it, and they are kept air-tight and labelled. The samples were filtered through 0.45-µm cellulose nitrate hydrophilic syringe filters. All the samples have been stored in refrigerator at a temperature of 4 °C until the laboratory analyses were completed. All the sampling and laboratory analysis has been undertaken as per the methods describe in APHA (American Public Health Association) guidelines (APHA 1995). The physicochemical parameters of the analytical results were compared with standard guideline values recommended by the WHO (World Health Organisation) and BIS (Bureau of Indian Standards) (WHO 2011; BIS 1991; Pande et al. 2018).

The portable water quality analyser, Aquameter (Eutech, Aqua read 2000 D), allows in situ monitoring of various parameters of water samples such as water Temperature, pH, Dissolved oxygen (DO), electrical conductivity (EC) and total dissolved solids (TDS). Chloride (Cl) and bicarbonate (HCO_3) was determined in the samples by volumetric titration. Sulphate (SO_4^{2-}) was determined by UV-Vis Spectrophotometer (Shimadzu UV-1800). Samples for cation and trace element analysis were acidified to a pH of <2 by adding nitric acid and they were analyzed by Microwave Plasma Atomic Emission Spectroscopy (4200 MP-AES/Agilent).

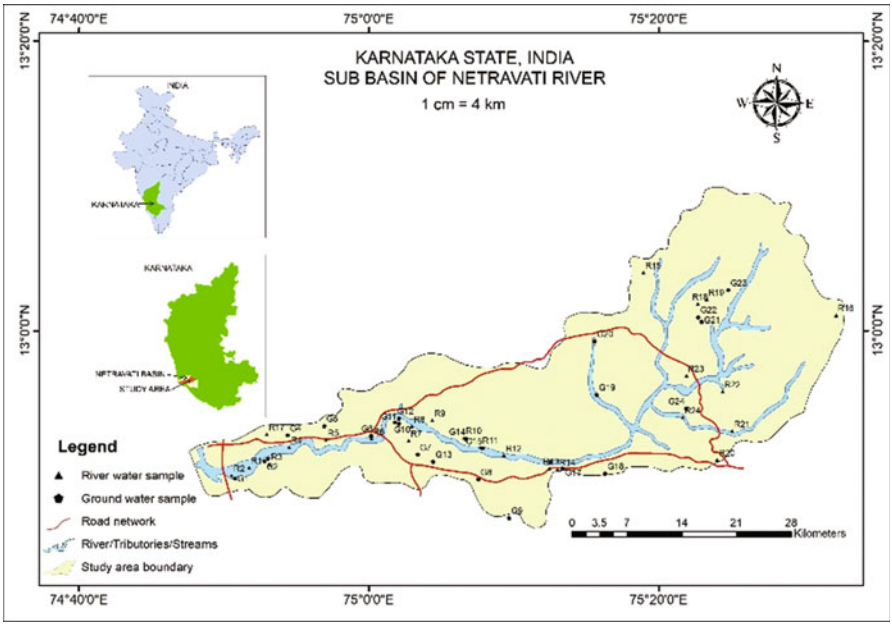

Fig. 16.1 Study area and sampling locations

Table 16.1 Standard equations used to determine irrigational status

Parameter	Equation	Reference
%Na	$\frac{(Na^+ + K^+)}{(Ca^{2+} + Mg^{2+} + Na^+ + K^+)} \times 100$	Wilcox (1995)
MAR	$\frac{Mg^+}{(Ca^{2+} + Mg^{2+})} \times 100$	Raghunath (1987)
SAR	$\frac{Na^+}{\sqrt{(Ca^{2+} + Mg^{2+})_2}}$	Richards (1954)
KR	$\frac{Na^+}{Ca^{2+} + Mg^{2+}}$	Kelley (1940)
RSC	$(CO_3 + HCO_3) - (Ca^{2+} + Mg^{2+})$	Eaton (1950)
PI	$\frac{(Na^+ + \sqrt{HCO_3})}{(Ca^{2+} + Mg^{2+} + Na^+)} \times 100$	Doneen (1964)

The estimation of nutrients such as total phosphate, total nitrate, nitrite and silicate were carried out using San^{++} Automated Wet Chemistry Analyzer Continuous Flow Analyzer (CFA). The software AquaChem version 2016 used to create geochemical plots. To assess the quality controlling mechanism and dominated hydrogeochemical facies of the study area Gibbs diagram was plotted. All instrumental analyses were carried out at the Central Chemical Laboratory of National Centre for Earth Science Studies.

To evaluate the drinking water quality and to assess the potential health risk to human, the microbial analyses were performed. Before sampling, the bottles were sterilized in an autoclave at 121 °C for 15 min. The membrane filtration technique was used to estimate the counts of coliforms in the water samples. Drinking water quality was evaluated using water quality Index method. The suitability of water samples for irrigation purpose was evaluated using various indices such as sodium adsorption ratio (SAR), percent sodium (%Na), residual sodium carbonate (RSC), magnesium adsorption ratio (MAR), Kelley's ratio (KR), and permeability index (PI). The equations are tabulated in Table 16.1.

16.4 Results and Discussion

The analytical results for all the physicochemical parameters of surface and groundwater in the Netravati River Basin are tabulated in Table 16.2. Surface water showed a maximum temperature of 31 °C and the minimum of 26 °C, average temperature is 28.5 °C. In groundwater, temperature ranges from 26 °C to 29 °C with a mean value of 27.5 °C.

16.4.1 Hydrogen Ion Concentration (pH)

The most frequently used parameter for water quality determination is pH. The permissible limit for pH in drinking water is 6.5–8.5 prescribed by WHO and BIS. In

Table 16.2 Statistical description of physicochemical parameters and trace elements of surface and groundwaters of study area

Parameters	Unit	Minimum		Maximum		Mean	
		SW	GW	SW	GW	SW	GW
Temp.	°C	26.9	26.8	31.8	29.6	29.07	28.34
pH		6.78	5.6	8.81	7.69	7.74	6.32
EC	µS/cm	44	48	4856	1443	511.12	192.29
TDS	mg/L	27	31	3164	942	332.12	124.04
TH	mg/L	9.19	0.98	296.11	112.12	75.81	28.08
Ca^{2+}	mg/L	2.15	0.33	24.72	24.63	5.51	7.7
Mg^{2+}	mg/L	0.93	0.04	56.96	12.3	6.64	2.14
Na^{+}	mg/L	2.64	1.46	379.65	13.52	41.46	6.54
K^{+}	mg/L	0.03	0.1	19.09	12.49	2.49	1.91
HCO_3^{-}	mg/L	14.64	4.88	39.04	180.56	20.13	43.11
Cl^{-}	mg/L	6.51	8.14	244.22	174.21	24.21	25.02
SO_4^{2-}	mg/L	0.32	0.13	15.8	13.31	1.99	0.92
NO_3^{-}	mg/L	10.84	3.74	381.27	861.96	153.44	248.07
PO_4^{-}	mg/L	1.06	0.15	37.78	49.44	5.95	6.59
Fe	mg/L	BDL	BDL	0.84	0.48	0.23	0.11
Zn	mg/L	BDL	BDL	0.05	0.05	0.03	0.03
Cd	mg/L	BDL	BDL	0.02	0.02	0.01	0.012
Cu	mg/L	BDL	BDL	0.01	0.01	0.01	0.01
Ni	mg/L	BDL	BDL	0.01	0.01	0.01	0.01
As	mg/L	BDL	BDL	0.01	0.1	0.01	0.055
Pb	mg/L	BDL	BDL	0.03	0.01	0.02	0.01
Mn	mg/L	0.01	BDL	0.11	0.12	0.03	0.036
Cr	mg/L	BDL	BDL	0.01	0.05	0.01	0.05
E. coli	CFU/100 mL	NG	NG	5300	NG	220.83	NG

SW surface water, *GW* groundwater, *EC* electrical conductivity, *TDS* total dissolved solids, *DO* dissolved oxygen, *TH* total hardness

the study area, pH varies from 6.78 to 8.81 (average 7.74) in surface water, therefore pH is generally alkaline/basic in nature. In groundwater, pH ranged from 5.6 to 7.69 (average 6.32) indicating slightly acidic to neutral nature. These acidic waters tend to corrode metals used for plumbing and it will increase the heavy metal content in water (Brindha et al. 2014). pH of groundwater is mainly controlled by dissolved carbon dioxide, carbonate, and bicarbonate (Kumar et al. 2007).

16.4.2 Electrical Conductivity (EC) and Total Dissolved Solids (TDS)

The measurement of EC is directly related to the concentration of dissolved solids present in water and it is also related to hardness and other mineral contamination.

Table 16.3 Classification of groundwater and surface water based on EC and TDS

Parameter	Ranges	Water type	% of samples	
			Surface water	Groundwater
EC (μS/cm)	<250	Excellent	83	92
	250–750	Good	4	4
	750–2250	Permissible	4	4
	2250–5000	Doubtful	8	NIL
	>5000	Unsuitable	NIL	NIL
TDS (mg/L)	<500	Desirable for drinking	88	96
	500–1000	Permissible for drinking	4	4
	<3000	Useful for irrigation	4	NIL
	>3000	Unfit for drinking and irrigation	4	NIL

Higher the dissolved material in water sample, higher is the EC. The electrical conductivity of surface water ranged from 44 to 4856 μS/cm and in groundwater values varied from 48 to 1443 μS/cm. The maximum permissible limit of EC in drinking water is prescribed as 1500 μS/cm. The variation of in EC is ascribed to the various levels of enrichment in depositional environment during accumulation (Nganje et al. 2014; Rimmer 2004). EC is directly linked with amount of dissolved salts in the samples. The maximum TDS (3164 mg/L) and maximum EC (4856 μS/cm) were measured in surface water. Due to the successive action of weathering and dissolution processes surface water samples showed higher TDS values in the study area. The water samples collected from the middle parts are located mainly in the suburban region with intense agricultural activity and are highly influenced by anthropogenic activities. The classification of the groundwater and surface water quality based on EC and TDS is shown in Table 16.3.

16.4.3 Total Hardness (TH)

TH of water is the sum of calcium and magnesium content of water. It is calculated using the formula given below (Sawyer and McCarty 1967).

$$\mathrm{TH\,(mg/l)} = 2.497\mathrm{Ca^{2+}\,(mg/l)} + 4.115\mathrm{Mg^{2+}\,(mg/l)}$$

The maximum permissible limit of TH for drinking water is 500 mg/L as per WHO international standards (2004) whereby this study has resulted in values ranging from 9.19 to 296.11 mg/L and thus all the samples were within the prescribed limit. Majority of surface and groundwaters in this area were soft in nature (Table 16.4). Calcium carbonate in water results in temporary hardness and permanent hardness is caused by Ca^{2+} and Mg^{2+}ions.

Table 16.4 Drinking water quality types in terms of total hardness (TH)

Total hardness as $CaCO_3$ (mg/L)	Type of water	% of samples	
		Surface water	Groundwater
<75	Soft	88	100
75–150	Moderately hard	4	NIL
150–300	Hard	8	NIL
>300	Very hard	NIL	NIL

Table 16.5 Drinking water quality types in terms of E. coli

E. coli (CFU/ml)	% of samples	
	Surface water	Groundwater
No risk	96	100
Low risk	NIL	NIL
Intermediate risk	NIL	NIL
High risk	NIL	NIL
Very high risk	4	NIL

16.4.4 E. coli

In terms of microbiological contamination in drinking water, all surface and groundwater samples were within the TC limit of WHO except one sample from surface water. According to WHO, *E. coli* contaminated water is categorized mainly into five types, described in Table 16.5. Presence of Escherichia indicates that the water is highly contaminated.

16.4.5 Water Quality Index (WQI)

Water quality index is defined as a rating reflecting the composite influence of different water quality parameters on the overall quality of water. Examples of different water quality indices developed worldwide are National Sanitation Foundation Water Quality Index (NSFWQI), Canadian Council of Ministers of the Environment Water Quality Index (CCMEWQI), British Columbia Water Quality Index (BCWQI), and Oregon Water Quality Index (OWQI). WQI has been used by many researchers to evaluate the water quality for drinking purposes in various geological terrains (Debels et al. 2005; Sener et al. 2017; Katyal and Bharti 2011). In this study, WQI was calculated by considering 14 water quality parameters (i.e., pH, EC, TDS, TH, HCO_3^-, Cl^-, SO_4, NO_3, Ca, Mg, Na, K, Fe, Pb) and assigned weights (wi) ranging from 2 to 5, and its selection depends on their significance in quality of water for drinking purposes, in order to assess the degree of water contamination and suitability (Pande et al. 2019).

Relative weight,

$$W_i = \frac{w_i}{\sum_{i=1}^{n} w_i} \tag{16.1}$$

where, w_i is the weight of each parameter and n is the number of parameters.

Quality rating,

$$q_i = \frac{C_i}{S_i} 100 \tag{16.2}$$

where, C_i is Concentration of each parameter in the water sample in mg/L, S_i is Standard limit for the respective parameter in mg/L.

Subindex of the *i*th parameter,

$$\mathrm{SI}_i = W_i \times q_i \tag{16.3}$$

Water quality index,

$$\mathrm{WQI} = \sum_{i=1}^{n} \mathrm{SI}_i \tag{16.4}$$

The current study reveals the results that water quality index (WQI) ranged between 15.02–94.65 and 11.75–95.11 in surface and groundwater (Table 16.6). Majority of water samples belongs to excellent category. Netravati catchment are extensively used for agriculture and the crops are fed with groundwater or surface water. Samples collected from Dakshina Kannada region is distinguished from the rest of the samples because of their higher concentration of EC, TDS and WQI values.

Table 16.6 Water quality classification based on WQI value

Class	WQI value	Water type	% of samples	
			Surface water	Groundwater
I	<50	Excellent	86	86
II	50–100	Good water	14	14
III	100–200	Poor water	NIL	NIL
IV	200–300	Very poor water	NIL	NIL
V	>300	Unsuitable for drinking	NIL	NIL

16.4.6 Hydrochemical Facies

The (Piper 1994) diagram is very useful in classification of water on the basis of its chemical characteristics. The hydrochemical evolution can be understood by plotting milliequivalent percentages of the major cations and anions in piper trilinear diagram. In the study area groundwater and surface water types were distinguished and grouped by their position in piper diagram. The central diamond field, provides the overall character of the water. Hydrochemical facies are identified for the surface water with majority of samples characterized by Na-Ca-HCO_3-Cl. The triangular cationic field showed Na + K dominant type whereas in an anionic triangle were in HCO_3 and Cl type. Surface water sample also proved that alkaline earth (Ca + Mg) exceeds alkalies (Na^+ + K^+) and strong acid (SO_4 + Cl) exceeds weak acids (CO_3 + HCO_3) (Fig. 16.2). Samples of groundwater, majority of triangular cationic field fell into no dominant type area and the anionic part in HCO_3 and Cl type. Most of the groundwater samples had more than 50% carbonate hardness, alkaline earth exceeds alkalies and weak acids exceed strong acids. Most of the samples reflect the mixing types of cations and anions.

16.4.7 Gibbs Plot

Gibbs plot (Gibbs 1970) determines the mechanisms that influence natural water chemistry, composition and origins of surface water. These are specified by the variation diagrams of TDS against the ratios Na/(Na + Ca) and TDS against Cl/(Cl + HCO_3) for both cations and anions groups (Fig.16.3). The natural mechanism controlling surface water chemistry are evaporation dominance, precipitation dominance and rock–water interaction dominance fields. Majority of surface water samples are controlled by rock dominance and a few by evaporation dominance of major cations and anions. In addition, a small portion of surface water samples were represented by evaporation–crystallization process. Samples which fall outside the diagram can be explained by the occurrence of anthropogenic activities (Srinivasamoorthy et al. 2008). Water samples in the rock dominance region indicate that the rock weathering as a primary factor controlling the water composition. This observation suggests that the dissolution of carbonate and silicate weathering are the dominant processes controlled by surface water chemistry in the study area.

16.4.8 Major Ion Characteristics and Hydrogeochemical Evolution

In surface water samples, cation contents were in the order $Na^+ > Mg^{2+} > Ca^{2+} > K^+$ and the order in groundwater was $Ca^{2+} > Na^+ > Mg^{2+} > K^+$ whereas, anions were in

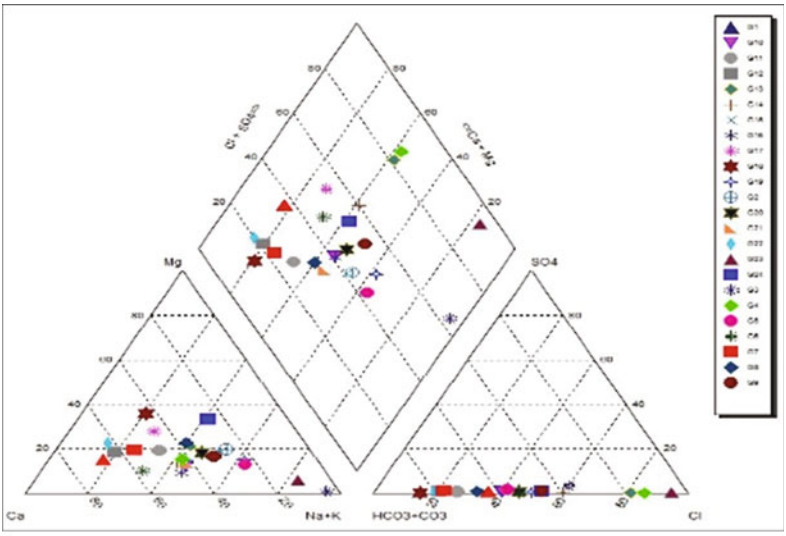

(a)

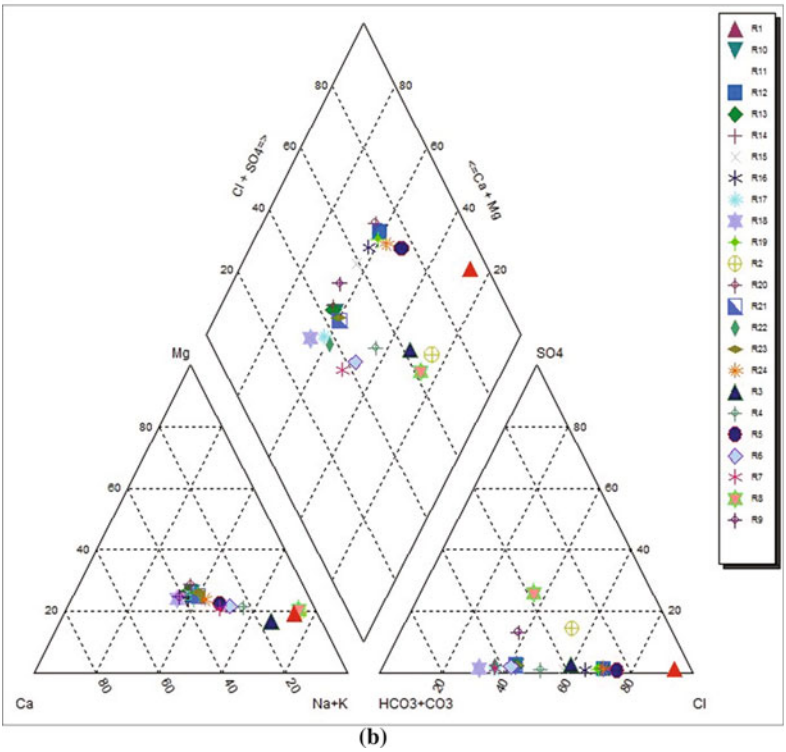

(b)

Fig. 16.2 (**a**, **b**) Piper diagram showing groundwater and surface water samples

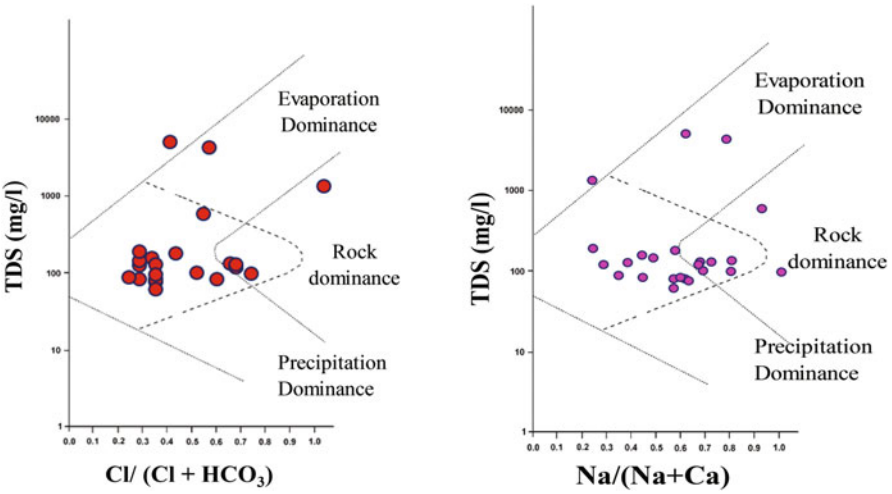

Fig. 16.3 Gibbs plot for surface water samples

the order Cl^- > HCO_3^- > SO_4^{2-} > NO_3^- for surface water and HCO_3^- > Cl^- SO_4^{2-} > NO_3^- for groundwater. As a result of different geological and hydrogeological conditions significant variations were observed in the order of ions. Ca^{2+} and Na^+ were the predominant cations, values varied from 0.33 to 23.63 mg/L and 2.64 to 379.65 mg/L in groundwater and surface water. The contact of water with ligneous rocks and weathering of salt deposits are the natural source of sodium. Increased concentration of calcium is found in groundwater due to leaching from rock forming limestones and silicates (Zhang et al. 2012). The range of Mg^{2+} varied from 0.93 to 56.93 mg/L and 0.04 to 12.3 mg/L and the concentration of K^+ ranged in between 0.03–19.09 and 0.1–12.49 mg/L in surface and groundwater samples. The low level of potassium may be owing to its fixation in the form of clay minerals and increased resistance to weathering (Berihu 2020). At station R8 (Bantwal) increased concentrations of all the major cations were observed for surface water samples. In contrast, at station G18 (Uppinangadi) maximum concentration of Ca^{2+}, Mg^{2+} were observed for groundwater.

Cl^- and HCO_3^- are the predominant anions in groundwater and surface water. The predominant natural form of the element chlorine is chloride and it is highly stable in water. They commonly originate from chloride mineral that occurs in the igneous rocks. Cl^- varies from 6.51 to 244.22 mg/L (at Mangalore region) and 8.14 to 174.21 mg/L whereas HCO_3^- ranges from 14.64 to 39.04 and 4.88 to 180.56n mg/L in surface and groundwater respectively. High concentration of bicarbonate originates from the oxidation and degradation of organic matter. In surface and groundwater lower concentration of SO_4^{2-} and NO_3^- were observed. Blue baby disease/Methaemoglobinae in children is mainly caused by increased concentration of nitrate in drinking water. The concentration of nitrate and sulphate lies within the permissible limit of 45 and 400 mg/L recommended by WHO.

Table 16.7 Interpretation of ion ratios (Hounslow 1995)

ID	Ca/ SO_4	Na/ Cl	Cl/ HCO_3	Mg/ (Ca + Mg)	Ca/ (Ca + SO_4)	(Ca + Mg)/ So_4	Cl/ ∑Anions
Min	0.06	0.01	0.17	0.15	0.06	0.07	0.15
Max	211.03	1.42	17.07	0.57	1.00	384.84	0.94
Avg	53.79	0.76	1.81	0.31	0.93	78.72	0.45
SD	44.10	0.40	3.52	0.10	0.19	73.80	0.20

Table 16.8 Ionic ratios

Ion ratio	Ranges	Origins
Ca/SO_4	<1	Ca^{2+} removed by ion exchange
	>1	Dissolution of silicates and carbonates
Na/Cl	<1	Dissolution of sodium
	>1	Silicate weathering
Cl/HCO_3	<1	Feeding way of limestone resources
	>2.8	Saltwater intrusion and evaporation
Mg/(ca + mg)	<0.5	Limestone-dolomite weathering
	>0.5	Dissolution of dolomite and calcite deposition
Ca/(ca + SO_4)	<0.5	Calcium removal by ion exchange
	>0.5	Calcium sources other than gypsum-carbonate or silicates
(ca + mg)/SO_4	>0.8 and < 1.2	Dedolomitization
Cl/∑anions	<0.8	Rock weathering

Ion ratios are helpful to describe the source of ions and the rocks impacting groundwater chemistry. Tables 16.7 and 16.8 represent ion ratios in the studied samples. In the water samples Na/Cl ratio varies from 0.01 to 1.42 with an average value of 0.75. This relation helps to identify the mechanism for acquiring salinity and also to determine the source of Na^+ in the water. Almost 66.66% of samples shows ratio < 1 which represents source of Na^+ is from dissolution of sodium and cation exchange reactions leading to leading to adsorption of Ca^{2+} on clay minerals. (Nganje et al. 2017). Cl/HCO_3 ratio also proved majority of samples (16 samples) belongs to <1, indicates the feeding way of limestone resource. A ratio value of Cl/∑Anions varies from 0.14 to 0.94 with an average value of 0.45, values less than 0.8 suggestive of rock weathering.

The resulting computed ratio values of Mg/(Ca + Mg) varied from 0.14 to 0.56 with mean value of 0.30, i.e., <0.5 indicating the limestone-dolomite weathering to be the dominant process. 95.83% of samples refers to higher concentration of calcium occurs due to limestone weathering. Calculated ratio value of Ca/(Ca + SO_4) less than 0.5 indicates the removal of calcium via ion exchange or calcite precipitation. In this study except one sample rest of the samples has obtained values less than 0.5 indicating Ca^{2+} removed by ion exchange or precipitation of calcite. 62.5% ratio value of Mg/(Ca + SO_4) is found to <0.5 indicating the influence of calcite and

gypsum. The excess of Ca indicates calcite dissolution or dissolution of silicate minerals (Kumar et al. 2006).

16.4.9 Chloro-Alkaline Indices (CAI)

Schoeller (1977) suggested CAI, indicating the ion exchange between water and its host environment during movement or residence processes, controlling factors towards water chemistry. The CAI used for the assessment of ion exchange is expressed as:

$$\mathrm{CAI} = (\mathrm{Cl}^- - (\mathrm{Na}^+ + \mathrm{K}^+))/\mathrm{Cl}^-$$

CAI shows 70.83% and 58.33% of surface and groundwater samples shows positive value of ratios indicates base exchange phenomenon i.e., Na^+ and K^+ exchange occurs in water with Mg^{2+} and Ca^{2+}. In contrast, 29.17% and 41.67% of samples showed negative CAI, indicating indirect ion exchange reaction (Shamsuddin et al. 2019). Chloro-alkaline disequilibrium and cation-anion exchange reaction is revealed by the negative values of CAI.

16.4.10 Trace Elements

The water samples were analysed for trace elements such as Fe, Zn, Cd, Cu, Ni, As, Pb, Mn, and Cr. Trace elements can be found naturally in bedrock and sediments or they be introduced into water from industrial sources and household chemicals. The sources of trace elements can be natural source which involves weathering of minerals and fall of atmospheric particulate matter and anthropogenic sources include fertilizers, domestic, and industrial effluents. The highest value of trace elements in surface water and groundwater was obtained for Mn (mean 0.02 ppm) and As (mean 0.05 ppm). Due to the chemical weathering process, slightly higher values of these elements were noted. The analytical results for all the elements were within the permissible limit.

16.5 Surface and Groundwater Quality Characteristics for Irrigation Purpose

Chemistry of water is an important factor determining its domestic and irrigation purposes. Quality of water is assuming great importance with the rising pressure on industries and agriculture and rise in standard of living. The water used for irrigation

Table 16.9 Classification of groundwater and surface water based on the suitability of water for irrigation purposes

Classification	Categories	Ranges	Number of samples % of samples			
			SW	GW	SW	GW
Sodium adsorption ratio (SAR)	Excellent	<10	24	24	100	100
	Good	10–18	4	0	17	0
	Doubtful	18–26	0	0	0	0
	Unsuitable	>26	0	0	0	0
Percent sodium (%Na)	Excellent	0–20	0	3	0	13
	Good	20–40	14	6	58	25
	Permissible	40–60	6	11	25	46
	Doubtful	60–80	4	2	17	8
	Unsuitable	>80	0	2	0	8
Residual sodium carbonate (RSC)	Permissible	<1.25	24	22	100	92
	Unsuitable	1.25–2.5	0	2	0	8
Magnesium hazard (MH)	Suitable	<50	20	23	83	96
	Unsuitable	>50	4	1	17	4
Kelly's ratio (KR)	Suitable	<1	23	22	96	92
	Unsuitable	≥1	1	2	4	8
Permeability index (PI)	Unsuitable	<25	0	0	0	0
	Good	25–75	0	0	0	0
	Excellent	>75	24	24	100	100

is an important factor in productivity of crop, its yield, and quality of irrigated crops. The chemical composition of water for irrigation impacts the crop production. High quality and quantity crops yield from the usage of high quality water. Classification of surface and groundwater samples on the basis parameters such as sodium adsorption ratio (SAR), percent sodium (%Na), residual sodium carbonate (RSC), magnesium hazard (MH), Kelley's ratio (KR), and permeability index (PI) are summarized in Table 16.9.

16.5.1 Sodium Adsorption Ratio (SAR)

Sodium adsorption ratio is an important parameter to determine the sodium hazard in connection with calcium and magnesium contents. SAR values predict the degree to which irrigation water involved in cation exchange reaction in soil. Excess sodium concentration decreases the soil structure and soil permeability via clay particle dispersion making the soil compact and impervious (Todd 1980). The suitability of surface and groundwater samples was evaluated for the determination of SAR shown in Table 16.9. According to SAR classification water attaining <10 is to be of excellent quality. In the study area SAR values ranged from 0.36 to 9.59 in surface

water and 0.24 to 1.56 in groundwater samples, whereby all 100% water samples were suitable for irrigation based on SAR.

16.5.2 Percent Sodium (%Na)

The sodium in water reacts with the soils and reduces its permeability which in turn affects the irrigation. The exchange process of sodium in water with that of calcium and magnesium results in the stark reduced permeability of the agricultural soil. % Na obtained has ranged between 33.72–75.09 with a mean value of 45.87 in surface water and 15.03–95.09 with mean value of 43.28 in groundwater. Fourteen surface water and 11 groundwater samples have 58% and 48% sodium belongs to good and permissible category.

16.5.3 Residual Sodium Carbonate (RSC)

In addition to SAR and %Na, the groundwater and surface water for irrigation purpose can be evaluated using the sum of carbonates and bicarbonates over the sum of calcium and magnesium in water, excessive presence of carbonates and bicarbonates tends to alter the soil properties and form, precipitates and increase soil salinity thus decreases its fertility. To quantify the suitability of water for irrigation, RSC index of water samples in the study area was computed. The lesser the value, the better the water is for irrigation. RSC remained negative for all surface water samples and in groundwater except two samples rest of the samples were within the limit (<2.5) for use in irrigation (Table 16.9).

16.5.4 Magnesium Hazard (MH)

Magnesium content of water is considered as one of the most important qualitative criteria in determining the suitability of water for irrigation. Excess of magnesium affects the quality of soil, rendering it alkaline resulting in poor yield of crops. The permissible limit of MH is 50 above which the water is harmful and unsuitable for irrigation. In surface water and groundwater, the calculated magnesium values vary from 36.19 to 79.16 and 14.93 to 56.74, respectively (Table 16.9). It was found that 17% and 4% of surface and groundwater samples had magnesium hazard values more than 50, indicating that they were unsuitable for irrigation.

16.5.5 Kelley's Ratio (KR)

An important parameter to evaluate irrigation water quality based on the concentration of sodium measured against calcium and magnesium was proposed by Kelley (1940). The statistical analysis of KR of the present study's groundwater ranges from −0.05 to 3.21 and surface water samples vary from −0.12 to 1.08, respectively. According to Kelley (1940) classification, except for one surface water sample and two groundwater sample, rest of the samples fall into the suitable category and are appropriate for irrigation (Table 16.9). Water samples yielding with >1 KR is indicative of excessive sodium level, hence unsuitable for irrigation and the water quality is good for irrigation, when Kelly's Ratio is <1.

16.5.6 Permeability Index (PI)

Irrigation water depends on various factors like total soluble salt, sodium, calcium, magnesium, and bicarbonate content of water. Doneen (1964) evaluated the suitability of water for irrigation based on permeability index (PI). Irrigation waters were classified into three main classes mainly Class I (<25), Class II (25–75), and Class III (>75). All the surface water (mean 153.94) and groundwater (mean 216.26) samples falls in the field of Class III and thus they are classified as having excellent permeability.

16.6 Conclusion

The study presents a general overview of hydrochemistry and water quality in Netravati river basin. The geological formations, anthropogenic point and non-point discharges that leads to the variations in surface and groundwater chemistry. The results of the study showed that the analyzed physiochemical parameters were found within the permissible limits of WHO with few exceptions. Based on calculated WQI, the water samples were assessed into two groups of "excellent" and "good" for drinking purpose. The type of water that predominates in the study area is Na-Ca-HCO_3-Cl. The plots of studied samples on Gibbs diagram supports the influence of rock–water interaction followed by evaporation dominance. In surface and groundwater the predominant cations were Na^+ and Ca^{2+} whereas HCO_3^- and Cl^- were the dominant anions. Ion relations suggested that ion exchange, limestone-dolomite weathering process yielding higher Na^+, Ca^{2+} and HCO_3^- ion concentrations. To evaluate the groundwater and surface water of the basin for irrigation purposes %Na, SAR, RSC, MH, PI and KR was determined. Irrigation water classified based on SAR and PI which classed all the water samples were excellent. As per the %Na and RSC surface water is more suitable for irrigation than

groundwater. Except few samples majority of water samples are suitable for drinking as well irrigation purpose. Continuous monitoring and development of management strategies for surface and groundwater is required to preserve this resource from further pollution.

Acknowledgments We are thankful to Dr. V. Nandakumar, Director, NCESS for providing laboratory and knowledge resource facilities and Dr. D. Padmalal, Scientist G and Group Head, Hydrological Processes Group & Atmospheric Processes Group, for the continuous support. The instrumental facilities in Central Chemical Laboratory, NCESS under the Ministry of Earth Sciences, Govt. of India is also acknowledged along with the NCESS-Core Project (W.P.3B.1).

References

APHA. (1995). *Standard methods for the examination of water and waste waters* (19th ed.). Washington, DC: American Public Health Association.

Berihu, A. B. (2020). Evaluation of groundwater and surface water quality suitability for drinking and agricultural purposes in Kombolcha town area, eastern Amhara region, Ethiopia. *Applied Water Science, 10*, 127. https://doi.org/10.1007/s13201-020-01210-6.

BIS. (1991). Specifications for drinking water IS: 10500:1991, Bureau of Indian Standards, New Delhi. In the soils of Tallinn (Estonia0). *Environmental Geochemistry and Health, 22*, 173–193.

BIS. (Bureau of Indian Standards) 10500. (2012). Indian Standard Drinking Water Specification.

Brindha, K., Neena Varman, K. V., Srinivasan, K., Babu, M. S., & Elango, L. (2014). Identification of surface water-groundwater interaction by hydrogeochemical indicators and assessing its suitability for drinking and irrigational purposes in Chennai, southern India. *Applied Water Science, 4*, 159–174.

Debels, P., Figueroa, R., Urrutia, R., Barra, R., & Niell, X. (2005). Evaluation of water quality in the Chillan River (Central Chile) using physicochemical parameters and a modified water quality index. *Environmental Monitoring and Assessment, 110*, 301–322.

Disli, E. (2017). Hydochemical characteristics of surface and groundwater and suitability for drinking and agricultural use in the upper Tigris Basin, Diyarbakir, Turkey. *Environmental Earth Sciences, 76*, 500. https://doi.org/10.1007/s12665-017-6820-5.

Doneen, L. D. (1964). Notes on water quality in Agriculture Published as a Water Science and Engineering Paper 4001, Department of Water Science and Engineering, University of California.

Eaton, F. M. (1950). Significance of carbonate irrigation water. *Soils Science 69*(2), 123–133.

Gibbs, R. J. (1970). Mechanism controlling world water chemistry. *Science, 170*, 1088–1090.

Gupta, S., Nayek, S., & Saha, R. N. (2012). Major ion chemistry and metal distribution in coal mine pit lake contaminated with industrial effluents: Constraints of weathering and anthropogenic inputs. *Environment and Earth Science, 67*, 2053–2061.

Gurumurthy, G. P., Balakrishna Jean, R. K., Braun, J. J., Stéphane, A., Udaya Shankar, H. N., & Manjunatha, B. R. (2012). Controls on intense silicate weathering in a tropical river, south-western India. *Chemical Geology, 300–301*, 61–69.

Hounslow, A. W. (1995). *Water quality data: Analysis and interpretation* (pp. 47–126). Boca Raton, FL: CRC Press.

Karthika, V. S., Mahadevan, H., Viswadas, V., Dev, V. V., & Krishnan, K. A. (2018). An integrated approach on evaluation of hydrochemical parameters of riverine system in Trivandrum urban area along with phosphate removal studies. *Bulletin of Pure and Applied Sciences Section C-Chemistry, 37*, 126–130.

Katyal, D., & Bharti, N. (2011). Water quality indices used for surface water vulnerability assessment. *International Journal of Environmental Sciences, 2*, 154–173.

Kelley, W. P. (1940). *Permissible composition and concentration of irrigation waters* (p. 66). Proc: ASCE.

Khadri, S. F. R., & Pande, C. (2015a). Ground Water Quality Mapping FOR Mahesh River Basin in Akola and Buldhana Districts of (MS) India using interpolation methods. *International Journal on Recent and Innovation Trends in Computing and Communication, 3*(2), 113–117.

Khadri, S. F. R., & Pande, C. (2015b). Analysis of hydro-geochemical characteristics of groundwater quality parameters in hard rocks of Mahesh River Basin, Akola, and Buldhana Dist. Maharashtra, India using geo-informatics techniques. *American Journal of Geophysics, Geochemistry and Geosystems, 1*(3), 105–114.

Khadri, S. F. R., & Pande, C. (2016). Ground water flow modeling for calibrating steady state using MODFLOW software: A case study of Mahesh River basin, India. *Model Earth System Environment, 2*, 39. https://doi.org/10.1007/s40808-015-0049-7.

Khadri, S. F. R., Pande, C., & Moharir, K. (2013). Groundwater quality mapping of PTU-1 Watershed in Akola district of Maharashtra India using geographic information system techniques. *International Journal of Scientific & Engineering Research, 4*(9), September-2013.

Kumar, M., Kumari, K., Ramanathan, A. L., & Saxena, R. (2007). A comparative evaluation of groundwater suitability for irrigation and drinking purposes in two intensively cultivated districts of Punjab, India. *Environmental Geology, 53*, 553–574.

Kumar, M., Ramanathan, A., Rao, S. O., & Kumar, B. (2006). Identification and evaluation of hydrogeochemical processes in the groundwater environment of Delhi, India. *Environmental Geology, 50*, 1025–1039.

Kumar, M. R., Krishnan, K. A., Das, R., & Vimexen, V. (2020). Seasonal phytoplankton succession in Netravathi-Gurupura estuary, Karnataka, India: Study on a three tier hydrographic platform. *Estuarine, Coastal and Shelf Science*. https://doi.org/10.1016/j.ecss.2020.106830.

Kumar, M. R., Vishnu, S. R., Sudhanandh, V. S., Faisal, A. K., Shibu, R., Vimexen, V., Ajmal, K., Aneesh, K. S., Antony, S., & Krishnan, K. A. (2014). Proliferation of dinoflagellates in Kochi estuary, Kerala. *Journal of Environmental Biology, 35*, 877–882.

Mahadevan, H., Krishnan, K. A., Pillai, R. R., & Sudhakaran, S. (2020). Assessment of urban river water quality and developing strategies for phosphate removal from water and wastewaters: Integrated monitoring and mitigation studies. *SN Applied Sciences, 2*. https://doi.org/10.1007/s42452-020-2571-0.

Kanak Moharir, Chaitanya Pande, and Sanjay Patil Inverse modeling of aquifer parameters in basaltic rock with the help of pumping test method using MODFLOW software, Geoscience Frontiers,86 1385-1395 (2017).

Moharir, K., Pande, C., Singh, S., Choudhari, P., Rawat, K., & Jeyakumar, L. (2019). Spatial interpolation approach-based appraisal of groundwater quality of arid regions in. *Aqua Journal, 68*(6), 431–447.

Nganje, T. N., Hursthouse, A. S., Edet, A., Stirling, D., & Adamu, C. I. (2014). Assessment of the Health Risk, Aesthetic and Agricultural Quality of Rainwater, Surface Water and Groundwater in the Shale Bedrock Areas, Southeastern Nigeria. *Water Quality, Exposure and Health, 7*(2), 153–178. https://doi.org/10.1007/s12403-014-0136-4.

Nganje, T. N., Hursthouse, A. S., Aniekan, E., Stirling, D., & Adamu, C. I. (2017). Hydrochemistry of surface water and groundwater in the shale bedrock, Cross River Basn and Niger Delta region, Nigeria. *Applied Water Science, 7*, 961–985.

Pande, C. B., Khadri, S. F. R., Moharir, K. N., & Patode, R. S. (2017). Assessment of groundwater potential zonation of Mahesh River basin Akola and Buldhana districts, Maharashtra, India using remote sensing and GIS techniques. *Sustainable Water Resources Management*. https://doi.org/10.1007/s40899-017-0193-5. ISSN 2363–5037.

Pande, C. B., & Moharir, K. (2018). Spatial analysis of groundwater quality mapping in hard rock area in the Akola and Buldhana districts of Maharashtra, India. *Applied Water Science, 8*(4), 1–17.

Pande, C. B., Moharir, K. N., Khadri, S. F. R., & Patil, S. (2018). Study of land use classification in the arid region using multispectral satellite images. *Applied Water Science, 8*(5), 1–11.

Pande, C. B., Moharir, K. N., Singh, S. K., & Dzwairo, B. (2019). Groundwater evaluation for drinking purposes using statistical index: Study of Akola and Buldhana districts of Maharashtra, India. *Environment, Development and Sustainability (A Multidisciplinary Approach to the Theory and Practice of Sustainable Development) Springer Journal, 22*, 7453. https://doi.org/10.1007/s10668-019-00531-0.

Piper, A. M. (1944). A graphic procedure in the geochemical interpretation of water analyses. *Transactions American Geophysical Union, 25*, 914–928.

Raghunath, H. M. (1987). *Groundwater* (pp. 344–369). New Delhi: Wiley Eastern Ltd..

Rajesh, R., Brindha, K., Murugan, R., & Elango, L. (2012). Influence of hydrogeochemical processes on temporal changes in groundwater quality in a part of Nalgonda district, Andhra Pradesh, India. *Environment and Earth Science, 65*, 1203–1213.

Rajesh, R., Sreedhara Murthy, T. R., & Raghavan, B. R. (2002). The utility of multivariate statistical techniques in hydrogeochemical studies: An example from Karnataka, India. *Water Research, 36*, 2437–2442.

Rao, N. S., Subrahmanyam, A., Kumar, S. R., Srinivasulu, N., Rao, G. B., Rao, P. S., & Reddy, G. V. (2012). Geochemistry and quality of groundwater of Gummanampadu sub-basin, GunturDistrict, Andhra Pradesh, India. *Environment and Earth Science, 67*, 1451–1471.

Richards, L. A. (1954). *Diagnosis and improvement of saline and alkali soils. Agricultural handbook no. 60* (pp. 98–99). New Delhi: USDA and IBH Publishing Co. Ltd..

Rimmer, S. M. (2004). Geochemical paleoredox indicators in Devonian-Mississipian black shales, central Application Basin (USA). *Chemical Geology, 206*, 373–398.

Sawyer, G. N., & McMcartly, D. L. (1967). *Chemistry of sanitary engineers* (2nd ed., p. 518). New York, NY: McGraw Hill.

Schoeller, H. (1977). Geochemistry of groundwater. In *Groundwater studies—An international guide for research and practice* (Vol. 15, pp. 1–18). Paris: UNESCO.

Sener, S., Sener, E., & Davraz, A. (2017). Evaluation of water quality index (WQI) method and GIS in Asku River (SW-Turkey). *Sci Total Environ, 584*, 131–144.

Shamsuddin, M. K., Azmin Sulaiman, W. N., Bin Ramli, M. F., & Mohd Kusin, F. (2019). Geochemical characteristic and water quality index of groundwater and surface water at lower river Muda Basin, Malaysia. *Arabian Journal of Geosciences, 12*, 309. https://doi.org/10.1007/s12517-019-4449-2.

Singh, K., Hundal, H. S., & Singh, D. (2011). Geochemistry and assessment of hydrogeochemical processes in groundwater in the southern part of Bathinda district of Punjab, Northwest India. *Environment and Earth Science, 64*, 1823–1833.

Srinivasamoorthy, K., Chidambaram, S., & Vasanthavigar, M. (2008). Geochemistry of fluorides in groundwater: Salem District, Tamilnadu, India. *Journal of Environmental Hydrology 1*, 16–25.

Tajabadi, M., Zare, M., & Chitsazan, M. (2018). The hydrogeochemical and isotopic investigation of the two-layered shiraz aquifer in the northwest of Maharlou saline lake, south of Iran. *Journal of African Earth Sciences, 139*, 241–244.

Todd, D. K. (1980). *Groundwater hydrology* (p. 535). Hoboken, NJ: John Wiley.

Udayakumar, P., Chandran, A., Jean, J. J., Shibu, R., & Krishnan, K. A. (2014a). *Journal of Marine Biology & Oceanography, 3*, 1–7.

Udayakumar, P., Jose, J. J., Krishnan, K. A., Kumar, C. S. R., Manju, M. N., & Salas, P. M. (2014b). Heavy metal accumulation in the surficial sediments along southwest coast of India. *Environment and Earth Science, 72*, 1887–1900.

WHO. (2011). *Guidelines for drinking-water quality* (4th ed.). Geneva: World Health Organization.

Wilcox, L. V. (1995). *Classification and use of irrigation waters. Circular no. 969*. Washington, DC: U.S. Department of Agriculture.

Zhang, B., Xianfang, S., Yinghua, Z., Dongmei, H., Changyuan, T., Yilei, Y., & Ying, M. (2012). Hydrochemical characteristics and water quality assessment of surface water and groundwater in Songnen plain, Northeast China. *Water Research, 46*, 2737–2748.

Chapter 17
Seasonal Variation of Groundwater Quality in the Kallada Basin, Southern Western Ghats of India

Uma Mohan and A. Krishnakumar

Contents

17.1 Introduction 335
17.2 Study Area 336
17.3 Materials and Methods 337
17.4 Results and Discussion 339
17.5 Water Quality Classification Using Piper Trilinear Diagram 343
17.6 Mechanism Controlling the Chemistry of Groundwater 343
17.7 Suitability of Water for Drinking Purpose Using Water Quality Index (WQI) and Pollution Index (PIG) 344
17.8 Pollution Index of Groundwater (PIG) 347
17.9 Conclusion 349
References 350

17.1 Introduction

Western Ghats also known as Sahyadri is a mountain range that runs parallel to the western coast of Indian peninsula, located entirely in India (Pande et al. 2019a, b; Khadri and Pande 2016; Chaitanya et al. 2017; Moharir et al. 2017, 2020). The Western Ghats perform important life sustaining functions (Khadri et al. 2013a; Khadri and Pande 2015a). Approximately 245 million people live in the peninsular Indian states that receive most of their water supply from rivers originating in the Western Ghats. Almost all rivers in Kerala originate from Western Ghats and flow towards the western side. From the point of view of water resources, Kerala is

U. Mohan · A. Krishnakumar (✉)
ESSO-National Centre for Earth Science Studies (NCESS), Ministry of Earth Sciences, Government of India, Thiruvananthapuram, Kerala, India

C. B. Pande, K. N. Moharir (eds.), *Groundwater Resources Development and Planning in the Semi-Arid Region*, https://doi.org/10.1007/978-3-030-68124-1_17

having both abundance and scarcity. Kerala has got 41 west-flowing and three east-flowing rivers originating from Western Ghats. Water, one of the most vital resources, is essential to sustain life. Based on the fundamental quality, water is used for domestic, agriculture, commercial and industrial purposes (Khadri et al. 2013b; Khadri and Pande 2015b, c, d). It is estimated that approximately one-third of the world's population use groundwater for drinking purposes. It is now widely accepted that the suitability of groundwater not only lies on its widespread occurrence, but also its quality which in turn is determined by different kinds of natural factors and man-made factors including the quality of the recharged water, atmospheric precipitation, and soil-rock weathering (Krishnakumar et al. 2017; Moharir et al. 2019). Continuous increase in water demands due to increasing population and developmental activities has resulted in more use of groundwater resources, which has led to groundwater depletion (Krishan et al. 2016). Besides this, the groundwater quality is deteriorating due to disposal of massive industrial effluents and mining activities. Groundwater resource is under threat from pollution either from human life style manifested by the low level of hygiene practiced or due to the use of fertilizers in agriculture (Ikem et al. 2002). Anthropogenic intervention in the river basins of Kerala is a major concern today because it is altering the health and quality of rivers, and thereby groundwater too. Therefore, determination of groundwater quality is important to observe the suitability of water for a particular use. Once the groundwater is contaminated, its quality cannot be restored by stopping the pollutants from the source therefore it becomes very important to regularly monitor the quality of groundwater. Water quality index (WQI) is one of the most effective, simple and easily understandable tools to assess water quality for its suitability for drinking purposes (Pande et al. 2019b). The present study has been conducted to quantify the types of pollution of groundwater in the study area by employing PIG. Due to the necessity of quality water, both in current process and for future environmental quality, water analysis is a critically important scientific process. The present study is aimed for the detailed investigation of the ground water systems of Kallada river basin during pre-monsoon, monsoon and post-monsoon seasons.

17.2 Study Area

The area selected for the study—the Kallada River Basin lies between 8°45′–9°15′ north latitude and 76°30′–77°20′ east longitude (Fig. 17.1). The Kallada river is one of the two major rivers that flow through the Kollam district of Kerala, India. It travels for 121 km, flowing through Punalur, Pathanapuram, Kunnathur, Kulakkada and Kallada before ending at Ashtamudi lake. It has a drainage area of 1717 km^2 and ranks fifth in terms of basinal area amongst the 41 west-flowing rivers of the State. The basin is bounded by Ithikara and Vamanapuram river basins in the south, Achenkovil and Pallikal river basins in the north, Lakshadweep Sea in the west and the Tambraparni river basin of Tamilnadu in the east. The Kallada basin is

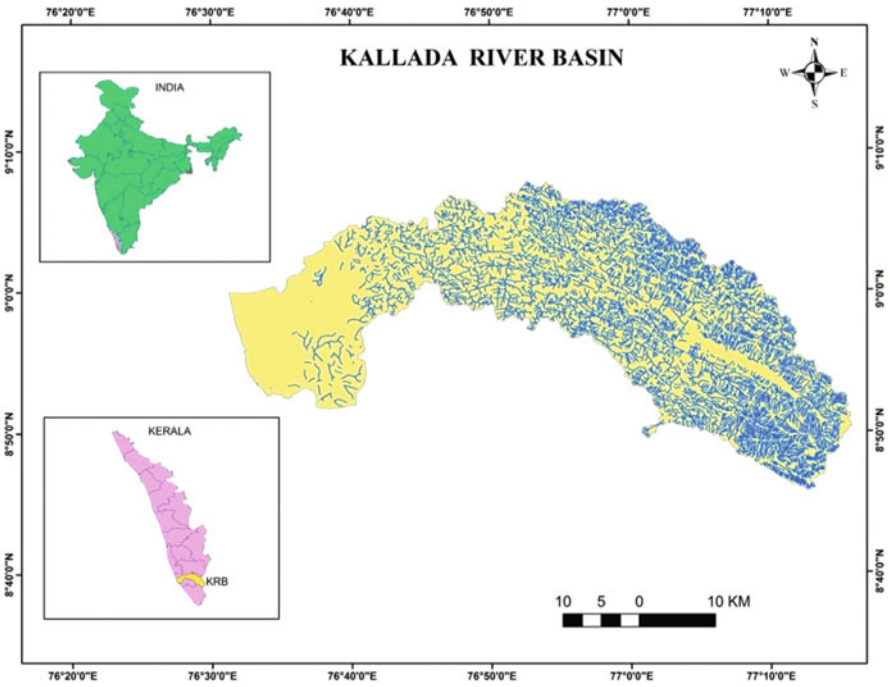

Fig. 17.1 Location map of the study area

almost rectangular with a length: width ratio 3:1. Two Ramsar sites, Ashtamudi Lake and Sasthamkota Lake are located in the study area. The river originating from the Western Ghats drains into Ashtamudi backwaters near Kollam.

17.3 Materials and Methods

Ground field survey was conducted for gathering preliminary data from the field by considering the aspects of environmental setting viz.; vegetation, drainage networks, soil and land use activities taking place in the areas. A total of 31 groundwater samples were collected both from Kallada river basin during monsoon, pre- and post-monsoon seasons. Well-cleaned plastic containers were taken for sample collection to analyse the physicochemical parameters. Utmost care was taken not to contaminate the samples during collection and preservation. The sampling sites are fixed along the river considering the physiography (Table 17.1). The location of sampling for ground water is shown in Fig. 17.2.

Table 17.1 General physiography of Kallada River Basin

Location name	Latitude	Longitude	General physiography
Thenmala (K_1)	N08°57′32.7″	E77°03′41.7″	Highland
Ottakkal (K_2)	N08°58′15.2″	E77°02′42.8″	Highland
Yeroor (K_3)	N08°59′09.7″	E076°59′33.3″	Highland
Anchal (K_4)	N08°54′24.1″	E076°55′27.8″	Highland
Karavalur (K_5)	N08°59′15.6″	E076°55′39.5″	Highland
Pathanapuram (K_6)	N09°05′01.1″	E076°51′50.3″	Highland
Edathara, Kalanjoor (K_7)	N09°05′58.3″	E076°51′05.6″	Highland
Koodal (K_8)	N09°08′12.4″	E076°51′24.7″	Highland
Neendakara (K_9)	N08°57′41.11″	E076°31′50.9″	Lowland
Chavara Kayal (K_{10})	N08°54′40.9″	E076°32′00.2″	Lowland
Sasthamcottah (K_{11})	N09°02′31.8″	E076°37′40.9″	Midland
Cheloor Lake (K_{12})	N09°02′27.2″	E076°39′21.5″	Midland
Bharanikavu (K_{13})	N09°03′03.9″	E076°38′12.6″	Midland
Kadavoor (K_{14})	N08°54′19.2″	E076°34′45.7″	Lowland
Ashtamudi (K_{15})	N08°57′33.3″	E076°35′51.9″	Lowland
Thekkumbhagom (K_{16})	N08°57′26.0″	E076°32′54.5″	Lowland
West Kallada (K_{17})	N09°01′51.0″	E076°37′23.1″	Midland
Kunnathur (K_{18})	N09°03′43.7″	E076°41′08.9″	Midland
Enathu, Puthoor (K_{19})	N09°05′23.6″	E076°45′20.1″	Midland
Kottarakara (K_{20})	N09°00′52.1″	E076°47′06.2″	Midland
Kovoor (K_{21})	N9°01′6.43″	E76°35′53.772″	Lowland
Kottukadu (K_{22})	N8°58′44.4″	E76°33′32.76″	Lowland
Perumon (K_{23})	N8°58′14.016″	E76°36′36.529″	Lowland
Chittumala (K_{24})	N9°0′37.116″	E76°39′37.31″	Midland
Puthoormukku (K_{25})	N9°5′3.34″	E76°45′25.27″	Midland
Cherupoika (K_{26})	N9°1′51.45″	E76°40′43.64″	Midland
Aarattupuzha (K_{27})	N9°4′59.49″	E76°46′49.36″	Midland
Kalayapuram (K_{28})	N9°3′3.395″	E76°46′17.1012″	Midland
Vettithitta (K_{29})	N9°2′26.24″	E76°55′14.29″	Midland
Manchallur (K_{30})	N9°4′42.697″	E76°51′22.08″	Midland
Munroe Island (K_{31})	N9°0′3.15″	E76°36′41.09″	Lowland

17.3.1 Parameters Analysed

The physical parameters such as pH, electrical conductivity (EC), dissolved oxygen (DO), total dissolved solids (TDS) and temperature were measured in the field using a portable water quality analyzer (PWQA). Other physicochemical parameters such as sodium, potassium, calcium, magnesium, total hardness, chloride, sulphate, carbonate, bicarbonate, nitrate, nitrite, silicate, phosphate and ammonia were estimated using standard procedures following the method of APHA (2012). The results obtained are compared with drinking water quality standards (BIS 2004). The suitability of the samples for drinking purpose was also determined.

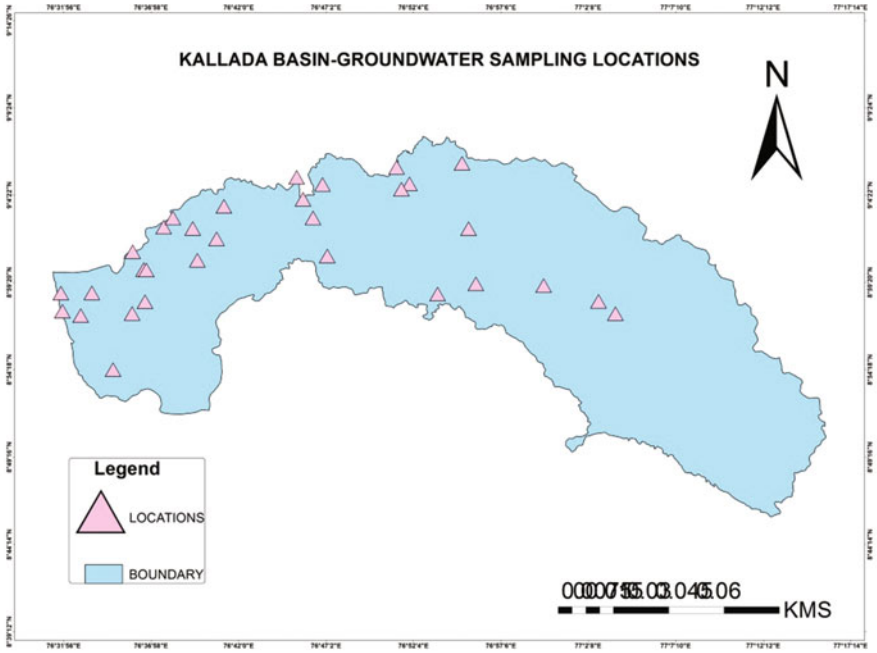

Fig. 17.2 Groundwater sampling locations

17.4 Results and Discussion

In this chapter focus on the 16 water quality parameters of Kallada basin were analysed for drinking suitability during pre-, post-monsoon seasons (2019–2020). The water quality is most important for the development of agriculture, drinking and industrial purposes in the semiarid region. Currently, so many parameters such as climate change factors and disaster activities may directly affect the groundwater quality, soil texture, and surface water quality in the semiarid area. The continuous groundwater quality monitoring is important for identification of water quality in the groundwater. The fresh water is only available in the groundwater or aquifer zones. In this context, this chapter is a play major role in the development and planning of groundwater in the semiarid area.

17.4.1 Seasonal Variation in Groundwater Quality

The seasonal variation of groundwater quality analysis is depicted by box plots in Fig. 17.3. The hydrogen ion concentration (pH) of the groundwater samples varied from 5.78 to 7.14, 6.33 to 6.63 and 5.36 to 9.44 during pre-post, monsoon seasons

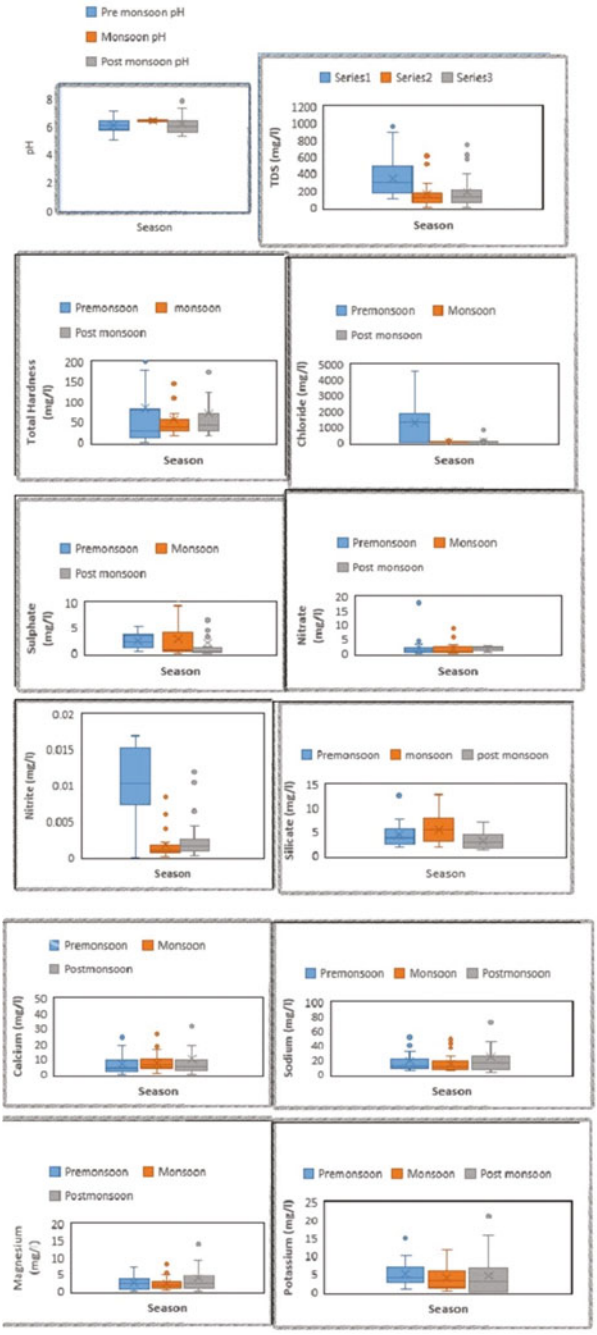

Fig. 17.3 Box plots of various water quality parameters showing seasonal variations

respectively. A few samples were observed with high TDS during the three seasons indicating the presence of high concentration of Na and Cl in groundwater. The results are in good agreement with the findings by Badusha and Santhosh (2017). The concentration of TDS was observed to be high at different sites, which might be due to the addition of solids from the surface runoff (Antony and Ignatius 2016). The hardness of a few samples exceeds the maximum limit of 300 mg/l (BIS 2004) in pre- and post-monsoon seasons. According to groundwater classification on the basis of total hardness, all groundwater samples falls in the category of soft (0–60 mg/l) and moderate hard (61–120 mg/l) type except a few samples which falls under the category of very hard type (>180 mg/l) (Sawyer et al. 2003). The total alkalinity (TA) was observed higher in post-monsoon and lower in monsoon and pre-monsoon seasons. Among the cations, Na is the dominant cation and it ranges from 5.8 to 52.3 mg/l (mean 17.9 mg/l), 5.2 to 49.5 mg/l (mean 14.7 mg/l) and 3.64 to 144 mg/l (mean 23.7 mg/l) during the pre-monsoon, monsoon and post-monsoon seasons respectively. It is followed by calcium, which ranges from 0.18 to 21.6 mg/l, 0.71 to 26.6 mg/l and 0.1 to 91.2 mg/l with average values being 6.61, 7.66 and 10.5 mg/l in pre-monsoon, monsoon and post-monsoon seasons respectively. The concentration of other cations like Mg and K falls well within the permissible limit recommended by BIS. These results are in good agreement with the observations by Abhisheka and Binoj Kumar in 2018. The chloride content of ground water samples of the study area varied from 3 to 4544 mg/l, 15.56 to 173.1 mg/l and 16.13 to 806.6 mg/l with average values of 1405, 44.55 and 73.95 mg/l in pre-monsoon, monsoon and post-monsoon seasons, respectively. Water containing less than 250 mg/l chloride is suitable for drinking purposes (Anderson 1979; Pande and Moharir 2018). In view of the above facts, the chloride content of ground water lies above the level recommended by BIS for drinking, household and other purposes. These results are in good agreement with the studies of Saranya and Lancelet (2019). The concentration of nitrates and phosphates are very less during the three seasons, which indicate that the groundwater has been less affected by these nutrients. The concentration of ammonia is found to be slightly higher in the three seasons. Anthropogenic activities such as urbanization is one of the major reasons that are responsible for the high ammonia content in the groundwater (Kamal et al. 2015). The silicate concentration is found to be within the permissible limit recommended by BIS and are in good agreement with the observations by Hema et al. (2015). The summary statistics of the hydrochemistry data for the monsoon (MON), post-monsoon (POM) and pre-monsoon (PRM) sampling of groundwater in Kallada river basin has been summarized in Table 17.2.

Table 17.2 Summary statistics of the hydrochemistry data for the monsoon (MON), post-monsoon (POM) and pre-monsoon (PRM) sampling of groundwater in Kallada River Basins. Grand mean is estimated as the mean of the three sampling seasons

	Parameters	pH	TDS	DO	TH	Cl	TA	SO_4	Ca	Mg	Na	K	NO_3	NO_2	Si	PO_4	NH_4
Season	Unit		mg/l	mg/l	mg/l	mg/l	mg/l	mg/l	mg/l	mg/l	mg/l	mg/l	mg/l	mg/l	mg/l	mg/l	mg/l
PRM	Mean	6.47	348.9	7.84	76.2	1405	38.9	2.3	6.61	2.38	17.9	4.75	1.65	0.01	4.11	0.02	0.12
	Max	7.14	974	12.1	700	4544	337	5.43	21.6	8.96	52.3	15.1	18.01	0.016	12.7	0.16	9.15
	Min	5.78	75	4.6	1.6	3	0	0.38	0.18	0.16	5.8	0.78	0.07	0.006	1.85	0	0.006
MON	Mean	6.46	162.3	7.4	57.2	44.55	35.9	2.81	7.66	2.08	14.7	4.07	1.78	0.002	5.48	0.02	0.24
	Max	6.63	654	9.31	244	173.1	254	9.48	26.6	8.12	49.5	11.9	10.44	0.009	12.9	0.17	1.43
	Min	6.33	0	6.34	16	15.56	0	0.1	0.71	0.31	5.2	0.25	0.052	8E-05	1.82	0	0.02
POM	Mean	6.28	187.4	6.38	71.7	73.95	60.1	2.15	10.5	3.96	23.7	5.23	1.71	0.021	3.11	0.03	0.24
	Max	9.44	746	8.06	420	806.6	793	37.4	91.2	25.6	144	15.9	2.484	0.586	6.94	0.76	1.69
	Min	5.36	17	3.17	16	16.13	1.22	0	0.1	0.09	3.64	0.13	0.48	3E-04	1.08	0	0.011
Grand mean		*6.4*	*232.8*	*7.2*	*49*	*3142*	*40.3*	*2.42*	*8.25*	*2.81*	*18.7*	*4.68*	*1.71*	*0.011*	*4.23*	*0.02*	*0.20*
BIS		*6.5–8.5*	*600*	*5*	*200*	*250*	*600*	*200*	*75*	*30*	*200*	*12*	*45*	*3*	*25*	*3*	*0.5*

TDS total dissolved solids, *TH* total hardness, *TA* total alkalinity. *DO* dissolved oxygen

17.5 Water Quality Classification Using Piper Trilinear Diagram

Piper trilinear diagrams (Piper 1994) were prepared to classify the water quality of selected sources of study area. The diagram classified the hydrochemical facies on account of prominent ions contributed the water quality. These diagrams graphically represent the chemical equilibrium between cations (Ca^2, Mg^{2+}, Na^+ and K^+) and anions (Cl^-, SO_4^{2-}, CO_3^{2-} and HCO_3^-) in water samples and also describe the presence of main contributor ions and chemical reactions taking place in the water. The diagram composed of two lower triangles of cations and anions and middle quadrilateral. Quadrilateral or diamond shape indicates the combined distribution of both ions (cations and anions) and final water type of sources. All the three fields have scales reading in % of meq/l. In the present study, water quality of 31 sites from Kallada basin during the three seasons has been characterized using Piper diagrams (Fig. 17.4). The Hill Piper diagram reveals that samples belong to the Ca-Na-Cl type in the pre-monsoon, Na-Cl type and mixed type in both monsoon and post-monsoon period. Improper sanitary conditions, fertilizers from agricultural land and irrigation return flow are the main contributing factors of Na and Cl in groundwater (Subba Rao 2012).

17.6 Mechanism Controlling the Chemistry of Groundwater

17.6.1 Gibbs Diagram and Water Rock Interaction

Gibbs (1970) proposed two diagrams to understand the hydrogeochemical procedures with reverence to atmospheric precipitation, rock–water interaction, and

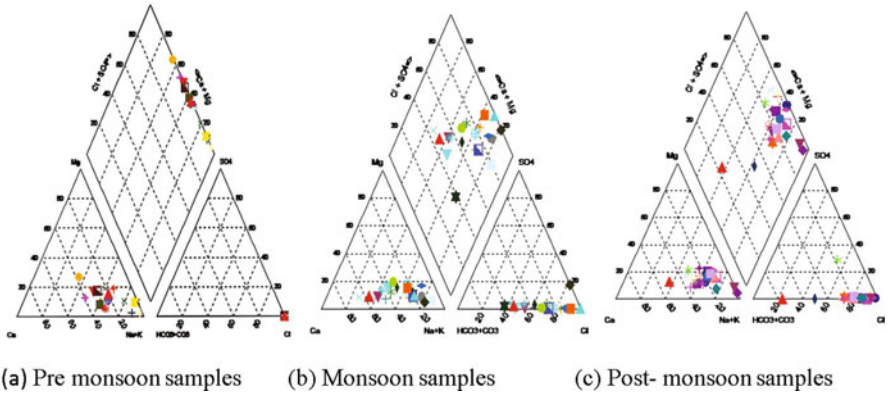

Fig. 17.4 Piper trilinear diagrams showing the groundwater characterization for Pre-post monsoon seasons. (**a**) Pre-monsoon samples. (**b**) Monsoon samples. (**c**) Post-monsoon samples

evaporation over the administration of geochemistry of groundwater. Gibbs plots are the graph of ratio of cations [(Na + K) / (Na + K + Ca)] and anions [Cl/ (Cl + HCO_3)] against TDS. The Gibbs plotting of chemical data (Fig. 17.5a–f) was mainly around rock dominance area and partly in precipitation dominance zone. It shows that water–rock interaction is the main factor controlling the chemical composition of groundwater samples of the study area.

17.7 Suitability of Water for Drinking Purpose Using Water Quality Index (WQI) and Pollution Index (PIG)

Water quality index determination (Tiwari and Mishra 1985; Pande et al. 2019b) for a set of 31 groundwater samples is undertaken with a major objective to determine the suitability of groundwater of the present study area with respect to drinking. The index classifies the water quality based on the purity of sample by using the most commonly measured water quality parameters. The standards for drinking purposes as recommended by WHO (2011) and BIS 10500 (2004) have been considered for the calculation of WQI. For computing WQI three steps are followed. In the first step, each of the 14 parameters (pH, TDS, DO, HCO_3, TH, Cl, SO_4, PO_4, NO_3, NO_2, Ca, Mg, Na and K) have been assigned a weight (wi) according to its relative importance in the overall quality of water for drinking purposes (Table 17.3). The maximum weight of 5 has been assigned to the parameters like nitrate and total dissolved solids due to their major importance in water quality assessment. Sodium and Potassium is given the minimum weight of 2 as it plays an insignificant role in the water quality assessment. Other parameters like calcium, magnesium, dissolved oxygen, total hardness, chloride, phosphate, sulphate, bicarbonate and nitrite were assigned weight between 2 and 5 depending on their importance in water quality determination. In the second step, the relative weight (Wi) is computed from the following Eq. 17.1:

$$\mathrm{Wi} = \mathrm{wi} / \sum_{i=1}^{n} \mathrm{wi} \tag{17.1}$$

where Wi is the relative weight, wi is the weight of each parameter and n is the number of parameters. Calculated relative weight (Wi) values of each parameter are given in Table 17.3.

In the third step, a quality rating scale (qi) for each parameter is assigned by dividing its concentration in each water sample by its respective standard according to the guidelines laid.

down in the BIS 10500 (2004) and the result is multiplied by 100 (Eq. 17.2):

$$\mathrm{qi} = (\mathrm{Ci}/\mathrm{Si}) \times 100, \tag{17.2}$$

where qi is the quality rating

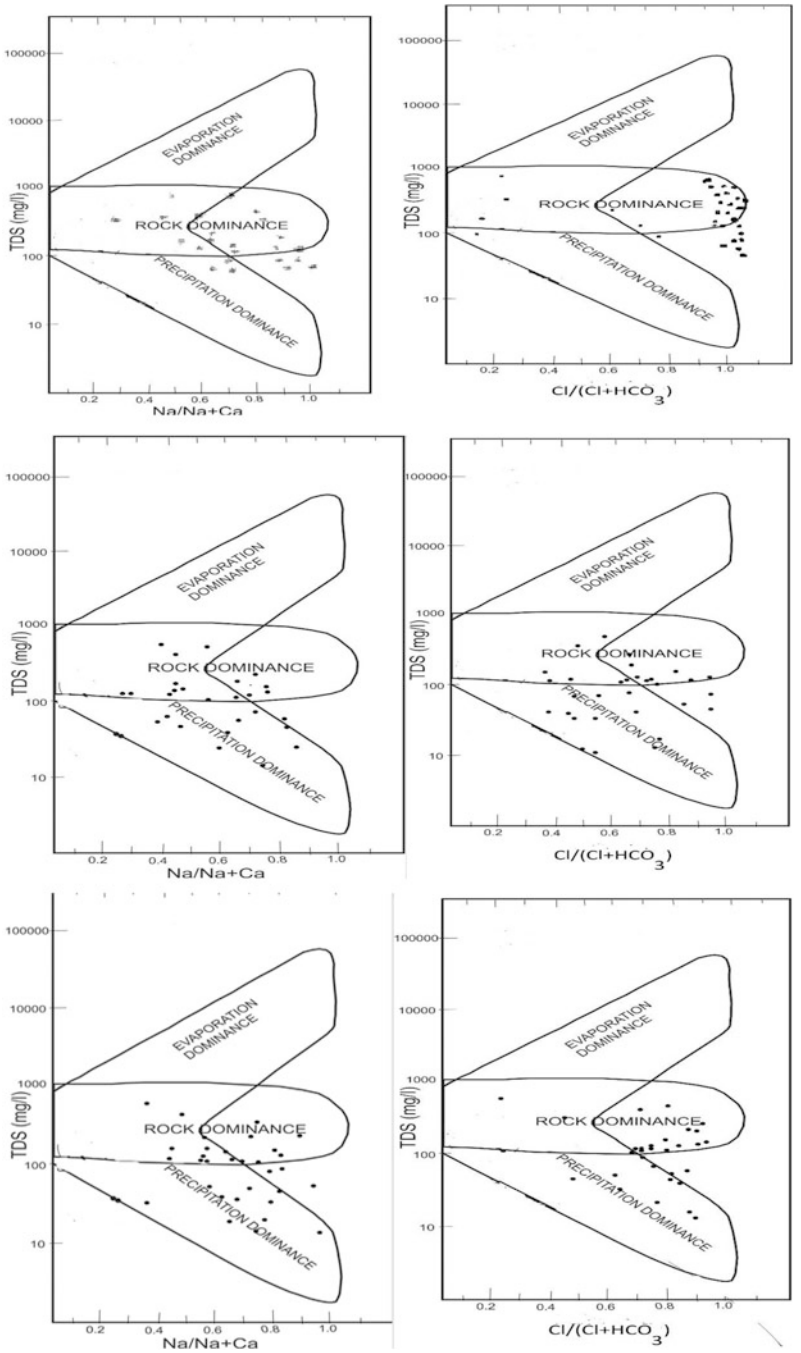

Fig. 17.5 Gibbs diagram (**a**) cations, (**b**) anions for pre-monsoon 2019, (**c**) cations, (**d**) anions for monsoon 2019, (**e**) cations, (**f**) anions for post-monsoon 2020

Table 17.3 Relative weight of chemical parameters

Parameters	Indian Standard (BIS 10500 2004)	Weight (wi)	Relative Weight (Wi)
pH	6.5–8.5	4	0.0727
TDS	500	5	0.091
DO	5	4	0.073
Alkalinity	200	3	0.055
Hardness	200	3	0.055
Chloride	250	4	0.073
Ca	75	3	0.055
Mg	30	3	0.055
Na	200	2	0.036
K	12	2	0.036
Sulphate	200	3	0.055
Nitrate(NO_3)	45	5	0.091
Nitrite(NO_2)	3	4	0.073
Phosphate	5	3	0.055
		$\Sigma wi = 55$	$\Sigma W_i = 0.8757$

Ci is the concentration of each chemical parameter in each water sample in mg/l.

Si is the Indian drinking water standard for each chemical parameter in mg/l according to the guidelines of the BIS 10500 (2004) (Eq. 17.3).

For computing the WQI, the Sub-Index (SI) is first determined for each chemical parameter, which is then used to determine the WQI as per the following Eq. 17.4:

$$\mathrm{SI}_i = \mathrm{Wi} \times q_i \tag{17.3}$$

$$\mathrm{WQI} = \Sigma \mathrm{SI}_i \tag{17.4}$$

where SI_i is the sub-index of *i*th parameter, q_i is the rating based on concentration of *i*th parameter and n is the number of parameters. Water quality types were determined on the basis of WQI. The computed water quality index ranges from 43.4 to 164.79 mg/l, 18.68 to 50.08 mg/l and 14.25 to 84.77 mg/l with average values being 86.69, 26.71 and 28.27 mg/l in pre-post monsoon seasons, respectively (17.6). Water of the study area and its classification based on WQI values are shown in Table 17.4. Only 25% of the pre-monsoon groundwater samples belong to 'Poor Water' category. Overall, the groundwater of the study area varies from excellent to good water and is suitable for drinking purposes in the three seasons (Table 17.4). Figure 17.6 indicates the comparative of Water Quality Index value in all the three seasons.

Table 17.4 Rating of water quality

WQI	Water quality	% of monsoon		
		Pre-monsoon (May 2019)	Monsoon (Sep 2019)	Post-monsoon (Feb 2020)
<50	Excellent	5	97	93.55
50–100	Good water	70	3	6.45
100–200	Poor water	25	0	0
200–300	Very poor water	0	0	0
>300	Unsuitable for drinking	0	0	0

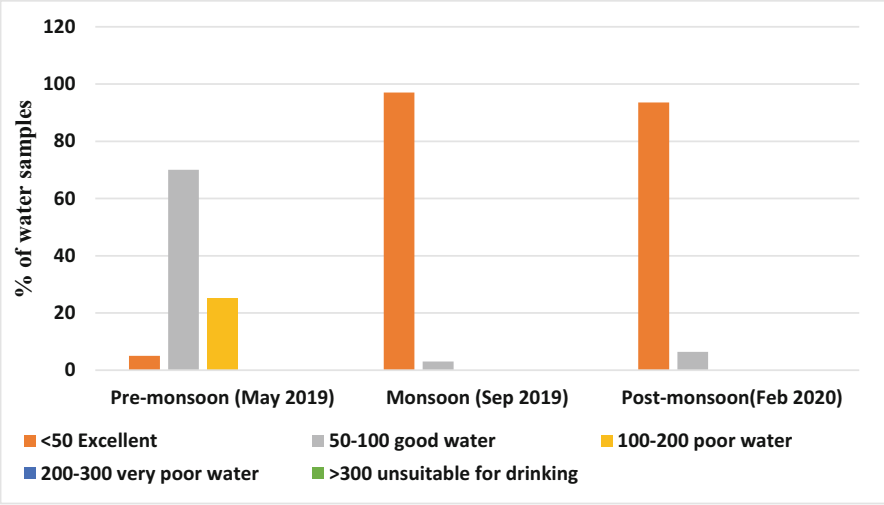

Fig. 17.6 Water Quality Index for the three seasons

17.8 Pollution Index of Groundwater (PIG)

For assessment of variation in groundwater quality caused by geogenic and anthropogenic sources, pollution index of groundwater (PIG) proposed by Subba Rao (2012) was used in the present study, which quantifies the status of relative impact of individual chemical variables (pH, TDS, Ca^{2+}, Mg^{2+}, Na^{+}, K^{+}, Cl^{-}, $SO_4{}^{2-}$, $NO_3{}^{-}$, $NO_2{}^{-}$ and $PO4^{-}$) on overall quality of groundwater. Computation of PIG is done in five steps. Based on the effects that the chemical parameters produce on the health of human being they were assigned a relative weight (Rw) (Table 17.5). The weight parameter (Wp) was calculated in the second step by the given equation.

$$\mathrm{Wp} = \mathrm{Rw} / \sum \mathrm{Rw}$$

Table 17.5 Relative weight of chemical parameters

Chemical parameter	Drinking water quality standards (BIS 2004)	Relative weight (Rw)	Weight parameter (Wp)
pH	7.5	5	0.098039
TDS	500	5	0.098039
HCO_3	300	3	0.058824
Hardness	200	4	0.078431
Cl	250	4	0.078431
Ca	75	4	0.078431
Mg	30	2	0.039216
Na	200	4	0.078431
K	10	1	0.019608
SO_4	150	4	0.078431
NO_3	45	5	0.098039
NO_2	3	4	0.078431
PO_4	3	2	0.039216
SiO_4	25	4	0.078431

Source: Subba Rao (2012)

In the third step, concentration status (Sc) for each parameter was estimated by dividing its respective water quality standard limit as prescribed by BIS, 2004 and Eq. 17.4.

$$\mathrm{Sc} = \mathrm{Ci}/\mathrm{Ds} \tag{17.5}$$

where Ci is the concentration of individual chemical parameters. Ds is the standard of drinking water quality for each chemical parameters. Overall chemical quality parameter (Ow) was first determined and then PIG was calculated as per the following Eqs. 17.6 and 17.7.

$$\mathrm{Ow} = \mathrm{Wp} \times \mathrm{Sc} \tag{17.6}$$

$$\mathrm{PIG} = \sum \mathrm{Ow} \tag{17.7}$$

Classification of PIG and types of pollution in the study area for the three seasons is given in Table 17.6. As per PIG classification, majority of the samples belong to insignificant pollution to low pollution in pre-monsoon season and 100% samples belong to insignificant pollution zone in monsoon and post-monsoon seasons. The rating of water quality as per the PIG value for the three seasons is shown in Fig. 17.7.

Table 17.6 Classification of Pollution Index of Groundwater (PIG)

Range of PIG	Classification	% of sample		
		Pre-monsoon	Monsoon	Post-monsoon
<1.0	Insignificant pollution	70	100	100
1.0–1.5	Low pollution	25	–	–
1.5–2.0	Moderate pollution	5	–	–
2.0–2.5	High pollution		–	–
>2.5	Very high pollution		–	–

Source: Subba Rao (2012)

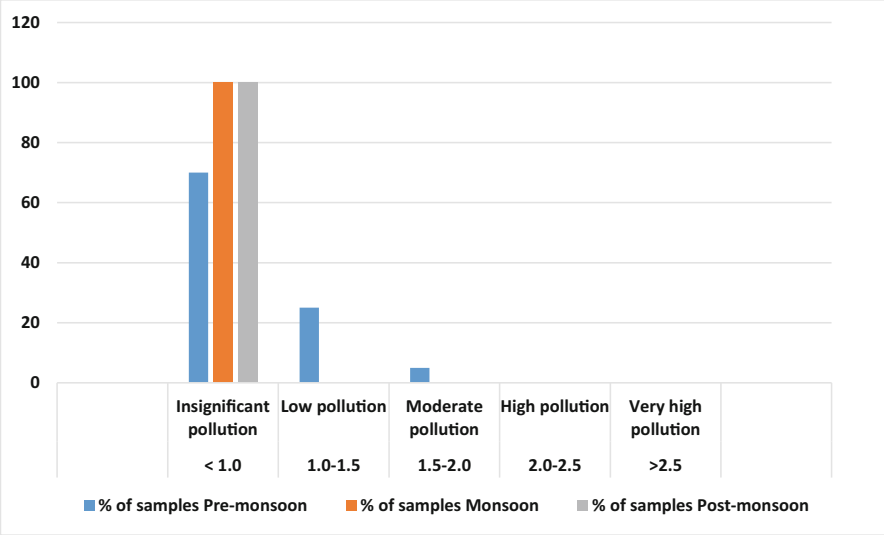

Fig. 17.7 Pollution Index for the three seasons

17.9 Conclusion

The present study was carried out with the aim of assessing the ground water resources of Kallada river basin during the monsoon and non-monsoon seasons for drinking purposes. The study provides an informative data and helps to understand the physicochemical characteristics of ground water samples in selected sites of the river basin. To find out the groundwater suitability for drinking purposes in Kallada river basin, 31 groundwater samples have been studied in detail during May 2019, September 2019 and January 2020. The results indicates that TDS, chloride, sodium, calcium, ammonia and hardness exceeds the maximum desirable limit as prescribed by BIS in majority of the samples in the three seasons. Dominant facies from Piper trilinear diagram are Ca-Na-Cl in pre-monsoon season and Na-Cl in monsoon and post-monsoon seasons. Chloride and Sodium are found to be higher at selected places compared to the permissible level owing to anthropogenic contribution which

might occur due to the seepage of polluted water from urban centres, sea water intrusion into lowland areas and insanitary practices in the study area. The samples fall in rock–water interaction dominant zone indicating chemical weathering of rock-forming minerals as the prime factor influencing the groundwater quality. Most of the samples fall in good water category in pre-monsoon and under excellent category in both monsoon and post-monsoon seasons indicating that the groundwater is suitable for drinking purposes according to WQI classification. As per the classification of PIG, majority of the samples are under insignificant pollution zone and a few samples show low to moderate pollution during pre-monsoon season. All the samples show insignificant pollution in the other two seasons. From this study, it is revealed that degradation of water quality is high at the downstream stretches of the river. Besides, a general increasing trend in usefulness is seen from pre-monsoon to post-monsoon seasons.

Acknowledgements The authors are grateful to the Director, NCESS for providing necessary facilities to do the work. One of the authors (U.M.) is thankful to the Director, Co-operative Academy of Professional Education (CAPE) for giving permission to do research under the Quality Improvement Programme (QIP) scheme of AICTE.

References

Abhisheka, V. R., & Binoj Kumar, R. B. (2018). Groundwater quality assessment for domestic and irrigational suitability in Kallada River Basin, South Kerala, India. *Nature Environment & Pollution Technology, 17*(1), 153–159.

Anderson, M. P. (1979). Using models to simulate the movement of contaminants through groundwater flow systems. *CRC Critical Reviews in Environmental Control, 9*(2), 97–156.

Antony, M. M., & Ignatius, J. (2016). A hydrological study of Ashtamudi Lake, Kerala, India with special reference to its ecological difference. *International Journal of Science and Research, 5* (8), 1841–1846.

APHA. (2012). *Standard methods for the examination of water and waste water* (21st ed., p. 948). Washington, DC: American Public Health Association.

Badusha, M., & Santhosh, S. (2017). Seasonal effects of water quality changes in Neyyar River, Kerala, India. *International Journal of Scientific and Research Publications, 7*(7), 703–710.

Bureau of Indian Standards, Indian Standards (IS:10550). (2004). *Drinking water specification*. New Delhi: BIS.

Chaitanya, B., Pande, S. F. R. K., Moharir, K. N., & Patode, R. S. (2017). Assessment of groundwater potential zonation of Mahesh River basin Akola and Buldhana districts, Maharashtra, India using remote sensing and GIS techniques. *Sustainable Water Resources Management*. https://doi.org/10.1007/s40899-017-0193-5.

Gibbs, R. J. (1970). Mechanisms controlling world water chemistry. *Science, 170*(3962), 10881090.

Hema, C. N., Padmalal, D., & Ammini, J. (2015). Hydro chemical assessment of tropical springs—a case study from SW India. *Environmental Monitoring and Assessment, 187*, 48. https://doi.org/10.1007/s10661-014-4164-0.

Ikem, A., Osibanjo, O., Sridhar, M. K. C., & Sobande, A. (2002). Evaluation of groundwater quality characteristics near two waste sites in Ibadan and Lagos, Nigeria. *Water, Air, & Soil Pollution, 140*(1–4), 307–333.

Kamal, M. Z. A. M., Hashim, D. M. M., & Zin, M. S. B. M. (2015). The effect of the ammonium concentration in the groundwater. *International Journal of Social Sciences, 2015*(Special Issue), 313–319.

Khadri, S. F. R., & Pande, C. (2015a). Remote sensing and GIS applications of linament mapping of Mahesh River Basin, Akola & Buldhana District, Maharashtra, India using multispectral satellite data. *International Journal of Research, 2*(10), October-2015.

Khadri, S. F. R., & Pande, C. (2015b). Groundwater quality mapping using hydrogen chemistry and geostatistical analyst of Mahesh River Basin, Akola and Buldhana District, Maharashtra, India. *International Journal of Research (IJR), 2*(10), October-2015.

Khadri, S. F. R., & Pande, C. (2015c). Analysis of hydro-geochemical characteristics of groundwater quality parameters in hard rocks of Mahesh River Basin, Akola, and Buldhana Dist. Maharashtra, India Using Geo-Informatics Techniques. *American Journal of Geophysics, Geochemistry and Geosystems, 1*(3), 105–114.

Khadri, S. F. R., & Pande, C. (2015d). Ground water quality mapping for Mahesh River Basin in Akola and Buldhana Districts of (MS) India using interpolation methods. *International Journal on Recent and Innovation Trends in Computing and Communication, 3*(2), 113–117.

Khadri, S. F. R., & Pande, C. (2016). Ground water flow modeling for calibrating steady state using MODFLOW software: A case study of Mahesh River basin, India. *Model Earth System Environment, 2*, 39. https://doi.org/10.1007/s40808-015-0049-7.

Khadri, S. F. R., Pande, C., & Moharir, K. (2013a). Geomorphological investigation of WRV-1 watershed management in Wardha district of Maharashtra India; using Remote sensing and Geographic Information System techniques. *International Journal of Pure and Applied Research in Engineering and Technology, 1*(10), 136.

Khadri, S. F. R., Pande, C., & Moharir, K. (2013b). Groundwater quality mapping of PTU-1 Watershed in Akola district of Maharashtra India using geographic information system techniques. *International Journal of Scientific & Engineering Research, 4*(9), September-2013 1856.

Krishan, G., Singh, S., Kumar, C. P., Gurjar, S., & Ghosh, N. C. (2016). Assessment of Water Quality Index (WQI) of groundwater in Rajkot District, Gujarat, India. *Journal of Earth Science and Climatic Change, 7*, 341.

Krishnakumar, A., Das, R., & Puthalath, S. (2017). Assessment of the quality of water resources in coastal urban lands of two small catchment rivers, Southwest India. *Management of Environmental Quality, 28*(3), 444–459.

Moharir, K. N., Pande, C. B., Singh, S. K., & Del Rio, R. A. (2020). *Evaluation of analytical methods to study aquifer properties with pumping test in Deccan Basalt Region of the Morna River Basin in Akola District of Maharashtra in India, groundwater hydrology*. London: Intec Open Publication. https://doi.org/10.5772/intechopen.84632.

Moharir, K., Pande, C., & Patil, S. (2017). Inverse modeling of Aquifer parameters in basaltic rock with the help of pumping test method using MODFLOW software. *Geoscience Frontiers, 8*(6), 1385–1395.

Moharir, K., Pande, C., Singh, S., Choudhari, P., Rawat, K., & Jeyakumar, L. (2019). Spatial interpolation approach-based appraisal of groundwater quality of arid regions. *Aqua Journal, 68*(6), 431–447.

Pande, C. B., & Moharir, K. (2018). Spatial analysis of groundwater quality mapping in hard rock area in the Akola and Buldhana districts of Maharashtra, India. *Applied Water Science, 8*(4), 1–17.

Pande, C. B., Moharir, K. N., Singh, S. K., & Dzwairo, B. (2019a). Groundwater evaluation for drinking purposes using statistical index: Study of Akola and Buldhana districts of Maharashtra, India, Environment. *Development and Sustainability (A Multidisciplinary Approach to the Theory and Practice of Sustainable Development)*. https://doi.org/10.1007/s10668-019-00531-0.

Pande, C. B., Moharir, K. N., Singh, S. K., & Varade, A. M. (2019b). An integrated approach to delineate the groundwater potential zones in Devdari watershed area of Akola district.

Maharashtra, Central India in Environment, Development, and Sustainability. https://doi.org/10.1007/s10668-019-00409-1.

Piper, A. M. (1994). A graphic procedure in the geochemical interpretation of water-analyses. *Eos, Transactions American Geophysical Union, 25*(6), 914–928.

Saranya, U., & Lancelet, T. S. (2019). A micro level study on the environmental issues of Munroe Island, Kollam, Kerala. *International Interdisciplinary Research Journal, 9*(1), 178–193.

Sawyer, G. N., Mccartly, D. L., & Parkin, G. F. (2003). *Chemistry for environmental engineering and science* (5th ed., pp. 587–590). New York, NY: McGraw-Hill.

Subba Rao, N. (2012). PIG: A numerical index for dissemination of groundwater contamination zones. *Hydrological Processes, 26*, 3344–3350.

Tiwari, T. N., & Mishra, M. (1985). A preliminary assignment of water quality index to major Indian rivers. *Indian Journal of Environmental Protection, 5*(4), 276–279.

WHO. (2011). *WHO guidelines for drinking water quality*. 4th edn. World Health Organization, Geneva, pp.1–564.

Chapter 18
GIS-Based Water Quality Assessment of Chalakudy River Basin, Southern Western Ghats, India

R. Resmi, A. Krishnakumar, and K. Anoop Krishnan

Contents

18.1 Introduction 353
18.2 Description of the Study Area 354
18.3 Materials and Methods 355
18.4 Results and Discussions 358
18.5 Hydrogeochemical Facies 364
18.6 Water Quality Index 365
18.7 Conclusion 365
References 367

18.1 Introduction

Water is vital basic resource for the sustenance of life (Pande et al. 2018a). The attitude of the humanity to water depends on its abundance, availability and quality. This resource becomes the most valuable commodity and a matter of public concern when portable water becomes scarce (Pande and Moharir 2018; Pande et al. 2017). The activities like industrialization, use of modern agriculture practices and other development programs coupled with population explosion pose great threat to this limited resource (Pande and Moharir 2015). Thus, the quality of water source may vary due to changing in source of pollution, increasing draw off good quality water, natural depletion of the resource and changing pattern of land use, etc. (Pande et al. 2018b). Ground water resources are varying with space and time. These resources

R. Resmi · A. Krishnakumar (✉) · K. A. Krishnan
ESSO (NCESS), Ministry of Earth Sciences, Govt of India, Thiruvananthapuram, Kerala, India
e-mail: resmi.ea@ncess.gov.in; sree.anoop@ncess.gov

C. B. Pande, K. N. Moharir (eds.), *Groundwater Resources Development and Planning in the Semi-Arid Region*, https://doi.org/10.1007/978-3-030-68124-1_18

are in the aquifers below the surface of the earth is one of the most important natural resources of our Country (Khadri and Moharir 2016; Khadri and Pande 2016; Moharir et al. 2017; Pande et al. 2019b). Ground water sources including open wells, springs, etc. are polluted due to anthropogenic activities. Over exploitation of these resources for various purposes like irrigation and drinking may lead to shrinkage of these resources. We have only one percentage of ground water resources that are managed in a proper way for its sustainable utilization. As our country is developing very fastly, the sustainable utilization of these natural resources is very important. Factors controlling ground water resources include, landuse/landcover, geochemistry of the regions, ground water recharge source, water–sediment interactions, etc. Ground water qualities are a major environmental aspect which needs to be analyzed and managed depending on its spatial distribution. Hence, Geographic Information System is widely used to produce ground water quality map and ground water potential zone demarcation. In addition to these, Water Quality Index is widely used to assess drinking water quality.

18.2 Description of the Study Area

The Western Ghats hosts various river basins of many rivers. Almost all rivers in Kerala originate from Western Ghats are flow towards the western side. Chalakudy River originate from Anamalai hills of the Western Ghats, and lies between 10°15′–10°35′ North latitude and 76°15′–76°55′ East longitude (Fig. 18.1). It is the fifth largest river in Kerala with a length of 144 km, and the Chalakudy river basins holds an area of 1704 km^2, falls in Trissur, Palakkad and Ernakulam districts and Coimbatore district of Tamil Nadu. Chalakudy and Periyar rivers are known as twin rivers. There are six dams on Chalakudy. Its major tributaries are the Sholayar, originating from the Anamalai in Tamil Nadu, the Parambikulam and Kuriarkutty originating from the Parambikulam plateau, and these after joining together flow down to first join with Sholayar at about 2 km above Orukombankooty, where Karappara, originating from Nelliyampathy hills, joins. From here, the river is known as Chalakudy puzha. The longest tributary Sholayar originates from the Valparai hills at an elevation of around 2000 m. The river has gained its name since it flows along the banks of the Chalakudy Town, the major settlement along the course of river. This study mainly concentrated in the downstream stretches of Chalakudy River Basin (224.2 km^2) where ground water is especially used for drinking water purposes. Location map of Chalakudy River Basin is shown in Fig. 18.1.

The extreme variation in rainfall pattern and distribution across different altitudes within the river basin has allowed niches for diverse vegetation types to evolve over time. Chalakudy River is one of the very few rivers in Kerala which is having relics of riparian vegetation in substantial level. One-third of the river's length is occupied by protected areas or forests that support wildlife. The Sholayar ranges hold a good percentage of Kerala's evergreen forests. Riparian vegetation is dominated by species such as *Syzigium occidentale*, *Barringtonia acutangula*, etc. these are

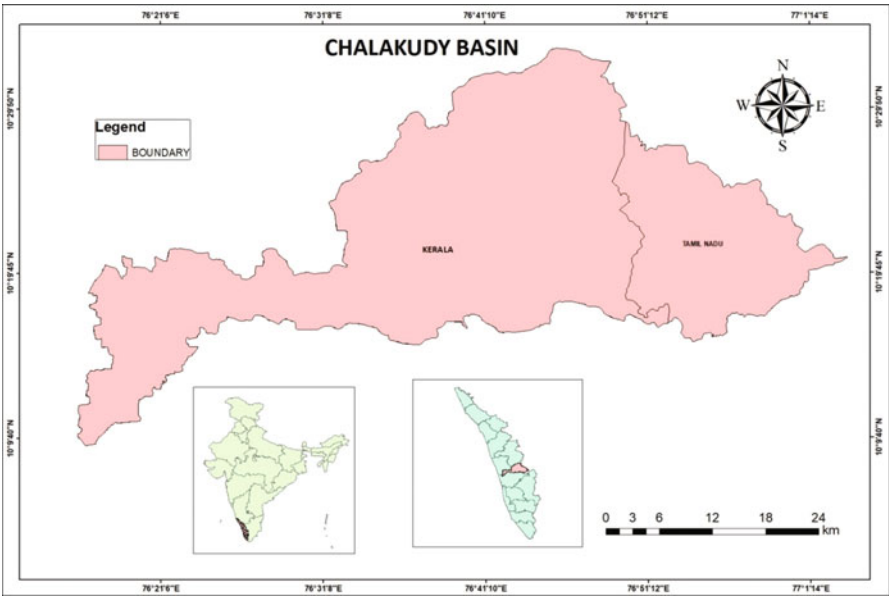

Fig. 18.1 Location map of Chalakudy River Basin

exclusive to riparian habitats. About 234 species of medicinal plants have been identified in this area of which 12 are threatened. Fish diversity in Chalakudy river is one of the highest among all rivers of Kerala, with the highest fish diversity index. Efforts are on to declare the Oxbow Lake at Vynthala near Mala town a Community Reserve. Also recorded are 170 species of butterflies and 231 species of birds from the river basin (Sreeja 2013).

18.3 Materials and Methods

The groundwater quality analysis is study on the geological, geochemistry and hydrogeological conditions. In this study selected 17 samples of groundwater were collected during pre-monsoon season in the month of May 2019. The location of sampling sites in the downstream stretches of CRB is shown in Fig. 18.2. All the samples have been stored in refrigerator at a temperature of 4 °C until the laboratory analyses were completed. The water quality parameters to be analyzed are categorized into cations, anions, nutrients followed by standard analytical techniques provides by APHA, 1998 and all the chemicals used were analytical grade. The physicochemical parameters of water are pH, Electrical Conductivity (EC), Turbidity, Total Dissolved Solids (TDS), alkalinity, Dissolved Oxygen, major cations ($Ca2^{+}$, Mg^{2+}, Na^{+}, K^{+}, and Fe^{2+}), trace elements, major anions ($Hco_{3,}$ Cl, and So_4^{2-}), dissolved silicates and other major nutrients ($Po_{4,}$ No_2, No_3).

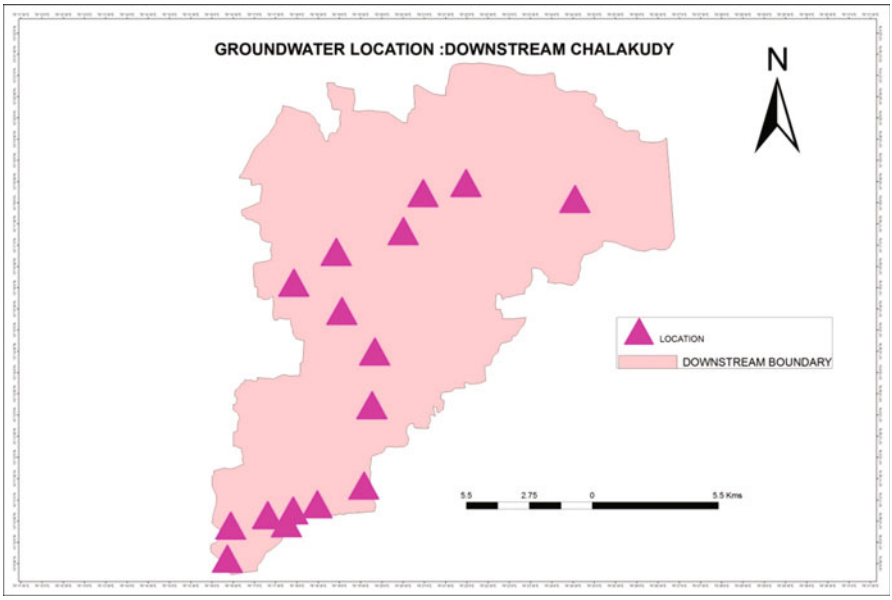

Fig. 18.2 Groundwater sampling location of downstream stretches of Chalakudy River Basin

In situ water quality measurements were done for the estimation of pH, Electrical Conductivity, Dissolved Oxygen, Biochemical Oxygen Demand (BOD), and TDS by using Portable Water Quality Analyzer. Sulphate (SO_4^{2-}) was determined by UV-Vis Spectrophotometer (Shimadzu UV-1800). Samples for cation and trace element analysis were acidified to a pH of <2 by adding nitric acid and they were analyzed by Microwave Plasma Atomic Emission Spectroscopy. The estimation of nutrients such as total phosphate, total nitrate, nitrite and silicate were carried out using San^{++} Automated Wet Chemistry Analyzer Continuous Flow Analyzer (CFA). The software Aqua Chem version 2016 used to create geochemical plots. To evaluate the drinking water quality and to assess the potential health risk to human, the microbial analyses were performed. There is no *E. coli* pollution in the groundwater samples. Hence, drinking water quality was evaluated using water quality Index method.

18.3.1 Spatial Modelling and Surface Interpolation Through IDW

GIS is an effective tool for the management of water resources, and monitoring of groundwater quality mapping also pollution in the air, water and soil on the earth surface (Khadri and Pande 2015c). These can be used to storing managing and displaying the spatial data often encountered in ground and surface water

management. The application of GIS in water resources management includes assessment of the water quality, determining water availability; prevent flooding, understanding the natural setting of the environment, etc. In the present study Spatial Interpolation technique through Inverse Distance Weighted has been used to delineate the distribution of ground water pollutants. Inverse Distance Weighted (IDW) is a method of Interpolation that estimates cell values by averaging the values of sample data points in the neighbourhood of each processing cell (Moharir et al. 2019). Hence GIS modelling gives us a visual representation in to the cause and relationship.

18.3.2 Estimation of Water Quality Index

18.3.2.1 Water Quality Index

Ground water quality index is a most effective tool to monitor the ground water pollution. This can be used effectively in ground water improvement programs. For evaluating Water Quality Index, the hydrochemical parameters of water samples are measured and noted. For calculating water quality index assigning of a weight for each ground water parameters (w_i), computing of relative weight (W_i) and quality rating scale (q_i) are needed (Pande et al. 2019a). Weight and Relative Weight determined for this study is shown in Table 18.1. Weighted values were assigned according to relative significance of comprehensive quality of water which range from 1 to 5 (Srinivasamoorthy et al. 2008). The highest weight of 5 was assigned to parameters, that have critical health effects and whose presence above the critical concentration limits could limit the usability of the resource for the domestic and

Table 18.1 Weight and relative weight for determined ground water parameters in this study

Parameters	Standard concentration	Weight (w_i)	Relative weight (W_i)
pH	6.5–8.5	4	0.08
TDS	500	4	0.08
Alkalinity	200	3	0.06
Hardness	200	4	0.08
Do	5	5	0.1
Ca	75	2	0.04
Mg	30	2	0.04
No_3	45	5	0.1
No_2	3	5	0.1
Phosphate	5	5	0.1
Chloride	250	3	0.06
Na	200	2	0.04
K	12	2	0.04
So_4	200	4	0.08

Table 18.2 Range of WQI and type of water (Srinivasamoorthy et al. 2008)

Range	Type of water
<50	Excellent water
50–100	Good water
100–200	Poor water
200–300	Very poor water
>300	Unsuitable

drinking purposes. DO, NO_2, NO_3, and PO_3 were assigned the highest weight because of their importance in the water quality assessment (Ramakrishnalah et al. 2009). The various classes of water quality index for drinking purpose is shown in the Table 18.2. Other parameters like pH, TA, TH, Cl, Ca, Mg, Na, K, TDS, and SO_4 were assigned weight between 1 and 5 depending on their importance in water quality determination. Fourteen physicochemical parameters in mg/L ($n = 14$) were used in this calculation.

$$W_i = w_i / \sum_{i=1}^{n} w_i \tag{18.1}$$

q_i was computed using determined concentration of groundwater parameter (c_i) and drinking water standard (S_i) values for each groundwater parameter based on WHO (2011). q_i was computed using Eq. (18.2)

$$q_i = \frac{c_i}{s_i} \times 100 \tag{18.2}$$

For calculating water quality index, the SI is first determined using the Eq. (18.3)

$$s_i = W_i \times q_i \tag{18.3}$$

Finally, WQI was computed using computed q_i and W_i as shown in the Eq. (18.4)

$$\mathrm{WQI} = \sum_{i=1}^{n} \mathrm{SI} \tag{18.4}$$

18.4 Results and Discussions

The groundwater analysis is so important for the nearby coastal zone with semiarid region. In this study, water quality index was measured based on the water quality parameters. In this context, piper trilinear diagram is an understanding of the

groundwater quality ranges with the known which groundwater quality changes in the area. The systematic understanding of the groundwater quality ranges and water quality index are measured for the development of groundwater planning and management in the semiarid region (Khadri and Pande 2015a).

18.4.1 Spatial Variation of Ground Water Parameters

18.4.1.1 pH

The nature of water in an aquatic environment can be determined by pH. It is the negative logarithm of the concentration of hydrogen ion in mole per litre. It is a measure of an acidic or basic (alkaline) nature of solution (Khadri et al. 2013). The principal component regulating ion pH in natural waters is the carbonate, which comprises CO_2, H_2CO_3, and HCO_3 (APHA 1995). In pure water, the dissociated molar concentrations of H^+ and OH^- ions are each being 10^{-7} moles per litre equivalent to pH of 7. If the H^+ ions exceed the OH^- as in acid solutions, the pH value is less than 7, while the pH is more than 7, if the OH^- ions exceed the H^+ ions as in basic solutions. High pH induces the formation of tri halomethanes, which are toxic. pH below 6.5 starts corrosion in pipes, thereby releasing toxic materials such as Zn, Pb, Cd and Cu. In the water supplies pH is an important factor in fixing alum dose in drinking water treatment. At Chalakudy, pH ranges from 4.51 to 7.34 mg/L. Most of the samples have lesser value than permissible limit and less than 6.5 (BIS 2012). pH value below 7 showed that all samples are slightly acidic in nature. The spatial variation map of about 70% of the study area is dominated with the pH that are slightly acidic in nature. The highest pH is observed in the Southern part of the study area (Fig. 18.3).

18.4.1.2 EC

Electrical conductivity is a measure of total ionic concentration of water. This parameter is influenced by Cl^-, Na^+, K^+ and so on. It is the numerical expression of aqueous solution to carry an electric current. The conductivity of water comes from ionisable of the dissolved salts and inorganic compounds in it. It was measured in the unit of μs cm^{-1}. Water with high conductivity is objectionable to both drinking and industrial purposes. In Chalakudy River Basin, the obtained EC value ranges from 106 to 2175 μs cm^{-1}. Out of the 17 ground water samples except three samples are under the permissible limit (WHO 2006). The low elevated region of the study area shows high values of EC. This is in the downstream stretches of Chalakudy river basin and EC values are comparatively lower in the northern stretches.

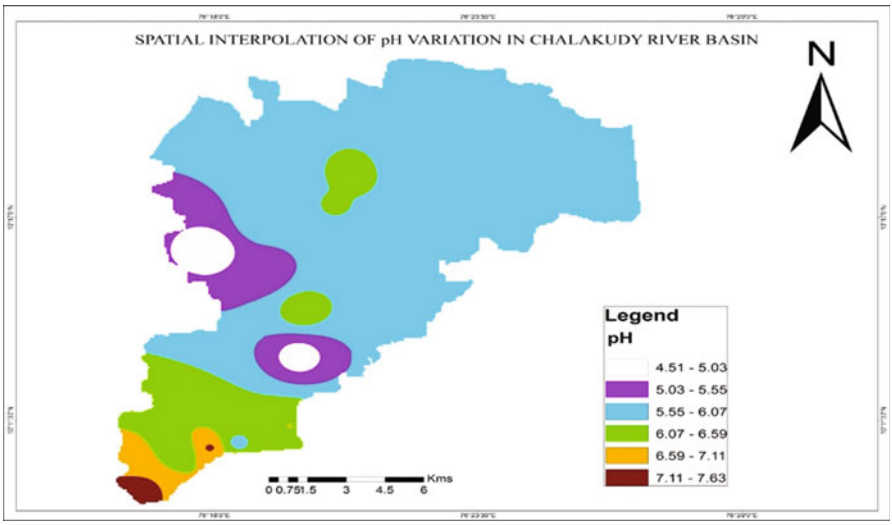

Fig. 18.3 Spatial variation map of pH

18.4.1.3 TDS

Dissolved solids denote mainly the various kinds of minerals present in the water. Natural waters, dissolved solids are composed mainly of carbonates, bicarbonates, chlorides, irons, phosphates, and nitrates of calcium, magnesium and iron. Concentration of dissolved solids is important parameter in drinking water and other water quality standard. In Chalakudy River Basin TDS values ranged from 66 to 1419 mg/L. Most of the samples are under permissible limit. Majority of the study area has TDS value less than 500 mg/L and falls in the fresh water group except some areas found in eastern part of the study area.

18.4.1.4 Turbidity

The degree of turbidity is often considered as measure of degree of pollution. The suspended particles, soil particles, discharge effluents, decomposed organic matter, total dissolved solids as well as the microscopic organisms increase the turbidity of water which interferes with the penetration of light (APHA 2005). Turbidity due to large volume of sediments will reduce light penetration, thereby suppressing photosynthetic activity of algae phytoplankton. It is actually expressed in terms of the optical property (Tyndall effect) in which the light is scattered by the suspended particles of the water column. In Chalakudy River Basin the turbidity ranges from 0.13 to 17.35 NTU. In Chalakudy River Basin most of the turbidity values are below permissible limit.

18.4.1.5 Salinity

A salinity problem related to water quality occurs if the total quantity of salts in the irrigation water is such that the salts accumulate in the root zone to the extent that crop yields are adversely affected. The salinity level of irrigation water can be determined directly by evaporation of a known quantity of water and measuring the residue of dissolved salts that remain. The Salinity of ground water samples of Chalakudy river basin ranges from 0.03 to 1.10 PSU. The values are within the permissible limit.

18.4.1.6 Alkalinity

Alkalinity or the buffering capacity of waters refers how well it can neutralize acidic pollution and resist changes in pH. Alkalinity measure the amount of alkaline compounds in the water, such as carbonates, bicarbonates and hydroxides. These compounds and natural buffers can remove excess hydrogen ions. The alkalinity of water is controlled by the sum of the titratable bases. It is mostly taken as an indication of the concentration of carbonate, bicarbonate and hydroxide, but may include contributions from borate, phosphates, silicates and other basic compounds. In Chalakudy river basin, alkalinity values ranges from 13.90 to 115.9 mg/L. The values are within the permissible limit proposed by WHO (2000).

18.4.1.7 Chloride

Chlorides occur naturally in all types of water. The presence of chloride in water is because of this solution of salt deposits, discharge of domestic sewage, irrigation drainage and sea water inclusion. It may create problems in boilers. Chloride in drinking water is not harmful to human beings. However, higher concentration may affect person suffering from heart and kidney diseases. In portable water, the salty taste produced by chloride concentration is variable and depends on the chemical composition of water. The chloride concentration at Chalakudy water sample ranged from 10.13 to 233.19 mg/L. In Chalakudy, all the groundwater samples are under permissible limit.

18.4.1.8 Total Hardness

The hardness of natural waters depends mainly on the presence of dissolved calcium and magnesium salts. The total content of these salts is known as general hardness, which can be further divided in to carbonate hardness (determined by concentration of calcium and magnesium hydrocarbonates), and non-carbonate hardness (determined by calcium and magnesium salts of strong acids). Hydrocarbonates are

transformed during the boiling of water into carbonates, which usually precipitate. Therefore carbonate hardness is also known as temporary hardness, whereas the hardness remaining in the water after boiling is called constant. Sulphates and chlorides of these cations can cause permanent hardness which cannot be removed by simple boiling. In general practice, the hardness is measured as concentration of only Ca and Mg (as $CaCO_3$) which are far high in concentration over other cations. In Chalakudy river basin, Total hardness ranges from 13.90 to 148 mg/L. The values are within the permissible and desirable values recommended by WHO.

18.4.1.9 Dissolved Oxygen

Dissolved oxygen is an important water quality parameter of aquatic environment as it sustains aquatic life. The amount of oxygen in water is called dissolved oxygen. It is an excellent indicator of physical, chemical and biological condition of water. It varies with temperature, salinity, turbulence, the photosynthetic activity of algae and plants and atmospheric pressure. Its presence is essential to maintain the higher forms of biological life in the water. Non polluted surface waters are normally saturated with dissolved oxygen, oxygen can be rapidly removed from the water by discharge of the oxygen demanding waters. Low oxygen concentration is generally associated with heavy contamination by organic matter. In Chalakudy river basin the dissolved oxygen values ranges from 2.86 to 7.39 mg/L. Almost all the values are out of the range of permissible value recommended by BIS.

18.4.1.10 Nitrate

Nitrite and nitrate are naturally occurring ions that are part of nitrogen cycle. Excess of *N* in any kind is the indication of pollution. High level of nitrate is generally due to excessive use of fertilizers in agriculture, domestic effluent, sewage disposal, industrial discharges, leachable form refuse dumps these all have become a serious problem. Nitrite ions are formed by the microbial reduction of nitrate or oxidation of ammonia. The presence nitrite indicates the presence of incomplete oxidation of organic matter or deficiency of oxygen or receiving excess quantity of contaminants in water system. In Chalakudy River Basin the nitrate and nitrite values range from 0.00 to 0.12 mg/L and 0.28 to 4.9 mg/L, respectively. These are within the permissible limit.

18.4.1.11 Phosphate

Phosphorus is one of the key elements necessary for growth of plants and animals. Phosphorus usually occurs in nature as phosphate. Phosphorus in elemental form is very toxic and is subject to bioaccumulation. They may exist in solution as particles, loose fragments or in bodies of aquatic organisms. Phosphate which is bond to plant

or animal tissue is known as organic phosphate, phosphate that is not associated with organic materials is known as inorganic phosphate. Both forms are present in aquatic systems and may be either dissolved in water or suspended. Rainfall can cause varying amounts of phosphates to wash from farm soils in to nearby waterways. Phosphates will stimulate the growth of plankton and aquatic plants which provide food for fish. This increased growth may cause an increase in the fish population and improve the overall water quality. However, if an excess of phosphates enters the water way, algal and aquatic plants will grow wildly, choke up the water way and use up large amounts of oxygen. This condition is known Eutrophication. Phosphate are not toxic to people or animals unless they are present in very high levels. Digestive problem could occur from extremely high level of phosphate (Kumar et al. 2014). In Chalakudy river basin phosphate values range from 0.0011 to 0.1194 mg/L The values are within the range recommended by WHO. The phosphate variation is slightly increasing from the northern side of the study area to the southern parts.

18.4.1.12 Sulphate

Most natural water contains sulphates. The origin of most sulphate compounds is due to the oxidation of sulphate ores, the presence of shales or the industrial wastes. A considerable amount of sulphate is added to hydrologic cycle through atmospheric precipitation (acid rain). Along with excessive calcium and magnesium dissolved in waters. Sulphate salts are mostly soluble and impart hardness to water. High concentration of SO_4^{2-} could cause a cathartic action on human beings and can also cause respiratory problems. In Chalakudy river basin the sulphate value ranges from 0.08 to2.8 mg/L. These are below the permissible limit.

18.4.1.13 Calcium

Calcium occurs in water naturally. One of the main reasons for the abundance of calcium in water is its natural occurrence in the earth's crust. Calcium is also a constituent of coral. Sea water contains approximately 400 ppm calcium. Rivers generally contain 1–2 ppm calcium, but in lime areas, rivers may contain calcium concentrations as high as 100 ppm. It may dissolve from rocks such as limestone, marble, calcite, dolomite, gypsum, fluorite and apatite. Calcium is determinant of water hardness, because it can be found in water as Ca^{2+} ions. Usually the concentration of Ca in freshwater is greater than that of Mg as the former is abundant in the earth crust compared to the later. In Chalakudy river basin Ca ranges from 2.96 to 142.95 mg/L. All most all samples are within permissible limit.

18.4.1.14 Magnesium

Magnesium is also an important cation in surface water. Magnesium is usually less abundant in water than calcium because magnesium is found in Earth's crust in much lower amounts as compared to calcium, the Ca to Mg reaches up to 10. Magnesium arises principally from the weathering of rocks containing ferromagnesium minerals and from some carbonate rocks. In Chalakudy river basin ground water samples magnesium varies from 1.32 to 27.65 mg/L. These magnesium values are within the permissible limit.

18.4.1.15 Sodium

Sodium is one of the most abundant alkali metals in natural waters. The sodium ion is ubiquitous in water. Salinity intrusion, mineral deposits, sea water spray, and sewage effluents, contribute significant quantities of sodium to water. In the study area, the quantity of sodium in the groundwater samples varies from 4.01 to 34.85 mg/L, under desirable limit. The natural contributors of sodium to the groundwater are the minerals present in the rocks of the region. The salts of sodium are highly soluble in water and impart softness to water (WHO 2000).

18.4.1.16 Potassium

Potassium though found comparatively in smaller amounts, it plays a vital role in the metabolic activity of freshwater organisms and hence considered to be an important macronutrient. It occurs widely in the environment including all-natural waters. The salts of K are highly soluble in water and impart softness. It plays a vital role in the metabolic activity of fresh water organisms. Potassium occurs in various minerals, from which it may be dissolved through weathering processes. In Chalakudy river basin the potassium in groundwater samples ranges from 0.25 to 6.74 mg/L. These are under permissible limit recommended by WHO (2011).

18.5 Hydrogeochemical Facies

The Piper (1944) diagram is very useful in classification of water on the basis of its chemical characteristics. The hydrochemical evolution can be understood by plotting milli equivalent percentages of the major cations and anions in piper trilinear diagram (Khadri and Pande 2015b). In the study area groundwater types were distinguished and grouped by their position in piper diagram. The central diamond field, provides the overall character of the water. Water types are identified using piper plot shown in Fig. 18.4. Based on the piper trilinear diagram the type of water

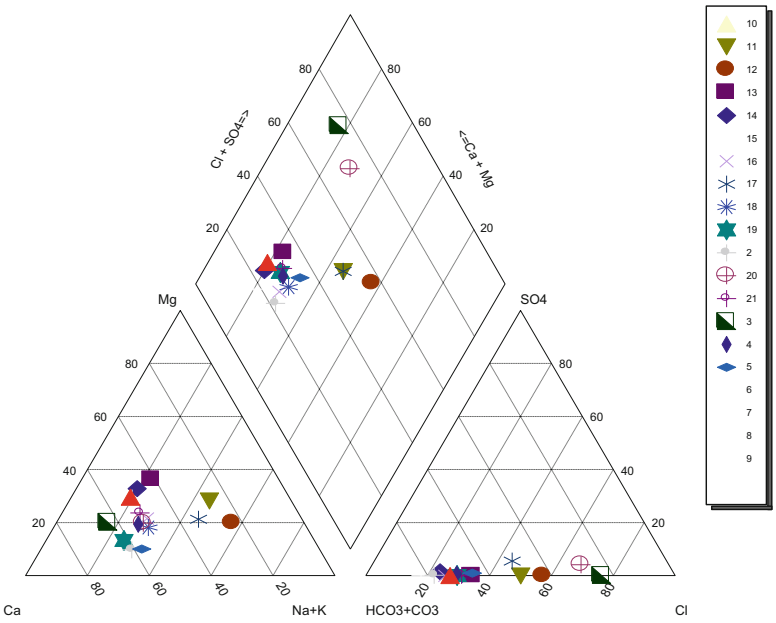

Fig. 18.4 Piper trilinear diagram

predominates in the study area is $CaHCO_3$ type. The hydrochemical facies indicates that alkaline earth exceeds alkalies and weak acid dominant chemical properties of groundwater.

18.6 Water Quality Index

The various classes of water quality index for drinking purpose is shown in the Table 18.1 and computed water quality index is shown in the Table 18.3. It shows that majority of samples fall in the class of excellent type. None of the samples fall in the class of unsuitable water type is shown in the Table 18.2. The Spatial Variation map of Water Quality Index in the downstream area of Chalakudy River Basin is shown in the Fig. 18.5.

18.7 Conclusion

The study mainly focuses on groundwater samples of downstream stretches of Chalakudy river basin. Experiments were conducted on the groundwater sample to find out the amount of physical and chemical parameters such as pH, EC, Turbidity,

Table 18.3 Computed water quality index for each ground water samples

Sample ID	Location name	WQI	Category
1	Manjali	39.8851	Excellent water
2	Kanakan Kadavu	67.7497	Good water
3	North Kuthiyathode	46.07582	Excellent water
4	Paithuruth	45.9643	Excellent water
5	Mozhikkadavu Bridge	45.1145	Excellent water
6	Ayiroor	35.3422	Excellent water
7	Puvathussery Ferry	41.2369	Excellent water
8	Pallisheri	20.7247	Excellent water
9	Annamanada Bridge	39.4781	Excellent water
10	Thikoottam Bridge	15.5639	Excellent water
11	Kadukutty Bridge	22.0067	Excellent water
12	Kudungapuzha	22.23131	Excellent water
13	Muringoor	32.9364	Excellent water
14	Meloor	27.6405	Excellent water
15	Bhagavatham Village	25.2015	Excellent water
16	Vettylappara	19.9790	Excellent water
17	Muzhikkakadavu	26.2671	Excellent water

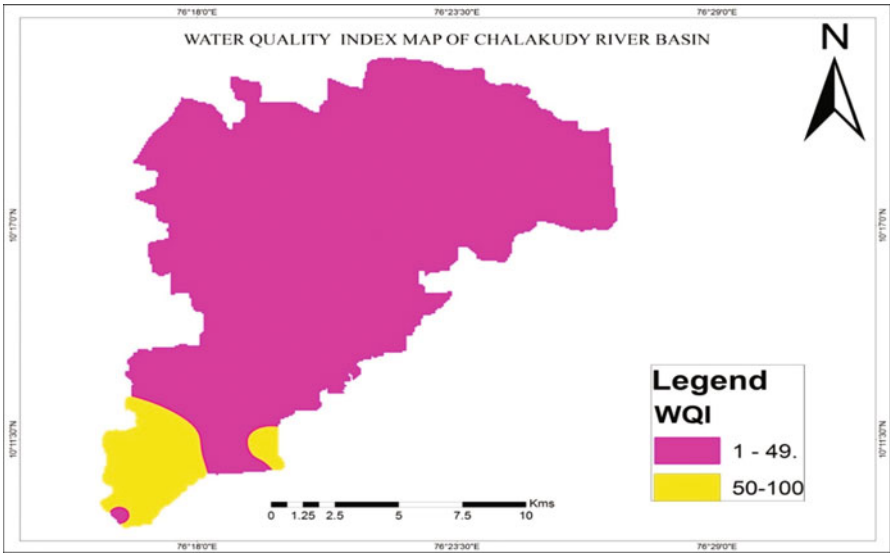

Fig. 18.5 Spatial variation of water quality index in Chalakudy River Basin

Salinity, alkalinity, Total dissolved salts, sodium, potassium, calcium, Magnesium, sulphate, phosphate, nitrate and nitrite. All parameters are tabulated. Then these values are checked with WHO standards. To evaluate suitability of ground water for drinking, 17 ground water samples were collected from selected wells and were

analyzed for various physicochemical parameters. Water Quality Index was computed using relative weight and quality rating scale. Due to the over exploitation and improper waste disposal, especially in urban areas, WQI is one of the most effective tools to communicate information on quality of water to the decision makers. WQI is an important parameter for the assessment and management of ground water resources. The water quality index ranges from 15.56 to 67.75. It shows that 95% of samples are under excellent and 5% of samples have good category. Therefore, there is a need of protection of this area from contamination. Based on the piper trilinear diagram the type of water predominates in the study area is $CaHCO_3$ type. The Spatial Variation map of computed WQI were produced using IDW interpolation techniques in GIS. Assessment of spatial variation of ground water quality led to a better understanding of ground water quality in Chalakudy River Basin. At present the quality of well water in the area is quite good for consumption.

Acknowledgements The authors are grateful to the Director, NCESS for providing necessary facilities and support to do the work. One of the authors (RR) is grateful to the University of Kerala for the University Research Fellowship to execute the research work.

References

APHA. (1995). *Standard methods for the examination of water and wastewater* (19th ed.). New York: American Public Health Association Inc.

APHA. (2005). *Standard methods for the examination of water and wastewater* (21st ed.). Washington, DC: American Public Health Association.

Bureau of Indian Standards. (2012). *Specification for drinking water. IS: 10500*. New Delhi: BIS.

Khadri, S. F. R., & Moharir, K. (2016). Characterization of aquifer parameter in basaltic hard rock region through pumping test methods: A case study of Man River basin in Akola and Buldhana Districts Maharashtra India. *Modeling Earth Systems and Environment, 2*, 33.

Khadri, S. F. R., & Pande, C. (2015a). Groundwater quality mapping using hydrogen chemistry and geostatistical analyst of Mahesh River Basin, Akola and Buldhana District, Maharashtra, India. *International Journal of Research, 2*(10), October-2015.

Khadri, S. F. R., & Pande, C. (2015b). Analysis of hydro-geochemical characteristics of groundwater quality parameters in hard rocks of Mahesh River Basin, Akola, and Buldhana Dist. Maharashtra, India, using geo-informatics techniques. *American Journal of Geophysics, Geochemistry and Geosystems, 1*(3), 105–114.

Khadri, S. F. R., & Pande, C. (2015c). Ground water quality mapping for Mahesh River Basin in Akola and Buldhana Districts of (MS) India using interpolation methods. *International Journal on Recent and Innovation Trends in Computing and Communication, 3*(2), 113–117.

Khadri, S. F. R., & Pande, C. (2016). Ground water flow modeling for calibrating steady state using MODFLOW software: a case study of Mahesh River basin, India. *Model Earth System Environment, 2*, 39. https://doi.org/10.1007/s40808-015-0049-7.

Khadri, S. F. R., Pande, C., & Moharir, K. (2013). Groundwater quality mapping of PTU-1 Watershed in Akola district of Maharashtra India using geographic information system techniques. *International Journal of Scientific & Engineering Research, 4*(9), September-2013 1856.

Kumar, R. P., Ranjan, R. K., Ramanathan, A. L., Singh, S. K., & Srivastava, P. K. (2014). Geochemical modeling to evaluate the mangrove forest water. *Arabian Journal of Geosciences, 13*, 1513–1523.

Moharir, K., Pande, C., & Patil, S. (2017). Inverse modeling of Aquifer parameters in basaltic rock with the help of pumping test method using MODFLOW software. *Geoscience Frontiers, 8*(6), 1385–1395.

Moharir, K., Pande, C., Singh, S., Choudhari, P., Rawat, K., & Jeyakumar, L. (2019). Spatial interpolation approach-based appraisal of groundwater quality of arid regions. *Aqua Journal, 68* (6), 431–447.

Pande, C. B., Khadri, S. F. R., Moharir, K. N., & Patode, R. S. (2017). Assessment of groundwater potential zonation of Mahesh River basin Akola and Buldhana districts, Maharashtra, India using remote sensing and GIS techniques. *Sustainable Water Resources Management*. https://doi.org/10.1007/s40899-017-0193-5. ISSN 2363-5037.

Pande, C. B., & Moharir, K. (2015). GIS-based quantitative morphometric analysis and its consequences: a case study from Shanur River Basin, Maharashtra India. *Applied Water Science, 7*(2), 23.

Pande, C. B., & Moharir, K. (2018). Spatial analysis of groundwater quality mapping in hard rock area in the Akola and Buldhana districts of Maharashtra, India. *Applied Water Science, 8*(4), 1–17.

Pande, C. B., Moharir, K. N., Singh, S. K., & Dzwairo, B. (2019a). Groundwater evaluation for drinking purposes using statistical index: Study of Akola and Buldhana districts of Maharashtra, India. *Environment, Development and Sustainability (A Multidisciplinary Approach to the Theory and Practice of Sustainable Development)*. https://doi.org/10.1007/s10668-019-00531-0.

Pande, C. B., Moharir, K. N., Singh, S. K., & Varade, A. M. (2019b). An integrated approach to delineate the groundwater potential zones in Devdari watershed area of Akola district, Maharashtra, Central India. *Environment, Development, and Sustainability*. https://doi.org/10.1007/s10668-019-00409-1.

Pande, C. B., Moharir, K. N., Khadri, S. F. R., & Patil, S. (2018b). Study of land use classification in the arid region using multispectral satellite images. *Applied Water Science, 8*(5), 1–11.

Pande, C. B., Moharir, K. N., & Pande, R. (2018a). Assessment of morphometric and hypsometric study for watershed development using spatial technology – A case study of Wardha river basin in the Maharashtra, India. *International Journal of River Basin Management*. https://doi.org/10.1080/15715124.2018.1505737.

Piper, A. M. (1944). A graphic procedure in the geochemical interpretation of water analyses. *Transactions American Geophysical Union, 25*, 914–928.

Ramakrishnalah, C. R., Hivalah, S., & Raganna, C. (2009). Assessment of water quality index for the ground water in Tumkur Taluk, Karnataka State, India. *European Journal of Chemistry, 6*, 523–530.

Sreeja, K. G. (2013). *Emergent non agrarian livelihoods and resource linkages in the agroecosystems of a river basin: A case study of Chalakudy river basin, Kerala, Thesis submitted to School of Natural Sciences and Engineering*. Bengaluru: National Institute of Advanced Studies, Indian Institute of Science.

Srinivasamoorthy, K., Chidambaram, M., Prasannaa, M. V., Vasanthavigar, M. P., & Anandhan, P. (2008). Identification of major sources controlling groundwater chemistry from a hard rock terrain, a case study from Metturtaluk, Salem district, Tamilnadu, India. *Journal of Earth System Science, 117*, 49–580.

World Health Organization. (2000). *Guidelines for drinking water quality* (3rd ed., p. 2000). Geneva: WHO.

World Health Organization. (2006). *Guidelines for drinking water quality, recommendations* (Vol. 1, 3rd ed.). Geneva: World Health Organization.

Chapter 19
Groundwater Resources Management Using Remote Sensing and GIS

Rohit Sambare, Vishal Singh, and Sanjay Kumar Jain

Contents

19.1 Introduction 369
19.2 Groundwater Mapping and Identification of Potential Groundwater Zones 371
19.3 Soil Moisture Estimation Using Remote Sensing Data 374
19.4 GRACE Data for Groundwater Mapping 376
19.5 SAR Interferometry in Groundwater Applications 380
19.6 Role of Geospatial Technology in Groundwater Modelling 381
19.7 Conclusion 382
References 383

19.1 Introduction

The advancement of RS technology since last few decades had opened various avenues for better and rapid management of natural resources (Cracknell 2018). Technological inventions had made data of satellite products from very course spatial resolution ranging from few kilometers to very high resolution data of submeter resolution. Due to these advancements the applications of these data had been increased (Cohen and Goward 2004; Patino and Duque 2013; Tang and Shao 2015). In combination with Geographic Information System (GIS), geospatial data became very easy to handle, process and to be worked upon (Jianping 1997; Xuejun 1997; Münch and Conrad 2007). The remotely sensed data is generally of four types like optical, microwave, thermal, and hyperspectral. The effective usage of

R. Sambare · V. Singh (✉) · S. K. Jain
National Institute of Hydrology, Roorkee, Uttarakhand, India
e-mail: rssambare.nihr@gov.in; vishal18.nihr@gov.in; sjain.nihr@gov.in

C. B. Pande, K. N. Moharir (eds.), *Groundwater Resources Development and Planning in the Semi-Arid Region*, https://doi.org/10.1007/978-3-030-68124-1_19

spatiotemporal, radiometric and spectral resolution of all data proved it to be best tool for rapid management of the natural resources on a large scale (Khadri et al. 2013; Kumar et al. 2015; Patode et al. 2017).

The demand of water is constantly increasing as population increases. There is high stress on all sources of water. Because of this reason today we can't utilize water in an irresponsible manner. So that its need of the hour to monitor and manage the water resources in better way. For effective water resources management, there should be integrated approach to go for it as it is understood water resource is a complex system. Field studies may give exact scenarios on ground but considering the scale of any management practices which are implemented in any nation, it is advisable to go for technologies which give acceptable picture of reality on larger scale. Geospatial technologies exactly come in to picture for this. The large scale, multitemporal, and rapid monitoring of the water resources can be done by this. The integration of EO (earth observation) data with hydrological models have been largely explored and they have yielded good results (Opolot 2013; Sood and Smakhtin 2015; Herman et al. 2018). The use of satellite data is very beneficial in data scarce regions for various inputs. The inventions and advancement of geospatial technology are able to provide various types input data for models like rainfall (TRMM, GPM missions), soil moisture (SMAP or SMOS), evapotranspiration (MODIS), etc. (Jackson et al. 2011; Kim et al. 2017; Running et al. 2017; Skofronick-Jackson et al. 2017; Chan et al. 2018). These satellite products can be used to run large scale hydrological models with good efficiency.

Groundwater adds approximately 35% of freshwater withdrawal from all sources worldwide (4300km^3/year during 1998–2002) (Döll et al., 2012). And its usage is 36% for households, 27% for manufacturing, and 42% for agriculture (Jing et al. 2020). Therefore, global stress on water resources has also affected severely to the quantity and quality of groundwater resources. Generally, remote sensing has the wider applications on the surface which are visible on the ground. Because the principle of remote sensing itself says it will provide the data carried by reflected electromagnetic waves. The majority of reflection generally occurs on surface. But with research in the geospatial technology and interpretation of remotely sensed indicators has led the researchers in finding out more usage of it in the groundwater also. The EO data has been useful in preparing the data inputs which are indicators of the potential groundwater recharge zones. Soil moisture which can be estimated by satellite data also indicates that water is available in vadose zone or shallow aquifers. There is continuous innovations and development of methodologies in this technology. In this book chapter, various applications of geospatial technology in the groundwater monitoring and its management will be discussed.

19.2 Groundwater Mapping and Identification of Potential Groundwater Zones

It is very important task in any drinking water management plan especially in arid regions that to identify the potable groundwater resources which can be sustainable for longer periods. It is well understood that remote sensing technology is directly used for mapping various features on surface of earth. The groundwater flow into the ground, interflow and aquifer characteristics is dependent on surface features. Therefore, this hidden water resource should be mapped based on derivative techniques. Hence monitoring surface features will helpful in groundwater prospect mapping. These maps can be very useful for field engineers and hydrogeologists. The hydrogeological features are mapped and monitored using high resolution satellite imageries. These maps are generally very course scaled like 1:1,00,000 to 1: 1,000,000 scale depending upon the application and scale of the project.

NRSC (National Remote Sensing Center) under the aegis of ISRO (Indian Space Research Organization), India have prepared countrywide HGM (Hydro Geo-Morphological) maps for groundwater prospect mapping on 1: 50,000 scale with the help of remote sensing and GIS technology. This work is done to support the National Drinking Water Project. In the process of making HGM maps there are five basic thematic maps are created. They are as follows

- Base map.
- Lithology map.
- Structural map.
- Geomorphology map.
- Hydrology map.

Base map is a map which contains general geographic information about region. Its main contents are name of the locations or boundaries which does not change their locations such as administrative boundaries, highways, roads, forests. In lithology, maps are prepared to give information about the geochemical, mineralogical, and physical properties of the rocks visible on the surface. Structural maps give the information regarding the geological structures such as folds, faults, lineaments, and fractures. In geomorphological maps, there is information regarding the landforms, surface and subsurface materials. Hydrological maps give the hydrological regimes of the area or watershed. There are many input layers for preparing the final groundwater prospects maps. These are administrative boundaries, settlement, road network, railway network, drainage, waterbody, spring rainfall data, wells, irrigated area, lithology, structures, and geomorphology. Then there are different layers which are derived from all these layers. The derivative layers are hydrogeology and recharge structures both in line and polygon layers. In final steps groundwater prospect maps are created (Fig. 19.1).

The contents of the final groundwater prospects maps three kinds of information: (1) reference information, (2) spatial data relevant to groundwater, (3) legend/index. All these information is categorized into 21 components. They are as follows:

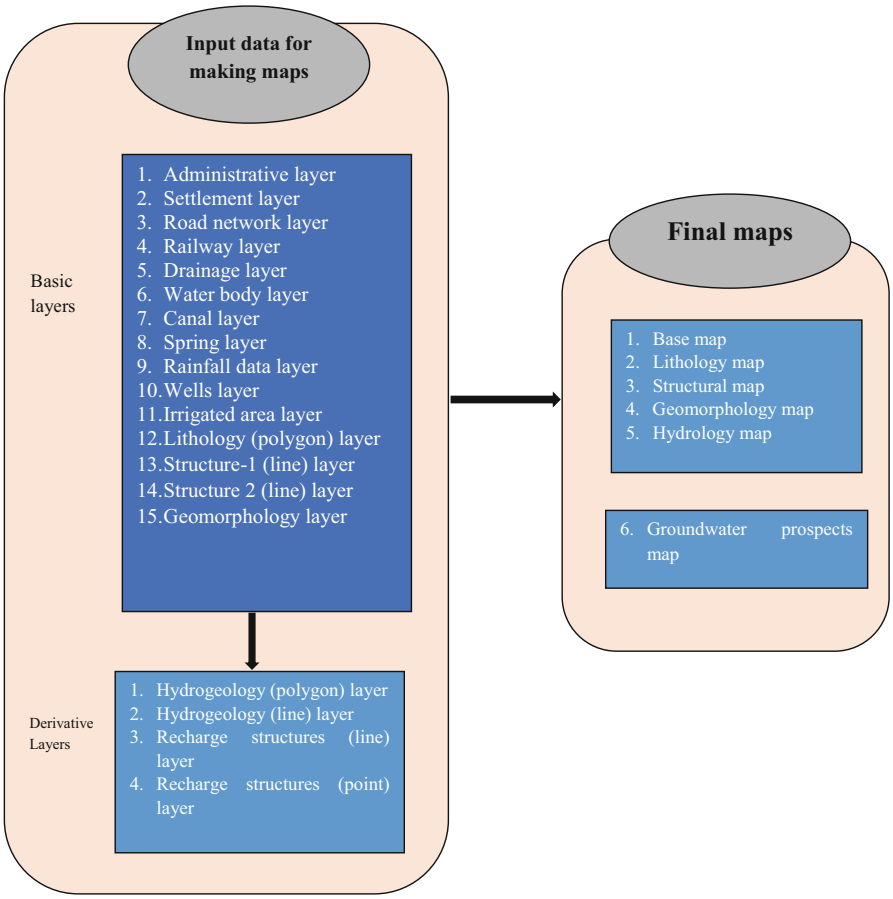

Fig. 19.1 Components of digital groundwater prospects maps (Reddy et al. 2011)

- Title of the Map.
- Method followed for preparing the Map.
- Scale of the Map.
- Map number—Survey of India 1:50,000 scale topo sheet index number.
- Administrative area covered by the map.
- Geographical directions of the map area.
- Organization which has copy right on the map.
- Input data used for preparing the map.
- Organization which has designed and developed the map layout.
- Organization which has prepared the map.
- Organization which has provided technical guidance for preparing map.
- Organizations which have participated in the preparation of the map.
- Organization which has provided methodology for preparation of the map.
- Organization which has sponsored the mapping work.

- Index for ground water prospect information—Fixed part of the legend.
- Index for hydrological Information—Fixed part of the legend.
- Index for structural Information—Fixed part of the legend.
- Index for base map Information—Fixed part of the legend.
- Body of the map.
- Main Legend of the map—Dynamic part of the legend describes body of the map taking symbols from the fixed part of the legend as well.
- Location map index.

These groundwater prospects map is mainly used for two purposes: (1) to locate the suitable area for groundwater source which can be used for drinking water source in the vicinity of the habitation area, and (2) to identify the suitable area for constructing artificial recharge structures. There is a detailed user manual prepared by NRSC freely available (https://jalshakti-ddws.gov.in/sites/default/files/User%20Manual-HGM%20maps_0.pdf) which had elaborated the detailed procedure of interpreting these HGM maps. Readers can go through this manual for detailed analysis of HGM maps.

According to NITI (National Institution of Transforming India) Aayog report which is the premier think tank of the Government of India in 2019, India will become water stress country by the year of 2025 and water scarce by year of 2050 if correct measures are not taken by authorities (NITI Aayog Report 2019). Therefore, new approaches should be adopted to tackle this problem. To identify the groundwater potential zones traditionally ground based surveys were preferred. But as these are very time taking process the use of remote sensing data and GIS becomes essential. These tools are very cost-effective methods. There are many studies carried out on the basis of MCDA (Multi-Criteria Decision Analysis) based AHP (Analytical Hierarchy Process) method (Arulbalaji et al. 2019). Satty (1980) first developed this AHP technique for the purpose of complex decision-making process. Since then this technique is used in various fields including hydrology. There are various hydrologic, geologic, and morphometric factors which affect the potential of area for groundwater recharge. Slope, rainfall, peak runoff, drainage density, LULC (Land Use Land Cover), soil cover, geologic structures like folds and faults are few of the most important factors which affect groundwater recharge. AHP method integrated with GIS is very effective tool for delineating the suitable area for constructing the groundwater recharge zones. In GIS, thematic layer of each factor is prepared and these all layers are assigned to weightage according to their influence on groundwater flow and storage. These weighing are assigned as per Satty's scale (1–9) by referring previous literatures and field knowledge also. The influence of thematic layer increases with the ascending order of their weightage. PCMs (Pairwise Comparison Matrices) are prepared by comparing all thematic layers. In PCMs, value of 1 is indicated that both thematic layers are equally important and if value increases it show that importance of one thematic layer is increasing with the layers to which it is comparing. Hence "9" is indicating extremely important when compared to another layer. After preparing PCMs, CI (Consistency Index) and CR

(Consistency Ratio) is calculated (Eqs. 19.1 and 19.2). The formula for these is given below.

$$\mathrm{CI} = \frac{\lambda_{\max} - n}{n - 1} \tag{19.1}$$

$\lambda_{\max}$ = Principle Eigen Value computed by Eigen vector technique.
n = Number of factors used in the analysis.

$$\mathrm{CR} = \frac{\mathrm{CI}}{\mathrm{RCI}} \tag{19.2}$$

RCI = Random consistency index value obtained Satty's standard (Saaty 1990).

According to the Satty, the value of the CR should always be less than 0.1, otherwise weightages need to reassessed whole process should be repeated. Now groundwater potential zones can be calculated using weighted overlay analysis method in GIS (Pande et al. 2017, 2018a, b, 2019). The final outputs can be overlaid on any remote sensing images or any georeferenced maps to identify most suitable, moderately suitable and less suitable area for groundwater recharge zones. In similar fashion groundwater potential mapping can be done by selecting proper thematic layers and assigning them proper weights. The summary of this method can be described in following points.

1. Selecting and prioritizing each influencing factor.
2. Preparing PCMs.
3. Calculation of CI and CR.
4. Weighted overlay analysis.

The general methodology is diagram for groundwater recharge zones is given in Fig. 19.2. High resolution optical remote sensing images like Cartosat, LISS 4, Worldview etc. can be used to derive few layers like LULC, lithology or geologic structures and DEM (Digital Elevation Model) can be used for slope, drainage density etc. GIS is effective tool to integrate all this data and process them to get.

19.3 Soil Moisture Estimation Using Remote Sensing Data

Soil moisture can be found in the unsaturated part of the soil column vadose zone of the soil and shallow aquifers (Kwast 2009). It is considered fundamental state variable which has role to play in the land atmosphere interaction including infiltration of water and other solutes (Sadeghi et al. 2015). The estimation of soil moisture by field-based methods will give accurate results but it is very incapable to map the spatial and temporal variability of soil moisture. Optical and thermal remote sensing has very limited capability to penetrate the surface to estimate the soil moisture. The spectra of across visible, near infrared and shortwave infrared ranges i.e., 0.4–2.5 μm

Fig. 19.2 General methodology for delineating potential groundwater recharge zones using AHP

can be used to estimate the soil moisture. There are many researches works since last century to estimate the soil moisture from the spectra of optical remote sensing (Curcio and Petty 1951; Bowers and Smith 1972; Price 1980; Kustas et al. 1994; Ben-Dor and Banin 1995). But microwave or radar technology is more robust method for soil moisture estimation. Any change in soil moisture causes the change in soil dielectric constant. Dielectric constant is one of the most important factors in the radar backscattering from soil. These methods give good results for soil moisture

Fig. 19.3 SMOS satellite (http://www.esa.int/Applications/Observing_the_Earth/SMOS)

estimation from bare earth but it gives poor results for vegetated area due to the scattering from the vegetation as backscattering occurs due to the moisture content of their own. European Space Agency (ESA) had launched SMOS (Soil moisture and Ocean Salinity) mission in 2009 which carried MIRAS (Microwave Imaging Radiometer with Aperture Synthesis) instrument. It detects the microwave waves in the L band (1.4 GHz) (Fig. 19.3). It is basically the telescope which directed toward the earth. SMOS data has been used in the numerous researches works for the soil moisture (Jackson et al. 2011; Kerr et al. 2012; Merlin et al. 2013; Kerr et al. 2016; Deng et al., 2019). SMAP (Soil Moisture Active Passive) is the latest addition in the satellites launched by NASA in 2015 which gives soil moisture products (Fig. 19.4). The satellite is placed in a near polar sun-synchronous orbit. It carries two instruments radar and radiometer which in together is used to measure the soil moisture globally. It gives global composite radar soil moisture product on 3 km resolution. Various research studies have been carried out using SMAP data since its launch (Colliander et al. 2019; Yueh et al. 2019; Mao et al. 2020; Zribi et al. 2020; Zhuang et al. 2020).

19.4 GRACE Data for Groundwater Mapping

GRACE (Gravity Recovery and Climate Experiment) is a unique satellite mission launched as a joint collaboration between NASA (National Aeronautics and Space Administration), USA and German space agency on 17th March 2002 (Fig. 19.5). Twin satellites (GRACE 1 and GRACE 2) are measuring the earth's gravity

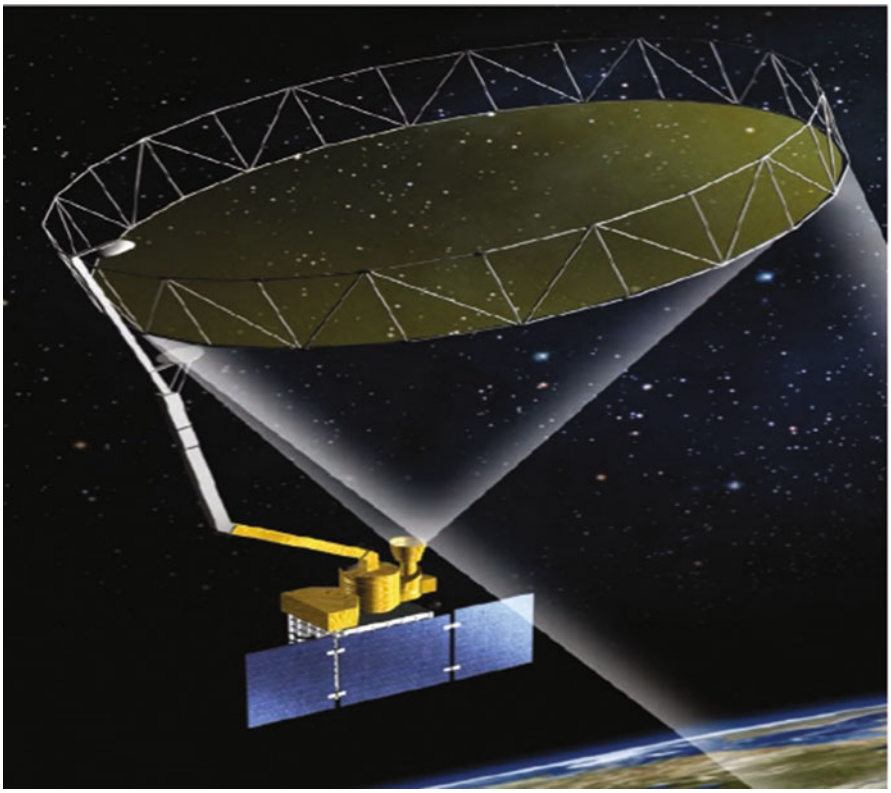

Fig. 19.4 SMAP satellite (https://smap.jpl.nasa.gov/resources/38/smap-large-antenna/)

anomalies on monthly basis with high accuracy (Chen et al. 2016). The earth's gravity changes due to the mass redistribution of the various physical components of the system for example oceans, snow, earth's features, etc. Contribution of the oceanic and atmospheric components can be removed from the GRACE data can be estimated and removed with the help of the numerical model. TWS (Terrestrial Water Storage) remains the factor which is one of the most significant for the earth's mass changes. So, if the change in the storage of the water in the ice, soil, and reservoirs are known then the gravity anomalies can be direct indicator of the groundwater changes.

Currently there many organizations which are responsible for monitoring of the groundwater resources. Instrumentation errors, less spatial coverage of monitoring stations, low frequency of collection of data can produce unreliable data. Remote sensing data integrated with hydrological modelling tools can be effectively used to map and monitor the groundwater scenario at larger scales and with high frequency. GRACE mission is a first of its kind satellite mission which is extensively used for groundwater mapping globally which is an invisible source of water. Its unique feature is that it does not use electromagnetic wave for collection of data. As water is

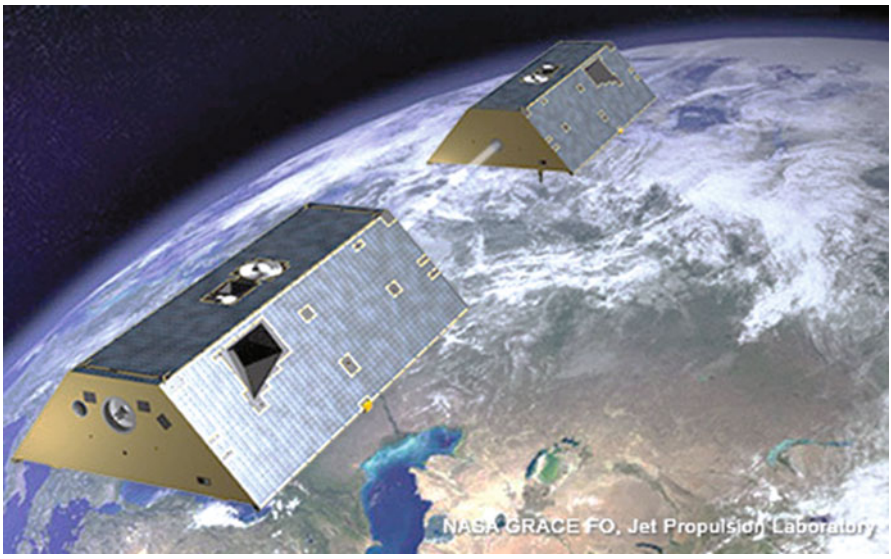

Fig. 19.5 Pictorial representation of GRACE satellites (https://grace.jpl.nasa.gov/mission/grace-fo/)

very difficult natural resource to monitor using traditional remote sensing tools but if studied for basin scale, the changes in mass storage can be highly related indicator for monitoring terrestrial water changes.

The constellation consists of two twin satellites flying in low earth orbit nearly 200 km part from each other in near polar orbit and measure the earth's gravity anomalies. The satellites take almost 30 days to map the whole earth's gravity field. Gravity redistribution of the earth can occur through various causes like changes in water balance, due to surface and deep currents in oceans, variations of mass on earth, glacier changes, etc. This variation in gravity causes the changes the orbital velocity of the satellite. If there is region of strong gravity, there will be acceleration of the leading satellite and distance will be increased between both satellites. When the trailing satellite comes above that region, it will also accelerate and covers the distance and decelerates when region is crossed. It is vice versa for low gravity regions. The distance between both satellites varies for few micrometers. It is estimated that if the water storage changes by 50 Gt, the distance between both satellites will change by 0.5 μm. The applications of GRACE data cover many aspects of hydrology i.e., ice mass changes, sea level changes, terrestrial water changes, etc. Due to course resolution of GRACE data, it is inefficient for the local studies. But in combination with terrestrial hydrological models, it can give insights on processes at higher spatial scale. The GRACE data can also be assimilated with land data assimilation models for greater accuracy.

Data from these satellites have been used in extensive studies and it had been used to monitor some of the biggest aquifer of the world. As mentioned earlier, 30 days are needed to measure earth's gravity field hence the gravity grids can be acquired on

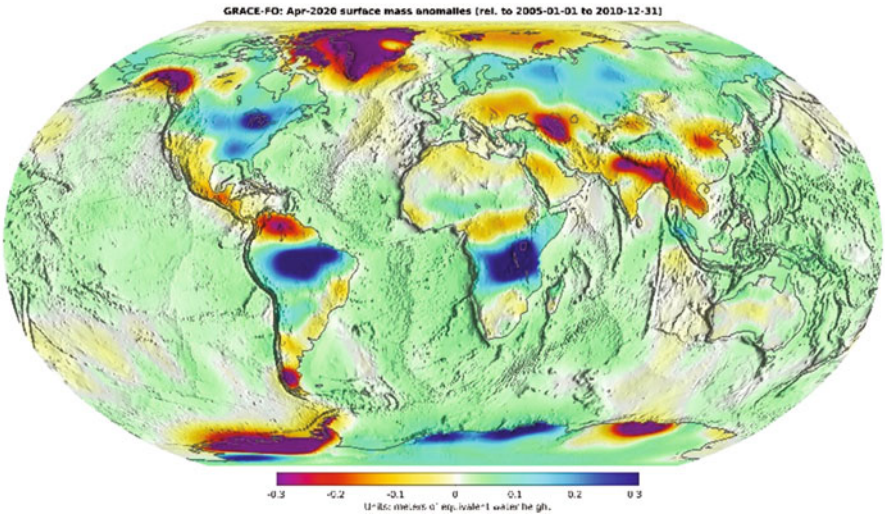

Fig. 19.6 Global surface gravity anomalies (https://gracefo.jpl.nasa.gov/data/grace-fo-data/)

monthly basis. But there are several organizations like CSR (Centre for Space Research), JPL (Jet Propulsion Laboratory), GFZ (GeoForschungZentrum) which process, prepare, and provide the GRACE data on daily, weekly, and monthly basis in terms of band limited spherical harmonic coefficients or global grids of mass change (Vishwakarma et al. 2018) which can be processed to get global grids of equivalent water height for different grid sizes (Fig. 19.6). The filtering of the GRACE data is the integral part of the data processing as it contains noise hence spatial data integration is done to receive useful information from the raw data. There are many research studies have been done for the filtering of the GRACE data (Swenson and Wahr 2006; Devaraju 2015; Vishwakarma 2017).

For using the GRACE data for groundwater applications, all other signals from needed to be filtered out. The GRACE data is generally used with integration of the other land surface models and field data to estimate the groundwater scenario in a region. This approach has also resulted in few research studies describing the effect of anthropogenic changes on groundwater depletion (Joodaki et al. 2014). There are several research studies that had been done since its inception in the orbit (Yeh et al. 2006; Swenson et al. 2008; Zaitchik et al. 2008; Feng et al. 2013). GRACE data can be assimilated into catchment land surface model to investigate to which extent gravity anomaly data can be used to improve modelling errors (Girotto et al. 2017). This data has been extensively used to estimate groundwater depletion in northwest India (Tiwari et al. 2009; Long et al. 2016; Girotto et al. 2017; Singh and Raju 2020). Therefore, GRACE data has advantage over other earth observation satellites is to capture the mass changes on surface and under the surface.

The GRACE mission is decommissioned in September 2017 due to the battery issue. The follow-up mission i.e., GRACE-FO (twin satellites nicknamed Tom and Jerry) was launched on 22 May, 2018. The GRACE-FO has the identical system and hardware to its predecessor. The GRACE satellites were using microwave ranging interferometer for measuring the distance between both satellites but in GRACE-FO use laser ranging interferometer in addition to previous one which has been put in it for experimental purpose for future missions. It provides monthly datasets of global gravity anomalies.

19.5 SAR Interferometry in Groundwater Applications

Land subsidence is the large region phenomenon which occurs due the excessive extraction of groundwater at large scale. It generally occurs in the valleys which contains the aquifer system of the fine grained sediments like silt and clay. These aquifer systems contain pore structures of granular skeleton and the groundwater which occupies the space between granules. When large quantities of groundwater are extracted, pore fluid pressure is reduced; stress is built up in the skeleton of whole system which causes deformation and some degree of compression. When these vertical changes become irreversible, land subsidence occurs. Thus, excessive groundwater pumping from the aquifers plays direct role in land subsidence accompanied by extraction of crude oil and natural gas (Carpenter et al. 2014). Since last century, land subsidence has become global problem as it causes damages in millions every year. Also, land subsidence will further shift aquifer downwards and water table with it. Hence land subsidence zones should be detected regularly for avoid excessive extraction of groundwater. In SAR (Interferometric Synthetic Aperture Radar) which is an advanced microwave remote sensing technique is very effective method for detecting vertical land surface changes (Zhang et al., 2019). This is an active remote sensing method in which SAR images are produced by the travel time of radar signal from sensor to target and back. Hence it can be understood that radar echo is directly proportional pulse's time of travel. For detecting height changes, one needs the two SAR images of same area but of different time periods. So, the phase difference in radar signals caused due to the vertical shift of the earth's surface from two different SAR images can be shown in interferograms. These phase differences can be caused by various other atmospheric factors such as water vapors (Zebker et al. 1997) which can be filtered out by independent interferograms. This range change is converted to the elevation difference with the help of the look angle of the sensor to the target. Vertical changes in land surface leads to the land subsidence. The interferometry should be done for large area as land subsidence is not local phenomenon.

There are several microwave remote sensing satellites launched by the different space agencies like ENVISAT, JERS, ERS 1/2, Sentinel-1, etc. The images obtained by these satellites are used for interferometry. There are many research studies

carried out globally to investigate the land subsidence (Sneed et al. 2003; Holzer and Galloway 2005; Yue et al. 2011; Ziwen et al. 2019; Brandt et al. 2020).

19.6 Role of Geospatial Technology in Groundwater Modelling

For the proper management of the groundwater, groundwater modelling is very effective tool to assess the effects of management strategies. Modelling is used to build the hypothetical scenario of the groundwater flow based on its principles. Informed management decisions can be made with the help of the robust groundwater model which is calibrated with correct data. These mathematical and numerical models require extensive amount of the data and it should be properly classified and prepared to feed into the models. Generally, groundwater modelling is done for the larger areas hence it needs the huge amount of the data (Moharir et al. 2017, 2020; Khadri and Moharir 2016; Khadri and Pande 2016).

The primary use of geospatial data in groundwater models are model grid setup, preparation of model boundaries, preparation of spatial inputs for the model (Fig. 19.7). Numerical model grids on the surface can be visualized on the satellite

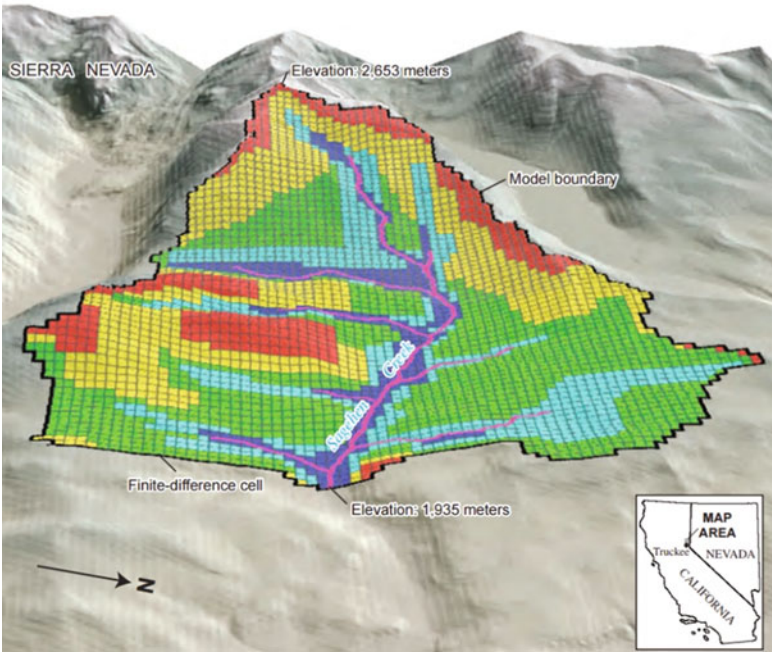

Fig. 19.7 Finite grid for groundwater model is shown on the DEM (https://www.usgs.gov/software/coupled-ground-water-and-surface-water-flow-model-gsflow)

images. Remote sensing data also used for deriving parameters related to the unsaturated zones, geomorphology, hydrogeological data etc. These types of data are used in the integrated modelling studies in which water flow is simulated in three mediums i.e., rivers, soil, and groundwater (Gogu et al. 2001; Chatterjee et al. 2005). Though remote sensing data do have very limited utility in the groundwater modelling GIS plays a very important role in data preparation, pre-processing, and post-processing.

GIS is a tool which can manage spatial data for larger area very efficiently. GIS is also useful in preparing the spatial data which can be further integrated into the hydrological models. Complex maps can be created and edited rapidly. There are two types of data, any groundwater model requires i.e., time constant parameters and time variant parameters. The time constant parameters are river network, land cover, soil, surface and subsurface hydrological data input, aquifer geometry (areal and vertical distribution of subsurface strata, aquifer thickness etc.). It also requires hydraulic parameters. These all datasets are thematic layers which are prepared in GIS and generated with the help of satellite images (Pande 2020a, b, c, d). The model also requires water table from the local wells to generate potentiometric maps of the unconfined aquifer. Here GIS does the interpolation of the point data to create the interpolated distribution map of the groundwater in the study area. All remote sensing data required for groundwater models are processed in GIS and then integrated into the models. It can also be used to identify the springs which is the outflow points of the groundwater flow and also calculate the flow length from the point of recharge to the outflow point. It also has utility in calculating the outflow, depleted outflow in the springs and measuring the effects of the groundwater abstraction (Jani 2012). GIS is used in post-processing of model results for visualization of results in map form. These types of results are more user friendly as they are very easy understand in spatial context. In few cases, GIS can do direct modelling of the groundwater properties such as recharge rates and contaminant plume migration with over-layered data layers. Also, GIS has widespread applications in groundwater contaminant transport modelling, saltwater intrusion in the groundwater. Thus, groundwater models can be set up with the help of geospatial technology with other variables.

19.7 Conclusion

In this chapter discussed on the various methods, software and satellite data can be used for effective analysis of Groundwater Resources Management in the semi-arid region. Currently so many researchers have been working on the various topics such as groundwater recharge, soil moisture analysis, soil and water conservation planning, and thematic maps of natural resources using Remote Sensing and GIS. This chapter is very important for understanding of the groundwater modelling, various types of satellite data, and hydrological modeling.

References

Arulbalaji, P., Padmalal, D., & Sreelash, K. (2019). GIS and AHP techniques based delineation of groundwater potential zones: a case study from southern Western Ghats, India. *Scientific Reports, 9*(1), 1–17. https://doi.org/10.1038/s41598-019-38567-x.

Ben-Dor, E., & Banin, A. (1995). Near-infrared analysis as a rapid method to simultaneously evaluate several soil properties. *Soil Science Society of America Journal, 59*(2), 364–372. https://doi.org/10.2136/sssaj1995.03615995005900020014x.

Bowers, S. A., & Smith, S. J. (1972). Spectrophotometric determination of soil water content. *Soil Science Society of America Journal, 36*(6), 978–980. https://doi.org/10.2136/sssaj1972.03615995003600060045x.

Brandt, J. T., Sneed, M., & Danskin, W. R. (2020). Detection and measurement of land subsidence and uplift using interferometric synthetic aperture radar, San Diego, California, USA, 2016–2018. *Proceedings of the International Association of Hydrological Sciences, 382*, 45–49.

Carpenter, J. W., M., Grabert, V. K., Dalgish, B., & Cannon, D., Luhdorff and Scalmanini Consulting Engineers, (2014). Land subsidence from groundwater use in California. California water foundation.

Chan, S. K., Bindlish, R., O'Neill, P., Jackson, T., Njoku, E., Dunbar, S., et al. (2018). Development and assessment of the SMAP enhanced passive soil moisture product. *Remote Sensing of Environment, 204*, 931–941. https://doi.org/10.1016/j.rse.2017.08.025.

Chatterjee, C., Kumar, R., Chakravorty, B., Lohani, A. K., & Kumar, S. (2005). Integrating remote sensing and GIS techniques with groundwater flow modeling for assessment of waterlogged areas. *Water Resources Management, 19*(5), 539–554. https://doi.org/10.1007/s11269-005-2071-4.

Chen, J., Famigliett, J. S., Scanlon, B. R., & Rodell, M. (2016). Groundwater storage changes: Present status from GRACE observations. *Surveys in Geophysics, 37*(2), 397–417. https://doi.org/10.1007/s10712-015-9332-4.

Cohen, W. B., & Goward, S. N. (2004). Landsat's role in ecological applications of remote sensing. *Bioscience, 54*(6), 535–545. https://doi.org/10.1641/0006-3568(2004)054[0535:lrieao]2.0.co;2.

Colliander, A., Cosh, M. H., Misra, S., Jackson, T. J., Crow, W. T., Powers, J., et al. (2019). Comparison of high-resolution airborne soil moisture retrievals to SMAP soil moisture during the SMAP validation experiment 2016 (SMAPVEX16). *Remote Sensing of Environment, 227*, 137–150. https://doi.org/10.1016/j.rse.2019.04.004.

Cracknell, A. P. (2018). The development of remote sensing in the last 40 years. *International Journal of Remote Sensing, 39*, 8387–8427. https://doi.org/10.1080/01431161.2018.1550919.

Curcio, J. A., & Petty, C. C. (1951). The near infrared absorption spectrum of liquid water. *Journal of the Optical Society of America, 41*(5), 302–304. https://doi.org/10.1364/JOSA.41.000302.

Deng, K. A. K., Lamine, S., Pavlides, A., Petropoulos, G. P., Bao, Y., Srivastava, P. K., & Guan, Y. (2019). Large scale operational soil moisture mapping from passive MW radiometry: SMOS product evaluation in Europe & USA. *International Journal of Applied Earth Observation and Geoinformation, 80*, 206–217.

Devaraju, B. (2015). *Understanding filtering on the sphere: Experiences from filtering GRACE data*. Stuttgart: Dissertation, University of Stuttgart.

Döll, P., Hoffmann-Dobrev, H., Portmann, F. T., Siebert, S., Eicker, A., Rodell, M., ... & Scanlon, B. R. (2012). Impact of water withdrawals from groundwater and surface water on continental water storage variations. *Journal of Geodynamics, 59*, 143–156.

Feng, W., Zhong, M., Lemoine, J. M., Biancale, R., Hsu, H. T., & Xia, J. (2013). Evaluation of groundwater depletion in North China using the Gravity Recovery and Climate Experiment (GRACE) data and ground-based measurements. *Water Resources Research, 49*(4), 2110–2118. https://doi.org/10.1002/wrcr.20192.

Girotto, M., De Lannoy, G. J., Reichle, R. H., Rodell, M., Draper, C., Bhanja, S. N., & Mukherjee, A. (2017). Benefits and pitfalls of GRACE data assimilation: A case study of terrestrial water

storage depletion in India. *Geophysical Research Letters, 44*(9), 4107–4115. https://doi.org/10.1002/2017GL072994.

Gogu, R., Carabin, G., Hallet, V., Peters, V., & Dassargues, A. (2001). GIS-based hydrogeological databases and groundwater modelling. *Hydrogeology Journal, 9*(6), 555–569. https://doi.org/10.1007/s10040-001-0167-3.

Herman, M. R., Nejadhashemi, A. P., Abouali, M., Hernandez-Suarez, J. S., Daneshvar, F., Zhang, Z., et al. (2018). Evaluating the role of evapotranspiration remote sensing data in improving hydrological modeling predictability. *Journal of Hydrology, 556*, 39–49. https://doi.org/10.1016/j.jhydrol.2017.11.009.

Holzer, T. L., & Galloway, D. L. (2005). Impacts of land subsidence caused by withdrawal of underground fluids in the United States. In J. Ehelen, W. Haneberg, & R. Larson (Eds.), *Humans as geologic agents* (Vol. 16, p. 87). Boulder, CO: Geological Society of America, Technology & Engineering.

Jackson, T. J., Bindlish, R., Cosh, M. H., Zhao, T., Starks, P. J., Bosch, D. D., et al. (2011). Validation of soil moisture and ocean salinity (SMOS) soil moisture over watershed networks in the US. *IEEE Transactions on Geoscience and Remote Sensing, 50*(5), 1530–1543. https://doi.org/10.1109/TGRS.2011.2168533.

Jani, J. (2012). GIS as a tool for modelling groundwater flow. *2012 IEEE Symposium on Business, Engineering and Industrial Applications, 2012*, 513–517. https://doi.org/10.1109/ISBEIA.2012.6422939.

Jianping, W., Anxin, M., Zhimu, C., & Jianzhong, S. (1997). Investigation of Landuse in Shanghai Using Aerial Remote Sensing. *Journal of Eastchina Normal University (Natural Science)*

Jing, M., Kumar, R., Heße, F., Thober, S., Rakovec, O., Samaniego, L., & Attinger, S. (2020). Assessing the response of groundwater quantity and travel time distribution to 1.5, 2, and 3° C global warming in a mesoscale central German basin. *Hydrology and Earth System Sciences, 24*(3), 1511–1526.

Joodaki, G., Wahr, J., & Swenson, S. (2014). Estimating the human contribution to groundwater depletion in the Middle East, from GRACE data, land surface models, and well observations. *Water Resources Research, 50*(3), 2679–2692. https://doi.org/10.1002/2013wr014633.

Kerr, Y. H., Al-Yaari, A., Rodriguez-Fernandez, N., Parrens, M., Molero, B., Leroux, D., et al. (2016). Overview of SMOS performance in terms of global soil moisture monitoring after six years in operation. *Remote Sensing of Environment, 180*, 40–63. https://doi.org/10.1016/j.rse.2016.02.042.

Kerr, Y. H., Waldteufel, P., Richaume, P., Wigneron, J. P., Ferrazzoli, P., Mahmoodi, A., et al. (2012). The SMOS soil moisture retrieval algorithm. *IEEE Transactions on Geoscience and Remote Sensing, 50*(5), 1384–1403. https://doi.org/10.1109/tgrs.2012.2184548.

Khadri, S. F. R., & Moharir, K. (2016). Characterization of aquifer parameter in basaltic hard rock region through pumping test methods: A case study of Man River basin in Akola and Buldhana Districts Maharashtra India. *Modeling Earth Systems and Environment, 2*, 33.

Khadri, S. F. R., & Moharir, K. N. (2013). Estimation of groundwater prospectus zone mapping and morphometric analysis of WRD-4 watershed in Wardha District of Maharashtra, India using Remote Sensing and GIS Techniques. *International Journal of Advancements in Research & Technology, 2*(5), 301–311.

Khadri, S. F. R., & Pande, C. (2016). Ground water flow modeling for calibrating steady state using MODFLOW software: A case study of Mahesh River basin, India. *Modeling Earth Systems and Environment, 2*, 39. https://doi.org/10.1007/s40808-015-0049-7.

Khadri, S. F. R., Pande, C., & Moharir, K. (2013). Geomorphological investigation of WRV-1 Watershed management in Wardha district of Maharashtra India; using remote sensing and geographic information system techniques. *International Journal of Pure and Applied Research in Engineering and Technology, 1*(10), 12.

Kim, K., Park, J., Baik, J., & Choi, M. (2017). Evaluation of topographical and seasonal feature using GPM IMERG and TRMM 3B42 over Far-East Asia. *Atmospheric Research, 187*, 95–105. https://doi.org/10.1016/j.atmosres.2016.12.007.

Kumar, N., Yamaç, S. S., & Velmurugan, A. (2015). Applications of remote sensing and GIS in natural resource management. *Journal of the Andaman Science Association, 20*(1), 1–6.

Kustas, W. P., Moran, M. S., Humes, K. S., Stannard, D. I., Pinter, P. J., Hipps, L. E., et al. (1994). Surface energy balance estimates at local and regional scales using optical remote sensing from an aircraft platform and atmospheric data collected over semiarid rangelands. *Water Resources Research, 30*(5), 1241–1259. https://doi.org/10.1029/93wr03038.

Kwast, Van der., J. (2009). Quantification of top soil moisture patterns: Evaluation of field methods, process-based modelling, remote sensing and an integrated approach. Utrecht University, Royal Dutch Geographical Society.

Long, D., Chen, X., Scanlon, B. R., Wada, Y., Hong, Y., Singh, V. P., et al. (2016). Have GRACE satellites overestimated groundwater depletion in the Northwest India Aquifer? *Scientific Reports, 6*, 24398. https://doi.org/10.1038/srep24398.

Mao, Y., Crow, W. T., & Nijssen, B. (2020). A unified data-driven method to derive hydrologic dynamics from global SMAP surface soil moisture and GPM precipitation data. *Water Resources Research, 56*(2), e2019WR024949. https://doi.org/10.1029/2019WR024949.

Merlin, O., Escorihuela, M. J., Mayoral, M. A., Hagolle, O., Al Bitar, A., & Kerr, Y. (2013). Self-calibrated evaporation-based disaggregation of SMOS soil moisture: An evaluation study at 3 km and 100 m resolution in Catalunya, Spain. *Remote Sensing of Environment, 130*, 25–38. https://doi.org/10.1016/j.rse.2012.11.008.

Moharir, K. N., Pande, C. B., Singh, S. K., & Del Rio, R. A. (2020). *Evaluation of analytical methods to study aquifer properties with pumping test in Deccan Basalt Region of the Morna River Basin in Akola District of Maharashtra in India, Groundwater Hydrology*. London: Intec Open Publication. https://doi.org/10.5772/intechopen.84632.

Moharir, K., Pande, C., & Patil, S. (2017). Inverse modeling of aquifer parameters in basaltic rock with the help of pumping test method using MODFLOW software. *Geoscience Frontiers, 8*(6), 1385–1395.

Münch, Z., & Conrad, J. (2007). Remote sensing and GIS based determination of groundwater dependent ecosystems in the Western Cape, South Africa. *Hydrogeology Journal, 15*(1), 19–28. https://doi.org/10.1007/s10040-006-0125-1.

NITI. (2019). Aayog – Composite water management index in association with Ministry of Jal Shakti and Ministry of Rural Development, Government of India. Retrieved July 4, 2020, from https://niti.gov.in/sites/default/files/2019-08/CWMI-2.0-latest.pdf.

Opolot, E. (2013). Application of remote sensing and geographical information systems in flood management: A review. *Research Journal of Applied Sciences Engineering and Technology, 6*(10), 1884–1894. https://doi.org/10.19026/rjaset.6.3920.

Pande, C. B. (2020a). Introduction. In *Sustainable watershed development. Springer briefs in water science and technology*. Cham: Springer. https://doi.org/10.1007/978-3-030-47244-3_1.

Pande, C. B. (2020b). Watershed management and development. In *Sustainable watershed development. Springer briefs in water science and technology*. Cham: Springer. https://doi.org/10.1007/978-3-030-47244-3_2.

Pande, C. B. (2020c). Thematic mapping for watershed development. In *Sustainable watershed development. Springer briefs in water science and technology*. Cham: Springer. https://doi.org/10.1007/978-3-030-47244-3_3.

Pande, C. B. (2020d). Sustainable watershed development planning. In *Sustainable watershed development. Springer briefs in water science and technology*. Cham: Springer. https://doi.org/10.1007/978-3-030-47244-3_4.

Pande, C. B., Khadri, S. F. R., Moharir, K. N., & Patode, R. S. (2017). Assessment of groundwater potential zonation of Mahesh River basin Akola and Buldhana districts, Maharashtra, India using remote sensing and GIS techniques. *Sustainable Water Resources Management*. https://doi.org/10.1007/s40899-017-0193-5, ISSN 2363-5037.

Pande, C. B., Moharir, K. N., Singh, S. K., & Varade, A. M. (2019). An integrated approach to delineate the groundwater potential zones in Devdari watershed area of Akola district,

Maharashtra, Central India. *Environment, Development, and Sustainability Springer Journal*. https://doi.org/10.1007/s10668-019-00409-1.

Pande, C. B., Moharir, K. N., Khadri, S. F. R., & Patil, S. (2018b). Study of land use classification in the arid region using multispectral satellite images. *Applied Water Science, 8*(5), 1–11.

Pande, C. B., Moharir, K. N., & Pande, R. (2018a). Assessment of morphometric and hypsometric study for watershed development using spatial technology – A case study of Wardha river basin in the Maharashtra, India. *International Journal of River Basin Management*. https://doi.org/10.1080/15715124.2018.1505737.

Patino, J. E., & Duque, J. C. (2013). A review of regional science applications of satellite remote sensing in urban settings. *Computers, Environment and Urban Systems, 37*, 1–17. https://doi.org/10.1016/j.compenvurbsys.2012.06.003.

Patode, R. S., Pande, C. B., Nagdeve, M. B., Moharir, K. N., & Wankhade, R. M. (2017). Planning of conservation measures for watershed management and development by using geospatial technology – A case study of Patur Watershed in Akola District of Maharashtra. *Current World Environment, 12*(3), 701–708.

Price, J. C. (1980). The potential of remotely sensed thermal infrared data to infer surface soil moisture and evaporation. *Water Resources Research, 16*(4), 787–795. https://doi.org/10.1029/wr016i004p00787.

Reddy, G. S., Behera, G., & Subramanian, S. K. (2011). *Ground water prospects maps – User manual*. Bengaluru: National Remote Sensing Agency, Indian Space Research Organization. Retrieved October, 2017, from https://www.nrsc.gov.in/sites/default/files/pdf/ebooks/RGNationalDrinkingWater_UserManual.pdf. Accessed Oct 2011.

Running, S. W., Mu, Q., Zhao, M., & Moreno, A. (2017). MODIS global terrestrial evapotranspiration (ET) product (NASA MOD16A2/A3) NASA earth observing system MODIS land algorithm. Retrieved July 4, 2017, from https://landweb.modaps.eosdis.nasa.gov/QA_WWW/forPage/user_guide/MOD16UsersGuide2016V1.52017May23.pdf.

Satty, T. L. (1980). *The analytical hierarch process*. New York, NY: McGraw-Hill.

Saaty, T. L. (1990). *Decision making for leaders: the analytic hierarchy process for decisions in a complex world*. Pittsburgh, PA: RWS Publications.

Sadeghi, M., Jones, S. B., & Philpot, W. D. (2015). A linear physically-based model for remote sensing of soil moisture using short wave infrared bands. *Remote Sensing of Environment, 164*, 66–76. https://doi.org/10.1016/j.rse.2015.04.007.

Singh, A., & Raju, A. (2020). Application of grace satellite data for assessment of groundwater resources in Central Ganga Alluvial Plain, Northern India. In V. Shukla & N. Kumar (Eds.), *Environmental concerns and sustainable development* (pp. 153–162). Singapore: Springer.

Skofronick-Jackson, G., Petersen, W. A., Berg, W., Kidd, C., Stocker, E. F., Kirschbaum, D. B., et al. (2017). The Global Precipitation Measurement (GPM) mission for science and society. *Bulletin of the American Meteorological Society, 98*(8), 1679–1695. https://doi.org/10.1175/BAMS-D-15-00306.1.

Sneed, M., Ikehara, M. E., Stork, S. V., Amelung, F., & Galloway, D. L. (2003). Detection and measurement of land subsidence using interferometric synthetic aperture radar and global positioning system, San Bernardino County, Mojave Desert, California. *Water-Resources Investigations Report, 3*, 4015. Retrieved from https://www.mojavewater.org/files/03-4015LandSubsidence.pdf.

Sood, A., & Smakhtin, V. (2015). Global hydrological models: A review. *Hydrological Sciences Journal, 60*(4), 549–565. https://doi.org/10.1080/02626667.2014.950580.

Swenson, S., Famiglietti, J., Basara, J., & Wahr, J. (2008). Estimating profile soil moisture and groundwater variations using GRACE and Oklahoma Mesonet soil moisture data. *Water Resources Research, 44*(1). https://doi.org/10.1029/2007WR006057.

Swenson, S., & Wahr, J. (2006). Post-processing removal of correlated errors in GRACE data. *Geophysical Research Letters, 33*(8). https://doi.org/10.1029/2005gl025285.

Tang, L., & Shao, G. (2015). Drone remote sensing for forestry research and practices. *Journal of Forestry Research, 26*(4), 91–797. https://doi.org/10.1007/s11676-015-0088-y.

Tiwari, V. M., Wahr, J., & Swenson, S. (2009). Dwindling groundwater resources in northern India, from satellite gravity observations. *Geophysical Research Letters, 36*(18). https://doi.org/10.1029/2009gl039401.

Vishwakarma, B. D. (2017). *Understanding and repairing the signal damage due to filtering of mass change estimates from the GRACE satellite mission*. Dissertation: University of Stuttgart.

Vishwakarma, B. D., Devaraju, B., & Sneeuw, N. (2018). What is the spatial resolution of GRACE satellite products for hydrology? *Remote Sensing, 10*(6), 852. https://doi.org/10.3390/rs10060852.

Xuejun, W. (1997). The combination of spatial analysistechnique and GIS [J]. *Geographical Research, 3*.

Yeh, P. J. F., Swenson, S. C., Famiglietti, J. S., & Rodell, M. (2006). Remote sensing of groundwater storage changes in Illinois using the Gravity Recovery and Climate Experiment (GRACE). *Water Resources Research, 42*(12). https://doi.org/10.1029/2006WR005374.

Yue, H., Liu, G., Guo, H., Li, X., Kang, Z., Wang, R., & Zhong, X. (2011). Coal mining induced land subsidence monitoring using multiband spaceborne differential interferometric synthetic aperture radar data. *Journal of Applied Remote Sensing, 5*(1), 053518. https://doi.org/10.1117/1.3571038.

Yueh, S., Shah, R., Xu, X., Elder, K., & Starr, B. (2019). Experimental demonstration of soil moisture remote sensing using P-band satellite signals of opportunity. *IEEE Geoscience and Remote Sensing Letters, 17*(2), 207–211. https://doi.org/10.1109/LGRS.2019.2918764.

Zaitchik, B. F., Rodell, M., & Reichle, R. H. (2008). Assimilation of GRACE terrestrial water storage data into a land surface model: Results for the Mississippi River basin. *Journal of Hydrometeorology, 9*(3), 535–548. https://doi.org/10.1175/2007jhm951.1.

Zebker, H. A., Rosen, P. A., & Hensley, S. (1997). Atmospheric effects in interferometric synthetic aperture radar surface deformation and topographic maps. *Journal of Geophysical Research: Solid Earth, 102*(B4), 7547–7563. https://doi.org/10.1029/96jb03804.

Zhang, B., Wang, R., Deng, Y., Ma, P., Lin, H., & Wang, J. (2019). Mapping the Yellow River Delta land subsidence with multitemporal SAR interferometry by exploiting both persistent and distributed scatterers. *ISPRS Journal of Photogrammetry and Remote Sensing, 148*, 157–173. https://doi.org/10.1016/j.isprsjprs.2018.12.008.

Zhuang, R., Zeng, Y., Manfreda, S., & Su, Z. (2020). Quantifying long-term land surface and root zone soil moisture over Tibetan Plateau. *Remote Sensing, 12*(3), 509. https://doi.org/10.3390/rs12030509.

Ziwen, Z., Liu, Y., Li, F., Li, Q., & Ye, W. (2019). Land subsidence monitoring based on InSAR and inversion of aquifer parameters. *EURASIP Journal on Wireless Communications and Networking, 2019*(1), 1–18. https://doi.org/10.1186/s13638-019-1602-2.

Zribi, M., Albergel, C., & Baghdadi, N. (2020). Soil moisture retrieval using radar remote sensing sensors. *Editorial for the Special Issue, 12*(7), 1100. https://doi.org/10.3390/rs12071100.

Chapter 20
Trend Analysis of Groundwater Level Using Innovative Trend Analysis

Mohammad Zakwan

Contents

20.1 Introduction 389
20.2 Materials and Methods 392
20.3 Results and Discussions 397
20.4 Conclusion 401
References 401

20.1 Introduction

Groundwater is the major source of freshwater as it contributes to about 30% of the total fresh water volume available on earth (Pande and Moharir 2018; Pande et al. 2019; Sharma et al. 2019). Groundwater is the lifeline for not only sustenance of human and animal life, but also the vegetal cover on the earth surface. Groundwater is the source of water supply for domestic, industrial and agricultural purposes (Birkinshaw et al. 2008; Li et al. 2013; Muzzammil et al. 2015; Pande et al. 2018). Groundwater is stored in pore spaces in various earth formations such as aquifer, aquitard, aquiclude and aquifuge. Earth formations are classified into aquifer, aquitard, aquiclude and aquifuge on the basis of permeability and porosity. However, these classifications are relative classifications depending on the availability of water in the region. Aquifers are further classified as confined aquifer and unconfined aquifer (Khadri and Moharir 2016; Khadri and Pande 2016a; Moharir et al. 2017, 2020). Water table or water level is the free water surface of unconfined aquifer and static level of well penetrating into the confined aquifer (Khadri and

M. Zakwan (✉)
Civil Engineering Department, IIT Roorkee, Roorkee, Uttarakhand, India

C. B. Pande, K. N. Moharir (eds.), *Groundwater Resources Development and Planning in the Semi-Arid Region*, https://doi.org/10.1007/978-3-030-68124-1_20

Pande 2016b; Pande et al. 2017). Water level continuously changes in response to recharge and withdrawal rate of water (Patle et al. 2015; Khadri and Pande 2016c; Patode et al. 2016; Zhou et al. 2017). Obviously if the recharge rate is higher than withdrawal rate water level will increase, otherwise, if the withdrawal rates are higher water level is bound to decline. Perpetual alteration in the water level is eminent if there is substantial withdrawal/ recharge. Ground water level fluctuates due to both natural and anthropogenic causes (Abiye et al. 2018; Alipour et al. 2018; Ndlovu and Demlie 2018; Zakwan 2019; Arshad and Umar 2020). Natural causes include alteration in the amount and pattern of rainfall and temperature while anthropogenic causes encompass changes in land-use pattern, type of irrigation, discharge of industrial effluents, ground water withdrawals and groundwater recharge, etc. (Patle et al. 2017; Ara and Zakwan 2018; Alexander et al. 2018; Marghade et al. 2020). Recently, it has been observed that both quality and quantity of groundwater are depleting in developing countries (Tsanis et al. 2008; Rodell et al. 2009; Jiao et al. 2015; Alexander et al. 2018; Salam et al. 2019; Sharma et al. 2019; Arshad and Umar 2020; Anand et al. 2020). Groundwater recharge can be natural or artificial. Natural recharge involves infiltration of water after rainfall (fraction that reaches the saturation zone), seepage from river beds, canal beds, irrigated lands, reservoirs and other water bodies. Recharge through infiltration resulting from rainfalls forms the major portion of natural recharge. Artificial recharge involves induced recharge from water bodies, recharge through rainwater harvesting techniques, check dams, subsurface dykes and reduction in saltwater intrusion. Growing population and their needs along with thrust for development and industrial growth has forced to substantial increase in the pumping rate of groundwater (Pande 2020a, d). At the same time these factors have also adversely affected hydrologic cycle leading to decline in rainfall in many regions of the world or decline in frequency of rainfall. Decline in rainfall further increases the dependency of agricultural sector on groundwater resources. Recently, a new term ground water drought has been introduced. Groundwater drought can be defined as a "lack of groundwater recharge or a lack of groundwater expressed in terms of storages or groundwater heads in a certain area and over a particular period of time" (Van Lanen and Peters 2000). The lack is usually determined in comparison to some "normal" or average amount or level derived from frequency analysis using historical data.

As an example, in most semiarid parts of India, agricultural sector faces serious water scarcity and liability of crop failure even with slight decrease or lag in the monsoon rainfalls. With advanced pumping technologies and their cheap accessibility, ground water utilization for irrigation across the country has witnessed enormous surge. However, rampant population increase and ground water utilization over the past few decades in majority of the regions of the country has resulted in the exploitation of groundwater at a rate far greater than the natural recharge, thereby, leading to decline in ground water level. This example also clearly demonstrates that alteration in ground water level is caused by both natural and anthropogenic reasons.

Several researchers have seen fluctuation in ground water level in connection with the trends in rainfall and river discharge and several studies have been

conducted by hydrologists to analyse the trends in discharge, rainfall and ground water level (Zakwan 2018). Among the trend analysis tests nonparametric Mann-Kendall and Spearman's Rho test have been used by many researchers to detect the trends in hydrologic variables (Daniel 1978; Crawford et al. 1983; El-Shaarawi et al. 1983; Hirsch and Slack 1984; Hirsch et al. 1982; Pilon et al. 1985; Cailas et al. 1986; Hipel et al. 1988; Demaree and Nicolis 1989; Zetterqvist 1991; Hipel and Mcleod 1994; McLeod and Hipel 1994; Keim et al. 1995; Douglas et al. 2000; Meade and Moody 2010; Zhang et al. 2011; Muzzammil et al. 2018; Pandey et al. 2018; Zakwan and Ara 2019; Sharma et al. 2019; Yilmaz et al. 2020).

Walling and Fang (2003) analysed the pattern of sediment discharge of nearly 150 rivers and reported that nearly 50% of them demonstrate statistically significant upward or downward trend. Milliman et al. (2008) investigated the water yield of over 100 rivers and reported that more than one-third of the river possesses alteration of over 30%. Lu et al. (2003) analyzed the seasonal discharge data in several tributaries of Yangtze River, China, reporting remarkable alteration in the hydrological parameters thereby projecting reasonable concern about flooding and water scarcity in different regions of Yangtze River basin. However, rivers of central Japan did not exhibit any remarkable trend in discharges (Siakeu et al. 2004).

Zakwan and Ara (2019) and Zakwan et al. (2019) analysed monthly precipitation data of Bihar, India and reported significant decline in rainfall over the region. Tsanis et al. (2008) developed an ANN framework to estimate groundwater level fluctuations based on rainfall data. Patle et al. (2015) used Mann-Kendall test and Sen's slope method to identify the trends in groundwater and reported a significant decline in water level for Karnal district of Haryana, India, both during pre-monsoon and post-monsoon season. Singh et al. (2019) applied both parametric (linear regression trend line) as well as nonparametric test (Mann-Kendall test and Sen's slope) to understand the trends in groundwater of Haryana, India, confirming significant decline in groundwater level. Pathak and Dodamani (2019) forwarded the concept of regional groundwater drought asserting significant decline in ground water level in Ghataprabha basin, India. Based on the results of Mann-Kendall trend test they reported that the decline in water level for more than 60% of the wells in the region is above 0.21 m on an average. Gibrilla et al. (2018) revealed increase in groundwater level in most of the wells of Ghana based on trend tests and ARIMA model. Ndlovu and Demlie (2018) analysed the trend in ground water level along with rainfall of KwaZulu-Natal Province, South Africa and found that the decline in groundwater level is directly linked with decline in rainfall. Lasagna et al. (2020) analysed the impact of natural and anthropogenic factors on the groundwater resources of Italy and reported that rainfall and irrigation pattern mainly influence the available groundwater resources. Anand et al. (2020) employed GIS along with trend tests to detect groundwater level fluctuations in India.

Analysis of pattern of water level plays a vital role in assessing the future scenario of available ground water resources in the region. Trend analysis could also be used to detect the successfulness of various groundwater recharge techniques. In this regard, trend analysis of water level of five wells was performed using Mann Kendall, Spearman-Rho, Sens slope and innovative trend analysis.

20.2 Materials and Methods

In the present study water level data of five wells of Churu district, Rajasthan, India (28°17′32″ N, 74°57′59″ E) were utilized for the trend analysis. The region comes under arid and semiarid regions of India. The wells were randomly selected for study area; however, care was taken to select those wells where longest time series of groundwater level was available. Three wells were located in Sadarshahar, one each in Ratangarh and Sujangarh tehsil of Churu. Map of the study area is shown in Fig. 20.1. The region faces acute shortage of water during summer or pre-monsoon season. The data was obtained from the website of Central Ground Water Board (http://cgwb.gov.in/GW-data-access.html). Water level data for the period 1994–2017 was available on the website. The statistical properties of the data are given in Table 20.1. It could be observed that water level does not show significant variation.

Generally, to analyse the temporal variation, parametric as well as nonparametric tests are used. Nonparametric tests have an advantage over parametric tests in way that they can be used for non-normal time series also. These nonparametric test does not require data series to follow normal distribution and yet are at par with other parametric trend tests (Yue et al. 2002; Ebadati et al. 2014; Tirkey et al. 2020). The preliminary assumption for conducting the test is that the data series is not serially correlated. Presence of auto correlation among data series might result in incorrect trend detection. Prewhittening of auto correlated series is one of the methods to avoid incorrect trend detection. But Bayazit and Onoz (2007), concluded that prewhitening should be avoided when coefficient of variation (C_v) of the data series is very low ($C_v = 0.1$) for all sample sizes or C_v is low ($C_v = 0.3$) and slope of linear trend (b) is high ($b > 0.006$) for moderate sample sizes, $n = 50$–75. The details of nonparametric used in present study are as follows.

20.2.1 Mann-Kendall Test

Mann-Kendall test (after Mann 1945; Kendall 1975) is a nonparametric statistical test used for the analysis of trend in climatologic and hydrologic time series (Hirsch et al. 1982; Yu et al. 1993; Gibbons and Chakraborti 2003; Sharma and Patel 2018). Mann-Kendall test is a rank based method used to analyse the trends in time series (Burn et al. 2004). This test has been found to be reliable even for non-normal time series (Lu 2005). Further, Mann-Kendall test statistics are not significantly affected by presence of outliers (Hirsch et al. 1982). In this test, the null hypothesis H_0 assumes that the realizations are independent that is no trend exists in data series which is tested against the alternative hypothesis H_1 that assumes that the monotonic trend exists in the time series (Pohlert 2017). Assuming X_i and X_j are two subsets of data series where $i = 1,2,3, \ldots n - 1$ and $j = i + 1, i + 2, i + 3, \ldots, n$.

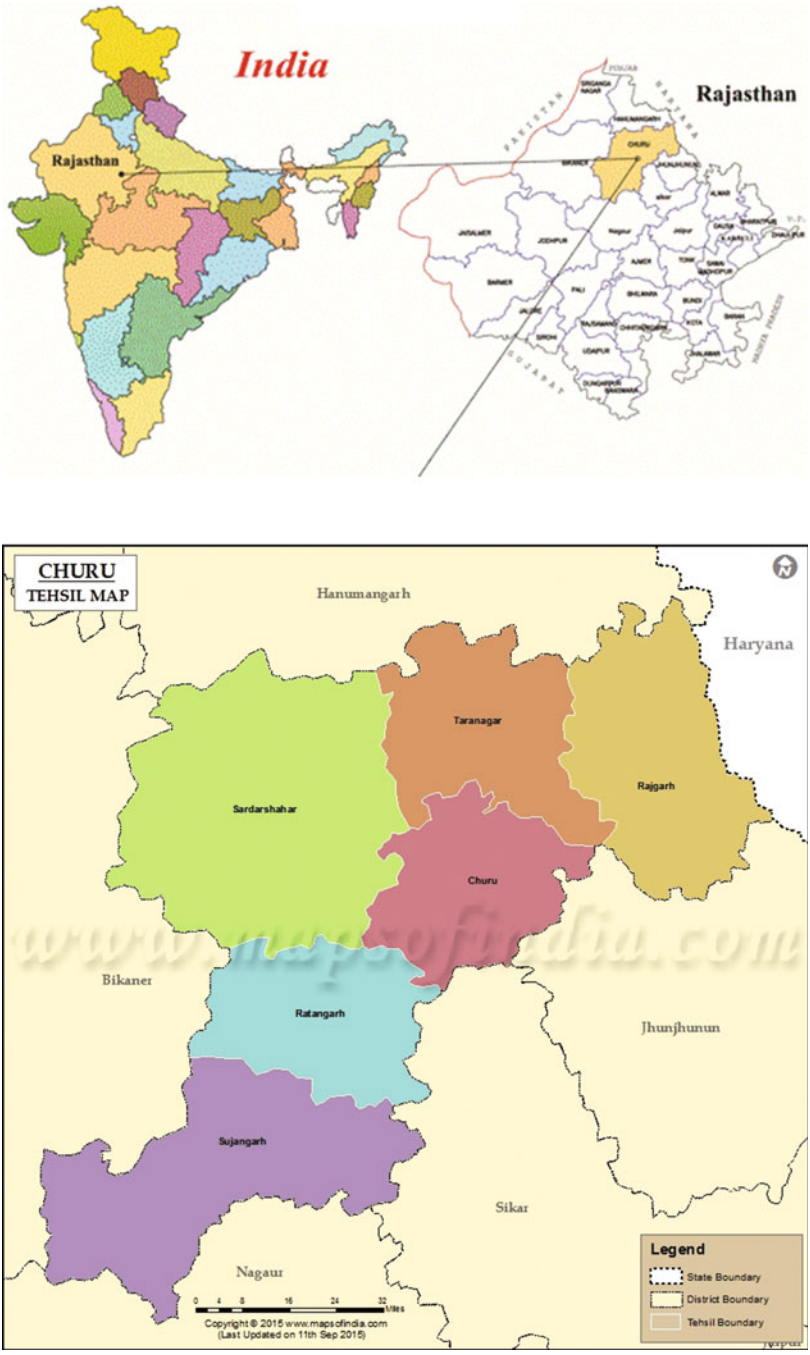

Fig. 20.1 Study area

Table 20.1 Statistical properties of groundwater data

Serial number	Location	Mean	Maximum	Minimum
W1	Ratangarh	37.47	39.50	35.86
W2	Sadarshahar	60.29	65.9	58.41
W3	Sadarshahar	56.32	63.17	52.98
W4	Sadarshahar	60.56	69.4	58.8
W5	Sujangarh	30.12	31.53	28.52

The Mann-Kendall S_m Statistic may be represented as follows:

$$S_m = \sum_{i=1}^{n-1} \sum_{j=i+1}^{n} \text{sign}(X_j - X_i) \tag{20.1}$$

$$\text{Sign}(T_j - T_i) = \begin{cases} 1 \text{ if } X_j - X_i > 0 \\ 0 \text{ if } X_j - X_i > 0 \\ -1 \text{ if } X_j - X_i > 0 \end{cases} \tag{20.2}$$

The variance (σ^2) for the S_m statistic is defined by:

$$\sigma^2 = \frac{[n(n-1)(2n+5)]}{18} \tag{20.3}$$

The standard test statistic Z_s is calculated as follows:

$$Z_S = \begin{cases} \dfrac{S_m - 1}{\sigma} & \text{for } S_m > 0 \\ 0 & \text{for } S_m = 0 \\ \dfrac{S_m + 1}{\sigma} & \text{for } S_m < 0 \end{cases} \tag{20.4}$$

If $|Zs|$ is greater than $Z_{100-\alpha}$, where α represents the chosen significance level (at 5% significance level or 95% confidence level with $Z_{95\%} = 1.96$) then the null hypothesis is invalid implying that the trend is significant (Zhang et al. 2011). Positive values of Z statistics indicate an increasing trend while negative values of Z statistics represent the negative trend (Timbadiya et al. 2013; Gebremicael et al. 2013).

20.2.2 Spearman's Rho Test

Spearman's Rho is a nonparametric test used to determine whether correlation exist between two classifications of the same series of observations (Esterby 1996). In

accordance with this test, the null hypothesis H_0 assumes that the population is independent and identically distributed which is tested against the alternative hypothesis H_1, which assumes that the trend exists. A time series of n data points X_i, where $i = 1$ to n, are ranked according to their value from highest to lowest as $R(\mathrm{X}_i)$.

Then the Spearman-Rho test statistics D_s is given by,

$$D_\mathrm{s} = 1 - \frac{6 \times \sum_{i=1}^{n} \{R(X_i) - i\}^2}{n(n^2 - 1)} \tag{20.5}$$

The standard test statistic Z is calculated as follows:

$$Z = D_\mathrm{s} \sqrt{\frac{(n-2)}{1 - {D_\mathrm{s}}^2}} \tag{20.6}$$

If $|Z|$ is greater than $t_{(1-\alpha/2,n-2)}$, where α represents the chosen significance level, then the null hypothesis is invalid implying that the trend is remarkable.

20.2.3 Sen's Slope Estimator

Sen (1968) proposed the nonparametric Sen's slope statistics. Slope for each pair may be calculated as

$$Q_i = \frac{\left(X_j - X_k\right)}{j - k} \text{ where } (\ j > k) \text{ (for } i = 1, 2, 3 \ldots n) \tag{20.7}$$

where X_j and X_k are the data values at times j and k ($j > k$), respectively.

Sens slope estimator can then be calculated as

$$Q_{\mathrm{med}} = \begin{cases} Q[(n+1)/2] \text{ if } n \text{ is odd} \\ \dfrac{Q_{n/2} + Q_{(\mathrm{n}+2)/2}}{2} \text{ if } n \text{ is even} \end{cases} \tag{20.8}$$

The Q_{med} sign reflects data trend, while its value indicates the steepness of the trend.

20.2.4 Innovative Trend Analysis

Innovative trend analysis was proposed by Şen (2012). The procedure for innovative trend analysis is as follows:

Divide the entire time series into two equal halves
Calculate the average of both the time series as $\overline{Y_1}$ and $\overline{Y_2}$.
Arrange both the time series in ascending order.
Plot a graph with first half of time series on abscissa and second half series on ordinate. Also plot the 1:1 (45°) line on the same plot.

Relative position of scatter point with respect to 45° line demarcates the trend. If all the points lie above the 45° line it represents monotonically increasing trend, on the other hand if all the points lie below the 45° line it would represent monotonically decreasing trend, otherwise trend may not be monotonic (Caloiero et al. 2018; Güçlü et al. 2019).

The magnitude of trend may be calculated (after Şen 2017) as

$$s = \frac{2\left(\overline{Y_2} - \overline{Y_1}\right)}{n} \tag{20.9}$$

Confidence limit (CL) of trend may be calculated using the following relationship

$$\mathrm{CL}(1-\alpha) = 0 \pm s_{\mathrm{cri}}\,\sigma_s \tag{20.10}$$

Where s_{cri} is critical slope; σ_{s} = Slope standard deviation.

$$\sigma_s^2 = \frac{8\sigma^2\left(1-\rho_{Y_2Y_1}\right)}{n^3} \tag{20.11}$$

where $\rho_{Y_2Y_1}$ = Cross-Correlation coefficient of averages of two halves given by

$$\rho_{Y_2Y_1} = \frac{E(Y_2Y_1) - E(Y_2)E(Y_1)}{\sigma_{Y_2}\sigma_{Y_1}} \tag{20.12}$$

Explains the innovative trend analysis. Figure 20.2 shows 1:1 line with two parts of time series on either axis. It may be observed that this graph shows low magnitude, moderate magnitude and high magnitude event and from the plotted points trends for low magnitude, moderate magnitude and high magnitude event can be understood separately. In this way innovative trend analysis have an advantage over nonparametric trend tests, nonparametric trends can only reveal monotonic trend; however, it may be possible that hydrological events of different magnitude may have different trends. As can be observed from Fig. 20.2, low magnitude events are trendless, while moderate magnitude events show significant negative trend and high magnitude events show slight positive trend.

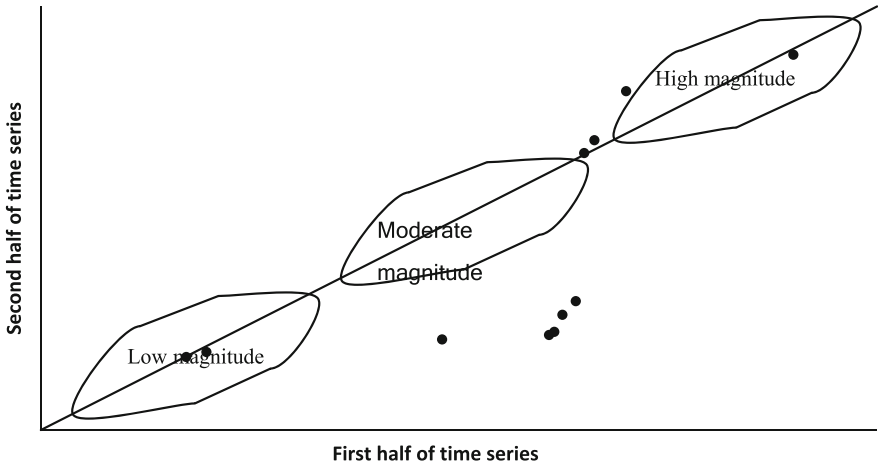

Fig. 20.2 Graphical representation of innovative trend analysis

20.3 Results and Discussions

In the present chapter time series of water level of five wells located in Churu, India, were analysed to recognize the temporal variation in water level. Trend analysis was performed using Mann-Kendall, Spearman-Rho, Sens slope estimator and innovative trend analysis. The results of trend of Mann-Kendall, Spearman-Rho and Sens slope are presented in Table 20.2 while the results of innovative trend analysis with statistical details can be found in Table 20.3. At four out of the five wells, water level was found to be declining significantly, only at one location water level showed positive trend. At Ratangarh and Sujangarh wells (W1 and W5 respectively), negative trend was observed which was insignificant at 5% significance level in accordance with the Mann-Kendall and Spearman-Rho test. However, as the magnitude of trend slope is higher than critical slope for innovative trend analysis as shown in Table 20.3, the trend is considered significant in accordance to innovative trend analysis. Out of the three wells (W2, W3 and W4) located in Sadarshahar, W2 and W4 presented significant negative trend but significant positive trend was observed at W3. Presence of positive trend at 5% significance level is confirmed from all the trend tests.

Perusal of Table 20.3 reveals that for all the location the magnitude of trend slope is higher than critical slope, thereby indicating presence of significant trend at all the locations. It may also be observed that the average of first half of time series is greater than average of second half of the time series for all the wells, except for the well W3, indicating presence of negative and positive trend respectively. Standard deviation at well W3 and W4 are higher as compared to other wells indicating greater fluctuations in water level these wells. On the other hand lowest deviation in water level is observed at well W5 signifying minimum fluctuation in water level.

Table 20.2 Results of trend analysis for water level

Serial number	Mann-Kendall	Spearman-rho	Sens slope
W1	−0.34	−0.17	−0.01
W2	−1.96[a]	−1.99[a]	−0.14
W3	3.47[a]	3.14[a]	0.20
W4	−2.34[a]	−2.54[a]	−0.10
W5	−1.76	−1.71	−0.04

[a]Significant trend at 5% significance level

Table 20.3 Statistical results of Innovative trend test

Serial number	Average of first half ($\overline{Y_1}$)	Average of second half ($\overline{Y_2}$)	Standard deviation (σ)	Cross-Correlation (ρ_{xy})	Trend slope (s)	Critical slope (Scr)
W1	37.84	37.10	1.26	0.65	−0.07[a]	0.04
W2	61.58	59.01	1.96	0.81	−0.23[a]	0.05
W3	55.11	57.53	2.93	0.72	0.22[a]	0.08
W4	61.13	59.99	2.36	0.35	−0.10[a]	0.09
W5	30.34	29.90	0.78	0.86	−0.04[a]	0.01

[a]Significant trend at 5% significance level

These observations are further supported by minimum and maximum water level observed at various wells as reported in Table 20.1.

Figure 20.3 shows the results of innovative trend analysis at various wells. At well W1 moderate water level show significantly downward trends while low and high water levels do not represent any significant trend. At well W2, all the points plot below the 1:1 line indicating that low, moderate and high water levels have declined during second half of the time series and therefore significant downward trend is observed at well W2. It may also be observed from Table 20.3 the trend slope for well W2 is −0.23 which is much smaller than critical slope 0.05.

At well W3, all the points plot above the 1:1 line indicating that low, moderate and high water levels have increased during second half of the time series and therefore significant upward trend is observed at well W3. Also, in Table 20.3 the trend slope for well W3 is reported as 0.22 which is much greater than critical slope 0.08. At wells W4 and W5 most of the points plot below 1:1 line indicating declining trend for these will which is further confirmed from trend and critical slopes as reported in Table 20.3.

Although no conflict was observed in the trend obtained from Mann-Kendall, Spearman-Rho, Sens slope estimator and innovative trend analysis, but, the innovative trend analysis provides the most exhaustive visualization of the changes taking place. In recent times, it has been a common observation that the number of rainy days is decreasing, overall rainfall is decreasing but the frequency of extreme rainfall is increasing (Rainfall is directly or indirectly related to most of the hydrologic observations such as streamflow, groundwater level and evaporation rate, etc.). In

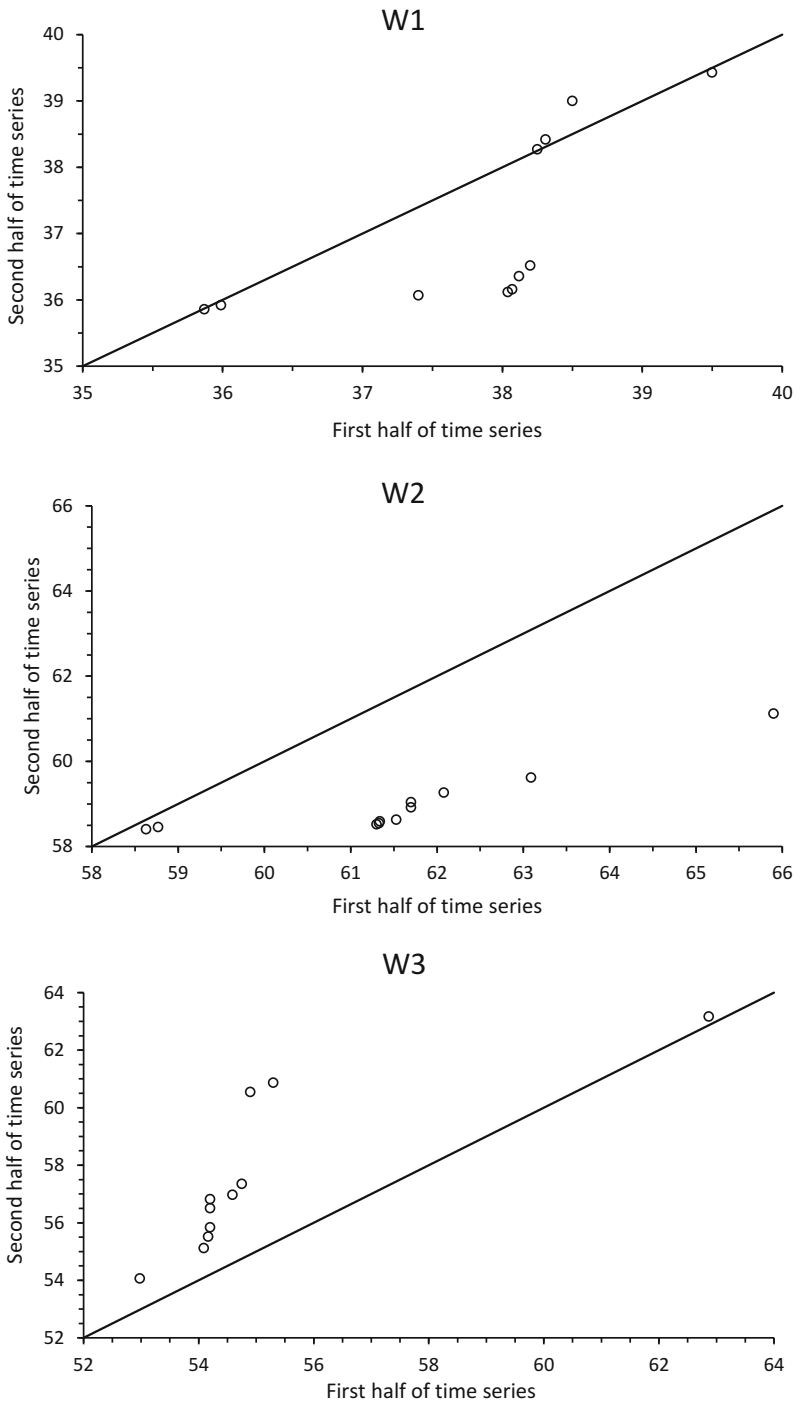

Fig. 20.3 Innovative trend graphs at various locations

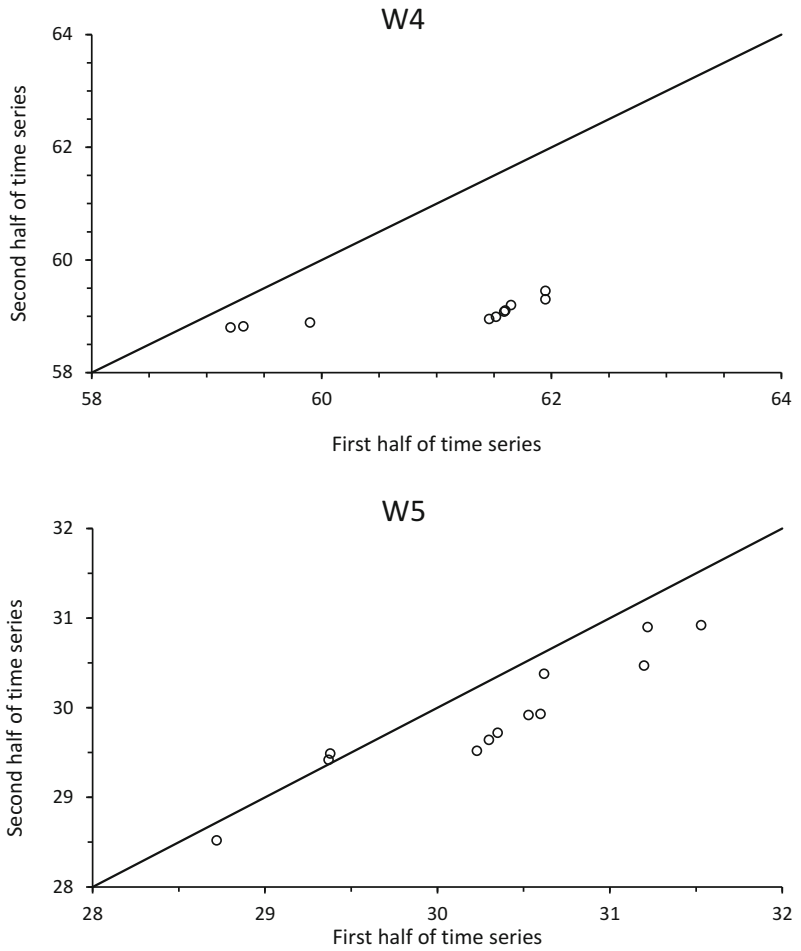

Fig. 20.3 (continued)

such cases Innovative trend analysis can help us to avoid extracting misleading knowledge from the trend results.

Further, with ever increasing population and fast tracked industrialisation declining trend in water level are very common all over the world. Recently, Arshad and Umar (2020) presented a comprehensive review of ground water resources in India. They emphasized that due to population surge and industrial expansion along with climate change has contributed to the decline in quantity as well as quality of groundwater in India. In past few years many parts of Rajasthan, India has experienced acute shortage of water. In this regard, planned and judicious use of available ground resource with every possible attempt for enhancing groundwater recharge could help to maintain sufficient groundwater resources for future.

20.4 Conclusion

Knowledge of available groundwater resource and its future potential provide an important input for the design and management of water supply system. Over the years reliability over groundwater resources has increased due to industrial expansion and dwindling rainfall patterns. In the present chapter, trend analysis of water level of five wells, located in Churu, Rajasthan, India, was performed using Mann-Kendall, Spearman-Rho, Sens slope estimator and innovative trend analysis. At four of the wells water level was found to be declining significantly, only at one location water level showed positive trend. The results of all the trend test were in good agreement with each other. However, unlike monotonic trends detected from other trend tests, innovative trend analysis revealed different trends for low, medium and high water levels. In this regard, it may be concluded that application of innovative trend analysis provides the comprehensive view of the ongoing hydrologic changes in the region. Over the years, many developing countries have experienced steady decline in groundwater resources. Planned and judicious use of available ground resource with every possible attempt for enhancing groundwater recharge could help to maintain sufficient groundwater resources for future.

References

Abiye, T., Masindi, K., Mengistu, H., & Demlie, M. (2018). Understanding the groundwater-level fluctuations for better management of groundwater resource: A case in the Johannesburg region. *Groundwater for Sustainable Development, 7*, 1–7.

Alexander, A. C., Ndambuki, J. M., Salim, R. W., & Manda, A. K. (2018). Groundwater remediation optimization using Solving Constraint Integer Program (SCIP). *Groundwater for Sustainable Development, 7*, 176–184.

Alipour, A., Hashemi, S., Shokri, S. B. S., & Moravej, M. (2018). Spatio-temporal analysis of groundwater level in an arid area. *International Journal of Water, 12*(1), 66–81.

Anand, B., Karunanidhi, D., Subramani, T., Srinivasamoorthy, K., & Suresh, M. (2020). Long-term trend detection and spatiotemporal analysis of groundwater levels using GIS techniques in Lower Bhavani River basin, Tamil Nadu, India. *Environment, Development and Sustainability, 22*, 2779–2800.

Ara, Z., & Zakwan, M. (2018). Estimating runoff using SCS curve number method. *International Journal of Emerging Technology and Advanced Engineering, 8*, 195–200.

Arshad, I., & Umar, R. (2020). Status of urban hydrogeology research with emphasis on India. *Hydrogeology Journal, 28*(2), 477–490.

Bayazit, M., & Onoz, B. (2007). To prewhiten or not to prewhiten in trend analysis. *Hydrological Sciences Journal, 52*(4), 611–624.

Birkinshaw, S. J., Parkin, G., & Rao, Z. (2008). A hybrid neural networks and numerical models approach for predicting groundwater abstraction impacts. *Journal of Hydroinformatics, 10*(2), 127–137.

Cailas, M. D., Cavadias, G., & Gehr, R. (1986). Application of a nonparametric approach for monitoring and detecting trends in water quality data of the St. Lawrence River. *Water Pollution Research Journal of Canada, 21*(2), 153–167.

Caloiero, T., Coscarelli, R., & Ferrari, E. (2018). Application of the innovative trend analysis method for the trend analysis of rainfall anomalies in southern Italy. *Water Resources Management, 32*(15), 4971–4983.

Crawford, C. G., Slack, J. R., & Hirsch, R. M. (1983). *Nonparametric tests for trends in water-quality data using the statistical analysis system* (p. 102). Washington, DC: US Geological Survey.

Daniel, W. W. (1978). *Applied nonparametric statistics*. Boston, MA: Houghton Mifflin.

Demaree, G. R., & Nicolis, C. (1989). Onset of sahelian drought viewed as a fluctuation-induced transition. *Quarterly Journal of the Royal Meteorological Society, 116*(491), 221–238.

Douglas, E. M., Vogel, R. M., & Kroll, C. N. (2000). Trends in floods and low flows in the United States: Impact of spatial correlation. *Journal of Hydrology, 240*(1-2), 90–105.

Ebadati, N., Hooshmandzadeh, M., & Behzad, N. (2014). A comparison of the correlation Matrix and Man-Kendal correlation statistical methods for analyzing the qualitative parameters of Dez River water. *Journal of Magnetic Resonance Report, 2*, 986–1001.

El-Shaarawi, A. H., Esterby, S. R., & Kuntz, K. W. (1983). A statistical evaluation of trends in the water quality of the Niagara River. *Journal of Great Lakes Research, 9*(2), 234–240.

Gibrilla, A., Anornu, G., & Adomako, D. (2018). Trend analysis and ARIMA modelling of recent groundwater levels in the White Volta River basin of Ghana. *Groundwater for Sustainable Development, 6*, 150–163.

Güçlü, Y. S., Dabanlı, İ., Şişman, E., & Şen, Z. (2019). Air quality (AQ) identification by innovative trend diagram and AQ index combinations in Istanbul megacity. *Atmospheric Pollution Research, 10*(1), 88–96.

Hipel, K. W., & McLeod, A. I. (1994). *Time series modelling of water resources and environmental systems* (Vol. 45). Amsterdam: Elsevier.

Hipel, K. W., McLeod, A. J., & Weller, R. R. (1988). Data analysis of water quality time series in Lake Erie. *JAWRA Journal of the American Water Resources Association, 24*(3), 533–544.

Hirsch, R. M., & Slack, J. R. (1984). A nonparametric trend test for seasonal data with serial dependence. *Water Resources Research, 20*(6), 727–732.

Hirsch, R. M., Slack, J. R., & Smith, R. A. (1982). Techniques of trend analysis for monthly water quality data. *Water Resources Research, 18*(1), 107–121.

Jiao, J. J., Zhang, X., & Wang, X. (2015). Satellite-based estimates of groundwater depletion in the Badain Jaran Desert, China. *Scientific Reports, 5*, 8960.

Keim, B. D., Faiers, G. E., Muller, R. A., Grymes, J. M., & Rohli, R. V. (1995). Long-term trends of precipitation and runoff in Louisiana, USA. *International Journal of Climatology, 15*(5), 531–541.

Kendall, M. G. (1975). *Rank correlation methods*. London: Griffin and Co.

Khadri, S. F. R., & Moharir, K. (2016). Characterization of aquifer parameter in basaltic hard rock region through pumping test methods: A case study of Man River basin in Akola and Buldhana Districts Maharashtra India. *Modeling Earth Systems and Environment, 2*, 33.

Khadri, S. F. R., & Pande, C. (2016a). Ground water flow modeling for calibrating steady state using MODFLOW software: A case study of Mahesh River basin, India. *Model Earth System Environment, 2*, 39. https://doi.org/10.1007/s40808-015-0049-7.

Khadri, S. F. R., & Pande, C. (2016b). GIS-based analysis of groundwater variation in Mahesh River Basin, Akola and Buldhana Districts, Maharashtra, India. *IJPRET, 4*(9), 127–136.

Khadri, S. F. R., & Pande, C. (2016c). Geo-environmental resource management in Mahesh River Basin in Akola and Buldhana districts, Maharashtra using remote sensing and GIS techniques. *IJPRET, 4*(9), 151–163.

Lasagna, M., Mancini, S., & De Luca, D. A. (2020). Groundwater hydrodynamic behaviours based on water table levels to identify natural and anthropic controlling factors in the Piedmont Plain (Italy). *Science of the Total Environment, 716*, 137051.

Lehmann, E. I. (1975). *Nonparametrics, Statistical Methods based on ranks*. San Francisco, CA: Holden-Day, Inc.

Li, F., Feng, P., Zhang, W., & Zhang, T. (2013). An integrated groundwater management mode based on control indexes of groundwater quantity and level. *Water Resources Management, 27* (9), 3273–3292.

Lu, X. X., Ashmore, P., & Wang, J. F. (2003). Seasonal water discharge and sediment load changes in the Upper Yangtze, China. *Mountain Research and Development, 23*(1), 56–64.

Mann, H. B. (1945). Nonparametric tests against trend. *Econometrica, 2*, 245–259.

Marghade, D., Malpe, D. B., Duraisamy, K., Patil, P. D., & Li, P. (2020). Hydrogeochemical evaluation, suitability, and health risk assessment of groundwater in the watershed of Godavari basin, Maharashtra, Central India. *Environmental Science and Pollution Research, 2020*, 1–24.

McLeod, A. I., & Hipel, K. W. (1994). Tests for monotonic trend. In *Stochastic and statistical methods in hydrology and environmental engineering* (pp. 245–270). Dordrecht: Springer.

Meade, R. H., & Moody, J. A. (2010). Causes for the decline of suspended-sediment discharge in the Mississippi River system, 1940–2007. *Hydrological Processes: An International Journal, 24*(1), 35–49.

Milliman, J. D., Farnsworth, K. L., Jones, P. D., Xu, K. H., & Smith, L. C. (2008). Climatic and anthropogenic factors affecting river discharge to the global ocean, 1951–2000. *Global and Planetary Change, 62*(3-4), 187–194.

Millimen, J. D., & Meade, R. H. (1983). Worldwide delivery of river sediments to the oceans. *Journal of Geology, 91*(1), 1–21.

Moharir, K. N., Pande, C. B., Singh, S. K., & Del Rio, R. A. (2020). *Evaluation of analytical methods to study aquifer properties with pumping test in Deccan Basalt Region of the Morna River Basin in Akola District of Maharashtra in India. Groundwater hydrology*. London: InTec Open Publication. https://doi.org/10.5772/intechopen.84632.

Moharir, K., Pande, C., & Patil, S. (2017). Inverse modeling of aquifer parameters in basaltic rock with the help of pumping test method using MODFLOW software. *Geoscience Frontiers, 8*(6), 1385–1395.

Muzzammil, M., Alam, J., & Zakwan, M. (2015). *An optimization technique for estimation of rating curve parameters* (pp. 234–240). New Delhi: National Symposium on Hydrology.

Muzzammil, M., Alam, J., & Zakwan, M. (2018). A spreadsheet approach for prediction of rating curve parameters. In *Hydrologic modeling* (pp. 525–533). Singapore: Springer.

Ndlovu, M. S., & Demlie, M. (2018). Statistical analysis of groundwater level variability across KwaZulu-Natal Province, South Africa. *Environmental Earth Sciences, 77*(21), 739.

Pande, C. B. (2020a). Introduction. In *Sustainable watershed development. Springer briefs in water science and technology*. Cham: Springer. https://doi.org/10.1007/978-3-030-47244-3_1.

Pande, C. B. (2020b). Watershed management and development. In *Sustainable watershed development. Springer briefs in water science and technology*. Cham: Springer. https://doi.org/10.1007/978-3-030-47244-3_2.

Pande, C. B. (2020c). Thematic mapping for watershed development. In *Sustainable watershed development. Springer briefs in water science and technology*. Cham: Springer. https://doi.org/10.1007/978-3-030-47244-3_3.

Pande, C. B. (2020d). Sustainable watershed development planning. In *Sustainable watershed development. Springer briefs in water science and technology*. Cham: Springer. https://doi.org/10.1007/978-3-030-47244-3_4.

Pande, C. B., Khadri, S. F. R., Moharir, K. N., & Patode, R. S. (2017). Assessment of groundwater potential zonation of Mahesh River basin Akola and Buldhana districts, Maharashtra, India using remote sensing and GIS techniques. *Sustainable Water Resources Management*. https://doi.org/10.1007/s40899-017-0193-5. ISSN 2363-5037.

Pande, C. B., & Moharir, K. (2018). Spatial analysis of groundwater quality mapping in hard rock area in the Akola and Buldhana districts of Maharashtra, India. *Applied Water Science, 8*(4), 1–17.

Pande, C. B., Moharir, K. N., & Pande, R. (2018). Assessment of morphometric and hypsometric study for watershed development using spatial technology – A case study of Wardha river basin

in the Maharashtra, India. *International Journal of River Basin Management*. https://doi.org/10.1080/15715124.2018.1505737.

Pande, C. B., Moharir, K. N., Singh, S. K., & Varade, A. M. (2019). An integrated approach to delineate the groundwater potential zones in Devdari watershed area of Akola district, Maharashtra, Central India. *Environment, Development, and Sustainability Springer Journal*. https://doi.org/10.1007/s10668-019-00409-1.

Pandey, M., Zakwan, M., Sharma, P. K., & Ahmad, Z. (2018). Multiple linear regression and genetic algorithm approaches to predict temporal scour depth near circular pier in non-cohesive sediment. *ISH Journal of Hydraulic Engineering, 26*, 1–8.

Pathak, A. A., & Dodamani, B. M. (2019). Trend analysis of groundwater levels and assessment of regional groundwater drought: Ghataprabha River Basin, India. *Natural Resources Research, 28*(3), 631–643.

Patle, G. T., Singh, D. K., Sarangi, A., Rai, A., Khanna, M., & Sahoo, R. N. (2015). Time series analysis of groundwater levels and projection of future trend. *Journal of the Geological Society of India, 85*(2), 232–242.

Patle, G. T., Singh, D. K., Sarangi, A., & Sahoo, R. N. (2017). Modelling of groundwater recharge potential from irrigated paddy field under changing climate. *Paddy and Water Environment, 15*(2), 413–423.

Patode, R. S., Nagdeve, M. B., & Pande, C. B. (2016). Groundwater level monitoring of Kajaleshwar-Warkhed Watershed, Tq. Barshitakli, Dist. Akola, India through GIS approach. *Advances in Life Sciences, 5*(24), 11207–11210.

Pilon, P. J., Condie, R., & Harvey, K. D. (1985). *Consolidated frequency analysis package: CFA user manual for version I: DEC PRO series*. Toronto, ON: Enviroment Canada, Water Resources Branch.

Rodell, M., Velicogna, I., & Famiglietti, J. S. (2009). Satellite-based estimates of groundwater depletion in India. *Nature, 460*(7258), 999–1002.

Salam, R., Islam, A. R. M. T., & Islam, S. (2019). Spatiotemporal distribution and prediction of groundwater level linked to ENSO teleconnection indices in the northwestern region of Bangladesh. *Environment, Development and Sustainability, 2019*, 1–27.

Şen, Z. (2012). Innovative trend analysis methodology. *Journal of Hydrologic Engineering, 17*(9), 1042–1046.

Şen, Z. (2017). Innovative trend significance test and applications. *Theoretical and Applied Climatology, 127*(3-4), 939–947.

Sharma, P., Machiwal, D., & Jha, M. K. (2019). *Overview, current status, and future prospect of stochastic time series modeling in subsurface hydrology*. New York, NY: Elsevier.

Siakeu, J., Oguchi, T., Aoki, T., Esaki, Y., & Jarvie, H. P. (2004). Change in riverine suspended sediment concentration in central Japan in response to late 20th century human activities. *Catena, 55*(2), 231–254.

Singh, O., Kasana, A., Singh, K. P., & Sarangi, A. (2019). Analysis of drivers of trends in groundwater levels under rice–wheat ecosystem in Haryana, India. *Natural Resources Research, 29*, 1101–1126.

Sneyers, J. R. (1990). *On statistical analysis of series on observations. Technical note no. 143, WMO no. 415*. Geneva: World Meterological Organization.

Tirkey, N., Parhi, P. K., Lohani, A. K., & Chandniha, S. K. (2020). Analysis of precipitation variability over Satluj Basin, Himachal Pradesh, India: 1901–2013. *Journal of Water and Climate Change, 2020*, jwc2020136.

Tsanis, I. K., Coulibaly, P., & Daliakopoulos, I. N. (2008). Improving groundwater level forecasting with a feedforward neural network and linearly regressed projected precipitation. *Journal of Hydroinformatics, 10*(4), 317–330.

Van Lanen, H. A. J., & Peters, E. (2000). Definition, effects and assessment of groundwater droughts. In *Drought and drought mitigation in Europe* (pp. 49–61). Dordrecht: Springer.

Walling, D. E., & Fang, D. (2003). Recent trends in suspended sediment loads of the world's rivers. *Global and Planetary Change., 39*, 111–126.

Yilmaz, A. G., Shanableh, A., Al-Ruzouq, R. I., & Kayemah, N. (2020). Spatio-temporal trend analysis of groundwater levels in Sharjah, UAE. *International Journal of Environmental Science and Development, 11*(1), 9–14.

Yue, S., Pilon, P., Phinney, B., & Cavadias, G. (2002). The influence of autocorrelation on the ability to detect trend in the hydrological series. *Hydrological Process, 16*, 1807–1829.

Zakwan, M. (2018). Spreadsheet-based modelling of hysteresis-affected curves. *Applied Water Science, 8*(4), 101–105. https://doi.org/10.1007/s13201-018-0745-3.

Zakwan, M. (2019). Comparative analysis of the novel infiltration model with other infiltration models. *Water and Environment Journal, 33*(4), 620–632.

Zakwan, M. (2020). Revisiting maximum observed precipitation and discharge envelope curves. *International Journal of Hydrology Science and Technology, 10*(3), 221–229. https://doi.org/10.1504/IJHST.2020.107215.

Zakwan, M., Ahmad, Z., & Sharief, S. M. V. (2018). Magnitude-frequency analysis for suspended sediment transport in the Ganga River. *Journal of Hydrologic Engineering, 23*(7), 05018013.

Zakwan, M., & Ara, Z. (2019). Statistical analysis of rainfall in Bihar. *Sustainable Water Resources Management, 5*(4), 1781–1789.

Zakwan, M., Khan, I., Ara, Z., Rahim, Z. A., & Sharief, S. M. V. (2019). Trend analysis of rainfall in Bihar. *Water Resources Management (WRM2019), 2019*, 79–85.

Zetterqvist, L. (1991). Statistical estimation and interpretation of trends in water quality time series. *Water Resources Research, 27*(7), 1637–1648.

Zhang, W., Shousheng, M. U., Zhang, Y., & Kaimin, C. H. E. N. (2011). Temporal variation of suspended sediment load in the Pearl River due to human activities. *International Journal of Sediment Research, 26*(4), 487–497.

Zhou, T., Wang, F., & Yang, Z. (2017). Comparative analysis of ANN and SVM models combined with wavelet preprocess for groundwater depth prediction. *Water, 9*(10), 781.

Chapter 21
Change Detection Analysis and Delineation of Artificial Groundwater Recharge Suitability Zone for Dindigul Block Using Geoinformatics Techniques

S. Arivazhagan, A. Karthi, M. Kirubakaran, and V. T. Mubasheer

Contents

21.1 Introduction 407
21.2 Study Area 409
21.3 Materials and Methods 410
21.4 Analysis of Artificial Recharge Potential Zones 412
21.5 Results and Discussion 418
21.6 Artificial Recharge Mapping 419
21.7 Conclusion 428
21.8 Recommendation for Suitable Recharge Structures 430
References 430

21.1 Introduction

Remote Sensing (RS) data are as important source which have been widely used for change detection analysis of vast areas in the past few decades (Pande and Moharir 2015). An unexpected city growth is an indicator of rapid industrialization, which may reduce the quality of the environmental health of a specific region. The urban

S. Arivazhagan (✉) · A. Karthi
Centre for Applied Geology, The Gandhigram Rural Institute-Deemed to be University, Dindigul, Tamilnadu, India

M. Kirubakaran
Sri Vickiy and Co., Erode, Tamil Nadu, India

V. T. Mubasheer
Kozhikode, Kerala, India

C. B. Pande, K. N. Moharir (eds.), *Groundwater Resources Development and Planning in the Semi-Arid Region*, https://doi.org/10.1007/978-3-030-68124-1_21

monitoring provides the planners and decision-makers required information regarding the current state-run of development and the nature of changes which have been occurred (Arivazhagan and Kirubakaran 2016; Kirubakaran et al. 2016; Arivazhagan et al. 2018; Pande 2020a). Change detection is the measure of the distinct data framework and thematic change information that can guide to more tangible insights into underlying process involving Land use/Land cover changes than the information obtained from continuous change (Ramachandra and Uttam 2004; Pande et al. 2018b). Groundwater storage and recharge are fundamental components of hydrological system (Samson and Elangovan 2015; Pande et al. 2018a, b) and also the management of both surface and subsurface water resources is very urgent need.

The artificial groundwater recharge plays a key role in the sustainable management of groundwater resources and practice of artificial recharging is increasingly emerging as a powerful tool in water resource management. The Artificial groundwater recharge is a process by which the groundwater reservoir is augmented at a rate exceeding the increasing rate under natural conditions of renewal (Bhattacharya 2010; Magesh et al. 2012; Pande et al. 2017; Balamurugan et al. 2020a, b; Kirubakaran et al. 2019, 2020).

The artificial recharge is the anthropological planned activity of supplementing the quality amount of groundwater avail through to increase the natural replenishment or percolation of surface waters into groundwater aquifers, which resulting in a corresponding increase in the amount of groundwater available for abstraction (Khadri and Moharir 2016; Khadri and Pande 2016; Moharir et al. 2017, 2020; Kumar and Balamurugan 2018). In India, these methods have been used for quite some time and its antique evolution is briefly outlined by many works in the field of groundwater studies (Prabhu and Venkateswaren 2015). The artificial recharge has been listed in many beneficial purposes although the primary objective of this technology is to preserve or enhance groundwater resources (Bastiaansen et al. 1998; Pande and Moharir 2018c; Pande 2020c; Patode et al. 2017). The artificial recharge study is mostly site-specific and descriptive in nature, which gives slight insight into the potential success of implementing this technology in other locations. The Geographic Information System (GIS) techniques have many advantages over older, improved georeferenced thematic map analysis and interpretations (Thapinta and Hudak 2003; Martin et al. 2005; Venkata et al. 2008; Chowdary et al. 2009; Singh et al. 2013; Malik and Rajeshwari 2015). The important consideration has been remunerated to artificial groundwater recharge in water resource management in arid and semi-arid regions (Ghayoumian et al. 2007; Prabhu and Venkateswaren 2015). In recent decades many researchers like Martin et al. (2005), Chowdhury et al. (2010), Singh et al. (2013); Prabhu and Venkateswaren (2015), and Malik and Rajeshwari (2015) are incorporated impeccable methodology to demarcate the artificial recharge zones as well as to find promising artificial recharge sites using integrated RS, GIS, and Multi-Criteria Decision Making (MCDM) techniques for augmenting groundwater resources (Pande 2020b, d).

Samson and Elangovan (2015) have tried to identify the groundwater recharge potential zones in Namakkal district of Tamilnadu state, India by using Weighted Index Overlay Analysis (WIOA) and the ArcGIS software used to integrate the thematic layers of soil, geology, geomorphology, lineament, land use/ land cover, rainfall, groundwater level, and slope. According to Sajikumar and Gigo (2013) integrated Analytic Hierarchy Process (AHP) and GIS techniques were the most suitable combination for groundwater prospects study. The prime purpose of AHP tool is to compute the weights of different parameters/ themes were computed using through Multi-Criteria Evaluation (MCE) technique (Pande et al. 2019). Dinesan et al. (2015) have been delineated groundwater prospect zones using RS and GIS for Melattur Grama Panchayat in Malappuram district of Kerala by using Landsat datasets. Anbazhagan et al. (2005) mapped the artificial recharge site and also estimated runoff for Ayyar basin by using of RS and GIS method. Muralitharan and Palanivel (2015) utilized integrated RS, GIS, and AHP technique for demarcation of Groundwater target zones at the Karur district.

The study aims to find out the changes occurred in the urban, water bodies, and to acquaint the best artificial recharge zones in the study area for ground water managements. The change detection analysis is required to study the reduction in surface water bodies and also urban sprawl in the Dindigul block, which would be the key factors for future water resources sustainability. So, this integrated approach will be utilized to investigate suitable recharge sites with special reference landuse changes (Pande et al. 2017). Hence, this study aims to map the artificial recharge structures suitable zones. The Artificial recharge purpose is to enhancing the natural replenishment of ground water storage by some method of construction, spreading of water, or by artificially changing natural conditions for the important areas which under water dearth. Therefore, the Pair wise comparison analytical hierarchical method applied to map the artificial structured zones in the study area.

21.2 Study Area

Dindigul block, Dindigul District in Tamilnadu is situated in the location between Latitude of 77°59′16.901″ E and Longitude of 10°21′41.11″ N, which is well known for the water scarcity of surface and subsurface water. The total aerial coverage of the study area is 253.21 km^2. The maximum abounded water bodies such as streams, bonds, Kodavanar river crosses over the study area. In summer season, most of the water bodies are drought then the water level is reduced. Morphologically, this area originated from denudational landforms with maximum abounded incept soils. In Dindigul block, the agricultural lands are conserved into built-up and industrial purposes. The minority of peoples are only utilizing the ground water for cultivating agricultural lands. In the study area, many buildings were constructed over water bodies. The ground water is contaminated with salty water which is used for agricultural purpose. The base map of the study area is shown in the Fig. 21.1.

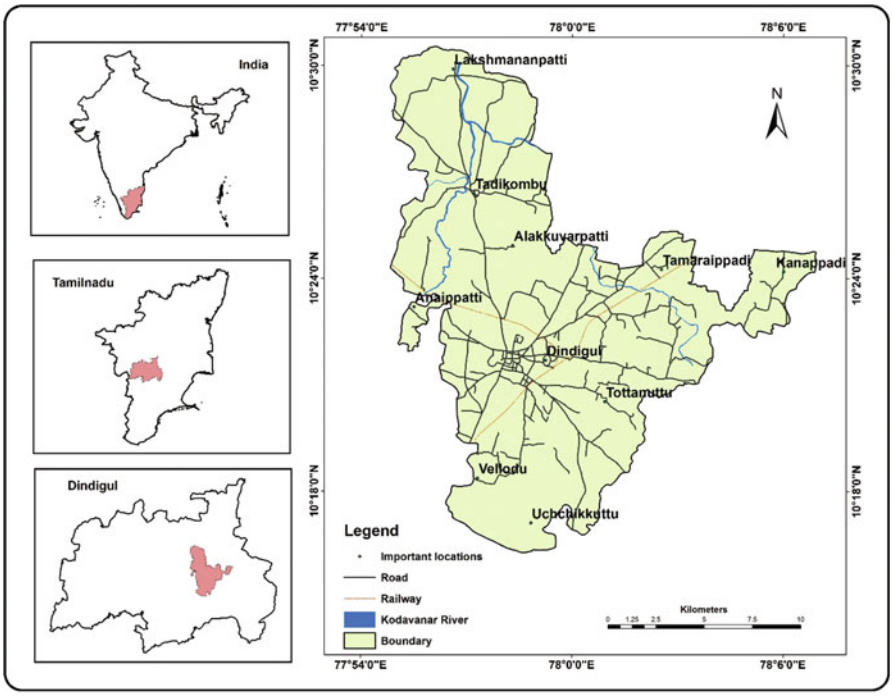

Fig. 21.1 Base map of the Dindigul block study area

21.2.1 Climate and Rainfall

Dindigul has a tropical climate and the average temperature is about 27.8 °C, where the rainfall averages 717 mm. The driest month is March, with 11 mm of rainfall. The greatest amount of precipitation occurs in October, with an average of 180 mm. The warmest month of the year is May, with an average temperature of 30.4 °C. The lowest average temperatures in the year occur in January, when it is around 24.8 °C. The difference in precipitation between the driest month and the wettest month is 169 mm. The variation in temperatures throughout the year is 5.6 °C (Dindigul climate Data n.d.).

21.3 Materials and Methods

The present methodology involves three major parts; (1) identifying the changes that occurred in between the different periods of Dindigul block, (2) AHP pairwise analysis process is used to find the artificial site suitable groundwater recharge

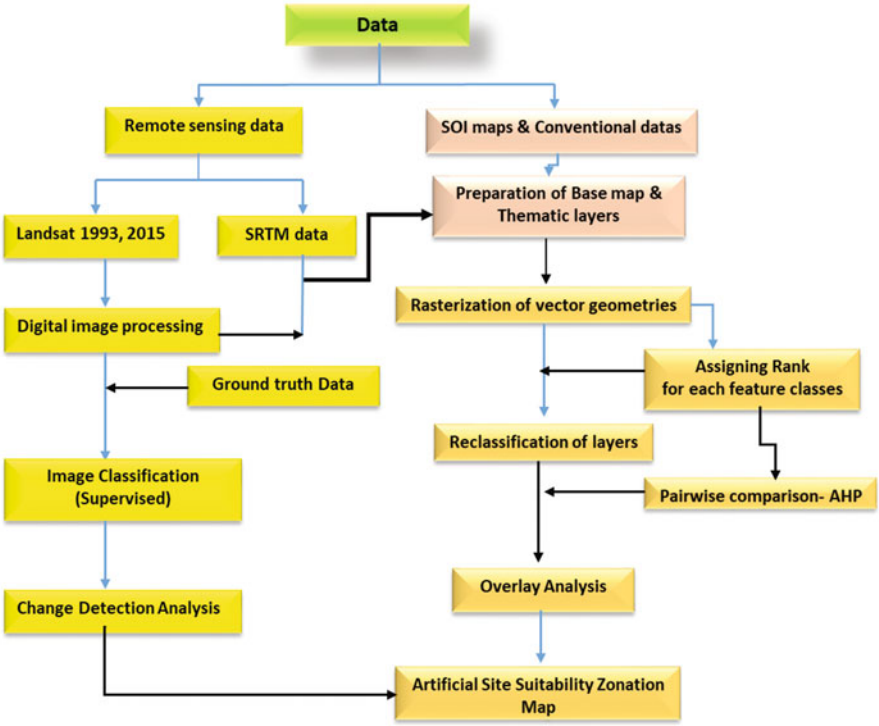

Fig. 21.2 The flow chart is showing the methodology adopted in the present study

zones, and (3) integrate both the results to arrive sustainable final resultant map. The methodology flow chart is shown in the Fig.21.2.

21.3.1 Materials

In the present study, the GIS platform spatial and conventional data sets which were collected from various sectors/organizations. The spatial data sets such as Landsat 5 (1993) and LANDSAT 8 OLI/TIRS (2015) are downloaded from USGS official server, Shuttle Radar Topographic Mission—Digital Elevation model (SRTM—30 m spatial resolution) data downloaded from USGS website, Geological Survey of India topographic maps with 1:50,000, the existing maps like European Soil Data Centre (ESDC) soil map and Survey of India's conventional data are collected from concern organizations for preparation of geology and geomorphology.

Table 21.1 Band combinations of LANDSAT 5 and LANDSAT 8 (USGS)

Composite name	LANDSAT 5	LANDSAT 8	Application
Color infrared	4,3,2	5,4,3	Vegetation
True color	3,2,1	4,3,2	Urban, water bodies
False color	5,4,3	6,5,4	Vegetation
False color	7,4,2	7,5,3	Vegetation
Pseudo color	5,4,2	6,5,3	Road networks and vegetation

21.3.2 Methodology

21.3.2.1 Digital Image Processing

The Arc GIS and Digital image processing (Envi, Erdas) softwares were used to digitally process the Landsat 5 (1993) and Landsat 8 (2015) datasets and generated various outputs. The image processing method involves elementary band combinations, such as True Color Composite (TCC), False Color Composite (FCC), and Pseudo Color Composite (PCC). The range of image enhancement techniques are broad but composite generation is one of the fundamental techniques were used in this study. Table 21.1 shows the different band combinations of Landsat 5 and Landsat 8. The False color composite image, True color composite image, and Pseudo color composite images shown in the Figs. 21.3, 21.4, and 21.5 respectively.

21.3.2.2 LULC Classification and Mapping

The land use and land cover (LULC) classification system described in this study involves first level classification. The LU/LC feature classes are selected based on National Remote Sensing Centre (NRSC) LU/LC classification approach used to classify Landsat 5 and Landsat 8 image (Pande 2014; Pande and Moharir 2014). The NRSC classification is Indian standard classification for land use land cover patterns which is given in the Table 21.2. The Landuse/Land cover map of the Landsat-5 (1993) and Landsat-8 (2015) and their overall changes were shown in the Fig. 21.6a, b, respectively.

21.4 Analysis of Artificial Recharge Potential Zones

21.4.1 Preparation of Thematic Layers

In the present study, we adopted the RS and GIS techniques for mapping artificial recharge zones, therefore we have taken seven different thematic layers such as Geology, Geomorphology, Soil, Slope, Landuse/Landcover, Lineament density, and

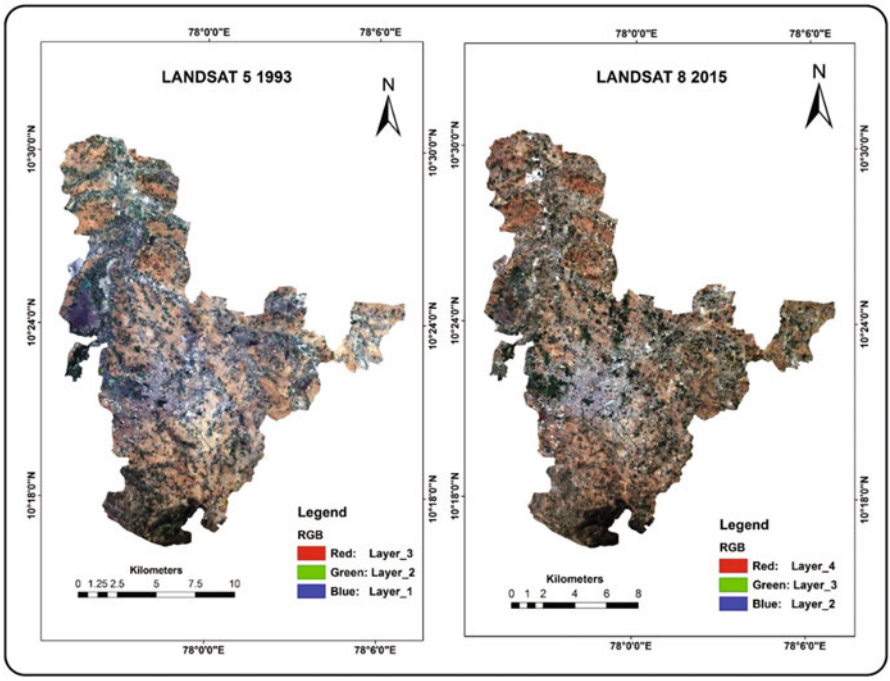

Fig. 21.3 True color composite (TCC) of Landsat 5 and Landsat 8 satellites data

Drainage density to map the potential artificial recharge zones. The geology, geomorphology maps were prepared by using Geological Survey of India existing data. The soil map of the study area has been generated through ESDC data. The Land use/Land cover map of the study area is generated from recent Landsat data. Slope map of the study area was prepared from SRTM–DEM data. The Lineament map of the study area was obtained from Bhuvan data center. Drainage map was digitized from Survey of India Toposheet (SOI).

21.4.2 AHP Pair Wise Analysis

Analytic Hierarchy Process (AHP) method is very helpful multi-parameter assessment can provide solutions for the complicated decision-making problems which was proposed by Saaty (1980, 1990). The influence in percentage of prepared layers can be derived from the pairwise comparison decision-making AHP technique. An approach to derive the weights for different factors is to draw a schematic sketch of the interrelationships of the different factors. The stronger influence of the one factor on other factors the larger its relative importance which hints to a superior weight

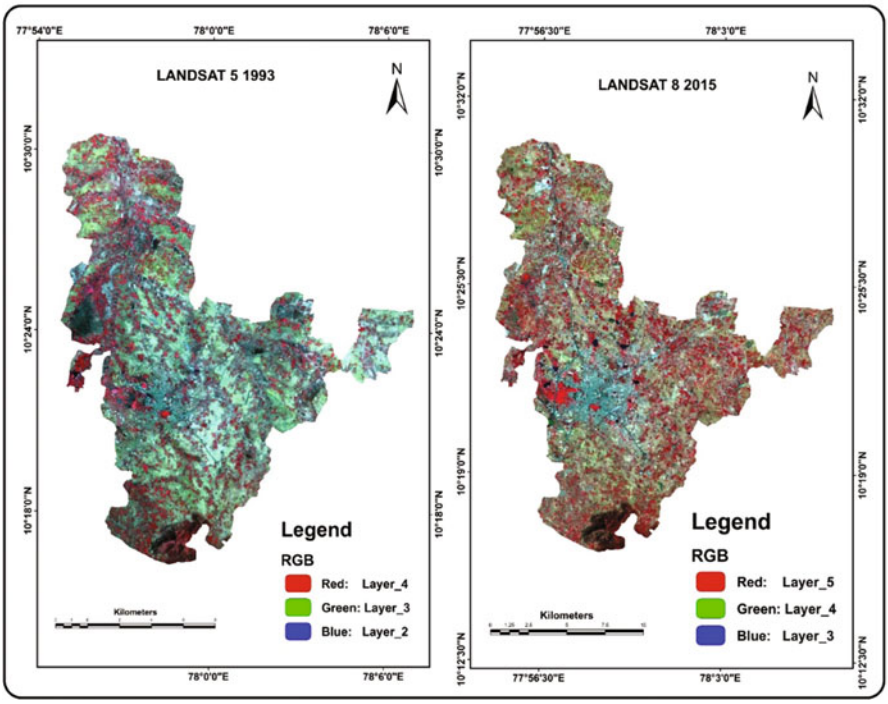

Fig. 21.4 False color composite (FCC) of Landsat 5 and Landsat 8 satellites data

(Yeh et al. 2016; Thapa et al. 2017). The Saaty's scale used to define the various themes with their scale of rank and priority which aids to establish the principles in analytic hierarchical order through a pairwise comparison matrix. The basic concept of Rank scale and their characters listed in the Table 21.3. The current study involves in the theory of hierarchies for demarcating the artificial groundwater potential zones.

The present study decision-making problem is defined with seven thematic layers and a parametric scale of the layers is assigned based on the direct and indirect influences of each parameter in the artificial groundwater recharge potential. Each layer correlated with remaining layers, and based on this comparison, pairwise relation matrices were generated and the weights of each thematic layer considered as the principal Eigen value of the generated matrix. The reliability of the result was referred by the calculated consistency index (CI) and consistency ratio (CR) values. Saaty (1990) and Kirubakaran et al. (2016) used the following formula for consistency analysis;

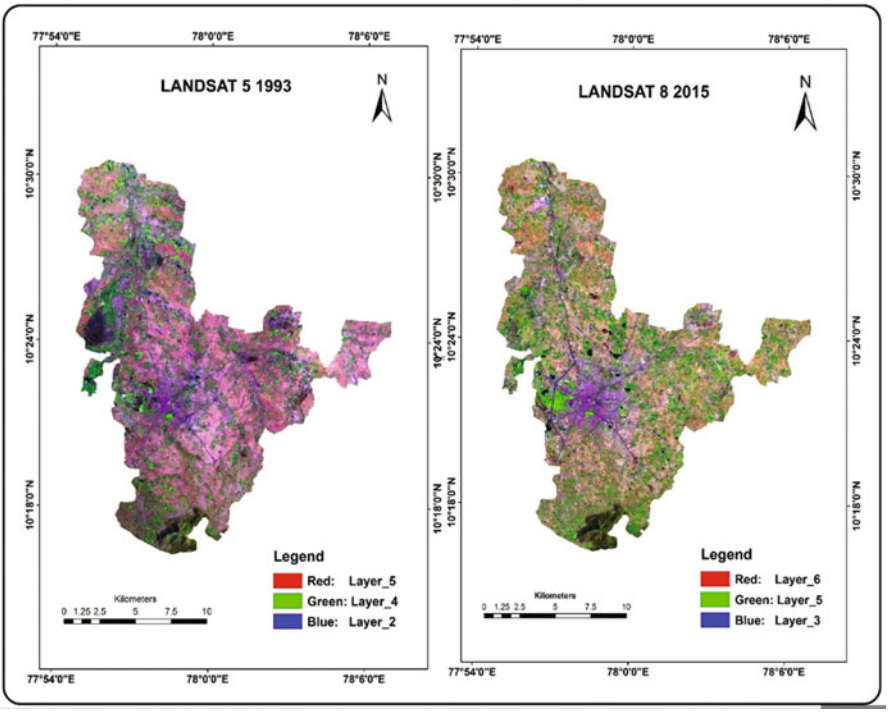

Fig. 21.5 Pseudo color composite (PCC) of Landsat 5 and Landsat 8 satellites data

Table 21.2 The classification scheme of present study area selected from NRSC classification

Sr. no	Classification (level 1)
1.	Agricultural land
2.	Built-up land
3.	Forest
4.	Waste land
5.	Water bodies

$$\text{Consistency Index (CI)} = \frac{\text{Maxprincipal Eignen Value} - \text{Number of factors}}{\text{Number of factors} - 1} \tag{21.1}$$

$$\text{Consistency ratio (CR)} = \frac{\text{Consistency index}}{\text{Random consistency index}} \tag{21.2}$$

Followed by each parameter and their respective classes are allocated the ranks and weights based on their comparative potential contribution by using pairwise normalized matrix which is shown in the Table 21.6. The raster calculation of all of these parameters incorporated via overlay weighted analysis into ArcGIS software and followed by the resulting map has been derived.

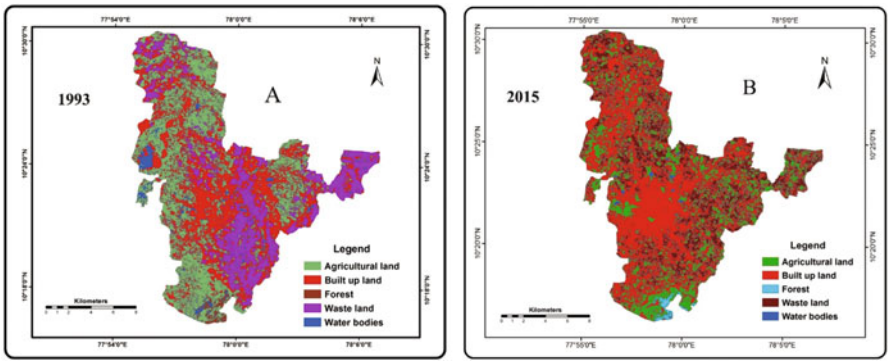

Fig. 21.6 The study area Dindigul block land use/land cover maps of 1993 (**a**) and 2015 (**b**)

Table 21.3 Rank scale and their definition

Ranks	Definition
1	Equal importance
2	Weak or slight
3	Moderate importance
4	Moderate plus
5	Strong importance
6	Strong plus
7	Very strong
8	Very very strong
9	Extreme importance

21.4.3 Identification of Artificial Recharge Zone

To delineate artificial recharge potential zones and suitable site structures for artificial recharge of groundwater, different thematic layer maps were prepared using remote sensing techniques or data collected by conventional methods. The selection and preparation of thematic layers of the study area is namely thematic layers include lithology, lineaments, geomorphology, landform, and drainage maps from remotely sensed data, and slope from topographic maps were prepared. By integrating the different thematic layers in the GIS environment, potential zones for artificial recharge to groundwater were specified.

Table 21.6 Pair-wise comparison matrix for the seven themes and calculation of normalized by the Analytic Hierarchy Process (AHP)

	Parameters						
Parameters	Geology	Lineament density	Land use	Geomorphology	Soil	Drainage density	Slope
Geology	8/8	8/6	8/7	8/9	8/6	8/7	8/6
Lineament density	6/8	6/6	6/7	6/9	6/6	6/7	6/8
Landuse/land cover	7/8	7/6	7/7	7/9	7/6	7/7	7/8
Geomorphology	9/8	9/6	9/7	9/9	9/6	9/7	9/8
Soil	6/8	6/6	6/7	6/9	6/6	6/7	6/8
Drainage density	7/8	7/6	7/7	7/9	7/3	7/7	7/8
Slope	6/8	6/6	6/7	6/9	6/6	6/7	6/8

21.5 Results and Discussion

21.5.1 Change Detection Analysis

In the present study, the change detection analysis is performed using Topo maps, Landsat 5, and Landsat 8 satellite images for the Dindigul block. It is observed that, the built-up area of Dindigul block has increased 47.05% (+44.02 km^2) within the study period (1993–2015). Dindigul is one of the most developing Districts in Tamil Nadu, India. Most of the major Education Institutions, Industries, etc. are situated and upcoming here. The results were observed based on Image classification and its interpretation. From the total area of 253.21 km^2, the following changes were obtained; The Agriculture land is drastically reduced in the area about 38.5% (36.55 km^2) within 22 years period whereas waste land is increased about 3.41% (1.81 km^2). The area covered by forest is reduced 25% (0.68 km^2) and more than 69.6% (6.64 km^2) of the water bodies are disappeared/or consumed for other purposes. The Land use/Land cover graphical interpretation is shown in the Fig. 21.7. The Landuse/Landcover different classes and their changes are shown listed in the Table 21.4.

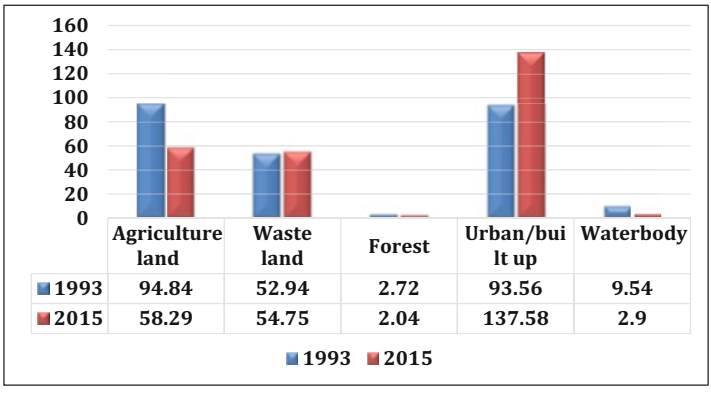

Fig. 21.7 The graphical interpretation of the land use/land cover changes in between 1993 and 2015

Table 21.4 The Land Use Land Cover different classes and their overall changes in the period of 1993–2015

S. no.	Classes	1993 (km^2)	2015 (km^2)	Changes in (km^2)	Changes (%)
1.	Agricultural land	94.84	58.29	36.55(−)	38.53
2.	Built-up land	93.56	137.58	44.02(+)	47.05
3.	Waste land	52.94	54.75	1.81(+)	3.41
4.	Forest	2.72	2.04	0.68(−)	25
5.	Water bodies	9.54	2.9	6.64(−)	69.6

21.6 Artificial Recharge Mapping

The Assessment of ranks to various thematic maps are based on the important toward the artificial recharge technique. The Geology is mostly underlain by Archean metamorphosed complex in the area. They composed of Hornblende biotite gneiss throughout the area and covers about 249.8 km^2 whereas small area covered by charnockite and quartzite i.e., 3.46 and 0.29 km^2 respectively. The geological map is shown in the Fig. 21.8. Based on their influence, the artificial recharge site containment is ranked as 8.

The majority of the area occupied moderately weathered Pediplain/moderately buried Pediplain and large ridge type of structural hill occurs in Inselberg and pediment/valley floor in the study area (Khadri and Pande 2015). Geomorphologically this area is formed in Denudational lands forms (Khadri et al. 2013). The Geomorphology map is shown in the Fig. 21.9. For artificial recharge site containment based it is ranked as 9. The study area is occupied by various types of soils such as red loam, sandy coastal alluvium, red sandy soil, and laterite. The Fig.21.10 is showing the soil map of the study area. The soil has been ranked as 6 for artificial recharge site structure arrangement based on its soil containment. Land use provides important indicators of the extent of groundwater requirements and groundwater utilization, as well as being an important indicator in the selection of sites for artificial recharge of groundwater. Land use and land cover are classified into five categories, (1) Agricultural land, (2) Built-up area, (3) Forest, (4) Waste land, (5) Water bodies. Based on their effect on the infiltration of surface water and suitability toward the artificial recharge site containment they are ranked as 7. Figure 21.11 is shown the land use land cover map of the study area.

The slope of an area is indicator of the infiltration rate. The places where the slope is more, the contact period of water with surface is less, hence, the infiltration rate will be less. In places where the slope is relatively less, the contact of water with the surface will be higher and the infiltration rate will be high, thus resulting in good groundwater potential infiltration. The study area was classified into five categories: nearly level (0–5°), gentle slope (5–10°), high slope (10–20°), and the other two classes represent the hills (20–30° and 30–49°). The slope map of the study area reveals that the slope was high in the hilly terrain which was situated in the southern parts of the study area. Major portion of the block falls under nearly level category (0–5°). Slope map is ranked as 6 based on their elevation difference with respect to the effect toward the artificial recharge zone delineation. Figure 21.12 is shown the slope distribution of the study area. The Lineaments image visualizes the three different types of lineaments such as drainage parallel lineament (Dominant), joint/fracture lineaments, and ridge parallel lineaments (less) in the study area which indicates that most of the surface of the study area is low grade in elevation and geologically less active spot. The orientation of the lineaments is NW-SE, W-E, NE-SW, N-S. From the lineaments, the lineament density map has generated and is shown in the Fig. 21.13. The lineament density indicates the relative infiltration capacity of an area. Places where the density is high, infiltration would be more and

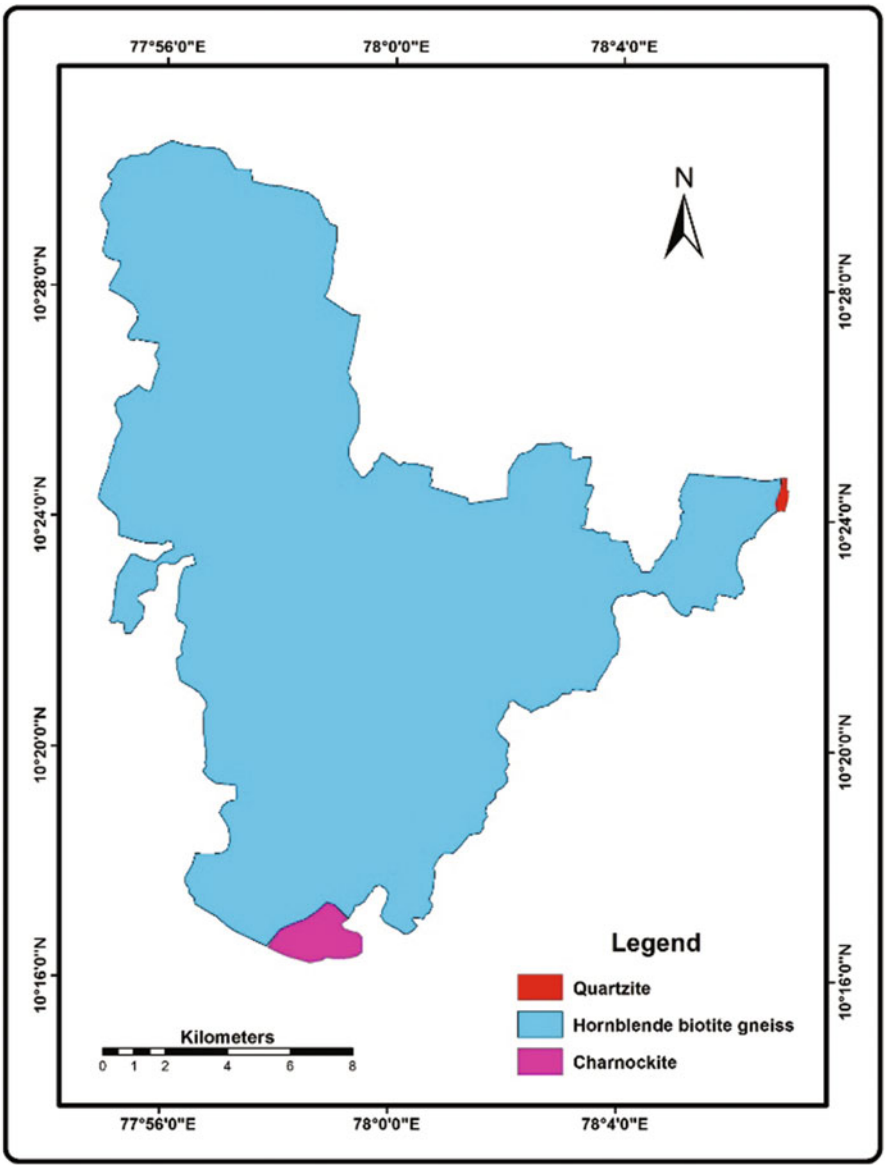

Fig. 21.8 The geology map

of less lineament density, infiltration would be less. Based on the effect of lineament density over the artificial recharge zone delineation has been ranked as 6.

The drainage layers via the drainage density was prepared and calculated using GIS environment (Integrated distance weighted (IDW) method). The drainage density directs the closeness of spacing of channels as well as nature of surface

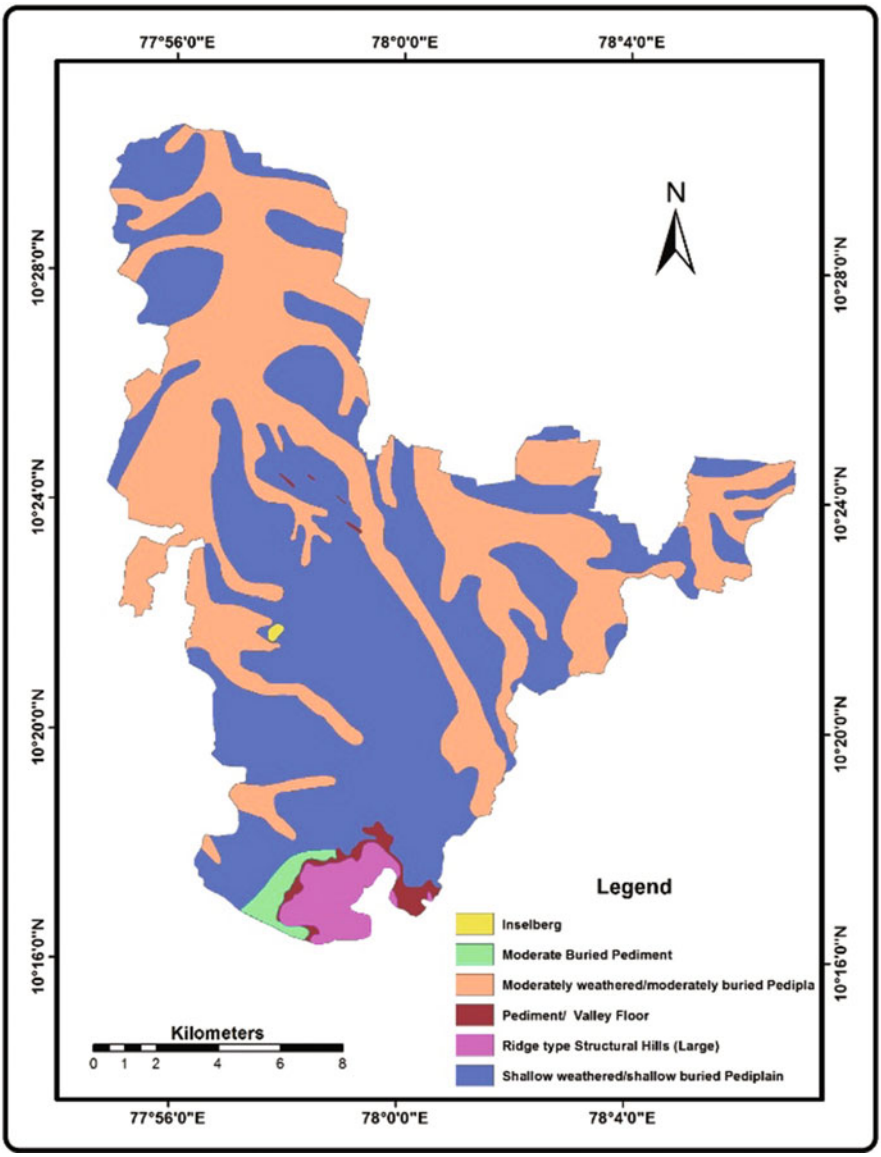

Fig. 21.9 The geomorphology map

material (Prasad et al. 2008). It was the measure of total length of the stream segment of all orders per unit area and it was affected by factors which control the characteristic length of the stream-like resistance to weathering, permeability of rock formation, climate, vegetation, etc., (Chopra et al. 2005). The drainage density indicates the relative run off of an area where the density is high, runoff would be

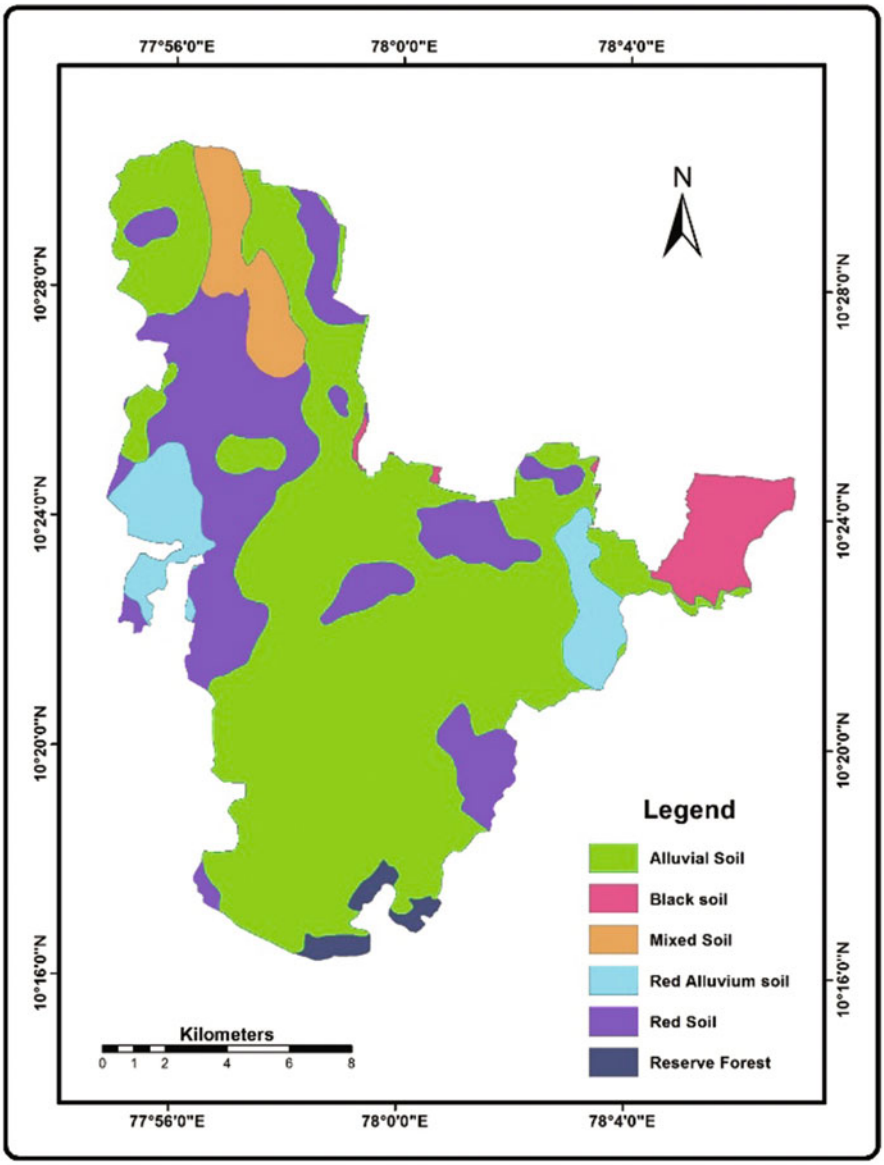

Fig. 21.10 The soil map

more, whereas less drainage density, run off would be less. The area having less drainage density is more suitable place artificial recharge site. The Drainage density ranked as 7 and their inter classes are weight based on their effect toward the infiltration. The Fig. 21.14 shows the drainage density map of the study area.

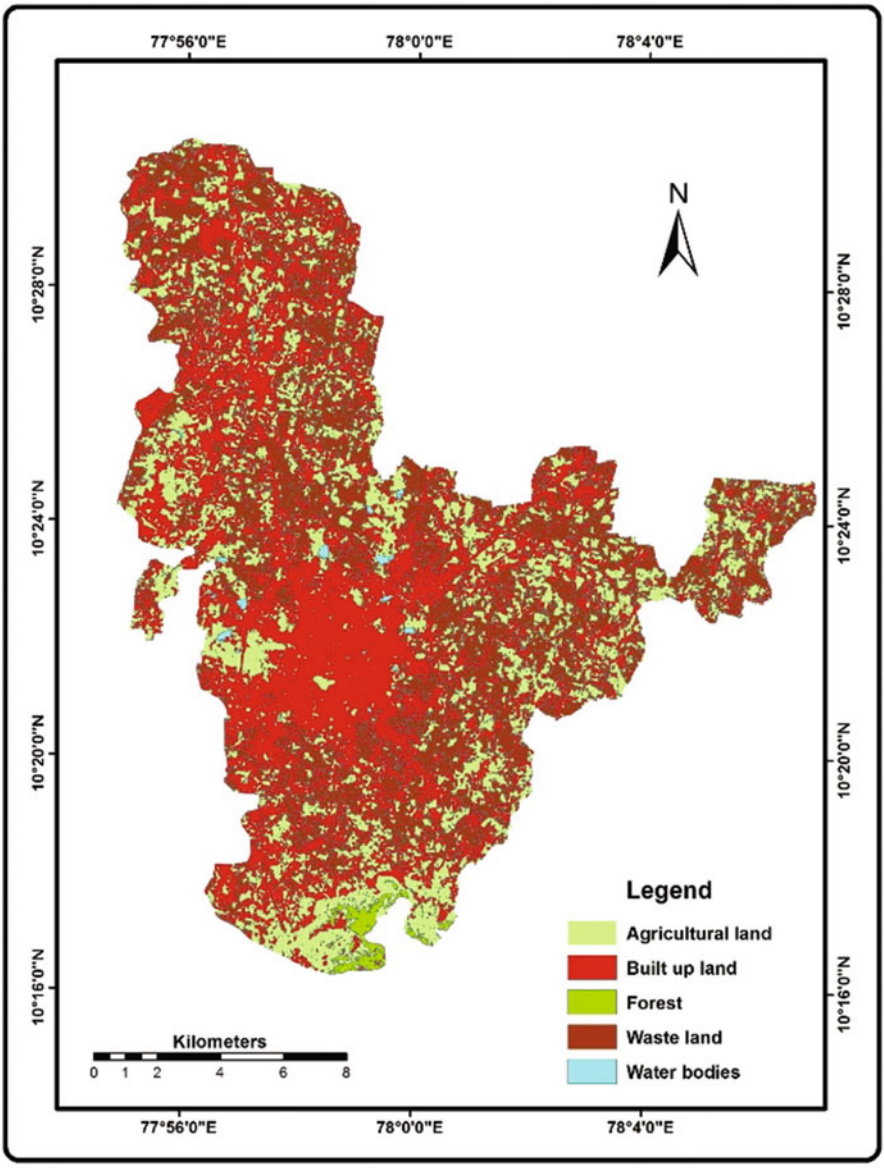

Fig. 21.11 Land use/land cover map

Based on literatures (Sajikumar and Gigo 2013; Singh et al. 2013; Malik and Rajeshwari 2015; Samson and Elangovan 2015; Dinesan et al. 2015) and expert's opinion the respective ranks were assigned. After ranks were given and their individual classes are considered and respective weights are assigned. For the pairwise AHP has been utilized to generate the artificial recharge zonation map.

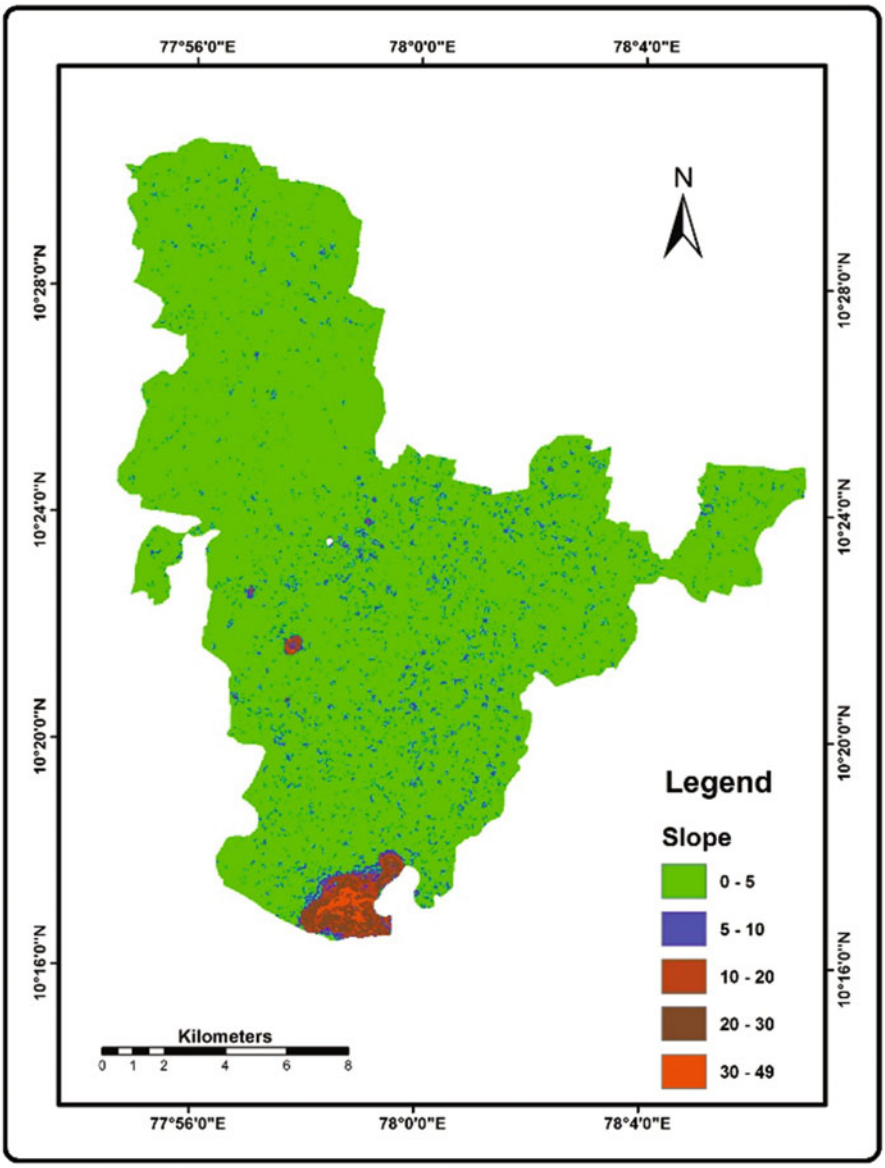

Fig. 21.12 Slope map

After assigning weight the maps in vector format should be converted into raster format and they are calculated based on the weights. Thus, the artificial map was created for the present study area. Figure 21.15 is shown the artificial recharge potential zone map of the study area. The study area is classified into five categories based on the recharging characteristics i.e., Excellent, Very Good, Good, Fair, Not

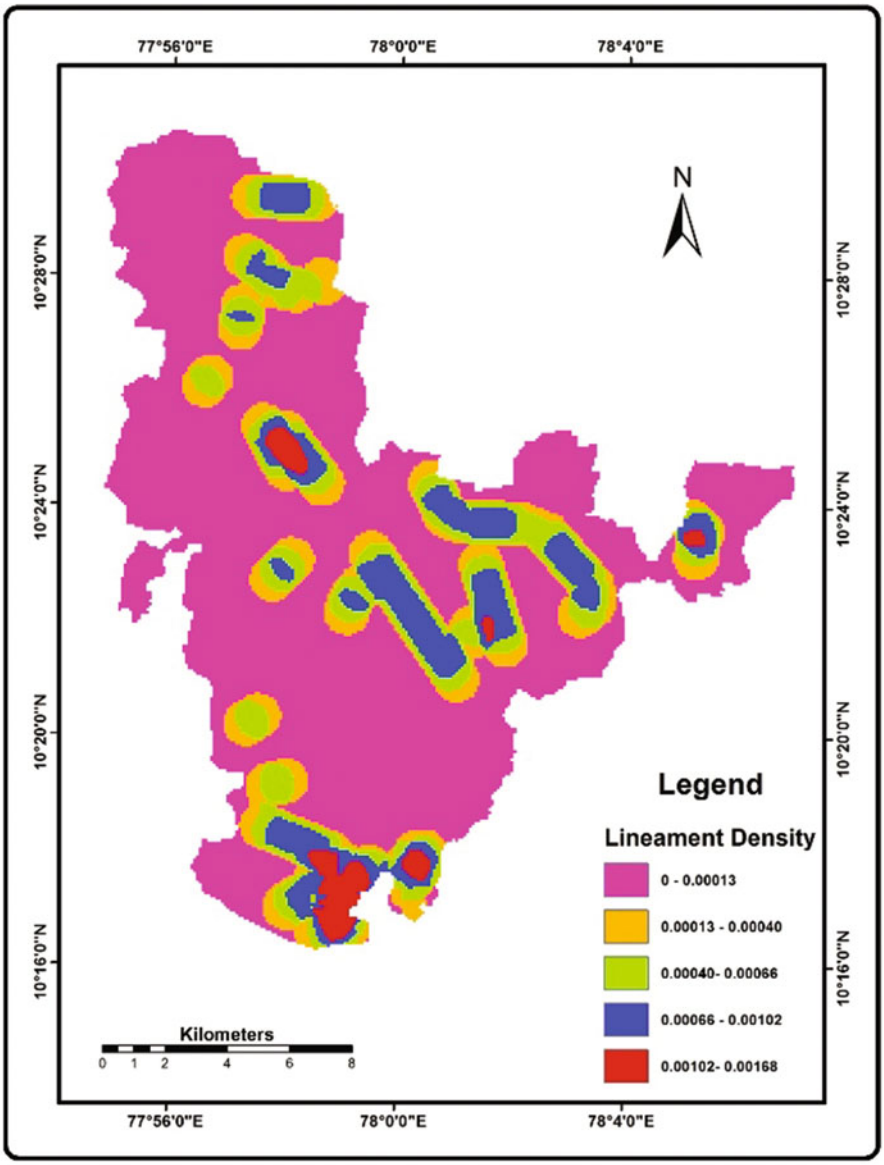

Fig. 21.13 Lineament density map

Suitable. Table 21.5 shows the score weight influence for artificial recharge management. Pairwise comparison matrix for the seven themes and calculation of normalized by the AHP is shown in Table 21.6. Table 21.7 shows normalization matrix for the thematic layers weights. Table 21.8 shows the artificial recharge zone delineation suitability aerial coverage of the present study.

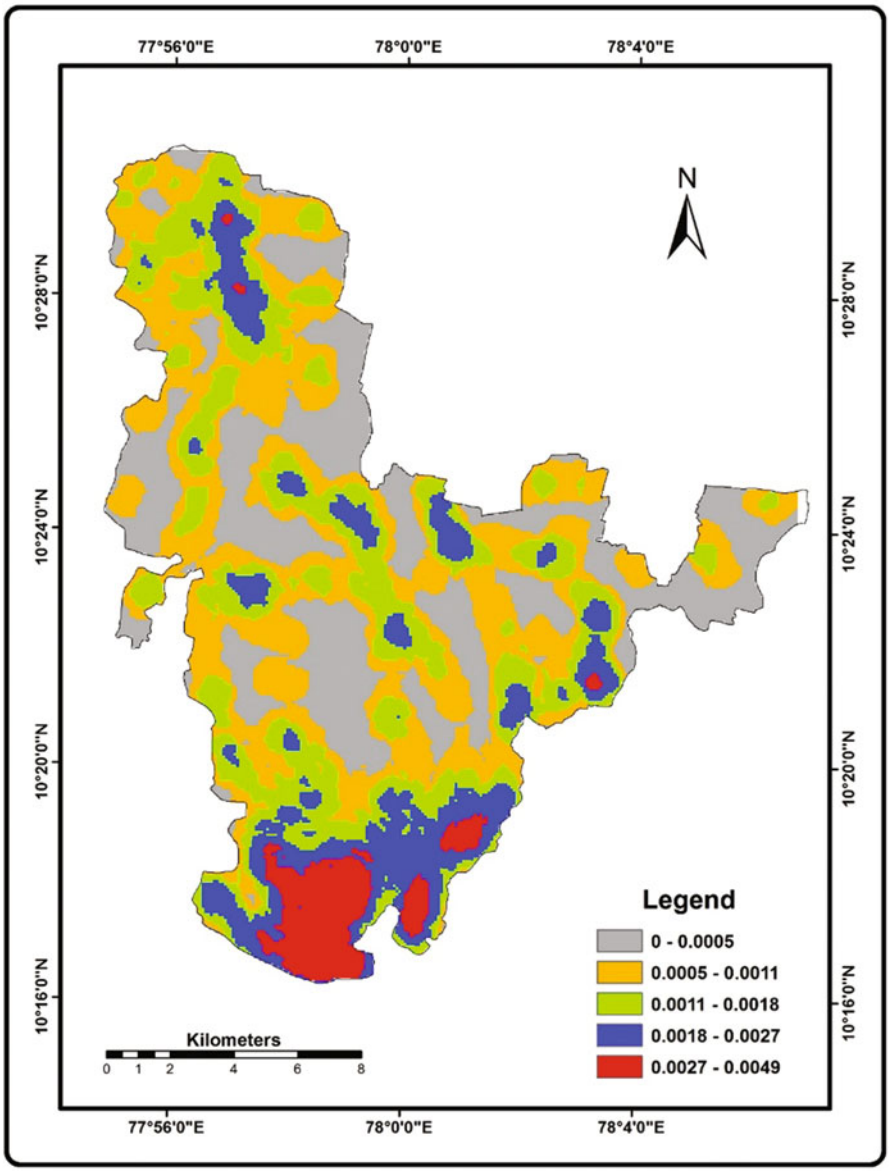

Fig. 21.14 Drainage density map of the study area

The best zones for artificial recharge to groundwater show in area having high storability, shallow depth to the water level and good water holding capacity; the pediment alluvial plain was the most suitable for the construction of an artificial recharge structure. Locations like Mullipadi, Settinaickenpatti, Periyakotta,

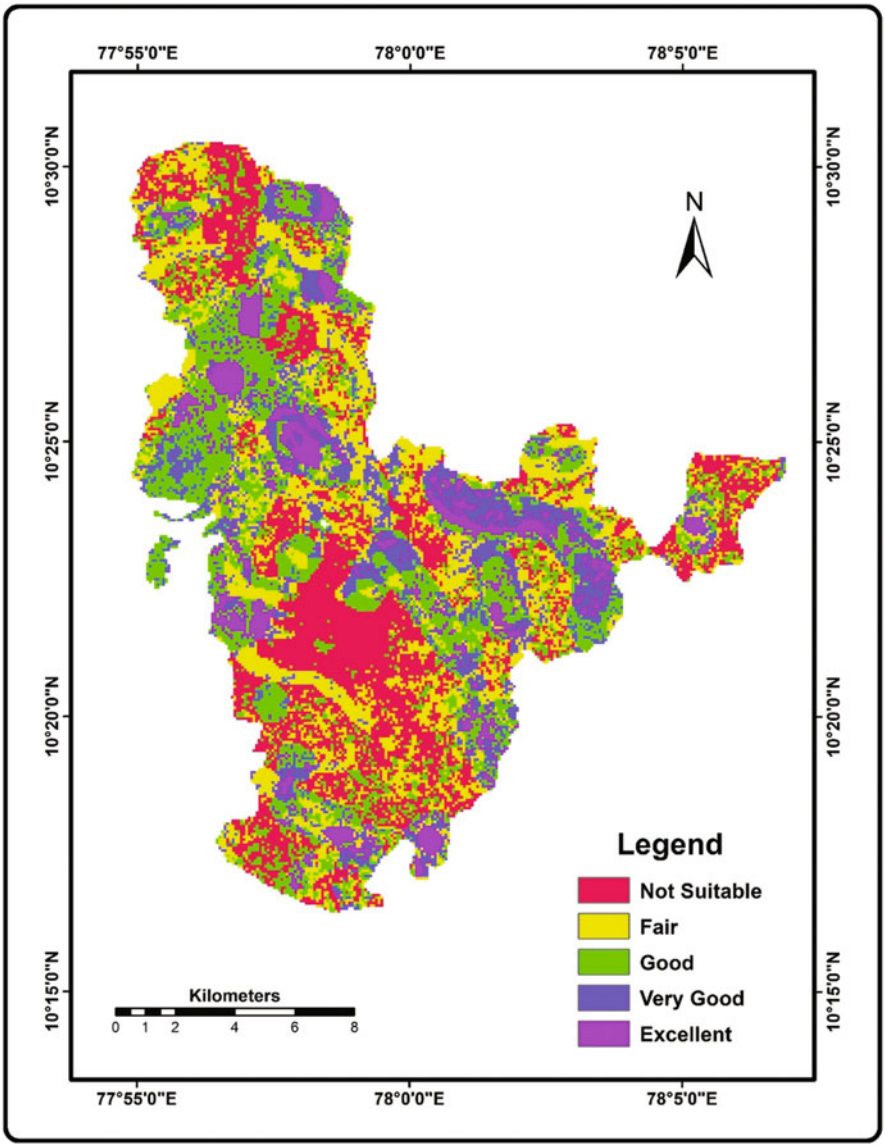

Fig. 21.15 The artificial groundwater recharge zone delineation map

Tottanuthu, Pallapatti, and south-east part of Agram (TP) are coming under excellent site for artificial recharge of groundwater which covers 24.03 km^2, whereas north-west part of study area mostly covers very good class around 32.20 km^2, good class covers in all parts of the Dindigul block in disseminated way, i.e., approximately

Table 21.5 Score weight influence for artificial recharge

Sr. no	Parameters	Score weight
1	Geology	8
2	Lineament density	6
3	Landuse/land cover	7
4	Geomorphology	9
5	Soil	6
6	Drainage density	7
7	Slope	6

about 66.84 km^2, fair class seen in west boarder of Balakrishnapuram and aerially covers 64.60 km^2 and Dindigul central town part comes under not suitable category along with northern border part between Agaram and Tadikombu and eastern part of Ramanathapuram area covers 65.53 km^2.

21.7 Conclusion

From the Landuse/Land cover changes and ground water artificial recharge zonation of the study using geomatic techniques and the change detection analysis shows the major changes in water bodies in the Dindigul block, which may have an alarm for the future water resources sustainability, the following finest conclusion were derived.

- The present study is focused to demarcate the changes occurred in the period from 1993–2015 for the Dindigul block, Dindigul district, south India. From the Landuse/Land cover change detection of the study area, it is evident that there is a decrease in the surface water shortage which is an alarm for the current situation and necessary steps has to be taken to conserve the presently available water bodies. The barren land/waste land may be converted to build the artificial recharge structures to improve the groundwater condition in the study area after necessary analysis. In the present study, the sites for artificial recharge structures were suggested which can be utilized for the improvement of the groundwater resources.
- In order to that, we have delineated artificial recharge potential zone map to identify the potential recharge zones which are come under the Good category (66.84 km^2), Very good category (32.20 km^2), Excellent category area (24.03 km^2) recommended to construct the wide form of artificial structures. The terrain type of the study area is most suitable because most of the area comes under the slope measure 0–5° under near level category which will be considered to construct the artificial recharge structures without any dispute. Not suitable category covers 65.53 km^2 and Fair category covers 64.60 km^2 from the study area, which are not recommended to construct the substantial artificial structures.

Table 21.7 The normalization matrix for the thematic layer's weights

Normalization matrix									
Parameters	Geology	Lineament density	Land use	Geomorphology	Soil	Drainage density	Slope	Weights	% Influence
Geology	0.163	0.163	0.163	0.163	0.143	0.163	0.206	0.167	16.7
Lineament density	0.122	0.122	0.122	0.122	0.107	0.122	0.116	0.119	11.9
Landuse/land cover	0.143	0.143	0.143	0.143	0.125	0.143	0.135	0.139	13.9
Geomorphology	0.184	0.184	0.184	0.184	0.161	0.184	0.174	0.179	17.9
Soil	0.122	0.122	0.122	0.122	0.107	0.122	0.116	0.119	11.9
Drainage density	0.143	0.143	0.143	0.143	0.250	0.143	0.135	0.157	15.7
Slope	0.122	0.122	0.122	0.122	0.107	0.122	0.116	0.119	11.9
Sum	1.000	1.000	1.000	1.000	1.000	1.000	1.000	1.000	100.0

Table 21.8 Artificial recharge zone delineation suitability aerial coverage of the present study

Sr. no	Class name	Area (km^2)
1	Excellent	24.03
2	Very good	32.20
3	Good	66.84
4	Fair	64.60
5	Not suitable	65.53

- In future, the further study can be made with higher spatial and spectral resolution remote sensing data along with geophysical studies and supplementary field works may give the superior and precision results.

21.8 Recommendation for Suitable Recharge Structures

To build the artificial recharge structures to enhance the ground and subsurface water sustainable yield in this study, we would like suggest and recommend that the following measurements can be taken up like,

- The small scale check dams can be endorsed in priority to build in excellent areas, percolation tanks may be constructed in the excellent or good regions to increase the groundwater level both in alluvial as well as hard rock formation which is very useful in agricultural practices to endure the accessibility of water entire a year.
- Farm ponds can be created adjacent to the agricultural fields for the augmentation of surface runoff, dug well recharge which can be built in alluvial as well as hard rock areas and can be used as structures directly recharge the dried aquifer.
- Recharge shafts are recommended for the poor permeable medium of aquifer and the existing village tanks are normally silted and damaged which can be modified to serve as recharge structure.
- This study will offer wealthy information to the government agencies, policy makers and farmers for framing development in water management.

References

Anbazhagan, S., Ramasamy, S. M., & Das Gupta, S. (2005). Remote sensing and GIS for artificial recharge study, runoff estimation and planning in Ayyar basin, Tamil Nadu, India. *Environmental Geology, 48*, 158–170. https://doi.org/10.1007/s00254-005-1284-4.

Arivazhagan, S., Karthi, A., & Kirubakaran, M. (2018). Change detection analysis and statistical site suitability mapping for Edappadi taluk using GIS techniques. *IJSART, 4*(4), 1562–1570.

Arivazhagan, S., & Kirubakaran, M. (2016). Detection of urban changes and statistical site suitability analysis in Tiruchencode taluk using geoinformatic techniques. *International Journal of Earth Sciences and Engineering, 9*(4), 1465–1473.

Balamurugan, P., Kumar, P. S., & Shankar, K. (2020a). Dataset on the suitability of groundwater for drinking and irrigation purposes in the Sarabanga River region, Tamil Nadu, India. *Data in Brief, 29*, 105255.

Balamurugan, P., Kumar, P. S., Shankar, K., Nagavinothini, R., & Vijayasurya, K. (2020b). Non-carcinogenic risk assessment of groundwater in southern part of Salem District in Tamil Nadu, India. *Journal of the Chilean Chemical Society, 65*(1), 4697–4707.

Bastiaansen, W., Menenti, R., Feddes, R., & Holtslag, A. (1998). A remote sensing surface energy balance algorithm for lands (SEBAL). *Journal of Hydrology, 212*, 198–229.

Bhattacharya, A. K. (2010). Artificial ground water recharge with a special reference to India. *IJRRAS, 4*(2), 214–221.

Chopra, R., Dhiman, R. D., & Sharma, P. K. (2005). Morphometric analysis of sub-watersheds in Gurdapur district, Punjab using remote sensing and GIS techniques. *Journal of the Indian Society of Remote Sensing, 33*(4), 531–539. https://doi.org/10.1007/BF02990738.

Chowdary, V. M., Ramakrishnan, D., Srivastava, Y. K., Chandran, V., & Jeyaram, A. (2009). Integrated water resource development plan for sustainable management of Mayurakshi Watershed, India using remote sensing and GIS. *Water Resources Management, 23*, 1581–1602. https://doi.org/10.1007/s11269-008-9342-9.

Chowdhury, A., Jha, M. K., & Chowdary, V. M. (2010). Delineation of groundwater recharge zones and identification of artificial recharge sites in West Medinipur district, West Bengal, using RS, GIS and MCDM techniques. *Environment and Earth Science, 59*, 1209–1222. https://doi.org/10.1007/s12665-009-0110-9.

Dindigul Climate Data. (n.d.) Dindigul climate data. https://en.climate-data.org/asia/india/tamil-nadu/dindigul-24012

Dinesan, V. P., Girish, G., & Ashitha, M. K. (2015). Application of geoinformatics for the delineation of groundwater prospects zones - A case study for Melattur Grama panchayat in Kerala, India. *Aquatic Procedia, 4*(2015), 1389–1396. https://doi.org/10.1016/j.aqpro.2015.02.180.

Ghayoumian, J., Mohseni Saravi, M., Feiznia, S., Nouri, B., & Malekian, A. (2007). Application of GIS techniques to determine areas most suitable for artificial groundwater recharge in a coastal aquifer in southern Iran. *Journal of Asian Earth Sciences, 30*(2), 364–374. https://doi.org/10.1016/j.jseaes.2006.11.002.

Khadri, S. F. R., Pande, C., & Moharir, K. (2013). Geomorphological investigation of WRV-1 watershed management in Wardha district of Maharashtra India; using remote sensing and geographic information system techniques. *International Journal of Pure and Applied Research in Engineering and Technology, 1*(10), 23.

Khadri, S. F. R., & Moharir, K. (2016). Characterization of aquifer parameter in basaltic hard rock region through pumping test methods: A case study of Man River basin in Akola and Buldhana districts Maharashtra India. *Modeling Earth Systems and Environment, 2*, 33.

Khadri, S. F. R., & Pande, C. (2015). Remote sensing based hydro-geomorphological mapping of Mahesh River Basin, Akola, and Buldhana districts, Maharashtra, India – Effects for water resource evaluation and management. *International Journal of Geology, Earth and Environmental Sciences, 5*(2), 178–187.

Khadri, S. F. R., & Pande, C. (2016). Ground water flow modeling for calibrating steady state using MODFLOW software: A case study of Mahesh River basin, India. *Model Earth System Environment, 2*, 39. https://doi.org/10.1007/s40808-015-0049-7.

Kirubakaran, M., Colins, J. J., & Ashokraj, C. (2019). Delineating the groundwater potential zone in Tirunelveli taluk, South Tamil Nadu, India, using remote sensing, geographical information system (GIS) and analytic hierarchy process (AHP) techniques. *Proceedings of the National Academy of Sciences, India Section A: Physical Sciences, 90*, 661. https://doi.org/10.1007/s40010-019-00608-5.

Kirubakaran, M., Colins, J. J., Ashokraj, C., & Arivazhagan, S. (2016). A geostatistical approach for delineating the potential groundwater recharge zones in the hard rock terrain of Tirunelveli

Taluk, Tamil Nadu, India. *Arabian Journal of Geosciences, 9*, 382. https://doi.org/10.1007/s12517-016-2419-5.

Kirubakaran, M., Samson, S., & Kumar, S. (2020). *A geospatial approach for delineating the artificial recharge sites in Salem city using AHP and CSI techniques. W& E international* (pp. 48–56). New Delhi: Water and Energy International (Water Resources Section).

Kumar, P. S., & Balamurugan, P. (2018). Evaluation of groundwater quality for irrigation purpose in Attur taluk, Salem, Tamil Nadu, India. *Water and Energy International, 61*(4), 59–64.

Magesh, N. S., Chandrasekar, N., & Soundranayagam, J. P. (2012). Delineation of groundwater potential zones in Theni district, Tamil Nadu, using remote sensing, GIS and MIF techniques. *Geoscience Frontiers, 3*(2), 189–196. https://doi.org/10.1016/j.gsf.2011.10.007.

Malik, & Rajeshwari, S. (2015). Identification of suitable sites for artificial recharge in Mewat District, Haryana. *Transactions, Indian Institute of Geographers, 37*(2), 245–257.

Martin, P. H., LeBoeuf, E. J., Dobbins, J. P., Daniel, E. B., & Abkowitz, M. D. (2005). Interfacing GIS with water resource models: A state-of the-art review. *Journal of the American Water Resources Association, 41*(6), 1471–1487.

Moharir, K. N., Pande, C. B., Singh, S. K., & Del Rio, R. A. (2020). Evaluation of analytical methods to study aquifer properties with pumping test in Deccan basalt region of the Morna River basin in Akola District of Maharashtra in India. *Groundwater Hydrology*. https://doi.org/10.5772/intechopen.84632.

Moharir, K., Pande, C., & Patil, S. (2017). Inverse modeling of aquifer parameters in basaltic rock with the help of pumping test method using MODFLOW software. *Geoscience Frontiers, 8*(6), 1385–1395.

Muralitharan, J., & Palanivel, K. (2015). Groundwater targeting using remote sensing, geographical information system and analytical hierarchy process method in hard rock aquifer system, Karur district, Tamil Nadu, India. *Earth Science Informatics, 8*(4), 827–842. https://doi.org/10.1007/s12145-015-0213.

Pande, C., & Moharir, K. (2014). Analysis of land use/land cover changes using remote sensing data and GIS techniques of Patur Taluka, Maharashtra, India. *International Journal of Pure and Applied Research in Engineering and Technology, 2*(12), 85–92.

Pande, C. B. (2020a). Introduction. In *Sustainable watershed development. Springer briefs in water science and technology*. Cham: Springer, Cham. https://doi.org/10.1007/978-3-030-47244-3_1.

Pande, C. B. (2020b). Watershed management and development. In *Sustainable watershed development. Springer briefs in water science and technology*. Cham: Springer. https://doi.org/10.1007/978-3-030-47244-3_2.

Pande, C. B. (2020c). Thematic mapping for watershed development. In *Sustainable watershed development. Springer briefs in water science and technology*. Cham: Springer. https://doi.org/10.1007/978-3-030-47244-3_3.

Pande, C. B. (2020d). Sustainable watershed development planning. In *Sustainable watershed development. Springer briefs in water science and technology*. Cham: Springer. https://doi.org/10.1007/978-3-030-47244-3_4.

Pande, C. (2014). Change detection in land use/land cover in Akola taluka using remote sensing and GIS technique. *International Journal of Research (IJR), 1*(8), September-2014.

Pande, C. B., Khadri, S. F. R., Moharir, K. N., & Patode, R. S. (2017). Assessment of groundwater potential zonation of Mahesh River basin Akola and Buldhana districts, Maharashtra, India using remote sensing and GIS techniques. *Sustainable Water Resources Management, 4*, 965–979. https://doi.org/10.1007/s40899-017-0193-5. ISSN 2363-5037.

Pande, C. B., & Moharir, K. (2015). GIS-based quantitative morphometric analysis and its consequences: A case study from Shanur River basin, Maharashtra India. *Applied Water Science, 7*(2), 861–871.

Pande, C. B., & Moharir, K. (2018). Spatial analysis of groundwater quality mapping in hard rock area in the Akola and Buldhana districts of Maharashtra, India. *Applied Water Science, 8*(4), 1–17.

Pande, C. B., Moharir, K. N., Singh, S. K., & Varade, A. M. (2019). An integrated approach to delineate the groundwater potential zones in Devdari watershed area of Akola district, Maharashtra, Central India. *Environment, Development, and Sustainability, 22*, 4867. https://doi.org/10.1007/s10668-019-00409-1.

Pande, C. B., Moharir, K. N., Khadri, S. F. R., & Patil, S. (2018b). Study of land use classification in the arid region using multispectral satellite images. *Applied Water Science, 8*(5), 1–11.

Pande, C. B., Moharir, K. N., & Pande, R. (2018a). Assessment of morphometric and hypsometric study for watershed development using spatial technology – A case study of Wardha river basin in the Maharashtra, India. *International Journal of River Basin Management*. https://doi.org/10.1080/15715124.2018.1505737.

Patode, R. S., Pande, C. B., Nagdeve, M. B., Moharir, K. N., & Wankhade, R. M. (2017). Planning of conservation measures for watershed management and development by using geospatial technology – A case study of Patur watershed in Akola District of Maharashtra. *Current World Environment, 12*, 3.

Prabhu, M. V., & Venkateswaren, S. (2015). Delineation of artificial recharge zones using geospatial techniques in Sarabanga Sub Basin Cauvery River, Tamil Nadu. International conference on water resources, coastal and ocean engineering (ICWRCOE 2015). *Aquatic Procedia, 4*, 1265–1274.

Prasad, R. K., Mondal, N. C., Banerjee, P., Nandakumar, M. V., & Singh, V. S. (2008). Deciphering potential groundwater zone in hard rock through the application of GIS. *Environmental Geology, 55*, 467–475. https://doi.org/10.1007/s00254-007-0992-3.

Ramachandra, T. V., & Uttam, K. (2004). Geographic resources decision support system for land use, land cover dynamics analysis. Proceedings of the FOSS/GRASS Users Conference.

Saaty, T. L. (1980). *The analytic hierarchy process: Planning, priority setting, resource allocation*. New York, NY: McGraw-Hill.

Saaty, T. L. (1990). An exposition of the AHP in reply to the paper, remarks on the analytic hierarchy process. *Management Science, 36*, 259–268.

Sajikumar, N., & Gigo, P. (2013). Integrated remote sensing and GIS approach for groundwater exploration using analytic hierarchy process (AHP) technique. *Proceedings of International Conference on Energy and Environment, 2*(Special Issue 1), 66–74.

Samson, S., & Elangovan, K. (2015). Delineation of groundwater recharge potential zones in Namakkal District, Tamilnadu, India using remote sensing and GIS. *Journal of the Indian Society of Remote Sensing, 43*(4), 769–778. https://doi.org/10.1007/s12524-014-0442-0.

Singh, A., Panda, S. N., Kumar, K. S., et al. (2013). Artificial groundwater recharge zones mapping using remote sensing and GIS: A case study in Indian Punjab. *Environmental Management*. https://doi.org/10.1007/s00267-013-0101-1. ISSN 0364-152X.

Thapa, R., Gupta, S., Guin, S., & Kaur, H. (2017). Assessment of groundwater potential zones using multi-influencing factor (MIF) and GIS: A case study from Birbhum district, West Bengal. *Applied Water Science, 7*(7), 4117–4131.

Thapinta, A., & Hudak, P. F. (2003). Use of geographic information systems for assessing groundwater pollution potential by pesticides in Central Thailand. *Environment International, 29*, 87–93.

Venkata, R. K., Eldho, T. I., Rao, E. P., & Chithra, N. R. (2008). A distribute kinematic wave–Philip infiltration watershed model using FEM, GIS and remotely sensed data. *Water Resources Management, 22*, 737–755. https://doi.org/10.1007/s11269-007-9189-5.

Yeh, H.-F., Cheng, Y.-S., Lin, H.-I., & Lee, C.-H. (2016). Mapping groundwater recharge potential zone using a GIS approach in hualian river, Taiwan. *Sustainable Environment Research, 26*(1), 33–43. https://doi.org/10.1016/j.serj.2015.09.005.

Chapter 22
Artificial Replenishment of Ground Water by Rain Water Harvesting: A Case Study

Sejal Desai

Contents

22.1 Introduction 435
22.2 Benefits of Artificial Recharge 436
22.3 Study Area 437
22.4 Methodology 438
22.5 Artificial Recharge Through Roof Top Rainwater Harvesting 439
22.6 Results and Analysis 444
22.7 Recharge Volume Validation 447
22.8 Summary and Conclusions 448
References 449

22.1 Introduction

Basic source of all recharge, natural or artificial is rainfall on land surface (Pande and Moharir 2015). The distribution of the same comes in the form of surface runoff, subsurface infiltration and returns back to atmosphere as evaporation or evapotranspiration losses from land surface or from root zone (Pande et al. 2017, 2018). Water reaching root zone supplements soil moisture and surplus if, any goes as deep percolation or recharge. In general recharge is that portion of infiltration that reaches ground water level. Athavale et al. (1994) have studied borehole injection recharging technique in Deccan Trap Basalts near Nagpur, India Athavale (2003) had given the detailed information regarding water harvesting and sustainable supply in India (Pande et al. 2019). The summary of artificial recharge is given in subsequent sections.

S. Desai (✉)
Sal Institute of Technology & Engineering Research, Ahmedabad, Gujarat, India

C. B. Pande, K. N. Moharir (eds.), *Groundwater Resources Development and Planning in the Semi-Arid Region*, https://doi.org/10.1007/978-3-030-68124-1_22

22.2 Benefits of Artificial Recharge

Artificial ground water recharge techniques have been used throughout the world for more than 200 years for variety of purposes. Some of the uses are: (1) Seasonal storage, (2) Agricultural water supply, (3) Long-term storage or water banking, (4) Nutrient reduction in Agricultural runoff, (5) Diurnal storage, (6) Reclaimed water storage for reuse, (7) Restore ground water levels, (8) Soil aquifer treatment, (9) Maintain distribution system pressure, (10) Store fresh water derived from rain and snow melt, (11) Maintain water temperature for fish hatcheries, (12) Improve water quality, (13) Reduce environmental effects of stream flow diversions, (14) Prevent salt water intrusion into aquifers, (15) Compensate for surface salinity barrier leakage losses, etc. (16) Reduction of land subsidence, (17) Renovation of waste water, (18) Improvement of ground water quality, (19) Storage of stream waters during period of high or excessive flow and thereby reduction of flood flows, (20) Increase well yield, and (21) Decrease the size of areas needed for water supply systems (Pande 2020d).

22.2.1 Various Rain Water Harvesting Techniques

Water harvesting means deliberate collection and storage of rain water from catchments and its storage including the methods or innovations which are adopted for its beneficial use like ground water recharge, drinking irrigation, agriculture, etc. and thereby, efficient utilization of limited water (Kokate et al. 2014). The ultimate intention of water harvesting is to provide supply of water at the most wanted period to its users. Conservation of rainwater by artificial means can be identified as water harvesting and the structures constructed or developed for collection of rainwater can be termed as Water Harvesting Structures (Athavale et al. 1994; Pande 2020a, b, c).

The Common method for rain water harvesting and structures related to artificial recharge of ground water can be widely classified as

1. Recharge through induced infiltration.
2. Recharge through water spreading.
   (a) Basins.
   (b) Flooding.
   (c) Ditches.
   (d) Natural channel modification.
   (e) Irrigation.
3. Recharge pits and shafts.
4. Hydrofracturing of borewells.
5. Farm ponds.

6. Storage tanks, medium irrigation tanks, medium irrigation schemes, village tanks.
7. Percolation tanks.
8. Recharge wells or injection wells.
9. Check dams.
10. Sub surface dykes or dams.
11. Gully plugging.
12. Contour bunding.
13. Contour trenching.
14. Roof top rain water harvesting.

(a) Recharge through abandoned dug well.
(b) Recharge through open well method.
(c) Rain water harvesting through bore well.
(d) Recharge through abandoned hand pump.
(e) Recharge pit.
(f) Recharge trench.
(g) Gravity head recharge tube wells.
(h) Recharge shaft.

While in this study percolation tank technique along with recharge tube well has been studied.

22.3 Study Area

The artificial recharging project included four tube wells in the factory premises at Vadodara, Gujarat. The factory layout plan and location of tubewells is shown in Fig. 22.1.

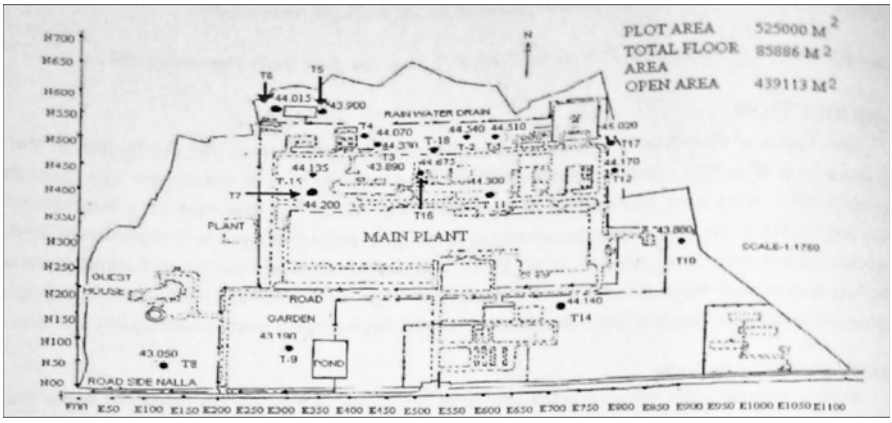

Fig. 22.1 Layout of the study area and the position of tubewells

The area falls under arid climatic conditions and temperature varies from 10 °C in winter to 45 °C in summer. Geologically this area falls under recent alluvial formation overlains the Deccan trap formation (Khadri et al. 2013; Khadri and Pande 2016). The geological strata consist of the over burden of 30–40 m in thickness and is composed of soil, silt and gravels (Khadri and Pande 2015b). The lower portion belongs to the rocky stratum of basalt, a formation of igneous and metamorphic rocks, with poor porosity and permeability (Moharir et al. 2017; Khadri and Moharir 2016). This formation contains negligible water circulation in it. Only in case of fractured rocks it gives higher yield of water during pumping (Athavale 2003; Khadri and Pande 2015a).

Hydrological, aquifers of this area are recharged by two rivers, which are semi perennial namely Vishwamitri and Dev. However, recharge capacity of these rivers is much less and there are no such efforts to store the surplus water in any form during non-monsoon period. Particularly in this area ground water occurs in two phases in alluvial formation as unconfined aquifer and in rock formation (Khadri and Pande 2015c; Moharir et al. 2020). In fine grained unconfined aquifer, gravity drainage of the pores is often not instantaneous; consequently, the water is released only, sometime after lowering of water table. So, it is called as unconfined aquifers with delayed yield. Such type of phenomenon is observed in this area, along with decreasing water level by 1–1.5 m every year. Hence it was decided to suggest suitable method for recharge by considering a pilot study at the factory premises. The factory area contains 17 tubewells out of which some of them are abandoned. The requirement of water during non-monsoon season particularly February to May every year had increased.

22.4 Methodology

22.4.1 Artificial Recharge Through Percolation Tank

22.4.1.1 Construction and Working of Percolation Tank

In between tubewells T-5 and T-6 percolation tank was excavated. As the water level in these two wells T-5 and T-6 had reached to 81 and 76.2 m below ground level respectively. In the recharge through percolation tank a trapezoidal tank of top width 45 m × 20 m and bottom width 35 m × 14 m with side slopes 1:1.67 along length and 1:1 slope along width in section and depth 3 m including 0.5 m freeboard was excavated as shown in Fig. 22.2. Water from nearby storm water drain was conveyed to the tank, through PVC pipe of 15 cm diameter and 50 m length. Change in water level of tank was daily monitored by measuring staff fitted in tank. Water percolated through bottom sides of tank in to the ground. Holes of 2–3 mm diameter and of 70 numbers were made in the casing pipes of tubewell which were covered by steel wire mesh to allow the water injection from the percolation tank in to the wells T-5 and T-6 from ground level up to 1.5 m depth as seen in section of the tank. A trench

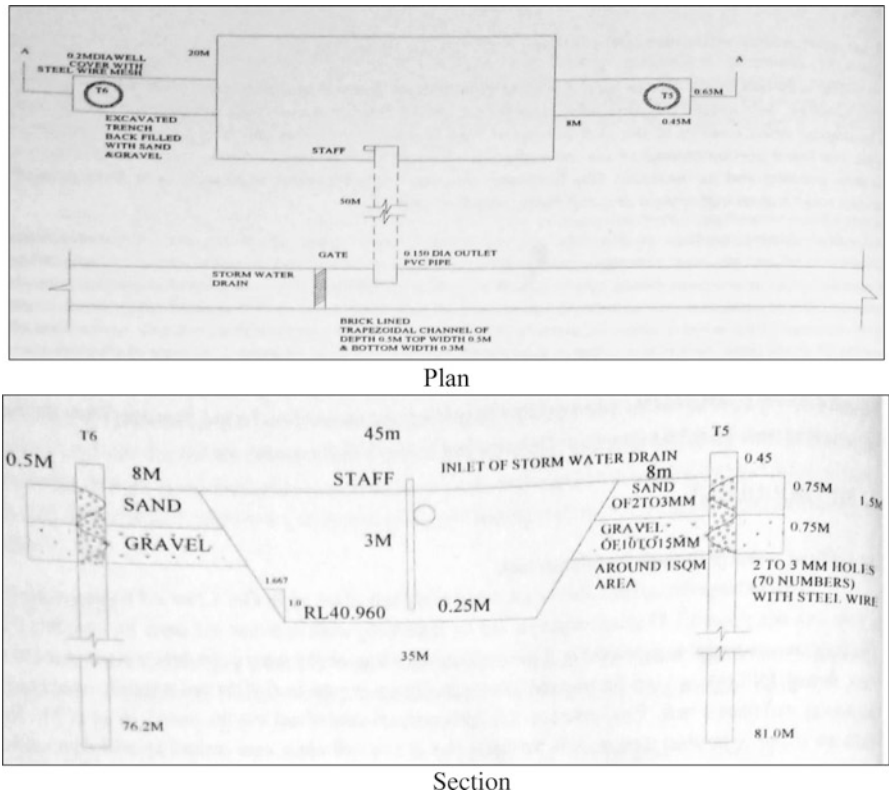

Fig. 22.2 Recharge through percolation tank in plan and section

was excavated and the filter material like gravel and sand was placed in it. Gravel layer with grain size of 10–15 mm underlies sand layer of grain size 2–3 mm. Water from the percolation tank before entering the holes of casing pipe of tubewells, was filtered through sand and gravel layer placed around the well (Khadri and Pande 2014; Patode et al. 2017).

22.5 Artificial Recharge Through Roof Top Rainwater Harvesting

22.5.1 Construction of Roof Top Rainwater Harvesting

As shown in Fig. 22.3 (in elevation), rain water was collected from the roof of the main building through mild steel drain pipe of diameter 0.3 m (Mishra and Singh 1999).

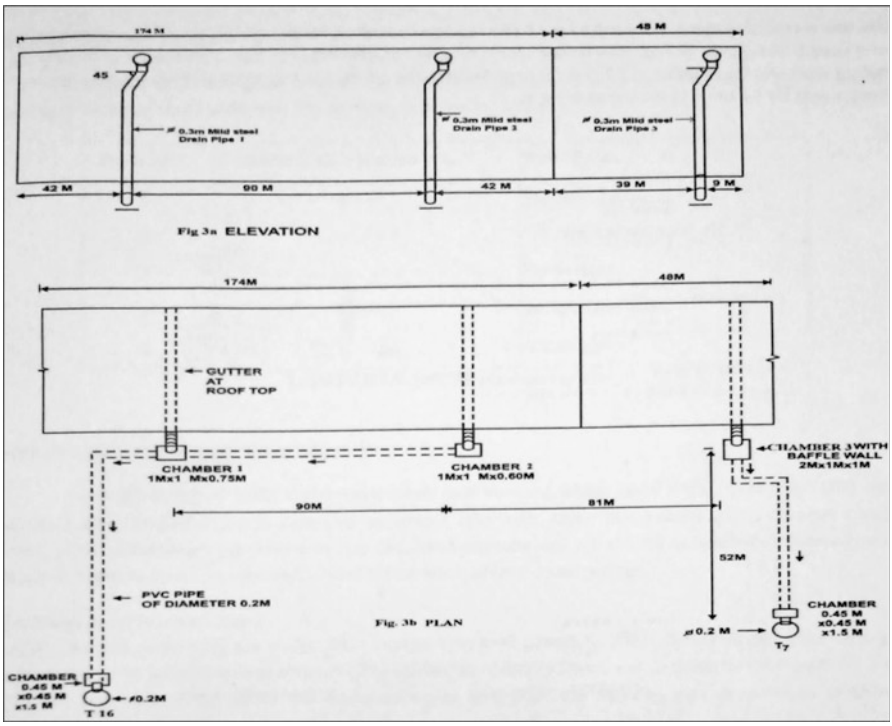

Fig. 22.3 Roof top harvesting system for recharge

These pipes had an inclination of 45° to the vertical for the purpose of maintenance and replacement. Height of the building was 11 m and height of the drain pipe was 10 m. Total length of the building was 222 m. The complete arrangement of such drain pipes are shown in Fig. 22.3 (in elevation). The tube wells T-7 and T-16 to be recharge by Roof Top Rain Water Harvesting (RWH) were having the depth of 85 and 78 m below ground level, respectively.

22.5.2 Working of Roof Top Rain Water Harvesting System

Roof water was collected in to the steel gutter as shown in Fig. 22.3 (in plan), from which it was transferred to the storm water drain pipe, and then it was collected into the chamber. Rain water was collected in to drain-2 and collected to chamber-2 of size 1 m × 1 m × 0.6 m ($L \times B \times D$) as shown in Fig. 22.3 (in plan). While storm water drain-1 transfers rain water in chamber-2 flow to chamber-1 under slope 1:600, through the underground PVC pipe of 20 cm diameter (Todd 1980).

From chamber-1 PVC pipe conveyed water to the chamber of size 0.45 m × 0.45 m × 1.5 m near T-16. A hole of diameter 20 cm was drilled into

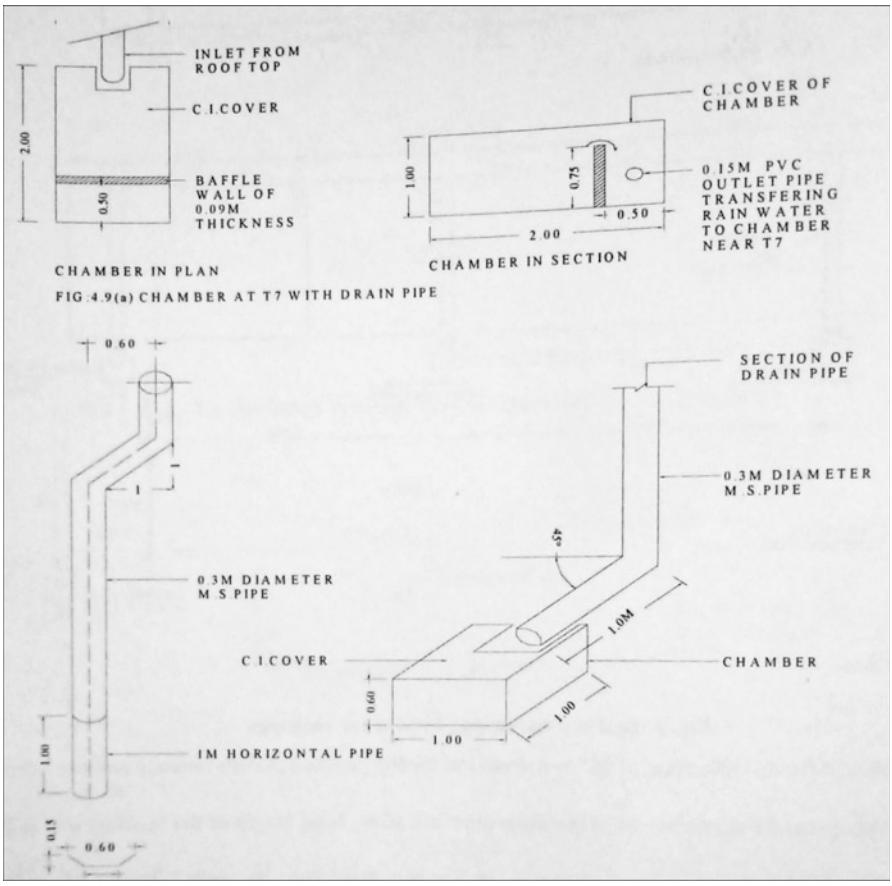

Fig. 22.4 Details of chamber and gutter of roof top harvesting system

the tubewell casing to introduce a PVC pipe of diameter 20 cm from chamber to tube well and thereby recharging T-16 (Athavale et al. 1994).

Drain pipe-3 collected the roof top rain water through roof gutter and transferred the water to chamber-3 as shown in Fig. 22.3 (Plan).This chamber of size 2 m × 1 m × 1 m is provided with baffle wall, so that silt and other suspended particles were arrested and clean water was available for recharging. Water from chamber-3 was conveyed to chamber constructed near T-7 of size 0.45 × 0.45 m × 1.5 m through underground PVC pipe of diameter 0.2 m with slope 1:104. Similar to T-16 after drilling hole in tube well another inlet PVC pipe was introduced to transfer the water collected in the chamber to T-7 in order to recharge it. The detailed arrangement of the roof top harvesting components for T-7 and T-16 are shown in Fig. 22.4.

22.5.3 Runoff Calculations by Soil Conservation Services Method (SCS)

The average rainfall in the study area ranges between 900 and 1000 mm, as per the data collected from Jilla Panchayat of Vadodara. The study was carried out based on the rainfall data available in 2001 that is 937 mm. SCS method, as used by (Mishra and Singh 1999) has been used in the present study. For the pasture, Curve no. (CN) = 84, $S = (1000/\text{CN}) - 10$, $R = (P - 0.25)^2/(P + 0.8\text{S})$. Total runoff for the pasture was calculated as 338.66 mm. SCS method for roof top, Curve no. (CN) = 98, $S = (1000/\text{CN}) - 10$, $R = (P - 0.25)^2/(P + 0.8S)$. Total runoff for the roof top was calculated as 843.30 mm.

22.5.4 Lithological and Resistivity Study

Resistivity and lithological survey of site was carried out and its data were analyzed to get an idea of average lithological strata of the site. The summary is shown in Table 22.1.

22.5.5 Permeability Calculations for the Tubewells

Drawdown (DD) was obtained from the difference of Static Water Level (SWL) and Pumping Water Level (PWL). Also the discharge was measured for various tube wells. Using Theim and Dupuit's equation (Todd 1980), permeability for various tubewells was calculated. For tubewells T-5 and T-6 its average permeability was found as 0.03 m/h. While for tubewell T-7 and T-16 it was 0.08 m/h on an average.

Table 22.1 Lithological strata chart of site

Strata no.	Thickness of each stratum in meter	Formations
1.	2.6–4.1	Top soil
2.	6.2–9.4	Silt, clay, kankar, sand, etc.
3.	8.2–16.6	Sandy strata
4.	4.0–6.0	Weathered basalt
5.	30–100	Massive trap

22.5.6 Rise in Tubewell Water Level Due to Recharging

Periodic water level was monitored in various tubewells (Trivedi 2002). Before installing the recharge system, reduced level of water level was measured as 21.600, 22.055, 24.0750 and 23.940 m for tube wells T-5, T-6, T-7 and T-16, respectively. While the maximum water level after the recharge was observed as 26.650, 25.265, 26.200 and 26.100 m.

Rise in water level in tubewells T-5, T-6 and T-7, T-16 was calculated by the difference between maximum water level and initial water level, which was obtained as 5.050, 3.210 and 1.450, 2.160 m respectively. Hence the average water level rise for T-5 and T-6 was obtained as 4.130 m, while for T-7 and T-16. It is 1.805 m.

22.5.7 Total Dissolved Solids (TDS) Reduction in Tubewells

Total Dissolved Solids (TDS) was monthly monitored for various tubewells (Trivedi 2002). Before caring out the recharging process, initial TDS values for tubewells T-5 and T-6 were measured as 1000 and 1100 ppm, respectively, on averaging it reduced to 1050 ppm. While for T-7 and T-16 tubewells TDS was 1500 and 1800 ppm which had averaged reduced to 1650 ppm.

After implementing recharging, TDS values for Tube wells T-5 and T-6 was found to be 730 and 715 ppm respectively, which averaged to 722 ppm. While for T-7 and T-16 tube wells it was 715 and 700 ppm respectively, which averaged to 707.5 ppm.

22.5.8 Replenishment of Ground Water Through Rain Water

Total volume of water recharged for percolation tank can be calculated by measuring daily water level fluctuating in the tank, amount of evaporation and the area of the tank for recharging (Trivedi 2002). It was found out as 2040 m^3. Recharging for roof top rain water harvesting system was found by multiplying the area of the roof with 90% (Mishra and Singh 1999) of runoff from the roof surfaces. It was found as 9466 m^3. Secondly the recharging capacity of tubewells through Roof Top Rain Water Harvesting was 601.43 m^3/day for T-7 and T-16 was 2268 m^3/day (Driscoll 1987) which was higher than the actual water injected in to the tubewells that is 57 and 206 m^3/day for T-7 and T-16, respectively.

22.6 Results and Analysis

22.6.1 Aquifer Strata

Aquifer characterization using lithological information was analyzed from Table 22.1. The analysis showed that an aquifer was divided in to five strata. First stratum was top soil consisting of thickness from ground level to 4.1 m maximum. While second strata was of variable thickness from 6.2 to 9.4 m which consists of different soil layers like silt, clay, kankar, sand, etc. Third stratum was sandy, which extended from thickness 8.2–16.6 m. Due to high porosity this strata held good amount of water. Weathered basalt of 4–3 m thickness contributing 20–25% of ground water. Last stratum was massive basalt or trap of thickness 38–69 m, which was highly compacted and contributing negligible amount of groundwater during pumping. The details of lithological formations are shown in the fence diagram as shown in Fig. 22.5.

22.6.2 Runoff for Roof Top Rainwater Harvesting and Percolation Tank

Total rainfall recorded in the year 2001 was 937 mm. Runoff for pasture, was 338.66 mm that is 34.3% runoff of the total rainfall. This can be observed graphically as shown in the Fig. 22.6. It matches with SCS condition for the pasture (Mishra and Singh 1999). Total runoff for the roof top was calculated as 843.30 mm

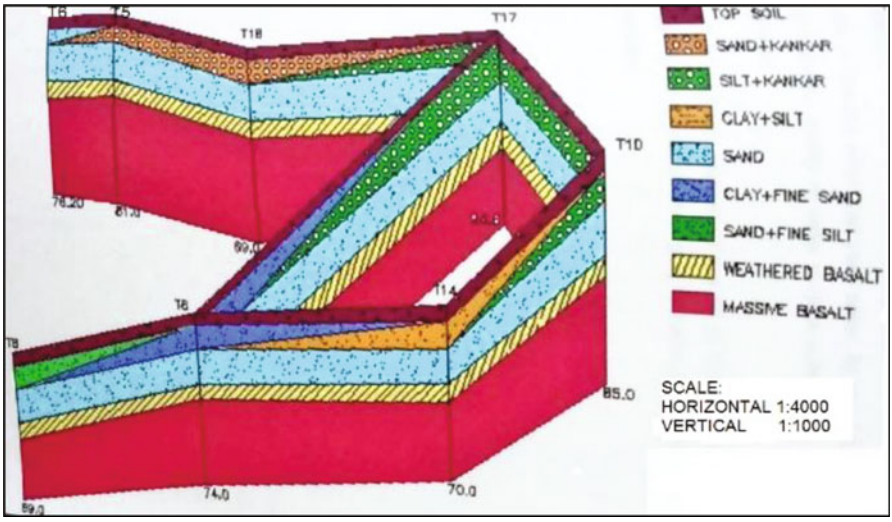

Fig. 22.5 Fence diagram

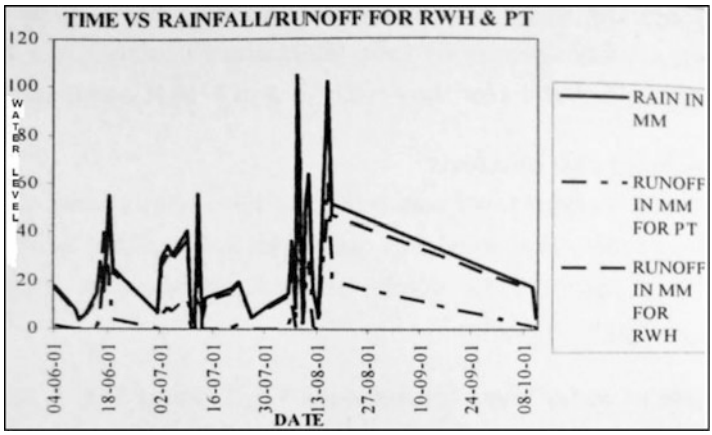

Fig. 22.6 Time vs. rainfall/runoff for RWH and percolation tank

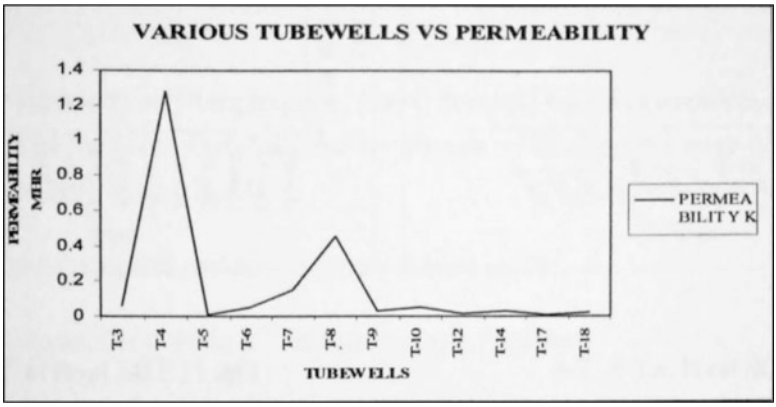

Fig. 22.7 Permeability vs. tubewells

that is 89.9%, runoff of the total rainfall (Fig. 22.6). This matches with SCS condition for pasture of 90% runoff for paved surfaces (Mishra and Singh 1999).

22.6.3 Permeability of Tubewells

Permeability graph as shown in Fig. 22.7 was plotted for various tube wells. It was observed that T-5, T-6, T-7, and T-16 had the permeability of 0.006, 0.053, 0.148 and 0.023 m/h, respectively. Whereas T-4 and T-8 tubewells had permeability of 1.27 and 0.45 m/h, respectively, highest permeability compared to any other tube wells and so for the next phase of recharging these two tubewells should be included in the system.

22.6.4 Water Level Rise in Tubewells

The average water level rise for T-5 and T-6 under percolation tank recharge was obtained as 4.13 m, while for T-7 and T-16 which was under roof top rain water harvesting recharge it was 1.805 m. Hence, from the above results it was analyzed that water level raised in T-5 and T-6 was twice than that of observed in T-7 and T-16. The comparison in this case was also made with tube well T-1 which was nonoperating. The rise in the water level of the same is shown in Figs. 22.8 and 22.9.

22.6.5 Total Dissolved Solids Due to Artificial Replenishment of Rain Water

Total Dissolved Solids for T-5 and T-6 level falls from 1050 to 722 ppm, percentage of reduction in TDS value was more than 32% by artificial recharging. While for T-7 and T-16 TDS reduced from 1650 to 707.5 ppm, which gave the reduction value of more than 58%.The comparative reduction is shown in Figs. 22.10 and 22.11. It was analyzed that TDS reduction in RWH was more by 26% as compared to percolation tank recharge (Trivedi 2002).

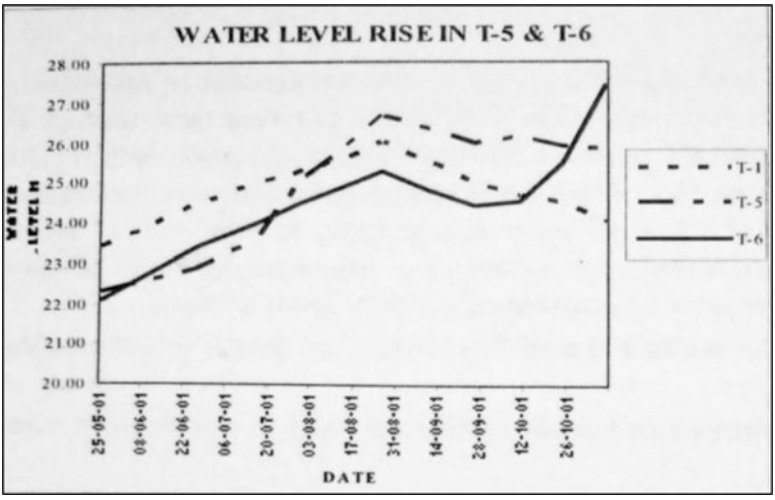

Fig. 22.8 Water level rise in T-5 and T-6

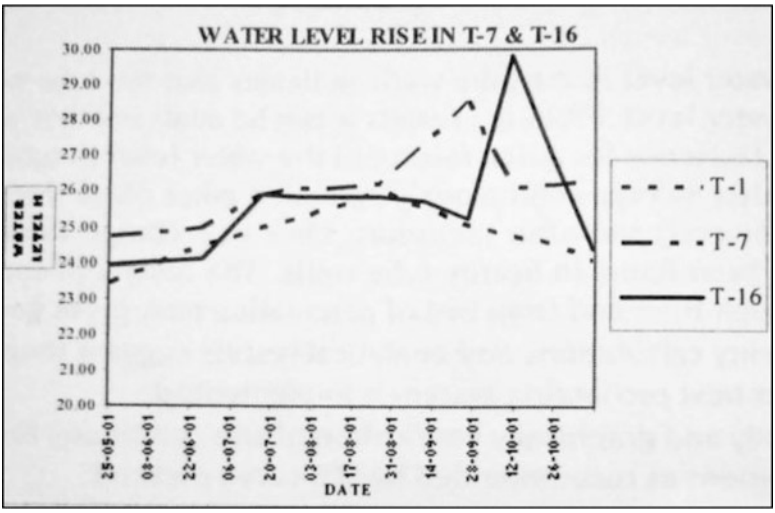

Fig. 22.9 Water level rise in T-7 and T-16

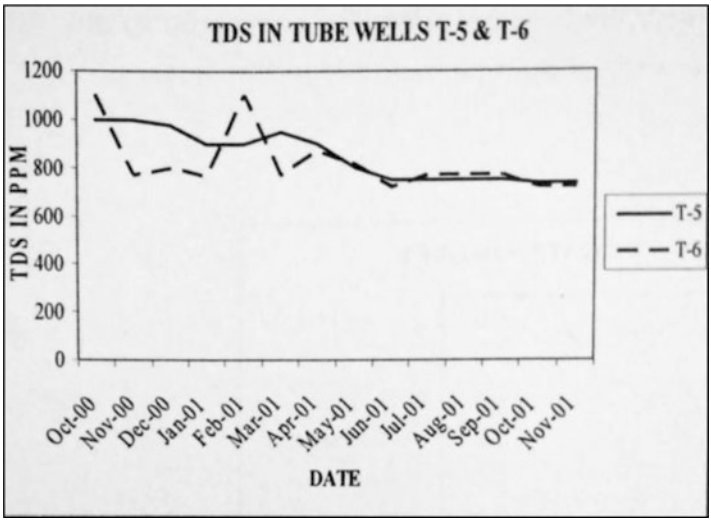

Fig. 22.10 TDS level in T-5 and T-6

22.7 Recharge Volume Validation

Total volume of water recharged by percolation tank was found as 2040 m^3, while by RWH it was 9466 m^3. Hence, the amount of recharge through RWH measured four times more than Percolation tank. From the above results it was found that for T-7 and T-16 the recharging capacity was 601.43 and 2268 m^3/day, respectively. This

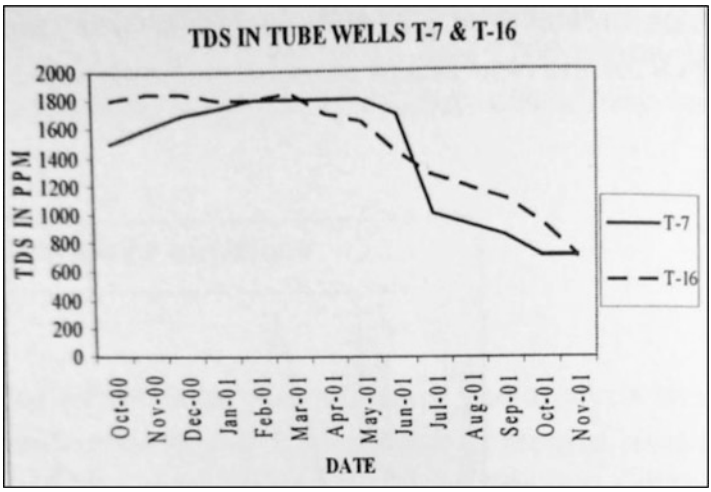

Fig. 22.11 TDS level in T-7 and T-16

was higher than the water injected in to the wells that is 57 and 206 m^3/day for both the tubewells, respectively. Thus, it was concluded that T-7 and T-16 tubewells have much more recharging capacity then the volume of water injected. This showed that the design capacity of T-7 and T-16 found to be ten times more than the actual recharging practiced. Hence, it will work much more efficiently in the heavy rains (Trivedi 2002).

22.8 Summary and Conclusions

1. Rise in water level in the tubewells indicates that the tubewell recharging technology was successful in replenishing ground water level. It was analyzed from the results that water level raised in T-5 and T-6 was twice than that of T-7 and T-16. Hence, for quick rising of the water level in tubewells percolation tank was much more effective. In percolation tank due to buffer storage continuous percolation takes place throughout the monsoon (even in between two successive rainfall intervals) and after monsoon. Thus, to recharge through the bed of percolation tank, higher rise in the level has been found nearby tubewells. The results of combined recharge system that is injection of water in tubewell through filter and from bed of percolation tank gives good results as compared to individual system.
2. Permeability calculation and analytical results suggested that tube wells T-4 and T-8 should be taken in recharging whenever next charging system implemented.

3. Through water budgeting method daily volume of ground water recharge was found out as 14 m^3/day. By pumping test average permeability of an aquifer system was estimated as 4 m/day.
4. Estimated volume of water recharged through Roof Top Rain Water harvesting was 9466 m^3. The calculated volume of water recharged through combination of percolation tank and two recharge wells was found as 2040 m^3.
5. An average recharge rate was of 16 mm/day was obtained by combined percolation tank and recharge wells system.
6. The total recharge volume in factory was about 10% of total pumping and total artificial recharge was about 2% of total pumping. Whereas total recharge was about 16% and artificial recharge was 3.5% of total rainfall.
7. Analytically and graphically verification site condition like amount of runoff of the site was in agreement with the conditions as recommended by SCS curve method.
8. The decrease in TDS value showed an effective artificial recharge in improving the water quality. Percentage reduction in TDS, in the RWH system in tubewells T-7 and T-16 was 26% higher as compared to tube wells T-5 and T-6 in percolation tank. Which suggest RWH is more effective than percolation tank for reducing TDS level in tubewells.
9. Least amount of evaporation losses takes place in RWH. Secondly, maximum recharge capacity was much more than the volume of water injected in to the tubewells. Thus, it can be concluded that the system would work effectively during the heavy rains.
10. It was concluded that there was a rise in water level on average of 0.4–3.5 m. Tube well recharging technique was successful in increasing ground water level and improving the quality of ground water. Roof top rain water harvesting technique was found to be more effective for recharging the ground water by tube wells.
11. Volume of water recharge through RWH was much more than percolation tank. Hence, whole roof top area of industry could be taken under RWH in the next phase of recharging.
12. Both the recharging system that is rooftop rainwater harvesting and percolation tank were compatible. Hence, further recharging of the entire site can be done which would be very beneficial to industry.

References

Athavale, R. N. (2003). *Water harvesting and sustainable supply in India*. Ahmedabad: Centre for Environment Education.

Athavale, R. N., Muralidharan, D., & Rangarajan, R. (1994). Borehole injection studies in Deccan trap basalts near Nagpur. *Proceedings of the Second International Symposium on Artificial Recharge of Ground Water, 1994*, 775–788.

Driscoll, F. G. (1987). *Ground water and wells* (2nd ed.). Beijing: Scientific Publishers.

Khadri, S. F. R., & Pande, C. (2016). Ground water flow modeling for calibrating steady state using MODFLOW software: A case study of Mahesh River basin, India. *Modeling Earth Systems and Environment, 2*, 39. https://doi.org/10.1007/s40808-015-0049-7.

Khadri, S. F. R., & Moharir, K. (2016). Characterization of aquifer parameter in basaltic hard rock region through pumping test methods: A case study of Man River basin in Akola and Buldhana districts Maharashtra India. *Modeling Earth Systems and Environment, 2*, 33.

Khadri, S. F. R., & Pande, C. B. (2014). Morphometric analysis of Mahesh River Basin exposed in Akola and Buldhana districts, Maharashtra, India using remote sensing & GIS techniques. *International Journal of Golden Research Thoughts, 3*(11), GRT-3768. ISSN 2231-5063.

Khadri, S. F. R., & Pande, C. (2015a). Remote sensing based hydro-geomorphological mapping of Mahesh River basin, Akola, and Buldhana districts, Maharashtra, India-effects for water resource evaluation and management. *International Journal of Geology, Earth and Environmental Sciences, 5*(2), 178–187.

Khadri, S. F. R., & Pande, C. (2015b). Analysis of hydro-geochemical characteristics of groundwater quality parameters in hard rocks of Mahesh River Basin, Akola, and Buldhana Dist. Maharashtra, India using geo-informatics techniques. *American Journal of Geophysics, Geochemistry and Geosystems, 1*(3), 105–114.

Khadri, S. F. R., & Pande, C. (2015c). Remote sensing and GIS applications of Linament mapping of Mahesh River basin, Akola & Buldhana District, Maharashtra, India using multispectral satellite data. *International Journal of Research (IJR), 2*(10), 85–90.

Khadri, S. F. R., Pande, C., & Moharir, K. (2013). Geomorphological investigation of WRV-1 watershed management in Wardha district of Maharashtra India; using remote sensing and geographic information system techniques. *International Journal of Pure and Applied Research in Engineering and Technology, 1*(10), 1–12.

Kokate, N. R., Moharir, K. N., & Pande, C. B. (2014). Morphometric analysis of Ural Khurd Nala watershed in Akola District of Maharashtra, India: Using remote sensing and geographic information system (GIS) techniques. *International Journal of Research (IJR), 1*(11), 387–397.

Mishra, S. K., & Singh, V. P. (1999). *Soil conservation service curve number (SCS-CN) methodology, Water Science and Technology* (Vol. 42). New York, NY: Springer.

Moharir, K. N., Pande, C. B., Singh, S. K., & Del Rio, R. A. (2020). *Evaluation of analytical methods to study aquifer properties with pumping test in Deccan basalt region of the Morna River basin in Akola District of Maharashtra in India. Groundwater hydrology*. London: Intec Open Publication. https://doi.org/10.5772/intechopen.84632.

Moharir, K., Pande, C., & Patil, S. (2017). Inverse modeling of aquifer parameters in basaltic rock with the help of pumping test method using MODFLOW software. *Geoscience Frontiers, 8*(6), 1385–1395.

Pande, C. B. (2020a). Introduction. In *Sustainable watershed development. Springer briefs in water science and technology*. Cham: Springer. https://doi.org/10.1007/978-3-030-47244-3_1.

Pande, C. B. (2020b). Watershed management and development. In *Sustainable watershed development. Springer briefs in water science and technology*. Cham: Springer. https://doi.org/10.1007/978-3-030-47244-3_2.

Pande, C. B. (2020c). Thematic mapping for watershed development. In *Sustainable watershed development. Springer briefs in water science and technology*. Cham: Springer. https://doi.org/10.1007/978-3-030-47244-3_3.

Pande, C. B. (2020d). Sustainable watershed development planning. In *Sustainable watershed development. Springer briefs in water science and technology*. Cham: Springer. https://doi.org/10.1007/978-3-030-47244-3_4.

Pande, C. B., Khadri, S. F. R., Moharir, K. N., & Patode, R. S. (2017). Assessment of groundwater potential zonation of Mahesh River basin Akola and Buldhana districts, Maharashtra, India using remote sensing and GIS techniques. *Sustainable Water Resources Management, 4*, 965. https://doi.org/10.1007/s40899-017-0193-5, ISSN 2363-5037.

Pande, C. B., & Moharir, K. (2015). GIS-based quantitative morphometric analysis and its consequences: A case study from Shanur River basin, Maharashtra India. *Applied Water Science, 7*(2), 861–871.

Pande, C. B., Moharir, K. N., Singh, S. K., & Dzwairo, B. (2019). Groundwater evaluation for drinking purposes using statistical index: study of Akola and Buldhana districts of Maharashtra, India. *Environment, Development and Sustainability (A Multidisciplinary Approach to the Theory and Practice of Sustainable Development)*. https://doi.org/10.1007/s10668-019-00531-0.

Pande, C. B., Moharir, K. N., & Pande, R. (2018). Assessment of morphometric and hypsometric study for watershed development using spatial technology – A case study of Wardha river basin in the Maharashtra, India. *International Journal of River Basin Management*, 1. https://doi.org/10.1080/15715124.2018.1505737.

Patode, R. S., Pande, C. B., Nagdeve, M. B., Moharir, K. N., & Wankhade, R. M. (2017). Planning of conservation measures for watershed management and development by using geospatial technology – A case study of Patur watershed in Akola District of Maharashtra. *Current World Environment, 12*(03), 708–716.

Todd, D. K. (1980). *Ground water hydrology* (2nd ed.). New York, NY: John Wiley.

Trivedi, S. H. (2002). *Artificial recharge by Tubewells and percolation tank: A case study Apollo Tyres industry at Waghodia taluka, Vadodara*. Baroda: master of engineering thesis M.S. University.

Chapter 23
Reservoir Sedimentation Assessment of Rihand Reservoir Using Remote Sensing Technique

Smrati Singh, Abhishek Kumar Yadav, and Arun Pratap Mishra

Contents

23.1 Introduction 453
23.2 Study Area 455
23.3 Data Used 456
23.4 Methodology 457
23.5 Result and Discussion 460
23.6 Conclusion 462
References 464

23.1 Introduction

Reservoirs are basically the water storage structures which can either be natural or man-made and have been in existence for centuries. Basically, the reservoir collects the inflows from several rivers and hence is constructed at the end of the catchment (Jorgensen et al. 2005; Khadri and Moharir 2016; Khadri and Pande 2016). Reservoirs provide water for various different activities such as for irrigational purpose, hydroelectricity production, drinking purpose, water supply, fishing, recreation, etc. and also helps in regulating the water level and controlling floods during the rainy season (Merina et al. 2016). The sedimentation of the reservoirs is one of the greatest

S. Singh
University of Lucknow, Lucknow, Uttar Pradesh, India

A. K. Yadav
Indian Institute of Remote Sensing, ISRO, Dehradun, Uttarakhand, India

A. P. Mishra (✉)
Northern Regional Centre, Botanical Survey of India, Dehradun, Uttarakhand, India

C. B. Pande, K. N. Moharir (eds.), *Groundwater Resources Development and Planning in the Semi-Arid Region*, https://doi.org/10.1007/978-3-030-68124-1_23

issues in managing these reservoirs and their applications all over the globe. The main cause of reservoir sedimentation is the process of soil erosion which is caused by the geomorphologic process but is accelerated by human activities like rapidly growing human population, deforestation, overgrazing, etc. (Pande 2014, 2020a, b; Pande and Moharir 2014). The flow of water into the reservoir is at a much less velocity and hence the sediments get trapped in the reservoirs at different levels which causes a decrease in capacity of transportation whereas the deposition of sediments increases leading to failure of reservoirs in performing with their designed capacity (Merina et al. 2016). Because of sedimentation, there is the formation of delta that results in blockage at the mouth of tributaries of rivers which causes the formation of pools and this decreases the storage capacity of reservoirs to a great extent (Mahto and Patil 2005; Murthy 1977). India being an agriculture-based economy has a great dependence on reservoirs thus it becomes much more important to keep a check on reservoirs for its proper maintenance (Pande and Moharir 2015; Pande et al. 2017, 2018a, 2019).

Reservoir sedimentation thus needs to be evaluated and monitored at regular time intervals. There are mainly two conventional methods used in the estimation of reservoir sedimentation which includes direct hydrographic survey method and indirect inflow-outflow sediment method, but both of these methods are high-priced and laborious (Jain 2002). Further with the arrival of remote sensing technique, assessment and continuous monitoring of the sedimentation process of reservoirs have become much more convenient with less time and money consumption.

Quantification of the sediment deposits for assessing the deposition and distribution pattern of sediments can be efficiently done by the application of remote sensing methods. Remote sensing makes it possible to determine water spread areas at different days having different reservoir elevation followed by preparation of revised the elevation-capacity curve which indicates the current scenario of the reservoir in terms of its storage capacity. Previously, many studies have been done based on remote sensing for estimation of reservoir sedimentation (Manvalan et al. 1991; Goel et al. 2002; Jain et al. 2002; Mukherjee et al. 2007). Studies have also been performed for soil erosion modelling by utilization of remote sensing data (Pandey et al. 2009). The assessment of regular change in water spread area along with the sediment deposition rate and distribution pattern of sediments in the reservoir can now be done effectively at regular intervals using high spatial, temporal and spectral resolution datasets (Jain et al. 2002; Narasayya 2013; Pande et al. 2018b) which are nowadays easily available in public domain free of cost. Hence, it can be said that a remote sensing-based study takes less time for analyzing the data and is a cost-effective method as compared to other conventional methods (Pande).

23.2 Study Area

Rihand Dam is the largest dam present in India in terms of its volume along with its largest man-made lake of India specifically known as Govind Ballabh Pant Sagar. It is present at a town named Pipri in the Sonbhadra District of Uttar Pradesh in between 23°56′00″ North latitude to 83°04′00″ East longitude (Fig. 23.1). Generally, the reservoir is located at the border of Uttar Pradesh and Madhya Pradesh. Rihand Dam was constructed on Rihand River itself which is a tributary of river Son. The dam was built during the years 1957–1962 and is a concrete gravity dam and has a length of 934.45 m (3066 ft) with its maximum height being 91.46 m (300 ft) (Table 23.1). The reservoir of the dam has a surface area of about 465.38 km^2 at FRL and at DSL the surface area is 137.6 km^2. The designed capacity of the reservoir is 10.6 billion m^3. Irrigation, flood control and hydropower generation are the main functions of this dam.

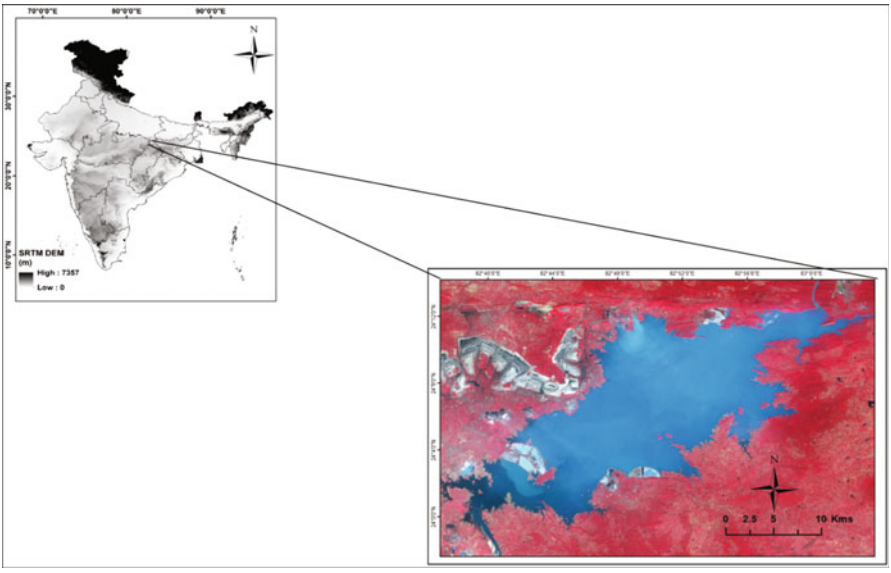

Fig. 23.1 Location of Rihand Reservoir

Table 23.1 Salient features of Rihand reservoir

Construction year	1962
Type of dam	Concrete gravity dam
Reservoir height	91.46 m
Length of reservoir	934.45 m
FRL (full reservoir level)	268 m above MSL
Catchment area	13,333.26 km^2
Annual inflow	6301 million m^3
Installed capacity	300 MW

23.3 Data Used

The data taken here for the assessment of reservoir sedimentation process is from Landsat 8 Earth observation satellite of the United States Geological Survey (USGS) which was launched on the 11th of February 2013 by NASA under its initial name Landsat Data Continuity Mission (LDCM). This satellite has a swath area of 185 kilometres and is equipped with other features like Operational Imager Sensor (OLI) and the Thermal InfraRed Sensor (TIRS) which helps in collecting image data for nine short wavelength bands and two with long wavelength thermal bands respectively. The detailed description of the satellite's payload and data provided by Landsat 8 is given in Table 23.2. The Landsat 8 optical data can be easily obtained from the USGS website (http://earthexplorer.usgs.gov) as provides cost-free data to its users. It provides a reasonable resolution of 30 m for visible and near-infrared regions which are being used in this study. Nine cloud-free images were acquired for this study from the period of May 2018 to May 2019. The images helped in mapping the water spread area in for the dates of image acquisition having maximum fluctuation in the water level. The details of the cloud-free data collected for 2018–2019 is given in Table 23.2. Band 3 (0.525–0.600 μm) and Band 4 (0.630–0.680 μm) which represent green and red bands respectively of the visible region along with Band 5 (0.845–0.885 μm) which is for the near-infrared region are taken in here for consideration. Landsat 8 OLI satellite acquired image data from May 2018 to May 2019 with path 142 and row 43 is used in this study (Table. 23.3 and Fig. 23.2).

Table 23.2 Characteristics Landsat 8 Satellite data

Sensors	Bands	Wavelength (μm)	Spatial resolution (m)	Swath width
Operational Land Imager (OLI)	Band 1—Coastal/ Aerosol	0.43–0.45	30	185 km
	Band 2—Blue	0.45–0.51	30	
	Band 3—Green	0.53–0.59	30	
	Band 4—Red	0.64–0.67	30	
	Band 5—Near-Infra-red (NIR)	0.85–0.88	30	
	Band 6—SWIR 1	1.57–1.65	30	
	Band 7—SWIR 2	2.11–2.29	30	
	Band 8—Panchromatic	0.50–0.68	15	
	Band 9—Cirrus	1.36–1.38	30	
Thermal Infrared Sensor (TIRS)	Band 10—Thermal Infrared 1	10.60–11.19	100	
	Band 11—Thermal Infrared 2	11.50–12.51	100	

Table 23.3 Satellite data with date of acquisition for the Rihand reservoir

Sr. no.	Date of acquisition	Satellite	Path/row	Elevation data (India-WRIS)
1.	16 Jun 2018	Landsat 8 OLI	142/43	255.21
2.	22 Oct 2018	Landsat 8 OLI	142/43	263.17
3.	7 Nov 2018	Landsat 8 OLI	142/43	262.5
4.	23 Nov 2018	Landsat 8 OLI	142/43	262.07
5.	9 Dec 2018	Landsat 8 OLI	142/43	261.73
6.	25 Dec 2018	Landsat 8 OLI	142/43	261.06
7.	10 Jan 2019	Landsat 8 OLI	142/43	260.33
8.	11 Feb 2019	Landsat 8 OLI	142/43	258.59
9.	31 Mar 2019	Landsat 8 OLI	142/43	256.52
10.	2 May 2019	Landsat 8 OLI	142/43	255.60
11.	18 May 2019	Landsat 8 OLI	142/43	255.70

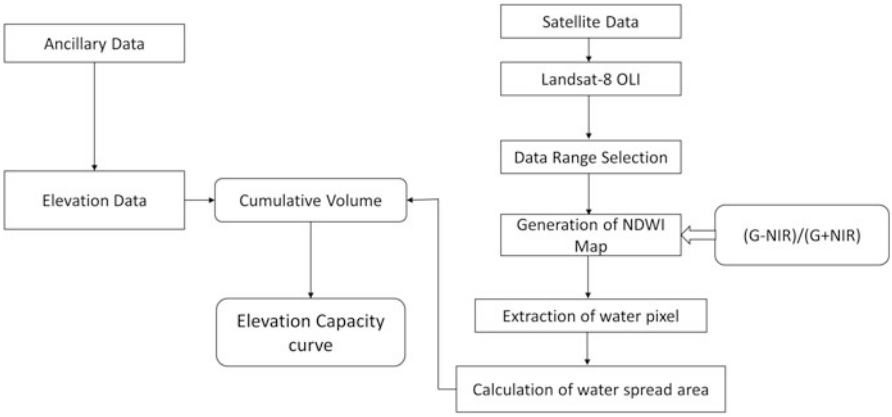

Fig. 23.2 Flow chart of methodology adopted

23.4 Methodology

23.4.1 Calculation of Water Spread Area

Satellite imagery is used in the assessment and estimation of the image data of the scene collected from the Landsat-8 OLI. For the assessment of sedimentation in the reservoir the water spread area of the reservoir is needed. Hence for this purpose, the remote sensing data having path and row numbers 142 and 43 respectively are processed. After this, the water body is extracted by the identification of the water pixels. For this, the water pixels are needed to be separated from the nearby features like vegetation, soil surface, built-up area, etc. However, the water pixels identification at land and water interface is a very critical task and therefore it needs proper interpretation from the analyst. Now, for recognition of the water pixels, NDWI (Normalized Differential Water Index) is been utilized for observing the alterations

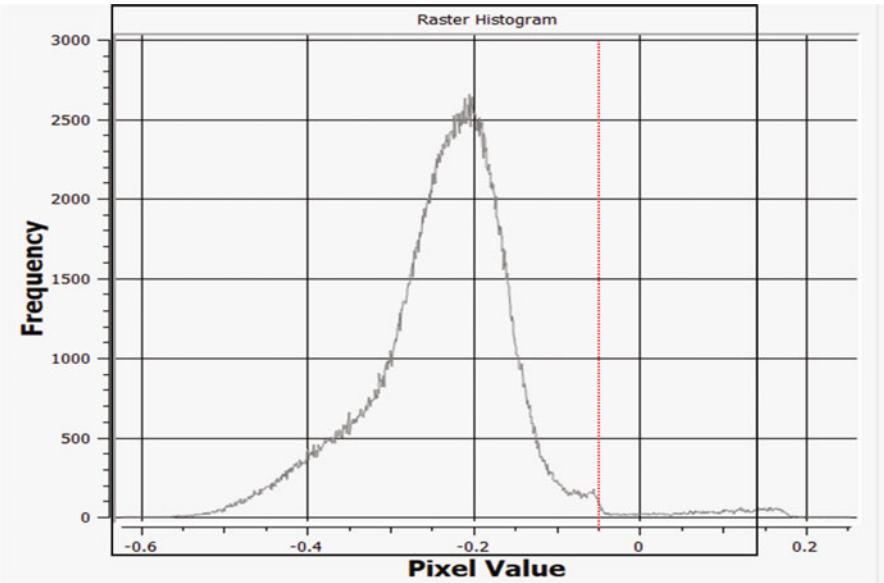

Fig. 23.3 Procedure of selecting threshold value using a Histogram of NDWI image. Red represents the value of the threshold selected

related to the water content in the reservoir using the NIR (Band 5) and Green (Band 3). The following equation is used for calculating NDWI (McFeeters 1996).

$$\text{NDWI} = (\text{Green} - \text{NIR})/(\text{Green} + \text{NIR})$$

where,Green wavelength—Band 3.NIR wavelength—Band 5.

The NDWI image of the reservoir area was generated and in case of NDWI image, the water has pixel value >0 while non-water pixels (vegetation, settlement, soil surface, etc.) have pixel value <0 (McFeeters 1996). The maximum absorption of electromagnetic radiation is done by water in the NIR (Near-Infrared) spectral region. Other features pixels (soil, vegetation, etc.) have a higher DN (Digital Number) than DN of water pixels. Hence, the threshold value of −0.05 was selected with the help of a histogram (Fig. 23.3) of the NDWI image for the extraction of water pixels. The pictorial representation of the NDWI image and output generated after applying the threshold value is shown in Fig. 23.4.

The water spread area of the eleven images acquired was estimated after extraction of water pixels by applying following equation:

$$\text{Water spread area} = \frac{\text{Number of water pixels} \times \text{Area of pixel}}{1,000,000}$$

Here, pixel area is taken as (30 × 30) m because the spatial resolution of landsat 8 OLI is 30 m.

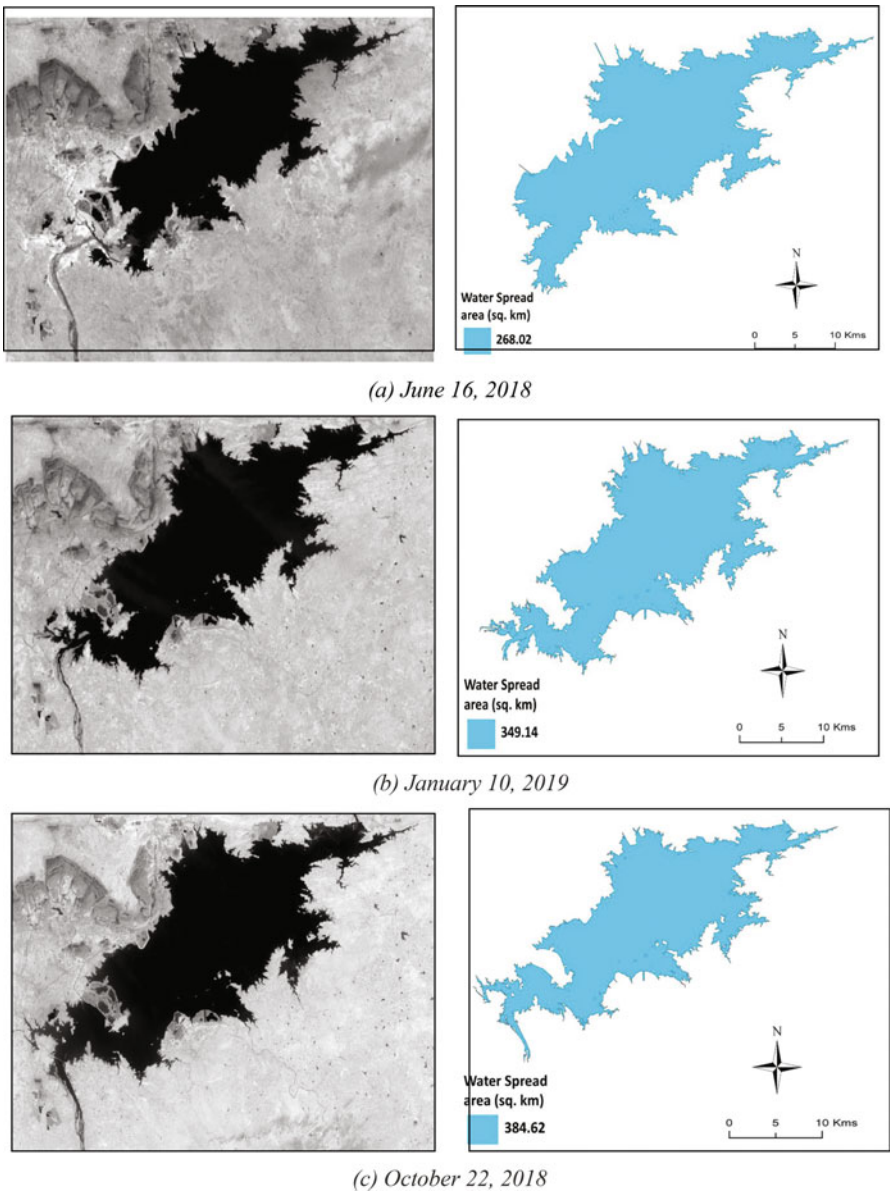

Fig. 23.4 Water pixel extracted from Landsat 8 data using NDWI image of Rihand Reservoir

23.4.2 Calculation of Revised Capacity

For analyzing the sedimentation in the reservoir by utilizing remote sensing technique, the principle used is that due to the deposition of the sediments in reservoir, the water spread area at specific height would decrease (Goel et al. 2002). Basically,

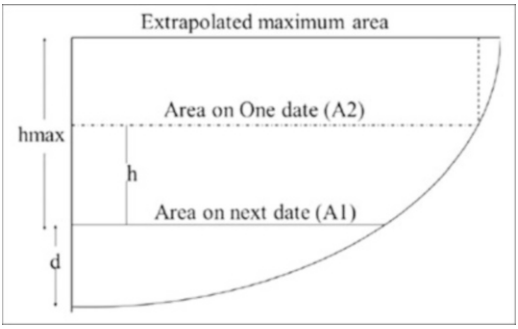

Fig. 23.5 Line diagram of trapezoidal method (Shukla et al. 2017)

there are three equations that could be used for calculation of capacity of the reservoir between two successive elevations, Trapezoidal equation, Prismoid equation, Simpson equation (Patra 2001). As for now in this study trapezoidal formula has been used by assuming the capacity of storage between two particular elevation or dates as a trapezoid (Fig. 23.5), the volume of water stored between the two particular elevations could be estimated simply by applying the trapezoidal formula (Jayapragasam and Muthuswamy 1980; Manvalan et al. 1991).

Trapezoidal formula is utilized for calculation of the reservoir volume at each elevation is shown below:

$$V = \frac{h}{3}\left(A_1 + A_2 + \sqrt{A_1 \times A_2}\right).$$

where,

$V =$ Volume of the reservoir between two heights.

$h =$ Difference between elevation.

A_1 and $A_2 =$ Water spread area of two dates calculated.

The revised cumulative volume of storage is then estimated by the addition of all the derived volume at every level taken into consideration. The deposition of sediments between the highest and lowest observed levels is derived by taking the difference between revised and original capacity.

23.5 Result and Discussion

The water spread area for the eleven cloud-free dates between the year 2018–2019 of the Rihand reservoir was calculated for the purpose of reservoir sedimentation estimation with the application of satellite imagery using LANDSAT 8 OLI sensor involving the calculation of NDWI using Green (Band 3) and NIR (Band 5) wavelength of the visible spectrum. The threshold value for the water pixels of the NDWI images was selected through histogram. Using water spread area of reservoir and elevation dataset the reservoir capacity is calculated by a trapezoidal formula and further the reservoir's cumulative volume is obtained.

Table 23.4 Estimation of cumulative volume and reservoir sedimentation using Trapezoidal method

Date	Area (km^2)	Elevation (m)	Volume (Mm^3)	Cumulative volume (Mm^3)
16/06/18	268.02	255.21		
18/05/19	270.37	255.7	131.9051	131.9051
2/05/19	273.89	255.76	16.32769	148.2328
31/03/19	289.85	256.52	214.1926	362.4254
11/02/19	320.26	258.59	631.2022	993.6276
10/01/19	349.14	260.33	582.1972	1575.825
25/12/18	359.46	261.06	258.6299	1834.455
9/12/18	366.3	261.73	243.126	2077.581
23/11/18	371.83	262.07	125.4809	2203.062
7/11/18	375.31	262.5	160.6345	2363.696
22/08/18	384.62	263.17	254.5702	2618.266

The volume between two successive reservoir levels was estimated by utilizing the trapezoidal equation with the help of a water spread area and its corresponding elevation data obtained through India-WRIS as shown in the methodology section. After computation of the volume between the reservoir levels, cumulative volume of the reservoir for the year 2018–2019 was calculated (Table 23.4). The water level fluctuation during the study period (16th June 2018 to 18th May 2019) was from 255.21 to 263.17 m. The difference between estimated cumulative capacity and original capacity provides the capacity loss of the reservoir caused by the sedimentation. Rihand reservoir was initially built with a total capacity of 10.6 billion cubic metres with the FRL of 268 m in the year 1962. According to the results of the hydrographic survey obtained from WRIS India, the live storage capacity in the year 2000–2001 of the Rihand reservoir was 2932.87 Mm^3 at 263.17 m water storage level. In the present study conducted using Landsat-8 optical data for the year 2018–2019, the water did not reach its FRL and the highest water level recorded was 263.17 m and the lowest water level was 255.21 m with the live storage capacity 2618.26 Mm^3 at 263.17 m level of water storage of the Rihand reservoir. The elevation data and cumulative capacity estimated for different days were plotted to get a revised elevation-capacity curve (Fig. 23.6). It could be observed from the graph that the storage capacity of the reservoir has decreased during 2018–2019 as was in 2000–2001, this loss in capacity has been attributed to the deposition of sediments in the reservoir over these years. This shows the continuous loss in the capacity of the reservoir since past 19 years due to the process of sedimentation in the catchment area of the reservoir and thus the loss in the reservoir capacity is assessed to be 314.61 Mm^3. And this capacity loss is associated with the sediment deposited in the zone of study i.e. 255.21–263.17 m, which is represented through the elevation-capacity curve shown in Fig. 23.7, it represents the comparison of reservoir capacities at given elevations for the current year of study 2018–2019 and the data of reservoir capacities versus elevations obtained back in the year

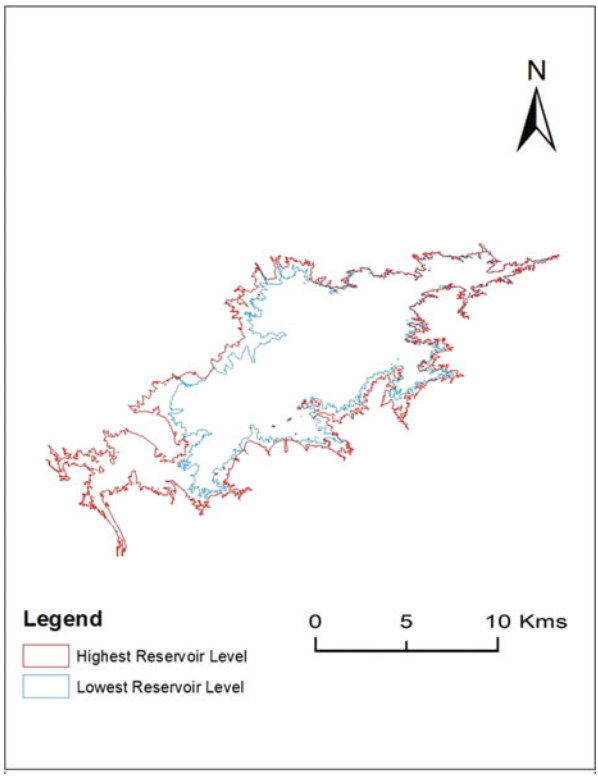

Fig. 23.6 Water spread area during highest and lowest elevation reservoir level

2000–2001. The average sedimentation rate from this study can be inferred to be about 16.52 Mm^3/year with a percentage loss of 10.73%.

The benefit of remote sensing technique is that at different elevation levels of the date of acquisition, water spread area and storage capacity could be estimated easily. And this further helps in plotting the elevation-capacity curve of the current scenario. It could be seen that the storage capacity has decreased nearly at each reservoir level in the zone of our study (255.21–263.17 m) while the decrease at higher levels is more as compared to lower levels. This is vital information for the reservoir/dam authorities which is necessary for the operation of the reservoir.

23.6 Conclusion

The current study was conducted for the estimation of the reservoir sedimentation in the Rihand reservoir using the remote sensing technology for the year 2018–2019. The results from the hydrographic survey of the year 2000–2001 obtained from WRIS India shows the live storage capacity of the Rihand reservoir to be 2932.87 Mm^3 at 263.17 m water storage level. The revised reservoir capacity

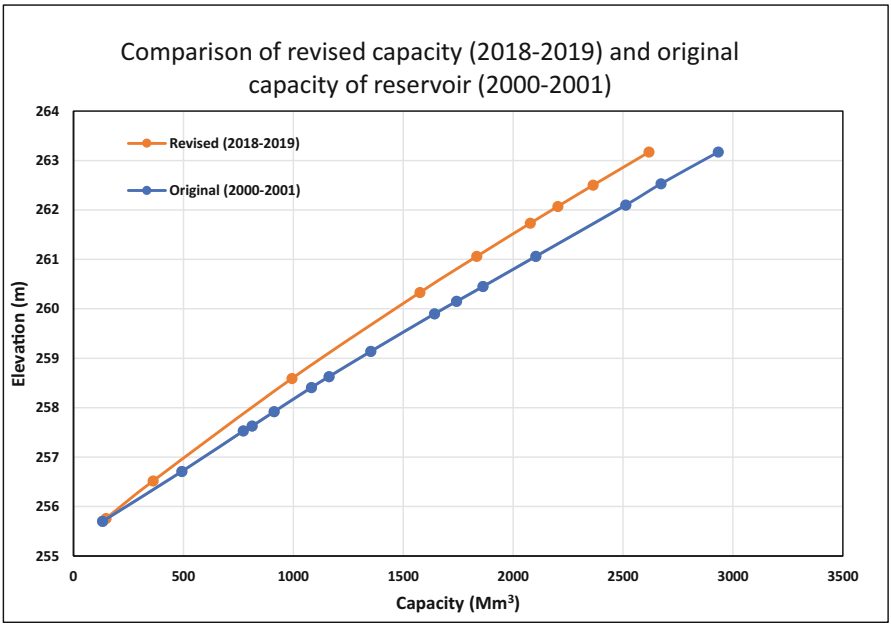

Fig. 23.7 Elevation-capacity curve for Rihand Reservoir (2018–2019)

assessed through the optical data for the year 2018–2019 was 2618.26 Mm^3 at 263.17 m. This shows that there has been a loss of 314.61 Mm^3 in the capacity of the reservoir due to the process of sedimentation in the last 19 years period. Further, the average rate of sedimentation thus estimated is 16.55 Mm^3/year and the percentage loss of the reservoir capacity is 10.73% between the reservoir levels considered. It means that reservoir is losing its capacity by 0.57% per year. It is to be noted that the water capacity of the Rihand reservoir did not reach to FRL in the year 2018–2019 (present study) of the sedimentation estimation which is carried out through the remote sensing technique therefore this rate of sedimentation estimated is in the zone of study (i.e. 255.21–263.17 m). The use of remote sensing in such estimations for reservoir sedimentation is not only rapid and less laborious but also low-cost and affordable in the long run which gives time to time systematic information about the fluctuations in the water level (live storage capacity) and the aggregate of sediments deposited in the reservoir. In terms of accuracy remote sensing technology can give slightly different results varying from those estimated through conventional methods such as hydrographic surveys as selection of threshold value is a difficult task which could lead to mixing of water and land pixels around the peripheral region of the reservoir. Since the pixels mixing generally happens for the interface of water and land which have a small proportion of water as compared to that of land, hence it might affect the capacity estimation of reservoir. To overcome this problem, high spatial and temporal resolution datasets need to be used such as SAR (Synthetic Aperture Radar) data which could give more accurate

results as compared to optical dataset. The remote sensing technology thus can be used to carry out for regular monitoring and assessment of the sedimentation in the reservoirs with simultaneous evaluations through hydrographic surveys which are carried after some fixed time intervals, this in future will ensure less consumption of time with low expenditure and high accuracy.

References

Goel, M. K., Jain, S. K., & Agarwal, P. K. (2002). Assessment of sediment deposition rate in Bargi Reservoir using digital image processing. *Hydrological Sciences Journal, 47*(S1), S81–S92.

Jain, S. K. (2002). Determination of reservoir storage capacity, 1–10. Retrieved from http://nihroorkee.gov.in/NHP/traning_Modules/Reservoir Sizing.pdf.

Jain, S. K., Singh, P., & Seth, S. M. (2002). Assessment of sedimentation in Bhakra Reservoir in the western Himalayan region using remotely sensed data. *Hydrological Sciences Journal, 47*(2), 203–212.

Jayapragasam, R., & Muthuswamy, K. (1980). Sedimentation studies in Vaigai Reservoir using grid system. *Water and Energy International, 37*(3), 337–350.

Jorgensen, S. E., Loffler, H., Rast, W., & Straskraba, M. (2005). *Lake and reservoir management*. Amsterdam: Elsevier.

Khadri, S. F. R., & Moharir, K. (2016). Characterization of aquifer parameter in basaltic hard rock region through pumping test methods: A case study of Man River basin in Akola and Buldhana Districts Maharashtra India. *Modeling Earth Systems and Environment, 2*, 33.

Khadri, S. F. R., & Pande, C. B. (2016). Ground water flow modeling for calibrating steady state using MODFLOW software: A case study of Mahesh River basin, India. *Model Earth System Environment, 2*, 39. https://doi.org/10.1007/s40808-015-0049-7.

Mahto, S., & Patil, T. S. (2005). Short term training programme on sedimentation planning for reservoir.

Manvalan, P., Rajegowda, G. E., & Srinivas, M. V. (1991). Capacity evaluation of Ghatprabha Reservoir using digital analysis of 1RS L1SS-II data. Project report no. B/003/91.

McFeeters, S. K. (1996). The use of the Normalized Difference Water Index (NDWI) in the delineation of open water features. *International Journal of Remote Sensing, 17*(7), 1425–1432.

Merina, N. R., Sashikkumar, M. C., Rizvana, N., & Adlin, R. (2016). Sedimentation study in a reservoir using remote sensing technique. *Applied Ecology and Environmental Research, 14*(4), 296–304.

Mukherjee, S., Veer, V., Tyagi, S. K., & Sharma, V. (2007). Sedimentation study of Hirakud Reservoir through remote sensing techniques. *Journal of Spatial Hydrology, 7*(1), 7.

Murthy, B. N. (1977). *Sedimentation studies in resevoirs* (Vol. 1). New Delhi: Central Board of Irrigation and Power.

Narasayya, K. (2013). Assessment of reservoir sedimentation using remote sensing satellite imageries. *Asian Journal of Geoinformatics, 12*(4), 711–718.

Pande, C., & Moharir, K. (2014). Analysis of land use/land cover changes using remote sensing data and GIS techniques of Patur Taluka, Maharashtra, India. *International Journal of Pure and Applied Research in Engineering and Technology, 2*(12), 85–92.

Pande, C. B. (2020a). Thematic mapping for watershed development. In *Sustainable watershed development. Springer briefs in water science and technology*. Cham: Springer. https://doi.org/10.1007/978-3-030-47244-3_3.

Pande, C. B. (2020b). Sustainable watershed development planning. In *Sustainable watershed development. Springer briefs in water science and technology*. Cham: Springer. https://doi.org/10.1007/978-3-030-47244-3_4.

Pande, C. B., Khadri, S. F. R., Moharir, K. N., & Patode, R. S. (2017). Assessment of groundwater potential zonation of Mahesh River basin Akola and Buldhana districts, Maharashtra, India using remote sensing and GIS techniques. *Sustainable Water Resources Management*. https://doi.org/10.1007/s40899-017-0193-5. ISSN 2363-5037.

Pande, C. (2014). Change detection in land use/land cover in Akola Taluka using remote sensing and GIS technique. *International Journal of Research (IJR), 1*(8), 1440–1450.

Pande, C. B., & Moharir, K. (2015). GIS-based quantitative morphometric analysis and its consequences: A case study from Shanur River Basin, Maharashtra, India. *Applied Water Science, 7*(2), 861–871.

Pande, C. B., Moharir, K. N., Singh, S. K., & Varade, A. M. (2019). An integrated approach to delineate the groundwater potential zones in Devdari watershed area of Akola district. *Maharashtra, Central India in Environment, Development, and Sustainability*. https://doi.org/10.1007/s10668-019-00409-1.

Pande, C. B., Moharir, K. N., Khadri, S. F. R., & Patil, S. (2018b). Study of land use classification in the arid region using multispectral satellite images. *Applied Water Science, 8*(5), 1–11.

Pande, C. B., Moharir, K. N., & Pande, R. (2018a). *Assessment of morphometric and hypsometric study for watershed development using spatial technology – A case study of Wardha river basin in the Maharashtra, India*. International Journal of River Basin Management. https://doi.org/10.1080/15715124.2018.1505737.

Pandey, A., Mathur, A., Mishra, S. K., & Mal, B. C. (2009). Soil erosion modeling of a Himalayan watershed using RS and GIS. *Environmental Earth Sciences, 59*(2), 399–410.

Patra, K. C. (2001). Design flood. *Hydrology and Water Resource Engineering, 2017*, 399–402.

Shukla, S., Jain, S. K., Kansal, M. L., & Chandniha, S. K. (2017). Assessment of sedimentation in Pong and Bhakra reservoirs in Himachal Pradesh, India, using geospatial technique. *Remote Sensing Applications: Society and Environment, 8*, 148–156.

Chapter 24
A Coupled Hydrological and Hydrodynamic Model for Flood Mitigation

Triambak Baghel, Manish Kumar Sinha, Ishtiyaq Ahmad, and M. K. Verma

Contents

24.1 Introduction 468
24.2 Materials and Methodology 471
24.3 Model Setting and Input Parameter Preparation 474
24.4 Hydrological Model Settings 474
24.5 Hydraulic Model Setting 477
24.6 Modification of Stream Cross-Section 479
24.7 Results and Discussions 479
24.8 Conclusion 482
References 483

T. Baghel
Water Engineering and Management, Asian Institute of Technology, Bangkok, Thailand

Department of Civil Engineering, National Institute of Technology, Raipur, Chhattisgarh, India

M. K. Sinha (✉)
Environmental and Water Resources Engineering, University Teaching Department, Chhattisgarh Swami Vivekanand Technical University, Bhilai, Chhattisgarh, India
e-mail: manishsinha200389@gmail.com

I. Ahmad · M. K. Verma
Department of Civil Engineering, National Institute of Technology, Raipur, Chhattisgarh, India
e-mail: iahmad.ce@nitrr.ac.in

C. B. Pande, K. N. Moharir (eds.), *Groundwater Resources Development and Planning in the Semi-Arid Region*, https://doi.org/10.1007/978-3-030-68124-1_24

24.1 Introduction

Estimation of flood hydrograph, peak flow computation and flood plain mapping have always been important role in flood inundation modelling in order to determine flood prone area for many design or flood management related studies (Todorovic and Zelenhasic 1970; Pedzisai 2010). Flood estimation is essential for saving human life and valuable properties beyond its use in several hydrologic and hydraulic studies (Hailegeorgis and Alfredsen 2017). Above 50 cities of different countries in the world are facing the problem of flood and India is one of them (World Meteorological Organization, WMO) (Jha et al. 2012). Recent catastrophic floods in Indian cities are, Ahmedabad (2001), Bangalore (almost every year since 2000), Chennai (2004), Delhi (2002, 2003, 2009, 2010), Hyderabad (2000, 2002, almost every year) Mumbai (2005, 2016), Surat (2006), Kolkata (2007), J, and Guwahati (2010) (Sengupta 2016). Keeping in view the above facts that the problem of flood has become more severe, these result in economic and structural losses that are mounting every year (Sayers et al. 2013). The occurrence of flood events can be measured and modelled with various hydro-spatial modelling platforms (Andrysiak and Maidment 2000; Marfai 2003). One of the worldwide used software is HEC-HMS & HEC-RAS (Hydrologic Engineering Center-Hydrologic Modelling System; River Analysis System) (Feldman 2000; Brunner 1995; Doan 2000). Most popular use of hydro-spatial modelling in identification of flood prone areas at catchment scale has focused on developing flood hydrographs. Many researches have been used and still using combined HEC-HMS-RAS to perform flood inundation modelling, to design flood hydrographs and corresponding floodplain, evaluating potential flood mitigation projects, and performing quasi-unsteady or full-unsteady flow analyses (Pistocchi and Mazzoli 2002; Heimhuber 2013; Hashemyan et al. 2015;). Using this modelling platform it is possible to obtain flood hydrographs by using HMS by developing basin geometric model with HEC-GeoHMS platform and then it can be imported in HEC-RAS from dynamic flood simulation (Quan 2006; Ahmad et al. 2015).

The study area shows the modelling strength of HEC-HMS-RAS software that can be easily applicable even for small size catchments when the area is highly influenced by flooding. Several attempts have been already made to determine flood hydrographs and identify flood plain areas using similar technique, especially GIS-based HMS and RAS (Wagener et al. 2004) explained in detail the step by step procedure for the use of HEC-RAS in the Rioni River in Georgia. With the use of topographic sheets and the data of observed ground points and not exactly extracted from the DEM, geometric data was rectified during this process. Pictures of the sites helped them to actual conclude for the exact Manning's coefficient values. After using the discharge values of different years observed repeatedly at different locations, the model was first run for Steady flow and then for Unsteady flows. For both the conditions results were analysed. Ackerman, Evans (Ackerman et al. 2000) explained HEC-GeoRAS, a suite of GIS for the pre and post-processing tools for the HEC-RAS, a 1-D river hydraulics model. This included the procedure

of importing roughness values along the cross-sections taken, exporting bank stations and velocities across the cross-sections of the river. These Manning's coefficient values were very much correlated with the polygon themes of landcover in attribute tables. Abera 2011 carried out the research work of Flood Mapping and Modeling for Fogera flood plains in Ethiopia. The watershed–hydrologic modelling was done in HEC-GeoHMS, the river modelling in HEC-GeoRAS and hydraulic modelling by HEC-RAS. All the results were procedurally complied and results were finally displayed in the form of the flood plain maps. The extent of area inundated is listed out in quantities given in the tables for 100 year storm flood (Bewsher et al. 2013). being the flood risk managers and consultants in Sydney, Australia, have summarized as to what basically these flood risks are, why these flood risk maps are prepared for and how to map these flood risks for better landuse planning. They have efficiently combined the flood risk precinct maps with the landuse planning policies. Alaghmand et al. (2010) carried out the research work of GIS-based River Flood Hazard Mapping for Kayu Ara River Basin, Malaysia. HEC-HMS and HEC-RAS were utilized as hydrologic and hydraulic models for river flood hazard mapping. The generated river flood risk was based on water depth and flow velocity maps which were prepared according to hydraulic model results in GIS. The results show that, magnitude of rainfall event and river basin land use development condition have significant influences on the river flood hazard maps pattern. Gül et al. 2009 combined hydrologic and hydraulic modelling approach for testing proposed Bostanli Dam in the study area for flood control plan of basin. The study area was examined by using the HEC-HMS and HEC-RAS modelling tools, both integrated with GIS functions for spatial operations. The results show that the dam construction as planned would have positive impact on potential flood control measure, this contribute to the overall flood mitigation performance in the basin. Heimhuber et al. 2015 has estimated the flood hazard of Onaville–Canaan–Haiti, the modelling is done in GIS (ArcMap) platform with combination of HEC-HMS and HEC-RAS for estimation of flood hazard area the result show that large areas of the settlement are currently exposed to a high level of flood related hazard. In the response, the artificial channels have been suggested to zones with the highest flood hazard. He has concluded that the suggested channels have enough capacity to convey a 100-year flood runoff safely.

Intensity-Duration-Frequency curves have been developed for the study using Gumbles extreme values theory. Bara et al. 2009 carried out a study to develop IDF characteristics of a short duration rainfall, a Gumbles extreme values theory was applied. The advantage of use of GEV allows the estimation of the design values of rainfall intensity for arbitrary durations using only normally available daily rainfall data. Similarly, Samarasinghea et al. 2010 derived flood extent from the flood extent obtained for the 50-year rainfall using HEC-HMS and HEC-RAS in Kalu-Ganga River, Sri Lanka. Meena (2012) introduces about the parameterization of hydrologic and hydraulic modelling for simulation of runoff and flood inundated for Kosi River Basin in Bihar, India. Various H&H models HEC-HMS, HEC-RAS, SCS-CN in addition to ANN models are performed for runoff and flood plain inundation modelling. The result shows that both the methods HEC-HMS and ANN may be

used for rainfall-runoff simulation depending on the data availability. The inundated area obtained using integrated approach can be graphically represented in DEM map of the study region and flood risk analysis can be done using stated approach. From the review of literature it is clear that Hydrological & Hydraulic model developed by U.S. Army Corps of Engineering's Hydrologic Engineering Center (HEC) is stable model for estimation of runoff and planning effective flood mitigation measures (Scharffenberg and Fleming 2006). It is a well-established method which is widely used in all over the world. Therefore, for present study distributed SCS-CN model in HEC-GeoHMS has prepared and applied to estimation of runoff in study area. Then the output obtains from HMS model is taken as input in RAS model for flood inundation modelling which results planning for flood mitigation measures in the study area. Various literatures, video lecture, documents were collected and reviewed keeping the object and requirement of the study, as the study is mainly focused on providing flood mitigation measures for a pooling station of electricity supplying station which was situated at confluence of three old natural drains. This station generates electricity for the region where it's located and its submergence was caused a huge economic loss to the electricity generation company. The site has been erroneously selected by the agency without proper survey of historical data.

The objective of this study was to develop hydrologic and hydraulic models for the Champa pooling station, Taga village, Janjgir Champa District, Chhattisgarh. Latitude and Longitude of the site is 21°57′57 N and 82°29′05 E respectively which is located in Fig. 24.1. Due to heavy rainfall on 1st Aug, 2014 to 10th Aug, 2014, the

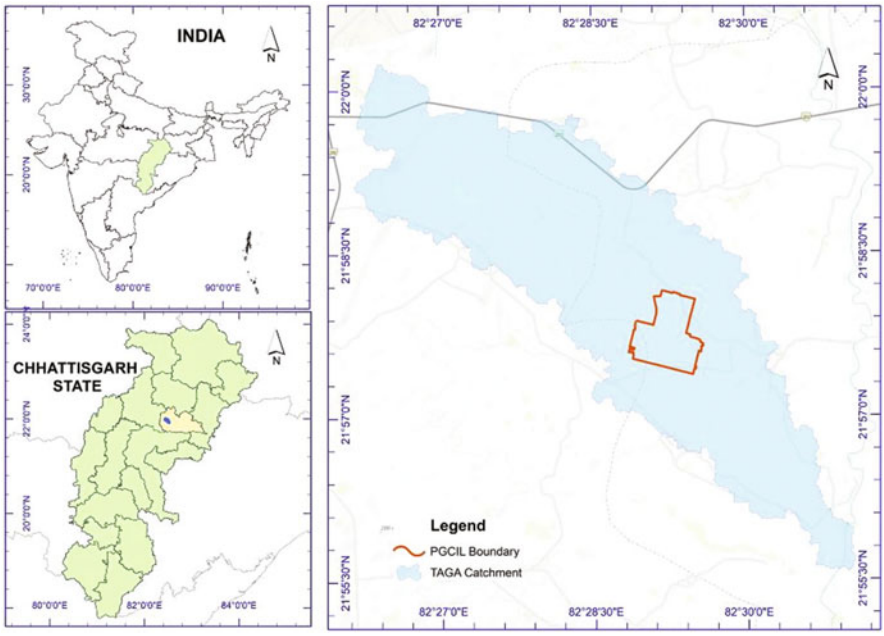

Fig. 24.1 Location map of the study area

Power Grid Corporation of India Limited—Champa pooling Station was flooded along with few parts of nearby villages. The flood problem in Taga village was cause due to alteration in natural drainage pattern and provision of improper artificial drainage. Historical satellite images shows that pooling station is located in confluence point of three streams that is also one of the causes for flooding. Flood occurs at time of construction of station. The station is installed with heavy electrical appliances such as capacitor banks and transformers. If water level rises about 50–100 cm it will cause damage to electrical appliances. This research work is based on the physical observations of the flood condition in and around the site and detailed watershed modelling and analysis of flood plan area to plan feasible remedial measures for flooding at Champa pooling station and its surrounding area.

24.2 Materials and Methodology

To generate flood inundation map for micro catchment, the basic requirement is to set up a model that replicate the Taga catchment. This has been achieved by coupling Hydrologic and Hydraulic model (H&H model) together (Pattison and Lane 2012). The hydrologic model is used to convert rainfall within the catchment boundaries into runoff (Mishra and Singh 2013). This runoff data obtained as result from hydrologic model serves as input for the hydraulic model and flow of flood wave in stream were simulated. Based on discharge in stream, the hydraulic model simulates water surface level and velocity at different locations of stream. By mapping geospatial distribution of water surface and velocities, flood inundation map were generated. Resulted flood inundation map has calibrated with field data obtained during the corresponding simulation period. Model parameters are altered and simulation was repeated till the flood inundation map imitates the observation flood map.

Although many flood control measures are available, each measure has its own site suitability characteristics. Based on site characters, model was modified such that it will have no flood inundation for the designed maximum flood. Following this flood mitigation framework is suggested, which is to be implemented in site to control flooding. The conceptual flowchart of methodology adopted is shown in Fig. 24.2.

24.2.1 Field Survey and Data Collection

The site was visited on Aug 11, 2014 from all the directions both inside and outside surrounding area. The site has the elevation variation from 295 to 272 m MSL. The major land use of upstream portion is agricultural land and fallow land. There are several small ditches and ponds that retain water. After site preparation, the normal flow path of flood water has been altered. High energy flood water in upstream has

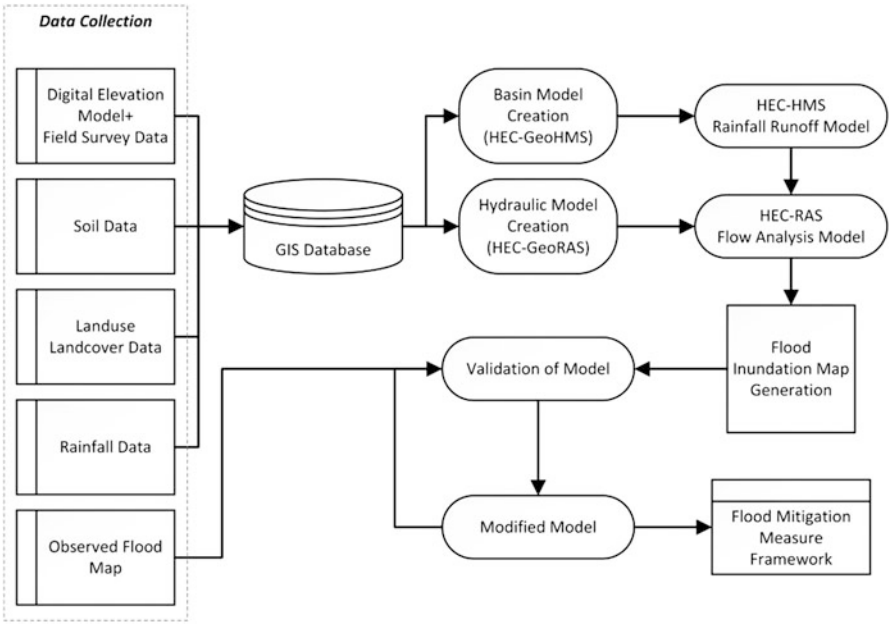

Fig. 24.2 Flow chart representing methodology adopted or flood mitigation strategies

created many new small fringes around the site. Water is obstructed to enter the site by boundary walls. But since the water energy is high, water started seeping below the wall and entered into the site. Poor drainage of upstream water is due to plain downstream condition with minimum slope.

Drainage provided in the site was designed for drainage of water inside the site and not for the extreme condition. Heavy rain for 10 days in the locality led to flooding condition. Since the prepared elevation is above surrounding area, improper diversion of flood water caused flooding in downstream villages. To reduce submergence in downstream village, water around boundary of site were diverted into the site and connected back to natural drain through outlet. Water diverted from ditch located at 21.967 N and 82.484 E through inlet which was connected with natural drainage at outlet. Since the newly prepared site's soil was not well compacted, many drainage fringes were formed due to rain inside site, which was widened further by water entering into site due to seepage under boundary wall. Water that entering via drain through the lower lying roads and connected with the outlet. This further increased the submergence of transformers, since outlet capacity is less, overland flow created submergence as show in Fig. 24.3.

Daily rainfall data is collected from State Data Centre, Raipur, Chhattisgarh. Rain gauge stations available around 50 km radius of the Taga Catchment are Kirari, Janjgir, Agaltara and Pamgarh stations. Among the three Kirari station was stopped functioning after 1998, Pamgarh and Agaltara stations were started functioning from 1997 and Janjgir is the only station that has continuous data from 1980 to 2014.

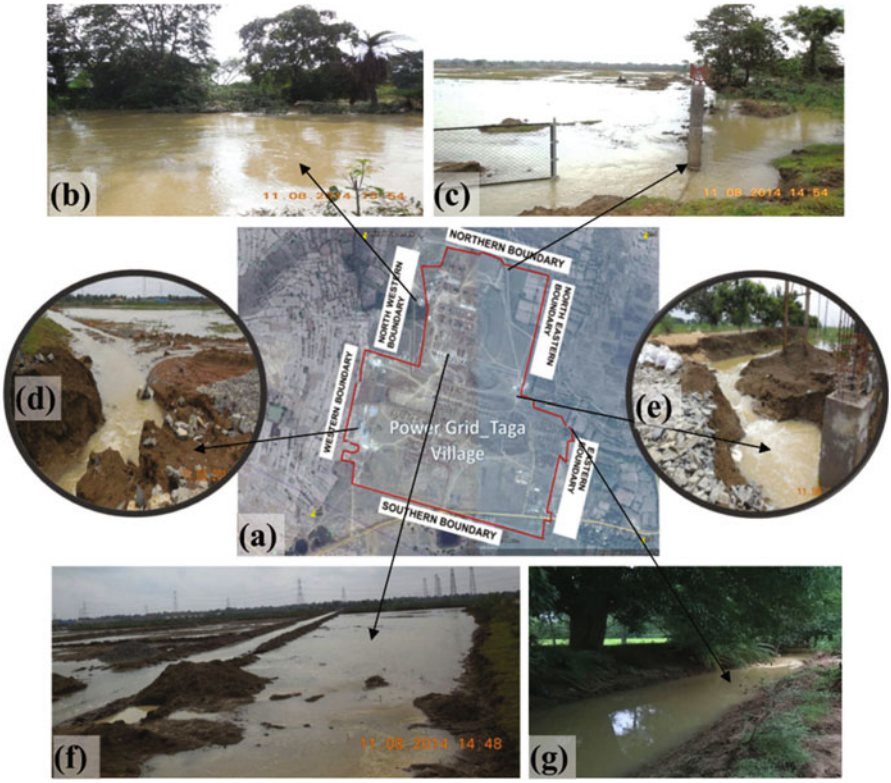

Fig. 24.3 Drainage conditions during field survey; where (**a**) PGCIL Champa pooling station map, (**b**) Inlet of Pawai Nalla in upstream, (**c**) Entry of flood water into site through gates at northern boundary, (**d**) Condition at entry of boundary wall at west channel, (**e**) At north eastern boundary wall, (**f**) Submergence area of main power distribution system install at site (**g**) Outlet of Pawai Nalla at the time of end of flood

Monsoon is the main source of rainfall in the study area and maximum precipitation falls between mid-June and September. The rainfall data are then used to prepare Intensity-Duration-Frequency (IDF) Curve.

Digital Elevation Model (DEM) of ASTER and Topographical survey conducted in and around the site are the main sources of terrain data. DEM of the watershed is used for Hydrologic Modelling. Topographical survey has been carried out with Differential global positioning system (DGPS) data are used in Hydraulic Modelling. Processed DEM from ASTER and survey both has been checked and validated during field survey to reduce temporal change in the topography, then has been used in preparation of basin characteristics.

Chhattisgarh State Soil Map and landuse-land cover was obtained from Survey of India, Raipur. The soil map was later cropped for the Taga catchment. Soil Map was classified into four hydrological soil groups (A, B, C and D) based on soil type. Since the State soil Map is wide scale, the whole catchment falls within the hydrological

soil group of 'D' which is also call 'kanhar' as local name. This is one of the constraints in preparing simulation model. LULC map was classified into five classes as Agricultural land, Water bodies, Wasteland, Build up and tree clads. Using soil group and landuse class curve number has been calculated, which is explained in hydrological modelling section.

24.3 Model Setting and Input Parameter Preparation

The flood assessment in the micro catchment Taga was performed based on Hydrologic and Hydraulic modelling and simulation. It is clear from recent researches that watershed level flood analysis and management is more efficient and reliable.

24.4 Hydrological Model Settings

Hydrologic model was developed in HEC-HMS 4.0 version software [10]. It is basically Rainfall-Runoff model. The hydrologic model was built with help of high spatial resolution DEM, Drainage network of the catchment, Soil Map and Land Use Land Cover Map. These geospatial data are initially processed using ArcMap 10.1. Purpose of building the hydrologic model is to convert rainfall in the catchment into runoff at different nodes of drainage network in and around site. Rainfall shedding in catchment is subjected to abstraction loss. SCS Curve Number technique was adopted to compute the loss. Geospatial distribution of Curve Number was developed based on combination of Soil Map and Land Use Land Cover Map (Sinha et al. 2019a, b; Dadhwal et al. 2010).

The SCS unit hydrograph method was used to transform direct rainfall to direct runoff. Since it is a micro catchment, base flow contribution to drainage was neglected (Leese 1973). Above methods are selected based on data availability and site suitability (Table 24.1). HEC-HMS requires three basic components for modelling that are basin component, meteorological component and control specification. Basin components were created using HEC-Geo-HMS extension of ArcMAP. ASTER 30 m Digital Elevation Model (DEM) of Taga micro catchment has been used as input data to generate basin morphometric features as show in Fig. 24.4.

Model setup is done by defining process and method adopted for computing runoff volume that are loss method, transform method, and routing method. Base flow method canopy method and surface method are not included in this basin model component since the analysis is only for short flood period and also lack of data required for each method. Though this will have impact in model simulation, but not including base flow provide additional factor of safety in design.

Table 24.1 Process, method used to generate HEC-HMS model

SN	Process	HMS model	Method used	Input data	Equation used
1	Computing run-off volume	Loss method	SCS-CN method	Initial abstraction Curve number Percent impervious	$Q = \frac{(P-\lambda S)^2}{P+(1-\lambda)S}$
2	Modelling direct runoff	Transform method	SCS unit hydrograph model	Basin lag	Lag time $= \frac{I^{0.8}\times(S+1)^{0.7}}{1900\times Y^{0.5}}$
3	Modelling channel flow	Routing method	Muskingum	Mannings 'n'	Continuity equation

Where,
P = daily rainfall in mm, λ = In the SCS method in Indian condition has the value of λ coefficient equal to 0.2, although for black soil region the value is taken as follows: (1) For black soil region AMC-I (Antecedent Moisture condition I) and for other regions: Ia = 0.3S. (2) For black soil region AMC-II & AMC-III: Ia = 0.1S

The potential maximum retention by the soil is given by dimensionless parameter known as curve number CN that depends upon the hydrologic soil groups, AMC and land use land cover factors of the catchment area.

S = 25,400/CN – 254,

I (in m.) = Hydraulic length of watershed,

Y = Average land slope.

Figure 24.5 shows a typical model setup in HEC-HMS, All the model processes are assigned in HEC-Geo-HMS and input parameters are assigned in HEC-HMS model.

24.4.1 Rainfall Frequency Analysis

Since design flood is target of the study, IDF curve was generated based on available data of Akaltara rain gauge station using 30-year daily rainfall data. Cumulative rainfall is calculated for 1, 2, 4 and 7 day for the return periods of 2, 5, 10, 30, 50 and 100 year. IDF curve was generated (Fig. 24.6) for maximum rainfall condition and the curve was fitted for Gumbel distribution (Chow 1964; Sinha et al. 2019a, b). DDF curve (Fig. 24.6) was generated from IDF curve which is the input of frequency storm method in model. Basin component has been imported in to HEC-HMS than frequency storm obtain from IDF curve was fed in Metrological component. The model was run for simulation period of 10 days with time step up 3 min. The model generated Peak discharge (runoff), Hydrograph and Time series data of the same.

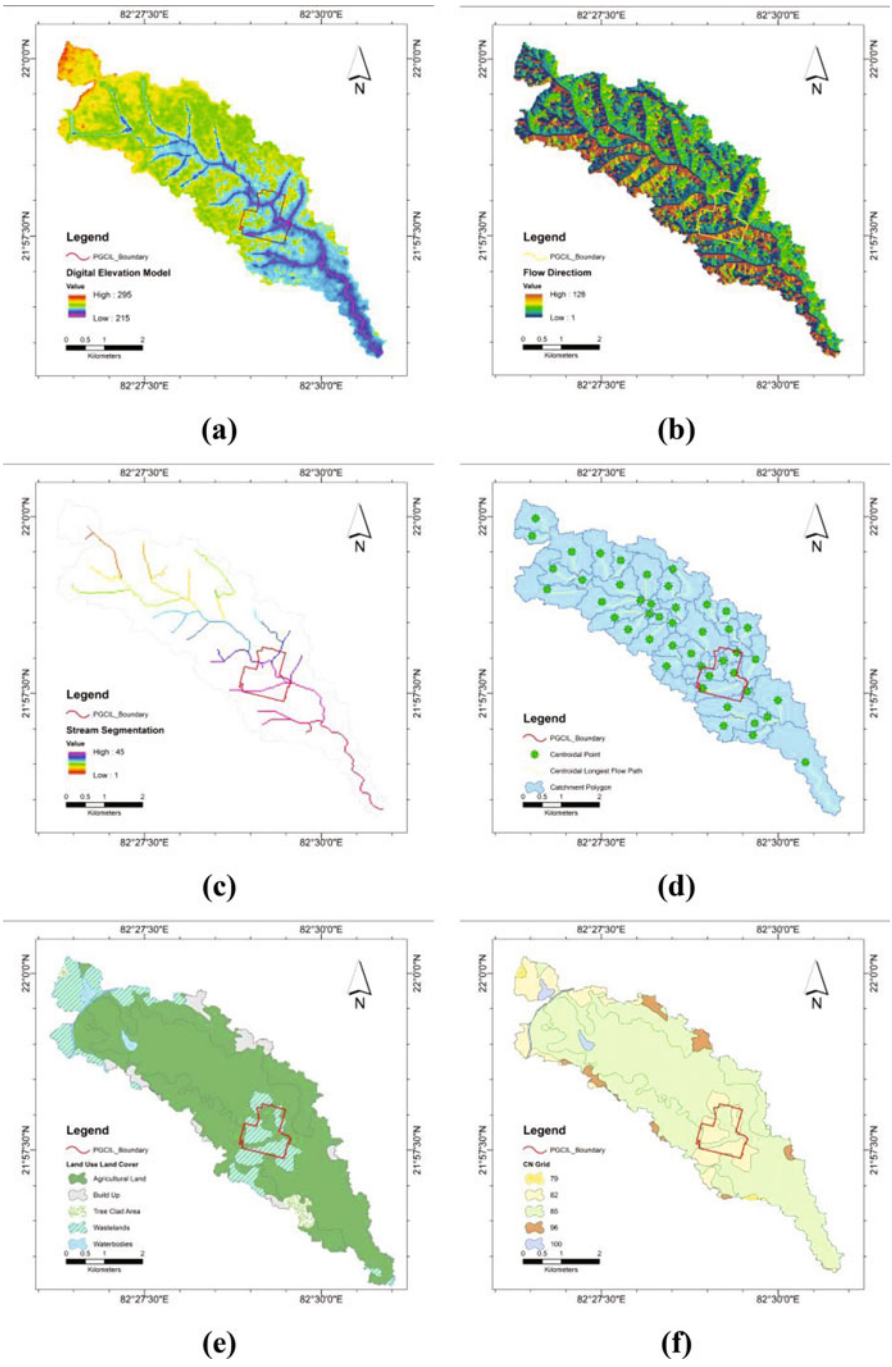

Fig. 24.4 Terrain pre-processing of Taga catchment; (**a**) digital elevation model, (**b**) flow direction, (**c**) streams, (**d**) centroid and longest flow path, (**e**) land use land cover and (**f**) curve number map

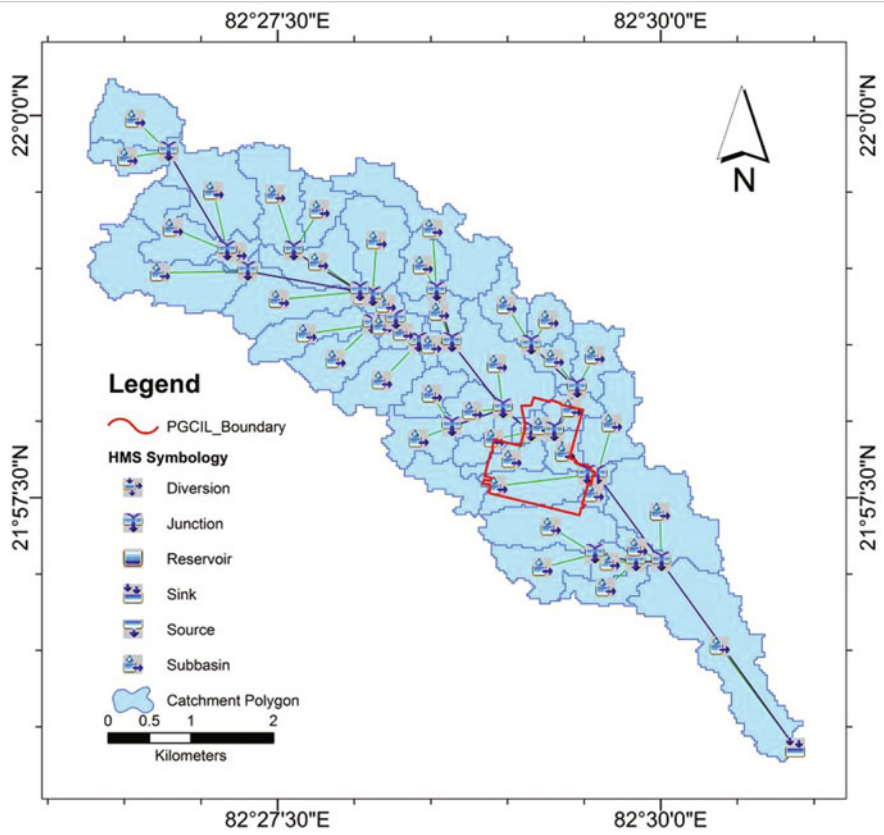

Fig. 24.5 Taga catchment HEC-HMS Basin Model

24.5 Hydraulic Model Setting

The Hydraulic model was developed in HEC-RAS 4.1.0 version software. Surveyed data has been used to produce Triangulated Irregular Network (TIN) using 3-D Analyst tool in Arc GIS, Geometry of hydraulic model (i.e. Stream, banks of stream, flow path of flood plain and cross-sections across flow path) that represent site are developed using HEC-Geo-RAS extension in Arc MAP. This geometric data was exported to HEC-RAS. Results of HEC-HMS were fed as flow data. The model was run and results obtained were water surface level along the flood plain. Figure 24.7 shows a typical model setup in HEC-Geo-RAS, and input parameters are assigned in HEC-RAS model. The RAS model is fed in with geometric model generated with HEC Geo RAS, Peak discharge obtain from HEC-HMS model for 100-year return period rainfall is taken input for steady flow (Table 24.2).

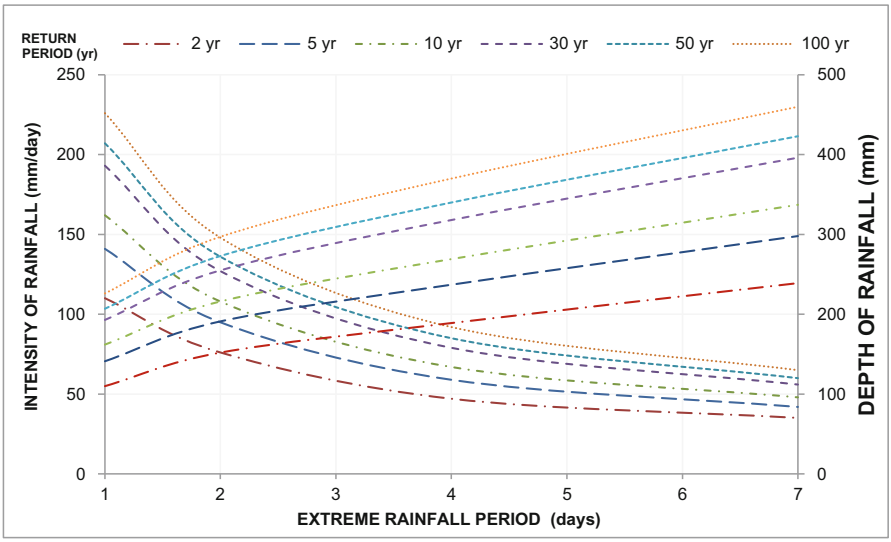

Fig. 24.6 Intensity-duration-frequency curve and depth-duration-frequency curves

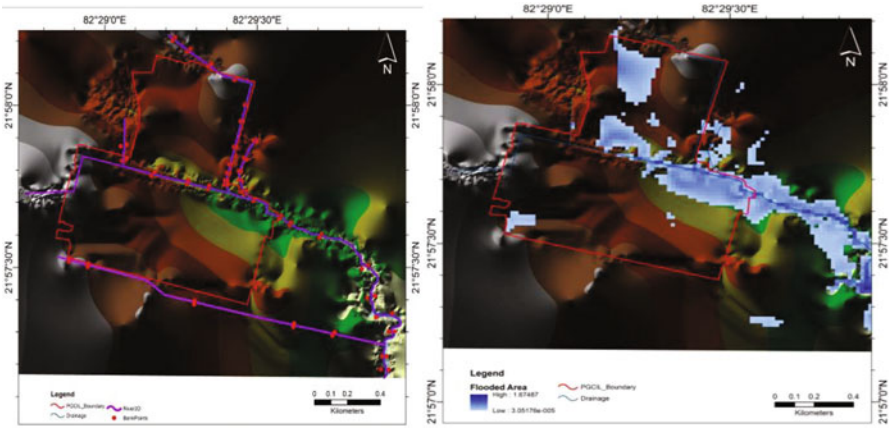

Fig. 24.7 PGCIL Boundary and Taga village HEC-RAS Model and Modelled flood inundated area for existing condition

Table 24.2 Peak design discharge input for RAS model

SN	Stream	Q (m^3/s)	Design Q (m^3/s)
1	Top	3.3	5
2	Main	26.4	33
3	West	1.8	5
4	Downstream	32.9	45
5	East	1.2	3

24.6 Modification of Stream Cross-Section

To reduce flood inundation in Champa pooling station site, stream cross-sections are modified by provision of rectangular and trapezoidal channel of different dimension in each stream. Cross-section dimensions of rectangular channel for different streams are computed using guidance provided in 'Open channel Hydraulics'. The formulas used in this computation are given below.

$$\text{Depth of rectangular channel}, y = \left(\frac{n \times Q \times 2^{\frac{2}{3}}}{1.49 \times 2 \times \sqrt{S}}\right)^{\frac{3}{8}} \tag{24.1}$$

$$\text{Free board FD} = \sqrt{1.5 \times y} \tag{24.2}$$

where, Q = Design discharge in stream (m^3/s), S = Channel bed slope, and n = Manning's roughness coefficient. Using Manning formula, discharges obtain by HEC-HMS model and velocity the cross-section of drainage is computed. In geometric data of HEC-RAS this cross-section of channel is fed and model is simulated till no flood condition obtained in model.

24.7 Results and Discussions

The Taga catchment is located in a semiarid region where the streams are non-perennial. Water will flow in streams only in monsoon season. Historical satellite images show that pooling station is located at confluence point of three streams. Alteration in natural drainage pattern and provision of improper artificial drainage system led to flooding in Taga village. Rainfall-runoff modelling of ungauged basin is done using HEC-HMS. The peak discharge obtained from HEC-HMS is input for HEC-RAS model and flood inundation map have generated. Results simulated from H&H model helped for proposing various flood protection measures in and around the station in Taga village. Result simulated after modification of streams as per proposed protection measures showed that there is no flooding in and around the station in Taga village as shown in Fig. 24.9b. Various alternative solutions are planned (Fig. 24.8) and results are simulated for no flood condition. Simulation result shows the inundation pattern which was validated during field survey. Inundation pattern is visualized in HEC-RAS and ArcMAP using RAS Mapper in Fig. 24.9.

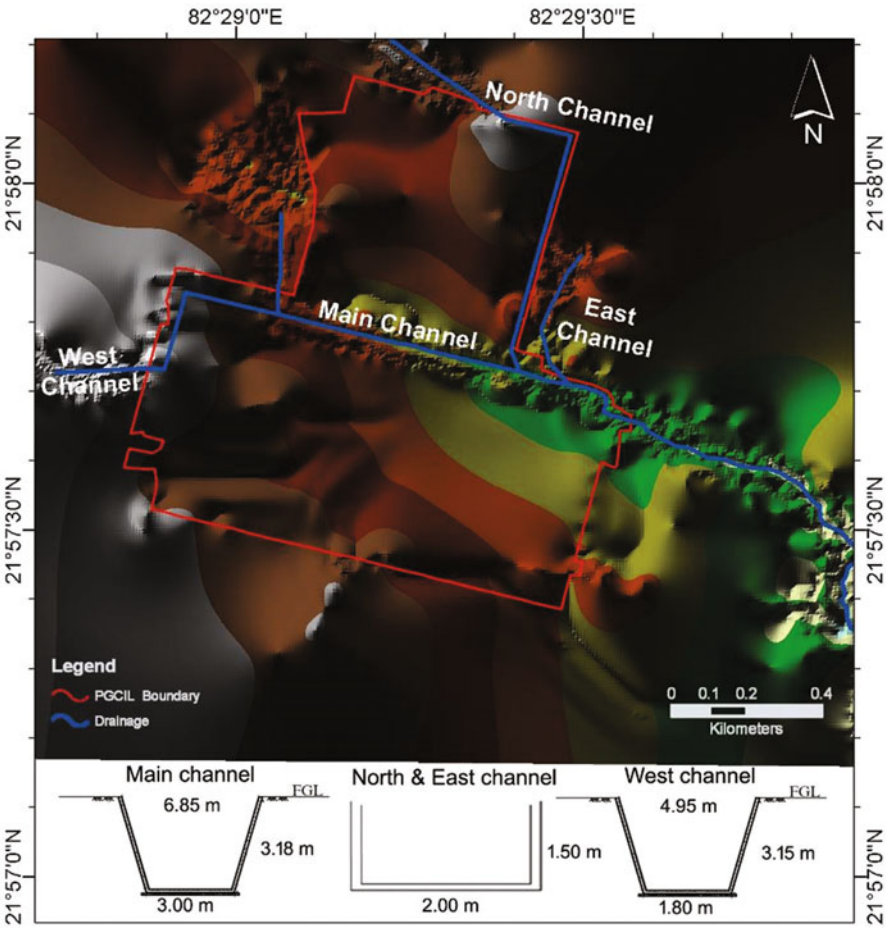

Fig. 24.8 Flood mitigation plan as per site suitability

24.7.1 Model Simulation Output

HEC-HMS model is fed in with basin model generated with HEC-Geo-HMS, storm frequency data with 100-year return period rainfall depth and control specification with simulation for 9 days with 12 hours' time step up. The peak runoff is obtained at sixth day 12.00 h for all stream for input depth of 100-year return period. Peak runoff for each stream is tabulated in Table 24.3.

To compensate ignorance of heterogeneity and irregularities of real system in model, factor of safety of 1.25 is adopted for computing design flood. The tabulations of discharges, and flow inputs for steady flow analysis at different cross-sections of streams are in Table 24.2. Then the modified design discharge has been used to re-simulate HEC-RAS model after channel modification. The flood

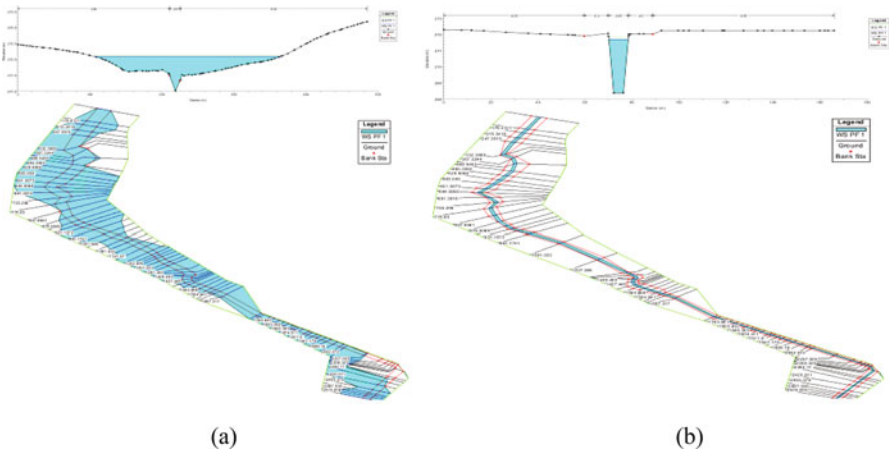

Fig. 24.9 Flood inundation of main stream and channel cross-section in HEC-RAS simulation for (**a**) existing condition and (**b**) after modification in channel section

Table 24.3 Modelled discharge of different channels during flood event simulated in HEC-HMS

Time	East u/s (m^3/s)	East d/s (m^3/s)	Main u/s (m^3/s)	Main d/s (m^3/s)	Top u/s and d/s (m^3/s)
01-08-2014 00:00	0	0	0	0	0
01-08-2014 12:00	0.1	0.8	1.1	0.1	0.1
02-08-2014 00:00	0.1	2.2	3.2	0.2	0.3
02-08-2014 12:00	0.2	3.5	5.2	0.2	0.4
03-08-2014 00:00	0.2	4.4	6.7	0.3	0.5
03-08-2014 12:00	0.2	5.1	7.8	0.3	0.5
04-08-2014 00:00	0.3	5.7	8.7	0.3	0.6
04-08-2014 12:00	0.3	6.2	9.6	0.4	0.6
05-08-2014 00:00	0.3	7.2	11	0.4	0.8
05-08-2014 12:00	0.5	10.1	15	0.7	1.1
06-08-2014 00:00	1.1	19.9	29.6	1.4	2.3
06-08-2014 12:00	1.2	24.5	37.3	1.5	2.6
07-08-2014 00:00	0.8	19.4	30.9	1	1.8
07-08-2014 12:00	0.5	13	21.4	0.4	1.1

inundation map obtain is shown in Fig. 24.9a, b. The inundation map is compared with the photographs taken during field visit (Fig. 24.3) and it is confirmed that the inundation pattern generated by model is similar to that of real site condition.

To reduce flood inundation in Champa pooling station site, stream cross-sections are modified by provision of rectangular and trapezoidal channel of different dimension in each stream Result simulated after modification of stream as per proposed protection measures showed that there is no flooding in and around the station in Taga village as shown in Fig. 24.8. Implementation of flood mitigation recommendations for upstream and downstream has been suggested to complete before commencement of monsoon. The recommended measure and designed channel have been constructed by PGCIL authority and since then Champa pooling station has been running successfully without affected by flood events.

24.8 Conclusion

This chapter comprises of possible causes and feasible remedial measures for flood at Champa pooling station and its surrounding area. In general, the following conclusion can be made based on this study: During selection of site for any project the hydrological factor should be considered including detailed topographic survey otherwise it may lead to natural disaster like flooding. HEC-GeoRAS and HEC-GeoHMS can be conveniently utilized for preparation of input geometric data for hydraulic model and hydrological model, respectively and also used for visualization of the hydraulic model results. HEC-HMS model can be used for generation of peak discharge for ungauged basin, when distributed or semi distributed modelling approach have been applied. The generated river flood inundation map of study area will help to validate the result of HEC- HMS model during the corresponding simulation period. Flood inundation maps are helpful in designing flood protection work measures. HEC-RAS model is efficient tool for design and simulate the flood control measures to analyse the difference of existing and modified flood protection schemes before its application in real field. H&H model is integrated tool for floodplain mapping and analyses, these tools provide more efficient, safe and standardized results to saves time and resources. For specific at PGCIL site, it has been seen that after the application of suggested flood protection measure, the pooling station is running without any effect of flooding since last 2 years. The design drains are enough efficient for draining the storm quickly from the pooling site at adverse rainfall condition.

Acknowledgement The authors would like to thank Power Grid Corporate India Limited (PGCIL) for funding and providing all the possible facilities during field survey at the time of data collection. The authors would like to thank Chhattisgarh water resources department for authorizing the use of data essentially for study and research purposes.

References

Abera, Z. (2011). *Flood mapping and modeling on fogera flood plain: A case study of Ribb River*. Addis Ababa: Addis Ababa Institute of Technology.

Ackerman, C. T., Evans, T. A., & Brunner, G. W. (2000). *HEC-GeoRAS: Linking GIS to hydraulic analysis using ARC/INFO and HEC-RAS. Hydrologic and hydraulic modeling support with geographic information systems*. New York, NY: ESRI Press.

Ahmad, I., Verma, V., & Verma, M. K. (2015). Application of curve number method for estimation of runoff potential in GIS environment. In *2nd International Conference on Geological and Civil Engineering, IPCBEE*. Singapore: IACSIT Press.

Alaghmand, S., et al. (2010). GIS-based river flood hazard mapping in urban area (a case study in Kayu Ara River basin, Malaysia). *International Journal of Engineering and Technology, 2*(6), 488–500.

Andrysiak, P. B., & Maidment, D. R. (2000). *Visual floodplain modeling with geographical information systems (GIS), CRWR online report 00-4*. Austin, TX: Center for Research in Water Resources: Bureau of Engineering Research, The University of Texas at Austin.

Bara, M., et al. (2009). Estimation of IDF curves of extreme rainfall by simple scaling in Slovakia. *Contributions to Geophysics and Geodesy, 39*(3), 187–206.

Bewsher, D., Grech, P., & Yeo, S. (2013). Hawkesbury's flood risk management plan: 15 years in the making. *Proceedings of the Floodplain Management Association National Conference*.

Brunner, G. W. (1995). *HEC-RAS river analysis system. hydraulic user's manual. Version 1.0*. Davis, CA: Hydrologic Engineering Center.

Chow, V. T. (1964). *Handbook of applied hydrology*. New York, NY: MacGraw Hill.

Dadhwal, V., Aggarwal, S., & Mishra, N. (2010). *Hydrological simulation of Mahanadi river basin and impact of land use/land cover change on surface runoff using a macro scale hydrological model*. Dehradun: IIRS.

Doan, J. (2000). *Geospatial hydrologic modeling extension HEC-GeoHMS-user's manual-version 1.0*. Davis, CA: US Army Corps of Engineers Hydrologic Engineering Center.

Feldman, A. (2000). *HEC-HMS technical reference manual*. Davis, CA: CPD-74B US Army Corps of Engineers.

Gül, G. O., Harmancıoğlu, N., & Gül, A. (2009). A combined hydrologic and hydraulic modeling approach for testing efficiency of structural flood control measures. *Natural Hazards, 54*(2), 245–260.

Hailegeorgis, T. T., & Alfredsen, K. (2017). Analyses of extreme precipitation and runoff events including uncertainties and reliability in design and management of urban water infrastructure. *Journal of Hydrology, 544*, 290–305.

Hashemyan, F., Khaleghi, M. R., & Kamyar, M. (2015). Combination of HEC-HMS and HEC-RAS models in GIS in order to simulate flood (Case study: Khoshke Rudan river in Fars province, Iran). *Research Journal of Recent Sciences, 4*(8), 122–127.

Heimhuber, V. (2013). *A case study in applying GIS (ArcMap) in combination with hydrologic (HEC-HMS) and hydraulic (HEC-RAS) modeling to estimate the flood Hazard of Onaville – Canaan – Haiti* (p. 129). Munchen: Technische Universitat Munchen.

Heimhuber, V., Hannemann, J.-C., & Rieger, W. (2015). Flood risk management in remote and impoverished areas—A case study of Onaville, Haiti. *Water, 7*(7), 3832–3860.

Jha, A. K., Bloch, R., & Lamond, J. (2012). *Cities and flooding: A guide to integrated urban flood risk management for the 21st century*. Washington, DC: World Bank Publications.

Leese, M. N. (1973). Use of censored data in the estimation of Gumbel distribution parameters for annual maximum flood series. *Water Resources Research, 9*(6), 1534–1542.

Marfai, M. A. (2003). *GIS modelling of river and tidal flood hazards in a waterfront city: Case study, Semarang City, Central Java, Indonesia* (pp. 1–123). Enschede: ITC.

Meena, R. S. (2012). *Simulation of runoff and flood inundation in Kosi River basin using hydrological models, ANN, remote sensing and GIS* (p. 101). Rourkela: Department of Civil Engineering, National Institute of Technology.

Mishra, S. K., & Singh, V. P. (2013). *Soil conservation service curve number (SCS-CN) methodology* (Vol. 42). Berlin: Springer Science & Business Media.

Pattison, I., & Lane, S. N. (2012). The link between land-use management and fluvial flood risk: A chaotic conception? *Progress in Physical Geography, 36*(1), 72–92.

Pedzisai, E. (2010). *Rainfall-runoff modelling for flashfloods in Cuong Thinh catchment, Yen Bai Province, Vietnam*. Enschede: International Institute for Geo-Information Science and Earth Observation.

Pistocchi, A., & Mazzoli, P. (2002). Use of HEC-RAS and HEC-HMS models with ArcView for hydrologic risk management. In *IEMS 2002-Proceedings of the International Environmental Modelling and Software Society Conference, Lugano*. Amsterdam: Elsevier.

Quan, N. H. (2006). *Rainfall-runoff modeling in the ungauged can Le catchment, Saigon river basin*. Enschede: International Institute for Geo-Information Science and Earth Observation.

Samarasinghea, S., et al. (2010). Application of remote sensing and GIS for flood risk analysis: A case study at Kalu-Ganga River, Sri Lanka. *International Archives of the Photogrammetry, Remote Sensing and Spatial Information Science, 38*(Pt 8), 110–115.

Sayers, P., et al. (2013). *Flood risk management: A strategic approach*. Mandaluyong: Asian Development Bank, GIWP, UNESCO and WWF-UK.

Scharffenberg, W. A., & Fleming, M. J. (2006). *Hydrologic modeling system HEC-HMS: User's manual*. Davis, CA: US Army Corps of Engineers, Hydrologic Engineering Center.

Sengupta, R. (2016). State of India's urban water bodies. In S. Narain (Ed.), *Why urban India floods Indian cities grow at the cost of their wetlands*. New Delhi: DownToEarth.

Sinha, M. K., et al. (2019a). *Impact of urbanization on surface runoff characteristics at catchment scale*. Singapore: Springer.

Sinha, M. K., et al. (2019b). *Semi-distributed modelling of stormwater drains using integrated hydrodynamic EPA-SWM model*. Singapore: Springer.

Todorovic, P., & Zelenhasic, E. A. (1970). A stochastic model for flood analysis. *Water Resources Research, 6*(6), 1641–1648.

Wagener, T., Wheater, H. S., & Gupta, H. V. (2004). *Rainfall-runoff modelling in gauged and ungauged catchments*. Singapore: World Scientific.

Chapter 25
Modelling and Assessment of Flood Discharge Based on Intensity-Duration-Frequency Curves in Kuttanad District, Kerala, India

J. Brema and Minnu K. Benny

Contents

25.1 Introduction 485
25.2 Study Area 487
25.3 Methodology 487
25.4 Flood Estimation (Hydrologic Modelling) 493
25.5 Results and Discussions 498
25.6 Flood Modelling 500
25.7 Comparison of Rainfall with Discharge 510
25.8 Conclusions 510
References 511

25.1 Introduction

Floods cause much loss of life and property, disruption of communication, damage to crops, famine, epidemic diseases and other indirect losses. Flood can be termed as the flow in the rivers and channels which cannot be contained within natural or artificial river banks. Floods are one of the major reasons for damage in many parts of the world due to natural disaster, which can be determined with help of causes in the environment. In order to understand the causes, it is very important to know the relationship between the flooded region and the factors which causes flood (Onus 2005). The floods in the rivers are due to sudden and high intensity rain or melting of

J. Brema (✉) · M. K. Benny
Karunya Institute of Technology and Sciences, Coimbatore, India
e-mail: bjayanarayanan@gmail.com

C. B. Pande, K. N. Moharir (eds.), *Groundwater Resources Development and Planning in the Semi-Arid Region*, https://doi.org/10.1007/978-3-030-68124-1_25

snow in the upper reaches of the basin. The reasons for floods may be due to mismanagement of under drainage systems and increased groundwater table level due to prolonged storm conditions. The flood detection services are active in developed countries, but the consequences faced in developing countries are larger. This study has been carried out to understand the characteristics of flood inundation in the Kuttanad region of Kerala. The Kuttanad region is fed by three rivers and it is a lowlying area, where paddy cultivation is carried out extensively. With this study, the area of submergence can be determined for a given discharge. HEC-RAS and HEC-GeoRAS have been widely used to develop flood inundation map in many research works (Hazarika 2007, Knebl et al. 2005, Hicks and Peacock 2005, Abera 2011, Khan 2009). The extent of flood and inundation depth has been determined using satellite imageries and GIS (Bhuiyan 2014; Islam et al. 2010; Hasan 2006). The results of the study can be used by planners to develop flood warning systems in order to reduce the destruction to infrastructure, environment and human beings. Flood modelling of Mangalam river was studied using GIS AND HEC-RAS (Sunil kumar Morais et al. 2018). The Mangalam river basin has experienced intense flash floods during heavy rainfall. The various changes preferably responsible for the floods were identified as release of water from Mangalam dam during monsoon season, encroachment of banks of river, improper planning and construction of hydraulic structures, change in land use. The flood inundated area was modelled in Hydrologic Engineering Centre's River Analysis System (HEC-RAS) software and inundation maps were developed in GIS. A study was conducted on flood modelling for computation of submergence area using ArcGIS, HEC-GEORAS & HEC-RAS. (Chudasama et al. 2018; Sudha 2012; Galoie et al. 2014; Edsel et al. 2011). This work presents a one-dimensional hydrodynamic modelling of a river network and floodplains. The marked seasonal flow regime and relative smooth hydrographs of River were quite well reproduced by the hydraulic model. The rainfall Intensity-Duration-Frequency (IDF) relationship is one of the most commonly used tools in water resources engineering, either for planning, designing and operating of water resource projects, or for various engineering projects against floods. The establishment of such relationships was done as early as in 1932. A novel regional framework based on quantile regression (QR) is used to estimate rainfall IDF curves at ungauged locations. Unlike standard regional approaches, such as index-storm and at-site ordinary least-squares regression, which are dependent on parametric distributional assumptions, the nonparametric QR approach directly estimates rainfall quantiles as a function of physiographic characteristics. A hydrologic cycle in a riverbasin is subjected to a complicated process that is affected by climate, topography, soil, vegetative cover, geomorphology, geology and human activities. Studies show that changes in streamflow is not only due to climate change, but also due to the landuse/landcover change induced by human activities. These changes considerably affect the stream flow in a river basin (Liang et al. 2013; Azeb et al. 2018). The changes in streamflow or runoff in a river basin can be assessed by carrying out a rainfall-runoff simulation (Naef et al. 2002; Joorabian et al. 2017; Iosub and Lesenciuc 2012; Iosub et al. 2014). The hydrological effects due to specific land

use changes in a river basin can be examined by including various land use scenarios including expansion of built-up land and decrease in vegetative cover (Pikounis et al. 2003). Kerala state has an average annual precipitation of about 3000 mm. The rainfall in the state is mainly due to the Southwest and Northeast monsoons. About 90% of the rainfall occurs during six monsoon months. The year 1920 witnessed unprecedented and very heavy floods in almost all rivers of Kerala. The year 1961 also witnessed heavy floods and rise in the water levels of reservoirs. Usually in the State, heavy precipitation is concentrated over a period of 7–10 days during the monsoon when the rivers rise above their established banks and inundate the low lying areas. But in 1961, floods were unusually heavy not only in duration, but also in the intensity of precipitation. The frequency of flooding has increased over the past few decades causing havoc to life and property.

25.2 Study Area

The study area, Kuttanad is the region covering parts of Alappuzha and Kottayam districts of Kerala, which are called as upper and lower Kuttanad. This is a well-known region for paddy cultivation, at a lowest altitude level (4–10 ft below sea level). Kuttanad is the major rice producer in the state. Kuttanad is known as the rice bowl of Kerala because of the vast extent of paddy cultivation. Kuttanad is basically divided into three regions namely Upper, Lower and North Kuttanad. This land is continuously affected by floods mostly during most southwest monsoon season. Major river basins in the study area include Achankovil, Pamba and Manimala as shown in Fig. 25.1 Achankovil originates in the southern tip of the peninsula due to the confluence of three tributaries namely Rishimala, Pasukidamettu, and Ramakkalteri. The Pamba river is the third longest river in Kerala. It has a length of 176 km, with an average elevation of 1650 m and basin area of 2235 km^2. The River Manimala has a length of 92 km and is a tributary of Pamba river.

25.3 Methodology

25.3.1 Intensity-Duration-Frequency Curve (IDF) Curve Analysis

The rainfall Intensity-Duration-Frequency (IDF) relationship is commonly required for planning and designing of various water resources projects. The IDF relationship is a mathematical relationship between the rainfall intensity, duration and return period.

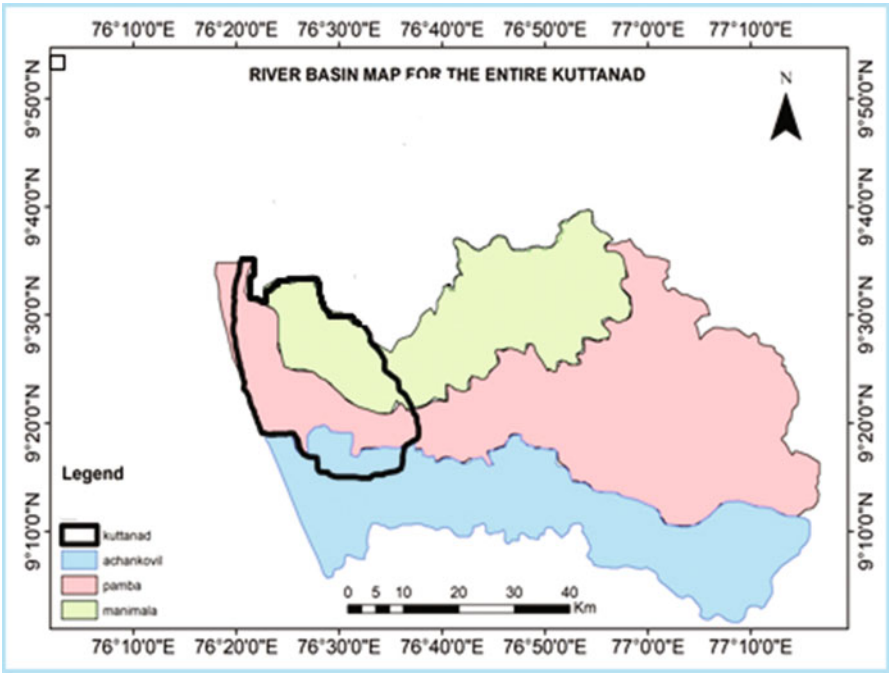

Fig. 25.1 Study area

$$K_T = -\frac{\sqrt{6}}{\pi}\left(0.5772 + \ln\left(\ln\left(\frac{T}{T-1}\right)\right)\right) \tag{25.1}$$

Where, K_T is the frequency factor and T is the return period. From the hourly rainfall measurements of Alappuzha station, the cumulative values for the durations 1, 2, 3, 6, 12 and 20 hours were obtained. The intensity was calculated by dividing the rainfall depths with the durations. Where, x is the intensity in mm/h, mean (μ) and standard deviation (S_d) of each of the durations are calculated. Once the frequency factor was calculated, the rainfall intensity was calculated using the Gumbel's distribution equation:

$$x = \mu + K_T S_d \tag{25.2}$$

For any given storm, the intensity increases with the return period. The shortest duration event shows the highest intensity. Sherman (1931) devised a method by which the intensity can be calculated without the rainfall data. An empirical equation was derived based on return period and duration.

$$i = \frac{k \times T^a}{(t+b)^n} \tag{25.3}$$

Where k, a, b and n are constants which depend on the geographical location, i is the rainfall intensity in cm/h. and T is the return period. Ram Babu et al. (1979) found the value of these constants for 42 stations. The values obtained were 6.672, 0.1536, 0.5 and 0.8158 for k, a, b and n respectively. Based on these data, the intensity-duration-frequency values for the various return periods were obtained.

25.3.2 Landuse Changes Studies

Landuse change is a process by which human activities transform the natural landscape, referring to how land has been used, usually emphasizing the functional role of land for economic activities. Landuse changes are often nonlinear and might trigger feedbacks to the system, stress living conditions, and threaten people with vulnerability. Therefore, not only do land use change categories affect the environmental conditions in a drastic manner especially runoff. In this study, attempts have been made to assess the changes in landuse and its effect on runoff. One of the detailed and useful ways to develop land use classification maps is to use geospatial techniques such as remote sensing and Geographic Information System (GIS) (Pande 2014, Pande and Moharir 2014; Pande et al. 2017; Patode et al. 2017; Reddy et al. 2017; Pande et al. 2018; Pande 2020a, b, c, d). It vastly improves the selection of areas designated as agricultural, industrial and/or urban sector of a region. Quantification of spatial and temporal dynamics of land use/cover changes was accomplished by using five satellite images, and classifying them using supervised classification algorithm technique. Landsat 8 data corresponding to the study area for the years 2014–2018 were obtained from USGS earth explorer. The following classes such as paddy field, vegetation, water body and built-up were considered for the supervised classification. Paddy field refers to rice cultivation, built-up includes the roads, buildings, etc., water body includes the lakes, rivers, streams, ponds, etc. and vegetation is used for other plants like banana, jack fruit, etc. as shown in Table 25.1. The classification of Landsat imageries has been carried out using maximum likelihood supervised classification. From these information, the area of each class has been calculated for different years and the percentage of each

Table 25.1 Landuse categories followed in the study

Sl. no	Categories	Description
1	Paddy field	Rice cultivation
2	Vegetation	All other crops and plants like coconut, banana, etc.
3	Water body	Rivers, streams, lakes, ponds, wells, etc.
4	Built-up	Residential, commercial, industrial, transportation, roads, mixed urban

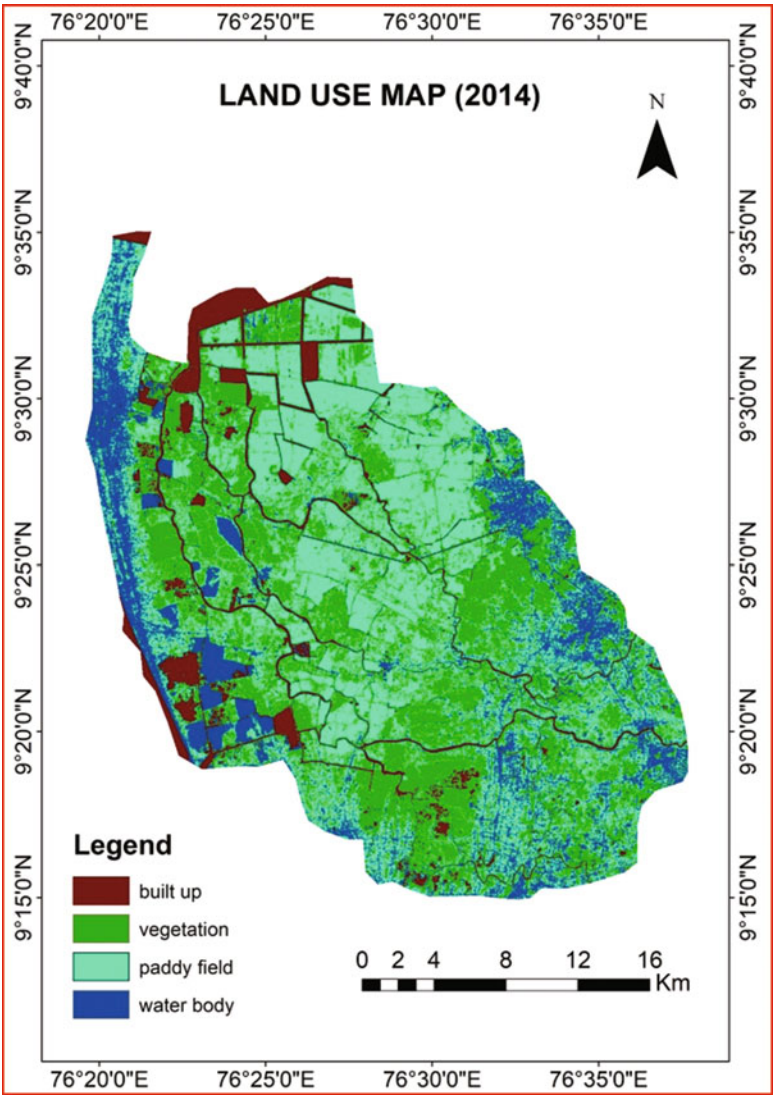

Fig. 25.2 Land use map of study area corresponding to 2014

class was calculated. These data were used to find the changes in values which may either be an increment or a decrement.

The Fig. 25.2, 25.3, 25.4, 25.5, and 25.6 show the variations in the landuse categories during the period 2014–2018. Significant changes have been observed in the land use categories during the study period. With the increase in built-up area, the paddy fields have decreased along with increase in vegetative area. Considerable increase in built-up area in the northeastern portion of the study area particularly in

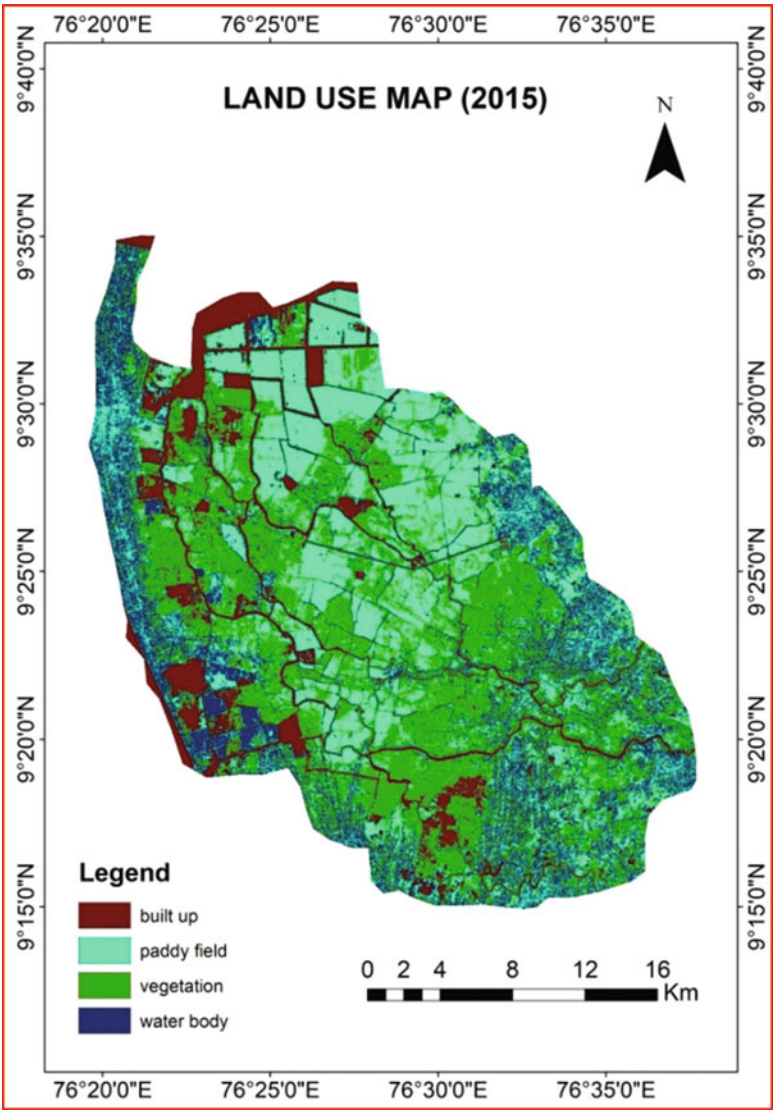

Fig. 25.3 Land use map of study area corresponding to 2015

the Vaikum taluk, western parts of Kottayam taluk and western parts of Changanacherry taluk in Kottayam district have been observed.

To analyze the impact of land use change, the percentage of variation in built-up land and paddy field were estimated as shown in Tables 25.2 and 25.3 and Fig. 25.7. It was observed that there was an increase in built-up land by 51.21% and a decrease in paddy field by 15.83% of the total area. This has increased the impermeability in

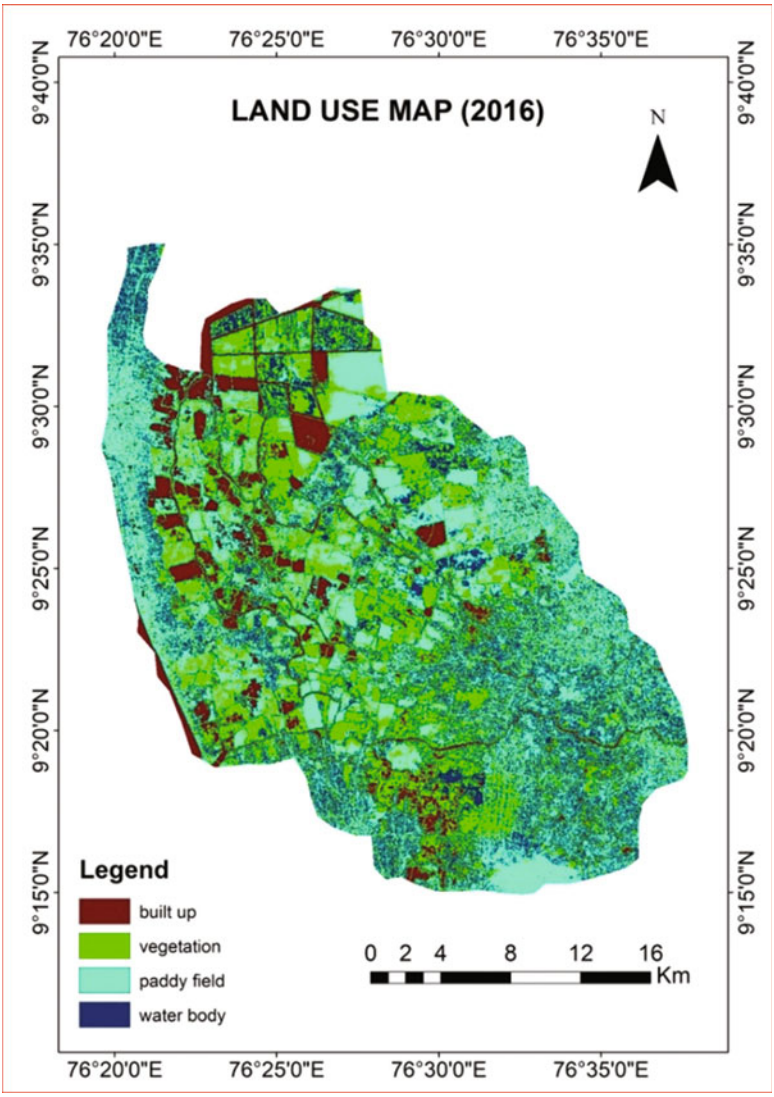

Fig. 25.4 Land use map of study area corresponding to 2016

the region and added to this since the region lies below mean sea level, the flood magnitude has increased considerably in the region.

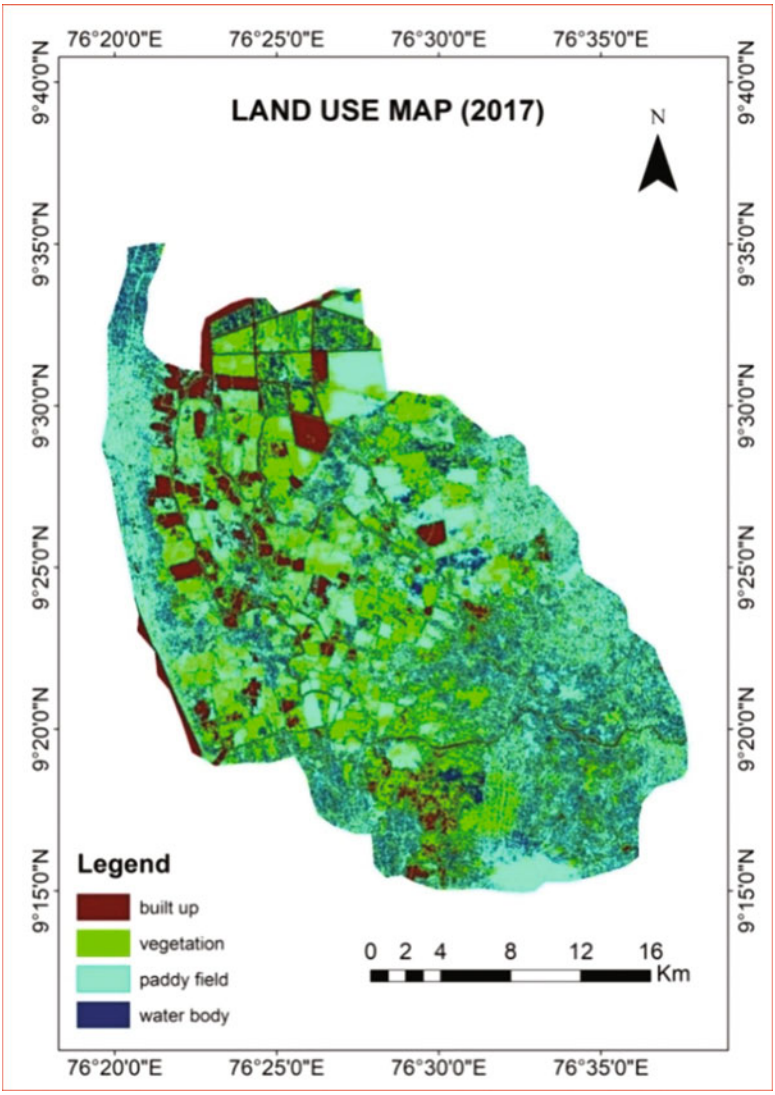

Fig. 25.5 Land use map of study area corresponding to 2017

25.4 Flood Estimation (Hydrologic Modelling)

The procedure followed for hydrologic modelling is as shown in Fig. 25.8. The results from IDF curve analysis along with land use change studies have been used in flood modelling. The curve number grid was generated utilizing the land use and hydrologic soil maps. The digital elevation model obtained from USGS Earth Explorer was used for the basin delineation using arc hydro tools. Basin

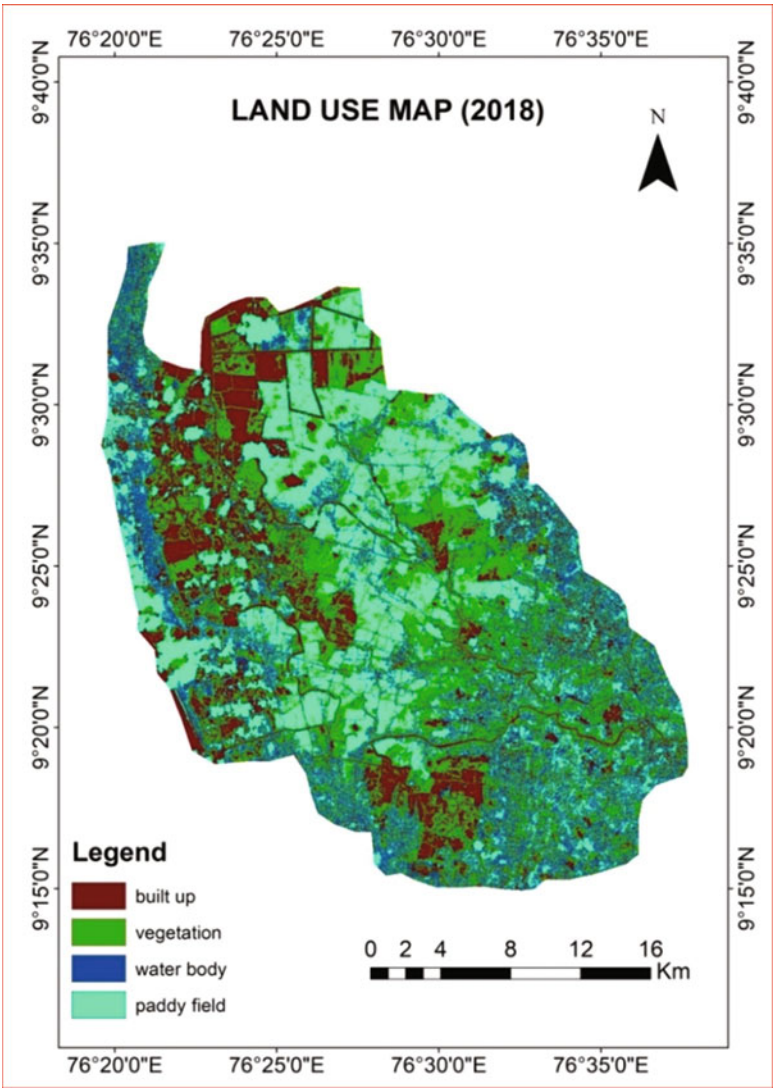

Fig. 25.6 Land use map of study area corresponding to 2018

Table 25.2 Land use changes for the period 2014–2018

Landuse category	2014 (km^2)	2015 (km^2)	2016 (km^2)	2017 (km^2)	2018 (km^2)
Built-up land	55.88	66.37	72.9	78.1	84.5
Paddy field	322.23	301.65	291.82	286.7	271.22
Water bodies	113.9	120.53	123.65	120.63	125.71
Vegetative cover	226.41	230.42	230.41	233.51	237.57

Table 25.3 Variation of land use from 2014 to 2018

Category	Changes in % from 2014 to 2018
Built-up land	+4.5
Paddy field	−7.5
Water bodies	+2.1
Vegetative cover	+1.12

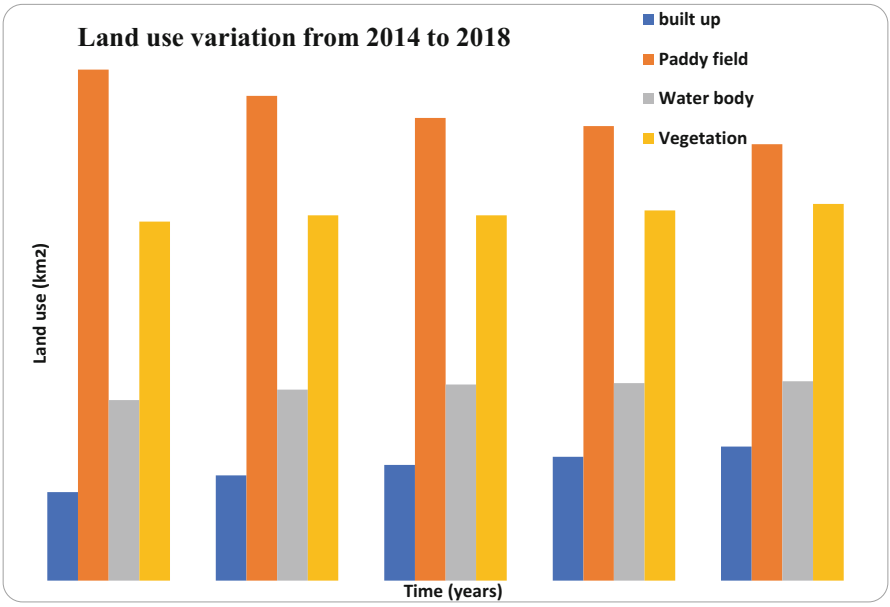

Fig. 25.7 Land use changes for the period 2014–2018

pre-processing was done for giving it as an input for HEC-HMS. The hourly rainfall data along with curve number grid were also given as input for HEC-HMS model. HEC-HMS model comprises of four components namely basin model, meteorological model, time series data and control specifications. After undergoing all these four processes, the calculated discharge was obtained. The observed discharge was obtained from central water commission, Ernakulam corresponding to 2, 8, 14 and 20 h. The calibration was carried out using the observed discharge values and the correlation coefficient was obtained. For flood estimation, hydrologic modelling followed by hydraulic modelling was carried out to estimate the discharge values. Hydrologic modelling requires data such as digital elevation model, daily rainfall, land use map, soil map and curve number grid.

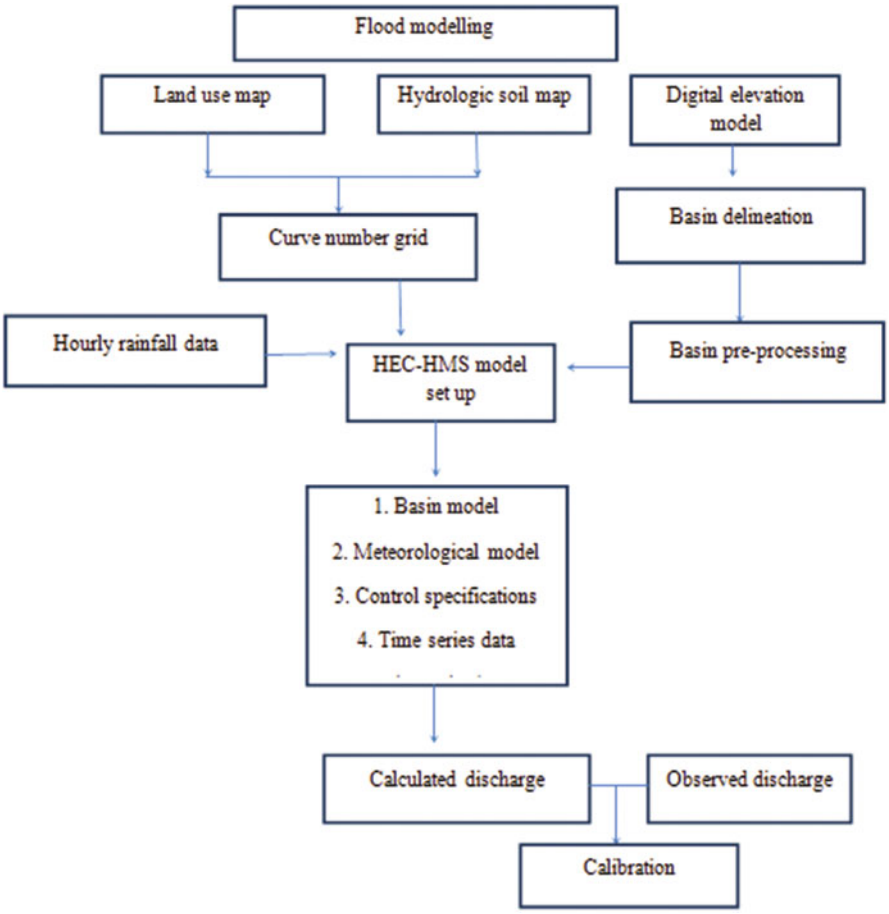

Fig. 25.8 Methodology for hydrologic modelling

25.4.1 Curve Number Grid Generation

The curve number is based on hydrologic soil group and land use types. The curve number is an efficient method for determining the approximate amount of direct runoff from a rainfall event. Soils are classified by the Natural Resource Conservation Service into four Hydrologic Soil Groups based on the soil's runoff potential. The four hydrologic soil groups are A, B, C and D. Where, soil A generally has the smallest runoff potential and soil D has the greatest. The curve number look up table which contains the curve number data corresponding to different soil groups and land use data obtained for the TR 55 model is given in Table 25.4. The final step is to generate the curve number grid using the soil-land use union polygon, the DEM of the study area and the Curve Number lookup table.

Table 25.4 Curve number lookup table

S. no	Description	Hydrologic soil groups			
		A	B	C	D
1	Water body	100	100	100	100
2	Vegetation	59	60	73	79
3	Paddy field	61	65	78	79
4	Built-up	67	70	80	85

Table 25.5 Time series data of rainfall from 14 to 20th August 2018

	Time (h)			
	2	8	14	20
Date	Rainfall (mm)			
14/08/2018	76	81	69	82
15/08/2018	142	159	170	175
16/08/2018	193	198	198	198
17/08/2018	190	185	181	181
18/08/2018	175	172	170	151
19/08/2018	142	136	136	130
20/08/2018	121	121	114	109

25.4.2 HEC-HMS Components

The four basic components of the HEC-HMS model are the basin model, meteorological model, control specifications and time series data. The basin model includes physical information about the basin. This includes ridgelines, location of river reaches, location of source and sinks. The meteorological model is used to specify the meteorological processes that take place in the basin such as precipitation. The meteorological model is used to model evapo-transpiration and snowmelt. In the present study, precipitation alone is modelled. Control specification is used to specify the start and end of the simulation. The control specification is dependent on the duration and time of the flood event which is being modelled. The time-series data manager can be used to specify the input data including rainfall and discharge data. The time series data for 2, 8, 14 and 20 h from 14 to 20 of August 2018, obtained from Indian meteorological department is given in Table 25.5.

Table 25.6 Values of frequency factors for different return periods

	Intensity values (mm/h) for return period of				
Duration (h)	2 Years	5 Years	10 Years	50 Years	100 Years
K_T	−0.16	0.71	1.30	2.59	3.13

Table 25.7 Intensity values using Gumbel's method

	Intensity values (mm/h) for return period of				
Duration (h)	2 Years	5 Years	10 Years	50 Years	100 Years
1	51.31	59.37	64.70	76.43	81.39
2	36.14	41.43	44.93	52.63	55.89
3	26.22	30.08	32.65	38.27	40.65
6	16.22	18.60	20.17	23.64	25.10
12	9.62	11.04	11.97	14.07	14.96
20	5.36	6.17	6.71	7.89	8.39

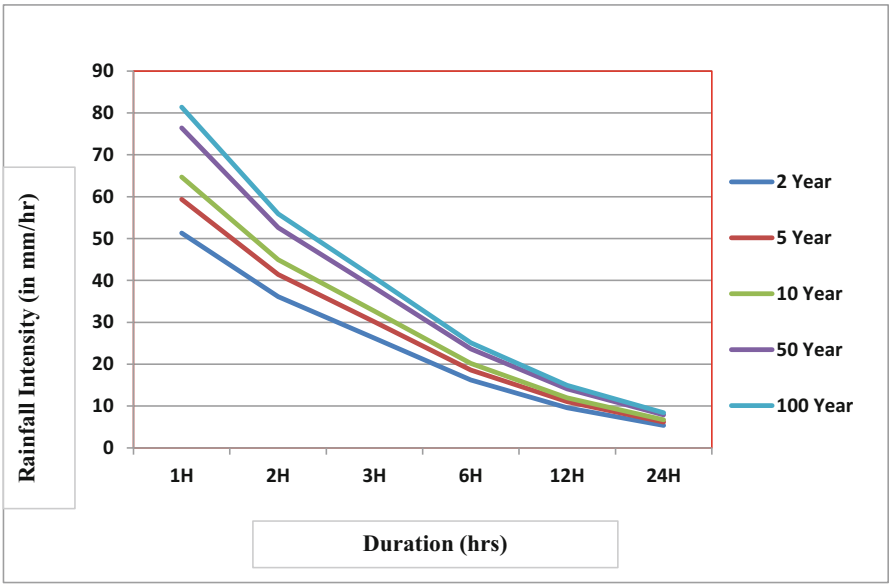

Fig. 25.9 Intensity-duration-frequency curve based on Gumbel's method calculation

25.5 Results and Discussions

25.5.1 Intensity-Duration-Frequency Curves

Intensity-Duration-Frequency (IDF) curves describe the relationship between rainfall intensity, rainfall duration, and return period. The frequency factors were

Table 25.8 Estimated rainfall intensity based on empirical equation

Duration (h)	Intensity values (mm/h) for return period of				
	2 Years	5 Years	10 Years	50 Years	100 Years
1	53.31	61.37	68.27	87.41	97.23
2	35.14	40.46	45.00	57.62	64.09
3	26.71	30.75	34.10	43.79	48.71
6	16.12	18.55	20.54	26.43	29.40
12	9.45	10.88	12.11	15.50	17.20
20	5.46	6.28	6.99	8.95	9.95

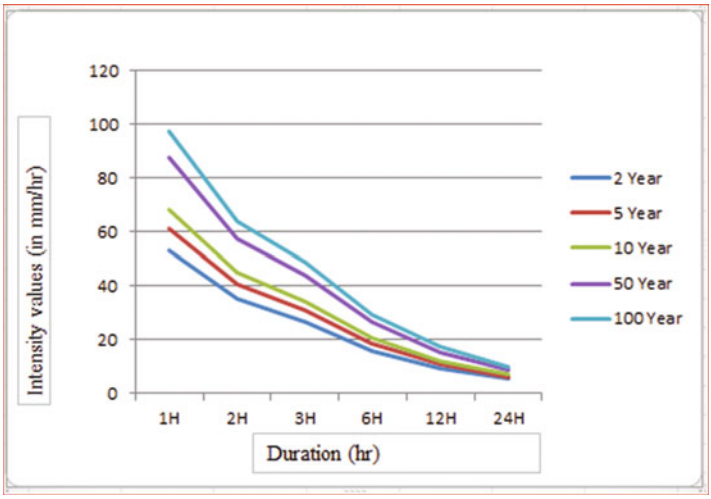

Fig. 25.10 Intensity-duration-frequency curve for the study area using empirical equation

estimated using Eq. 25.1 for various return periods and are given in Table 25.6. The rainfall intensity values based on Gumbel's method were estimated using Eq. 25.2 and are given in Table 25.7. Based on these values, the Intensity-Duration-Frequency (IDF) curves were generated as shown in Fig. 25.9.

The rainfall intensity values were estimated based on empirical equation method as given in Eq. 25.3 and it is displayed in Table 25.8. Based on these values, the Intensity-Duration-Frequency (IDF) curves were generated as shown in Fig. 25.10.

While comparing the results, it was observed that the values obtained from the Gumbel distribution and the empirical equations are more or less the same. It was also observed that for development of IDF curves, frequency analysis has to be performed for each set of annual rainfall data associated with each of the rainfall duration.

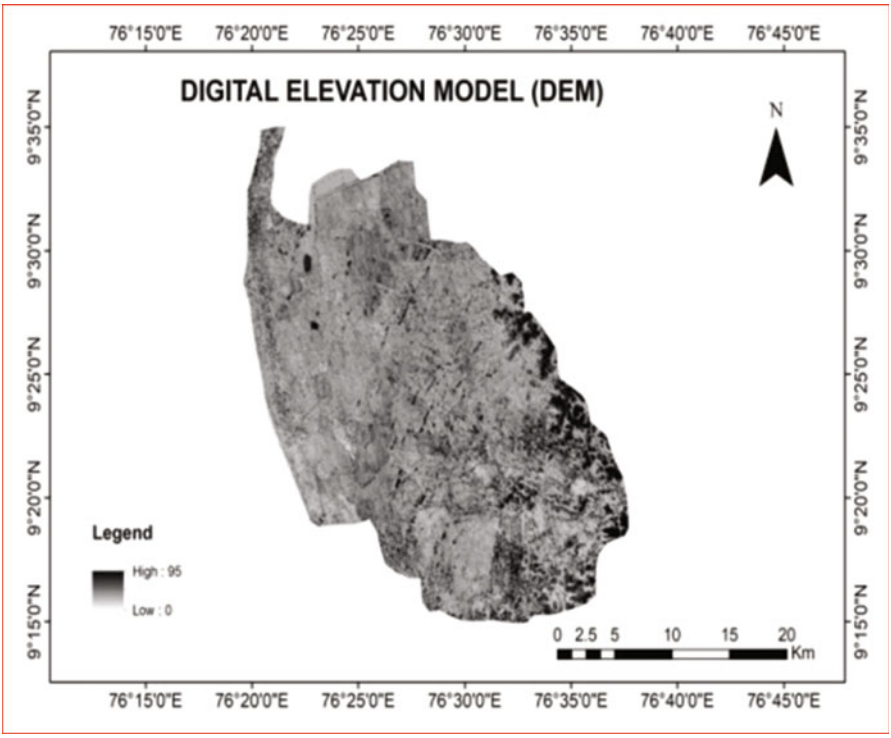

Fig. 25.11 Digital elevation model of the study area

25.6 Flood Modelling

25.6.1 Basin Delineation

The digital elevation model of the study area is shown in Fig. 25.11. The DEM used in this study is shuttle radar topographic mission (SRTM) with a resolution of 30 m. The elevation varies from a minimum elevation of 0 m to a maximum elevation of 95 m.

25.6.2 Basin Pre-processing

For giving the input in HEC-HMS model, a set of steps has to be followed which will result in the generation of catchment, drainage lines, etc. Figure 25.12 shows the flow direction map which is the basis for generation of the catchment map as shown in Fig. 25.13.

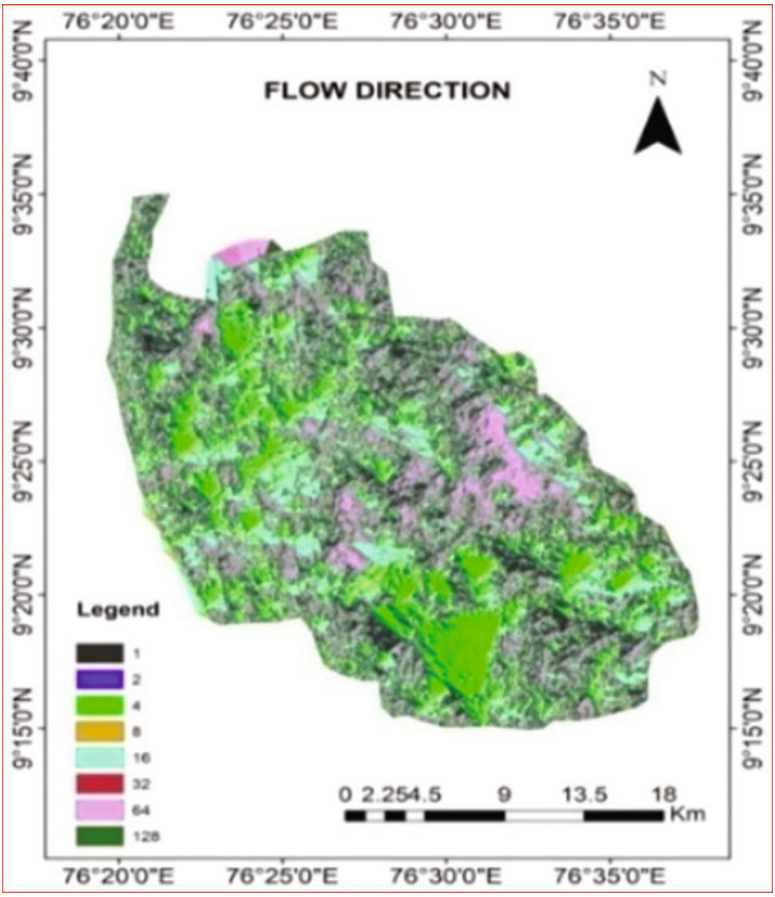

Fig. 25.12 Flow direction

The flow direction map is an integer raster whose values range from 1 to 255. If a cell is lower than its eight neighbours, that cell is given the value of its lowest neighbour and flow is defined towards this cell. Flow direction map shows the flow direction from each cell to its down slope neighbour, or neighbours.

By the catchment delineation process, the catchment grid was obtained. The catchment has 278 sub-catchments. The sub-catchment 8 has the lowest area and sub-catchment 216 has the highest area of about 87.35 $km^{2.}$

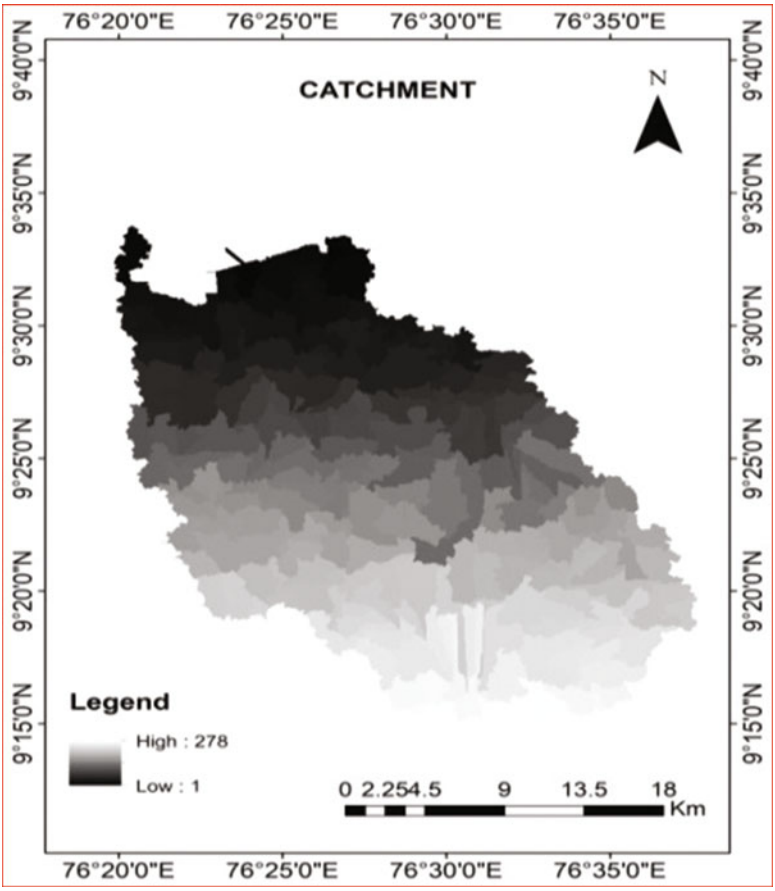

Fig. 25.13 Catchment grid

25.6.3 HEC-HMS Model Set Up

Once the hydrologic model is set, the model is imported to HEC-HMS. In the meteorological model, type of precipitation input is specified as specified hyetograph. The required time series data such as rainfall data and reservoir release data are given in the time series data manager. The control specifications are set accordingly by selecting a suitable computational time interval for running the model. The inputs for HEC-HMS model is curve number grid and that was obtained from land use and hydrologic soil maps.

The study area has three different classes of soils namely B, C and D based on the hydrologic soil group classification. Larger portion of the study are is covered by hydrologic soil D which consists of clay loam, silty clay loam, sandy clay, silty clay or clay as shown in Fig. 25.14. This soil has the highest runoff potential.

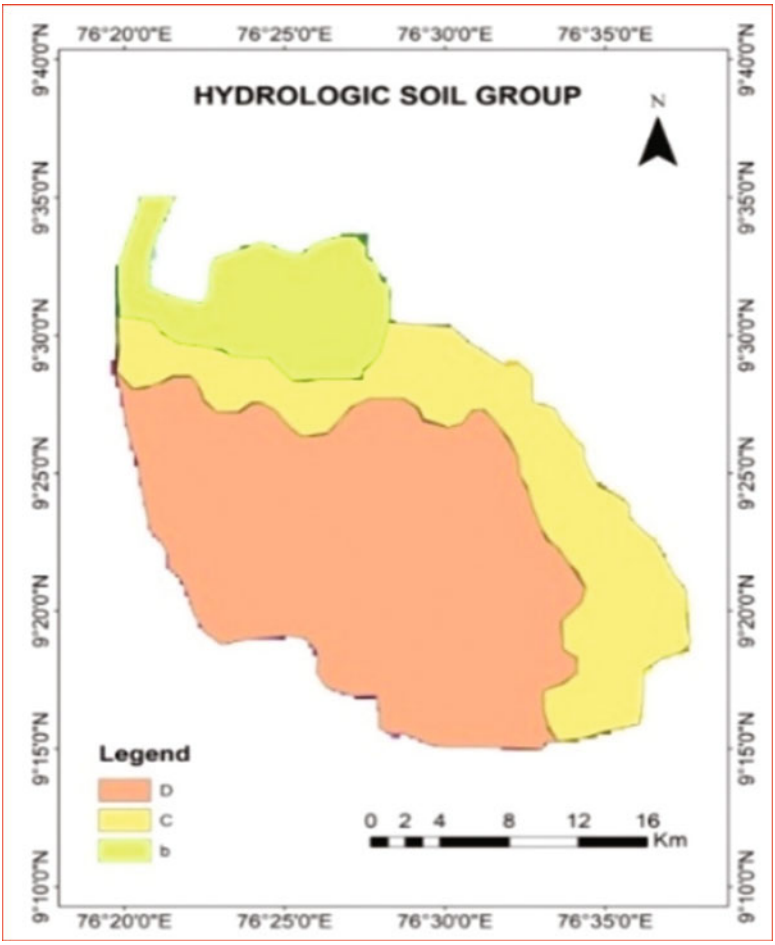

Fig. 25.14 Hydrologic soil map

The CN is 100 for water bodies and it decreases as the perviousness increases. The curve number 100 can be seen in most of the study area which is water body combined with any soil group and the lowest curve number is 85 which is a combination of built-up area with soil group D as shown in Fig. 25.15.

25.6.4 Estimated Discharges

The rainstorm of 16–18, July 1920 was caused by the Southwest monsoon that extended to the south of peninsula on 15th July and caused heavy downpour in the Malabar region. Under its influence, heavy rainfall occurred in almost entire Kerala.

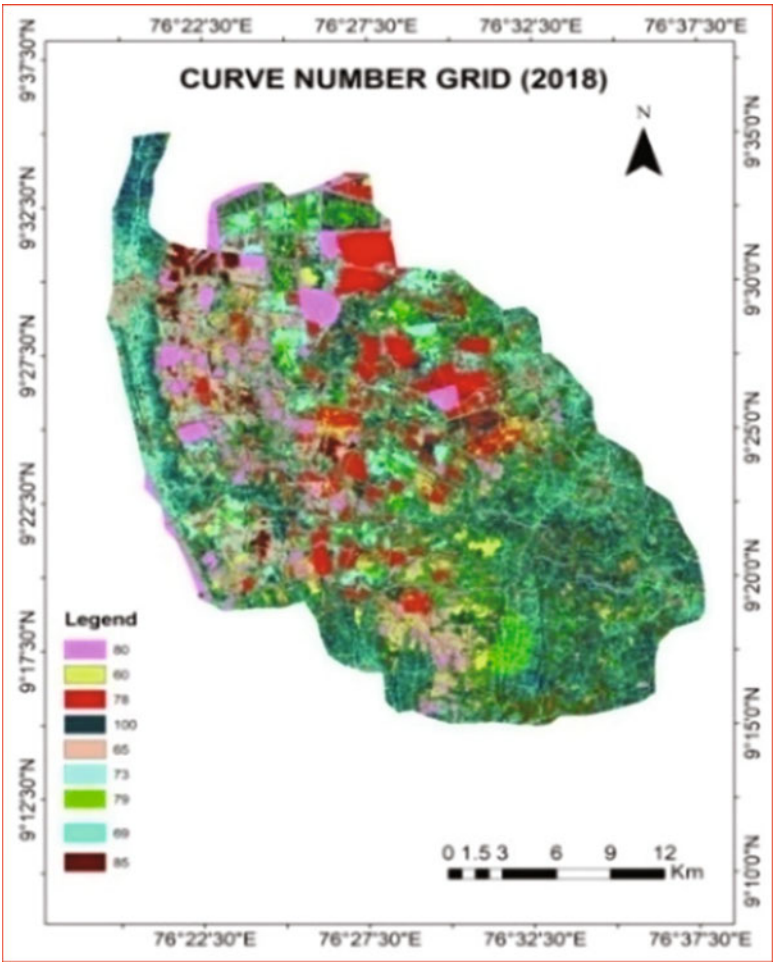

Fig. 25.15 Curve number map for the year 2018

Table 25.9 Estimated discharge values based on the simulated model

	Time (h)			
Calculated discharge (cumecs)	2	8	14	20
14/08/2018	470	490	460	510
15/08/2018	830	1320	1870	2310
16/08/2018	2680	2840	2840	2790
17/08/2018	2590	2360	2320	2330
18/08/2018	2310	2020	1860	1360
19/08/2018	890	680	660	630
20/08/2018	610	570	490	430

Table 25.10 Observed discharge values corresponding to various durations

	Time (h)			
Observed discharge (cumecs)	2	8	14	20
14/08/2018	500	530	490	540
15/08/2018	1000	1500	2000	2500
16/08/2018	2900	3000	3000	3000
17/08/2018	2800	2700	2600	2600
18/08/2018	2500	2300	2000	1500
19/08/2018	1000	800	800	790
20/08/2018	750	750	700	680

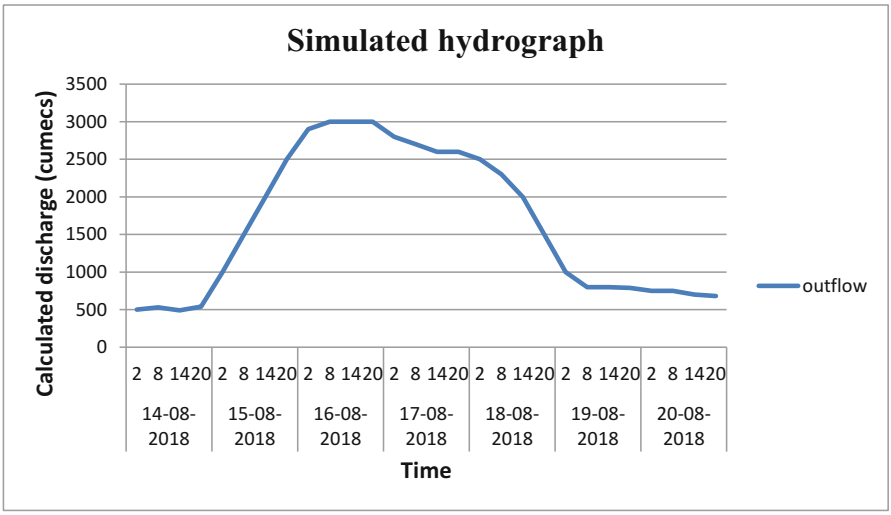

Fig. 25.16 Simulated hydrograph corresponding to the calculated discharge values

The area under the storm recorded 1-day maximum rainfall on 17th of July, 2-day maximum rainfall for 16–17, July 1920 and 3-day maximum rainfall for 16–18, July 1920. The storm centre of the 1-day and 2-day storms was located at Devikulam in Kerala which recorded 484 mm and 751 mm of rainfall respectively. The storm centre of 3-day storm was located at Munnar in Kerala which recorded a rainfall of 897 mm in 3 days. The discharge values were estimated based on the hourly rainfall data obtained from Indian meteorological department corresponding to 2, 8, 14 and 20 h for the study period 14–20 of August 2018. A hydrograph is a graph showing the rate of flow (discharge) versus time past a specific point in a river, channel, or conduit carrying flow. The estimated discharge values are given in Table 25.9.

For the purpose of validation of the model, observed discharge data was obtained from Central Water Commission, Ernakulum for the study period 17/08/2018 to 20/08/2018 as shown in Table 25.10.

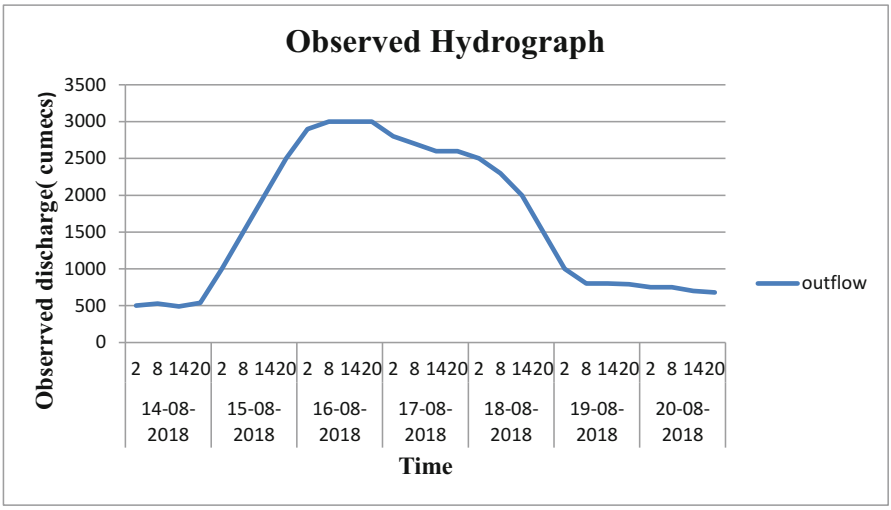

Fig. 25.17 Hydrograph corresponding to observed values

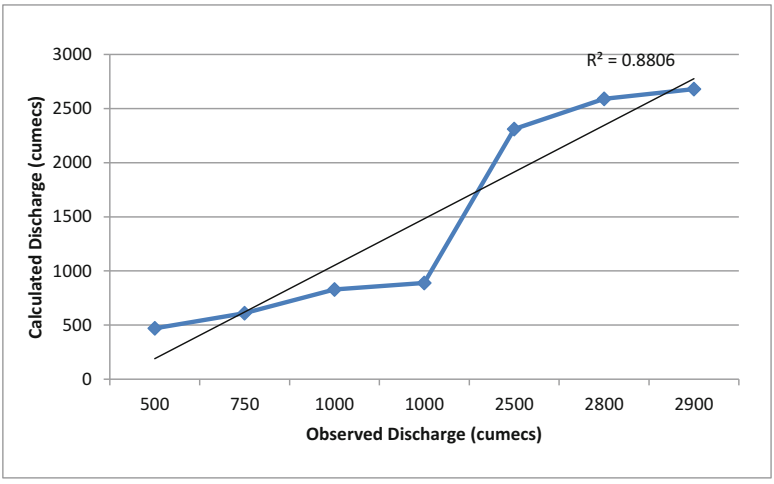

Fig. 25.18 Observed vs. calculated discharge corresponding to second hour of the storm

From the hydrograph as shown in Fig. 25.16 corresponding to estimated discharge, it can be seen that the rising limb of the hydrograph, reflects a prolonged increase in discharge from a catchment area, typically in response to a rainfall event. Here the rising limb starts from 14/08/2018 to 16/08/2018 and the peak discharge is obtained at 16/08/2018 at eighth and 14th hour. The recession limb extends from the peak flow rate onward. The end of storm and the return to groundwater-derived flow

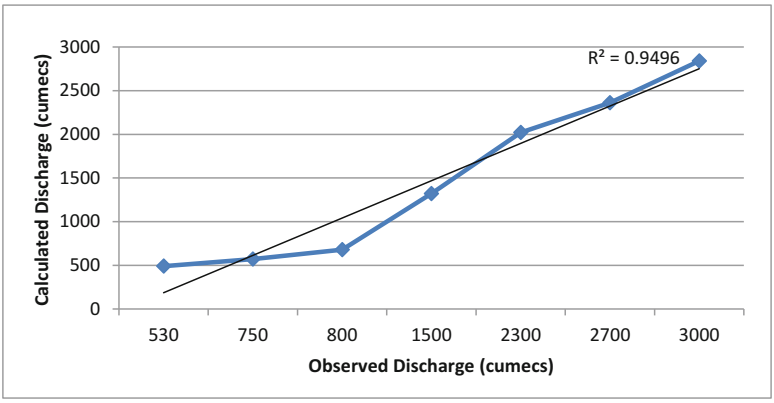

Fig. 25.19 Observed vs. calculated discharge corresponding to eighth hour of the storm

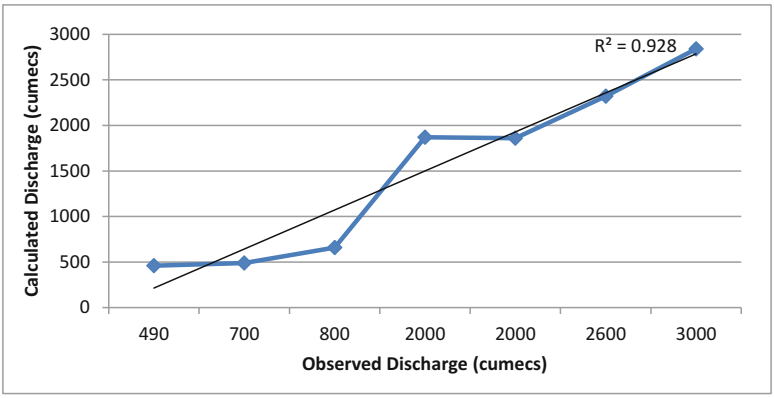

Fig. 25.20 Observed vs. calculated discharge corresponding to 14th hour of the storm

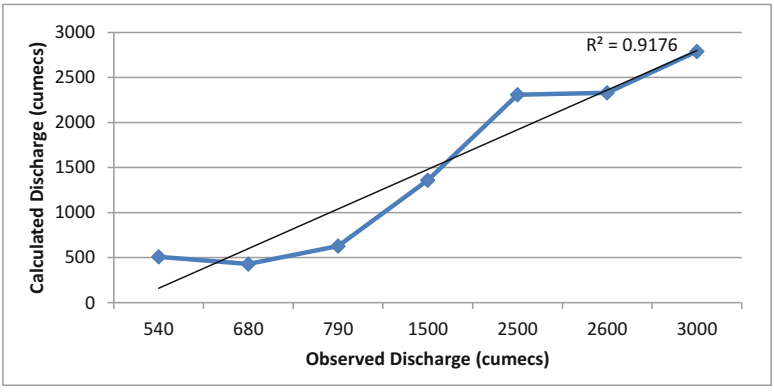

Fig. 25.21 Observed vs. calculated discharge corresponding to 20th hour

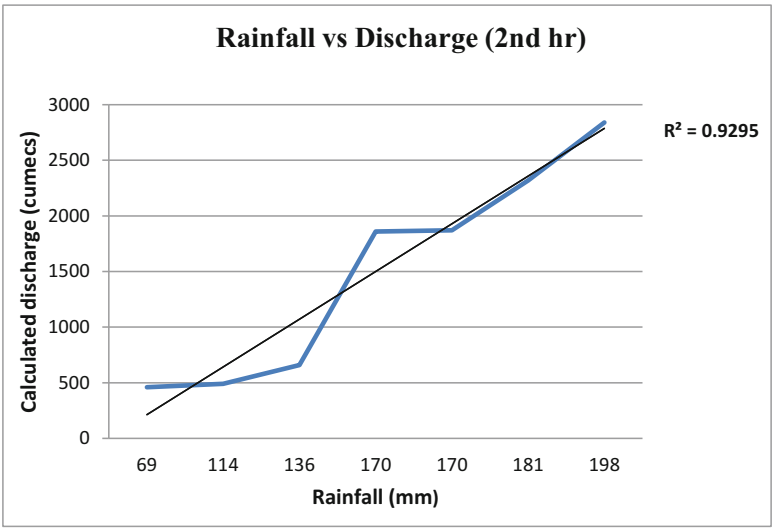

Fig. 25.22 Rainfall vs. discharge corresponding to second hour

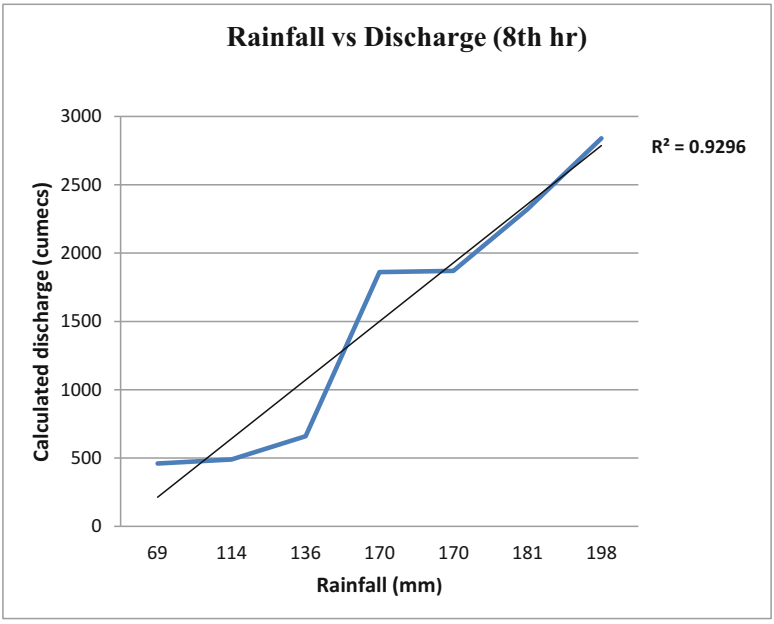

Fig. 25.23 Rainfall vs. discharge corresponding to eighth hour

(base flow) is often taken as the point of inflection of the recession limb. Here the recession limb starts from 16/08/2018 at 20th hour to 20/08/2018.

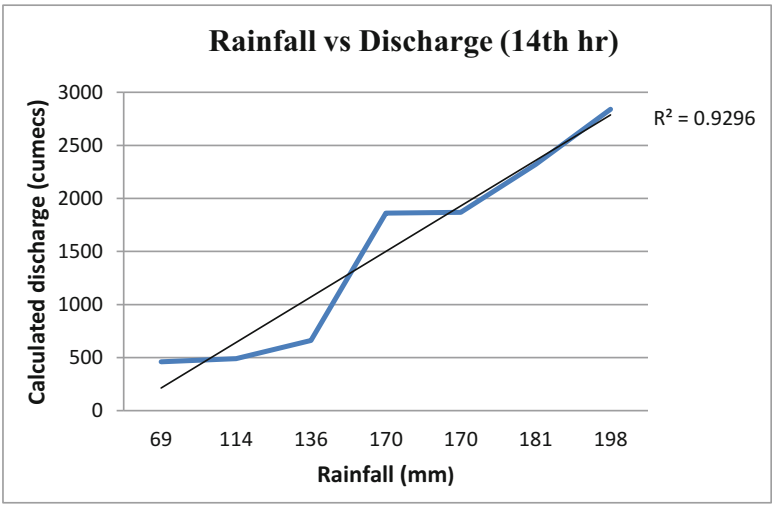

Fig. 25.24 Rainfall vs. discharge corresponding to 14th hour

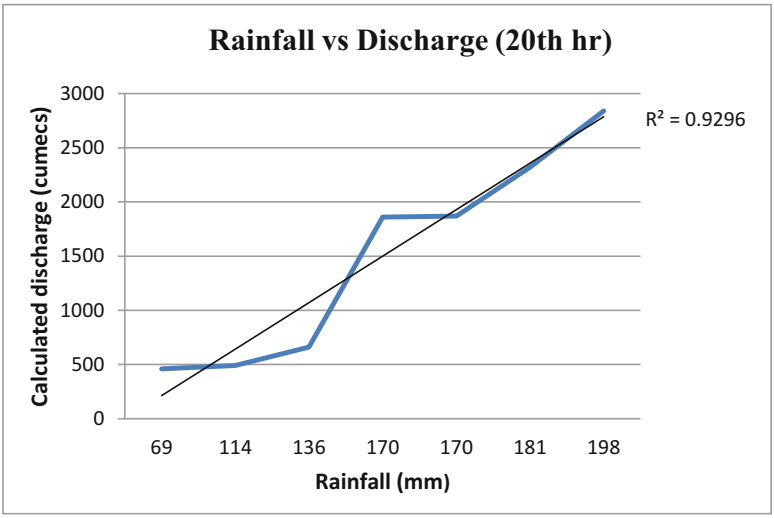

Fig. 25.25 Rainfall vs. discharge for corresponding to 20th hour

The calibration was carried out by considering the estimated and observed discharge for each day after carrying out the regression analysis. The hydrograph generated from the observed discharge data is shown in Fig. 25.17. The highest discharge occurs on 16.08.18.

Figures 25.18, 25.19, 25.20, and 25.21 shows the correlation between the calculated discharge and observed discharge for 2, 8, 24 and 20 h respectively. The correlation coefficient between the discharge values varies between 0.88 and 0.949.

25.7 Comparison of Rainfall with Discharge

Figures 25.22, 25.23, 25.24, and 25.25 show the correlation between rainfall and estimated discharge value corresponding to second, eighth, 14th and 20th hour. The graphs show that rainfall and estimated discharge are found to be directly proportional**.**

25.8 Conclusions

The present work depicts a methodology for the development of IDF curves from daily rainfall data. The analysis of the IDF curves showed very slight deviations between the Gumbel's and Empirical method. Analyzing the growing factor K_T, it is possible to identify the frequency of extreme events. The spatial distributed hydrological model HEC-HMS was coupled with the IDF analysis for simulation of inundation in the lower Kuttanad area of Kerala. The HEC-HMS model predicted flood flows and was applied, calibrated, and validated for which topography, land use, and soil data were utilized in the raster format. HEC-HMS model was applied in the downstream floodplain of the Kuttanad using the predicted discharge series and the model was calibrated and verified corresponding to the observed stage hydrographs in the floodplain. The model developed in this study can be used to simulate floods in river basin, and can aid in the development of strategies towards mitigation of impact of floods. The following conclusions can be drawn:

- Inundation of floodplains can be visualized by three-dimensional (3D) graphical representation and it shows that the model is suitable for predicting inundation and assessing flood risks.
- Coupling of hydrological model along with IDF analysis can form an important tool for the management of flood control and for real-time simulation of inundation in Kuttanad to prevent or reduce damage in terms of lives, property, and infrastructure.
- The study shows that modelling approach can easily be applied in practice to predict flood inundation, since the model requires only common basin characteristics such as topography, soil type and landuse and this can be easily handled by GIS (Geographical Information System) tools.
- The land use change in the study area should not be neglected especially during flood season. The effects of human activities including land use change should be

considered during the study to assess the variations in water resources and reasonable measures or policies should be adopted.

References

Abera, Z. (2011). *Flood mapping and modeling on Fogera flood plain: A case study of Ribb River*. Addis Ababa: M.Sc thesis, Depatment of Civil Engineering, Addis Ababa University.

Azeb, W., Florian, Z., & Wolfram, M. (2018). Assessing land use and land cover changes and agricultural farmland expansions in Gambella region, Ethiopia, using Landsat 5 and sentinel 2a multispectral data. *Helyon, 8*(4), 1–28.

Bhuiyan, M. S. R. (2014). *Flood Hazard and vulnerability assessment in a riverine flood prone area: A case study*. Dhaka: M.Sc. thesis, Institute of Water and Flood Management (IWFM), Bangladesh University of Engineering and Technology (BUET).

Chudasama, M. K., Dihora, G. V., & Chauhan, D. R. (2018). Flood modeling for computation of submergence area using arc GIS, HEC Georas & Hecras. *International Journal for Research in Applied Science & Engineering Technology, Issue, 6*, 4.

Edsel, B., Janey, V., Camp, E., LeBoeuf, J., Penrod, J. P., Dobbins, M., & Abkowitz, D. (2011). Watershed modelling and its applications: A state-of-the-art review. *The Open Hydrology Journal, 5*, 26–50.

Galoie, M., Eslamian, S., & Motamedi, A. (2014). An investigation of the influence of a retention dam on flood control in a small catchment area in Austria. *Journal of Flood Engineering, 5* (1–2), 1–15.

Hasan, S. M. I. (2006). *Application of geoinformatics for flood study at Tarapur Union of Gaibandha*. Dhaka: M.Sc, thesis, Institute of Water and Flood Management (IWFM), Bangladesh University of Engineering and Technology (BUET).

Hazarika, M. (2007). *Capacity building in applications of geoinformatics in flood hazard mapping fo bagmati river in Nepal. Technical report*. Bangkok: Geoinformatics Center (GIC), Asian Institute of Technology (AIT).

Hicks, F. E., & Peacock, T. (2005). Suitability of hec-ras for flood forecasting. *Canadian Water Resources Journal, 30*(2), 159–174.

Iosub, M., Enea, A., Hapciuc, O. E., Romanescu, G., & Minea, I. (2014). Flood risk assessment for the Ozana river sector corresponding to Leghin village, Romania. In *14th SGEM GeoConference on Water Resources: Forest, Marine And Ocean Ecosystems, SGEM2014 Conference Proceedings* (Vol. 1, pp. 315–322). Sofia: Secretariat Bureau. ISBN 978-619-7105-13-1/ISSN 1314-2704, June 19–25.

Iosub, M., & Lesenciuc, D. (2012). Hydrological risk characteristics of the Ozana river valley. *Universităţii Iaşi, 6*(2), 210.

Islam, A. S., Bala, S. K., & Haque, M. A. (2010). Flood inundation map of Bangladesh using modis time-series images. *Journal of Flood Risk Management, 3*(3), 210–222.

Joorabian, S. S., Kamran, S., Gholamalifard, M., Azari, M., SerranoNotivoli, R., & Ignacio López-Moreno, J. (2017). Impacts of future land cover and climate change on the water balance in northern Iran. *Hydrological Sciences Journal*, 2150–3435.

Khan, S. A. (2009). *Flood management in bangladesh*. Tampere: M.Sc. thesis, Department of Environmental Engineering, Tampere Polytechnic University of Applied Sciences.

Knebl, M. R., Yang, Z. L., Hutchison, K., & Maidment, D. R. (2005). Regional scale flood modeling using nexrad rainfall, gis, and hec-hms/ras: A case study for the San Antonio river basin summer 2002 storm event. *Journal of Environmental Managemen, 75*(4), 325–336.

Liang, K., Liu, C., & Song, X. (2013). Impacts of climate variability and human activity on streamflow decrease in a sediment concentrated region in the middle Yellow River. *Stochastic Environmental Research and Risk Assessment, 27*, 1741–1749.

Naef, F., Scherrer, S., & Weiler, M. (2002). A process based assessment of the potential to reduce flood runoff by land use change. *Journal of Hydrology, 267*, 74–79.

Onus, G. L. (2005). *Floodplain management based on HEC-RAS modelling system*. Izmir: Ph.D. thesis, Dokuz Eyl¨ul Universitesi fen ¨ Bilimleri Enstit¨us¨u.

Pande, C., & Moharir, K. (2014). Analysis of land use/land cover changes using remote sensing data and GIS techniques of Patur Taluka, Maharashtra, India. *International Journal of Pure and Applied Research in Engineering and Technology, 2*(12), 85–92.

Pande, C. B. (2020a). Introduction. In *Sustainable watershed development. Springer briefs in water science and technology*. Cham: Springer. https://doi.org/10.1007/978-3-030-47244-3_1.

Pande, C. B. (2020b). Watershed management and development. In *Sustainable watershed development. Springer briefs in water science and technology*. Cham: Springer. https://doi.org/10.1007/978-3-030-47244-3_2.

Pande, C. B. (2020c). Thematic mapping for watershed development. In *Sustainable watershed development. Springer briefs in water science and technology*. Cham: Springer. https://doi.org/10.1007/978-3-030-47244-3_3.

Pande, C. B. (2020d). Sustainable watershed development planning. In *Sustainable watershed development. Springer briefs in water science and technology*. Cham: Springer. https://doi.org/10.1007/978-3-030-47244-3_4.

Pande, C. (2014). Change detection in land use/land cover in Akola taluka using remote sensing and GIS technique. *International Journal of Research (IJR), 1*(8), ISSN 2348-6848.

Pande, C. B., Khadri, S. F. R., Moharir, K. N., & Patode, R. S. (2017). Assessment of groundwater potential zonation of Mahesh River basin Akola and Buldhana districts, Maharashtra, India using remote sensing and GIS techniques. *Sustainable Water Resources Management, 4*, 965–979. https://doi.org/10.1007/s40899-017-0193-5. ISSN 2363-5037.

Pande, C. B., Moharir, K. N., Khadri, S. F. R., & Patil, S. (2018). Study of land use classification in the arid region using multispectral satellite images. *Applied Water Science, 8*(5), 1–11.

Patode, R. S., Nagdeve, M. B., Pande, C. B., & Moharir, K. N. (2017). Land use and land cover changes in Devdari watershed Tq. Patur, Distt. Akola, of Vidarbha region in Maharashtra. *Trends in Biosciences, 10*(8), 1622–1625.

Pikounis, M., Varanou, E., Baltas, E., Dassaklis, A., & Mimikou, M. (2003). Application of the SWAT model in the Pinios River basin under different land use scenarios. *Global Nest: The International Journal, 5*, 71–79.

Ram Babu, Tejwani, K. G., Agarwal, M. C. & Bhushan, L. S. (1979). Rainfall Intensity Duration - return period equations and nomographs of India, CSWCRTI, ICAR, India.

Reddy, D. M., Patode, R. S., Nagdeve, M. B., Satpute, G. U., & Pande, C. B. (2017). Land use mapping of the Warkhed micro-watershed with geo-spatial technology. *Contemporary Research in India, 7*(3), ISSN 2231–2137.

Sherman, C. W. (1931). Frequency and intensity of excessive rainfall at Boston, Massachusetts, *Transaction paper, 95*, 951–960.

Sudha, Y. (2012). A hybrid approach of integrating HEC RAS and GIS towards the identification and assessment of flood risk vulnerability in the city of Jackson. *American journal of Geographic Information System, 1*(1), 7–16.

Sunil kumar Morais, C., Girish, T. E., Baburaj, M. S., & Abhilash Kumar, R. G. (2018). On the spatial variations of Rainfall in Kerala during the Great Floods in the year 1924. *International Journal of Scientific Research and Reviews, 7*(4), 1700–1709.

Chapter 26
Groundwater Development and Planning Through Rainwater Harvesting Structures: A Case Study of Semi-arid Micro-watershed of Vidharbha Region in Maharashtra, India

R. S. Patode, Ranee Wankhade, Sumiran Dabrase, M. B. Nagdeve, Chaitanya B. Pande, V. V. Gabhane, A. B. Turkhede, R. S. Mali, and V. P. Pandagale

Contents

26.1 Introduction 514
26.2 Material and Methods 514
26.3 Soil Classification 517
26.4 Survey, Nala Deepening, and Widening with CNB Work, 2015–2016 518
26.5 Results and Dicussion 518
26.6 Groundwater Level Monitoring, 2015–2016 519
26.7 Groundwater Level Analysis, 2016–2017 519
26.8 Groundwater Level Analysis, 2017–2018 519
26.9 Groundwater Level Analysis, 2018–2019 520
26.10 Monthly Groundwater Map During 2018–2019 521
26.11 Monitoring of CNB 525
26.12 Groundwater Level Analysis, 2019–2020 536
26.13 Conclusion 554
References 557

R. S. Patode (✉) · R. Wankhade · V. V. Gabhane · A. B. Turkhede · R. S. Mali · V. P. Pandagale
All India Coordinated Research Project for Dryland Agriculture, Akola, Maharashtra, India

S. Dabrase
Post Graduate Institute of Dr. PDKV, Akola, Maharashtra, India

M. B. Nagdeve
Faculty of Agricultural Engineering, Dr. Panjabrao Deshmukh Krishi Vidyapeeth, Akola, Maharashtra, India

C. B. Pande
Sant Gadge Baba Amravati University, Amravati, Maharashtra, India

All India Coordinated Research Project for Dryland Agriculture, Akola, Maharashtra, India

C. B. Pande, K. N. Moharir (eds.), *Groundwater Resources Development and Planning in the Semi-Arid Region*, https://doi.org/10.1007/978-3-030-68124-1_26

26.1 Introduction

Groundwater decreases daily due to human activities and climate change factors. Currently only 2.5% of the world's water is freshwater that is available for human consumption, agricultural, and industrial purposes (Pande 2020a, 2020b, 2020c, 2020d). In several parts of the world, however, water is being used at a much faster rate than can be replenished by rainfall (Pande and Moharir 2015). In 2025, the per capita water availability in India will be reduced to 1500 m^3 5000 m^3 in 1950 (Sharma 2010). Groundwater resources play an important role in planning natural resources management (Pande et al. 2017, 2018, 2019). There has been tremendous increases in the demand for groundwater due to increases in population, advanced irrigation practices, and industrial usages (Jha et al. 2007, 2010; Khadri and Pande 2016; Moharir et al. 2017). The occurrence and movement of groundwater are governed by several factors, such as lithology, geological structures, soil, lineament features, slope, drainage patterns, geomorphology, land use/land cover, and the interrelationships among these factors (Jaiswal et al. 2003; Jha et al. 2007; Jha et al. 2010; Chowdhury et al. 2010; Patode et al. 2017). Many researchers have investigated groundwater development and sustainable planning in semi-arid areas and have used modeling, remote sensing, and GIS methods to determine groundwater potential zones in their areas of interest (Saraf and Choudhury 1998; Jha and Peiffer 2006; Jaiswal et al. 2003; Al-Adamat et al. 2003; Solomon and Quiel 2006; Jha et al. 2007). Several factors, such as rock types and their structural properties, topography, drainage networks, landform patterns, land use/land cover patterns, and meteorological conditions, impact agricultural crop growth and groundwater development (Jaiswal et al. 2003; Ali et al. 2015; Yeh et al. 2016; Golla et al. 2018). Detailed knowledge about aquifers, recharge, and potentiality are a principal requirement for sustainable groundwater planning, management, and development in semi-arid regions.

The delineation of potential zones of groundwater recharge is one of the key processes for the enhancement, management, and development of groundwater resources. Remote sensing in combination with GIS has been widely used for groundwater prospect mapping (Krishnamurthy et al. 1996; Srinivasa Rao and Jugran 2003; Elbeih 2015; Moharir et al. 2020). In 2019, the average depth of observation wells increased by 0.92 m compared with 2018 depths.

26.2 Material and Methods

26.2.1 Study Area

The watershed is situated in Barshitakli Taluka, Akola District, Maharashtra state, between 20°13′59″ N latitude and 77°13′23″ E longitude and at an altitude of 337 m above mean sea level (MSL), with an average annual rainfall of 850 mm. The

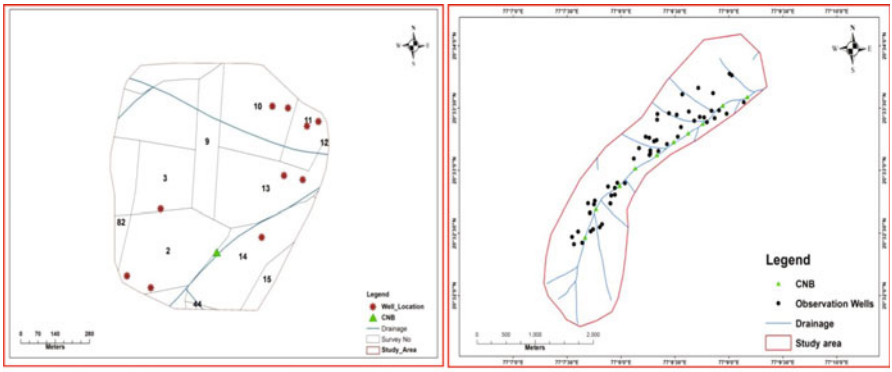

Fig. 26.1 Location map of previous (**a**) and extended watershed area (**b**)

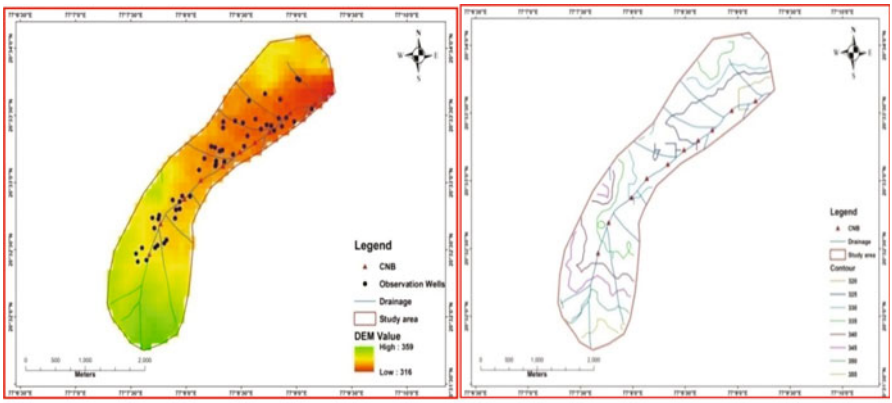

Fig. 26.2 DEM map (**a**) and contour map (**b**) of extended watershed

important aquifers in the area are basalt rock. Basalt, when weathered and fractured, contains considerable amounts of groundwater. The location map is shown in Figs. 26.1a, b.

The study area elevation is 316–359 m. The length of the drainage line dips around 5000 m as it moves from Kajaleshwar to Warkhed villages. A contour map was prepared from digital elevation model (DEM) data (Fig. 26.2). The scaling up of work done in Kajaleshwar-Warkhed Watershed was completed in 2018–2019 years. The area increased by 504.4 ha. (Fig. 26.1b).

26.2.2 Topography

The SRTM (30 m) data set of the Space Shuttle Endeavour satellite was used to create a DEM. DEM data are a very effective tool for terrain analysis, and many terrain attributes (such as slope, aspect, relief, and watershed hill shade and flow direction) can be used to locate rainwater structures. The following methodology was used to derive contour maps from the aforementioned data set, and they are used as layers in the GIS domain for further analysis. A contour map with 1 m intervals was generated from the DEM using surface analysis tools in ArcGIS software 10.1. A contour map is very useful for designing rainwater harvesting structures. The lowest and highest elevations were observed in a range of 325–337 m (Fig. 26.2a). The contour map of the area is given in Fig. 26.2b.

26.2.3 Agricultural Land

Agricultural land is defined as land primarily used for farming and for the production of food, fiber, and other commercial and horticultural crops. It includes land under crops (such as irrigated and non-irrigated, fallow, plantations). In the study area, agricultural land includes mostly cropland. Cropland includes those lands with standing crop as of the date of satellite overpass. The crops can be of either kharif or rabi or kharif-rabi seasons. Cropland appears in bright red to red in colour with varying shapes and sizes in a contiguous to non-contiguous pattern. In this study, agricultural land occupies about 286.71 ha (85.06%). Dryland cultivation is the dominant land use category in the study area. Large amounts of cotton, red gram, soybean, green gram, onion, jawar, and other pulse crops have been grown in this watershed.

26.2.4 Climate

The study area comes under the central Maharashtra plateau zone and is characterized by a subtropical, monsoonal, semi-arid type of climate divided into four seasons: a cold season from November to February, a hot season from March to May, a south-west monsoon period from June to September, and a post-monsoon period from October to November. The climate of the study area is mainly hot and dry except during the monsoon period. The highest relative humidity observed in April 16% higher than the 38%. The highest wind speed observed is about 14.7 km/h in June during the south-west monsoon period and the lowest is 4.4 km/h in December during the winter period. The average wind speed for the year is 8.6 km/h (source IMD).

26.2.5 Soil Types and Slope

Soil slope is considered an important factor in soil genesis and land use. In the demonstration site, the soil slope ranges from 1% to 5% was observed using multispectral satellite image. The soil slope map was prepared from LISS-III satellite images and ground verification using visual interpretation techniques in GIS 10.1 software.

26.3 Soil Classification

Among the aforementioned soil types of the Kajaleshwar watershed the soil classification is done. A soil map was created using GIS software with ground-truth verification. Spatial soil maps (shape file) for the soil types of the Kajaleshwar watershed generally identify five types of soil groups according to their texture: clay, clay loam, gravelly clay loam, gravelly sandy clay loam, and sandy clay loam (Fig. 26.3).

Most of the Kajaleshwar watershed area is covered with a clay-type soil. Soils that have a high clay content do not allow very much infiltration and thus have relatively high run-off coefficients, while soils with high gravel content have higher infiltration rates and low run-off coefficients. Clay soil has high run-off coefficients, so more surface run-off can occur during rainfall. The area in the Kajaleshwar watershed is very fertile but lacks moisture, so the soil tends to be degraded.

Fig. 26.3 Soil texture map of micro watersheds

26.4 Survey, Nala Deepening, and Widening with CNB Work, 2015–2016

The site of the rainwater harvesting structure for this study was selected based on the drainage line and was finalized on the basis of expert advice from IIT, Kharagpur. In this watershed area, initial 100 m widening and deepening work was constructed on the existing drainage line. It has been used in a rainwater management strategy through water conservation structures in the Kajaleshewar and Warkhed watersheds. Digging work for nala deepening and widening was done and the CNB was repaired during the summer season in 2015–2016 under rainfed conditions. Rainwater and runoff water were collected in the water conservation structure and the stored water used for sustainable irrigation of agricultural crops under rainfed conditions. Water conservation structures are helpful for the development of a groundwater regime and agricultural sector.

It was observed that the surrounding groundwater level was increasing due to the nala deepening and widening work on the drainage line in the watershed area. The excess runoff was stored in the rainwater harvesting structure (CNB) during kharif seasons. The total cumulative quantity of the stored water was measured using a water level indicator, and the total quantity of water available during the nala widening and deepening work was obtained every month. Before the project, the area had suffered from various climatic conditions, such high percolation, evaporation, and seepage rates, and high run-off, and water in the nala was not available for irrigation at the peak pod development stage of the soybean crop. However, following construction of the CNB for rainwater harvesting in the rainwater harvesting structure on the lower layer, the moisture availability in the bottom toposequence increased and the crop yield of soybean was increased by one and two protective irrigation methods.

26.5 Results and Dicussion

The observation well location maps were prepared using ArcGIS 10.1 software and the maps showing the variation in groundwater level were prepared using the IDW method and GIS technique. The locations of the observation wells were transformed on the base map in GIS software. This chapter is concerned with rainwater harvesting activities' impact on the groundwater level and aquifer zones. Semi-arid regions have a great need for rainwater harvesting activites to increase water levels and improve agriculture yields. Such activities are important for farmers because in the last five decades climate change factors have directly affected crop yields, water availability, and ecosystems in semi-arid regions. Soil and water conservation is one of the methods for environmental protection, preventing soil erosion, and maintaining water quality and groundwater levels in semi-arid regions. Water levels were observed in the study area in the period 2015–2019.

26.6 Groundwater Level Monitoring, 2015–2016

GPS was used to locate the exact coordinates of wells, allowing well levels to be monitored using water level indicators (Table 26.1). The well level data were transferred to the base map in a GIS environment. Groundwater level changes were calculated on the basis of observation wells around the deepened and widened nala/CNB. Groundwater level maps were prepared using differences in well levels in 2015 and 2016 (Figs. 26.4 and 26.5).

26.7 Groundwater Level Analysis, 2016–2017

Groundwater level monitoring was done in October, November, and December 2016 and January and February 2017 (Table 26.2). Groundwater level maps were prepared in ArcGIS (Figs. 26.6, 26.7, 26.8, 26.9, and 26.10).

26.8 Groundwater Level Analysis, 2017–2018

Groundwater level data were collected from 35 observation wells. It was observed that in 2015 and 2017, water levels ranged between 3.65 and 9.1 m and 2.2–8.3 m, respectively (Figs. 26.11 and 26.12). Groundwater level fluctuations in 2017 compared to 2015 were observed (Fig. 26.13). Well water levels increased in 2017 over 2015.

Table 26.1 Ground water levels during the year 2015–2016

	Water levels in well (m)	
Well no.	Pre-monsoon (2015)	Pre-monsoon (2016)
1	8.6	3.25
2	9.8	4.95
3	8	5.68
4	8	4.38
5	6.7	5.2
6	6.7	5.96
7	6.7	5.6
8	14.0	9.40
9	13.0	9.60
10	14.21	8.5

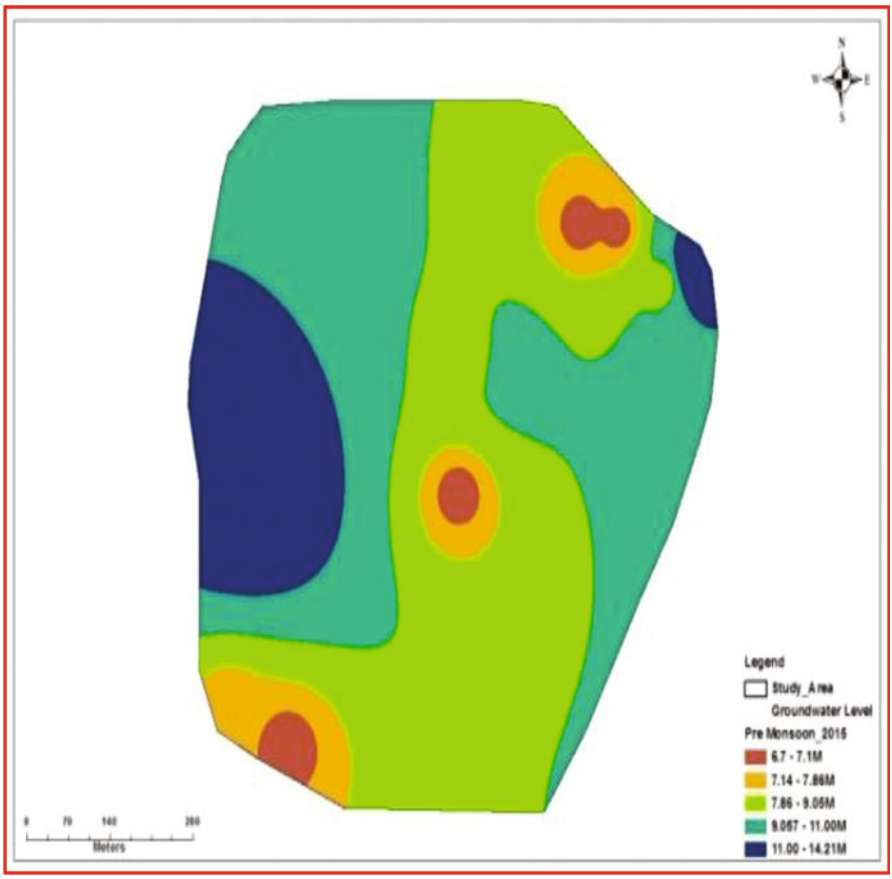

Fig. 26.4 Groundwater level map in pre-monsoon 2015

26.9 Groundwater Level Analysis, 2018–2019

Groundwater level data were collected from 51 observation wells in the vicinity of 10 CNBs for the analysis of rainwater harvesting's impact on the groundwater regime in the watershed area. In 2017 (35 wells), the average depth of the water level (Fig. 26.14) was 4.07 m, and in 2018 (36 + 15 = 51 wells), the average depth of the water level (Fig. 26.15) was 3.60 m (Table 26.3). Groundwater level were increased in 2018 compared to 2017 were observed (Fig. 26.16).

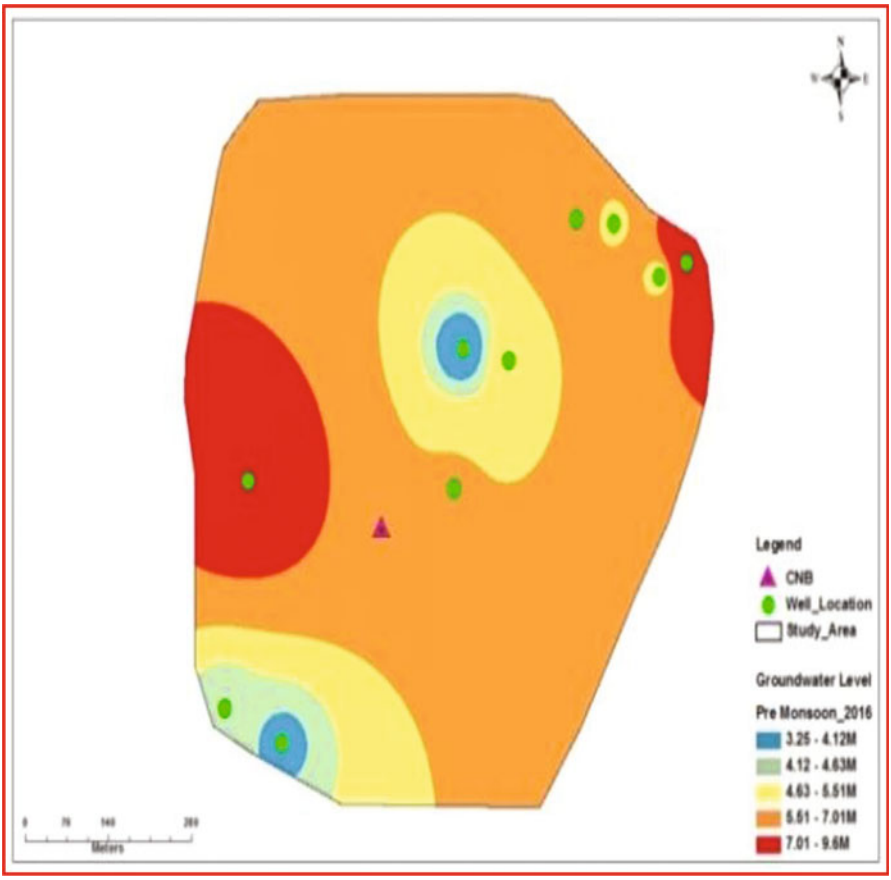

Fig. 26.5 Groundwater level map in pre-monsoon 2016

26.10 Monthly Groundwater Map During 2018–2019

In the period 2018–2019, 51 observation wells were selected for monthly data collection in watershed area. The map shows the depth to groundwater level. The monthly groundwater level maps were generated using the inverse distance–weighted method in ArcGIS. The water levels were observed to increase in 2018 vs. 2017. Figure 26.17 shows a groundwater level map from July in which the depth to groundwater level ranges between 2 and 8.5 m. Figure 26.18 shows a groundwater level map from August in which the depth to groundwater level ranges between 0.5 and 8.5 m. Figure 26.19 shows a groundwater level map from September in which the depth to groundwater level ranges between 2 and 5.9 m. Figure 26.20 shows a groundwater level map from October in which the depth to groundwater level ranges between 2.4 and 5.9 m. Figure 26.21 shows a groundwater level map from November in which the depth to groundwater level ranges between

Table 26.2 Groundwater levels during rabi season 2016–2017

Observation well no.	Depth of water level (m), Oct. 2016	Depth of water level (m), Nov. 2016	Depth of water level (m), Dec. 2016	Depth of water level (m), Jan. 2017	Depth of water level (m), Feb. 2017
1	3.5	4.2	4.9	5.3	6.2
2	1.2	2.2	3.2	3.9	5.4
3	3.2	4.1	5.2	5.8	7.3
4	2.4	2.9	3.5	4.3	6.4
5	3.6	3.9	4.8	5.8	7.8
6	4.9	5.2	5.9	6.8	8.2
7	1	1.5	2.2	3.9	5.4
8	1.85	2.36	3.1	4.7	6.7
9	2.8	3.1	4.1	5.6	7.9
10	1.60	2.6	3.2	4.1	6.1
11	2.6	3.4	4.2	5.4	6.9
12	0.9	1.3	2.5	3.7	5.5
13	1.2	1.7	2.8	3.5	6.4
14	0.5	1.3	2.3	3.6	6.7
15	6.3	7.2	8.3	9.2	11.5
16	2.3	2.9	4.2	5.7	7.8
17	2.2	3.5	4.3	5.1	8.2
18	0.9	1.3	2.7	3.9	6.1
19	2.50	3.1	3.9	4.5	5.3
20	1.5	1.9	2.3	3.5	5.3
21	2.25	2.8	3.2	4.5	6.7
22	1.75	2.3	3.2	4.8	7.4
23	2.5	3.3	4.4	5.8	8.3
24	4.6	5.4	6.3	7.5	9.7
25	2.3	2.7	3.4	4.8	5.8
26	2.4	3.2	4.1	5.1	7.6
27	2.5	3.4	4.3	6.2	8.5
28	3.2	3.9	4.9	5.6	8.1
29	2.8	2.9	3.7	4.8	7.9
30	2.90	3.1	3.8	5.2	9.2
31	4.1	4.6	5.2	6.4	9.4
32	1.90	2.1	3.3	4.3	8.6
33	1.60	2.1	3.1	5.1	8.1
34	2.2	2.8	3.8	4.8	7.3
35	8.7	9.7	10.5	11.2	12.5

1.3 and 6.45 m. Figure 26.22 shows a groundwater level map from December in which the depth to groundwater level ranges between 2.35 and 7.5 m. Figure 26.23 shows a groundwater level map from January in which the depth to groundwater level ranges between 4.4 and 9.3 m. Figure 26.24 shows a groundwater level map

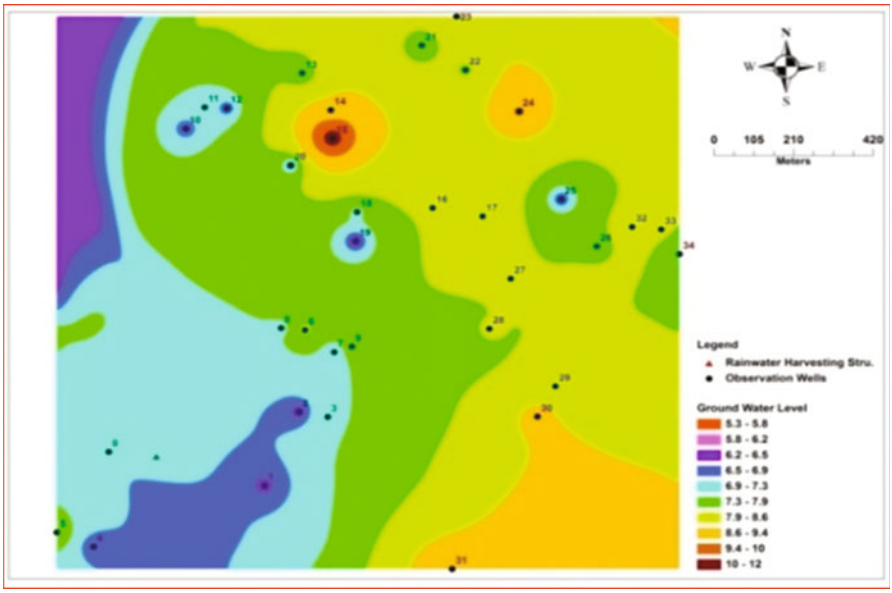

Fig. 26.6 Depth of groundwater levels, October 2016

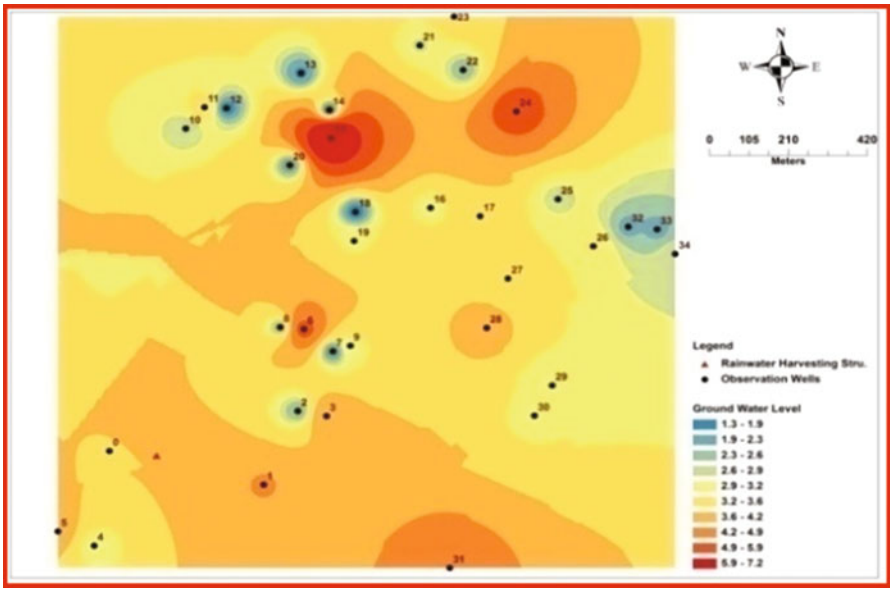

Fig. 26.7 Depth of groundwater levels, November 2016

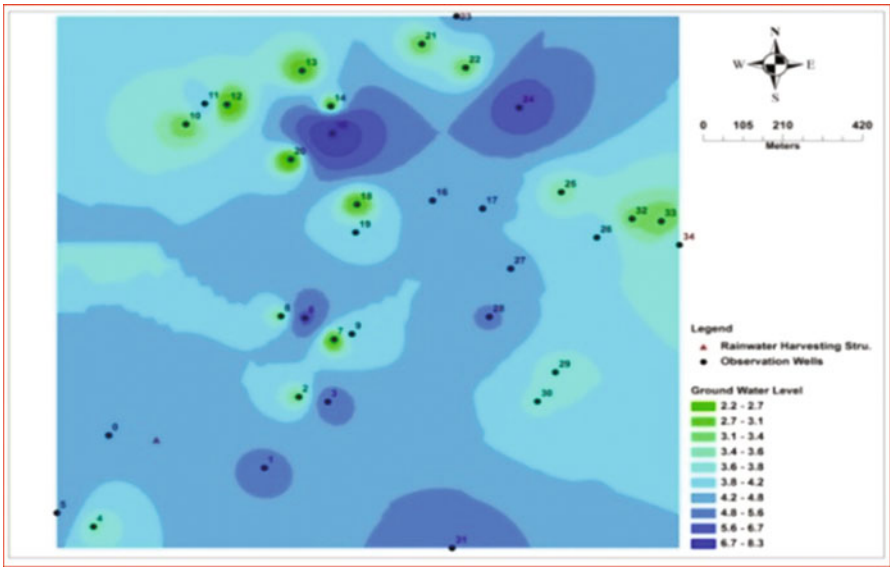

Fig. 26.8 Depth of groundwater levels, December 2016

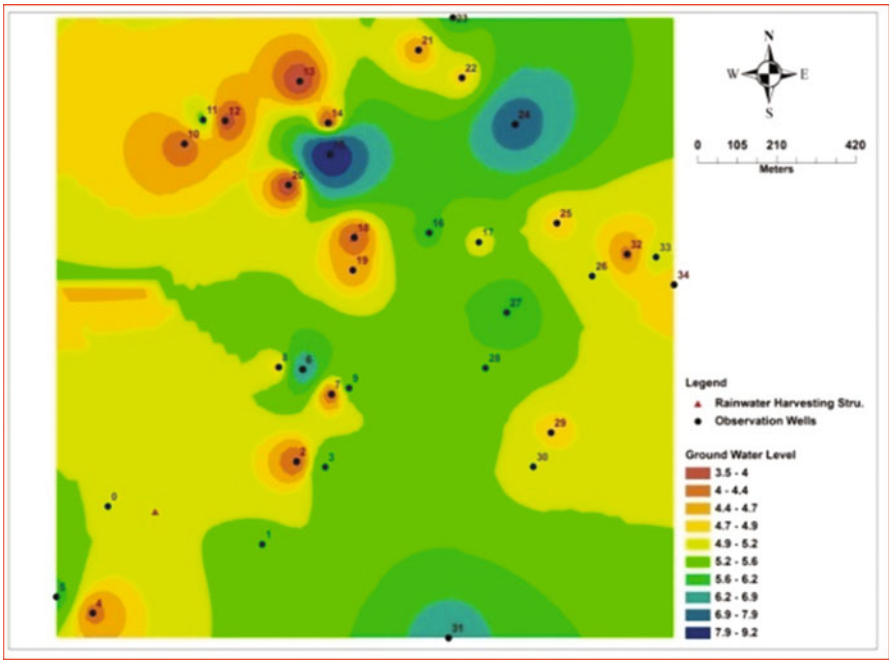

Fig. 26.9 Depth of groundwater levels, January 2017

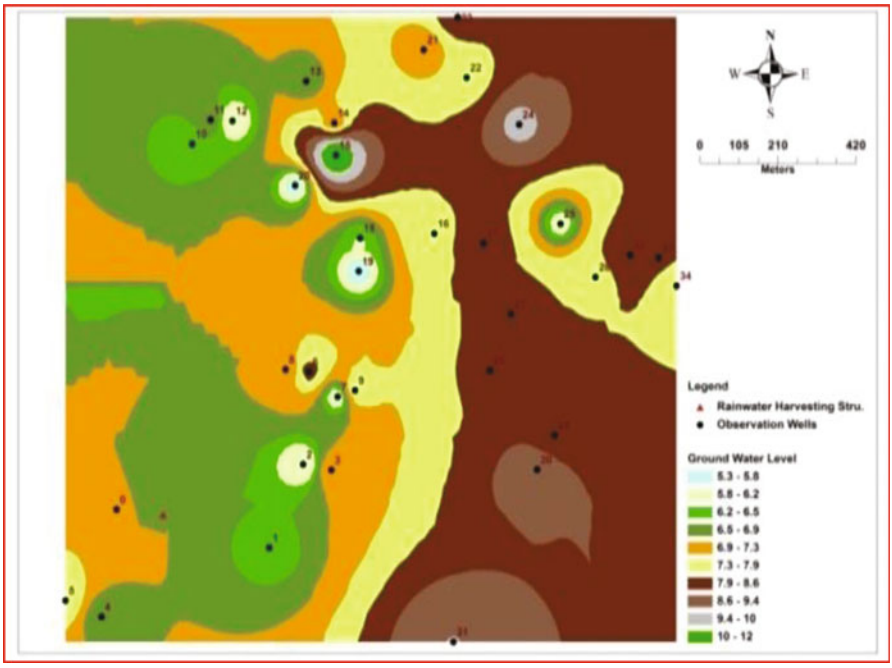

Fig. 26.10 Depth of groundwater levels, February 2017

from February in which the depth to groundwater level ranges between 3.7 and 10.3 m. Figure 26.25 shows a groundwater level map from March in which the depth to groundwater level ranges between 4.44 and 12.8 m. Figure 26.26 shows a groundwater level map from April in which the depth to groundwater level ranges between 5.45 and 14. 31 m. The groundwater levels in July, August, September, October, November, and December are in good condition. Starting in January, however, the levels decline.

26.11 Monitoring of CNB

A total of 10 CNBs were selected for impact analysis of rainwater harvesting in the study area. Water storage characteristics in the cement nala bund were studied by monitoring the depth of water storage in epy cement nala bund and the extent of water spread. The capacities of the CNBs were determined and are given in Table 26.4. Table 26.4 shows that CNB 1 and CNB 3 have the same storage capacity, which was the highest among all the CNBs, i.e. 2016 m^3, and the lowest storage capacity was observed in CNB 10, i.e. 1680 m^3. Accordingly, monthly water storage in the CNBs was observed. Tables 26.5, 26.6, 26.7, 26.8, 26.9, 26.10, 26.11, 26.12, 26.13, and 26.14 show the monthly water storage of CNBs 1–10 respectively.

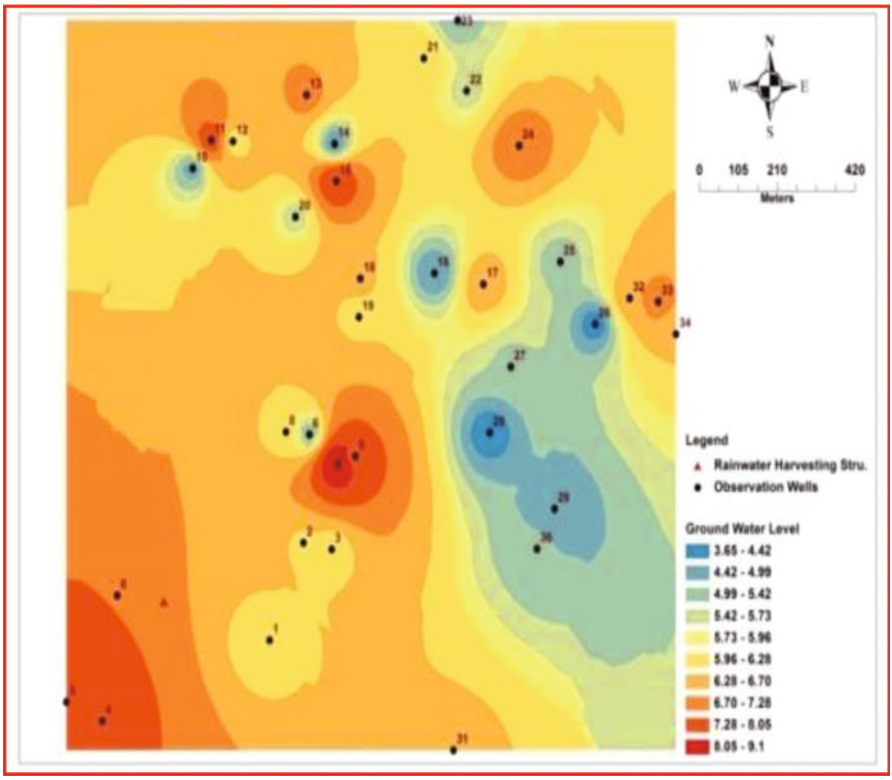

Fig. 26.11 Depth of groundwater levels, 2015

Generally, in July and August, due to consistent rainfall, the CNBs overflow and are dry during summer. CNB 7 was damaged, so its water storage capacity was poor and generally went dry sooner than the other CNBs. It was observed that CNB storage increased due to widening and deepening of the nalas. Farmers benefitted from the water storage in the CNBs. Farmers have used the water stored in the CNBs as protective irrigation for different crops in different seasons.

Table 26.5 shows storage in CNB 1 in the period 2018–2019. The capacity of CNB 1 is 2016 m^3. The maximum rainfall was collected in July, August, and September in that period, and CNB overflowed twice. The CNB was dry in April, May, and June of 2018 and also in February, March, and April of 2019.

Table 26.6 shows storage in CNB 2 in the period 2018–2019. The capacity of CNB 2 is 1980 m^3. The maximum rainfall was collected in July, August, and September, and in that period the CNB overflowed twice. The CNB was dry in April, May, and June of 2018 and in February, March, and April of 2019.

Table 26.7 shows storage in CNB 3 in the period 2018–2019. The capacity of CNB 3 is 2016 m^3. The maximum rainfall was collected in July, August, and

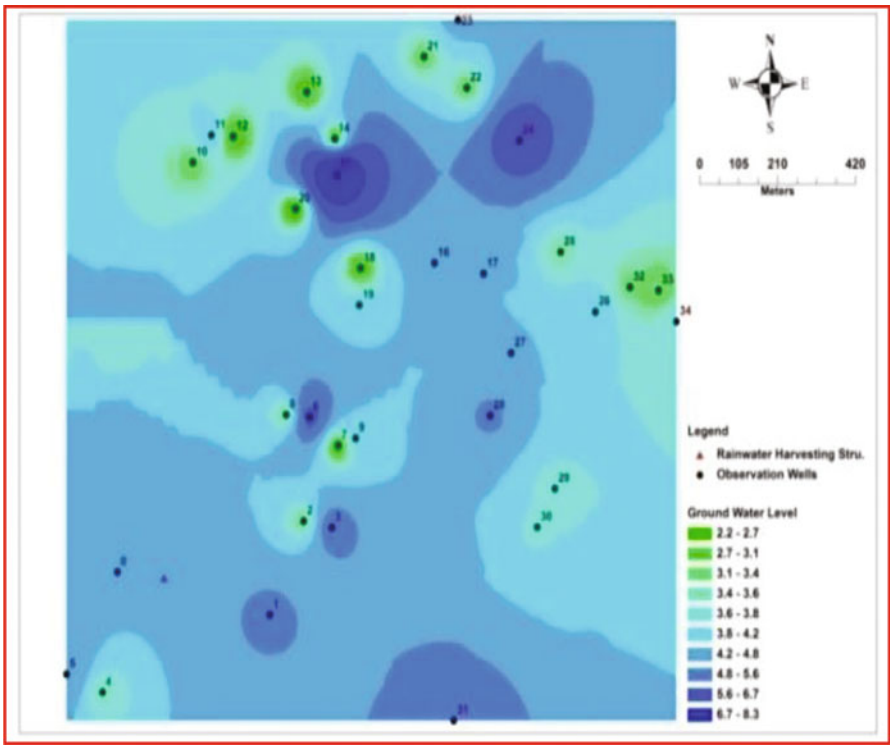

Fig. 26.12 Depth of groundwater levels, 2017

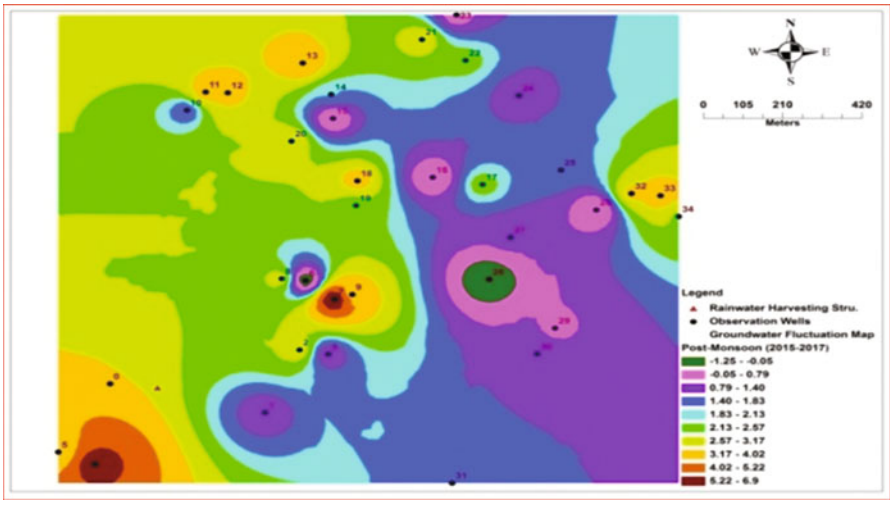

Fig. 26.13 Groundwater level fluctuations, 2015–2017

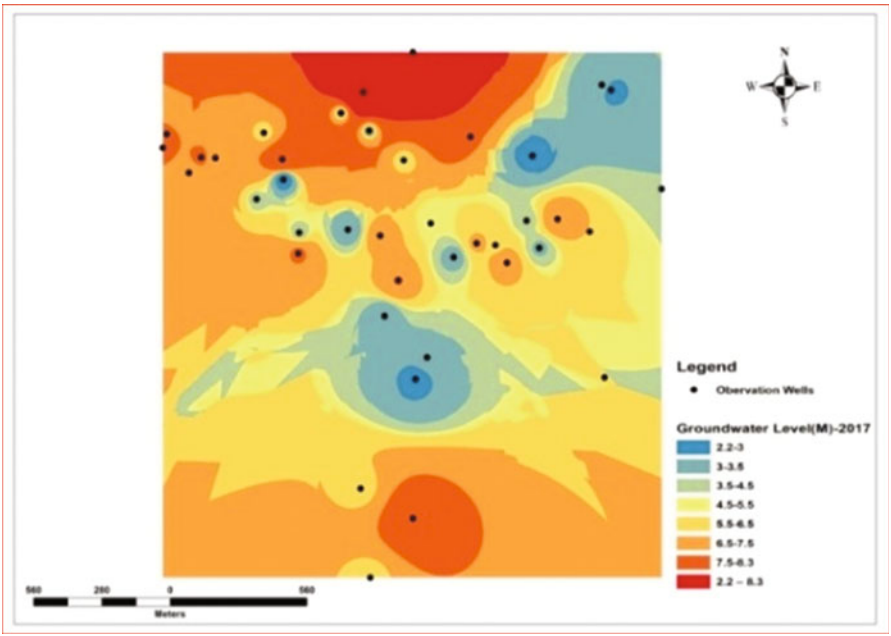

Fig. 26.14 Depth of groundwater levels, 2017

September, and in that period the CNB overflowed twice. The CNB was dry in April, May, and June of 2018 and in February, March, and April of 2019.

Table 26.8 shows storage in CNB 4 in the period 2018–2019. The capacity of CNB 5 is 1920 m^3. The maximum rainfall was collected in July, August, and September, and in that period the CNB overflowed twice. The CNB was dry in April, May, and June of 2018 and in February, March, and April of 2019.

Table 26.9 shows storage in CNB 5 in the period 2018–2019. The capacity of CNB 5 is 1831 m^3. The maximum rainfall was collected in July, August, and September. The CNB was observed to overflow once and was dry in January, February, March, April, May, and June of 2018 and in February, March, April, and May of 2019.

Table 26.10 shows storage in CNB 6 in the period 2018–2019. The capacity of CNB 6 is 1800 m^3. The maximum rainfall was collected in July, August, and September. The CNB overflowed once and was dry in January, February, March, April, May, and June of 2018 and in February, March, April, and May of 2019.

Table 26.11 shows storage in CNB 7 in the period 2018–2019. The capacity of CNB 7 is 1800 m^3. The maximum rainfall was collected in July, August, and September. CNB 7 is damaged, which is why it overflowed twice. The CNB was dry in January, February, March, April, May, and June of 2018 and in December, January, February, March, April, and May of 2019.

Table 26.12 shows storage in CNB 8 in the period 2018–2019. The capacity of CNB 8 is 1794 m^3. The maximum rainfall was collected in July, August, and

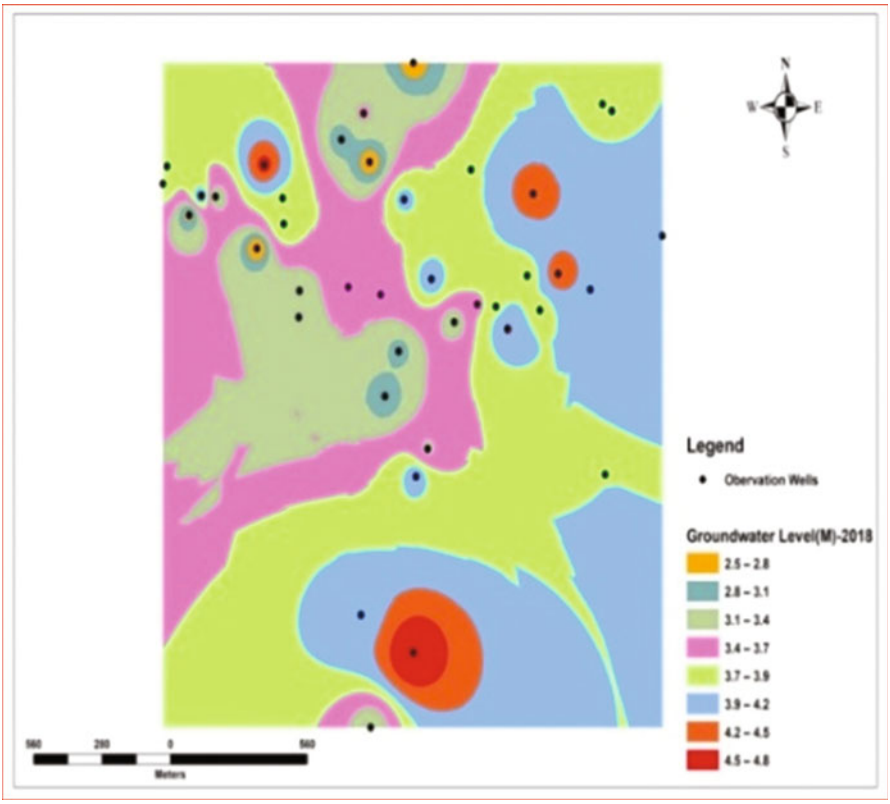

Fig. 26.15 Depth of groundwater levels, 2018

September. The CNB overflowed once and was dry in January, February, March, April, May, and June of 2018 and in February, March, April, and May of 2019.

Table 26.13 shows storage in CNB 9 in the period 2018–2019. The capacity of CNB 9 is 1716 m^3. The maximum rainfall was collected in July, August, and September. The CNB overflowed once and was dry in January, February, March, April, May, and June of 2018 and in February, March, April, and May of 2019.

Table 26.14 shows storage in CNB 10 in the period 2018–2019. The capacity of CNB 10 is 1680 m^3. The maximum rainfall was collected in July, August, and September. The CNB overflowed once and was dry in January, February, March, April, May, and June of 2018 and in February, March, April, and May of 2019.

Table 26.3 Groundwater Level Fluctuations, 2018 vs. 2017

Well no.	Average depth of water level (m), 2017	Average depth of water level (m), 2018	Depth of groundwater fluctuations (m), 2018 vs. 2017
1	4.9	3.87	1.03
2	3.2	2.66	0.54
3	5.2	4.15	1.05
4	3.5	3.08	0.42
5	4.8	4.58	0.22
6	5.9	3.92	1.98
7	2.2	3.96	−1.76
8	3.1	3.6	−0.5
9	4.1	3.38	0.72
10	3.2	3.2	0
11	4.2	3.17	1.03
12	2.5	2.48	0.02
13	2.8	2.92	−0.12
14	2.3	2.55	−0.25
15	8.3	3.4	4.9
16	4.2	4.02	0.18
17	4.3	4.13	0.17
18	2.7	3.08	−0.38
19	3.9	2.97	0.93
20	2.3	2.82	−0.52
21	3.2	3.33	−0.13
22	3.2	4.07	−0.87
23	4.4	4.13	0.27
24	6.3	4.78	1.52
25	3.4	3.17	0.23
26	4.1	3.59	0.51
27	4.3	3.92	0.38
28	4.9	4.25	0.65
29	3.7	3.83	−0.13
30	3.8	3.8	0
31	5.2	4.38	0.82
32	3.3	4.4	−1.1
33	3.1	3.95	−0.85
34	3.8	3.87	−0.07
35	8.2	2.66	5.54
Average	4.07	3.60	0.47

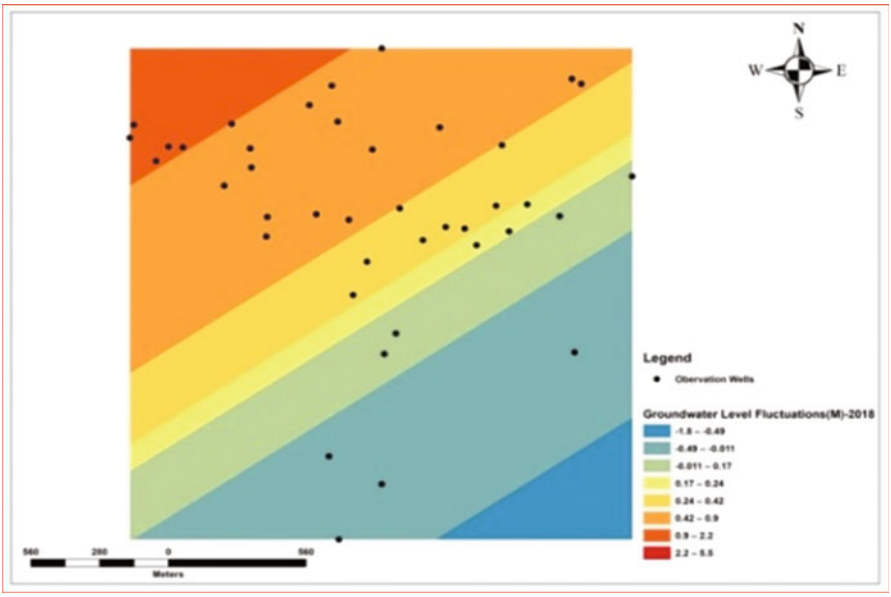

Fig. 26.16 Groundwater level fluctuations, 2018 vs. 2017

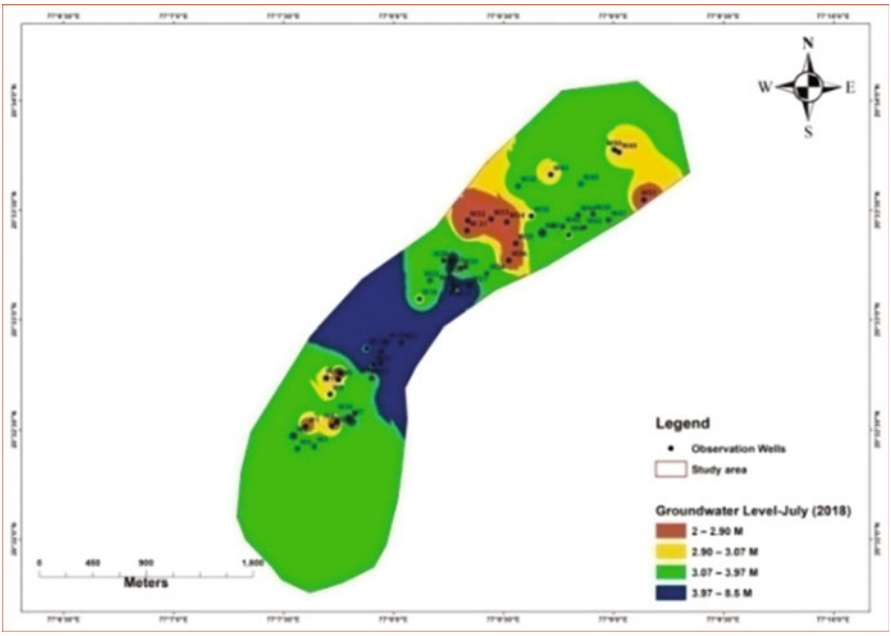

Fig. 26.17 Depth of groundwater levels, July

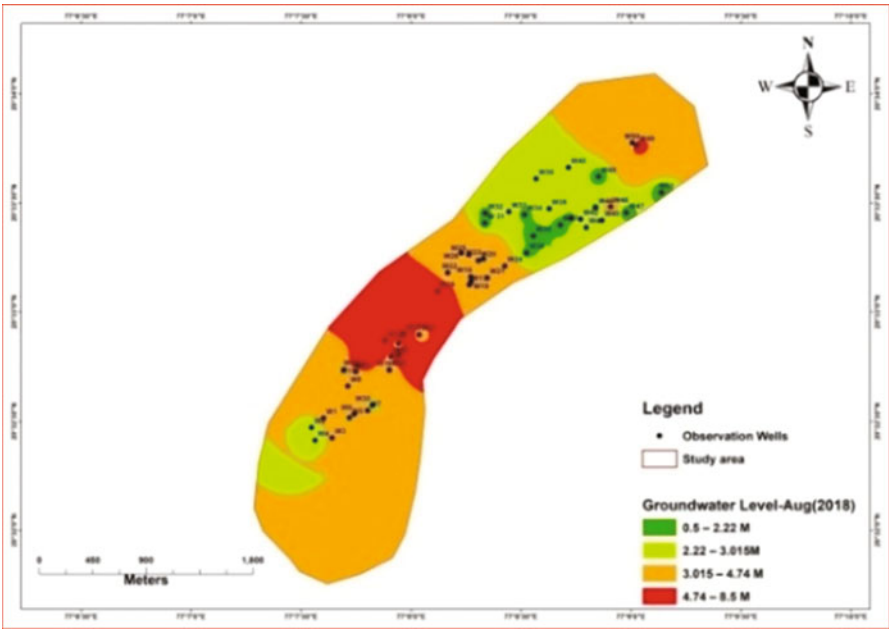

Fig. 26.18 Depth of groundwater levels, August

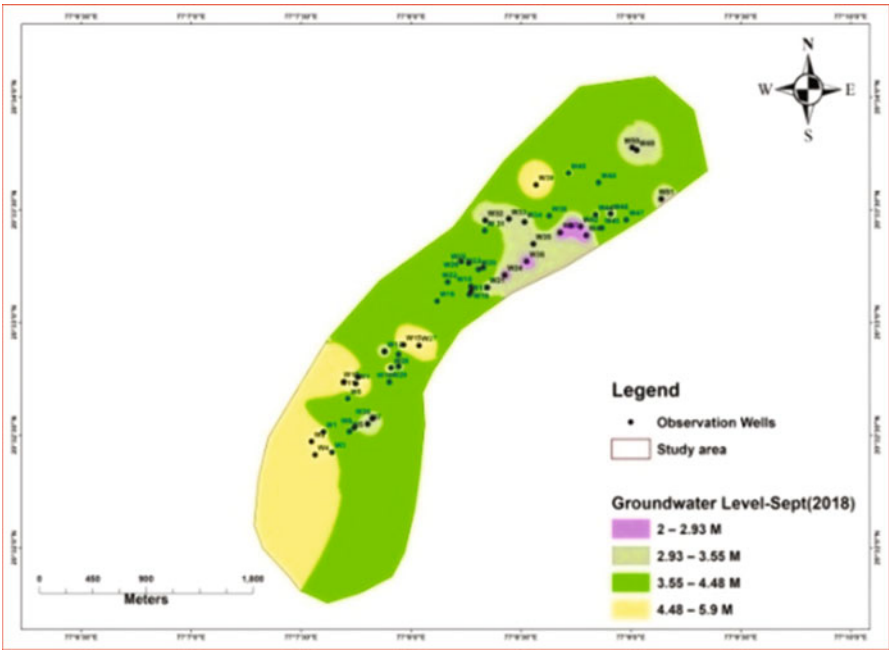

Fig. 26.19 Depth of groundwater levels, September

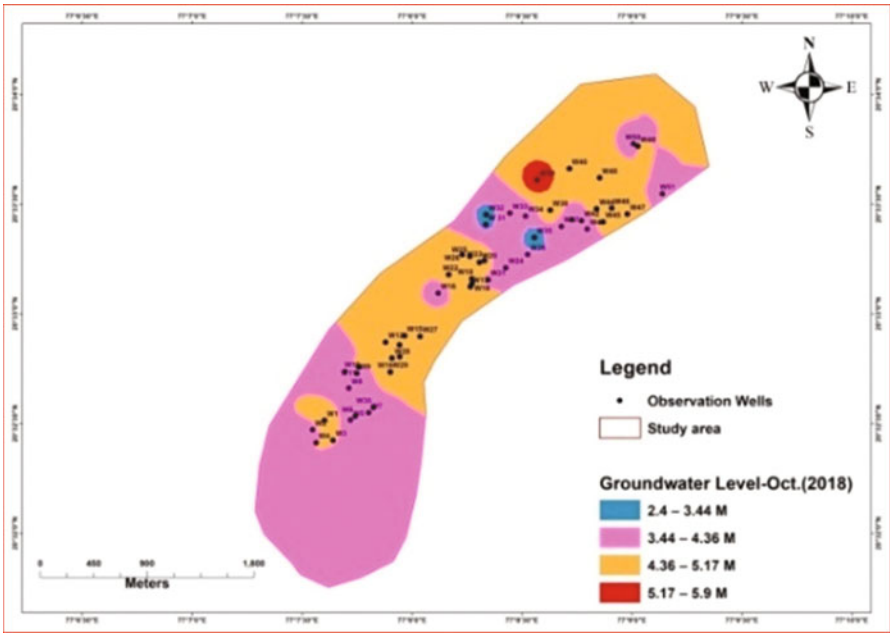

Fig. 26.20 Depth of groundwater levels, October

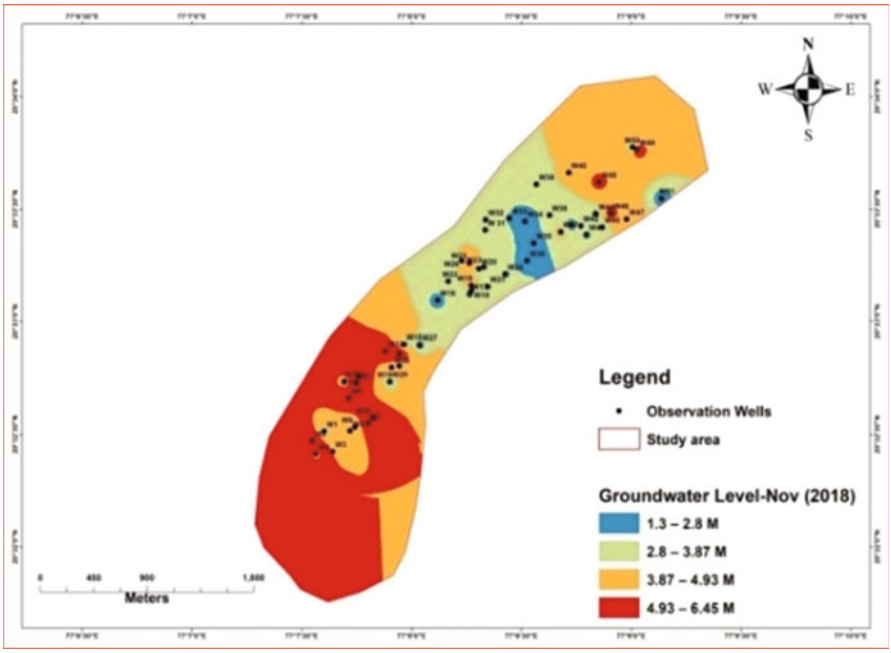

Fig. 26.21 Depth of groundwater levels, November

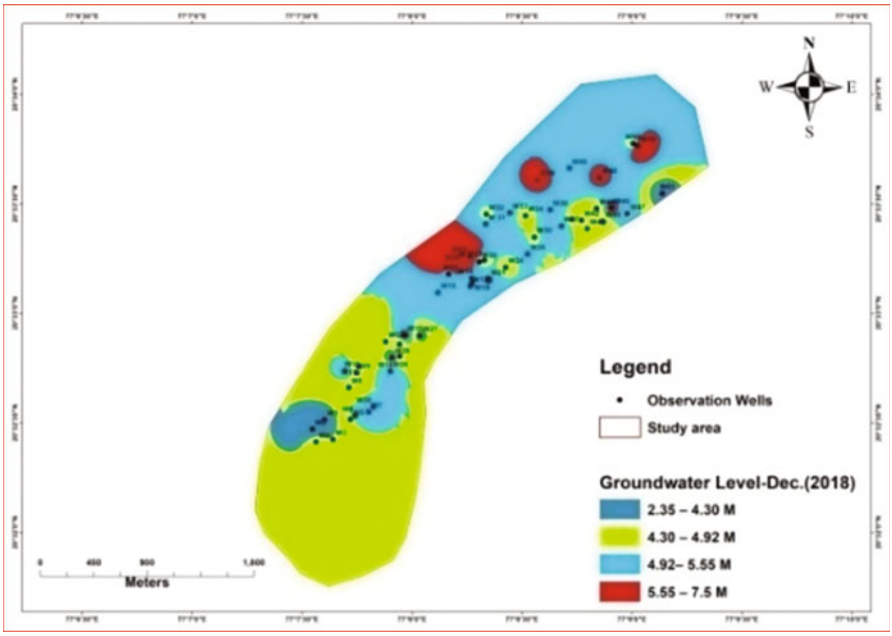

Fig. 26.22 Depth of groundwater levels, December

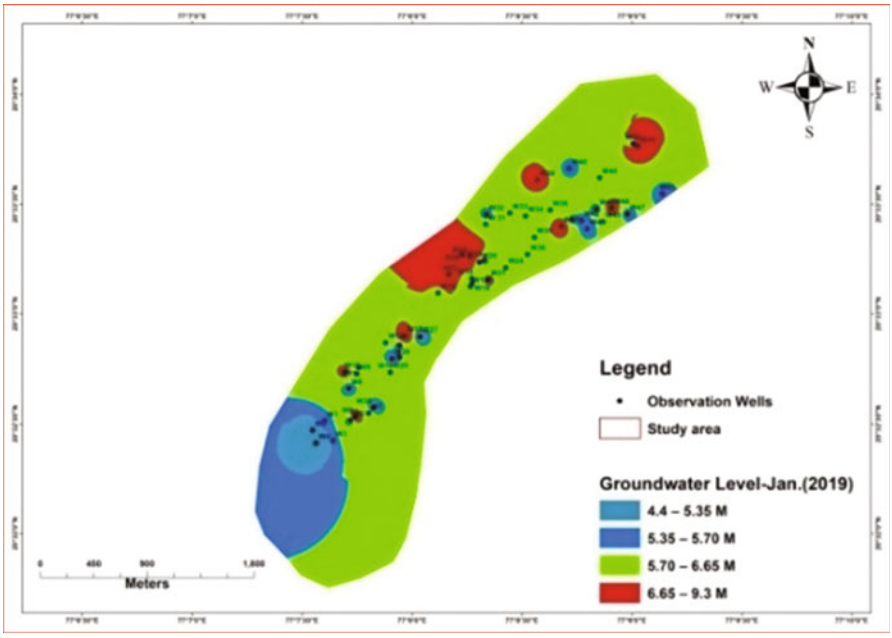

Fig. 26.23 Depth of groundwater levels, January 2019

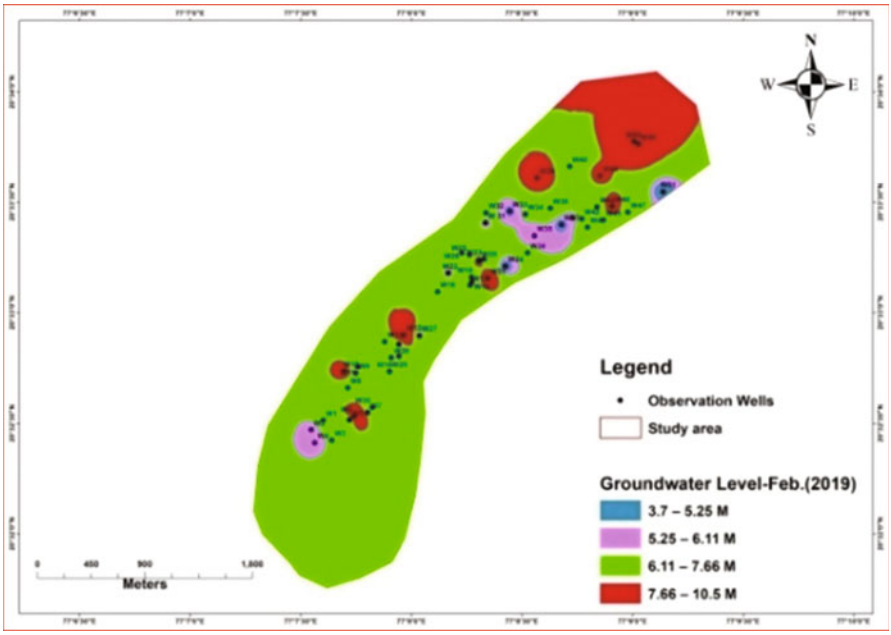

Fig. 26.24 Depth of groundwater levels, February 2019

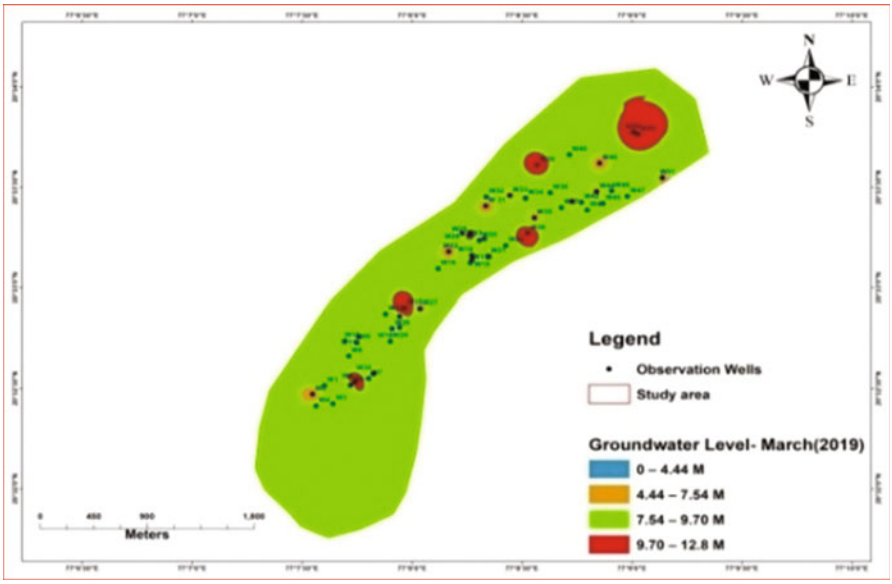

Fig. 26.25 Depth of groundwater levels, March 2019

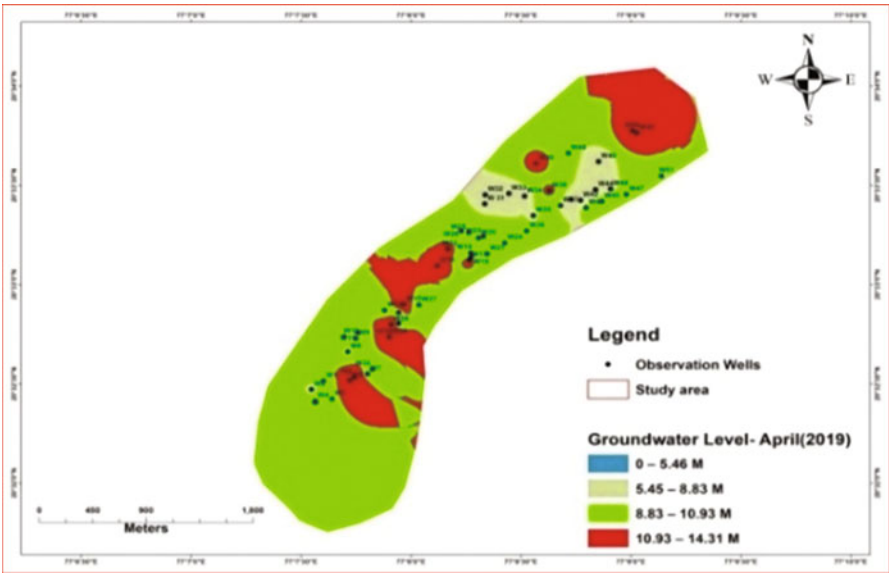

Fig. 26.26 Depth of groundwater levels, April 2019

Table 26.4 Storage capacity of CNB

CNB no.	Width (m)	Effective height (m)	Extent of water spread (m)	Effective storage capacity (m^3)
1	12	1.2	140	2016
2	12	1.33	124	1980
3	12	1.4	120	2016
4	12	1.3	123	1920
5	12	1.35	113	1831
6	12	1.35	113	1831
7	12	1.5	100	1800
8	12	1.4	115	1794
9	12	1.3	110	1716
10	12	1.4	100	1680

26.12 Groundwater Level Analysis, 2019–2020

Groundwater level data was collected from 51 observation wells in the vicinity of 10 CNBs for the analysis of rainwater harvesting's impact on the groundwater regime in the watershed area. In 2018 (51 wells) the average depth of the water level (Fig. 26.27) was 3.73 m and in 2019 (51wells) it (Fig. 26.28) was 2.81 (Table 26.15). Groundwater level fluctuations in 2019 vs. 2018 were observed.

Table 26.5 Monthly storage in CNB 1, 2018–2019

Monthwise duration	Rainfall (mm)	Initial water vol. (m^3)	Volume of rainwater stored (m^3)	Total vol. of water available during this period (m^3)	Water usage/ overflow/ losses (m^3)	Remarks
15/Jan/ 2018 to 15/Feb/ 2018	0	332.8	0	333	214	Usage, seepage, and other losses
16/Feb/ 2018 to 15/Mar/ 2018	0	119	0	119	85	Usage, seepage, and other losses
16/Mar/ 2018 to 15/Apr/ 2018	0	34	0	34	34	Seepage and other losses
16/Apr/ 2018 to 15/May/ 2018	0	0	0	0	0	Dry
16/May/ 2018 to 15/June/ 2018	0	0	0	0	0	Dry
16/June/ 2018 to 15/July/ 2018	338	0	1400	1400	215	Usage, seepage, and other losses
16/July/ 2018 to 15/Aug/ 2018	231	1186	1325	2511	495	Overflow
16/Aug/ 2018 to 15/Sept/ 2018	351	2016	1100	3116	1100	Overflow
16/Sept/ 2018 to 15/Oct/ 2018	43	2016	0	2016	714	Usage, seepage, and other losses
16/Oct/ 2018 to 15/Nov/ 2018	0	1302	0	1302	534	Usage
16/Nov/ 2018 to 15/Dec/ 2018	0	768	0	768	307	Usage

(continued)

Table 26.5 (continued)

Monthwise duration	Rainfall (mm)	Initial water vol. (m^3)	Volume of rainwater stored (m^3)	Total vol. of water available during this period (m^3)	Water usage/ overflow/ losses (m^3)	Remarks
16/Dec/ 2018 to 15/Jan/ 2019	0	461	0	461	268	Usage +losses
16/Jan/ 2019 to 15/Feb/ 2019	0	193	0	193	182	Seepage and other losses
16/Feb/ 2019 to 15/Mar/ 2019	0	11	0	11	11	Dry
16/Mar/ 2019 to 15/Apr/ 2019	0	0	0	0	0	Dry
16/Apr/ 2019 to 15/May/ 2019	60.1	0	300	300	0	Stormwater

Table 26.6 Monthly storage of CNB 2, 2018–2019

Monthwise duration	Rainfall (mm)	Initial water vol. (m^3)	Volume of rainwater stored (m^3)	Total vol. of water available during this period (m^3)	Water usage/ overflow/ losses (m^3)	Remarks
15/Jan/ 2018 to 15/Feb/ 2018	0	314	0	314	197	Usage, seepage, and other losses
16/Feb/ 2018 to 15/Mar/ 2018	0	117	0	117	91	Usage, seepage, and other losses
16/Mar/ 2018 to 15/Apr/ 2018	0	26	0	26	26	Seepage and other losses
16/Apr/ 2018 to 15/May/ 2018	0	0	0	0	0	Dry

(continued)

Table 26.6 (continued)

Monthwise duration	Rainfall (mm)	Initial water vol. (m^3)	Volume of rainwater stored (m^3)	Total vol. of water available during this period (m^3)	Water usage/ overflow/ losses (m^3)	Remarks
16/May/ 2018 to 15/June/ 2018	0	0	0	0	0	Dry
16/June/ 2018 to 15/July/ 2018	338	0	1420	1420	215	Usage, seepage, and other losses
16/July/ 2018 to 15/Aug/ 2018	231	1205	1300	2505	525	Overflow
16/Aug/ 2018 to 15/Sept/ 2018	351	1980	1085	3065	1085	Overflow
16/Sept/ 2018 to 15/Oct/ 2018	43	1980	0	1980	809	Usage, seepage, and other losses
16/Oct/ 2018 to 15/Nov/ 2018	0	1171	0	1171	603	Usage
16/Nov/ 2018 to 15/Dec/ 2018	0	568	0	568	315	Usage
16/Dec/ 2018 to 15/Jan/ 2019	0	253	0	253	125	Usage + losses
16/Jan/ 2019 to 15/Feb/ 2019	0	128	0	128	44	Seepage and other losses
16/Feb/ 2019 to 15/Mar/ 2019	0	84	0	84	84	Dry

(continued)

Table 26.6 (continued)

Monthwise duration	Rainfall (mm)	Initial water vol. (m^3)	Volume of rainwater stored (m^3)	Total vol. of water available during this period (m^3)	Water usage/ overflow/ losses (m^3)	Remarks
16/Mar/ 2019 to 15/Apr/ 2019	0	0	0	0	0	Dry
16/Apr/ 2019 to 15/May/ 2019	60.1	0	220	220	0	Stormwater

Table 26.7 Monthly storage of CNB 3, 2018–2019

Monthwise duration	Rainfall (mm)	Initial water vol. (m^3)	Volume of rainwater stored (m^3)	Total vol. of water available during this period (m^3)	Water usage/ overflow/ losses (m^3)	Remarks
15/Jan/ 2018 to 15/Feb/ 2018	0	303	0	303	184	Usage, seepage, and other losses
16/Feb/ 2018 to 15/Mar/ 2018	0	119	0	119	79	Usage, seepage, and other losses
16/Mar/ 2018 to 15/Apr/ 2018	0	40	0	40	40	Seepage and other losses
16/Apr/ 2018 to 15/May/ 2018	0	0	0	0	0	Dry
16/May/ 2018 to 15/June/ 2018	0	0	0	0	0	Dry
16/June/ 2018 to 15/July/ 2018	338	0	1450	1450	208	Usage, seepage, and other losses
16/July/ 2018 to 15/Aug/ 2018	231	1242	1329	2571	555	Overflow

(continued)

Table 26.7 (continued)

Monthwise duration	Rainfall (mm)	Initial water vol. (m^3)	Volume of rainwater stored (m^3)	Total vol. of water available during this period (m^3)	Water usage/ overflow/ losses (m^3)	Remarks
16/Aug/ 2018 to 15/Sept/ 2018	351	2016	1065	3081	1065	Overflow
16/Sept/ 2018 to 15/Oct/ 2018	43	2016	0	2016	725	Usage, seepage, and other losses
16/Oct/ 2018 to 15/Nov/ 2018	0	1291	0	1291	586	Usage
16/Nov/ 2018 to 15/Dec/ 2018	0	705	0	705	324	Usage
16/Dec/ 2018 to 15/Jan/ 2019	0	381	0	381	274	Usage + losses
16/Jan/ 2019 to 15/Feb/ 2019	0	107	0	107	103	Seepage and other losses
16/Feb/ 2019 to 15/Mar/ 2019	0	4	0	4	4	Dry
16/Mar/ 2019 to 15/Apr/ 2019	0	0	0	0	0	Dry
16/Apr/ 2019 to 15/May/ 2019	60.1	0	190	190	0	Stormwater

Table 26.8 Monthly storage of CNB 4, 2018–2019

Month wise duration	Rainfall (mm)	Initial water vol. (m^3)	Volume of rainwater stored (m^3)	Total vol. of water available during this period (m^3)	Water usage/ overflow/ losses (m^3)	Remarks
15/Jan/ 2018 to 15/Feb/ 2018	0	290	0	290	170	Usage, seepage, and other losses
16/Feb/ 2018 to 15/Mar/ 2018	0	120	0	120	120	Usage, seepage, and other losses
16/Mar/ 2018 to 15/Apr/ 2018	0	0	0	0	0	Dry
16/Apr/ 2018 to 15/May/ 2018	0	0	0	0	0	Dry
16/May/ 2018 to 15/June/ 2018	0	0	0	0	0	Dry
16/June/ 2018 to 15/July/ 2018	338	0	1436	1436	554	Usage, seepage, and other losses
16/July/ 2018 to 15/Aug/ 2018	231	882	1190	2072	845	Overflow
16/Aug/ 2018 to 15/Sept/ 2018	351	1227	992	2219	784	Overflow
16/Sept/ 2018 to 15/Oct/ 2018	43	1435	0	1435	601	Usage, seepage, and other losses
16/Oct/ 2018 to 15/Nov/ 2018	0	834	0	834	253	Usage
16/Nov/ 2018 to 15/Dec/ 2018	0	581	0	581	201	Usage

(continued)

Table 26.8 (continued)

Month wise duration	Rainfall (mm)	Initial water vol. (m^3)	Volume of rainwater stored (m^3)	Total vol. of water available during this period (m^3)	Water usage/ overflow/ losses (m^3)	Remarks
16/Dec/ 2018 to 15/Jan/ 2019	0	380	0	380	196	Usage, losses
16/Jan/ 2019 to 15/Feb/ 2019	0	184	0	184	184	Seepage and other Losses
16/Feb/ 2019 to 15/Mar/ 2019	0	0	0	0	0	Dry
16/Mar/ 2019 to 15/Apr/ 2019	0	0	0	0	0	Dry
16/Apr/ 2019 to 15/May/ 2019	60.1	0	160	160	0	Stormwater

Table 26.9 Monthly storage of CNB 5, 2018–2019

Monthwise duration	Rainfall (mm)	Initial water vol. (m^3)	Volume of rainwater stored (m^3)	Total vol. of water available during this period (m^3)	Water usage/ overflow/ losses (m^3)	Remarks
15/Jan/ 2018 to 15/Feb/ 2018	0	0	0	0	0	Dry
16/Feb/ 2018 to 15/Mar/ 2018	0	0	0	0	0	Dry
16/Mar/ 2018 to 15/Apr/ 2018	0	0	0	0	0	Dry
16/Apr/ 2018 to 15/May/ 2018	0	0	0	0	0	Dry

(continued)

Table 26.9 (continued)

Monthwise duration	Rainfall (mm)	Initial water vol. (m^3)	Volume of rainwater stored (m^3)	Total vol. of water available during this period (m^3)	Water usage/ overflow/ losses (m^3)	Remarks
16/May/ 2018 to 15/June/ 2018	0	0	0	0	0	Dry
16/June/ 2018 to 15/July/ 2018	338	0	1350	1350	204	Usage, seepage, and other losses
16/July/ 2018 to 15/Aug/ 2018	231	1146	1000	2146	321	Usage, seepage, and other losses
16/Aug/ 2018 to 15/Sept/ 2018	351	1825	1045	2870	1067	overflow
16/Sept/ 2018 to 15/Oct/ 2018	43	1803	0	1803	719	Usage, seepage, and other losses
16/Oct/ 2018 to 15/Nov/ 2018	0	1084	0	1084	559	Usage
16/Nov/ 2018 to 15/Dec/ 2018	0	525	0	525	315	Usage
16/Dec/ 2018 to 15/Jan/ 2019	0	210	0	210	150	Usage + losses
16/Jan/ 2019 to 15/Feb/ 2019	0	60	0	60	60	Seepage and other losses
16/Feb/ 2019 to 15/Mar/ 2019	0	0	0	0	0	Dry

(continued)

Table 26.9 (continued)

Monthwise duration	Rainfall (mm)	Initial water vol. (m^3)	Volume of rainwater stored (m^3)	Total vol. of water available during this period (m^3)	Water usage/ overflow/ losses (m^3)	Remarks
16/Mar/ 2019 to 15/Apr/ 2019	0	0	0	0	0	Dry
16/Apr/ 2019 to 15/May/ 2019	60.1	0	0	0	0	Dry

Table 26.10 Monthly storage of CNB 6, 2018–2019

Monthwise duration	Rainfall (mm)	Initial water vol. (m^3)	Volume of rainwater stored (m^3)	Total vol. of water available during this period (m^3)	Water usage/ overflow/ losses (m^3)	Remarks
15/Jan/ 2018 to 15/Feb/ 2018	0	0	0	0	0	Dry
16/Feb/ 2018 to 15/Mar/ 2018	0	0	0	0	0	Dry
16/Mar/ 2018 to 15/Apr/ 2018	0	0	0	0	0	Dry
16/Apr/ 2018 to 15/May/ 2018	0	0	0	0	0	Dry
16/May/ 2018 to 15/June/ 2018	0	0	0	0	0	Dry
16/June/ 2018 to 15/July/ 2018	338	0	1275	1275	203	Usage, seepage, and other losses
16/July/ 2018 to 15/Aug/ 2018	231	1072	1036	2108	311	Usage, seepage, and other losses

(continued)

Table 26.10 (continued)

Monthwise duration	Rainfall (mm)	Initial water vol. (m^3)	Volume of rainwater stored (m^3)	Total vol. of water available during this period (m^3)	Water usage/ overflow/ losses (m^3)	Remarks
16/Aug/ 2018 to 15/Sept/ 2018	351	1797	1040	2837	1086	Overflow
16/Sept/ 2018 to 15/Oct/ 2018	43	1751	0	1751	752	Usage, seepage, and other losses
16/Oct/ 2018 to 15/Nov/ 2018	0	999	0	999	576	Usage
16/Nov/ 2018 to 15/Dec/ 2018	0	423	0	423	323	Usage
16/Dec/ 2018 to 15/Jan/ 2019	0	100	0	100	80	Usage + losses
16/Jan/ 2019 to 15/Feb/ 2019	0	20	0	20	20	Seepage and other losses
16/Feb/ 2019 to 15/Mar/ 2019	0	0	0	0	0	Dry
16/Mar/ 2019 to 15/Apr/ 2019	0	0	0	0	0	Dry
16/Apr/ 2019 to 15/May/ 2019	60.1	0	0	0	0	Dry

Table 26.11 Monthly storage of CNB 7, 2018–2019

Monthwise duration	Rainfall (mm)	Initial water vol. (m^3)	Volume of rainwater stored (m^3)	Total vol. of water available during this period (m^3)	Water usage/ overflow/ losses (m^3)	Remarks
15/Jan/ 2018 to 15/Feb/ 2018	0	0	0	0	0	Dry
16/Feb/ 2018 to 15/Mar/ 2018	0	0	0	0	0	Dry
16/Mar/ 2018 to 15/Apr/ 2018	0	0	0	0	0	Dry
16/Apr/ 2018 to 15/May/ 2018	0	0	0	0	0	Dry
16/May/ 2018 to 15/June/ 2018	0	0	0	0	0	Dry
16/June/ 2018 to 15/July/ 2018	338	0	625	625	150	Usage, seepage, and other losses
16/July/ 2018 to 15/Aug/ 2018	231	475	523	998	359	Overflow
16/Aug/ 2018 to 15/Sept/ 2018	351	639	496	1135	629	Overflow
16/Sept/ 2018 to 15/Oct/ 2018	43	506	0	506	403	Usage, seepage, and other losses
16/Oct/ 2018 to 15/Nov/ 2018	0	103	0	103	85	Usage
16/Nov/ 2018 to 15/Dec/ 2018	0	18	0	18	18	Usage + losses

(continued)

Table 26.11 (continued)

Monthwise duration	Rainfall (mm)	Initial water vol. (m^3)	Volume of rainwater stored (m^3)	Total vol. of water available during this period (m^3)	Water usage/ overflow/ losses (m^3)	Remarks
16/Dec/ 2018 to 15/Jan/ 2019	0	0	0	0	0	Dry
16/Jan/ 2019 to 15/Feb/ 2019	0	0	0	0	0	Dry
16/Feb/ 2019 to 15/Mar/ 2019	0	0	0	0	0	Dry
16/Mar/ 2019 to 15/Apr/ 2019	0	0	0	0	0	Dry
16/Apr/ 2019 to 15/May/ 2019	60.1	0	0	0	0	Dry

Table 26.12 Monthly storage of CNB 8, 2018–2019

Month wise duration	Rainfall (mm)	Initial water vol. (m^3)	Volume of rainwater stored (m^3)	Total vol. of water available during this period (m^3)	Water usage/ overflow/ losses (m^3)	Remarks
15/Jan/ 2018 to 15/Feb/ 2018	0	0	0	0	0	Dry
16/Feb/ 2018 to 15/Mar/ 2018	0	0	0	0	0	Dry
16/Mar/ 2018 to 15/Apr/ 2018	0	0	0	0	0	Dry
16/Apr/ 2018 to 15/May/ 2018	0	0	0	0	0	Dry

(continued)

Table 26.12 (continued)

Month wise duration	Rainfall (mm)	Initial water vol. (m^3)	Volume of rainwater stored (m^3)	Total vol. of water available during this period (m^3)	Water usage/ overflow/ losses (m^3)	Remarks
16/May/ 2018 to 15/June/ 2018	0	0	0	0	0	Dry
16/June/ 2018 to 15/July/ 2018	338	0	1036	1036	198	Usage, seepage, and other losses
16/July/ 2018 to 15/Aug/ 2018	231	838	839	1677	420	Usage, seepage, and other losses
16/Aug/ 2018 to 15/Sept/ 2018	351	1257	1030	2287	1027	Overflow
16/Sept/ 2018 to 15/Oct/ 2018	43	1260	0	1260	668	Usage, seepage, and other losses
16/Oct/ 2018 to 15/Nov/ 2018	0	592	0	592	416	Usage
16/Nov/ 2018 to 15/Dec/ 2018	0	176	0	176	101	Usage
16/Dec/ 2018 to 15/Jan/ 2019	0	75	0	75	64	Usage + losses
16/Jan/ 2019 to 15/Feb/ 2019	0	11	0	11	11	Seepage and other losses
16/Feb/ 2019 to 15/Mar/ 2019	0	0	0	0	0	Dry

(continued)

Table 26.12 (continued)

Month wise duration	Rainfall (mm)	Initial water vol. (m^3)	Volume of rainwater stored (m^3)	Total vol. of water available during this period (m^3)	Water usage/ overflow/ losses (m^3)	Remarks
16/Mar/ 2019 to 15/Apr/ 2019	0	0	0	0	0	Dry
16/Apr/ 2019 to 15/May/ 2019	60.1	0	0	0	0	Dry

Table 26.13 Monthly storage of CNB9, 2018–2019

Month wise duration	Rainfall (mm)	Initial water vol. (m^3)	Volume of rainwater stored (m^3)	Total vol. of water available during this period (m^3)	Water usage/ overflow/ losses (m^3)	Remarks
15/Jan/ 2018 to 15/Feb/ 2018	0	0	0	0	0	Dry
16/Feb/ 2018 to 15/Mar/ 2018	0	0	0	0	0	Dry
16/Mar/ 2018 to 15/Apr/ 2018	0	0	0	0	0	Dry
16/Apr/ 2018 to 15/May/ 2018	0	0	0	0	0	Dry
16/May/ 2018 to 15/June/ 2018	0	0	0	0	0	Dry
16/June/ 2018 to 15/July/ 2018	338	0	910	910	199	Usage, seepage, and other losses
16/July/ 2018 to 15/Aug/ 2018	231	711	618	1329	354	Usage, seepage, and other losses

(continued)

Table 26.13 (continued)

Month wise duration	Rainfall (mm)	Initial water vol. (m^3)	Volume of rainwater stored (m^3)	Total vol. of water available during this period (m^3)	Water usage/ overflow/ losses (m^3)	Remarks
16/Aug/ 2018 to 15/Sept/ 2018	351	975	1020	1995	818	overflow
16/Sept/ 2018 to 15/Oct/ 2018	43	1177	0	1177	662	Usage, seepage, and other losses
16/Oct/ 2018 to 15/Nov/ 2018	0	515	0	515	310	Usage
16/Nov/ 2018 to 15/Dec/ 2018	0	205	0	205	106	Usage
16/Dec/ 2018 to 15/Jan/ 2019	0	99	0	99	63	Usage + losses
16/Jan/ 2019 to 15/Feb/ 2019	0	36	0	36	36	Seepage and other losses
16/Feb/ 2019 to 15/Mar/ 2019	0	0	0	0	0	Dry
16/Mar/ 2019 to 15/Apr/ 2019	0	0	0	0	0	Dry
16/Apr/ 2019 to 15/May/ 2019	60.1	0	0	0	0	Dry

Table 26.14 Monthly storage of CNB 10, 2018–2019

Month wise duration	Rainfall (mm)	Initial water vol. (m^3)	Volume of rainwater stored (m^3)	Total vol. of water available during this period (m^3)	Water usage/ overflow/ losses (m^3)	Remarks
15/Jan/ 2018 to 15/Feb/ 2018	0	0	0	0	0	Dry
16/Feb/ 2018 to 15/Mar/ 2018	0	0	0	0	0	Dry
16/Mar/ 2018 to15/Apr/ 2018	0	0	0	0	0	Dry
16/Apr/ 2018 to 15/May/ 2018	0	0	0	0	0	Dry
16/May/ 2018 to 15/June/ 2018	0	0	0	0	0	Dry
16/June/ 2018 to 15/July/ 2018	338	0	892	892	195	Usage, seepage, and other losses
16/July/ 2018 to 15/Aug/ 2018	231	697	606	1303	347	Usage, seepage, and other losses
16/Aug/ 2018 to 15/Sept/ 2018	351	956	1000	1956	802	Overflow
16/Sept/ 2018 to 15/Oct/ 2018	43	1154	0	1154	649	Usage, seepage, and other losses
16/Oct/ 2018 to 15/Nov/ 2018	0	505	0	505	304	Usage
16/Nov/ 2018 to 15/Dec/ 2018	0	201	0	201	98	Usage

(continued)

Table 26.14 (continued)

Month wise duration	Rainfall (mm)	Initial water vol. (m^3)	Volume of rainwater stored (m^3)	Total vol. of water available during this period (m^3)	Water usage/ overflow/ losses (m^3)	Remarks
16/Dec/ 2018 to 15/Jan/ 2019	0	103	0	103	62	Usage + losses
16/Jan/ 2019 to 15/Feb/ 2019	0	41	0	41	41	Seepage and other losses
16/Feb/ 2019 to 15/Mar/ 2019	0	0	0	0	0	Dry
16/Mar/ 2019 to 15/Apr/ 2019	0	0	0	0	0	Dry
16/Apr/ 2019 to 15/May/ 2019	60.1	0	0	0	0	Dry

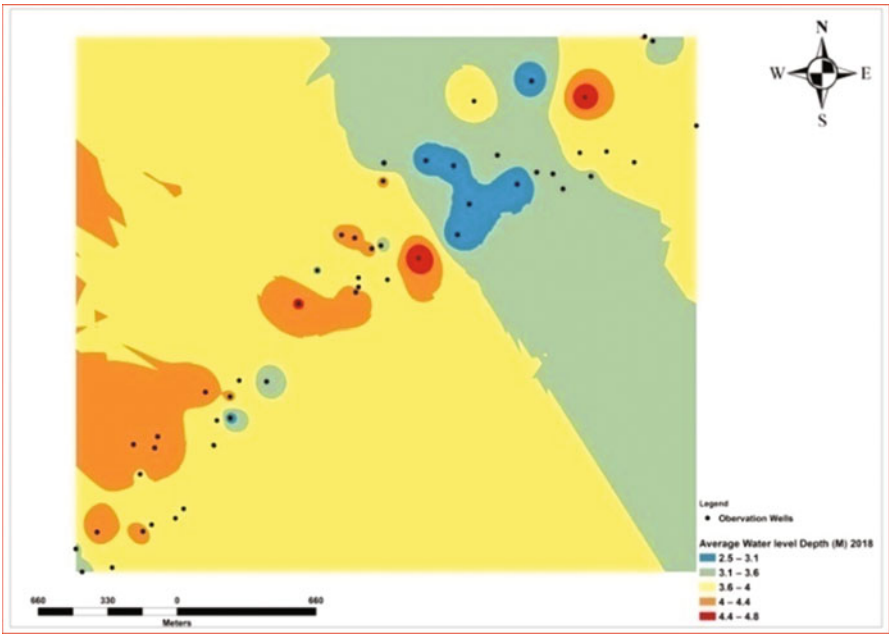

Fig. 26.27 Average depth of water level (m), 2018

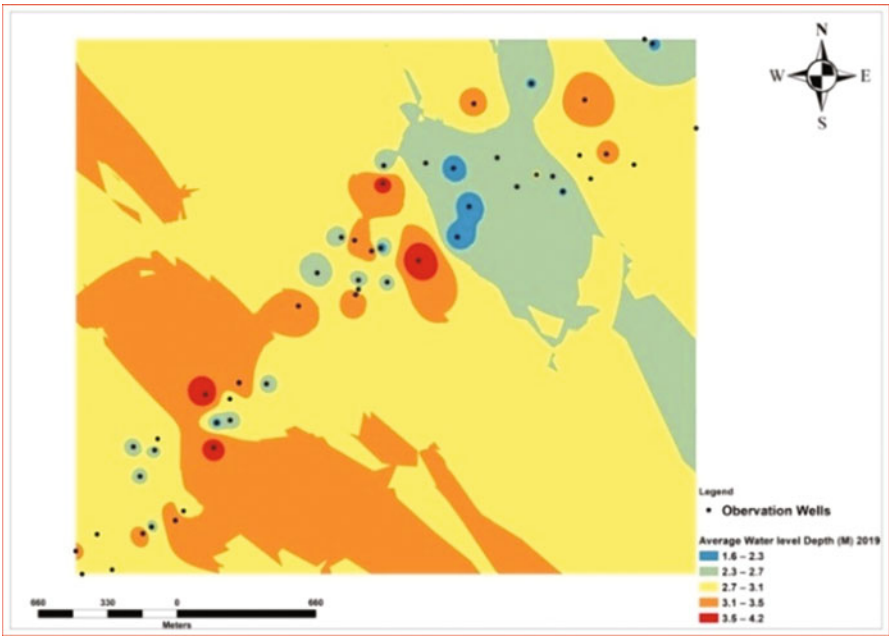

Fig. 26.28 Average depth of water level (m), 2019

Well water levels were observed to increase in 2019 vs. 2018 in the largest wells. The average depth in the wells in 2019 increased by 0.92 m with respect to 2018 levels and by 3.44 m compared to 2016 levels (Table 26.16 and Fig. 26.29).

The yearly increase in average well water depth compared to the project implementation year are given in Table 26.17. The well water levels increased by 2.18, 2.52, and 3.44 m respectively in 2017, 2018, and 2019 vs. 2016.

26.13 Conclusion

Nala widening and deepening was carried out on an existing 500 m drainage line which originates in Kajaleshwar and runs toward Warkhed village, Barshitakli Taluka, Akola District. Existing rainwater harvesting structures (CNB) constructed on the drainage line were repaired, the monthly water level in the wells coming in the vicinity of 10 CNBs was monitored using a water level indicator, and monthly well water level maps were prepared in ArcGIS 10.1 by IDW interpolation. It was observed that the average well water levels of the monitored wells increased by 2.18, 2.52, and 3.44 m respectively in 2017, 2018, and 2019 over the initial year, 2016. Farmers use the stored water in the kharif season to cope with stressed conditions and in the rabi season it was used for protective irrigation at the pod initiation stage and pod development stage on chickpeas, wheat, and other crops.

Table 26.15 Groundwater level fluctuations in 2019 vs. 2018

Well no.	Average depth of water level (m), 2018	Average depth of water level (m), 2019	Fluctuations in depth (m), 2019 vs. 2018
1	3.87	2.90	0.97
2	2.66	2.23	0.43
3	4.15	2.63	1.52
4	3.08	2.13	0.95
5	4.58	3.47	1.11
6	3.92	3.14	0.78
7	3.96	3.07	0.89
8	3.6	2.96	0.64
9	3.38	2.21	1.17
10	3.2	2.53	0.67
11	3.17	2.75	0.42
12	2.48	1.76	0.72
13	2.92	2.04	0.88
14	2.55	2.26	0.29
15	3.4	2.57	0.83
16	4.02	3.21	0.81
17	4.13	3.73	0.4
18	3.08	2.40	0.68
19	2.97	2.02	0.95
20	2.82	2.29	0.53
21	3.33	2.54	0.79
22	4.07	2.22	1.85
23	4.13	3.53	0.6
24	4.78	4.16	0.62
25	3.17	1.63	1.54
26	3.59	2.24	1.35
27	3.92	2.54	1.38
28	4.25	3.43	0.82
29	3.83	2.63	1.2
30	3.8	2.30	1.5
31	4.38	3.54	0.84
32	4.4	3.29	1.11
33	3.95	3.66	0.29
34	3.87	3.55	0.32
35	2.66	2.39	0.27
36	4.12	2.73	1.39
37	4.32	3.98	0.34
38	4.31	2.90	1.41
39	4.26	2.66	1.6
40	4.2	2.63	1.57
41	4.03	2.66	1.37
42	4.04	3.50	0.54

(continued)

Table 26.15 (continued)

Well no.	Average depth of water level (m), 2018	Average depth of water level (m), 2019	Fluctuations in depth (m), 2019 vs. 2018
43	3.85	2.43	1.42
44	4.16	3.26	0.9
45	3.42	3.00	0.42
46	3.57	3.12	0.45
47	4.26	2.75	1.51
48	3.95	2.00	1.95
49	3.68	2.90	0.78
50	4.02	3.70	0.32
51	3.84	2.94	0.9
Average	3.73	2.81	0.92

Table 26.16 Yearly average depths of water levels in wells (m)

Average depth of water levels in wells (m), 2016	Average depth of water levels in wells (m), 2017	Average depth of water levels in wells (m), 2018	Average depth of water levels in wells (m), 2019
6.25	4.07	3.73	2.81

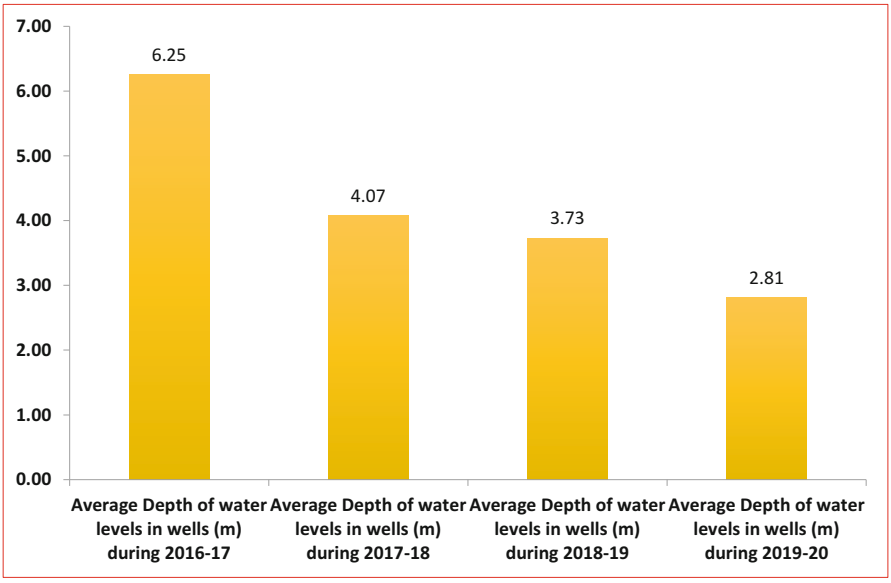

Fig. 26.29 Yearly average depth of water levels in wells (m)

Previously, an area of only 8 ha was irrigated during the rabi season, but now, thanks to the CNB water, this area has increased to 42.6 ha. Similarly, earlier an area of only 105 ha was irrigated using well water, but this has increased to 211 ha.

Table 26.17 Yearly increase in average water levels in wells, 2016–2017 (initial year)

Increase over 2016 (m)		
2017	2018	2019
2.18 m	2.52 m	3.44 m

References

Al-Adamat, R. A., Foster, I. D., & Baban, S. M. (2003). Groundwater vulnerability and risk mapping for the Basaltic aquifer of the Azraq basin of Jordan using GIS, remote sensing and DRASTIC. *Applied Geography, 23*(4), 303–324.

Ali, H. Y., Priju, C. P., & Prasad, N. N. (2015). Delineation of groundwater potential zones in deep midland aquifers along Bharathapuzha river basin, Kerala using geophysical methods. *Aquatic Procedia, 4*, 1039–1046.

Chowdhury, A., Jha, M. K., & Chowdary, V. M. (2010). Delineation of groundwater recharge zones and identification of artificial recharge sites in West Medinipur District, West Bengal using RS, GIS, and MCDM techniques. *Environmental Earth Sciences, 59*(6), 1209–1222.

Elbeih, S. F. (2015). An overview of integrated remote sensing and GIS for groundwater mapping in Egypt. *Ain Shams Engineering Journal, 6*(1), 1–15.

Golla, V., Etikala, B., Veeranjaneyulu, A., Subbarao, M., Surekha, A., & Narasimhlu, K. (2018). Data sets on delineation of groundwater potential zones identified by geospatial tool in Gudur area, Nellore district, Andhra Pradesh, India. *Data in Brief, 20*, 1984–1991.

Jaiswal, R. K., Mukherjee, S., Krishnamurthy, J., & Saxena, R. (2003). Role of remote sensing and GIS techniques for generation of groundwater prospect zones towards rural development–An approach. *International Journal of Remote Sensing, 24*(5), 993–1008.

Jha, M. K., & Chowdary, V. M. (2007). Challenges of using remote sensing and GIS in developing nations. *Hydrogeology Journal, 15*(1), 197–200.

Jha, M. K., Chowdary, V. M., & Chowdhury, A. (2010). *Groundwater assessment in Salboni Block, West Bengal (India) using remote sensing, geographical information system, and multi-criteria decision analysis techniques*. New York, NY: Springer.

Jha, M. K., Chowdhury, A., Chowdary, V. M., & Peiffer, S. (2007). Groundwater management and development by integrated remote sensing and geographic information systems: Prospects and constraints. *Water Resources Management, 21*(2), 427–467.

Jha, M. K., & Peiffer, S. (2006). *Applications of remote sensing and GIS technologies in groundwater hydrology: Past, present, and future*. Bayreuth: BayCEER.

Khadri, S. F. R., & Pande, C. (2016). Ground water flow modeling for calibrating steady state using MODFLOW software: A case study of Mahesh River basin, India. *Model Earth System Environment, 2*, 39. https://doi.org/10.1007/s40808-015-0049-7.

Krishnamurthy, J., Kumar, N. V., Jayaraman, V., & Manivel, M. (1996). An approach to demarcate groundwater potential zones through remote sensing and a geographic information system. *International Journal of Remote Sensing, 17*(10), 1867–1884.

Moharir, K. N., Pande, C. B., Singh, S. K., & Del Rio, R. A. (2020). Evaluation of analytical methods to study aquifer properties with pumping test in Deccan Basalt Region of the Morna River Basin in Akola District of Maharashtra in India. *Groundwater Hydrology*. https://doi.org/10.5772/intechopen.84632.

Moharir, K., Pande, C., & Patil, S. (2017). Inverse modeling of Aquifer parameters in basaltic rock with the help of pumping test method using MODFLOW software. *Geoscience Frontiers, 8*(6), 1385–1395.

Pande, C. B. (2020a). Introduction. In *Sustainable watershed development. Springer briefs in water science and technology*. Cham: Springer. https://doi.org/10.1007/978-3-030-47244-3_1.

Pande, C. B. (2020b). Watershed management and development. In *Sustainable watershed development. Springer briefs in water science and technology*. Cham: Springer. https://doi.org/10.1007/978-3-030-47244-3_2.

Pande, C. B. (2020c). Thematic mapping for watershed development. In *Sustainable watershed development. Springer briefs in water science and technology*. Cham: Springer. https://doi.org/10.1007/978-3-030-47244-3_3.

Pande, C. B. (2020d). Sustainable watershed development planning. In *Sustainable watershed development. Springer briefs in water science and technology*. Cham: Springer. https://doi.org/10.1007/978-3-030-47244-3_4.

Pande, C. B., Khadri, S. F. R., Moharir, K. N., & Patode, R. S. (2017). Assessment of groundwater potential zonation of Mahesh River basin Akola and Buldhana districts, Maharashtra, India using remote sensing and GIS techniques. *Sustainable Water Resources Management*. https://doi.org/10.1007/s40899-017-0193-5.

Pande, C. B., & Moharir, K. (2015). GIS-based quantitative morphometric analysis and its consequences: A case study from Shanur River Basin, Maharashtra India. *Applied Water Science, 7*(2), 861–871.

Pande, C. B., Moharir, K. N., Singh, S. K., & Varade, A. M. (2019). An integrated approach to delineate the groundwater potential zones in Devdari watershed area of Akola district, Maharashtra, Central India. *Environment, Development, and Sustainability*. https://doi.org/10.1007/s10668-019-00409-1.

Pande, C. B., Moharir, K. N., & Pande, R. (2018). Assessment of morphometric and hypsometric study for watershed development using spatial technology – A case study of Wardha river basin in the Maharashtra, India. *International Journal of River Basin Management*. https://doi.org/10.1080/15715124.2018.1505737.

Patode, R. S., Pande, C. B., Nagdeve, M. B., Moharir, K. N., & Wankhade, R. M. (2017). Planning of conservation measures for watershed management and development by using geospatial technology – A case study of Patur Watershed in Akola District of Maharashtra. *Current World Environment, 12*(3), 2017.

Saraf, A. K., & Choudhury, P. R. (1998). Integrated remote sensing and GIS for groundwater exploration and identification of artificial recharge sites. *International Journal of Remote Sensing, 19*(10), 1825–1841.

Sharma R.K. (2010). *Rainwater harvesting at National Institute of Technology, Rourkela*. Bachelor of Technology in Civil Engineering thesis, 14.

Solomon, S., & Quiel, F. (2006). *Groundwater study using remote sensing and geographic information systems (GIS) in central highlands of Eritrea*. New York, NY: Springer.

Srinivasa Rao, Y., & Jugran, D. K. (2003). Delineation of groundwater potential zones and zones of groundwater quality suitable for domestic purposes using remote sensing and GIS. *Hydrological Sciences Journal, 48*(5), 821–833.

Yeh, H. F., Cheng, Y. S., Lin, H. I., & Lee, C. H. (2016). Mapping groundwater recharge potential zone using a GIS approach in Hualian River, Taiwan. *Sustainable Environment Research, 26*(1), 33–43.

Index

A
Adaptive numerical homogenization, 152
Advanced very-high-resolution radiometer (AVHRR), 222
Agricultural lands, 409, 516
Agricultural pollution, 8
Agricultural practises, 316
Agriculture, 1
Agro-ecology, 11
Alkalinity, 361
Amaravathi River basin
  dissolved oxygen (DO), 276
  DO concentration, 282
  downstream, 281
  draining, 272
  geology and hydrogeology, 274, 275
  geomorphology, 273
  groundwater quality, 270
  groundwater samples, 275
  HCA, 277
  irrigation practices, 274
  location, 271
  physicochemical parameters, 277, 279–281
  rainfall and climate, 274
  red soil, 273
  soil and vegetation area, 273
  statistical analysis, 277
  and subbasin, 274
  turbidity, 276
  water flow, 272
  WQI, 276
Amhara National Regional State (ANRS), 75
Ammonia, 341
Analytic hierarchy process (AHP), 25, 39, 44, 47, 413–415
Anthropogenic activities, 341
Anthropogenic intervention, 336
AquaChem version 2016, 319
Aquifers, 2, 63, 515
  as confined and unconfined, 389
  characteristics, 38, 43
  characterization, 444
  geometry, 382
  hydraulic conductivity, 183
  pollution, 8
  systems, 380
  zones, 339
Aquifer Test software, 97
Aquifer vulnerability
  coast belt on Nagapattinam Taluk, 193
  GALDIT vulnerability classes, 190
  groundwater balance and sea water interruption, 180
  variables, 182
ArcGIS software, 154–156, 409
Arid climatic conditions, 438
Artificial groundwater recharge, 436
  AHP method, 413–415
  anthropological planned activity, 408
  aquifers, 438
  Ayyar basin, 409
  change detection analysis, 418
  classification, 436
  conservation, 436
  Dindigul block, 409
  drain pipes, 440
  GIS techniques, 408

C. B. Pande, K. N. Moharir (eds.), *Groundwater Resources Development and Planning in the Semi-Arid Region*, https://doi.org/10.1007/978-3-030-68124-1

Artificial groundwater recharge (*cont.*)
IDW method, 420
land use and cover, 419
lineament density map, 419
pairwise AHP, 423
pairwise comparison matrix, 425
percolation tank, 437–439
preparation, thematic layers, 412
PVC pipe, 441
rainfall, 444
rain water, 440
roof top rain, 443
SCS method, 442
site containment, 419
and structures, 436
sustainable management, 408
TDS values, 443
thematic layers, 416
trapezoidal tank, 438
tubewells, 437
unconfined aquifers, 438
water level in tubewells, 443
zones, 419, 426
Artificial neural network (ANN), 56, 57
advantage, 131
algorithms techniques, 131
dynamic nonlinear modelling system, 130
layers, 131, 132
performance, 130, 132
sigmoidal activation function, 132
simulation of precipitation, 130
training process, 132
Artificial recharge, 166, 168, 390, 419

B

Bar plot displaying, 32
Basin model component, 474
Bicarbonate ions, 253
Biochemical oxygen demand (BOD), 276, 310
Biological oxygen demand (BOD), 152
Bioretention, 6
Boolean logic, 39
Bostanli Dam, 469

C

Calcium, 250, 363
Calibration, 509
Canadian Council of Ministers of the Environment Water quality Index (CCMEWQI), 295, 300, 301, 304, 307, 309
Carbonate, 253
Carbonate geological formations, 45
Carbonate-rich minerals, 253
Catastrophic floods, 468
Catchment grid, 502
C-factor, 79
Chalakudy River Basin
Chalakudy puzha, 354
dams, 354
groundwater analysis, 358
groundwater quality analysis, 355
location, 354–356
origin, 354
and Periyar rivers, 354
physicochemical parameters, 355
piper trilinear diagram, 358, 364, 365, 367
rainfall pattern and distribution, 354
spatial modelling and surface interpolation, 356–357
spatial variation, ground water
alkalinity, 361
calcium, 363
chlorides, 361
dissolved oxygen, 362
EC, 359
hydrogeochemical facies, 364, 365
magnesium, 364
nitrite and nitrate, 362
pH, 359, 360
phosphate, 363
potassium, 364
salinity, 361
sodium, 364
sulphates, 363
TDS values, 360
total hardness, 361, 362
turbidity, 360
WQI, 357, 358
drinking purpose, 365
spatial variation map, 365
Chamber-1 PVC pipe, 440
Champa pooling station, 482
Change detection analysis, 407, 409, 418, 428
Chemical oxygen demand (COD), 130, 276
Chhattisgarh State Soil Map, 473
Chlorides, 252, 361
Chloro-alkaline indices (CAI), 328
Classification algorithm technique, 489
Clay soil, 517
Climate, 516
Climate change, 5, 6, 514
Cluster analysis (CA), 285, 286
CNB monitoring

monthly water storage, 2018–2019, 526, 528, 529, 537, 538, 540, 542, 543, 545, 547, 548, 550, 552
rainwater harvesting, study area, 525
storage capacity, 536
water storage characteristics, 525
Coefficient of determination, 59, 138
Coefficient of Efficiency, 137
Conceptual flowchart, 471
Conceptual model
boundary condition, 155
calibrated model, 159, 160
detection, groundwater movement, 152
Dharsiwa block, 153, 161
digitization, 154
flow budget, 159
grids of different head values, 159
isotopic, hydrochemical and hydrogeological approach, 152
modflow, 158
nitrate contamination, 153
parameters, 151
rainfall, 156, 157
source and sinks coverage, 155
transport modelling, 152
upscaling, 152, 162
Conductance, 155, 156, 162
Confined aquifer, 109, 112, 113
Contaminants, 152, 153, 170
Conventional drainage systems, 12, 13
Correlation between LST and NDVI
1995
2D scatterplot, 226, 227
N-S and E-W profiles, 226, 228
study areas, 226
2000
2D scatterplots, 227, 229
N-S and E-W profiles, 227, 230
study areas, 227
2005
2D scatterplot, 229, 231
N-S and E-W profiles, 229, 232
study areas, 229
2010
2D scatterplots, 231, 233
N-S and E-W profile, 231, 234
study areas, 231
2015
2D scatterplot, 233, 235
N-S and E-W profile, 233, 236
study areas, 231
DN value conversion to spatial radiance, 225
Landsat OLI data, 226
Landsat TM, 226
LST maps, 224
Nagapattinam, 222
objectives, 223
research methodology, 224
study area map, 223
Vedaranyam, 222
vegetation index, 226
Correlation coefficient, 59
Cost-benefit, 43
Cropland, 516
Cuddalore aquifer, 167
Curve number map, 504

D
Daily rainfall data, 472
Deccan trap formation, 438
Decision-making problem, 414
Decision-making process, 24
Decision rules, 43, 44
Decontamination process, 114, 115, 118, 122
Deep aquifers, 8, 14
Deep confined aquifers, 7
Deep structures, 22
Diffusive interface approach, 54
Digital elevation model (DEM), 202, 208, 209, 473, 474, 515
Digital groundwater prospects maps, 372
Digital image processing, 412
Digital numbers (DNs), 224
Digitization, 154, 155
Dindigul block, 407–430
location, 409
methodology, 410
satellite images, 418
tropical climate, 410
Discharge values, 504, 505
Dissolved oxygen (DO), 152, 282, 302, 309, 362
Drainage network, 474
Drain pipe-3, 441
Drawdown (DD), 442
Drinking potential
PIG, 344, 346, 347
WQI, 344, 346, 347
Drinking purposes, 316, 322, 331
Drinking water quality, 319, 322
Drip irrigation, 10–12
Dryland cultivation, 516

E
Earth formations, 389
E. coli contaminated water, 322
Ecosystem natural attenuation, 294
Efficiency index, 137
Electrical conductivity (EC), 249, 310, 359
Erosion risk mapping, 82
Ethylenediaminetetraacetic acid (EDTA), 243
Exchangeable sodium percentage (ESP), 262

F
False color composite (FCC), 414
Fecal coliform (FColi), 310
Feedforward neural network (FFNN), 131, 133, 141, 142, 144
Finite element method (FEM)
  groundwater flow, 111
  and Meshfree method, 109
  numerical analysis, 111
  numerical method in aquifer modelling, 108
  with optimization tools, 109
Fletcher-Reeves conjugate gradient algorithm, 134, 135
Flood discharge
  hydraulic model, 486
  IDF, 487
  Kuttanad region, 486
  life and property, 485, 487
  Mangalam river basin, 486
  QR approach, 486
  study area, 487
Flood estimation, 468
Flood hazard mapping, 469
Flood hydrograph, 468
Flood mitigation, 472
  ASTER, 473
  conceptual flowchart, 471
  DDF curve, 475
  DEM, 473
  flood inundation map, 471
  HEC-HMS and HEC-RAS modelling tools, 469
  HEC-HMS-RAS software, 468
  hydro-spatial modelling, 468
  IDF curve, 475
  LULC map, 474
  Manning's coefficient, 469
  runoff data, 471
  SCS-CN model, 470
Flood modelling
  catchment delineation process, 501
  digital elevation model, 500
  flow direction map, 501
  HEC-HMS model, 500
  hydrologic model, 502
Flood risk management, 12
Floods, 13, 14
Fluoride, 253
Fluoride pollution index (FPI), 245, 246, 255, 256
Flushing method, 114, 118, 122
Fresh water, 316
  flushing, 122
  demand, 5

G
GALDIT Index, 189, 190
GALDIT model, 181, 184, 187, 190–192
Galerkin's finite element method, 108, 111, 112
Gaussian process regression (GPR), 55, 56, 58, 65, 67
General hardness, 361
Genetic programming (GP), 57
Geographical distribution, 26
Geographical patterns, 41, 42
Geographic information systems (GIS), 23, 489
  advantages, 408
  Arc GIS 10.2, 248
  Chalakudy river basin, 357
  and digital image processing, 412
  EO data with hydrological models, 370
  geospatial data, 369
  in groundwater modelling, 381, 382
  IDW interpolation, water quality data, 248
  MAR (*see* Managed aquifer recharge (MAR))
  and MCDM, 408
  Nilakottai taluk, 248
  software, 514, 517
  spatial data sets, 411
  ulagalla tank cascade landscape, 240
Georeferencing, 154
Geospatial methods, 179
Geospatial technologies, 370, 381
Gibbs diagram, 343–345
Gibbs plot, 324
Global MAR Inventory Database, 41
Global Positioning System (GPS), 76
Google earth images, 154
GRACE-FO (twin satellites), 380
GRACE satellites, 378
Gradient descent with momentum (GDM), 136
Gravity Recovery and Climate Experiment (GRACE), 376–380

Gravity redistribution of the earth, 378
Ground field survey, 337
Groundwater, 20, 28, 42
abuse, 179
characterization, 343
contaminants, 108
environment, 108
forced contaminant load, 180
hydrogeological conditions, 182, 183
natural sources, 240
numerical modelling, 95
physical characteristics
EC, 249
pH, 248
TDS, 250
TH, 250
in Punnam village, 270
purposes, 129
quality, 107, 168
in Raipur city, 309
SAR interferometry, 380
and seawater interruption, 180, 182
simulation, 144
source of water supply, 389
Groundwater chemistry
Gibbs diagram, 343–345
KRB (*see* Kallada river basin (KRB))
resources, 336
water rock interaction, 343–345
Groundwater contamination, 240
Groundwater development and sustainable planning, 514
Groundwater drought, 390
Groundwater flow, 168
conceptual model, 161 (*see also* Conceptual model)
flow budget, 158, 159
Kharun River flows, 153
modflow, 158
multiphase flow, 152
and transport modelling, 169
and transport processes, 166
well flow rate, 155
Ground water forecasting, 130, 139
Groundwater level
ANNs, 142
depletion, 130
fluctuation, 390
model development, 139
modelling
ANNs, 131, 132
conjugate gradient algorithm, 134, 136
FFNN, 131
GDM, 136
learning rate, 136
LM training algorithm, 133
OSS technique, 135
resilient backpropagation algorithm, 133
SCG algorithm, 134
straining algorithms, 133
natural causes, 390
performance, calibrated network model, 137
trend analysis, 391, 397, 398
WA-SVR, 142
Groundwater management, semi-arid regions
irrigation agriculture, 6
irrigation networks, 6
mechanized pumping technologies, 7
overexploitation, groundwater sources (*see* Overexploitation of groundwater sources)
rainwater, 6
wells, 6
Groundwater mapping
derivative layers, 371
GRACE, 376–380
HGM, 371
hydrological maps, 371
in lithology, 371
RS technology, 371
Groundwater modelling, 166, 381
Groundwater pollution, 8
Groundwater potential zone (GPZ) mapping, 130
Groundwater prospect mapping, 514
Groundwater qualities, 240, 354
for drinking, 240
factors, 269
human health risk assessment, 240
irrigation purpose, 240
Raipur city, 309
seasonal variation, 339, 341, 342
Groundwater recharge, 514
artificial recharge, 165, 166, 168, 390
borehole locations, 170, 171
boundary conditions, 172
calibration, 172
conceptual model design, 171
Cuddalore aquifer in Tamil Nadu, 167
geoelectrical resistivity survey, 167
in India, 166
MT3D model, 168–170
natural recharge, 390
validation, 172
Groundwater remediation
finite element formulation

Groundwater remediation (*cont.*)
for contaminant transport, 112
for groundwater flow, 111, 112
flow and contaminant transport, 109, 110
multiobjective spatial pumping optimization, 109
removal, contaminants/pollutants, 108
strategies, aquifer remediation, 114
two-dimensional flow and transport models, 112–114
Groundwater resources, 353, 354, 514
Groundwater salinity predictions
accuracy, 55
aquifer, 63
barrier wells, 61
coastal aquifers, 53
parameters, 61
systems, 55
complex-coupled, 54
complex 3D groundwater flow, 66
development dataset, 62
diffusive interface approach, 54
Discipulus GP Software, 63
domestic consumption, 61
draught, 66
efficiency, 55
ensemble prediction models, 55
flooding, 66
fluids, 54
high-resolution discretization, 61
homogeneous ensemble models, 54, 66
homogeneous model, 60
hydrological studies, 66
Latin Hypercube sampling strategy, 62
machine learning algorithms, 55
machine learning-based prediction models, 54, 55, 62
MATLAB parameters, 63
methodology
ANN, 56, 57
GMDH, 58
GP, 57
GPR, 58
SVMR, 57
3D numerical simulation, 56
models, 58, 59, 63
monitoring wells, 61
performances evaluation, 59, 60, 64, 65
phases, 58, 59
pumping patterns, 66
saltwater intrusion, 53
sharp interface approach, 54
statistical indices, 65
3D numerical simulation, 61, 67
3D transient simulation, 62
transition zone, 54
transport model, 66
Groundwater table, 7
Group method of data handling (GMDH), 58
Gumbel distribution, 475, 488
Gumbles extreme values theory, 469
Guna-tana watershed, 74
analytical approach, 76
cover and management factor, 83
data source, 76
description, 75
erosion risk mapping, 82
Lake tana, 87
land degradation, 87
land use and land cover change, 80, 81
LULC, 86
RUSLE model, 77–80
sediment yield, 85, 88
slope length, 83
soil and water conservation, 85, 86
soil erosion, 87
soil loss, 83, 84, 88
steepness factor, 83
support factor, 83
validation, 86

H
HEC-GeoHMS, 468–470
HEC-GeoRAS, 468
HEC-HMS model, 480, 482, 497
HEC-HMS-RAS software, 468
High energy flood water, 471
Hill Piper diagram, 343
Homogeneous and heterogeneous aquifer systems, 54
Homogeneous model, 60
Horton index, 294
Human activities, 514
Human health risk assessment (HHRA), 247, 248, 255, 256
Hydraulic conductivity, 157, 160, 172
Hydraulic model, 477
geometry, 477
HEC-Geo-RAS extension, 477
RAS model, 478
Hydrochemical evolution, 364
Hydrochemical facies, 316, 324, 343
Hydrochemistry, 331
Hydrogeochemical process, 240

Hydro geo-morphological (HGM) maps, 371, 373
Hydrological maps, 371
Hydrologic cycle, 3
Hydrologic model, 471, 474, 493
Hydrologic soil map, 503
Hydro-meteorology, 38
Hypothetical pumping well, 96

I
IDW interpolation method, 248
Impact assessment, 43
Induced bank filtration systems, 22
Industrial effluents, 107
Industrialization, 353
Innovative stormwater management techniques, 5
Innovative trend analysis, 396–398
Integrated distance weighted (IDW) method, 420
Intensity-duration-frequency (IDF)
  curves, 469, 498, 499
  curve number, 496
  empirical equation, 488
  HEC-HMS, 495
  land use changes, 495
  relationship, 487
Inundation, 486, 510
Inundation pattern, 479
Inverse distance weighted (IDW), 248, 357
Ionic balance error (IBE), 243
Irrigation, 6, 7
  chemistry of water, 328
  factors, 331
  groundwater and surface water, 330
  KR, 331
  magnesium content of water, 330
  practices, 274
  SAR values, 329
  sodium in water, 330
Irrigation indexes
  ESP, 262
  KR, 262
  K value, 260, 261
  magnesium hazards, 258
  percentage sodium (%Na), 257, 260
  PI, 258
  PS, 260
  RBSC, 260
  RSC, 258
  SAR, 257
Irrigation water quality indexes (IWQI), 240, 246, 247

K
Kallada River Basin (KRB)
  ground field survey, 337
  groundwater, 337, 339, 342
  location map, 336, 337
  parameters, 338, 339, 341, 342
  physiography, 337, 338
  sampling sites, 337
  well-cleaned plastic containers, 337
Karl Pearson correlation matrix analysis, 277
Karur
  Amaravathi River (*see* Amaravathi River basin)
  dyeing industry, 270
  major product groups, 270
  river, geomorphology, soil and geology, 272
  textile center, 270
Kelley's ratio (KR), 262, 331
K-factor, 78
k-means clustering algorithm, 28
Köppen-Geiger climate classification, 26, 30

L
Lakshadweep Sea, 336
Landsat 8 optical data, 456
Landsat 8 satellite data, 456
Landscape-based LID techniques, 6
Land subsidence, 380, 381
Land surface temperature (LST), 221
Land use and land cover (LULC), 76, 423
  categories, 419
  classification system, 412
  Dindigul block, 416, 428
  graphical interpretation, 418
Landuse change, 489
Latin Hypercube sampling strategy, 62
Latitude filtered, 30
Levenberg–Marquardt (LM) algorithm, 130, 133
Low impact development (LID), 6

M
Machine learning-based prediction models, 55
Magnesium, 251, 364
Magnesium hazards (MH), 258, 330
Magnitude of trend, 396
Managed aquifer recharge (MAR), 240
  agricultural impact, 39
  arithmetic means, 38
  boxplot of weights, 38, 39
  climate change, 20

Managed aquifer recharge (MAR) (*cont.*)
criteria selection, 33, 39, 42, 43
data, 27
database, 27, 29, 30
decision rules, 36, 39, 40, 43, 44
demand, 20
evaporation, 39
geographical patterns, 41, 42
geophysics, 39
implementation, 20
induced bank filtration, 38
k-means clustering, 40
objectives, 36
paper review, 29, 31, 32
paper selection, 27, 28
remote sensing, 23
review process, 28
scatter plot, 41
scope, 25, 26
SDG, 20
semi-arid regions, 20, 44–46
spreading methods, 40
suitability mapping, 23–25, 46, 47
techniques, 20–23, 33
weight distribution, 42, 43
weighting methods, 36, 39, 40, 43, 44
Management criteria, 46
Manning formula, 479
Mean absolute error (MAE), 59
Mann-Kendall test, 391, 392, 394, 397, 398
Mean sea level (MSL), 514
Metrological component, 475
Micro-irrigation techniques
advantages, 10
agricultural growth, 11
benefits, 11
crop yields, 9
drip irrigation, 10, 12
implementation, 10
real water savings, 11, 12
sprinkler irrigation, 10
type, 11
Microwave Imaging Radiometer with Aperture Synthesis (MIRAS), 376
Microwave remote sensing satellites, 380
Model discretization, 171
MODFLOW (modular flow) model, 166, 168, 173
finite difference grids, 96
numerical modelling, 96, 101, 104
software package, 170
Modular three-dimensional transport model (MT 3D), 168–170
Monotonic trend, 392, 396, 401
Monsoon (MON), 341, 342
Most extreme GALDIT-Index, 189
Multi-criteria decision analysis, 23
Multi-criteria decision making (MCDM), 408
Multi-criteria evaluation (MCE) technique, 409
Multi-influencing factor (MIF), 24, 44, 47
Multiphase flow, 152
Multiwell pumping aquifer tests, 93–105

N

Nash–Sutcliffe efficiency (NE), 59
Nash–Sutcliffe Efficiency Index, 137
National Drinking Water Project, 371
National Sanitation Foundation Water Quality Index (NSFWQI), 295, 297, 300, 301, 304, 308
National urban sanitation policy, 294
Natural environment, 81
Natural recharge, 390
Near-infrared (NIR), 226
Netravati River basin
geological and hydrogeological conditions, 326
irrigational status, 319
in situ monitoring, parameters of water sample, 318
location, 317
physicochemical parameters and trace elements, 320
post-monsoon season, 318
rocks, 317
surface and groundwater, 319
CAI, 328
EC, 320
Gibbs plot, 324
hydrochemical facies, 324
pH, 319
TDS, 321
trace elements, 328
WQI, 322, 323
watershed, 317
Neuman curve fitting method, 97
Neuman β parameter, 95
Neuman solution, 96, 98–104
Nilakottai taluk in Dindigul
cumulative rainfall, 241
FPI, 245, 246
groundwater contamination, 241
HHRA, 247, 248
IWQI, 246, 247
locations, 241, 242

NPI, 244, 245
Quartzite, 242
sampling and analysis, 242, 243
WQI method, 243
Nitrate, 152, 153, 162, 253
Nitrate nitrogen (NO_3), 310
Nitrate pollution index (NPI), 244, 245, 254, 256
Nondominated sorting genetic algorithm II (NSGA II), 109
Nonparametric tests, 392
Normalized difference vegetation index (NDVI), 222
Numerical groundwater models, 168
Numerical modelling, 95

O
One-step secant (OSS) backpropagation, 135, 142
Open channel Hydraulics, 479
Ordered weighted averaging (OWA), 25
Organic matter, 310
Overexploitation of groundwater sources
aquifers pollution, 8
declining groundwater tables, 8
deep confined aquifers, 7
groundwater recharge, 7
groundwater table, 7
impacts, 7
irrigation, 7
semi-arid regions, 7

P
Pairwise comparison, 24
Pairwise comparison matrices (PCMs), 373, 374
Pearson's correlation coefficient, 277
Per capita water availability, India, 514
Percentage sodium (%Na), 257, 260, 330
Periodic water level, 443
Permeability graph, 445
Permeability index (PI), 258, 331
Pesticides, 153
P-factor, 79
Phosphate, 362
Phosphorus, 362
Physical geography, 32, 38, 46
Piper trilinear diagrams, 340, 343, 358, 364, 365, 367
Planning natural resources management, 514
Polluted water, 246
Pollution index of groundwater (PIG), 344, 346–349
POM season, 341
Poor Water category, 346
Post-monsoon (POM), 341, 342
Potassium, 252, 364
Precipitation, 180
Pre-monsoon (PRM), 341, 342
Pre-post monsoon seasons, 343
Principal component analysis (PCA), 25, 277, 284, 285
PRM season, 341
Pseudo color composite (PCC), 415
Pumping aquifer tests, 93, 95, 96, 98, 99, 101
Pumping wells
contaminated aquifer, 118
in flow domain, 114
and flushing, 114
PSO technique, 109
remediation strategy, 115
simulation period, 118
two-dimensional flow and transport models, 114

Q
Q-mode hierarchical cluster analysis, 287
Quality of water, 316, 322, 328
Quantile regression (QR), 486
Quartzite, 242

R
Rainfall, 156, 157, 391
Rainfall and runoff harvesting, 23
Rainfall erosivity factor (R), 77
Rainfall-runoff modelling, 479
Rainwater, 14
Rainwater harvesting structures, semi-arid regions
agricultural land, 516
agriculture yields, 518
average depths, water levels in wells, 554, 556
Barshitakli Taluka, Maharashtra, 514, 515
climate, 516
drainage line, 518
groundwater level monitoring
2015–2016, 519
2016–2017, 519, 522–525
2017–2018, 519, 527
2018–2019, 520, 528–531
2019 *vs*. 2018, 555

Rainwater harvesting structures (*cont.*)
2019–2020, 536
IDW method, 518
Kajaleshwar-Warkhed watersheds, 515, 518
monthly groundwater map (2018–2019), 521, 525, 531–536
Nala deepening, 518
observation well location maps, 518
soil and water conservation, 518
soil classification, 517
soil slope, 517
soil texture map, micro watersheds, 517
soil types, 517
topography, 516
water levels, 518
well water levels, 2016–2017, 554, 557
Rainwater management strategy, 518
Raipur city
CCMEWQI, 297
groundwater quality, 295, 297, 300
Kharun River flows, 294
lakes, 295
location, 294
NSFWQI Map, 295
spatial distribution
of BOD, 304
pH and nitrate, 303, 310
water quality parameters, 297
WQI and parameters, 307
Ranking methods, 24
Rank-reversal issue, 44
Rating methods, 24, 47
Red soil, 273
Remote sensing (RS), 23, 200, 209, 211, 373, 454, 514
AHP method, 373
MIRAS, 376
soil moisture, 374, 376
technique, 462
technology, 369, 464
urban monitoring, 407
Reservoir sedimentation, 453, 454
elevation-capacity curve, 454
features, 455
location, 455
quantification, 454
remote sensing technique, 459
satellite data, 457
temporal and spectral resolution datasets, 454
Residual sodium bicarbonate (RBSC), 260
Residual sodium carbonate (RSC), 258, 330
Resilient backpropagation algorithm, 133, 134
Resistivity and lithological survey, 442
Revised Universal Soil Loss Equation (RUSLE), 77–80
R-factor, 78
Rihand Dam, 455
Rihand reservoir, 460–463
Rihand River, 455
Riparian vegetation, 354
R-mode hierarchical cluster analysis, 286, 288
Roof top rain water harvesting (RWH), 440
Roof water, 440
Root mean square error (RMSE), 59
Root zone supplements, 435

S
Safe drinking water, 270
Sahyadri, 335
Saline soils, 262
Saline water intrusion, 196
Salinization, 180
Saltwater intrusion, 54
SAR (Interferometric Synthetic Aperture Radar), 380
Satellite data, 370
Satellite imagery, 457
Scaled conjugate gradient (SCG), 134
Scaling methods, 25
SCS Curve Number technique, 474
Seasonal variation in groundwater quality, 339, 341, 342
Seawater-freshwater intersection, 54
Sea water intrusion, 179, 185, 187, 188
Sediment delivery ratio (SDR), 80, 85
Sediment transport, 74
Sediment yield, 79
Semi-arid regions, 20, 25, 29, 30, 32, 44–46
fissured rocks, 4
groundwater, 4
groundwater development and sustainable planning, 514
river basins, 4
water scarcity, 4
Sens slope methods, 391, 395, 398, 401
Shallow and deep aquifers, 22
Shallow aquifers, 370, 374
Sharp interface approach, 54
Silicate concentration, 341
Single layer model, 151
Small-scale structures, 22
SMAP satellite, 377
SMOS satellite, 376
Sodium, 252, 364

Sodium adsorption ratio (SAR), 257, 329
Soil and water conservation (SWC) practice, 79
Soils, 517
  classification, 517
  conservation, 74
  erodibility factor, 78
  erosion, 74, 81
  moisture, 370, 374, 376
  slope, 517
  texture map, micro watersheds, 517
Soil moisture active passive (SMAP), 376
Soil moisture and ocean salinity (SMOS), 376
Solar electromagnetic radiation, 226
Solute-transport modelling, 173
Source pumping well, 103, 104
Sources of pollution, 8
South Gondar Zone, 75
Spatial analysis tools, 211
Spatial distributed hydrological model, 510
Spatial distribution, 82, 174
  BOD in Amaravathi River basin, 279, 280, 282, 283
  cation exchange process, 281
  of Fecal Coliform, 305
  HCO_3^- concentration, 281
  turbidity in water, 279
Spatial Interpolation technique, 357
Spearman's Rho test, 394, 395, 397, 398, 401
Spreading methods, 21, 29
Spring thickness, 187, 188
Spring water-driven conductivity, 183
Stable isotopes, 152
Standard SCG backpropagation algorithm, 134
Stormwater, 13
Structural and non-structural best management practices (BMPs), 6
Sub-index (SI), 346
Subsurface water, 3
Successive reservoir levels, 461
Sulfate, 253
Support vector machine regression (SVMR), 57
Support vector regression (SVR)
  and FFNN, 131
  parameters, 140
  WA-SVR model (*see* Wavelet support vector machine (WA-SVR) model)
Surface erosion, 74
Surface water, 32
  alkaline earth, 324
  cation contents, 324
  Cl^- and HCO_3^-, 326
  on EC and TDS, 321
  E. coli contaminated water, 322
  electrical conductivity, 321
  Gibbs plot, 324
  and groundwater interchange, 316
  and groundwater samples, 329
  magnesium values, 330
  Netravati River, 317, 319
  post-monsoon season, 318
  quality, 5
  resources, 3
Surface water sources
  conventional drainage systems, 13
  drainage systems, 13
  extreme flood events, 12
  flood risk management, 12
  floods, 13
  large dams, 12
  pollution, 14
  reservoir siltation, 12
  stormwater, 13
  SUDS, 13, 14
  urbanization, 13
Sustainable Development Goals (SDGs), 9, 20, 47
Sustainable groundwater management, 93
  agro-ecology, 11
  aquifer recharge, 10
  challenges, 9
  drip irrigation, 10–12
  hydro-meteorology, 11
  India, 9, 11
  Indian agriculture, 9
  irrigation techniques, 9
  Legislation, 10
  micro-irrigation, 9–12
  SDGs, 12
  sustainable agricultural demand, 9
Sustainable land management, 74
Sustainable management, 167
Sustainable urban drainage systems (SUDS), 13
Sustainable water management, 2, 9
Synthetic harmful coefficient (K), 260, 261

T

Taga catchment, 479
Taga Catchment HEC-HMS Basin Model, 477
Temperature, 277, 309
Terrestrial water storage (TWS), 377
Theim and Dupuit's equation, 442
Thermal infrared radiation (TIR), 221
Three-dimensional groundwater flow, 166
Topography, 516
Total alkalinity (TA), 341

Total coliform (Tcoli), 311
Total dissolved solids (TDS), 311, 341, 443
Training algorithms, 133
Transition zone, 54
Transmissivity, 94, 96, 98–105
Transport model
  MODFLOW model, 173
  MT3D model, 168, 169
  solute-transport modelling, 173
  steps in flow and transport modelling, 169
Trapezoidal formula, 460
Trapezoidal method, 460, 461
Trend analysis, 391
True color composite (TCC), 412, 413
Turbidity, 311

U
Unconfined aquifers
  during pumping aquifer test, 93
  homogeneous and isotropic, 97
  isotropic and homogeneous, 96, 104
  Neuman method, 94
  time-drawdown, 94, 95, 97–99, 101, 103
  transmissivity and specific yield, 94
  unconfined well function, 94
Universal Soil Loss Equation (USLE), 76
Upscaling, 152, 162
Urbanization, 4, 13, 293
Urban groundwater pollution potential, 294
Urban pollution, 8
Urban stormwater runoff, 6

V
Vegetation, 222

W
Waste management, 240
Wastewater disposal, 294
Water, 1–5
  analysis, 336
  balance, 170
  conservation structures, 518
  demand, 270
  harvesting, 436
  management techniques, 3
  pixel, 459
Water quality, 294, 316
  agriculture, 339
  classification, 340, 343
  domestic, agriculture, commercial and industrial, 336
  drinking and industrial purposes, 339
  natural factors and man-made factors, 336
  parameters, 340
Water quality index (WQI), 344, 346, 347, 354, 367
  Amaravathi River basin, 276, 283
  assessment and management, 367
  in Chalakudy river basin, 357, 358
  classification, water type, 254
  computed qi and Wi, 358
  for drinking purpose, 365
  in Germany, 294
  Netravati River basin, 322, 323
  Nilakottai taluk, 243
  spatial variation map, 367
  suitability, drinking purposes, 336
  and type of water, 358
Water quality management, 5
Water rock interaction, 343–345
Water scarcity, 2, 5
Watershed, 75, 85, 86
Watershed development
  annual temperature fluctuates, 202
  aquifer zones, 202
  automatic stream ordering, 211
  basaltic rock formation, 202
  computing drainage and geomorphic parameters, 200
  conventional and automatic techniques, 212
  crops, 201
  DEM values, 214
  dendritic and sub-dendritic system, 210
  drainage and basin characteristics, 216
  drainage and network basin parameters, 209
  drainage parameters, 200
  elevation values, 212
  elongation ratio, 212
  flow direction, 214
  geomorphic landforms, 209
  geomorphological structures, 200
  GIS methods, 200
  GIS techniques, 211
  hydrological system processes, 209
  innovative techniques, 211
  land and water resources, 210
  land cover, 215
  land use, 215
  linear and aerial factors, 200
  logarithm graph, 200
  methodology, 202
  mild winters, 202

morphological parameters, 200
morphometric parameters, 200
agriculture field, 204
basin area, 208
basin perimeter, 208
bifurcation ratio, 206
calculations, 202
digital elevation model, 209
ecosystem management, 204
land cover, 209
land use, 209
length area relation, 208
linear elements, 202
mean stream length, 206
rho coefficient, 207
river basin management, 204
soil and water conservation activates, 204
stream length, 206
stream length ratio, 207
stream number, 206
stream order, 205
policymakers, 199, 212
quantitative characteristics, 203
remote sensing techniques, 200
RS and GIS systems, 213
soil slope, 216
stream density, 210
stream length, 211
stream network, 212
stream orders, 203, 212, 213
stream-order maps, 211
stream patterns, 209
warm summers, 202
water and soil resource management, 199
water conservation planning, 212
water resources, 217
watershed planning method, 209
Watershed management planning, 202
Watershed planning method, 209
Water spread area, 454
Water storage characteristics, 525
Wavelet support vector machine (WA-SVR) model
MATLAB, 139
performance measures, 145
structure, 139, 140
SVR parameters, 140
wavelet decomposition series, 140
Weighted Index Overlay Analysis (WIOA), 409
Weighted linear combination (WLC), 25, 39, 44
Weighted overlay combination (WOL), 25
Weighting methods, 43, 44
Wells of Churu district, 392
Western Ghats, 335
east-flowing rivers, 336
Kerala, 335
life sustaining functions, 335